

THE ALKALINE ROCKS OF PORT CYGNET,
TASMANIA

By

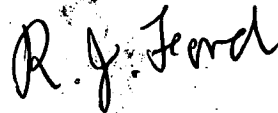
RAMSAY J. FORD

Submitted in fulfilment of the requirements
for the degree of Doctor of Philosophy

University of Tasmania
HOBART

1983

This thesis contains no material which has been accepted for the award of any other degree or diploma in any university, and to the best of my knowledge and belief, contains no copy or paraphrase of material previously published or written by another person, except where due reference is made in the text of this thesis.

A handwritten signature in dark ink, appearing to read 'R.J. Ford'. The signature is written in a cursive, slightly slanted style.

R.J. Ford

University of Tasmania,
March, 1983.

USE OF THESES

THIS VOLUME is the property of the University of Tasmania, but the literary rights of the author must be respected. Passages must not be copied or closely paraphrased without the written consent of the author. If the reader obtains any assistance from ^{the} volume he must give proper credit.

...has

FRONTISPIECE

Port des Cygnes, explored by C.F.
Beautemps-Beaupré, February 1793



Port Cygnet looking to the southeast. Regatta Point is at centre, and Langdon's Point is at the extreme right of the near shoreline. Pyrrhotite nodules occur near the building on far shore at half-left of centre.

TABLE OF CONTENTS

	Page No.
Frontispiece	
List of Tables	i
List of Figures	iii
List of Plates	viii
ABSTRACT	
CHAPTER I INTRODUCTION	I-1
Previous work and literature	I-3
Acknowledgements	I-10
Geological setting	I-11
Geology of Port Cygnet district	I-14
Geological structure	I-16
The main rock types	I-18
CHAPTER II MICROSCOPIC PETROGRAPHY	II-1
Syenite porphyry	II-1
Sanidine porphyries	II-15
Variants of the sanidine porphyries	II-28
Summary of alkaline rocks	II-40
Hybrid rocks	II-41
Summary of hybrid rocks	II-59
CHAPTER III MINERALOGY	III-1
The nepheline geothermometer	III-1
The two feldspar geothermometer	III-10
The biotite thermometer	III-22
Melanite mineralogy	III-29
Amphibole mineralogy	III-36
Pyroxene mineralogy	III-50
Pyroxenes in the hybrid rocks	III-64
Feldspathoid mineralogy	III-66
Feldspar mineralogy	III-69
Scapolite mineralogy	III-96

	Page No.
CHAPTER IV MAJOR ELEMENT CHEMISTRY	IV-1
The alkaline intrusive rocks	IV-7
Syenite porphyries	IV-14
Sanidine rocks	IV-23
Comparisons	IV-27
Summary of major element data for the alkaline rocks	IV-40
The hybrid rocks	IV-43
CHAPTER V MINOR ELEMENT CHEMISTRY	V-1
The alkaline rocks	V-1
The hybrid rocks	V-32
The amphibole inclusions	V-40
Summary of minor element data	V-44
CHAPTER VI ISOTOPE GEOLOGY	VI-1
Sulphur isotopes	VI-1
Strontium isotopes	VI-5
Summary	VI-12
CHAPTER VII THE ORIGIN OF THE PORT CYGNET ALKALINE ROCKS	VII-1
Summary of mechanisms	VII-4
Syenite porphyries	VII-8
Sanidine rocks	VII-16
A basaltic source of the rocks	VII-20
Evidence of parental material	VII-28
The depth of formation of the alkaline rocks	VII-30
The heat source	VII-33
Note on Cape Portland rocks	VII-35
Origin of the garnet trachyte	VII-36
Experimental test of the model	VII-47
Formation of the epidote	VII-50
Origins of other rocks	VII-56
CHAPTER VIII SUMMARY AND CONCLUSIONS	VIII-1
Alkaline rocks	VIII-1
Major element data	VIII-2
Minor element data	VIII-3
Mineralogical data	VIII-5

	Page No.
Isotopic data	VIII-5
Origin of sanidine rocks	VIII-6
Origin of other rocks	VIII-7
Hybrid rocks	VIII-9
Conclusions	VIII-10
Further investigations	VIII-11
REFERENCES	1
REFERENCES ADDENDUM	25

APPENDIX VOLUME

APPENDIX 1	SOME TYPICAL SYENITE ASSOCIATIONS AND OCCURRENCES
APPENDIX 2	X-RAY FLUORESCENCE ANALYTICAL DATA
APPENDIX 3	NORMATIVE DATA
APPENDIX 4	ELECTRON MICROPROBE DATA
APPENDIX 5	SPECIMEN LIST
APPENDIX 6	GEOLOGICAL AND LOCALITY MAPS

LIST OF TABLES

Table No.		Page No.
II-1	Microprobe analyses of Fe-micas from inclusions in sanidine porphyry dyke X50.	II-30
III-1	Nepheline geothermometer data for nephelines and co-existing alkali feldspars.	III-6
III-2	The two feldspar geothermometer data for co-existing plagioclase and alkali feldspars.	III-11
III-3	Distribution data for the Ab molecule from Table III-2.	III-21
III-4	Analyses of biotite from altered dolerite at Regatta Point.	III-23
III-5	Analyses of biotites from re-crystallized hybrid rocks.	III-25
III-6	Analyses of melanite garnets.	III-31
III-7	Debye-Scherrer data and XRF analyses of melanite garnet from the hybrids of Port Cygnet.	
III-8	Analyses of amphiboles.	III-37
III-9	Analyses of pyroxenes.	III-55
III-10	Partial analyses of hauynite and analcime.	III-68
III-11	Structural state data for sanidine phenocrysts.	III-74
III-12	Compositions of feldspars with structural state data.	III-75
III-13	Analyses of cores and rims of feldspar phenocrysts and crystals.	III-86
III-14	Analyses of phases from CY44.	III-97
IV-1	Chemical analyses of some syenite porphyries from Port Cygnet.	IV-2
IV-2	Chemical analyses of some sanidine porphyries from Port Cygnet.	IV-3
IV-3	Average alkaline igneous rock compositions from Le Maitre (1976).	IV-4
IV-4	Average alkaline igneous rock chemical compositions from Nockolds (1954), plus T541, the felsic matrix of amphibolite inclusions from Port Cygnet.	IV-5
IV-5	Chemical analyses of some hybrid rocks from Port Cygnet.	IV-46
V-1	Rare earth element values (ppm) for Port Cygnet rocks.	V-27
V-2	Determination of trace elements in standard rocks.	V-38 - V-39
V-3	Analytical and comparative data for amphibolite inclusions.	V-43

Table No.		Page No.
VI-1	$\delta^{34}\text{S}$ values relative to Canyon Diablo Troilite.	VI-4
VI-2	Initial strontium isotope values.	VI-8
VII-1	Comparison of chemical compositions of typical Port Cygnet alkaline rocks with mixes of amphibolite matrix (T541), tinguaitite, amphibole and syenites.	VII-12a
VII-2	Parental compositions from Helz (1976) compared with Port Cygnet amphibolite.	VII-13
VII-3	Partial melt compositions and CIPW norms at 875°C from Helz (1976) at 5 kbar water pressure.	VII-14
VII-4	Compositions of typical alkaline rocks, alkali olivine basalt and basanite and Port Cygnet tinguaitite.	VII-21
VII-5	Comparison of Cape Portland rocks with experimental partial melt from Helz (1976).	VII-37
VII-6	Electron microprobe analyses of garnet and epidote from garnet trachyte.	VII-43
VII-7	Comparison of garnet trachyte and tinguaitite analyses.	VII-49
VII-8	Electron probe microanalyses of synthetic garnets and a feldspar from experiment T860.	VII-51
VII-9	Analysis of spessartite garnet-composite.	VII-52
VII-10	Microprobe analyses of core plagioclase and zeolite alteration in garnet trachyte.	VII-53

LIST OF FIGURES

Figure No.		Page No.
I-1	Location of the Port Cygnet area.	I-2
I-2	Inset area of Figure I-1 with Port Cygnet localities.	I-4
I-3	Maps of Port Cygnet and Regatta Point after Edwards (1947).	I-8
I-4	A summary of the hybrid rocks at Regatta Point after Edwards (1947).	I-33
III-1	Plot of excess silica in nepheline geothermometer after Hamilton (1961).	III-2
III-2	Perchuk and Ryabchikov (1968) plot for distribution of sodium between co-existing nepheline and alkali feldspar of hybrid rocks. Randomised structure model.	III-3
III-3	Perchuk and Ryabchikov (1968) plot of distribution of K between co-existing potassium nepheline and alkali feldspar. Ordered structure model.	III-5
III-4	Powell and Powell (1977) geothermometer for co-existing nepheline and alkali feldspar.	III-9
III-5	Stormer geothermometer plot for Ab distribution between co-existing feldspars.	III-18
III-6	Powell and Powell geothermometer plot of distribution of Ab between co-existing plagioclase and alkali feldspar.	III-20
III-7	Wones-Eugster $\log_{10} fO_2$ - temperature plot for biotites from the hybrid rocks.	III-26
III-8	Plot of hybrid melanite garnet data on main $\log fO_2$ - silica undersaturation diagram of Huckenholz et al. (1976).	III-35
III-9	Amphibole compositions superimposed on nomenclature recommended by the IMA.	III-42
III-10	Tetrahedral Al-alkali metal plot for amphiboles from the amphibole-bearing rocks.	III-43
III-11	Site occupancy of Al in amphibolite, amphiboles and syenite porphyry.	III-45
III-12	Ca-Mg-Fe plot for amphiboles and pyroxenes of all rocks.	III-46
III-13	The variation of K/Na and Si atoms for amphiboles, amphibolites and alkaline rocks.	III-48
III-14	The main compositional field of pyroxenes for all rocks superimposed on the pyroxene nomenclature scheme of Poldervaart and Hess (1951).	III-51

Figure No.

Page No.

III-15	Replacement of Ca by Na in pyroxenes, particularly those from the hybrid rocks.	III-53
III-16	Di-Hd-Ac molecular plot of pyroxenes from Port Cygnet rocks, compared with other trends.	III-54
III-17	Ternary feldspar plot for feldspars from the alkaline rocks with the solvus for the 900° isotherm and 0.5 kbar pH_2O .	III-70
III-18	Structural states of alkaline feldspars from sanidine porphyries after Wright (1968).	III-77
III-19	Ternary feldspar plot for feldspars from the hybrid rocks.	III-79
III-20	Core-rim compositions for co-existing feldspars in syenite porphyry CY49.	III-81
III-21	Core-rim compositions for co-existing feldspars in syenite porphyry CY70.	III-83
III-22	Core-rim compositions for co-existing phenocrysts in CY61 and CY92.	III-85
III-23	Core-rim compositions for feldspar phenocrysts from the sanidine porphyries.	III-93
III-24	Averaged values of co-existing feldspars from the syenite porphyries compared with other groups on a Ternary feldspar triangle.	III-95
IV-1	Albite-quartz-orthoclase-nepheline normative plot for all rock types.	IV-6
IV-2	Thornton-Tuttle differentiation index - normative quartz or nepheline plot for all rocks.	IV-8
IV-3	Potash-silica plot for the alkaline rocks.	IV-9
IV-4	Thornton-Tuttle differentiation index plot of SiO_2 , Al_2O_3 , and TiO_2 for all rocks.	IV-10
IV-5	Thornton-Tuttle differentiation index plot of K_2O , Na_2O and CaO for all rocks.	IV-11
IV-6	Thornton-Tuttle differentiation index plot of Fe_2O_3 and MgO for all rocks.	IV-12
IV-6a	Harker Plot for Al_2O_3 and K_2O .	IV-12a
IV-6b	Harker Plot for Na_2O and CaO .	IV-12b
IV-6c	Harker Plot for Fe_2O_3 and FeO .	IV-12c
IV-6d	Harker Plot for MgO and TiO_2 .	IV-12d
IV-7	Normative plagioclase-quartz-orthoclase plot for syenite porphyries.	IV-15
IV-8	Nepheline-quartz-kalsilite plot for syenite porphyries and sanidine porphyries.	IV-17
IV-9	NaAlSiO_4 - SiO_2 - KAlSiO_4 plot for syenite porphyries and sanidine porphyries. Main phase boundaries at 1 bar, 1 kbar and 5 kbar pH_2O are shown.	IV-18

Figure No.

Page No.

IV-9a	Fractionation trends for selected rocks of Fig. IV-9.	IV-18a
IV-10	Ab-Q-Or normative plot of syenite porphyries with minima in the system Ab-Q-Or from 0.5 to 10 kbar added.	IV-19
IV-11	Winkler plot for normative Quaternary Ab-Or-Q-An.	IV-21
IV-12	Position of CY85 on the $\text{NaAlSi}_2\text{O}_6$ - KAlSi_2O_6 join at one kbar (from Edgar, 1978).	IV-28
IV-13	Bailey-McDonald Al_2O_3 - SiO_2 -($\text{K}_2\text{O}+\text{Na}_2\text{O}$) plot of Port Cygnet alkaline rocks.	IV-30
IV-14	Section across Al_2O_3 - SiO_2 - Na_2O - K_2O tetrahedron corresponding to the general trend of Fig. IV-13.	IV-31
IV-15	AFM plot for the Port Cygnet alkaline rocks with amphibolite inclusions and their amphibole added.	IV-33
IV-16	Comparative AFM plots for other areas with Port Cygnet plot added.	IV-34
IV-17	AFM plot comparing the Port Cygnet potassium-rich rocks with those of Finmark and eastern Ontario (after Appleyard, 1974).	IV-36
IV-18	Total alkali plot for all rocks with trends for other areas added.	IV-37
IV-19	Total alkali plot comparing the Port Cygnet potassium-rich rocks with those of Finmark and eastern Ontario (after Appleyard, 1974).	IV-39
IV-20	Niggli QLM plot for alkaline rocks and their inclusions.	IV-41
IV-21	Niggli QLM plot of Phalaborwa Complex showing the relation between syenite, feldspathic pyroxenite and pyroxenite.	IV-42
IV-22	Fe_2O_3 - $\text{K}_2\text{O}/\text{MgO}$ plot for all rocks showing the relationships of dolerite, melanocratic hybrids and alkaline rocks including leucocratic hybrids.	IV-45
IV-23	K_2O - Fe_2O_3 - MgO molar plot for the alkaline and hybrid rocks.	IV-47
V-1	Thornton-Tuttle differentiation index plot of Rb, Ba, and Sr for all rocks.	V-2
V-2	Thornton-Tuttle differentiation index plot of Sc, Ga, Cs, and Zn for all rocks.	V-3
V-3	Thornton-Tuttle differentiation index plot of Cu, Y, Zr, and Ni for all rocks.	V-4
V-4	K-Rb plot for alkaline rocks and melanocratic hybrids.	V-5
V-5	Shaw plot of K/Rb for the main rock types at Port Cygnet.	V-7

Figure No.

Page No.

V-6	K-Ba plot for syenite porphyries and sanidine porphyries.	V-9
V-7	Sr-Ca plot for all rocks.	V-10
V-8	Ba-Sr plot for all rocks.	V-12
V-9	FeO-Sc plot for all rocks.	V-14
V-10	Agpaitic coefficient-Y plot for all rocks.	V-16
V-11	Ti-Y plot for all rocks.	V-17
V-12	Zr-Y plot for all rocks.	V-19
V-13	Nb-Ti plot for all rocks.	V-20
V-14	Ga-Al ₂ O ₃ plot for the alkaline rocks.	V-23
V-15	Chondrite normalised REE plots for sanidine rocks.	V-25
V-16	Chondrite normalised REE plots for syenite porphyries.	V-26
V-17	Chondrite normalised REE plots for syenite porphyry, sanidine porphyry and amphibolite inclusions.	V-28
V-18	Chondrite normalised REE plots of brown matrix rocks CY61 and CY92.	V-30
V-19	Ba-K plot for melanocratic hybrid rocks.	V-33
V-20	Ba-Sr plot for melanocratic hybrid rocks showing their relationship to unaltered dolerite.	V-35
V-21	Chondrite normalised REE plot for sanidine porphyry, hybrid (CY29), altered dolerite (CY119) and Red Hill dolerite.	V-36
V-22	Plot of immobile discriminate elements for amphibolite inclusions.	V-41
V-23	Leake plot for differentiation of the amphibolites.	V-42
V-24	Plot of Nb-Rb for alkaline rocks and amphibolite inclusions together with the reciprocal plot.	V-46
VI-1	Strontium isotope mixing curve and reciprocal plot for sanidine rocks, syenite porphyries and amphibolite inclusions.	VI-10
VII-1	Niggli QLM plot for alkaline rocks and their inclusions.	VII-9
VII-2	Ab-Q-Or plot of 5 kbar partial melts of basalts after Helz (1976). Port Cygnet data added.	VII-11
VII-3	Ab-Q-An plot of 5 kbar partial melts of basalts after Helz (1976). Port Cygnet data added.	VII-12
VII-4	Model of crust-granite surface.	VII-26

Figure No.		Page No.
VII-5	Aeromagnetic traverse line 18 with its magnetic profile from Finney and Shelley (1966).	VII-31
VII-6	Compositions of spessartite garnets from garnet trachyte plotted on Winchell (1951) variation diagram.	VII-40
VIII-1	Possible zone of initial formation of syenite porphyry.	VIII-4
VIII-2	Flow sheet showing possible evolution of the Port Cygnet alkaline complex.	VIII-12

LIST OF PLATES

Plate No.		Page No.
1	Syenite porphyry with amphibolite inclusions.	I-19
2	Holland's Quarry showing succession of dykes.	I-19
3	Porphyritic texture of sanidine dyke rocks.	I-21
4	Tinguaite dyke at Langdon's Point.	I-21
5	Close-up from Plate 4 showing swirl patterns.	I-23
6	Gold fragment from tinguaite X44.	I-23
7	Magpie rock. Sanidine porphyry with grey groundmass.	I-24
8	Plagioclase phenocrysts with sanidine in brown groundmass.	I-24
9	Oligoclase crystals with K-feldspar overgrowths.	I-25
10	Garnet trachyte dyke near Langdon's Point.	I-27
11	Details of spessartite phenocrysts in garnet trachyte.	I-28
12	Details of epidote phenocrysts in garnet trachyte.	I-29
13	Melanocratic hybrid rock cut by aplite veins.	I-31
14	Core crystal of oligoclase with regular overgrowth.	I-31
15	Deformed oligoclase crystal in syenite porphyry.	II-2
16	Oligoclase crystal overgrowth with inclusions in the core	II-2
17	Cumulus of euhedral oligoclase crystals in syenite porphyry.	II-5
18	Embayed quartz crystal with inclusions of amphibole and sphene.	II-5
19	Marble inclusion in syenite porphyry.	II-7
20	Quartzite fragment in syenite porphyry.	II-7
21	Inclusion of andesine in oligoclase feldspar.	II-9
22	Epidote core with amphibole reaction rim enclosed in K-feldspar.	II-11
23	K-feldspar enclosing epidote with amphibole reaction rim.	II-12
24	Hornblende porphyry from Petchey's Bay.	II-12
25	Amphiboles and pyroxenes in feldspathic groundmass.	II-14
26	Inner part of amphibolite inclusions.	II-14
27	Rim amphiboles from amphibolite inclusion.	II-16
28	Multiple twinning and overgrowths in sanidine crystal.	II-16

Plate No.		Page No.
29	Calcite reaction rim on melanite crystal.	II-19
30	Fibrous cancrinite crystals in groundmass.	II-19
31	Allanite (inclusion?) with included melanite crystals.	II-21
32	Groundmass from CY85.	II-23
33	Sanidine tablet showing multiple growth.	II-23
34	Eudialyte surrounded by sanidine crystals.	II-25
35	Muscovite pseudomorph of andalusite? crystal.	II-25
36	Pectolite patch in groundmass of feldspar laths.	II-27
37	Zoned brown melanite enclosing pyroxene in CY73.	II-27
38	Glomeroporphyritic zoned melanites with scapolite rims.	II-31
39	Melanite garnets in various stages of alteration.	II-33
40	Xenolith of iron-muscovite included in sanidine crystal from X50.	II-34
41	Sanidine phenocryst from CY92 with included oligoclase.	II-34
42	Garnet trachyte with spessartite and epidote phenocrysts.	II-37
43	Potash feldspar crystallized on to edge of epidote.	II-38
44	Zeolitized labradorite crystal on spessartite.	II-39
45	Fresh dolerite with glomeroporphyritic exsolved pyroxene.	II-44
46	Exsolved pyroxene with peripheral dusting of magnetite altered to green hornblende and biotite.	II-46
47	Altered dolerite (RP10).	II-48
48	Recrystallized hybrid rock.	II-49
49	Hybrid rock with intergrowing pyroxene and green-brown biotite.	II-51
50	Hybrid rock RP18.	II-51
51	Hybrid rock RP6.	II-53
52	Hybrid rock RP18.	II-53
53	Hybrid rock 70-221.	II-56
54	Hybrid rock CY29.	II-56
55	Syenite aplite with exsolved alkali feldspars.	II-57
56	Syenite aplite with exsolved potash feldspar overgrowth on plagioclase core crystal.	II-57
57	Garnet orthoclasite.	II-60

ABSTRACT

The Port Cygnet alkaline complex consists of small scattered concordant and discordant intrusions of Cretaceous age emplaced in Jurassic dolerite and Permian fluvioglacial sediments in the vicinity of Port Cygnet, southern Tasmania.

The alkaline rocks are miaskitic and fall into two main groups: one is a group of slightly oversaturated syenites with a porphyritic texture rich in phenocrysts of oligoclase (syenite porphyries), and the other consists of nepheline syenites, characteristically with a flow structure and containing phenocrysts of euhedral sanidine crystals, with feldspathoids in the groundmass, and occasionally as phenocrysts. These are the sanidine rocks or sanidine porphyries.

The primary magma was a potash-rich upper mantle or lower crustal, partial melt (of a mafic alkali parent) probably equivalent ultimately to a tinguaitite which began crystallizing in a magma chamber with subsequent successive injections of magma containing coarser sanidine phenocrysts. This gave rise to the nepheline syenites.

The intrusion of the potassic magma was accompanied by volatiles with evidence of the presence of water, carbon dioxide, sulphur dioxide and hydrogen sulphide, demonstrated by the presence of both primary and secondary reaction mineral products.

The porphyritic syenites seem to have been derived by the mixing of a potassic upper mantle or lower crustal partial melt, with a crustal partial melt of the feldspathic matrix of an amphibolite followed by subsequent initial crystallization at depth before injection into the country rocks.

The model is based on microscopic and textural characteristics, chemical compositions, mineralogy and initial strontium isotope ratios.

Variation of the syenite porphyries due to addition of recrystallized amphibole from the parent amphibolite formed a horn-

blende porphyry. Fractionation of the syenitic melt has resulted in a group of mixed feldspar phenocryst rocks showing potash feldspar reacting with plagioclase phenocrysts in a brown matrix.

Assimilation of mineralized carbonates by the magma has produced one rock unique in having phenocrysts of spessartite and epidote. Sulphur from the country rocks was mobilized by this intrusion.

At Regatta Point, on the western shore of Port Cygnet, the potassic magma reacted with Jurassic dolerite to form hybrid rocks. These were most likely produced within the temperature range of 710°C to 810°C and a log fO_2 in the range -11 to -13.

The alkaline intrusion was probably associated with the break-up of Gondwanaland.

CHAPTER I

INTRODUCTION

The alkaline rocks of Port Cygnet in Tasmania occur within an area of approximately 200 km² forming a rectangle extending from the western bank of the Huon River opposite Petchey's Bay in a north-easterly direction to Kettering on the western bank of D'Entrecasteaux Channel (Figs. I-1 and I-2). Approximately 50 km south west of Hobart, the town of Cygnet is near the centre of the area of interest at the head of Port Cygnet which is an inlet branching off the main estuary of the Huon River. Port Cygnet was discovered and named by C.F. Beautemps-Beaupré, surveyor with the expedition of Admiral Bruni D'Entrecasteaux, during 1793.

Access to the area is via sealed highways. The country has moderate relief up to about 500 metres with numerous steep sided valleys containing streams draining into Port Cygnet. The hilltops are well forested and the lower slopes of open grassland are used for cattle grazing, orcharding and grape-growing on a thick sandy soil. The average annual rainfall is about 75 cm.

Alkaline rocks have always been of interest to geologists by virtue of their highly varied nature and possible modes of origin. They have formed from melts which are usually due to fractional crystallization, partial melting or other processes, of some parent material and are always associated with significant amounts of volatiles, particularly H₂O and to a lesser extent CO₂, SO₂, Cl₂ and F. As a consequence of their derivative nature most bodies of alkaline rocks are emplaced as small intrusives. The alkaline rocks of the Port Cygnet area are a typical example with a multitude of small irregular intrusions of Cretaceous syenite porphyry and

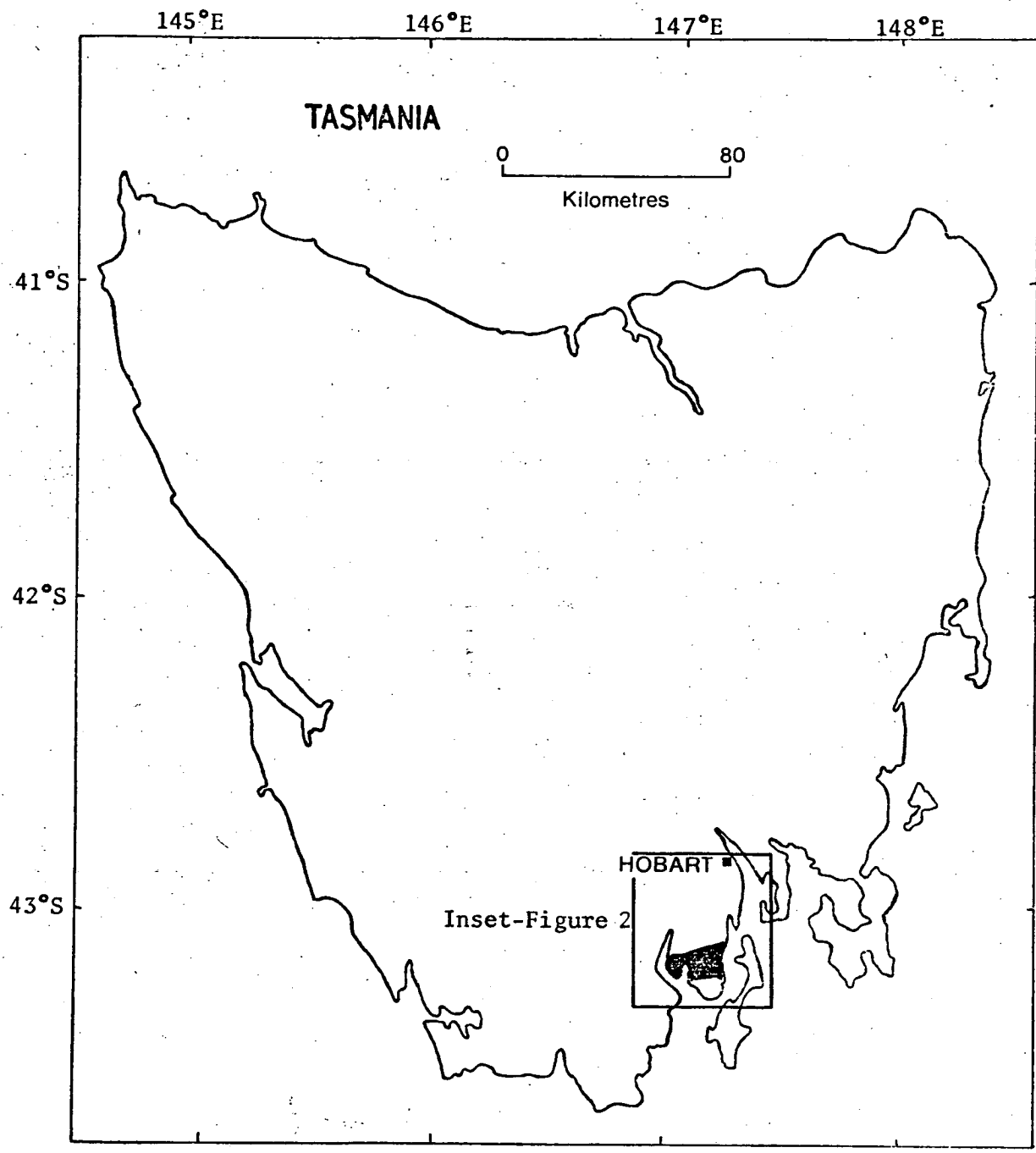


Figure I-1 Location of the Port Cygnet area.

sanidine bearing dykes intruding relatively flat lying Permian fluvio-glacial sediments and Jurassic dolerite intrusions.

The earliest observation of the geology of Port Cygnet was probably due to Peron (1807) when a rock was thrown at him by a native during the sojourn of Nicolas Baudin's expedition in 1801. Specimens were collected and later described by von Buch. During the early months of 1804, the mineralogist A.W. Humphrey, having arrived in the River Derwent with David Collins' settlers, visited the area with the eminent botanist Robert Brown and collected samples of the garnet trachyte from near Langdon's Point (Vallance 1981). Von Buch visited the Council of Mines in Paris during 1810 for the purpose of studying the geological collection made by members of Baudin's expedition. His descriptions (1814) of specimens collected by Bailly refer to augite in a basaltic greenstone and augite with booklets of mica and white needle-like crystals of feldspar comparable with basaltic greenstone. These descriptions ostensibly refer to dolerite, however if the recognition of the mica booklets is accurate then this specimen may have been collected from the hybrid rocks of the Regatta Point area.

PREVIOUS WORK AND LITERATURE

After the visit of Humphrey to Port Cygnet the next significant observations were made by Milligan (1852) who observed reddish golden mica from Port Cygnet. This may well have been a reference to the hybrid rocks. Milligan (1855) also reported the presence of a feldspathic rock with tourmaline and granitic structure south of Oyster Cove.. Both sanidine bearing rocks and syenite porphyry occur here. The "discovery of gold" and subsequent rush to Mr. Piguenit's farm at

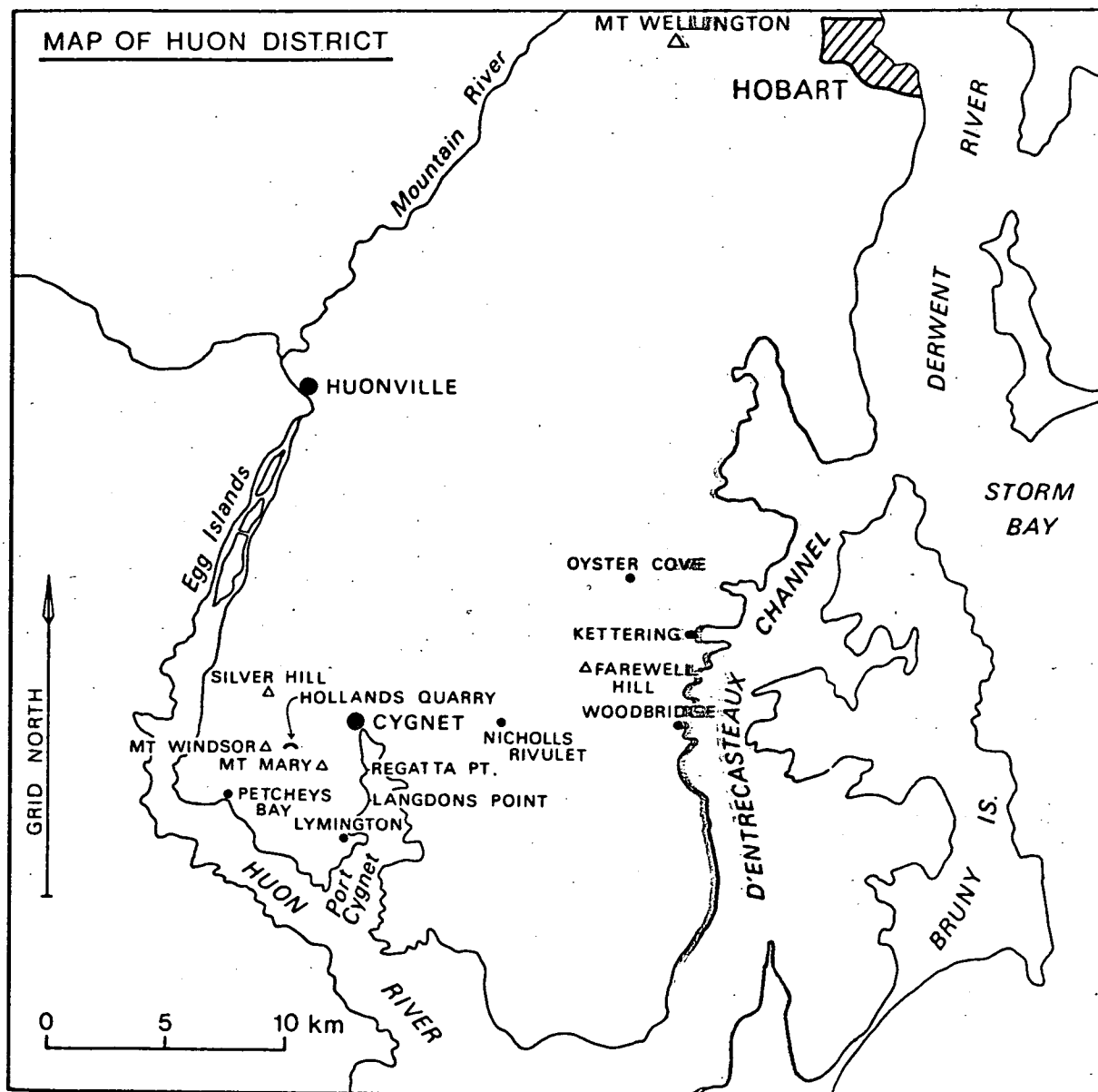


Figure I-2 Inset area of Figure I-1 showing localities referred to in text.

Little Oyster Cove (Kettering) in 1857 may have revealed an association with the alkaline rocks but this was never published. In The Geology of Tasmania (1888), R.M. Johnston later showed a series of intrusions from Port Cygnet in a northeasterly direction to Oyster Cove. There was no accompanying petrographical description given by Johnston.

The first formal description of the alkaline rocks of the district was given by Twelvetrees and Petterd (1898). They recognized three major groups, namely:-

(a) Effusive or soda trachyte group consisting of haüyne trachyte, aegirine trachyte, melanite trachyte and trachyte.

(b) Intrusive or soda aplite group with sanidine-augite-haüyne aplite, sanidine-augite-biotite aplite and malchite (diorite).

(c) Plutonic group comprising alkali augite syenite with micro-perthite and analcime or elaeolite.

It was also established that they were intruded into Permo-Carboniferous country rocks. McLeod and White (1898) described a new species of garnet from Port Cygnet. Twelvetrees offered a classification and mineralogical summary of the Port Cygnet rocks for the Australian Association for the Advancement of Science in 1902. In this he recognised two main groups with associated variants. These were alkali syenite ($\text{SiO}_2 = 52-60\%$) and elaeolite syenite ($\text{SiO}_2 = 45-60\%$). In this way Twelvetrees recognised the presence of a saturated quartz-bearing group and another group of undersaturated, feldspathoid-bearing rocks.

Twelvetrees included descriptions of the rocks from Rosenbusch, to whom he had sent some specimens, and there follows a brief summary of the rocks recognised by these workers:-

Alkali syenite:

Quartz augite syenite (alkali feldspar - augite - quartz); alkali

syenite (orthoclase and albitic feldspar - augite - amphibole with accessory biotite quartz, sphene and apatite); often porphyritic texture.

Elaeolite syenite:

Alkali feldspar - elaeolite - alkaline pyroxene - amphibole with accessory melanite, biotite, hydronephelite, sphene and apatite.

Elaeolite syenite porphyry:

Orthoclase and some triclinic feldspar phenocrysts, alkaline pyroxene and amphibole, melanite and iron ore after nosean and garnet with natrolite pseudomorphs after nepheline (or sodalite). Fluidal feldspathic groundmass.

Nosean rock:

Sanidine, amphibole, alkaline pyroxene, melanite, and nosean or haüyne. Aggregates of natrolite after small crystals of nepheline.

Mica solvsbergite:

Orthoclase and albite with brownish yellow mica, garnet, and pyrochlore.

Solvsbergite porphyry:

Sanidine, aegirine and natrolite after aegirine. Groundmass of acicular aegirine, sanidine, analcime and a little nepheline.

Tinguaite porphyry:

Phenocrysts of aegirine-augite, melanite, sanidine, sphene and nepheline. Groundmass of sanidine, acicular aegirine and analcime.

Jacupirangite:

Nepheline and augite.

Essexite:

Labradorite and andesine feldspar with augite, amphibole and quartz.

Mica nephelinite:

Nepheline, augite, biotite, amphibole and accessory apatite.

Twelvetreets (1903) published a "Note on Jacupirangite in Tasmania", describing the occurrence of this rock at Port Cygnet, as being

associated with the margins of a central spur of elaeolite syenite on "the promontory at Regatta Point". He described the rock thus: "The elaeolite is in large hypidiomorphic plates. Sphene is in fair quantity in wedge shaped crystals. Melanite garnet, which is characteristic of all the Port Cygnet eruptive is not absent from this, and is occasionally rather plentiful. Apatite is present in the forms of prisms and grains, magnetite in scattered grains and a little brown biotite. In order of quantity, the minerals are elaeolite, augite, sphene, garnet, apatite, magnetite, biotite." This was regarded as having its origin by differentiation through progressive crystallization of the cooling mass with the more basic (darker) parts crystallizing at the edge of the intrusion. The central (lighter) portion crystallized later, after cooling of the periphery.

In 1906 Dr. F.P. Paul described foyaite - theralite rocks from Tasmania and figured some sanidine crystals. Twelvetrees (1907) associated gold in the area with quartz veins developed in contact-metamorphosed sediments at the edges of the intrusions. Jensen (1908) noted their resemblance to other Australian alkaline rocks and speculated as to their possible Lower Mesozoic age. David and Skeats (1914) also thought they might be Lower Mesozoic. Daly (1914) in his list of alkaline rocks of Australia, associated the Port Cygnet rocks with Palaeozoic limestone probably apropos of his theory of assimilation of limestone being the cause of formation of alkaline feldspathoidal rocks. Only minor limestone occurs at Cygnet (Map No. 4). Skeats (1917) demonstrated that the alkaline rocks intrude Jurassic dolerite in Little Oyster Cove (Kettering) at the eastern limit of the area. Reid (1922) also agreed that they were intrusive into dolerite.

A.B. Edwards (1947) showed the Regatta Point rocks to have been

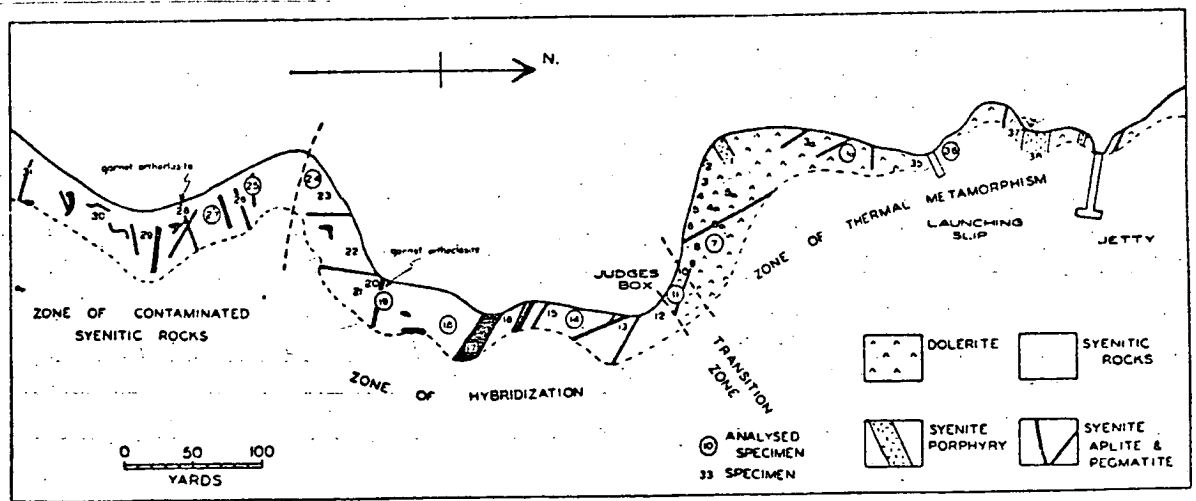
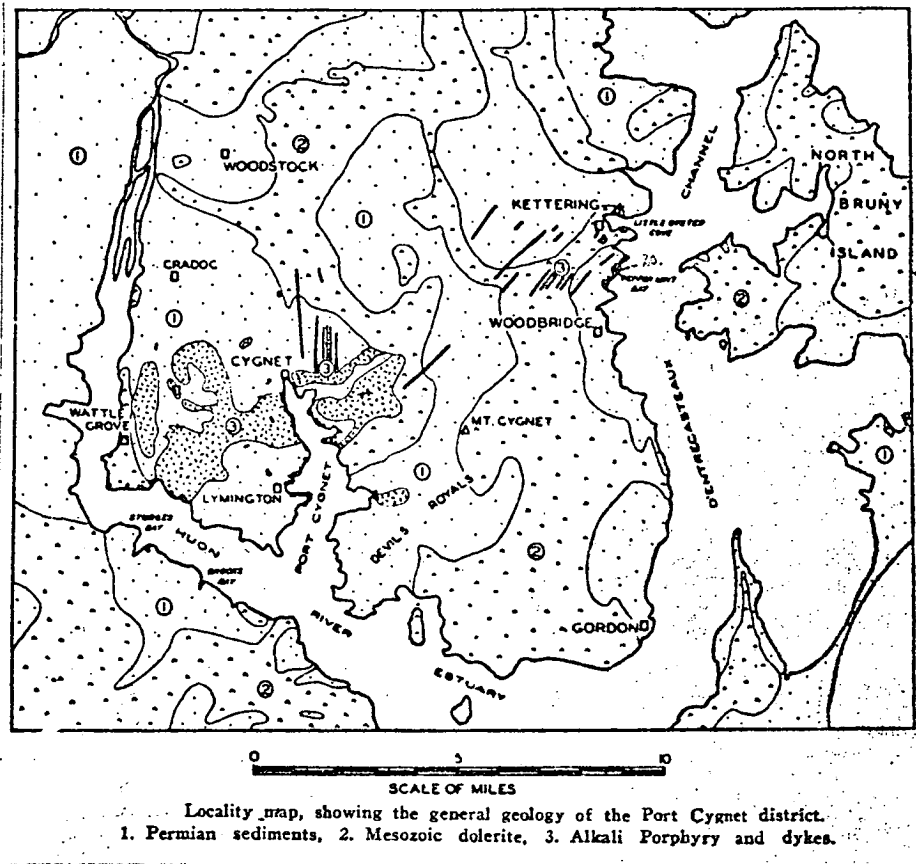


Figure I-3 The general geology of Port Cygnet (top) and the detailed geology of the shore-line at Regatta Point (from Edwards 1947).

formed by reaction of a potash rich alkaline magma, of syenitic composition, with pre-existing dolerite. Fig. 1-3 shows Edwards' regional map of the area together with his map of Regatta Point. Edwards considered the main intrusion to be a stock of syenite porphyry (banatite) with later stage intrusions of numerous porphyritic dykes of varying compositions. Edwards recognised the following rock types: syenite porphyry, h  yne sanidine garnet porphyry, sanidine garnet porphyry, sanidine biotite porphyry, sanidine porphyry, sanidine tinguaitite, syenite aplite. He came to the conclusion that the alkaline rocks represented a differentiated syenite stock derived from a parent monzonitic magma.

Robertson and Hastie (1961) presented palaeomagnetic data suggesting that the syenite porphyry and dolerite were related.

Evernden and Richards (1962) measured K-Ar ages ranging from 99 m.yr. (sanidine and biotite) to 109 m.yr. (hornblende) for the rocks.

McDougall and Leggo (1965) remeasured the hornblende sample of Evernden and Richards at 95 m.yr. and also found an age of 98 m.yr. for their own sample.

Leaman and Naqvi (1967) studied the structure and stratigraphy of the area using geophysical methods. They suggested the general structure to be a dome of faulted Permian sediments and Jurassic dolerite, intruded by the alkaline rocks as a laccolithic tongue having an associated dyke swarm.

Ford (1967) showed that the johnstonotite garnet of McLeod and White was essentially spessartite.

The Tasmanian Geological Survey has completed a map of the area as part of the Kingborough sheet (Appendix Map No. 4) from which it is apparent that the intrusions are scattered with no continuous surface

outcrop as suggested by the original sketch map of A.B. Edwards (Fig. I-3).

ACKNOWLEDGEMENTS

I would like to acknowledge the early interest of Dr. G.A. Joplin who encouraged me to continue with the project. The generous assistance of the staff of the Tasmanian Department of Mines, particularly Dr. E. Williams, Dr. N. Farmer and Mr. P. Baillie, in allowing me access to their specimens and maps, is gratefully acknowledged. I am grateful to the University of Tasmania for a special research grant to enable strontium isotope analyses to be carried out, and to Professor H. Bloom from the Department of Chemistry for enabling me to obtain an A.I.N.S.I.E. Grant for the determination of the rare earth elements by spark source mass spectrometry at Lucas Heights, N.S.W. I would also like to thank Mrs. J. Reeve for the careful drafting of the diagrams, Dr. Varne and Dr. Ellis for suggestions and improvements, Dr. M.R. Banks for information concerning the early explorers and geologists in Tasmania, and Mrs. Byers and Mrs. Pongratz for the typing of the manuscript.

THE GEOLOGICAL SETTING

Tasmania is an island with an area of 64,409 km², the geology of which is shown on the 1:500,000 geological map included as map no. 5 in the appendix section. In addition (Appendix Map No. 4) there is a copy of the Kingborough sheet of the Department of Mines Geological Atlas 1:50,000 series illustrating the detailed geology of the country surrounding Port Cygnet. A synopsis of the information shown on both maps is given in the following paragraphs.

The geological record begins with Precambrian metaquartzites and pelites with occasional associated amphibolites and mafic dykes, which collectively constitute the ancient core of the island, upon which most of the subsequent systems have been deposited. This core has been referred to as the Tyennan nucleus.

Younger Precambrian unmetamorphosed orthoquartzite and mudstone with associated dolomite as well as turbidite sequences and some basalts, overlie the older rocks.

With the advent of the Palaeozoic Era and the Cambrian Period there was the development of a trough marginal to the Tyennan core and another further towards the north-west extremity of Tasmania. Within these troughs, particularly that one adjacent to the core, were deposited unfossiliferous orthoquartzite, greywacke and turbidite sequences followed by acid-intermediate volcanics, including ophiolite and alpine ultramafic complexes. Fossiliferous greywacke-turbidite sequences occur near the top of the succession with a Middle-Late Cambrian age. These, together with some granitoid stocks, constitute the Cambrian System in Tasmania.

Near the end of the Cambrian Period there were small movements and the formation of minor unconformities with the deposition of

talus breccias and siliceous conglomerates as alluvial fans, followed in the Early Ordovician by marine sandstones, siltstones and extensive deposits of limestone. Sedimentation continued through the Silurian into the Early Devonian Period with no great discontinuity in the succession which changed in the Late Ordovician Period from limestone to sandstones, siltstones and shales with minor limestone.

While the succession described above refers essentially to Western and Central Tasmania, in the same time span, i.e. from possibly as early as the Cambrian until the Early Devonian Period, in eastern Tasmania the stratigraphic record was quite different, consisting of an uninterrupted sequence of quartzwackes and turbidites together with mudstones and siltstones, limestones being conspicuously absent.

During the Middle Devonian Period extensive folding occurred, followed by emplacement, extending into the Early Carboniferous Period, of granitoid batholiths into the pre-existing Palaeozoic rocks of both eastern and western Tasmania. These events are correlated with the Tabberabberan Orogeny of eastern Australia. The basis of later Tasmanian fault patterns may also have been set by this orogeny.

Apart from occasional small superficial deposits, Tasmania then became a land surface subject to erosion until the Late Carboniferous Period when, with the onset of glaciation, a new period of sedimentation began which extended with minor interruptions into the Triassic. The basal beds are usually tillites with glacio-marine sequences which may include pebbly mudstones and sandstones and oil shale. Formed later, were restricted areas of freshwater sandstones and siltstones containing coal measures which subsequently gave way to another glacio-marine interlude with the formation of pebbly sandstones and mudstones with associated cold water limestones. Another development of freshwater sequences with coal measures of Late Permian and Triassic age, followed. In the Middle and Late Triassic coal

measures were deposited and included volcanic litharenites.

With the ending of the Triassic Period the last great sedimentary cycle had been completed in Tasmania, and the older rocks, especially in the central and southeastern regions were blanketed by the flat-lying younger sediments to a total thickness of about two kilometres.

In the Jurassic Period, the injection of large volumes of tholeiitic magma formed extensive sills and dykes of dolerite intrusive into the Permo-Triassic System. These rocks collectively, i.e. the Permo-Triassic and dolerite, formed the country rocks into which the Port Cygnet alkaline rocks were intruded.

After the consolidation of the Jurassic dolerite there was a long period with no significant events until the intrusion about 100 million years ago, of the Port Cygnet alkaline rocks and the Cape Portland appinites of north-eastern Tasmania.

During the Late Cretaceous Period normal faulting, and probably also reactivation of older fault lines, commenced. The fault troughs filled with fresh water muds, silts and lignites. Some marine limestones were formed at coastal margins during the Middle Tertiary Period.

Following this faulting, the out-pouring of flood olivine basalts in the northwestern area particularly, but also as sporadic flows and tephra vents, often associated with earlier faulting, occurred throughout the island.

Glaciation in the Pleistocene Epoch gave rise to morphological sculpturing of the areas of higher relief and formation of associated tills, outwash and periglacial deposits which represent the last substantial features of the geological record, to which must be added recent alluvium, talus and other superficial deposits.

THE GEOLOGY OF THE PORT CYGNET DISTRICT

The geology is covered by the Kingborough sheet (Appendix Map No. 4). The essential stratigraphy is restricted to the Permian, Triassic and Jurassic systems as well as the alkaline rocks of Cretaceous age. The sedimentary rocks belong to the Parmeener Supergroup which is split into upper and lower divisions with the lower one representing the Lower Permian and possibly Upper Carboniferous systems while the upper division covers the Upper Permian and Lower Triassic systems.

The Permian System

There is no direct evidence of the substrate of the Permian System in the Port Cygnet area where the thickness of the basal tillite is at least 300 metres.

The lowest formation of the sequence which dominates the sediments of the area is the Truro tillite, which may be Upper Carboniferous. This is a poorly sorted rock with many and varied erratics as constituents. These may range up to 30 cm or greater in size with faceting, but only occasionally are striated quartzite pebbles found. Rock fragments abundant in the tillite are quartzite, conglomerate, and granite. The fragments are not sorted nor is there any evidence of bedding. With the matrix being essentially rock flour the rock disintegrates very readily thus leading in part to the thick soil cover in the Port Cygnet area. Occasional beds of pebble-free dark mudstone may also occur.

Overlying the Truro tillite in the Port Cygnet area the remaining formations of the Permian system total some 645 metres and consist of a succession of marine mudstones and siltstones with

associated dropstones. Many of the lower beds are pyritic with nodules abundant in some horizons. Fossils occur in most of the constituent formations.

A coarse feldspar-bearing sandstone, which may grade up to granule and pebbly conglomerates, is a prominent marker bed approximately 8.5 m thick occurring two thirds of the way up the sequence. This is the Risdon Sandstone Formation.

The only limestone recognized in the Port Cygnet area is a thin lens at Silver Hill.

The top of the Permian System is largely represented by approximately 20 metres of Cygnet Coal Measures with some coal seams which can vary laterally into feldspathic sandstones and minor mudstone.

Triassic System

The top part of the Upper Parmeener Supergroup lies within the Triassic System, which is here represented by medium to coarse grained, cross-bedded quartz sandstones. Mudstones and minor clay pellet layers occur as subsidiary beds. The total thickness of this System is somewhat greater than 280 metres in this area.

Jurassic System

This is represented by dolerite which has intruded as a tholeiitic magma forming dykes and sills with an exposed thickness of at least 500 metres on Grey Mountain, north of Cygnet. The dolerite has very little contact metamorphism associated with its intrusion, in spite of the large amounts of magma involved. This is also a consequence of the siliceous nature of the country rocks and the lack of associated carbonates together with a relative lack

of volatiles associated with the dolerite. Baking of sediments near contacts and narrow chilled margins are the usual contact phenomena observed. Some granophyric differentiates are present on large dykes to the east but there is no sign of these at Port Cygnet, nor is there any evidence of Cretaceous alkaline rocks intruding them.

Cretaceous System

The alkaline rocks are the only representatives of this system and occur as irregular dykes and sills piercing the Permian country rocks and the Jurassic dolerite. The largest of the intrusions occur at Farewell Hill and Helliwell's Point to the east and on Black Jack Ridge, Mt. Mary and Mt. Windsor in the western part of the area. No intrusions have been observed in the Triassic rocks.

GEOLOGICAL STRUCTURE

The structure is simple with the flat-lying country rocks having low angles of dip with a maximum value of about 19° . The dips have a radial disposition about the Cygnet Peninsula which could be described as a dome. The time of formation of the dome and its relation to the dolerite and alkaline rocks is unknown although it would be expected that the former would have had a more profound effect than the alkaline rocks at the time of intrusion. On the basis of gravity data, Leaman and Naqvi (1967) have suggested that there is a basin-shaped dolerite sheet beneath the Cygnet Peninsula.

The area is traversed by a well developed fault pattern. Many faults are inferred and cannot be mapped adequately because of the nature of the overburden and the deep weathering profile at Port Cygnet. It is normal faulting with two dominant components giving

one system striking about north west and the other set about north east. The relative ages of these faults is not known but some terminate the syenite porphyries and some dykes have also been strongly disrupted and slickensided so that many of the faults at least post-date the alkaline rocks and are probably of Early Tertiary age conforming to other areas in Tasmania. The relation between the dolerite and faulting would suggest most of the faults are later than the dolerite, however, note can be made of the thin dolerite dyke striking approximately north along grid line 513000E (Appendix Map No. 4) which is associated with a concomittant fault along its line of outcrop, with the upthrown block to the west. The estuary of Port Cygnet is probably fault controlled and may be a small graben but this cannot be determined unequivocally because of superficial cover.

The alkaline dykes range from a few centimetres, in the hybrid zone, up to 10 metres wide in the more dispersed areas. Intersections are rare and thermal metamorphism is confined to the few centimetres of the country rock bordering the dyke. Such baked margins may persist as remnant dyke walls where weathering and erosion have removed the dyke material such as on the sea shore. Around some dykes, e.g. the garnet trachyte, where there has been a high proportion of volatiles and the country rock contains carbonate fossils, the contact metamorphism has been somewhat more pronounced. The most spectacular metamorphism has occurred at Regatta Point where the potassium rich alkaline magma has reacted with the Jurassic dolerite, producing the hybrid rocks.

There is no pronounced relationship of the dyke trends to the fault pattern but there is a preferred north-west-southeast trend over other directions (Leaman and Naqvi, 1967). Most of the dykes are vertical or near vertical and others usually have dips greater than 45°.

THE MAIN ROCK TYPES OF THE PORT CYGNET ALKALINE COMPLEX

This complex is represented by three main groups of rocks which may be summarised:

(a) A plagioclase-potash feldspar bearing group having a porphyritic texture which may be referred to as syenite porphyry.

(b) The second group consist dominantly of potash feldspar rich rocks which in most cases have phenocrysts of sanidine with varying amounts of feldspathoids in the groundmass. These will be generally referred to as sanidine porphyries or sanidine rocks. There are variants of these rocks, which will also be described.

(c) The third group is that of hybrid rocks produced by the reaction of a potassic magma with pre-existing Jurassic dolerite.

The syenite porphyries fall into Streckeisen's (1967, 1976) syenite field, whereas the feldspathoidal content of the sanidine porphyries would classify them as foid-bearing (nepheline) alkali syenite if they were plutonic.

The Syenite Porphyries

These occur commonly as small sills, dykes and rarely as boss-like bodies, which are best shown at Farewell Hill where the intrusion is about 500 metres in diameter. The textures only become apparent on weathering when the phenocrysts become cloudy and can be seen embedded in the groundmass. The fresh rock is grey to blue-grey in colour with a rind of weathered material which may be up to 30 cm thick. Macroscopically it consists of pale pink phenocrysts of glassy feldspars, usually of oligoclase but in some cases also of orthoclase. The crystals are euhedral to subhedral having an equidimensional habit with the grainsize varying from about 5 mm up



Plate 1 Syenite porphyry containing small amphibolite inclusions. CY18 from Petchey's Bay Road on northwest slope of Mt. Windsor.



Plate 2 Hollands Quarry. Coarse syenite porphyry (left) is cut by fine grained sanidine porphyry (centre) which is itself cut by coarse sanidine porphyry (right).

to 2.5 cm for occasional phenocrysts. Both growth zoning and twinning can be detected with a hand lens. Ferromagnesian minerals are not abundant and in most samples contribute less than one percent of the rock. They usually appear as black needles of hornblende with some grains of pale green pyroxene. Hornblende is more abundant in some rock (Pl. 1) with occasional clots ranging up to 5 cm in diameter. Occasionally there may be small feldspar rich veins within the rock. In many samples there are numerous pyrite grains present. The groundmass consists of very fine-grained feldspars which are not resolvable in the hand specimen. There is no glass apparent.

At the western limit of Petchey's Bay is a dyke containing lath shaped dark green hornblende phenocrysts of dimensions up to 2.5 x 0.2 cm which define a flow structure (Pl. 38). In addition the groundmass has a patchy appearance with each patch containing scattered fragments of pale pyroxene (Pl. 39). This rock has been called hornblende porphyry. The hornblende porphyries are related to the more hornblende-rich of the syenite porphyries but have euhedral lath-shaped hornblende crystals and less potash feldspar and oligoclase phenocrysts.

Inclusions are not very abundant in the syenite porphyries but when present are almost exclusively of dark green amphibolite xenoliths (Pl. 1). These occur in greatest abundance at Mt. Windsor on the Petchey's Bay road. Some also occur at Farewell Hill where one pyroxenite inclusion was also found. Occasional rafted blocks of Permian sediments up to one metre in diameter can be seen near some contacts, particularly near Petchey's Bay.



Plate 3 Typical porphyritic texture of sandine dyke rocks.
This specimen from X44 at Langdons Point.



Plate 4 Tinguaita dyke (X44) at Langdons Point. On shoreline
looking south.

The Sanidine-bearing Rocks

This group of intrusives which can be seen to intersect the syenite porphyry near the western end of Silver Hill Road, and at Holland's Quarry (Pl. 2) consists of a system of relatively isolated dykes from about 1 to 10 metres in width. These show a degree of mineralogical variability. Usually they have a porphyritic texture where the phenocrysts consist of euhedral (010) tablets of potash feldspar, variety sanidine, occurring in a finer ground-mass of soda-potash feldspars (Pl. 3). The larger crystals may have up to 5 cm by 0.5 cm limiting dimensions. The fresh feldspars have a vitreous lustre and are colourless. Simple twinning is easily discernable. There may be signs of corrosion at the edges of the crystals which also tend to alter first. The groundmass consists predominantly of finer grained potash feldspars which always show a flow structure of varying degrees of development. The flow structure is always apparent due to alignment of the sanidine phenocrysts. This reaches maximum development with dyke (No. X44) (Pl. 4) near Langdons Point, where turbulent flow swirls are clearly observable in the rock (Pl. 5).

The characteristics of these rocks are somewhat variable, due to the groundmass which is mostly of feldspar is usually dark grey. There may be small pitchy-black grains of melanite garnet up to about 2 mm diameter. An abundance of these together with the phenocrysts and grey groundmass produce the magpie rock, so-called by the early gold miners (Pl. 7). When the rocks contain large sanidine phenocrysts and little melanite they were labelled "biscuit rock" by the miners.

If large amounts of aegirine occur as small laths in the ground-

Plate 6 Gold fragment from X44. x1400 SEM photograph.

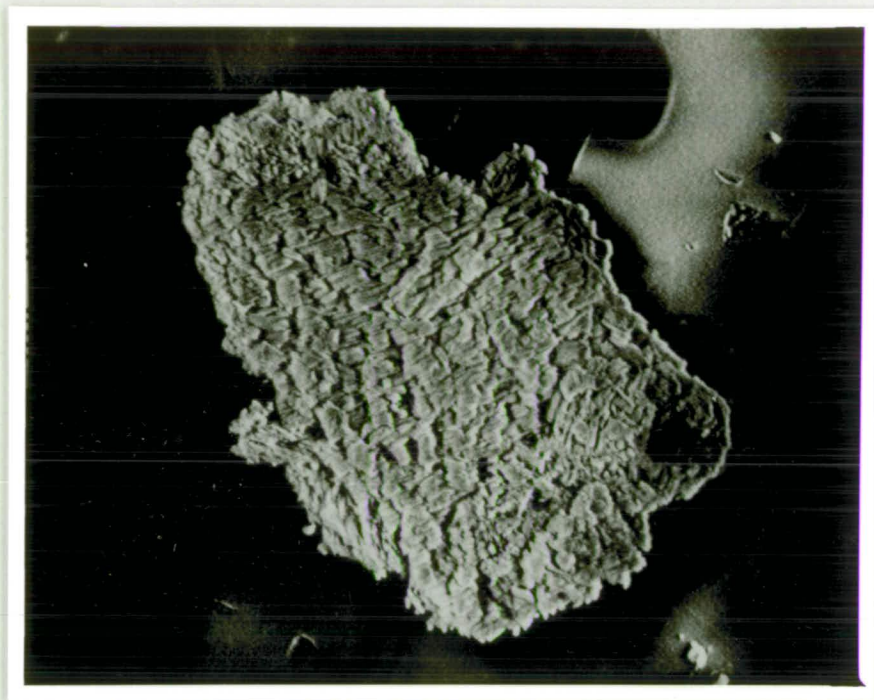


Plate 5 Close up from Plate 4 showing swirl flow patterns in the sandstone crystals.





Plate 7 "Magpie rock". Sanidine porphyry with grey groundmass. Sanidine tablets with black grains of melanite.



Plate 8 Plagioclase phenocrysts with sanidine in brown groundmass. CY92.

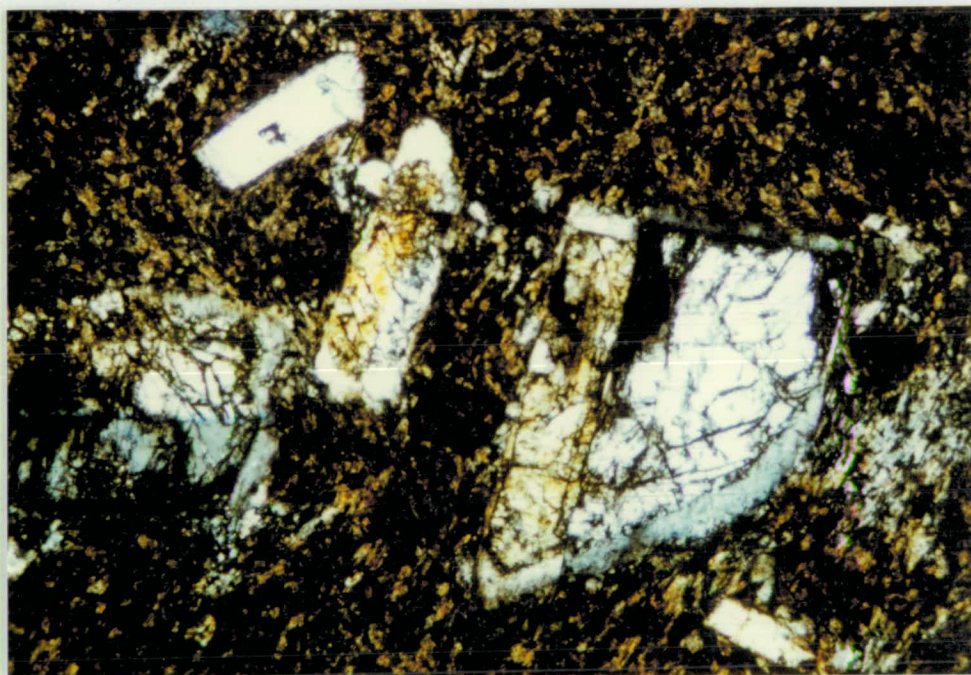


Plate 9 Oligoclase crystals with potash feldspar overgrowths. CY61. Crossed nicols. x75.

mass, the matrix is green in colour with the white to glassy phenocrysts enclosed by it. This is the tinguaitite described earlier by A.B. Edwards (1947) (Pl. 4). Other dykes may have small glassy crystals of feldspathoid usually less than 0.5 mm diameter together with melanite grains in a groundmass of green aegirine and potash feldspar laths.

Another rare group of dyke rocks is superficially very similar to those already described but they have a brown groundmass (Pl. 8) of fine grained potash feldspar laths containing tabular euhedral phenocrysts of oligoclase-andesine which may have potash feldspar overgrowths (Pl. 9). The rocks are very tough and are known from two localities at Silver Hill and in the Huon River at the western limit of Petchey's Bay.

An unusual potash feldspar rich rock which cannot be conveniently classified as above, occurs near Langdon's Point where a dyke (Pl. 10) contains rounded phenocrysts of brown spessartitic garnet (Pl. 11) and green epidote (Pl. 12b) with feldspar crystallised onto them producing a white rim in a grey groundmass of fine grained feldspar laths (Pl. 12a). This is the garnet trachyte of MacLeod and White (1898).

Inclusions are generally absent from the sanidine rocks, but small inclusions of phengitic mica together with small (0.5 cm) vugs of pyrite crystals occur in dyke X50 from the western slope of Mt. Mary. This may be the sanidine biotite rock described by Edwards (1947) but otherwise not identified at Port Cygnet.

In the field it is possible to recognise the main groups of the sanidine porphyries by noting the colour of the groundmass as grey, green or brown.



Plate 10 Garnet trachyte dyke near
Langdon's Point.



Plate 11a Detail of Plate 10 showing brown spessartite crystals with white feldspathic rims.



Plate 11b Some larger spessartite phenocrysts and their feldspathic rims, in the garnet trachyte.



Plate 12a Garnet trachyte showing epidote phenocrysts.
Some of these enclose brown spessartite crystals
and have white rims of potash feldspar.



Plate 12b Detail from above specimen showing epidote
overgrowth on spessartite.

The Hybrid Rocks

These formed from the reaction between the potassic magma and fragmented pre-existing Jurassic dolerite. The rocks so produced were labelled hybrid rocks by Edwards (op. cit.). They outcrop along the western coastal strip of Port Cygnet from about 0.5 km north to a point about 0.5 km south of the judges box at Regatta Point. The most intense alteration has taken place in the area around the judges box and does not appear to extend inland but this cannot be determined precisely due to superficial soil cover. However the magnetitic measurements of Leaman (1977) and the presence of thermally metamorphosed sediments on the eastern shore of Port Cygnet opposite Regatta Point indicate a metamorphosed zone within the estuary. Following the nomenclature of Edwards it is possible to recognise both melanocratic (dark) and leucocratic (light) types.

The melanocratic rocks have granular textures with average grain size about 1 mm but somewhat variable. They are composed of green pyroxene, dark green amphibole, potash and soda-lime feldspar, magnetite, biotite, melanite and occasional nepheline. There can be clots of biotite up to 5 cm in diameter and occasional large melanite aggregates up to 2 cm. A sequence of alteration can be recognized, beginning with unaltered dolerite.

The leucocratic rocks are usually in the form of veins varying from 1 cm to 1 m in width. These have sub-rectangular allotriomorphic crystals of potash feldspar and some lime-soda feldspar, together with some ferromagnesium minerals. The average grain size is near 2 mm. Some of these were originally fissure fillings so that tabular potash feldspar crystals can be seen growing off the original walls which have been completely filled with both coarse and fine grained feldspar (Pl. 13). Edwards called these rocks aplites. Other veins and dykes contain coarse potash feldspar crystals almost



Plate 13 Melanocratic hybrid rock cut by feldspathic aplite veins at Regatta Point.

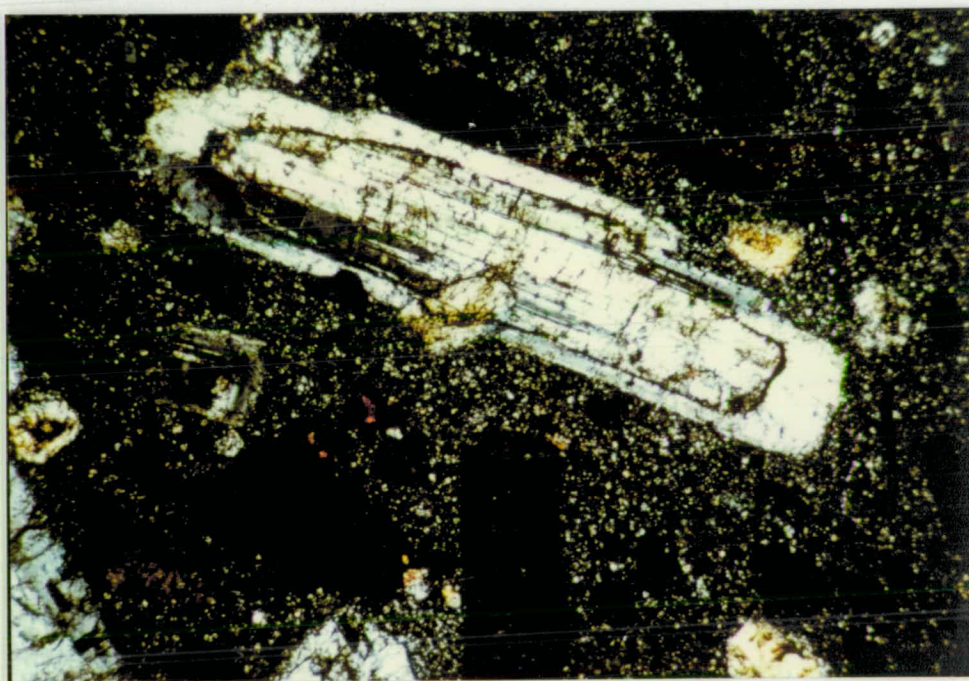


Plate 14 Syenite porphyry (CY45C) core crystal of oligoclase with a regular overgrowth. Crossed nicols. x75.

exclusively with little groundmass and occasional melanite garnets. These are the garnet orthoclasites of Edwards, who recognised several zones of alteration at Regatta Point. With increasing heating and metasomatism of the dolerite, and addition of alkaline magma, hybrid rocks containing sanidine tablets with mafic minerals as interstitial constituents are produced.

Thus beginning with fresh dolerite there are successive zones of thermal metamorphism, transition, and hybridization to the zone of contaminated syenite. While the essentials of Edwards' metamorphic sequence are not in dispute it is clear that the zones do not occur as specifically suggested by him. From his work a general east-west trend for the contact can be inferred, however as magnetite is produced during the metamorphic transformations this is useful in delineating the contact zone using a magnetometer. This work has been carried out by Leaman (1977) and shows that the contact bears approximately parallel to the present shoreline at Regatta Point, within Port Cygnet estuary.

A summary of Edwards' work at Regatta Point is given in Figure I-4.

Figure I-4: A SUMMARY OF THE HYBRID ROCKS AT REGATTA POINT (After A.B. Edwards, 1947)

ROCK OR ZONE	MINERALOGY						TEXTURE
Dolerite	Labradorite $mNaAlSi_3O_8$			Magnetite Fe_3O_4	Ilmenite $FeTiO_3$	Quartz SiO_2	Ophitic
Zone of Thermal Metamorphism	$nCaAl_2Si_2O_8$		Augite $Ca(Mg,Fe,Al)(SiAl)_2O_6$	Magnetite	Biotite $K(Mg,Fe)_3(OH)_2(AlSi_3O_{10})$	Sphene $CaTiSiO_5$	Ophitic
Transition Zone	Albite $NaAlSi_3O_8$		Hornblende $Ca(Mg,Fe,Al)_5(OH)_2[(Si,Al)_4O_{11}]_2$				Granular
Zone of Hybridization	Albite $NaAlSi_3O_8$		Augite	Pyrite (FeS_2)		Apatite $Ca_5(PO_4)_3F$	Granular
Zone of Contamination	Albite Nepheline $Na_3K(AlSiO_4)_4$ Zeolites		Melanite $Ca_3Fe_2(SiO_4)_3$				
Syenite	Andesine	Hornblende	Augite	Orthoclase Quartz	Sphene	Magnetite	Apatite

CHAPTER II

MICROSCOPIC PETROGRAPHY

The thin sections described in this chapter have been incorporated into the Geology Department, University of Tasmania collection. Their departmental numbers, together with field numbers are listed in Appendix (6) where the outcrop co-ordinates on the Kingborough sheet (Map No. 5) are also recorded. These have been transposed onto transparent overlays for ease of identification on the geological base map.

THE ALKALINE ROCKS

SYENITE PORPHYRY

The microscopic characteristics of the syenite porphyry can be summarized from several thin sections of rocks collected in the eastern part of the area around Farewell Hill and Helliwell's Point at Woodbridge, and the western part is represented by specimens from the Huon River, Dineen's spur, King's Hill, Silver Hill, and in the vicinity of Mt. Windsor (Fig. I-2). The rocks all have a characteristic porphyritic texture. It is very difficult to obtain absolutely fresh material due to very weathered outcrops and the possibility that late stage hydrothermal activity has also produced hydration changes in the feldspars. These rocks average about 25 percent modal plagioclase with the remainder consisting mainly of potash feldspar, and subsidiary ferromagnesian minerals and quartz. Having a porphyritic texture they can be labelled syenite porphyry in accordance with the classification of Streckeisen (1967, 1976) and used by Sørensen (1974).

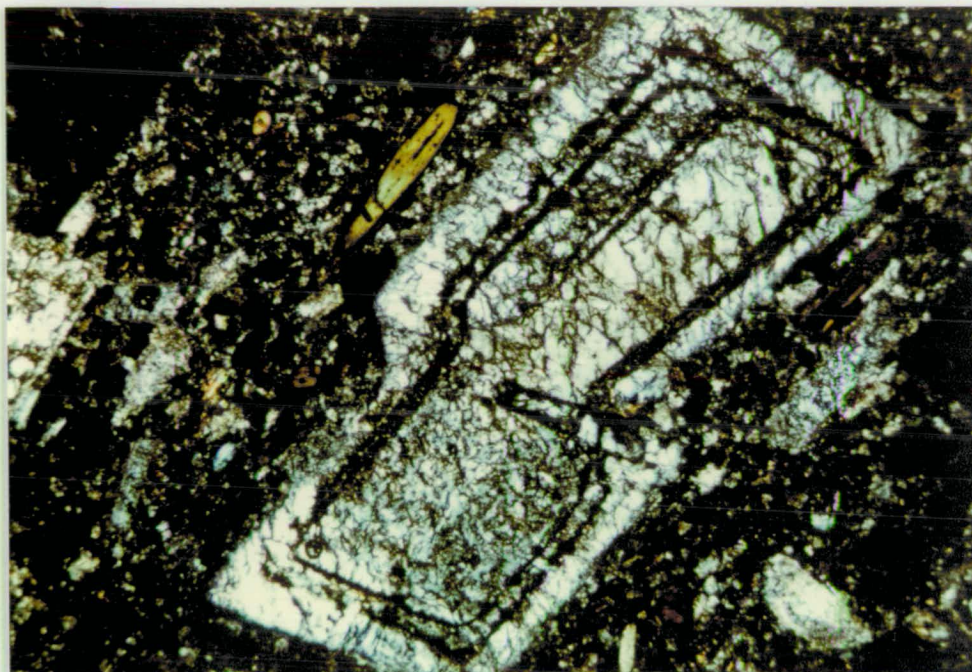


Plate 15 Syenite porphyry (CY71). Deformed oligoclase crystal. Rows of inclusions suggest three stages of growth. Crossed nicols. x75.

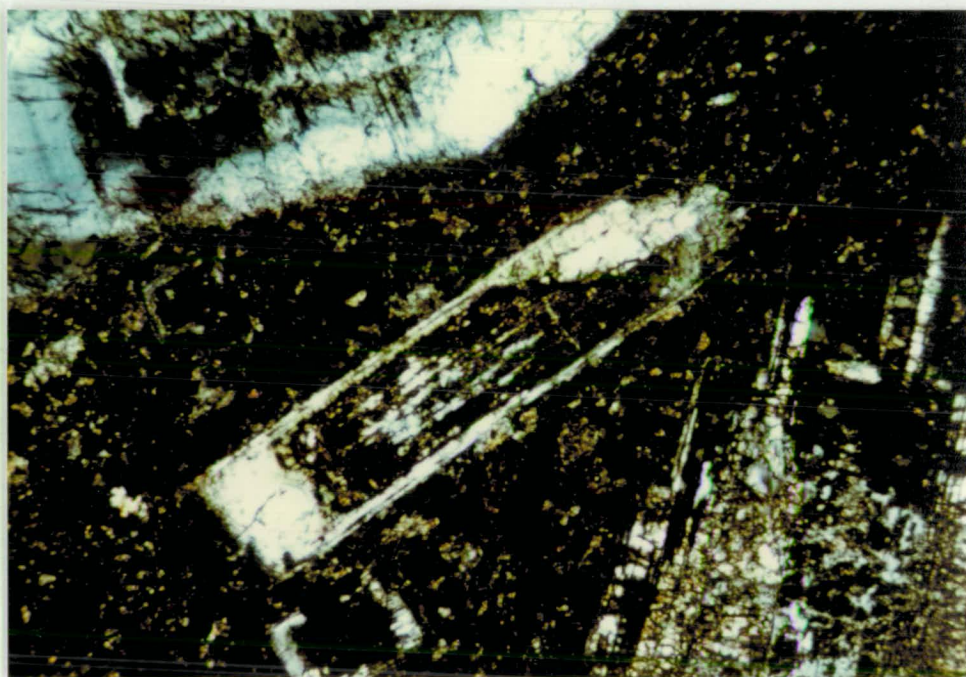


Plate 16 Syenite porphyry (CY71). Oligoclase crystal overgrowth with many inclusions in core. Crossed nicols. x75.

The phenocrysts consist of oligoclase recognised by its small extinction angle in the albite twin zone and also determined by electron probe analysis (see later). The compositions range from near andesine (An_{30}) to near albite (An_{10}) with some crystals being albite rich at the rims, but most not showing great composition changes across the crystal even though optical zoning may be prominent. The crystals are euhedral equidimensional, ranging in diameter from 1 mm to 5 mm, or subhedral rectangular crystals with no terminations. There can be some degree of alteration at the edges to small patches of micaceous material. Many crystals show evidence of overgrowths with respect to linear accumulations of semi-translucent unresolvable inclusions. An irregular core crystal may have regular overgrowth (see Pl. 14) indicating at least two stages of growth and also some distorted crystals show subsequent overgrowth (Pl. 15). Many crystals have inclusions of small green rod shaped crystals of pyroxene. In many feldspars the mantling feldspar is relatively clear but the core crystal has many dark inclusions (Pl. 16). Sporadic potash feldspar crystals occur with inclusions of oligoclase.

Some crystals of plagioclase tend to clump together to produce a glomeroporphyritic texture, but the overall textural relationships can approximate a cumulate texture (Pl. 17). Occasional potash feldspar phenocrysts occur but usually do not have crystal faces as well developed as the plagioclase crystals.

Amphibole is variable in quantity reaching a maximum in some specimens of 5 percent. It occurs in lath shaped crystals 1 mm x 0.2 mm, strongly pleochroic from Z = dark green, Y = green, to X = yellow green. The crystals are euhedral with colour zoning and twinning, however many have been shattered and there may be some

rounding of crystal edges. The amphibole may be agglomerated into small clots and is usually quite fresh. Some pyrite inclusions are present.

There is some pyroxene present which is pale green to colourless and usually strongly altered with opaque minerals at the margin. In many specimens it occurs as small phenocrysts but relatively unaltered crystals may occur as high relief, highly birefringent irregular grains in the groundmass.

There are a few larger grains of quartz occurring as rounded resorbed xenocrysts with a grainsize up to 4 mm (Pl. 18) and occasionally containing pargasite hornblende crystals. Apart from these, quartz is always a groundmass phase. Also typical of the rocks are numerous small euhedral crystals of sphene and apatite. These show the characteristic wedge-shape of sphene and the typical hexagonal cross-section or terminated lath of apatite. They are 0.1 mm diameter although some sphene crystals may be much larger, close to 0.5 mm.

The groundmass is always crystalline with no suggestion of development of any glass. It is often obscured by cloudy alteration but in fresh specimens consists of an interlocking mesh of potash feldspar grains with re-entrant contacts. Distributed through these are clear grains of quartz. The grain size is very uniform at 0.01 mm diameter.

Inclusions occur in the rocks from the eastern part of the area. They include fragments of marble (Pl. 19) quartzite (Pl. 20) and some calcite grains in the groundmass. In addition some large amphibole clots are present with some alteration to epidote. The marble inclusions occur in the rocks outcropping at Helliwell's Point (Woodbridge). The specimens described include CY5, 6, 25, 47C, 48, 49, 53.

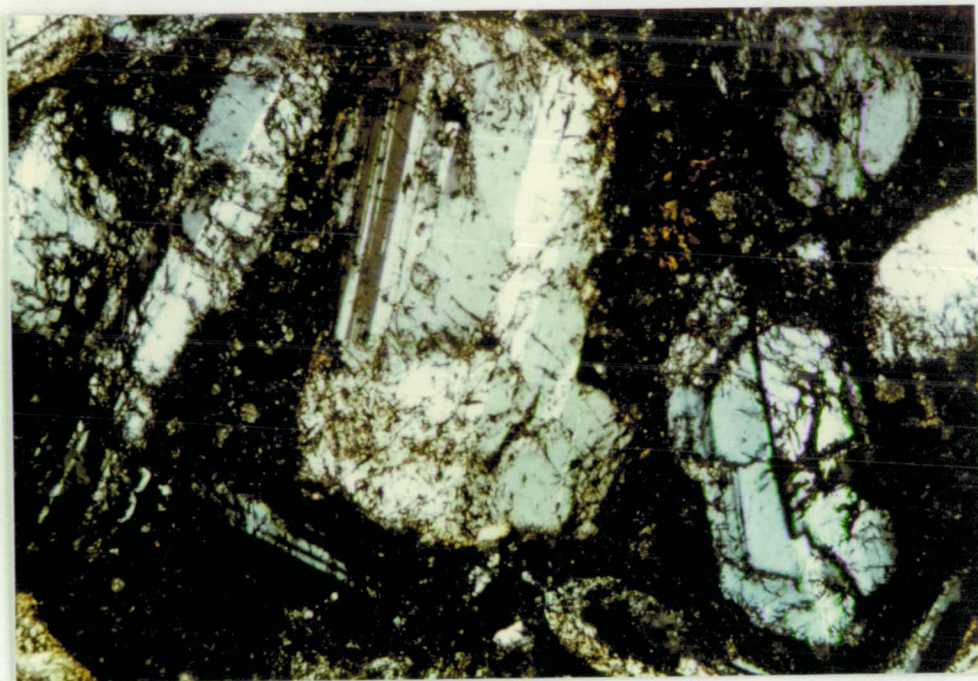


Plate 17 Syenite porphyry (CY70). Cumulus of euhedral oligoclase crystals with multiple growth and welding together evident. Crossed nicols. x75.

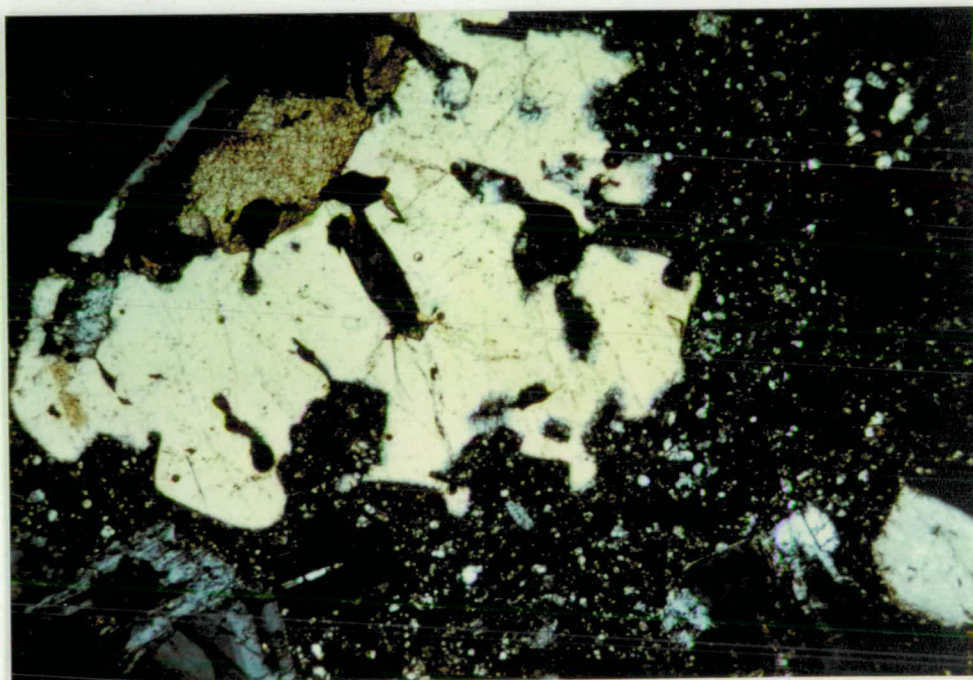


Plate 18 Syenite porphyry (CY60) embayed quartz crystal with inclusions of amphibole and sphene. Crossed nicols. x75.

A large mass of syenite porphyry occurs as a dyke on the north-west slopes of Mt. Windsor, south of Mt. Windsor and the western slopes of Silver Hill. There are also smaller dykes on King's Hill on the south east spur of Mt. Windsor and small sill-like intrusions occur on the east bank of the Huon River south of Petchey's Bay. Once again the rocks have euhedral phenocrysts of oligoclase with grainsize of the order of 2 mm x 1 mm width (010) tablets showing multiple twinning. There is some micaceous alteration at the edge of the crystals with second order colours. Some opaque minerals, mainly pyrite are present. The oligoclase has some inclusions of andesine present (Pl. 21) and zoning is well developed. Some of the feldspars contain rods of a green mineral which is probably aegirine. There are small inclusions of amphiboles in some of the feldspars. Once again there is evidence of two stages of growth with a central core of altered material mantled by a layer of fresh clear feldspar, both of which are oligoclase.

Two distinct groups of syenite porphyry can be recognized. One of these has slightly smaller phenocrysts, in a fine grained altered groundmass, which are dominantly of euhedral plagioclase (usually oligoclase) although crystals with compositions close to albite (An_{10}) do occur. Extinction angles in the symmetrical zone give ambiguous results in this range, however many crystals have slightly greater extinction angles on their margins, have refractive index less than canada balsam and are more albite-rich where analysed. Some small potash feldspar (sanidine with a low 2v) phenocrysts are present but not abundant.

Those with the larger phenocrysts having dimensions varying from 5 mm to 1 cm have a coarser groundmass with more abundant potash feldspar crystals occasionally with included oligoclase crystals. The included plagioclase may have less well-defined twin lamellae and non-symmetrical extinction. Plagioclase phenocrysts are euhedral

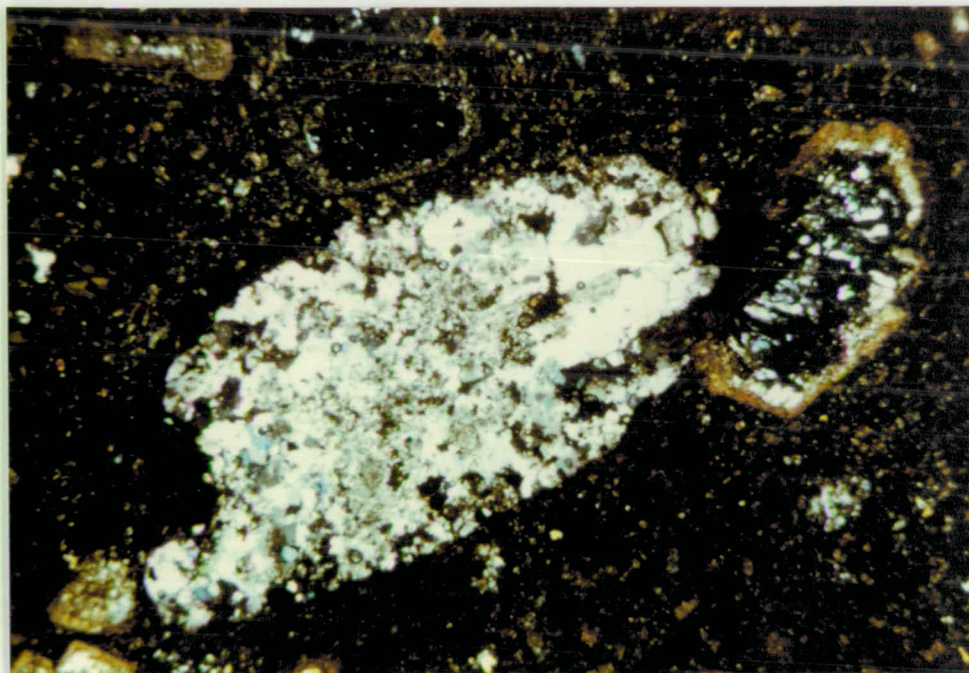


Plate 19 Syenite porphyry (CY25). Inclusion of marble.
Crossed nicols. x30.

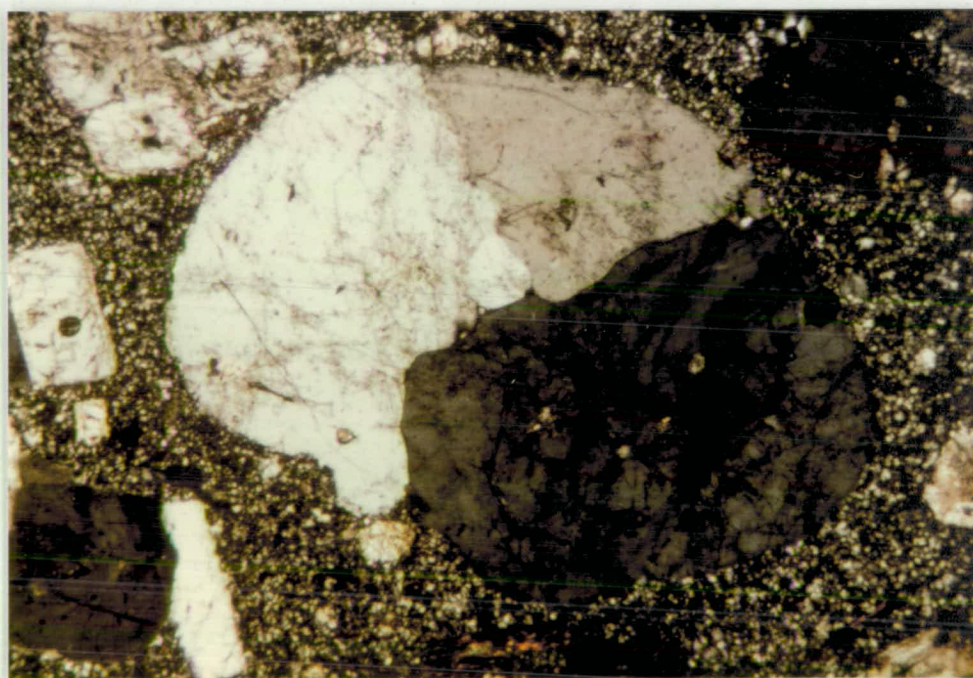


Plate 20 Quartzite fragment in syenite porphyry.
Crossed nicols. x75.

and terminated. The potash feldspar tends to be rectangular in habit with few prismatic terminations. The feldspar phenocrysts have always some degree of cloudy alteration. This is platey material with second order colours. Some crystals have a zeolitic alteration. Inclusions also indicate at least two stages of crystal growth with the occurrence of distinct altered cores in some crystals (Pl. 22, 23). Inclusions of epidote occur in one or two feldspar phenocrysts. These rocks have few ferromagnesian minerals, and where these are present they have been chloritized leaving skeletal remains of euhedral crystals defined by released magnetite grains and pseudomorphed by green chlorite tufts and small crystal remnants. From the forms of the pseudomorphs it appears that both pyroxene and amphibole have been altered.

The smaller phenocryst-bearing rocks are characterised by the presence of fresh euhedral phenocrysts of amphibole. These are lath shaped, 2 mm x 0.1 mm, and many have been shattered. Some multiple twinning is present. The amphibole is strongly pleochroic X = yellow green, Y = green, Z = very dark green. Some colour zoning is present.

In all cases the rocks have a few embayed quartz crystals up to 2 mm in diameter.

The groundmass of the rocks has a grain size of 0.025 mm consisting of granular interlocking grains of potash-soda feldspar showing some degree of alteration and undulose extinction and also having interlocking quartz crystals of apparently primary origin. There is no sign of glass in the groundmass, within which, occurring as small phenocrysts are euhedral crystals of apatite and sphene, the latter occasionally showing simple twinning. Opaque minerals, usually pyrite are scattered through the matrix.



Plate 21 Syenite porphyry (CY83). Inclusion of andesine
in oligoclase feldspar. Crossed nicols. x75.

Also present are odd interstitial grains which have been identified as barite, calcite and aragonite. In one specimen mordenite has formed as a late stage vein filling.

The syenite porphyries have varying amounts of ferromagnesian minerals which are usually only in accessory amounts. Some of the syenite porphyries (CY2, CY91) have rather more amphibole with the usual phenocrysts of oligoclase and potash feldspar which may have inclusions of oligoclase. CY91 which outcrops on the western headland of Petchey's Bay represents the ultimate evolution of these rocks, with large feldspar phenocrysts absent. CY2 outcrops on the Nicolls Rivulet road at Oyster Cove. These particular rocks are called hornblende porphyries.

The Petchey's Bay rock in the hand specimen is a grey porphyritic rock with an unresolvable groundmass which has a mottled appearance due to lighter patches of ovoid shape scattered through a slightly darker groundmass. The phenocrysts are composed of dark laths of amphiboles of uniform grain size with dimensions approximately 1 cm x 0.2 cm and having a preferred alignment in the rock (Pl. 24). The amphiboles of the finer grained dyke (CY2) are smaller, appearing as fine needles in a somewhat weathered groundmass.

The groundmass is more uniform than that of CY91 and the rock does not have the same patchy appearance, however within the rock an inclusion of pale green pyroxene has been found with a diameter of 3 cm. Feldspar phenocrysts are absent from this rock.

In CY91 the amphibole consists of crystals which are strongly pleochroic with X = yellow green, Y = dark yellow green and Z = dark green. Some colour zoning and twinning also are present. The amphibole is fresh with very few inclusions and is pargasitic in composition (Table III-8). In thin section it is apparent that the lighter patches consist of accumulations of fragmented pale green

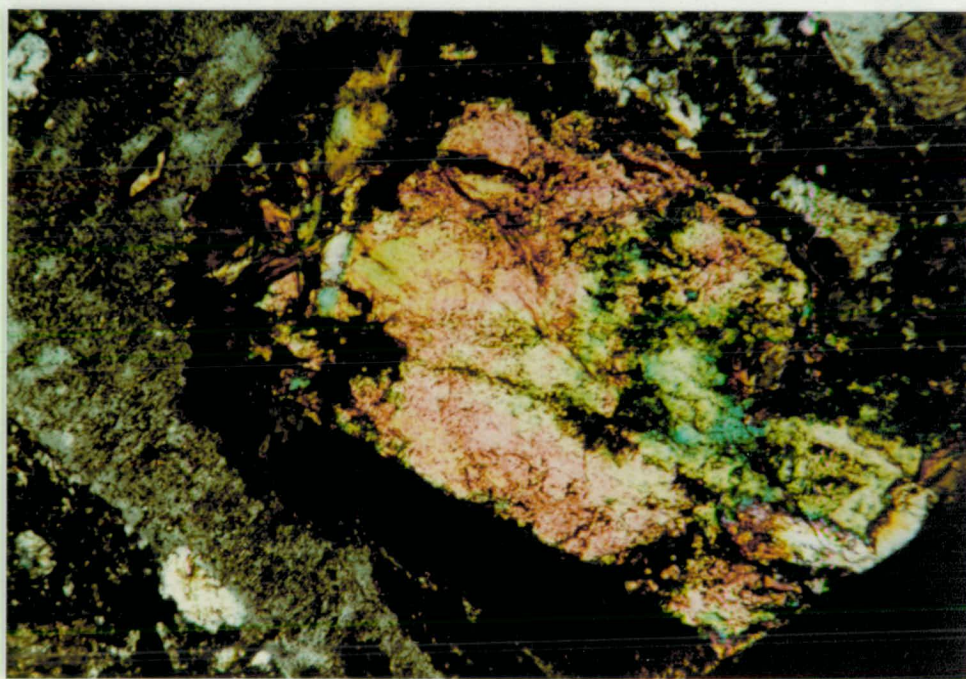
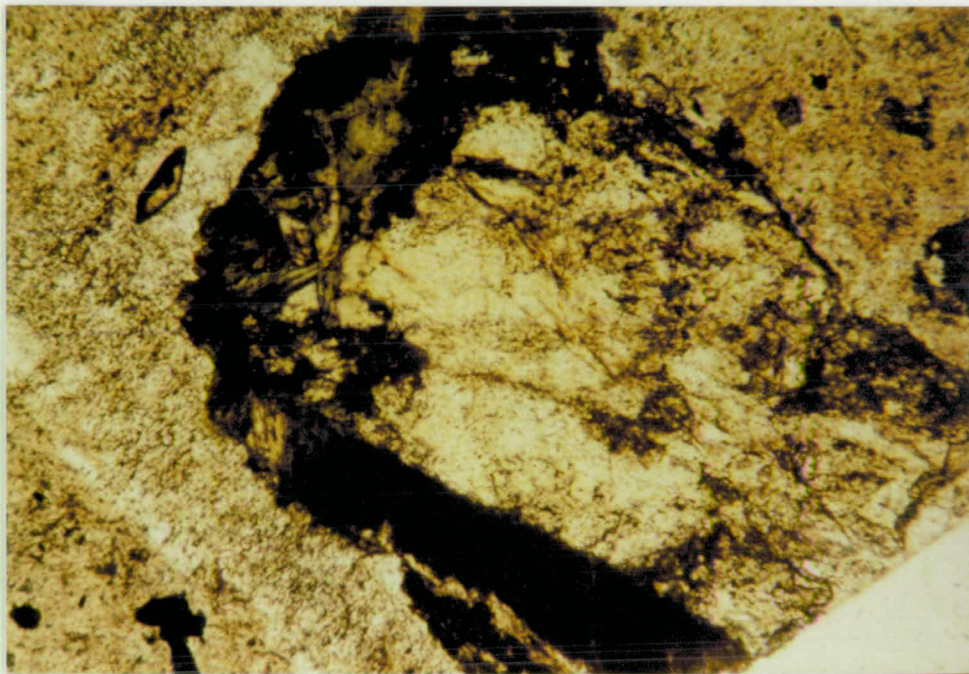


Plate 22 Syenite porphyry (CY76). Epidote core with amphibole reaction rim enclosed in potash feldspar. x190.

Top - plane polarised light
Bottom - crossed nicols.

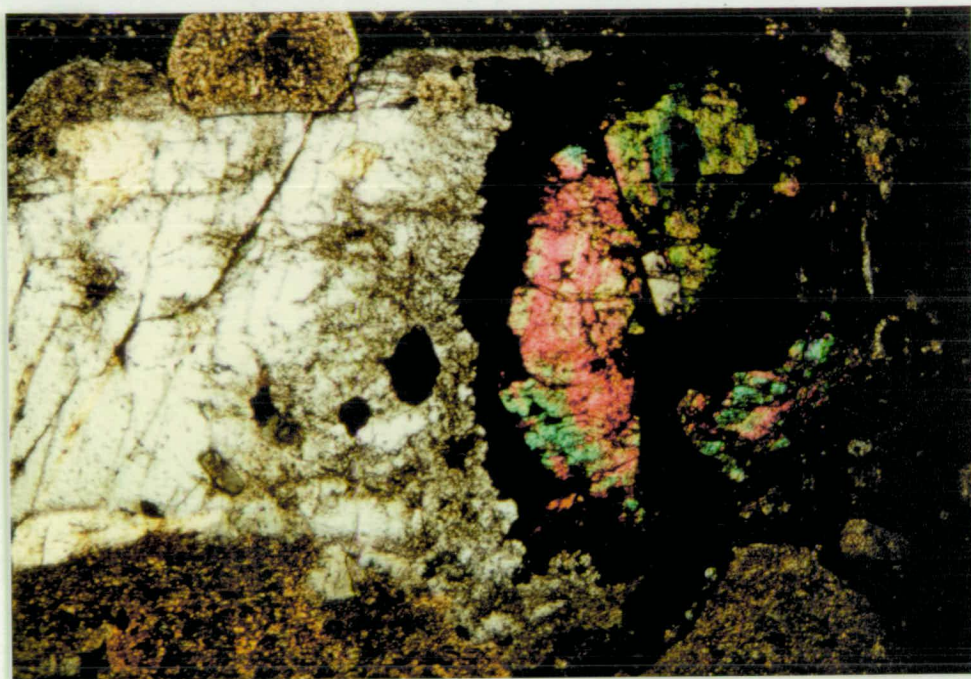


Plate 23 Syenite porphyry (CY76). Epidote with amphibole reaction rim and potash feldspar growing off it. Crossed nicols. x60.

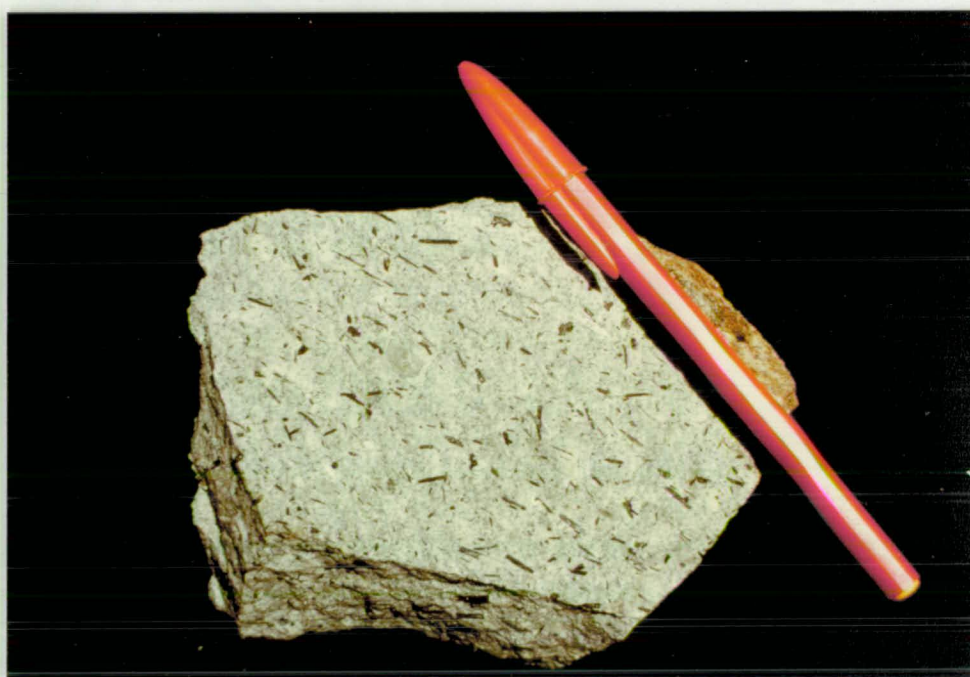


Plate 24 Hornblende porphyry, Petchey's Bay. Note lighter patches in the matrix.

pyroxene tablets and laths of maximum dimensions about 1 mm x 0.05 mm (Pl. 25). In the groundmass which constitutes about 70% of the rock are a few small euhedral apatite crystals and sphene crystals up to 1 mm long. Small magnetite grains occur throughout the groundmass, which is composed of a dense mesh of altered potash feldspar laths which have a trachytic texture. The feldspars are sericitized.

CY2 is similar to above with a generally finer grain size. The amphibole is similar as is also the scattered euhedral granular crystals of pale green pyroxene. These pyroxenes are similar to those comprising a pyroxenite inclusion occurring in the rock. The inclusion has granular pyroxenes, very pale green in colour with weak pleochroism but having darker rims, particularly at the margin of the inclusion. The inclusion has sharp contacts with the enclosing rock. Thus the indication is that the pyroxenes in these rocks are derived from disrupted inclusions of foreign origin from their similar compositions, fragmental nature, and occurrence as clumps of crystals. The groundmass consists of pilotaxitic potash feldspar laths with some micaceous alteration ranging up to high first order interference colours. Some amygdules are present, containing radiating fibrous zeolite crystals. These are both length slow and length fast with oblique extinction.

Inclusions in the Syenite Porphyries

Apart from occasional rafted blocks of Permian country rocks the only abundant inclusions are the amphibolite xenoliths occurring in the syenite porphyry on the north west slopes of Mt. Windsor, and exposed in road cuttings on the Petchey's Bay road. Hand specimens reveal these to consist of angular fragments with well defined margins varying from about 1 cm to 10 cm maximum dimension. They consist



Plate 25 Amphiboles (dark green) and pyroxenes (light green) in feldspathic groundmass. Note pyroxenes associated with lighter patches in groundmass. CY91. Plane polarised light. x75.

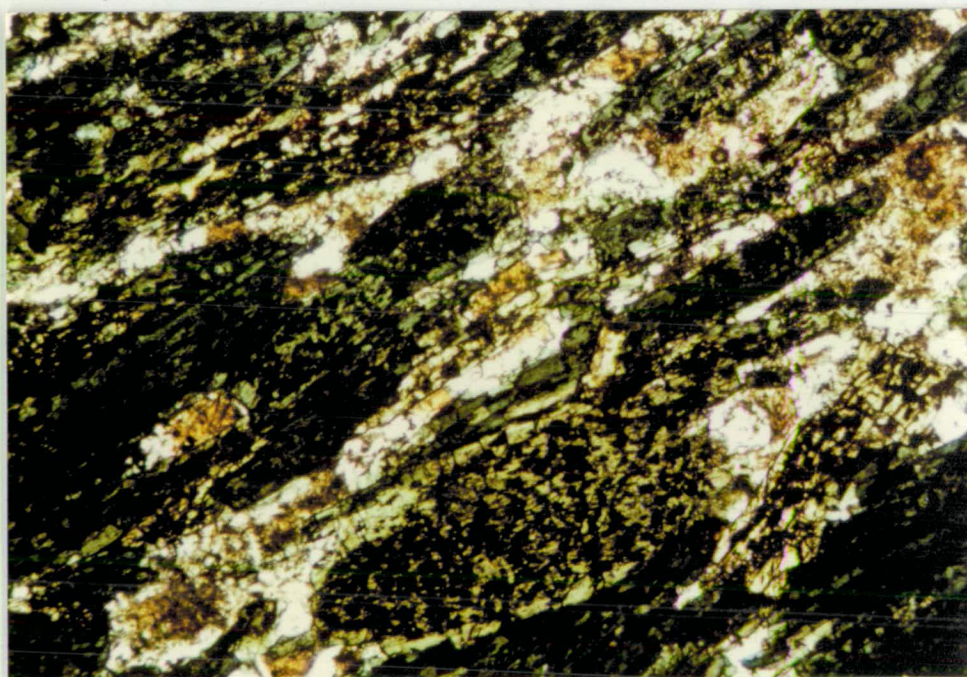


Plate 26 Amphibolite inclusions, Petcheys Bay Road, Mt. Windsor. Inner part of inclusion showing amphibole with many inclusions and clear quartz-feldspar matrix. Plane polarised light. x75.

either of massive dark green amphibole, or more commonly having a black and white striped appearance due to interlayering of darker amphibole with light coloured matrix.

Microscopically the xenoliths have a foliated texture showing green amphibole crystals interlayered with a colourless matrix of irregularly shaped equigranular crystals of clear untwinned plagioclase, having the composition of andesine, and quartz, together with patches of iron-stained unresolvable material. The matrix occupies about 30% of the rock.

The amphibole is negative with 2V of about 60° and pleochroic having X = pale green, Y = green, Z = dark green. The amphiboles comprising the inner parts of the inclusions have a larger number of opaque inclusions (Pl. 26). There are also small brown inclusions which have high relief, are strongly birefringent and are probably zircon.

The rims of the inclusions are characterised by a lack of matrix, possibly because of being melted out, the amphibole now being recrystallised to give a dense mass with a more hornfelsic (equigranular) texture but still with an orientation (Pl. 27). The pleochroic scheme does not change. The inclusions, particularly the opaque ones, have virtually disappeared leaving a few rectangular to rhomboidal grains of high relief and high birefringence (about 0.1 mm diameter). These are probably small zircons. The compositions of the amphiboles are summarised in Table III-8 and Figs. III-9 and III-10 where it can be seen they are related to pargasite with the rim compositions richer in iron than the cores.

SANIDINE PORPHYRIES

In contrast to the syenite porphyry which contains phenocrysts of

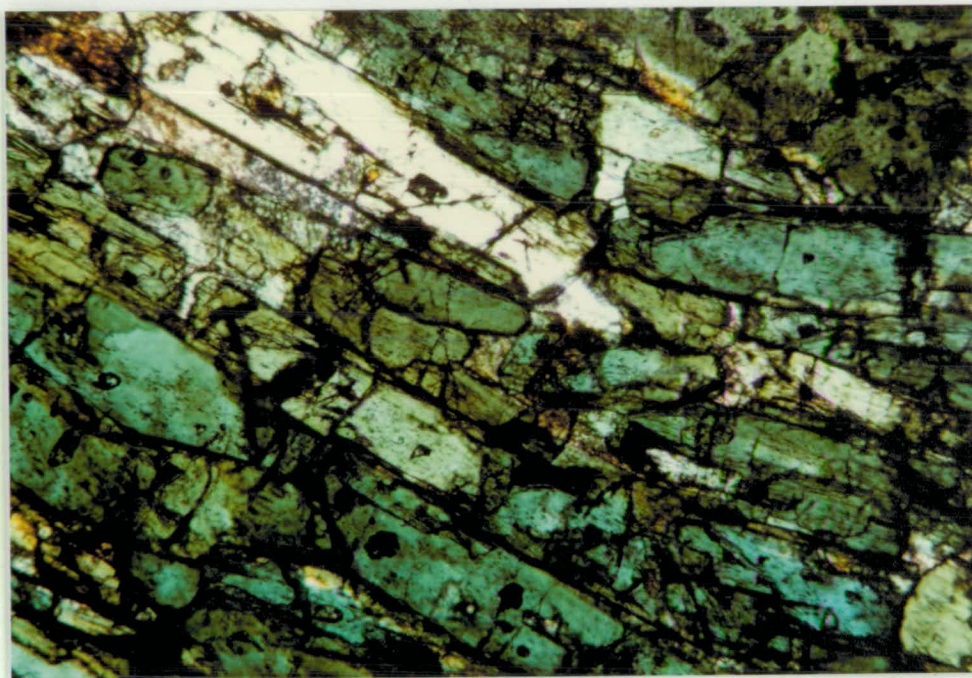


Plate 27 Rim amphiboles from inclusion of Plate 24. Amphiboles are devoid of inclusions, less elongated and there is very little feldspathic matrix. Plane polarised light. x190.

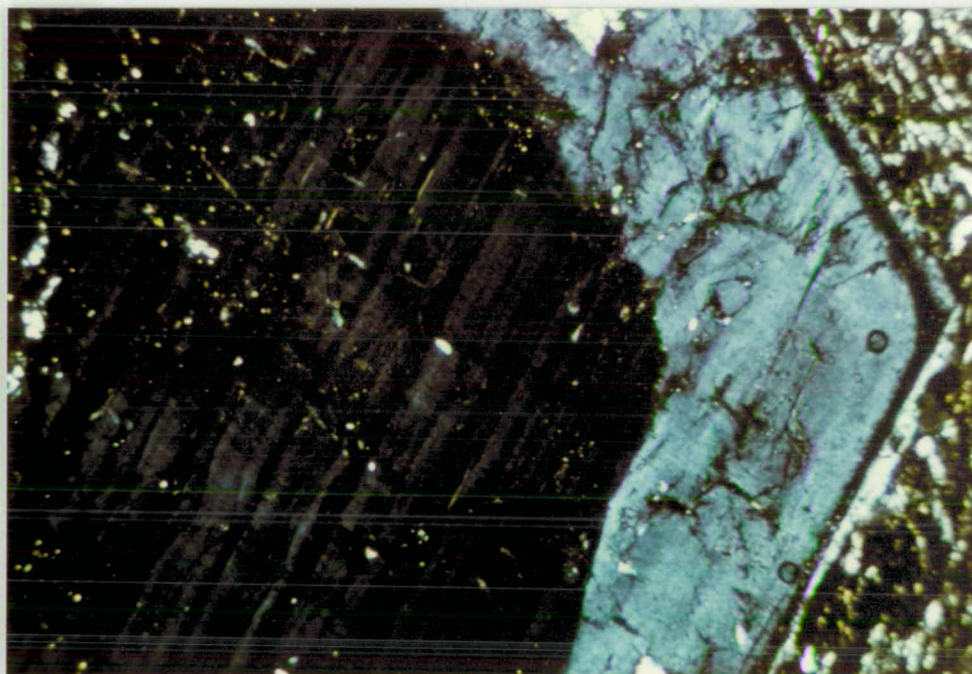


Plate 28 Fine multiple twinning and evidence of second and third stage overgrowths with rim inclusions in a sanidine crystal from CY74. Crossed nicols. x75.

oligoclase, this group of rocks is of somewhat greater mineralogical variation but with phenocrysts of mainly sanidine. Also grouped with them for descriptive purposes are dykes containing phenocrysts of oligoclase and sanidine with the potash feldspar of later generation than the plagioclase. These sanidine rocks occur as dykes, usually no wider than about 2 m, and are much more consistent in their form than are the syenite porphyry intrusions. That these rocks are later than the syenite porphyry is shown by their intrusion into the syenite porphyry at the western end of Silver Hill road, and at Hollands Quarry (Pl. 2).

The early descriptions of Twelvetrees and Petterd (1898) together with those of Edwards (1947) referred to the sanidine-bearing rocks with the largest phenocrysts as "biscuit" rock. No fresh specimens of this rock could be collected.

Grey Groundmass Rocks

The rocks originally described as "magpie" rock occur in several dykes throughout the area. The best exposure occurs on the Huon River south of Petchey's Bay (CY74). Here the rock contains large clear euhedral sanidine crystals up to 3 cm x 0.5 cm maximum dimensions with a poorly defined alignment. These have little alteration but may have small inclusions within the crystal rims which are cloudy and barely translucent. The optic axial planes are perpendicular to (010) with a low 2V. Some very fine multiple twinning appears in one crystal (Pl. 28) clearly showing an overgrowth of potash feldspar. This crystal has 3.22% Na₂O and is approaching anorthoclase. The other phenocrysts contain from 1-2% Na₂O. Euhedral isotropic melanite crystals from 1-2 mm diameter showing colour zoning in plane polarized light occur in the groundmass. These include euhedral crystals of yellow-green to green pleochroic pyroxene, suggesting a

later formation for the melanite. A few pyroxenes include grains of magnetite with no reaction relationship but many of the melanite crystals from CY74 have grown as euhedral zoned phenocrysts and have opaque areas of alteration at their margins. The opaque material is dense, consisting of an unresolvable opaque mixture having iron and titanium as major components as well as silica, alumina, lime and potash. In spite of its opaque nature the material does not analyse as ilmenite and must be a very fine mixture of decomposition products of the melanite. Several grains (Pl. 29) have a clear reaction rim of calcite grains. Cancrinite occurs in patches of fibrous crystals in the groundmass of CY74 (Pl. 30). These together with calcite reaction rims in melanite grains and calcite grains in the groundmass, indicate the presence of late stage fluids rich in CO_2 . Some sulphur is also present in the cancrinite.

The groundmass which comprises about 80% of the rock consists mainly of pilotaxitic laths of small sanidine crystals. These appear to have some sericitic alteration, and also crystallised with them are small granules of very dark green pyroxene, euhedral melanite and grains of titaniferous magnetite. Small irregular segregations of analcime occur in the groundmass. No analcime has been found as euhedral crystals, but two or three small wedge shaped isotropic crystals of high negative relief in the groundmass of CY74 appear to have a composition between natrolite and analcime. The compositions could not be accurately determined because of boiling of the specimen in the electron probe. This phenomenon did not occur with probing of the larger analcime crystals. The form of these is very similar to those reported for analcime in the Dippin Sill Arran by Henderson and Gibb (1977). The analcime may be intergrown with a fibrous mineral which is length slow, and has upper first order

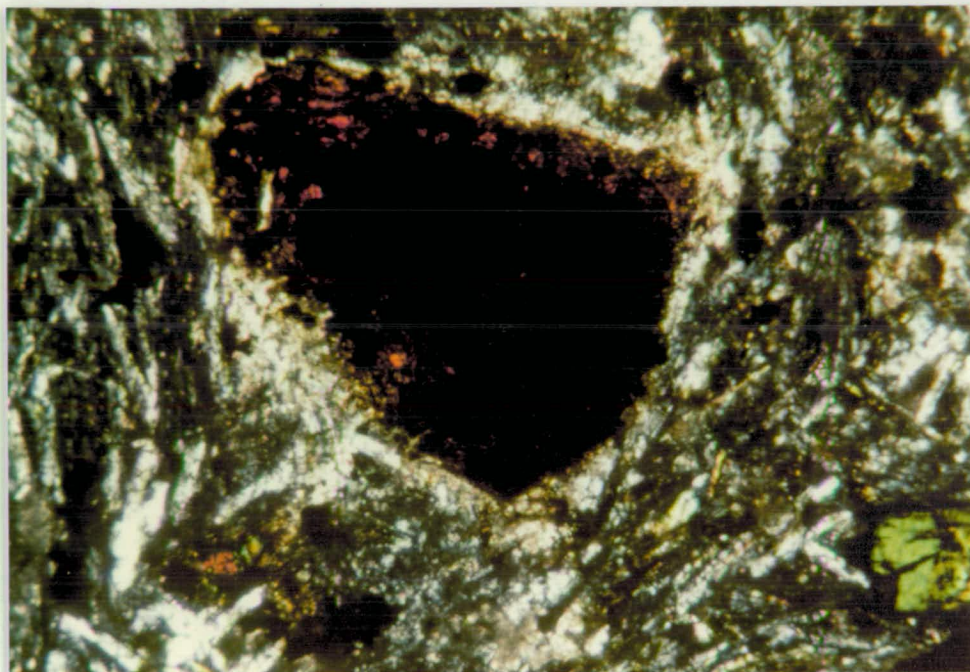


Plate 29 Calcite reaction rim around altered melanite crystal. CY74. Crossed nicols. x75.



Plate 30 Fibrous cancrinite crystals in the groundmass of CY74. Crossed nicols. x190.

interference colours. A very small inclusion of sodalite within pyroxene was found in CY74 using the electron probe. It is quite probable that it represents an irregular spot in the original crystal face in which the feldspathoid had crystallized. The groundmass of these rocks appears grey in the hand specimen.

Other examples have phenocrysts with some inclusions giving the appearance of growth zoning. Some dark green amphibole is rarely present and is pleochroic, X = yellow, Y = green, Z = dark green. Two examples were found showing melanite crystals in reaction relationship with allanite grains (Pl. 31) which could be inclusions as no others were observed. Small euhedral melanite grains occur in the groundmass with relatively rare small needles of aegirine. Interstitial calcite grains can occur.

In the groundmass are occasional small resorbed plagioclase crystals, small apatite and sphene grains and small opaque rectangular grains are mainly of pyrite. No glass is present in any rock. One old slide from the area (A.D. Mackay No. 19) shows altered euhedral hexagonal hauynite included in sanidine laths. In this slide appears a clot of melanite crystals with a rim of scapolite which suggests it is equivalent to CY44 of the present collection. A melanite-bearing rock with grey groundmass (CY86) intersects two dykes with a green groundmass (CY85) between Copper Alley and Langdon's Point.

Green Groundmass Rocks

These latter dykes contain euhedral glassy rectangular sanidine phenocrysts showing alignment parallel to their walls. The crystals are 0.3 cm long. The edges of many sanidine phenocrysts may appear diffuse due to the inclusion of aegirine laths. This is due to further growth of the initial phenocryst by addition of material

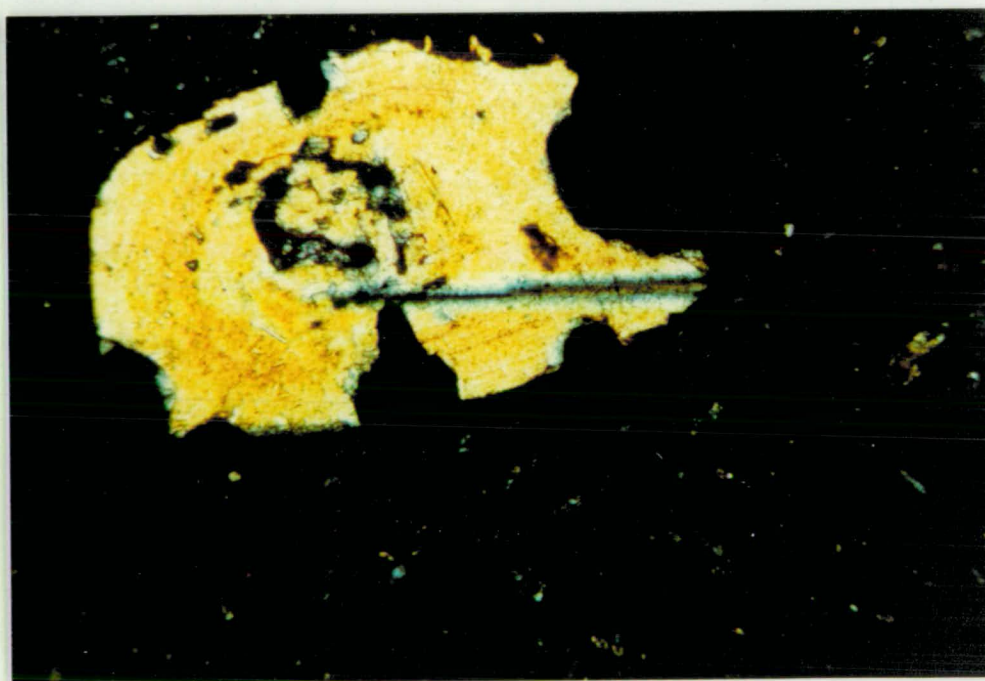
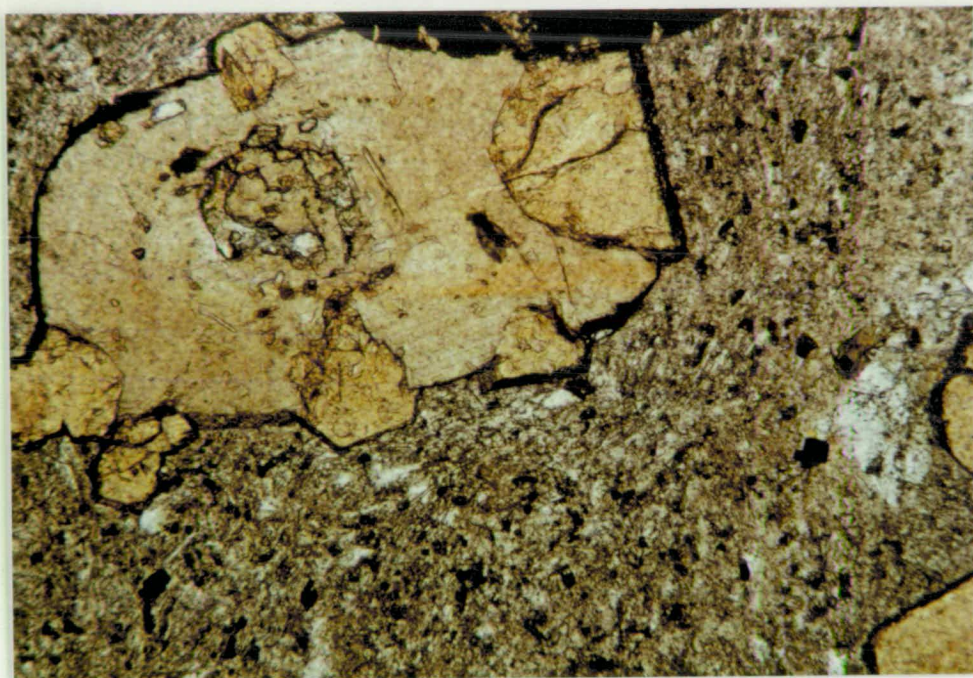


Plate 31 Allanite (inclusion?) from CY19 with included melanite crystals. x190

Top - plane polarised light
Bottom - crossed nicls.

from the feldspathic component of the groundmass. Small euhedral phenocrysts of pyroxene with yellow-green pleochroism occur in the groundmass, which occupies about 80% of the rock. These show columnar prismatic and rectangular basal sections. Grainsize has a 1 mm maximum. Melanite occurs in these as small sporadic euhedral crystals. There are rare subhedral crystals of late stage pectolite in the groundmass which consists of a very dense fine grained intergrowth of aegirine needles intergrown with potash feldspar laths. There is a flow structure present but the texture is more that of a "spotted slate" type due to the presence of numerous small rounded uniaxial negative crystals of nepheline, potash feldspar and possibly pseudoleucite (Pl. 32). There are occasional larger grains with a development of some crystal faces, many of which have undergone a cloudy micaceous alteration which gives a pink tinge to them.

On the shore about 100 metres north of the site of the old Port Cygnet deep water jetty at Langdon's Point is another dyke with a green groundmass, and another about 30 cm thick, 200 metres to the north, which is the sanidine tinguaite described by Edwards (1947). The most striking aspect of this dyke in the field is the beautiful swirl structures, presumably indicating turbulent flow, which are exhibited by the orientation of large plates of sanidine (Pl. 5). These are typical euhedral (010) tablets, about 3 cm long, embedded in a fine grained (but non-glassy) green matrix. It does not have a glassy chilled margin but is finer grained at the contact and maintains its porphyritic texture. The dyke has only a small zone (about 5 cm wide) where obvious baking has taken place although the Permian country rock in the area is generally thermally metamorphosed.

Microscopically the rock contains large clear euhedral rectangular phenocrysts of sanidine, which are biaxial negative with low 2V.

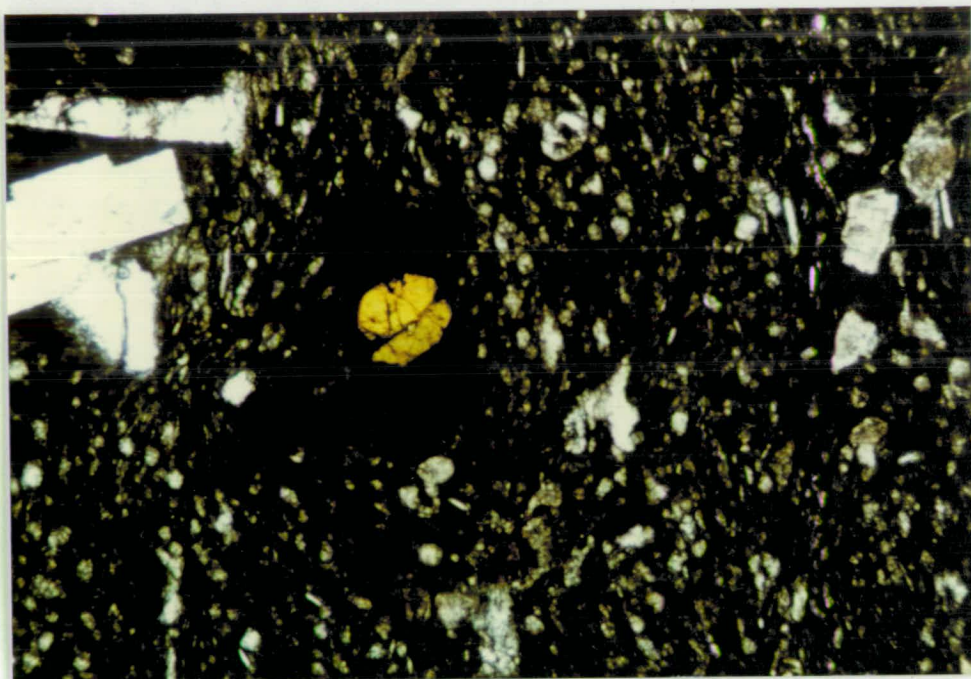


Plate 32 Detail of groundmass from CY85 showing sanidine laths, pyroxene included in dark melanite, rounded grains of nepheline and dense aegirine needles. Plane polarised light. x75.



Plate 33 Small tablet of sanidine from X44 showing evidence of multiple growth with inclusions of aegirine needles. Crossed nicols. x190.

Some crystals have cloudy cores and quite a few are broken or cracked. There is evidence of multiple growth shown by aegirine inclusions (Pl. 33). Most crystals are quite homogeneous but in some, particularly in the cores, there is evidence of microperthitic exsolution lamellae. Smaller subhedral sanidines occur in the groundmass and many of these are uniaxial negative. They may be distinguished from nepheline by their development of partial crystal faces producing a lath-like form. Their composition has been checked by electron probe analysis. Some feldspars have been altered to small clumps of radiating, length-fast zeolite? crystals. There are occasional patches of a purple coloured mineral, usually as a groundmass segregation, which is identified as eudialyte (Pl. 34) intergrown with aegirine needles. Evidence of discrete andalusite crystals is present as muscovite pseudomorphs in the groundmass (Pl. 35). Melanite is scarce in this rock. Small euhedral crystals of yellow-green pleochroic pyroxene (0.1 mm diameter) are present having colour zoning with lighter cores. The rims on some pyroxene are very dark and it is difficult to ascertain if this is due to opaque oxides from alteration, or simply a very dense colour border. Most pyroxene appears fresh and unaltered. Pyroxenes are also included in some of the potash feldspar phenocrysts. These also have very dark rims.

The groundmass consists of small rectangular potash feldspar laths with pilotaxitic texture. These are also associated with laths of pectolite showing high second order interference colours (Pl. 36). The groundmass has a dense mesh of fine grained aegirine laths which grow between and through the feldspar laths of the matrix. Also present are rounded, irregular grains of nepheline, intergrown with the aegirine crystals. These are not as abundant as in the first group (i.e. CY85) described above. The groundmass occupies about 50% of the rock.

On the road from Lymington to Mt. Windsor occurs another dyke (CY73) with a green groundmass but showing a mineralogy significantly different from those described above. The outcrop is poor but fresh samples have a prominent parallel alignment of euhedral glassy sanidine tablets. These may be up to 5 cm x 0.5 cm in length and thickness. Also obvious in the hand specimen are small black euhedral phenocrysts of melanite garnet up to 3 mm diameter.

The phenocrysts of sanidine are unaltered with clean rims. They contain occasional small inclusions of euhedral yellow-green pleochroic pyroxene and euhedral hexagonal isotropic hauynite which does show some alteration. There may be some small sphene inclusions in both the pyroxene and sanidine. Smaller subhedral crystals of sanidine consisting of angular fragments of crystals occur as a smaller generation of phenocrysts (approx. 1 mm diameter). Some sphene laths with terminations up to 2 mm in length are present as phenocrysts as well as occasional apatite crystals.

The melanite crystals are euhedral isotropic with strong colour zoning. They contain some unaltered inclusions of pyroxene and are square to pseudo-hexagonal in cross section with a brown colour and high relief. There are a large number of well formed hexagonal sections of isotropic phenocrysts of hauynite (Pl. 37). They are approximately 1 mm in diameter, characteristically have a distinct dodecahedral cleavage and are quite fresh with little alteration.

In addition to hauynite there are rather irregular anhedral masses of fresh analcime in the rock. This can vary from 1 cm for the largest mass, which has a reaction relationship to a sanidine phenocryst, down to 0.5 mm as small segregations in the groundmass. There are smaller anhedral isotropic grains in the groundmass which are also analcime. They are associated with aegirine needles. These

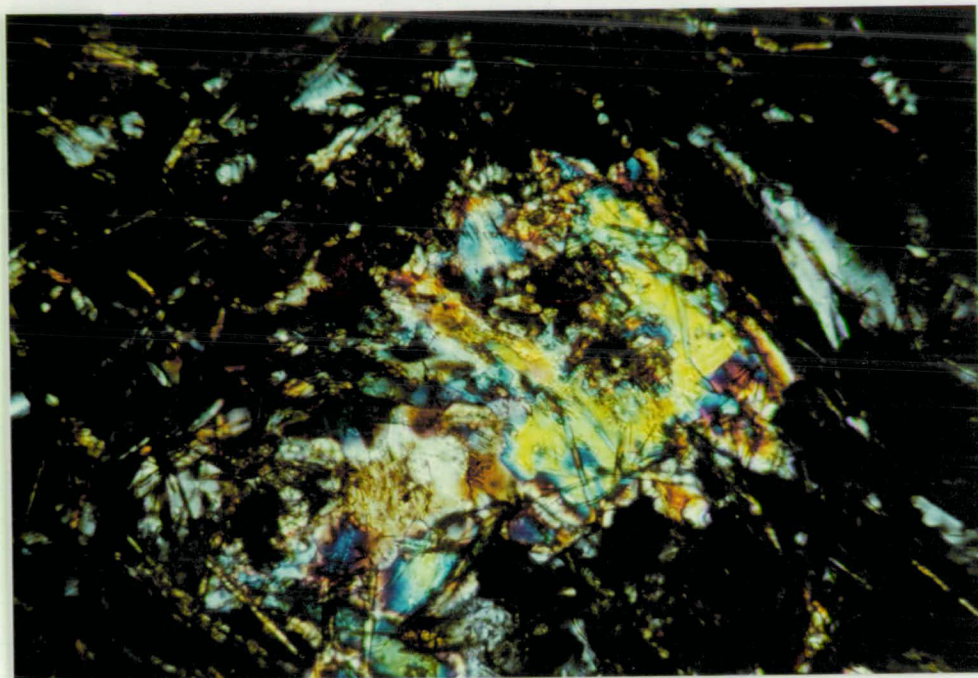


Plate 36 X44 - patch of pectolite in groundmass of feldspar laths. Crossed nicols. x480.

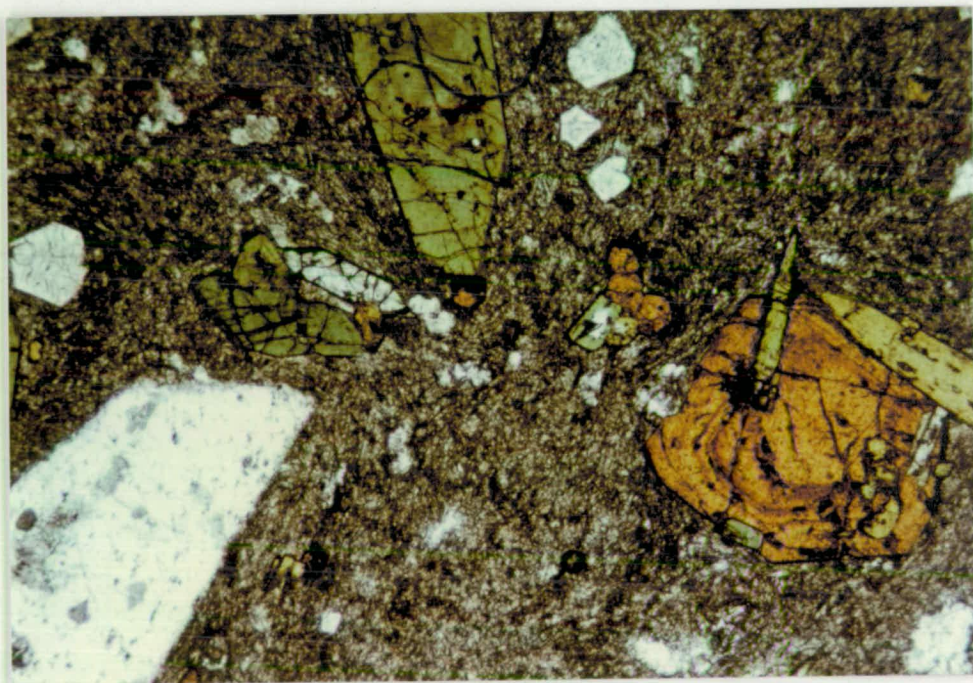


Plate 37 CY73 - Zoned brown melanite enclosing pyroxene. Large clear crystal is sanidine. Euhedral clear small crystals are hauynite. Euhedral elongated clear crystal between green pyroxenes is sphene. Irregular small anhedral crystals in groundmass are analcime. Plane polarised light. x75.

minerals have had their compositions checked using electron probe analysis (Table III-10). The groundmass which constitutes about 75% of the rock is composed of pilotaxitic potash feldspar laths which are closely intergrown with a close mesh of aegirine needles.

The crystallisation order for the sanidine rocks is: apatite, sphene, magnetite and zircon together followed by melanite, and pyroxene which crystallised concurrently with the feldspar phenocrysts and hauynite and finally the feldspathic groundmass with nepheline and analcime.

VARIANTS OF THE SANIDINE PORPHYRIES

Scapolite-bearing Dyke Rock

On the western shore of Port Cygnet about 300 m north of Langdon's Point outcrops a dyke (CY44) with sanidine phenocrysts aligned parallel to its margins, appearing as white crystals in a grey groundmass. This rock appears to represent an altered equivalent of "magpie" rock (i.e. grey groundmass rock). The sanidine phenocrysts are euhedral, approximately 1 cm x 0.25 cm, and have some included altered feldspathoid crystals and garnet grains. Euhedral feldspathoid crystals included in the sanidine are altered to scapolite. The sanidines show some sericitic alteration and microperthitic exsolution. Biotite and small sphene grains are sometimes also included. Glomeroporphyritic melanite crystals with strong colour zoning and original euhedral form, are present. They have a maximum diameter of 3 mm. Many melanites show typical light to dark brown colour-zoned cores, but some have colourless to pale pink rims which are weakly anisotropic with a dusting of small highly birefringent grains of sphene, and calcite due to alteration. In many grains there is a further outer reaction rim of

well crystallized scapolite plates with included grains of pyrite (Pls. 38 & 39). Occasional anhedral plates of scapolite, with diffuse margins, occur separately in the groundmass. In some examples there may exist a further zone of small platy crystals of brown and green biotite recognized by its high birefringence and uniaxial negative sign. The pale pink garnets are frequently pseudomorphed by patches of remnant garnet, sphene grains, green-brown biotite plates and pyrite grains. These may or may not have associated scapolitic reaction. Pink garnets with opaque inclusions and alteration occur in the groundmass, and as unaltered inclusions in sanidine crystals. Probe analyses of these garnets shows that the lighter grains have less iron oxide and more alumina than the darker melanite core. It would appear that the alteration is due to sulphur reacting with the melanite to produce scapolite, pyrite and sphene. In the groundmass are also areas where pyrite has reacted to produce biotite. Associated with one pink garnet is a low birefringent pink mineral of high relief, almost uniaxial negative with 2V of about 5°. Its composition is similar to the pink garnet and pyrite with brown-green biotite and sphene grains may be pseudomorphs of melanite. Some dark green amphibole crystals, both fresh and altered, are also present. When altered they have been converted to an accumulation of green biotite grains. The groundmass which constitutes about 70% of the rock, consists of pilotaxitic feldspar laths with scattered high birefringence sphene grains probably derived from the alteration of the garnets.

Iron-muscovite bearing rock

Another variant of the potash-feldspar-bearing dykes outcrops on King's Hill road near the saddle of Mt. Mary (X50). In hand specimen

TABLE II-1

Electron Microprobe Analyses of Fe-Micas from Inclusions in Sanidine
Porphyry Dyke. X50.

Na ₂ O	0.22	0.26	0.00	0.22	0.00	0.00
MgO	1.15	1.19	1.42	0.25	0.57	0.25
Al ₂ O ₃	34.76	34.63	34.16	36.13	35.86	35.98
SiO ₂	45.07	45.48	45.45	45.85	46.12	46.32
K ₂ O	10.99	11.20	11.19	10.94	11.06	11.00
CaO	0.17	0.00	0.10	0.00	0.13	0.13
TiO ₂	0.49	0.36	0.29	0.13	0.14	0.00
FeO	5.28	4.62	4.90	4.31	4.31	3.23
Un-normalised Total	98.12	97.85	97.51	97.82	98.19	96.90

Atomic Proportions on basis of 22 Oxygen

K	1.857	1.895	1.901	1.838	1.853	1.855
Na	0.056	0.067	0.000	0.056	0.000	0.000
Ca	0.024	0.000	0.014	0.000	0.019	0.018
Site Total	1.937	1.962	1.915	1.894	1.872	1.873
Ti	0.049	0.036	0.030	0.012	0.013	0.000
Mg	0.227	0.236	0.281	0.048	0.111	0.049
Fe*	0.390	0.342	0.363	0.317	0.316	0.238
Al	3.393	3.442	3.407	3.655	3.610	3.726
Site Total	4.054	4.056	4.081	4.032	4.050	4.013
Al	2.032	1.969	1.951	1.958	1.941	1.878
Si	5.968	6.031	6.049	6.042	6.059	6.122
Site Total	8.000	8.000	8.000	8.000	8.000	8.000
O	22.000	22.000	22.000	22.000	22.000	22.000

*Fe Calculated as Fe³⁺

The lack of pleochroism in these relatively high iron micas indicates oxidised iron (Fe³⁺) where the d₅ octahedral electronic configuration is associated with colourless ions.

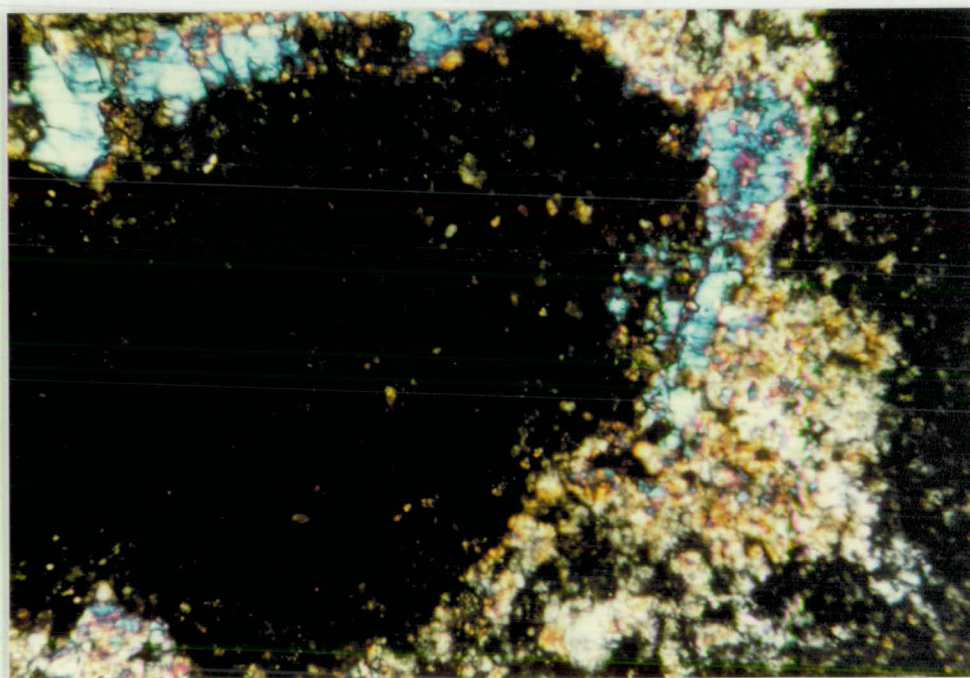
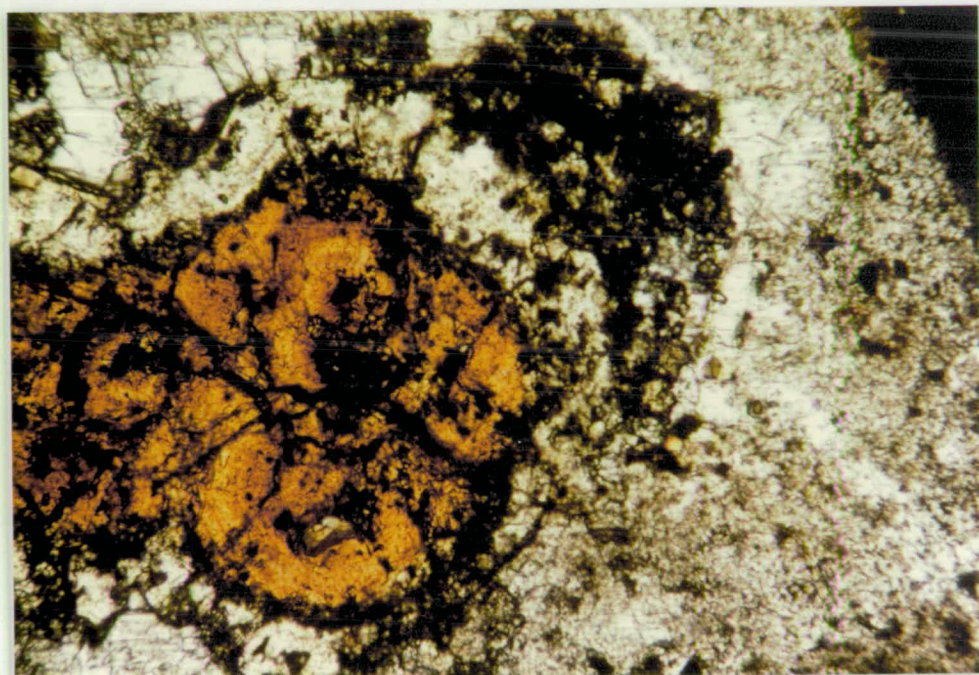


Plate 38 From CY44. Glomeroporphyritic zoned melanite crystals with clear rim surrounded by a reaction rim of platey scapolite with included pyrite grains with some associated biotite. xl90.

Top - plane polarised light.
Bottom - crossed nicols.

the rock appears to have an aphanitic texture with small vugs containing pyrite crystals. It is heavily iron-stained on numerous joint surfaces. In thin section euhedral fresh rectangular and terminated sanidine crystals occur. These have dimensions up to 1 cm x 0.25 cm in a groundmass of pilotaxitic sanidine laths (0.1 x 0.01 mm) which are partially sericitized. Within the rock are xenoliths of ferriiferous muscovite with the largest up to 1 cm in diameter. These consist of well crystallized plates (up to 1 mm) of iron-muscovite biaxial negative with 2V about 30°. Some uniaxial plates also occur. They show high second-third order maximum interference colours and are colourless in plane polarized light. Sanidine crystals have crystallised about some of the inclusions (Pl. 40). Opaque grains of pyrite are scattered through the groundmass. This may be the sanidine biotite dyke referred to by Edwards (1947). Mica compositions by electron probe are given in Table II-1.

Mixed Feldspar Rocks

Two dykes of interest occur, one on the King's Hill road near the base of Mt. Mary (CY61) and the other as a small outcrop which can only be sampled at low tide in the Huon River, off the north-western headland of Petchey's Bay (CY92). They have characteristics between those of the syenite porphyry and the more potassic rocks. These dykes have tabular feldspar phenocrysts, but are composed of plagioclase as well as sanidine with plagioclase more abundant. The larger phenocrysts are subhedral rectangular, being poorly terminated and having maximum dimensions of 1 cm x 0.25 cm. Smaller crystals tend to be euhedral in form. The plagioclase is oligoclase with some crystals having larger extinction angles at the rims, indicating albite enrichment. The compositions from electron probe do extend into the

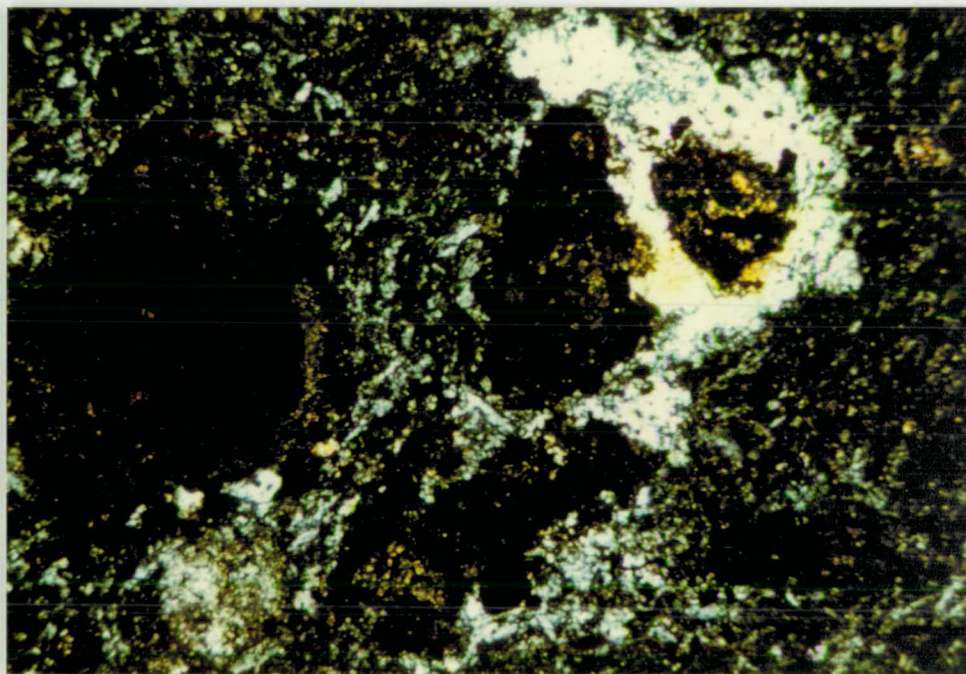
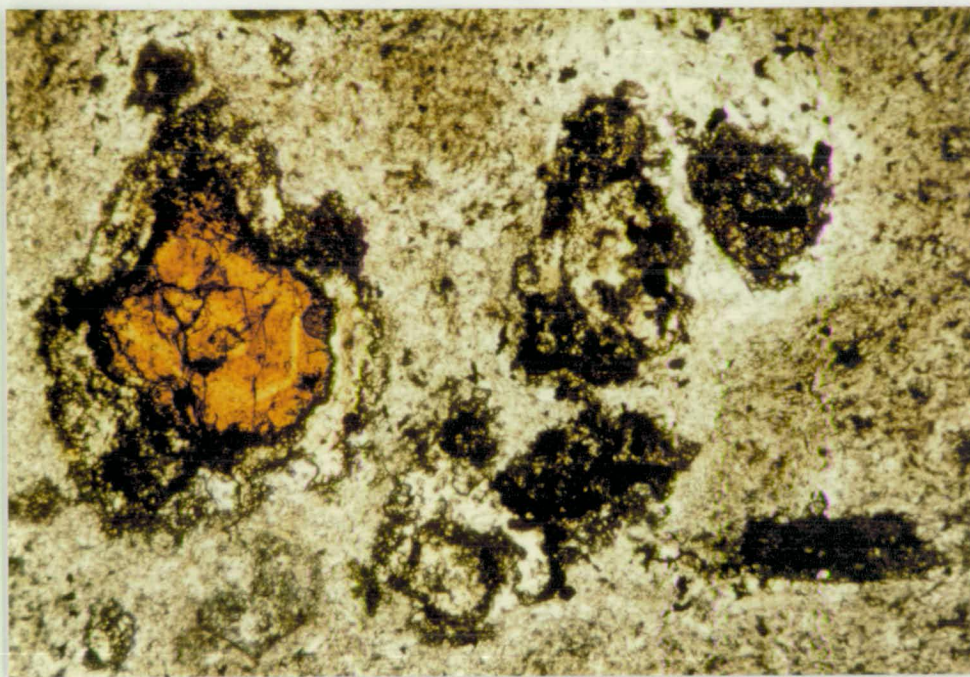


Plate 39 Melanite garnets in various stages of alteration. Growth-zoned melanite with clear rim and included dusting of sphene. Other garnets are altered to pyrite aggregates with surrounding reaction rims of scapolite. x77. CY44.

Top - plane polarised light.
Bottom - crossed nicols.

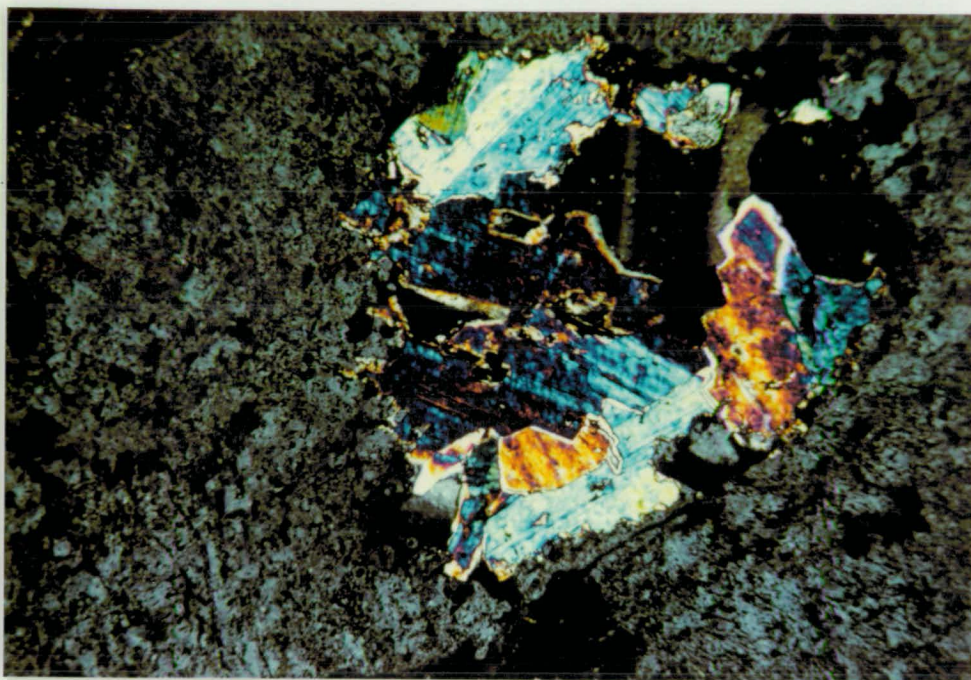


Plate 40 Xenolith of iron-muscovite included in a sanidine crystal from X50. Crossed nicols. x60.

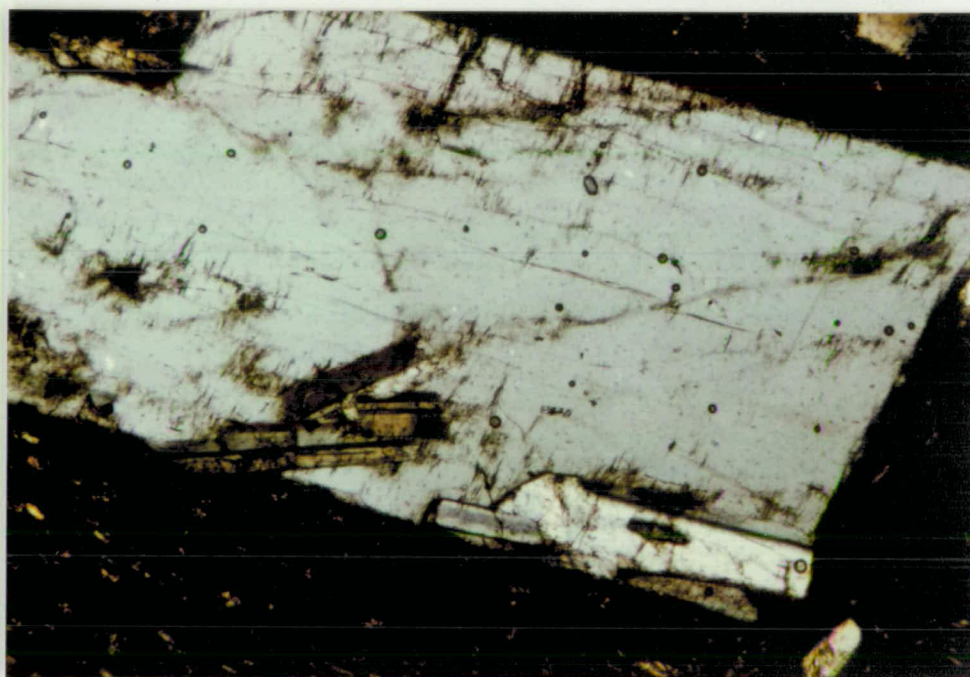


Plate 41 Sanidine phenocryst from CY92 with included oligoclase crystals. Crossed nicols. x75.

albite field. Well defined fine lamellar twinning as well as coarser twin lamellae are present, with many of these having undulose and unsymmetrical extinction. The sanidine crystals may have small rectangular oligoclase inclusions present (Pl. 41) and sanidine overgrowths occur on a few of the larger oligoclase phenocrysts (Pl. 8).

A few dark green-yellow euhedral crystals of pyroxene with 1 mm diameter are present together with sporadic euhedral melanite and occasional sphene crystals. Some small grains of pyroxene and melanite may be scattered through the groundmass which is made up of pilotaxitic feldspar laths and rectangles. Some of these show multiple twinning and also a tendency to microperthitic exsolution. Small opaque grains of magnetite are scattered throughout the rock. The groundmass constitutes about 70% of the rock and is light brown, hence the name of brown matrix rocks.

Garnet Trachyte

Between the outcrops of the tinguaita dykes with the swirl structures there occurs one of the most unusual rocks of the area. This is the rock referred to as a garnet trachyte by Macleod and White (1898). The dyke (Pl. 10) is about 40 cm wide with some evidence of multiple intrusion at the margins, and has caused some thermal metamorphism of the surrounding Permian country rock. The rock is dense, dark grey with a porphyritic texture produced by the presence of rounded phenocrysts of pinkish brown garnet and green epidote with diameters up to one centimetre. The garnets are much more abundant than the epidotes. The phenocrysts are rimmed with a white halo of sanidine crystals.

A thin section shows phenocrysts of spessartite garnet, which are euhedral to subhedral rounded, colourless to slightly pink, weakly-

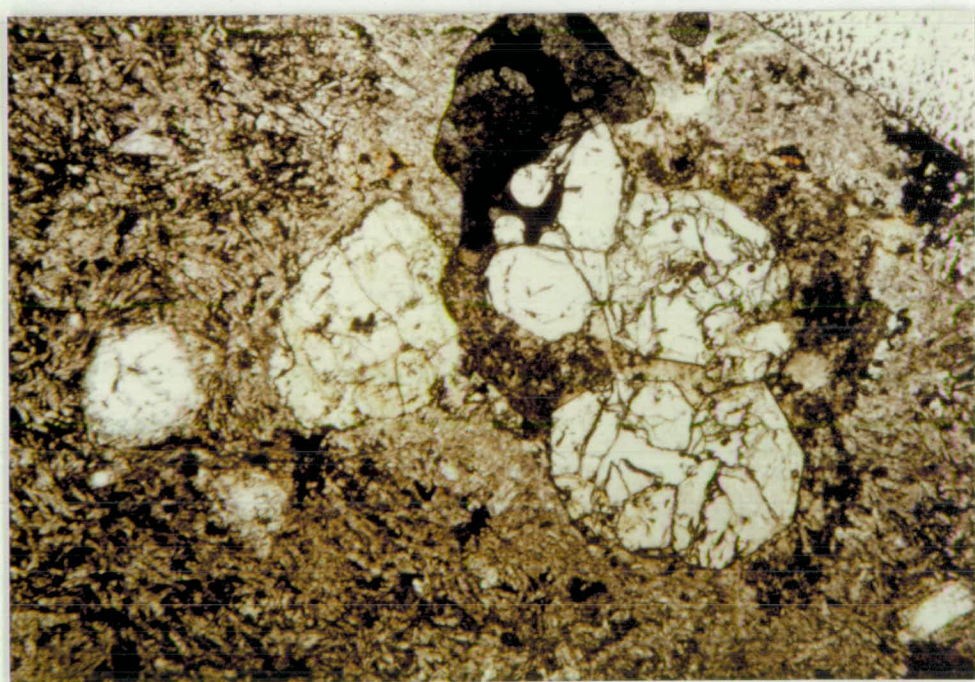
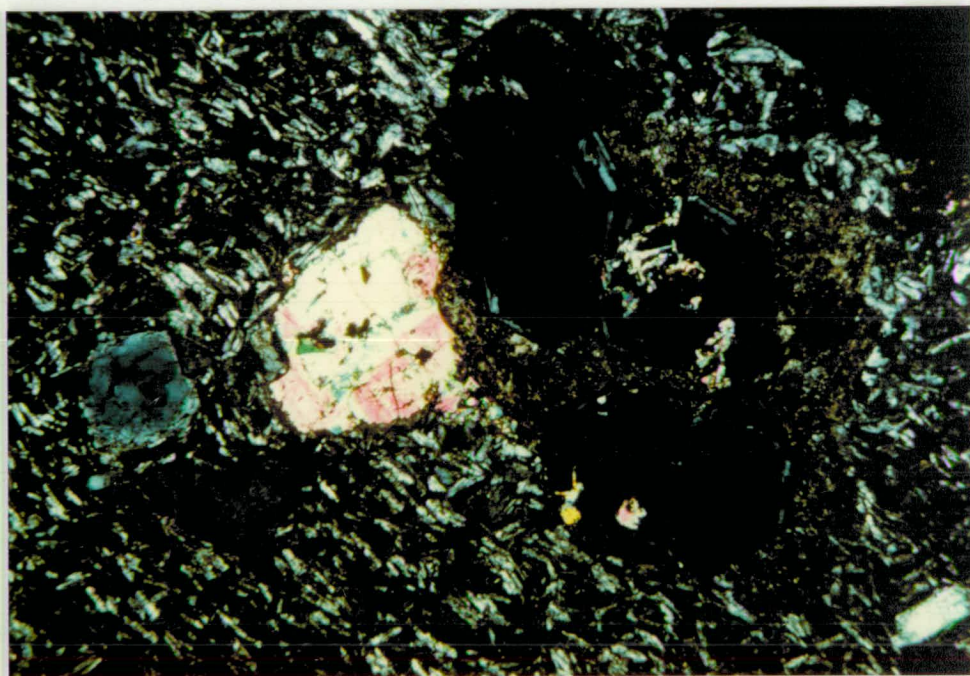
strongly anisotropic and having clearly defined growth zones (Pl. 42).

The epidote phenocrysts are not usually composed of small grains, but many are multigranular with large, constituent crystals. The epidote and spessartite occur as distinct phenocrysts. In some cases the epidote may enclose or overgrow the spessartite crystals (Pl. 12) but with no evidence of reaction between them. One crystal of epidote had a form suggesting it may have pseudomorphed a spessartite crystal. Both sets of phenocrysts range in sizes from 2 cm maximum to smaller grains which may occur in the groundmass. The crystals of epidote are mostly unaltered but rarely may have small needles of amphibole reaction rims with the groundmass. Both sets of phenocrysts have white rims due to the subsequent crystallization of potash feldspars on to them from the fluid medium (Pl. 11 and Pl. 43).

Pyrite crystals accompany many of the spessartite crystals but are always of later formation with no evidence of the spessartite having pyrite inclusions. Minor pyrrhotite occurs in the groundmass. The epidote may enclose pyrite crystallized with the spessartite. Some epidotes have enclosed individual pyrite grains formed in the groundmass. The textural evidence suggests the sequence spessartite-pyrite-epidote-potash feldspar. Phenocrysts of sanidine are rare in this rock. The largest would only be 3 mm x 0.25 mm with a rectangular habit and some showing evidence of two stages of growth. Occasional square habits occur.

One garnet phenocryst shows an overgrowth of a low birefringent mineral which is pseudomorphing an original crystal. A remnant core of the original is present having a higher first order birefringence (Pl. 44). This core has a composition close to labradorite (Table VII-6). Its alteration product is a zeolite, probably chabazite whose composition is also given in Table VII-6. Both the garnet and its altered over-

Plate 42 Garnet trachyte with spessartite garnet and epidote
phenocrysts in trachytic feldspar matrix. x30.
Top - plane polarised light
Bottom - crossed nicols.



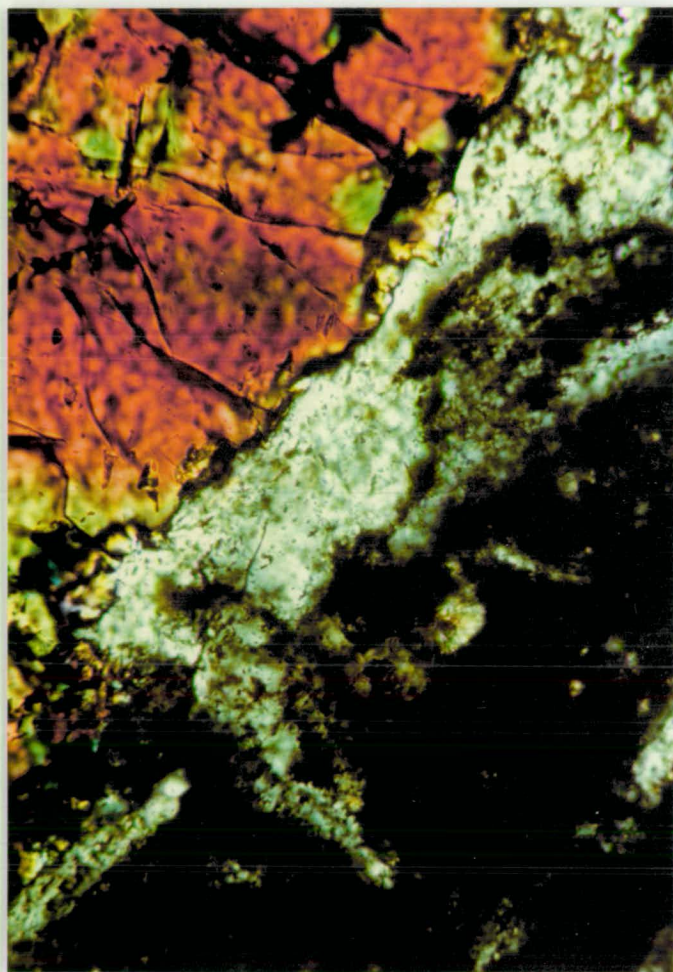


Plate 43 Detail of garnet trachyte with potash feldspar crystallised on to edge of epidote crystal. Crossed nicols. x380.

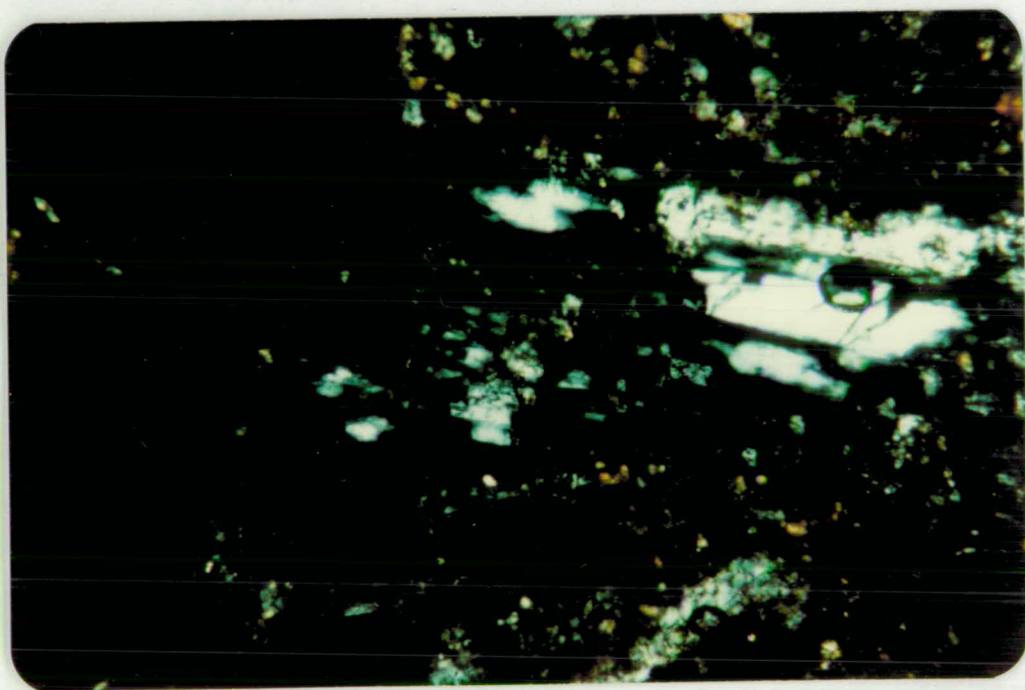
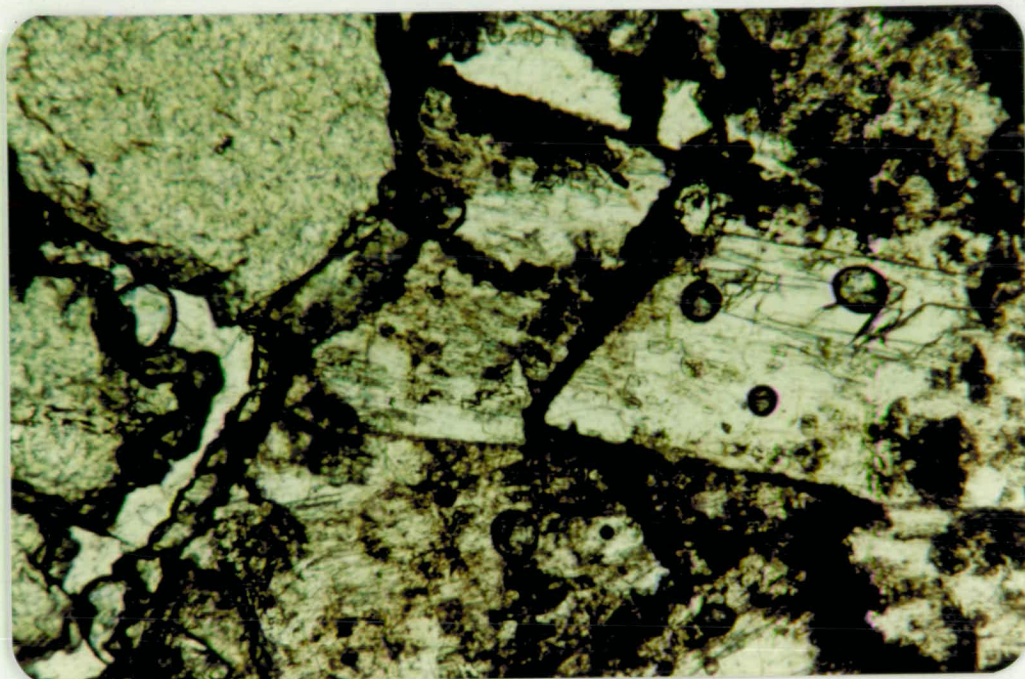


Plate 44 Zeolitized labradorite crystal growing off
spessartite garnet in garnet trachyte. x75.

Top - plane polarised light.
Bottom - crossed nicols showing unaltered
core.

growth have a further rim of small green epidote grains and potash feldspar laths. The texture may be interpreted as the garnet developed a rim crystal of labradorite followed by an overgrowth of epidote and feldspars after which the labradorite was hydrolysed to zeolite by high water activity with the epidote remaining stable.

The groundmass is 80% of the rock or greater due to the uneven distribution of phenocrysts in the rock. It is mainly of lath-shaped crystals of sanidine, with simple twinning, having a trachytic texture. In the groundmass scattered between the feldspars are numerous small grains of highly birefringent epidote and small plates of chlorite which may vary in colour from green to brown to reddish brown. The chlorite is only confined to the groundmass and does not appear as larger crystals or phenocrysts.

SUMMARY OF THE ALKALINE ROCKS

The syenite porphyries have euhedral phenocrysts of oligoclase which may show growth zoning from Ab_{60} to Ab_{90} . There is evidence of multiple growth of the phenocrysts. These occur in a groundmass of potash feldspar and quartz grains which may vary from very fine grained (less than 0.025 mm) to a relatively coarse grained (2 mm) aggregate. Occasional embayed quartz grains are present. Ferromagnesian minerals are not abundant but are represented by pargasitic hornblende which varies in quantity but reaches its greatest development in the variant referred to as hornblende porphyry.

Inclusions of marble and quartzite are present but the most abundant inclusions consist of amphibolite occurring in the syenite porphyry near Mt. Windsor.

The sanidine porphyries are later than the syenite porphyries.

They all show flow structure and may be loosely grouped into grey groundmass and green groundmass rocks.

The grey groundmass rocks have euhedral sanidine phenocrysts with melanite and occasional pyroxene with sphene and apatite. The groundmass is of fine grained sanidine laths with some interstitial analcime and cancrinite.

The green groundmass rocks have a felted mass of aegirine and sanidine laths in the groundmass, hence the colour, and the name, tinguaitite, applied to these by A.B. Edwards (1947). Variations of these have:

sanidine-nepheline-aegirine-eudialyte

sanidine-melanite-nepheline-aegirine

sanidine-hauynite-melanite-analcime-aegirine

Variants of the sanidine porphyries are represented by the dyke (CY44), containing scapolitized garnets, the muscovite bearing dyke (X50) and the mixed phenocryst, brown groundmass rocks (CY61 and CY92) containing euhedral plagioclase with overgrowths and associated phenocrysts of sanidine.

The garnet trachyte with phenocrysts of spessartite and epidote in a groundmass of sanidine laths is regarded as a modification of the parent magma of the sanidine rocks (see later chapter), and is a unique rock.

THE HYBRID ROCKS

In hand specimen two main groups can be recognised: melanocratic rocks whose composition is dominated by ferromagnesian minerals giving them a dark appearance while the lighter coloured leucocratic rocks are dominated by potash feldspar to the exclusion of most of the ferromagnesian minerals. The melanocratic rocks have

been derived largely from dolerite and the leucocratic rocks from the alkaline magma.

A multitude of names was given to specimens from the Regatta Point by Twelvetrees and Petterd (1898) where Edwards (1947) was subsequently able to show that the variation was due to reaction between an intrusive potash-rich magma and pre-existing fractured dolerite to produce a series of hybrid rocks, rather than a differentiation sequence as suggested by Twelvetrees et al. Edwards' main mineralogical conclusions are still valid, but his mapping of different zones of alteration striking approximately perpendicular to the shoreline, may be an over-simplification. Magnetite is generated as part of the reaction process, and consequently the hybrid rocks are associated with a significant magnetic anomaly. Leaman and Naqvi (1965) and Leaman (1977) have shown that the Regatta Point area is marginal to a marine magnetic anomaly located within Port Cygnet and bearing approximately NNW-SSE. This area is the only place where large scale reaction and alteration of dolerite has occurred and where there is evidence of thermal metamorphism of country rocks on both sides of the Port Cygnet estuary.

The Dolerite

The fresh unaltered dolerite is medium to coarse grained. The pyroxenes occur as glomerophyritic anhedral aggregates with ragged edges up to 3 mm in diameter and showing some ophitic texture with respect to the feldspars. The pyroxenes are colourless with some unexsolved cores. Most however are completely exsolved with regular exsolution lamellae, some of which appear to be rod shaped opaque material. Where twinning occurs this gives them a 'herringbone' appearance. With a 2V in the range of 0° to 10° the pyroxenes are

pigeonite. Occasional subhedral magnetite grains are scattered through the rock. Subhedral laths of plagioclase feldspar with a composition ranging from andesine to labradorite ($An_{40}-An_{58}$) are present. Some small potash feldspars are present, crystallized between plagioclase laths with quartz in the mesostasis (Pl. 45).

Melanocratic Rocks

These have been formed as a result of the alteration of dolerite. Pyroxene is the first mineral affected, most changing colour from colourless to green, with an increase in positive 2V, and a few to a somewhat bluish tinge with a small negative 2V, which represents a chloritic and later amphibolitic alteration. At the same time the original pyroxene develops a dust of included magnetite, often concentrated about the margin (Pl. 46). It appears that the orthopyroxene component of the exsolved pair is relatively unstable and breaks down.

The plagioclase feldspars of the dolerite do not show significant alteration at this stage and the dolerite texture is preserved. There is recrystallization of the mesostasis to produce relatively large clear anhedral grains of quartz which consequently are much more prominent than is normally so with unaltered dolerite. The grainsize of these is 0.25 mm. Small rounded grains of a dark green to brown pleochroic biotite may also occur here. The grainsize of these is near 25 microns. The clinopyroxene component of the exsolved pyroxene has high second order interference colours and may be altered to relatively coarse, anhedral, rimming, crystals of yellow green - pale green - very dark green hornblende. Both the hornblende and remnant pyroxene may be altered to fine grained rounded aggregates of green biotite. There may also be occasional larger plates of biotite

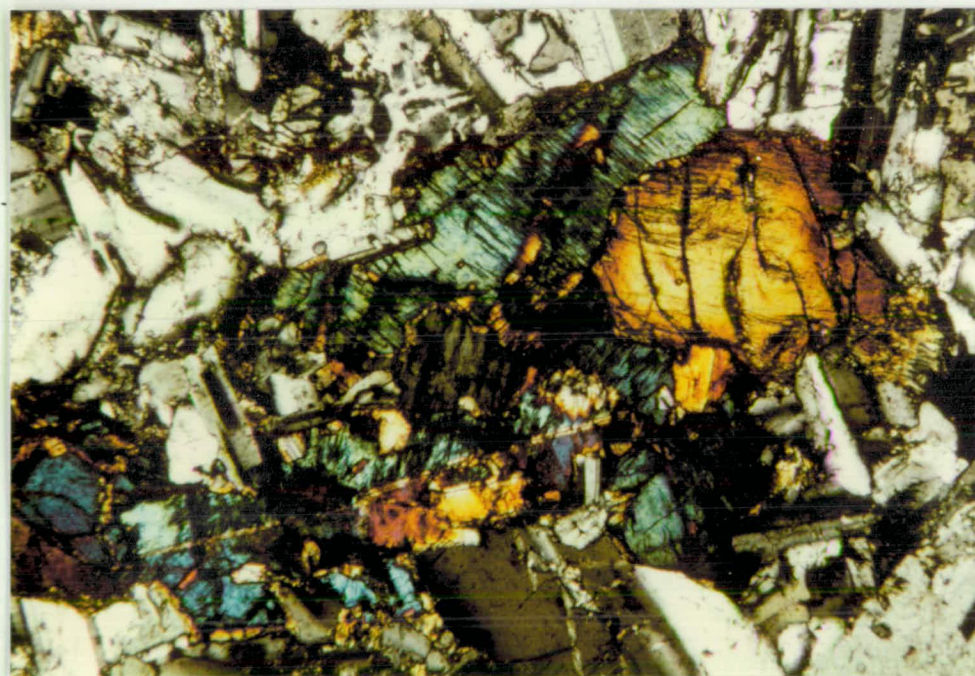
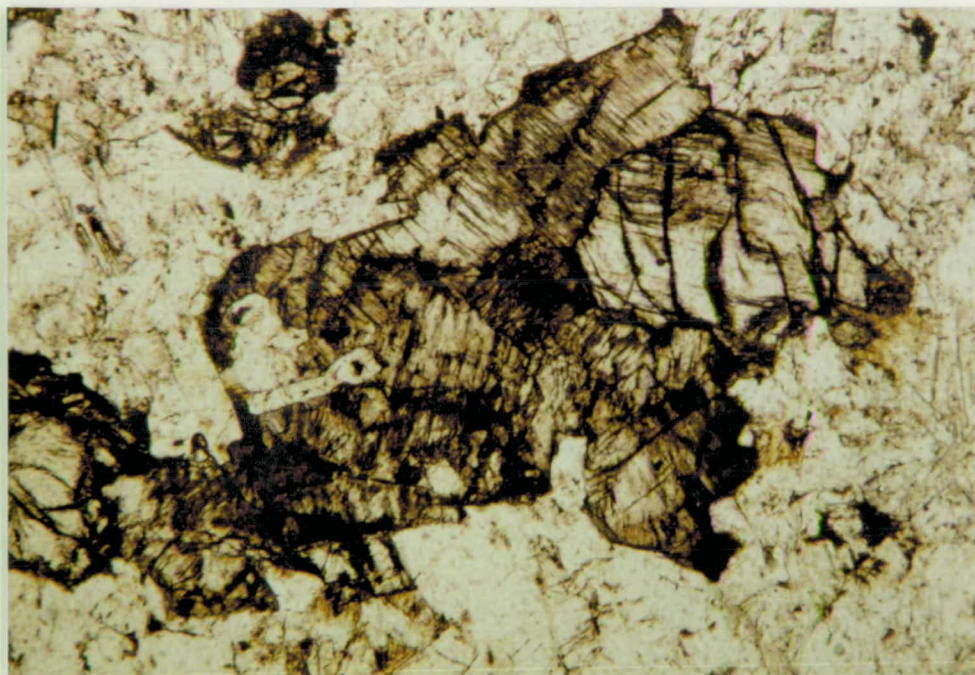


Plate 45 Fresh dolerite (CY57) showing glomeroporphyritic exsolved pyroxene with plagioclase (An₄₀₋₅₀) laths and occasional magnetite grains. x190.

Top - plane polarised light.
Bottom - crossed nicols.

which are recognized by their strong pleochroism, uniaxial negative sign and high birefringence.

The next stage of alteration shows the development of reaction rims of subhedral rectangular plates of brown biotite about magnetite grains, both those of the original matrix and those produced during alteration of the pyroxene. The larger magnetite grains in the rock may also have small reaction rims of sphene grains surrounding them.

At this point the beginning of change of the feldspar crystals occurs. The original feldspar laths with multiple twin lamellae now begin to lose their precise extinction characteristics with the lamellae becoming coarser and showing undulose extinction in the albite twin zone.

A further development which is seen readily with plane polarized light appears when the original feldspar which usually shows a typical cloudy surface now develops clear rims of fresh feldspars which may be soda or potash rich, with the soda derived from plagioclase breakdown. The lime component is absorbed by the formation of melanite, sphene and pyroxene. The original laths have now lost most of their structure to become untwinned granular feldspars of sanidine and albite compositions (Pl. 47). The resulting rock develops a granular hornfelsic texture in which the mineralogical composition consists of a pale green granular pyroxene with some original traces of the pyroxene exsolution structure. It is non ophitic. There are subhedral biotite plates having pleochroism from light brown to very dark brown. Hornblende is present in occasional clots. Euhedral to subhedral opaque magnetite grains are abundant throughout the rock. The feldspars have largely lost their lath-like habit and now have a granular interlocking texture with occasional evidence of an original core. There is some fresh multiple twinning in some grains giving composition ranging from

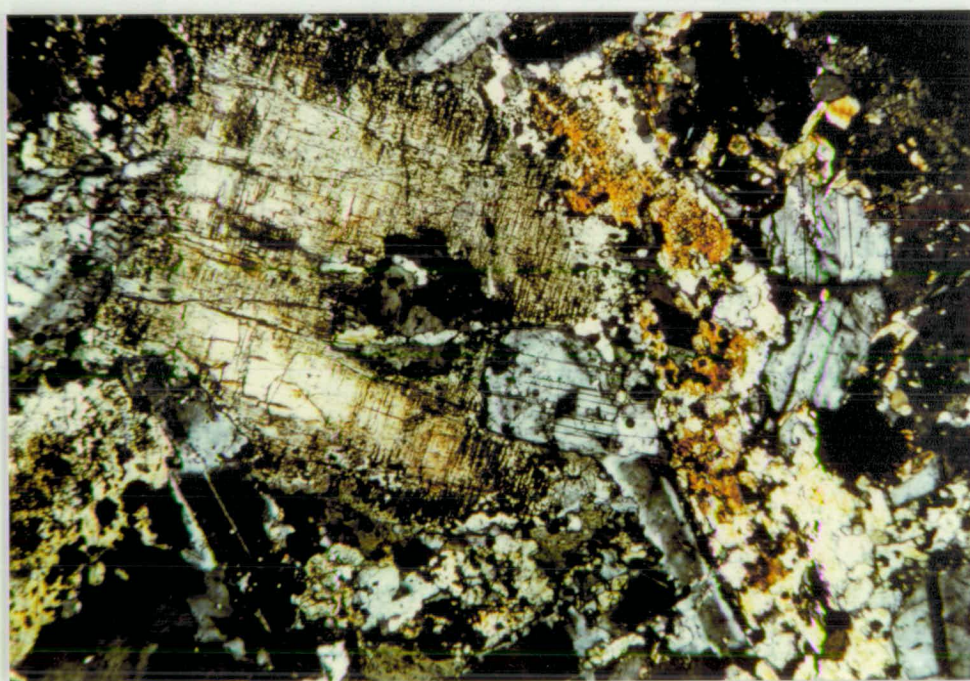
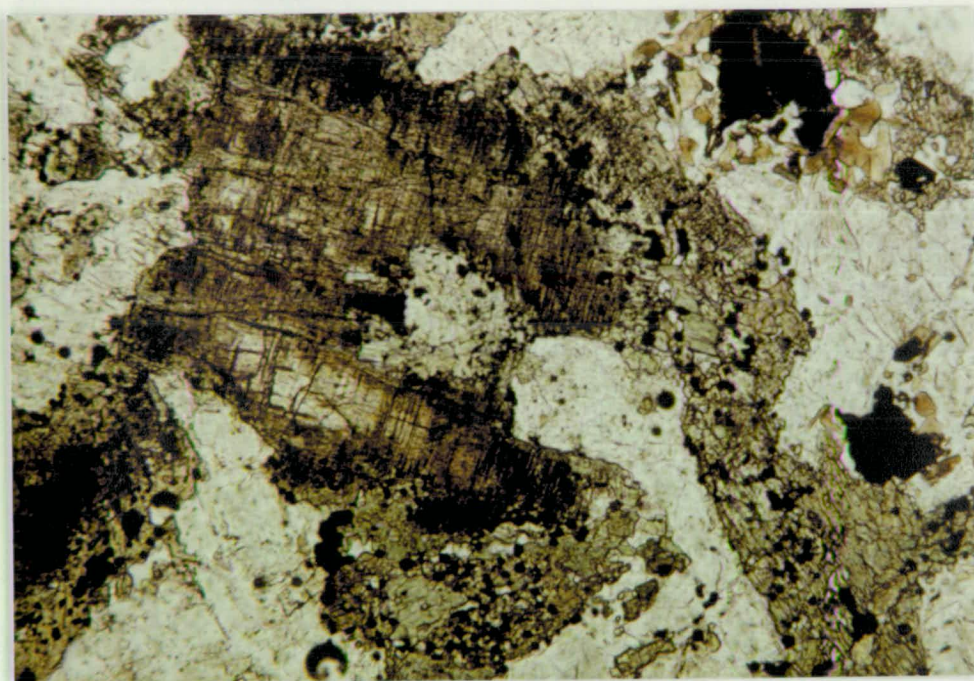


Plate 46 Exsolved pyroxene (70-209) with peripheral dusting of magnetite altered to green hornblende and biotite. Note brown biotite reactions about large magnetite grains. Dolerite plagioclase still intact. x190.

Top - plane polarised light.
Bottom - crossed nicols.

An₂₀-An₃₄ (oligoclase). Some veins of coarser potash feldspar with evidence of exsolution and having sutured borders can intersect the altered dolerite. The total development of feldspar compositions is summarised in Fig. III-23. Some large apatite and sphene crystals may be developed.

The subsequent evolution of the system is mainly due to additional increments of essentially potash feldspar-rich material to, and with consequent dilution of, the material of doleritic origin. Thus there is an addition and dilution process which leads to the leucocratic rocks, regarded by Edwards as contaminated variants of the parent "syenite porphyry", consisting of aplitic and pegmatitic veins intersecting and mixing with the altered dolerite. In the coarser varieties, laths of subhedral sanidine may crystallize with the material derived from the altered dolerite being squeezed between the coarser feldspar crystals giving rise to a schlieren texture.

In the more uniform grainsize rocks the texture is one of interlocking potash feldspar crystals of grainsize near 2 mm and having sutured margins. These crystals invariably have a cloudy alteration, seen best in plane polarized light, which tends to etch potential exsolution zones, not always observable with analysed light. There are variable degrees of mixing with the coarser feldspar grains now often exhibiting ophitic texture by enclosing grains of recrystallised sodium bearing pyroxene. The pyroxene may be euhedral showing laths of tabular form up to 1 mm in length as well as typical basal sections (Pl. 48). Pyroxene grains may also be included within light brown - very dark brown biotite (Pl. 49). The interstices between the pyroxene grains may be filled with iron stained zeolitic material. This material is in fibrous aggregates with first order grey-straw interference and length fast with straight extinction. It is probably thomsonite.

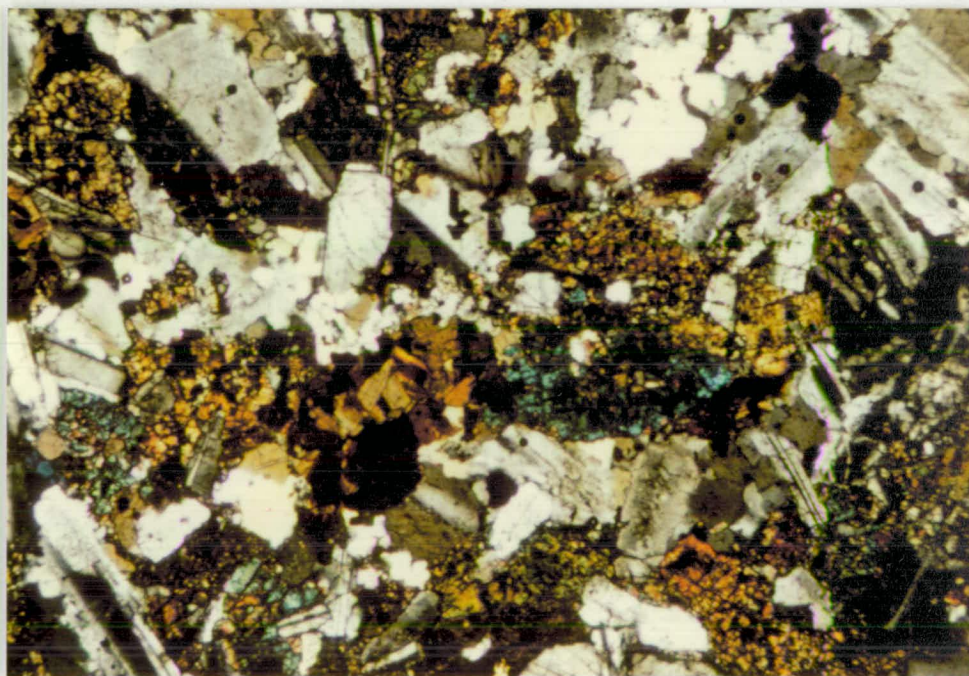
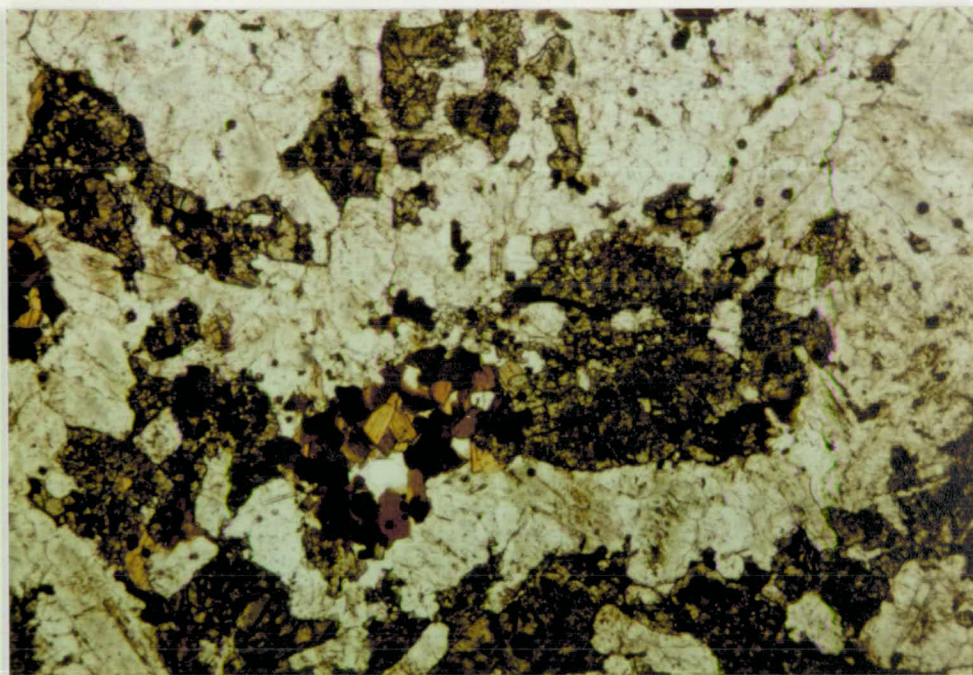


Plate 47 Altered dolerite (RP10). Pyroxene altered. Biotite reaction rim around magnetite. Feldspars beginning to alter with some undulose extinction, formation of clear rims and granular alkali feldspar. x75.

Top - plane polarised light.
Bottom - crossed nicols.

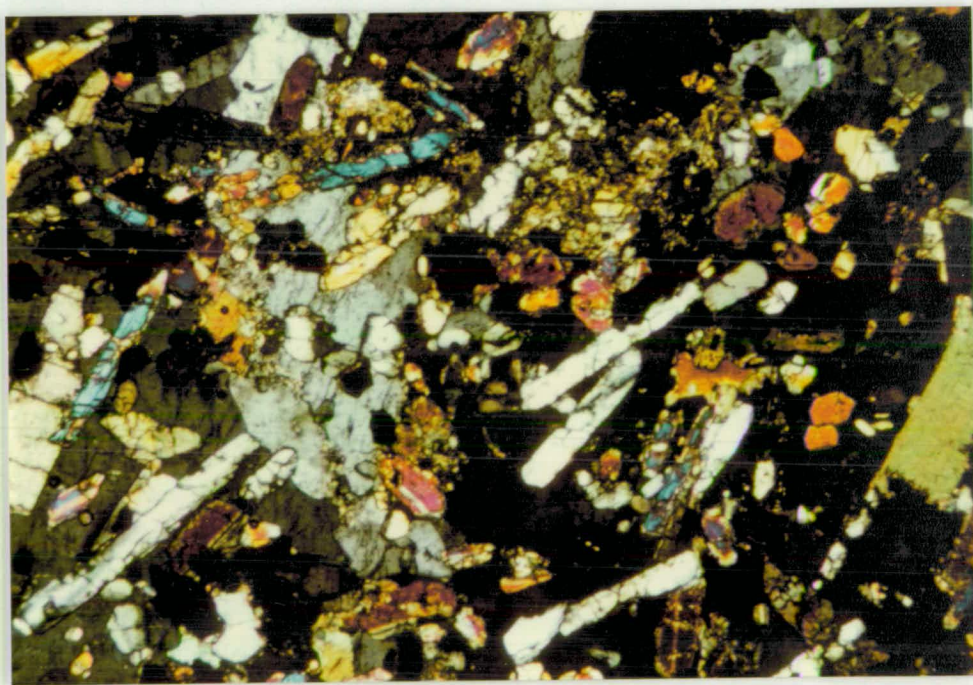
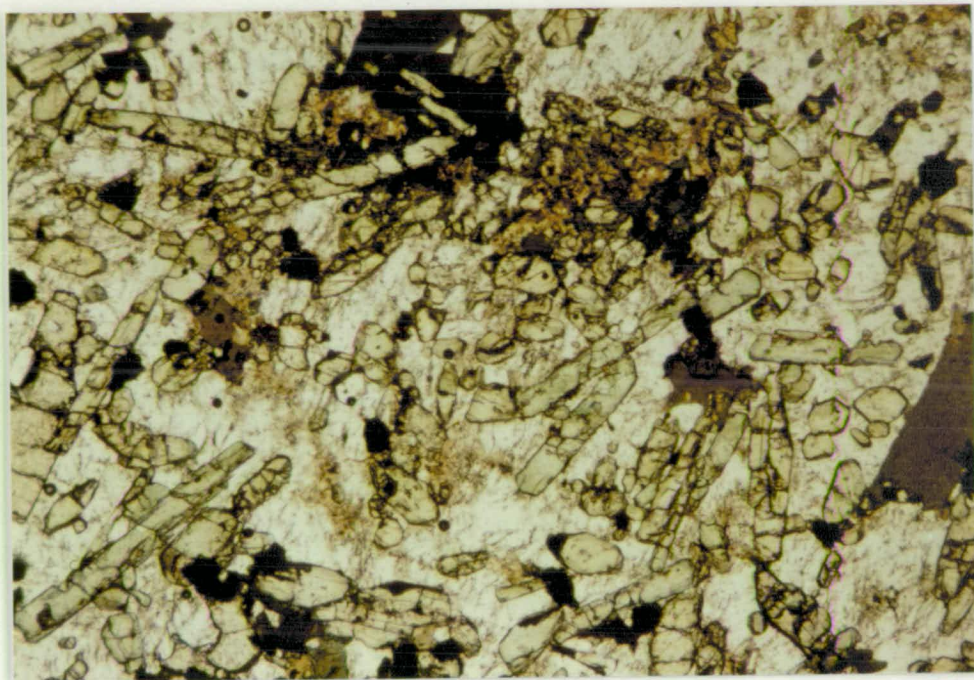


Plate 48 Recrystallised hybrid rock (S6) with pyroxene laths, biotite plates, granular and lath feldspars. x75.

Top - plane polarised light.
Bottom - crossed nicols.

The pyroxene may be mantled by dark green - light brown pleochroic hornblende. Where there is a large amount of hornblende there is zeolite (Pl. 50) present, but the zeolite does not always have the amphibole associated with it. Biotite is usually associated with magnetite grains but may also occur with amphibole and pyroxene. Some large euhedral apatite and anhedral sphene grains can occur in the rock. These well-crystallized granular-textured hornfels-type rocks represent the extreme recrystallization product.

The presence of excess dark minerals leads to the formation of a deeper green coloured pyroxene (CY34, S2). The pyroxenes may still have pale cores, but these are not abundant. Grainsize is up to 5 mm x 2 mm. With an extinction angle of 28°C , the pyroxene is aegirine-augite, and has an electron-probe analysis of 4% Na_2O . The pyroxenes are mainly anhedral laths with rims containing biotite and small grains of melanite (Pl. 51). Included in the rock may be inclusions of subhedral aggregates of lath shaped pale green pyroxenes which may have a rosette arrangement of crystals due to their initial mode of crystallization. These also have a groundmass of interlocking feldspar crystals. Some dark-brown to light-brown biotite is crystallized with the pyroxene but does not appear to have a reaction relationship with it. It may contain small included crystals of melanite.

The groundmass of the hybrid rock consists of an interlocking mass of anhedral grains of sanidine and albite as well as laths of sanidine within which are aggregates of somewhat coarser lath-like subhedral, simply twinned crystals. These latter have very few other minerals in them and suggest a mixing process. The feldspathic groundmass of the hybrid is peppered with a dusting of small melanite dodecahedra, having perfectly developed crystals with 0.05 mm maximum diameter. Occasional euhedral sphene crystals of similar size occur.

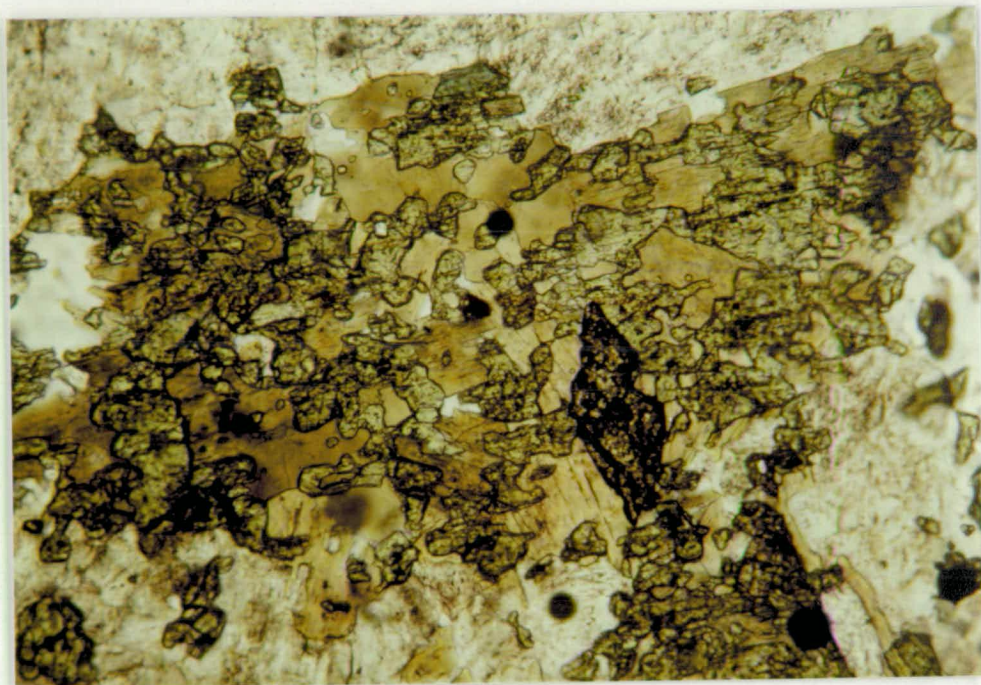


Plate 49 Hybrid rock (70-187) with intergrowing pyroxene and green-brown biotite. Sphene grain near centre and alkali feldspar matrix. Plane polarised light. x75..

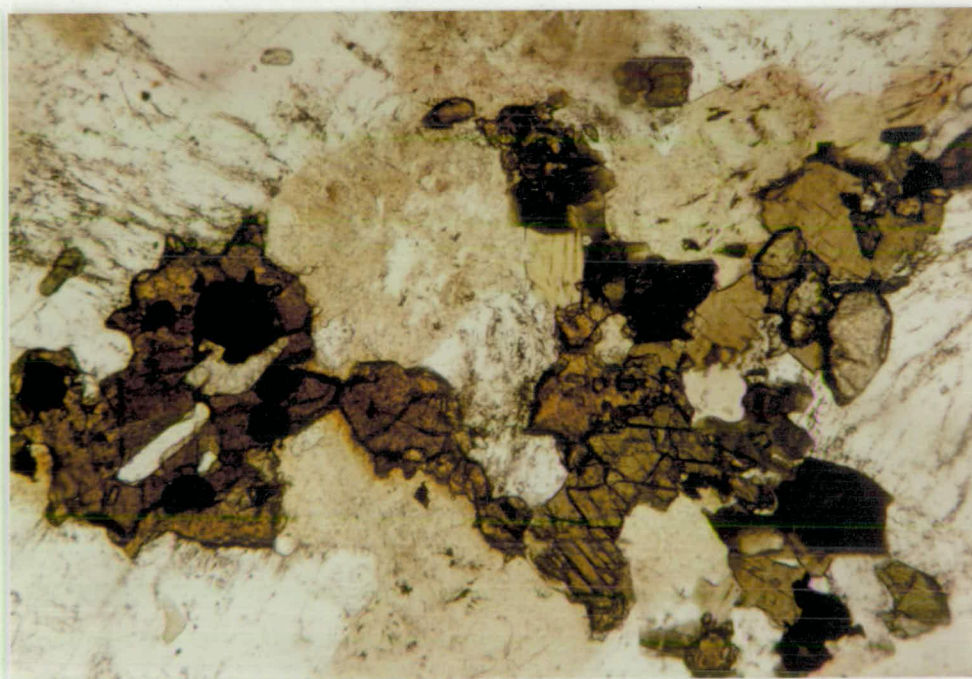


Plate 50 Hybrid rock (RP18). Hornblende (yellow brown), melanite (orange brown), biotite (dark-light brown), zeolite (light brown patchy), sphene (euhedral high relief), light brown), apatite (clear lath), and potash feldspar (clear). Plane polarised light. x190.

Small green-brown biotite plates tend to crystallize about the melanite crystals and also about the pyroxene (Pl. 52). Larger euhedral melanite crystals with diameters of 2 mm occur throughout the rock.

A typical hybrid rock contains coarse sutured-edge potash feldspars. These have a low 2V (30°) and are sanidine in spite of their anhedral form. Their average grainsize is from 2 to 3 mm. Between the grains may be formed irregular aggregates of melanite, hornblende, biotite, sphene and magnetite grains, together with some zeolite. The biotite ranges from very light brown to very dark green-brown pleochroism. It is usually associated with magnetite and hornblende of similar pleochroism. There appears to be a band of biotite between the hornblende and associated melanite, with sphene rods in the melanite. These are all associated with fresh zeolite which is length fast and in fibrous aggregates. The ferromagnesian minerals and associated zeolite occur in interstices between the much coarser sanidine crystal-grain groups.

Melanite has a complex relationship to the green pyroxene. They appear to have crystallized concurrently (Pl. 53). Because of the crystal growing power of the melanite it is difficult to assess if it pseudomorphs original pyroxene as claimed by Edwards (op. cit.). In these rocks melanite garnet appears more frequently than in those more closely allied to the original dolerite.

In some rocks it may be concentrated enough to produce aggregates up to 2 cm maximum dimension. Single euhedral melanite crystals may be up to 5 mm in diameter, with a very dense colouring (suggesting a relatively high titania content, if due to $\text{Fe}^{3+} + \text{Ti}^{3+} \rightleftharpoons \text{Fe}^{2+} + \text{Ti}^{4+}$), although probe analysis does not indicate this. Colour zoning is present and the most frequent inclusions are sphene and occasional apatite. In most cases the melanite is associated with dark green and

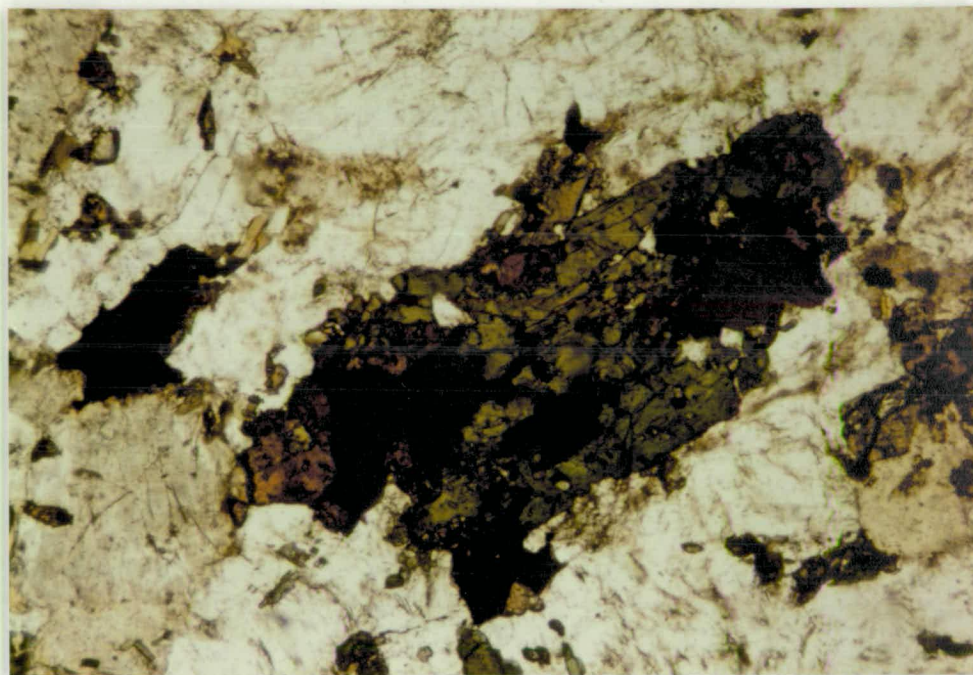


Plate 51 Hybrid rock (RP6). Anhedral green pyroxene with grains of melanite and dark green biotite included. Matrix is alkali feldspar (clear) and nepheline (cloudy). Plane polarised light. x75.

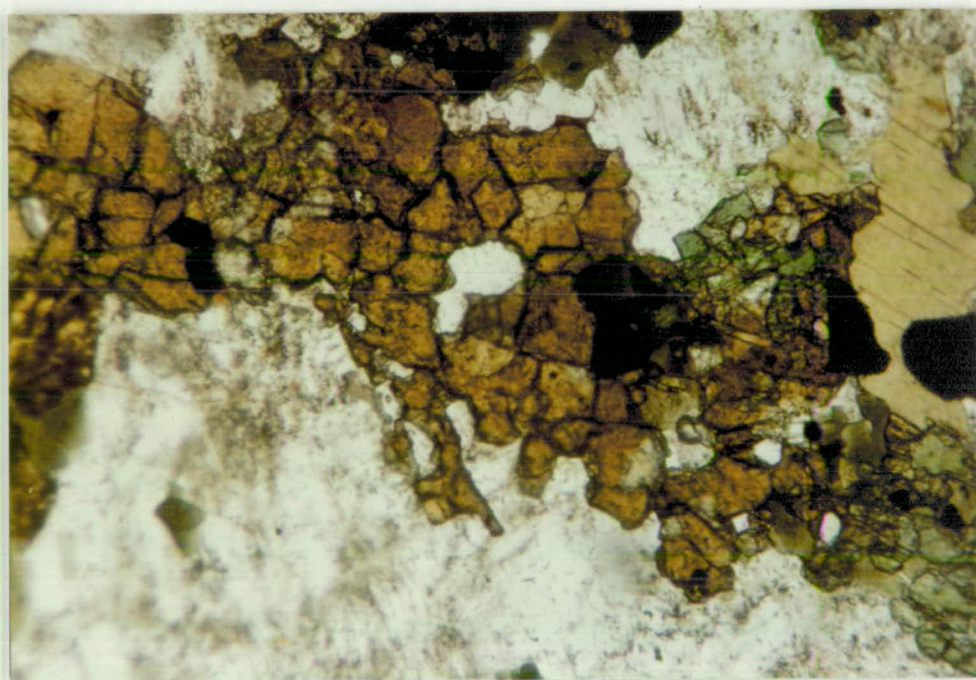


Plate 52 Hybrid rock (RP18). Brown biotite, dark green biotite, light green pyroxene, melanite (dark brown), magnetite (black) in matrix of clear alkali feldspar. Plane polarised light. x190.

light green pyroxene and biotite. Those rocks with the largest melanite crystals usually have the largest grainsize feldspars in their matrix.

Co-crystallized with the sanidine in CY29 is nepheline. Superficially and texturally the mineral may be confused with sanidine because it develops rectangular forms similar to sanidine which may also be uniaxial negative. The basal sections have hexagonal symmetry emphasised by zoning due to minute inclusions (Pl. 54). The normal rectangular sections which have a maximum dimension of about 1 mm also contain numerous small inclusions. The nepheline may contain small inclusions many of which are small melanite crystals and green pyroxenes, usually aegirine-augite. The rock may contain up to 20% nepheline. In less fresh specimens the mineral is very cloudy and gives a poor interference figure - probably due to the inclusions, however these together with the basal sections are distinctive. Probe analyses of the nepheline (Table III-1) are invariably slightly non-stoichiometric, which is a characteristic feature of stuffed derivatives of the tridymite structure. Repeated analyses show no alkali loss. Some nepheline is altered to irregular patches of fibrous zeolite. It could well be that the zeolite of the pyroxene rocks may represent original nepheline as this also tends to have sub-rectangular form.

Irregular grains of sphene and euhedral apatite may also be present. This rock is probably the ijolite of Twelvetrees and Petterd (1898).

Leucocratic Rocks

The leucocratic rocks are composed of potash feldspar with a variety of grainsizes. They can range in composition from almost pure potash feldspar rocks to those in which there is a significant proportion of pyroxene and to a lesser extent, biotite and melanite.

In the field the contact relations of the leucocratic rocks are very complicated with both fine and coarse grained veins intersecting each other. The fine grained rocks generally form the smaller veins while the coarser pegmatitic phases are fissure fillings with crystals growing off the walls. Pegmatite dykes up to 30 cm in width occur in the area, but in these there is no obvious growth of crystals from the dyke wall.

Feldspar Rocks

These rocks may be classified following Streckeisen (1976) as syenite pegmatite and syenite aplites according to grain size, with prefixes if any other characteristic minerals are present. The finest grained veins are composed of close-packed granules of potash feldspar approximately 0.1 mm in diameter, in a granuloblastic mosaic. These are untwinned, unexsolved and show little surface alteration and permeate the Regatta Point area.

Coarser grained aplites occur and are of two types: potash feldspar aplites and potash feldspar-plagioclase aplites. The potash feldspar aplites consist of anhedral grains having diameters of approximately 1 mm. These are close packed with strongly sutured edges. In some of these, surface alteration suggests exsolution lamellae but these are not obvious with crossed nicols. Other examples show feldspars with clear cores and exsolved borders (Pl. 55). Some specimens show completely perthitic feldspars and these are perhaps correctly classified as perthosites. In these rocks there is also about 10% quartz present.

Other aplites have textures which can be described as mixtures of the above types, thus there are aplites with a type of glomeroporphyritic texture with aggregates of larger feldspars with sutured margins, in a groundmass of the finer interlocking granular material.

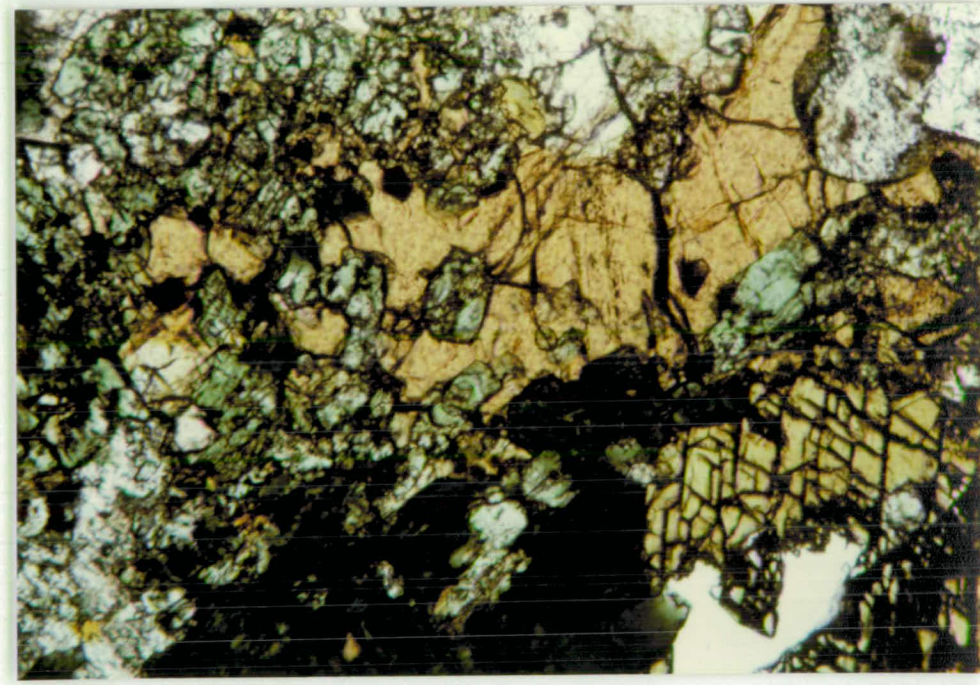


Plate 53 Hybrid rock (70-221). Melanite (brown), pyroxene (light green), biotite (dark green), hornblende (yellow), and feldspar (clear). Plane polarised light. x75.

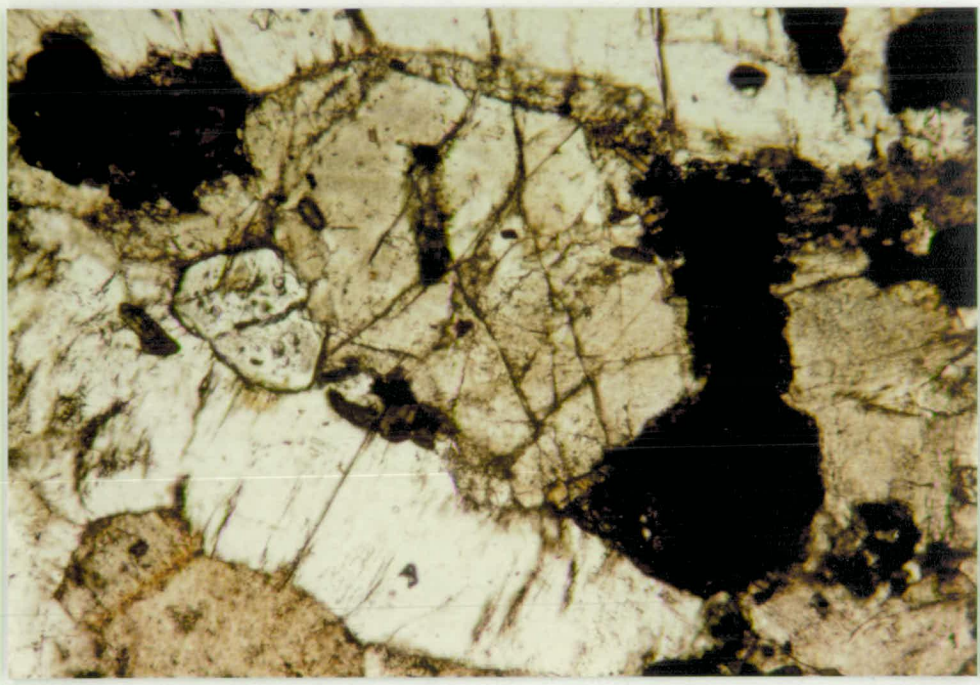


Plate 54 Hybrid rock (CY29). Melanite (black), nepheline (cloudy large hexagonal crystal with alteration), apatite (small clear hexagonal crystal), and clear potash feldspars (subhedral laths). Plane polarised light. x190.

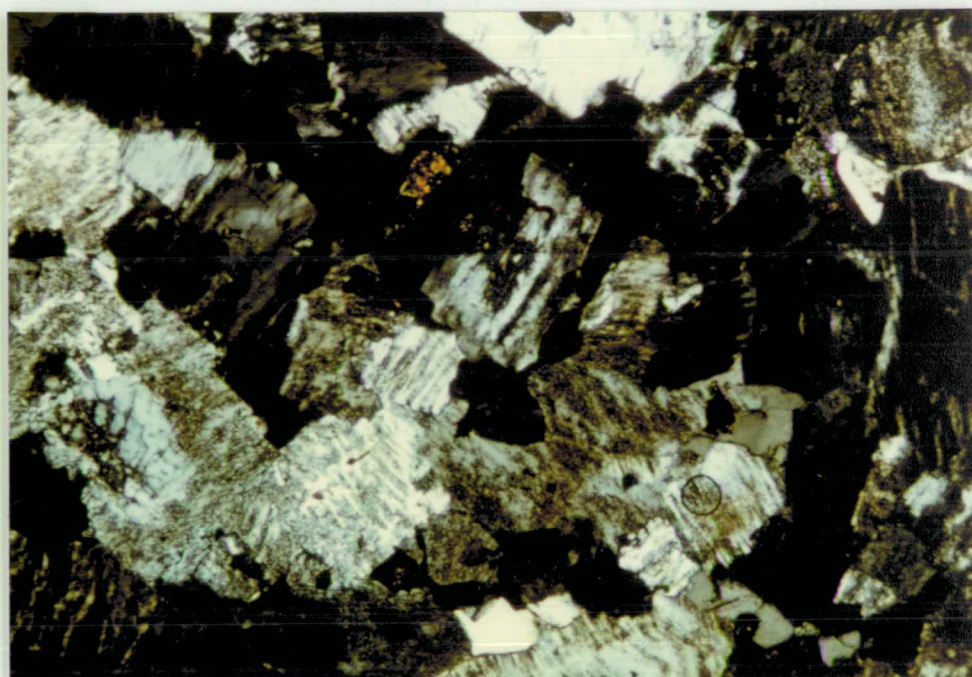


Plate 55 Syenite aplite (71-311) with exsolved alkali feldspars and some clear cores. Crossed nicols. x75.

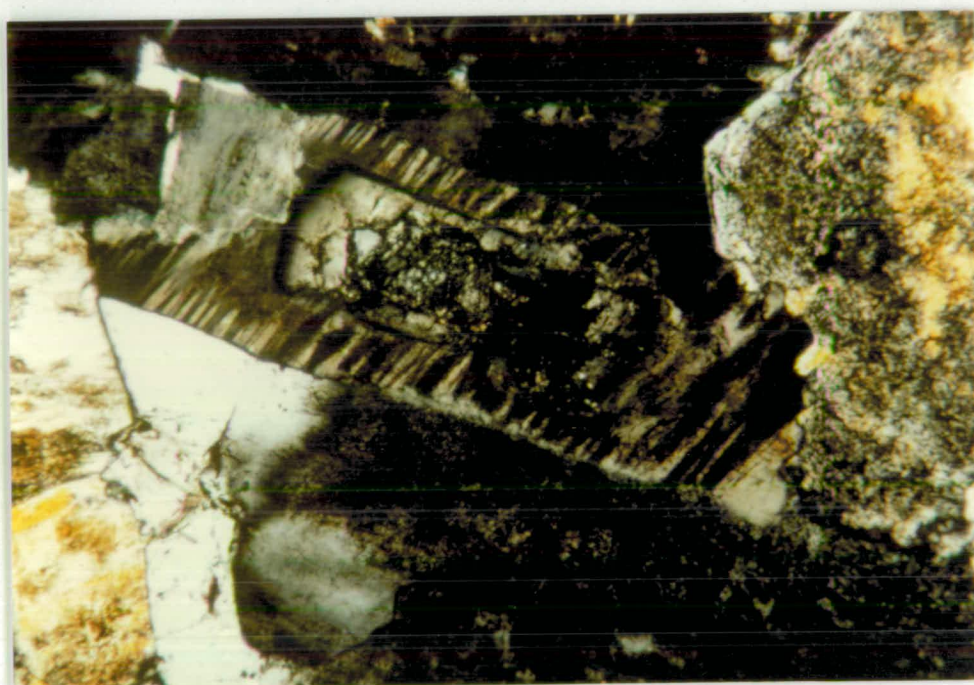


Plate 56 Syenite aplite, Regatta Point, with exsolved potash feldspar overgrowth on plagioclase core crystal. Crossed nicols, x75.

These are mainly sanidine but albite grains also are present. Some of the grains in these rocks have a tendency to form rectangular subhedral crystals seen as its most extreme in the syenite pegmatites.

The plagioclase-bearing aplites occur as two dyke-like intrusions outcropping near the centre of the Regatta Point area. These are the rocks originally described by Twelvetrees and Petterd (1898) as the alkaline members of a differentiation sequence. It is interesting to note that the texture of these aplites is very similar to the groundmass textures of the syenite porphyry occurring elsewhere in the area. These aplites contain subhedral tabular sanidine crystals with fresh rims and altered cores, making up about 70% of the rock. Oligoclase crystals also occur constituting about 20% of the rock and may have potash feldspar overgrowths (Pl. 56). There is also about 5% of quartz in the rock. The grainsize averages 1 mm. Within the rock are occasional small clots (5 cm x 1 cm) of green pyroxene (often colour zoned with clear cores) and magnetite grains. Small subhedral to euhedral pale green pyroxene grains (0.5 mm) are scattered through the rock together with occasional melanite and brown to dark green amphibole grains.

The grainsize of the aplites is usually about a few millimetres but the coarsest phases contain tabular potash feldspar crystals up to 2.5 cm x 0.5 cm. It is impossible to collect completely fresh specimens of this rock. These are euhedral to subhedral with complete terminations absent, when viewed with the microscope. The crystals show no overall preferred arrangement, but groups of them have grown parallel. The feldspars are sanidines with 2V ranging from 0° to about 30° with some alteration. Because of their overall lack of orientation groups of crystals tend to abut each other perpendicularly, in bundles. Optically there is a slight disorientation hence there is probably

some degree of micro-exsolution present. The groundmass makes up less than 10% of the rock, and in most cases is now heavily sericitized, with the crystallization of some larger muscovite laths. The best resolved parts of the groundmass contain the remains of magnetite grains and biotite plates. Some small melanites occur in the sanidine. The groundmass is quite subordinate so that the rocks do not have a porphyritic texture. These are the rocks named garnet orthoclasite by Edwards (1947) (Pl. 57).

SUMMARY OF HYBRID ROCKS

The hybrid rocks have formed by potassium metasomatism associated with thermal metamorphism of dolerite by a potassic alkaline magma. Two groups of rocks may be recognized in the resulting assemblage. The first group consists of melanocratic (dark) rocks which have been derived largely from dolerite minerals by reaction with potash to form biotite from magnetite and augite. Addition of water also produced hornblende. Breakdown of plagioclase and original pyroxene also formed melanite garnet and sphene from ilmenite as well as a new generation of pyroxenes. Soda from the plagioclase formed albite and nepheline with further addition of water producing zeolite. Potash feldspar also crystallized producing a granular hornfelsic rock which could also have sanidine laths present.

The second group consists of leucocratic (light) rocks whose dominant component is potash feldspar, occasionally with oligoclase as well as varying amounts of pyroxene, biotite and melanite. The feldspar rocks occur as fine to coarse grained aplites intruded as veins in the melanocratic rocks and associated with two larger alkaline dykes through Regatta Point. Many of the potash feldspars are perthitic and

occur as overgrowths on core plagioclase crystals. In some dykes larger tablets of sanidine with little groundmass have formed the sanidine rich rocks originally described as orthoclasites by Edwards (1947).

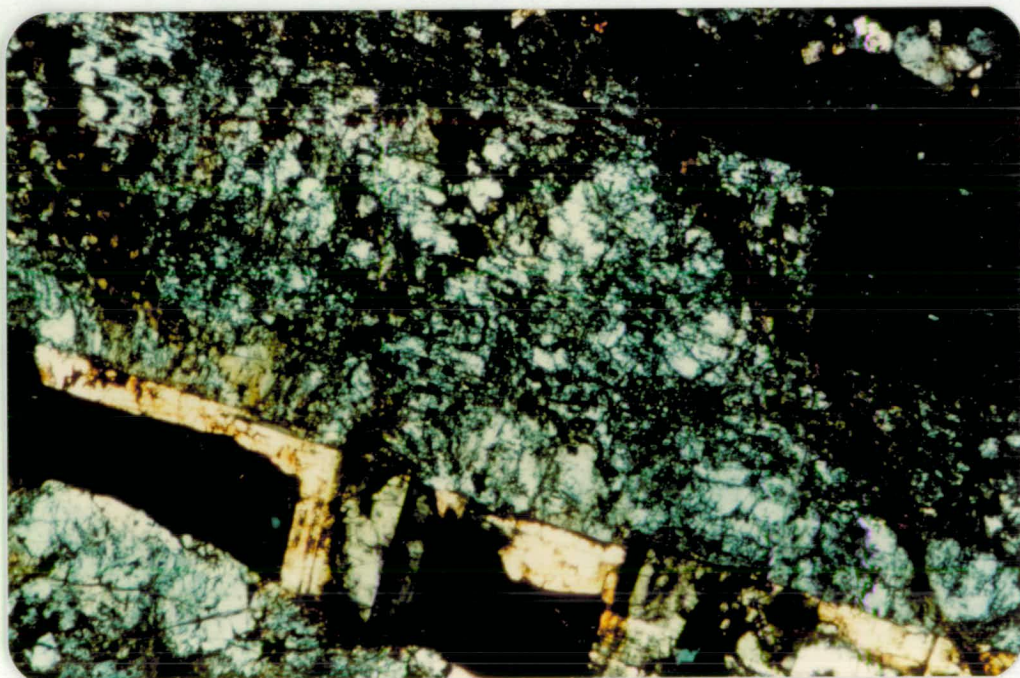


Plate 57 Garnet orthoclasite (CY31), x75. Crossed nicols. Sanidine crystals with melanite (black) and interstitial oligoclase (yellow).

CHAPTER III

MINERALOGY

The mineralogy of the rocks reflects the conditions under which formation occurred with respect to the physical and chemical parameters existing at that time. One important parameter is the temperature of formation of the rocks. Mineralogical geothermometers which could be applicable to the Port Cygnet rocks are: nepheline, nepheline-feldspar, sanidine-biotite-magnetite and plagioclase-alkali feldspar. The first three geothermometers may apply to the hybrid rocks while the plagioclase-alkali feldspar method might be applicable to the coarser grained alkaline rocks.

THE NEPHELINE GEOTHERMOMETER

Nepheline occurs in the hybrid rocks and also in the groundmass of the tinguaitite dykes, e.g. CY85. Nepheline may be used in two modes as a geothermometer; using the presence of excess silica and the kalsilite mole-fraction which is the development of the method of Hamilton (1961) and Hamilton and McKenzie (1965), and also using the distribution of soda between co-existing alkali feldspar and nepheline. The theoretical basis and outline of the latter method has been given by Perchuk and Ryabchikov (1968) and subsequently modified by Powell and Powell (1977).

Nepheline belongs to a group referred to as stuffed silica structures in which the mode of linking of the tetrahedra in one of the high temperature forms of silica (in this case β -tridymite) is retained, but some silicon is replaced by aluminium and cations (alkali or alkaline earth ions) are accommodated in the interstices to maintain electrical neutrality. The interstices in the β -tridymite structure

are big enough to accept larger ions (e.g. potassium) which is a typical constituent of nepheline. Thus while electrostatic neutrality is maintained, atomic proportions may vary considerably from the simple ratios expressed in the basic formula $\text{NaAlSi}_3\text{O}_8$, and such variations cause non-stoichiometry with respect to these.

The excess silica diagram (Fig. III-1), following the method of Hamilton (1961) has been constructed using weight percent of the K-Na equivalent molecules and determining the excess of silica over these. Because of the low amount of calcium present; the observation by Gupta and Edgar (1974) that there is no preferential acceptance of calcium or potassium into the nepheline structure; and that it probably has a negligible thermodynamic effect (Grover 1977), calcium has been included with sodium in the calculation of silica excess. Repeated probe analysis has indicated no appreciable alkali loss due to interaction with the electron beam.

In the hybrid rocks, nepheline and potash feldspar have crystallized together in an apparently equilibrium coarse grained hornfels texture. Assuming that these minerals have formed an equilibrium assemblage then the Perchuk and Ryabchikov geothermometer might be applicable. As there is no evidence of exsolution in the feldspars crystallizing with the nepheline it can be assumed that whatever the original structural state might have been, there has been no physical or chemical redistribution and the original would have been at least a relatively high temperature polymorph.

The data for nephelines from the Pt. Cygnet hybrids zone, in particular CY29, are given in Table III-1. These are plotted on the excess silica diagram of Hamilton (Fig. III-1) where it can be seen that the data group well about the 775°C isotherm. If calcium is subtracted from the analyses and the data recalculated for Na and K molecules only,

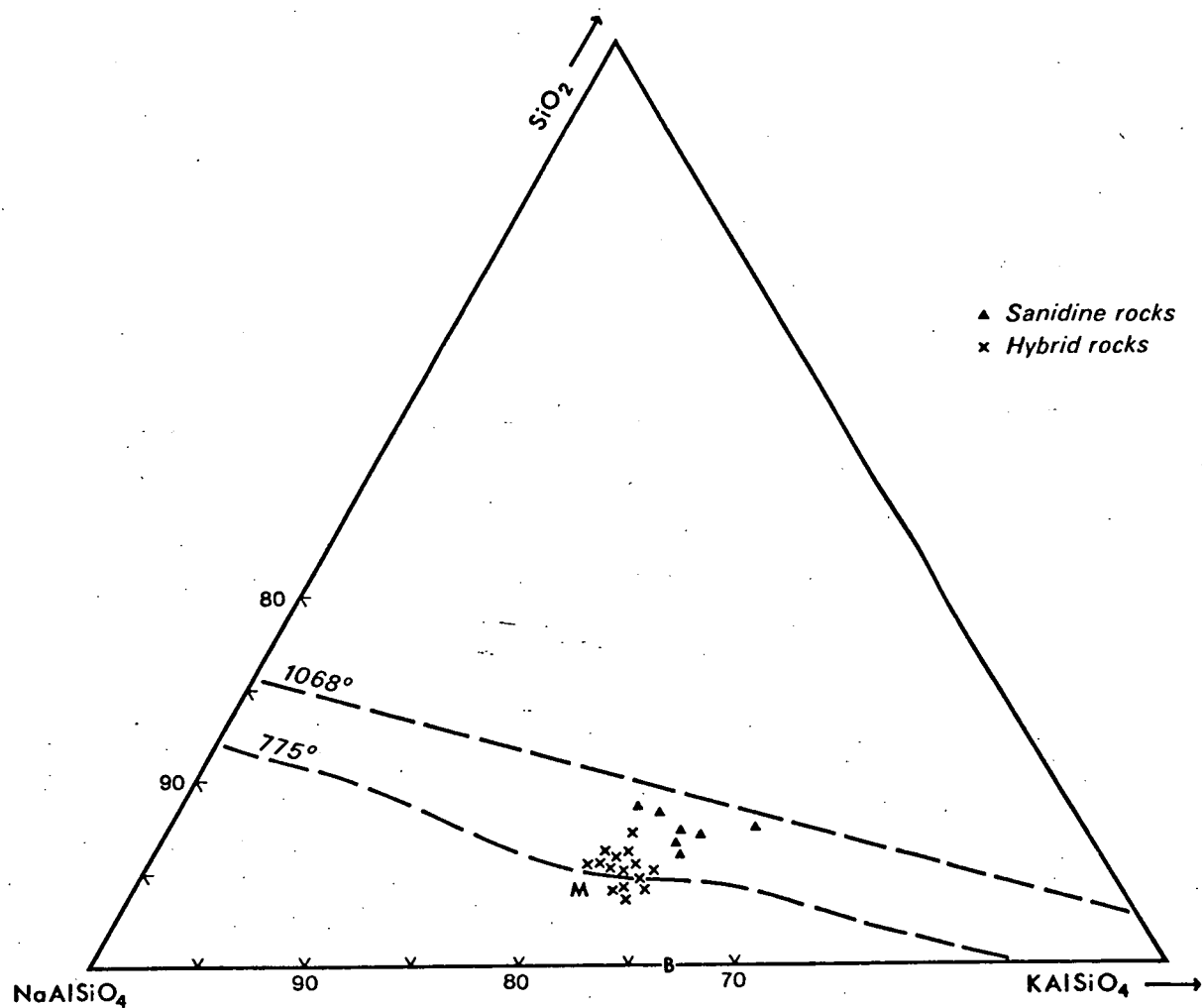


Figure III-1 Plot of excess silica in nepheline geothermometer after Hamilton (1961). M is the Morozeuricz nepheline composition of Tilley (1958); B is the Buerger composition for nepheline from Buerger (1954). Molecules plotted as wt. percent.

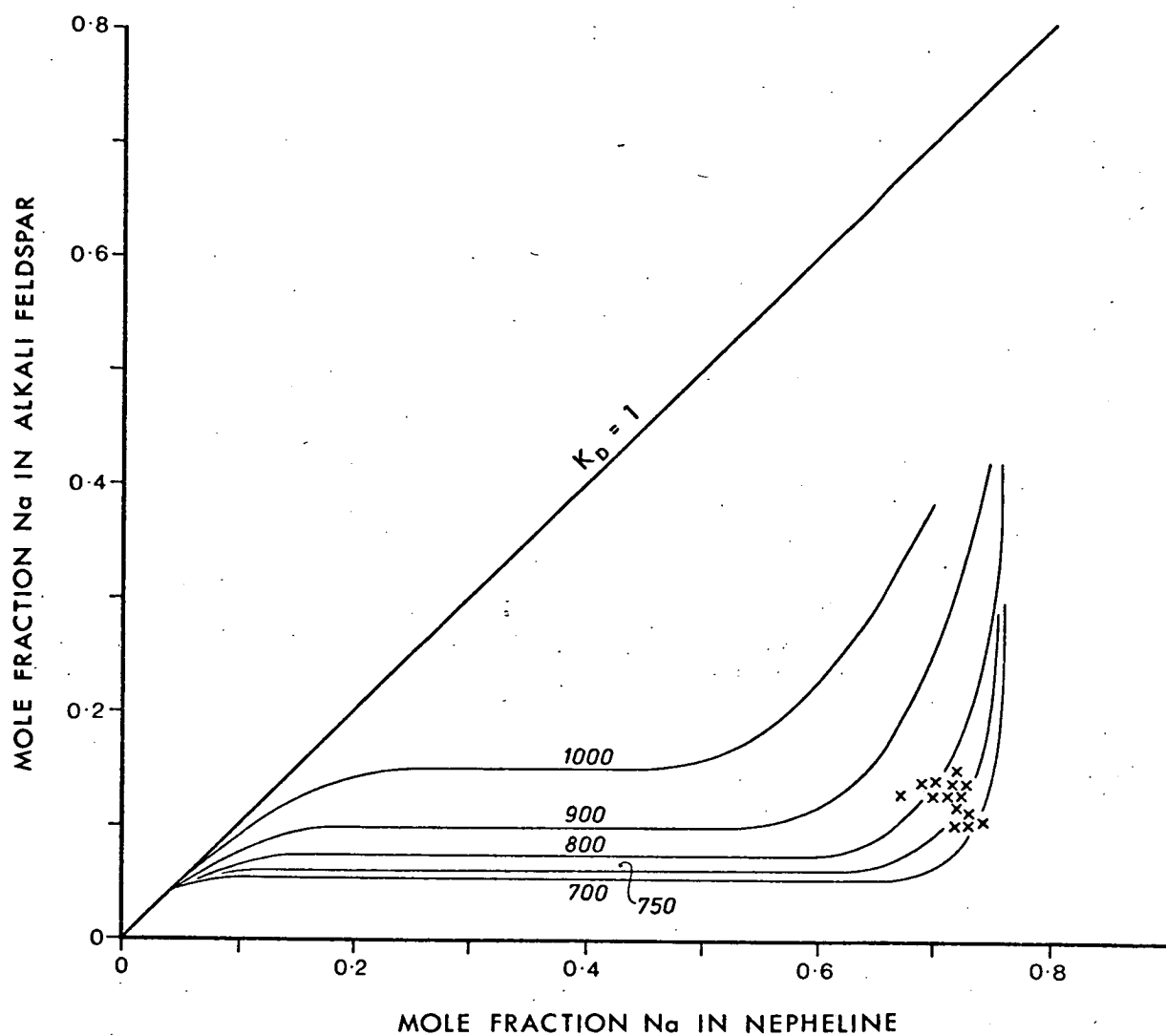


Figure III-2 Perchuk and Ryabchikov (1968) plot for distribution of sodium between co-existing nepheline and alkali feldspar of hybrid rocks. This plot is for the randomised structure model.

the apparent temperature falls to approximately 500°C and the compositions fall into the field between the Morozewicz and Buerger compositions which Hamilton (op. cit.) regarded as unreliable.

The data for the nepheline in the groundmass of the tinguaitite dyke are somewhat more scattered and more difficult to obtain because of the intimate intergrowth with potash feldspar and aegirine. The excess silica in these minerals is greater than in the hybrid rocks and would suggest a temperature greater than that of the hybrid rocks, possibly as high as 900°C, but with a relatively wide scatter due to the close isotherms in this part of the diagram.

If the method of Perchuk and Ryabchikov (1968) is applied, the mole fractions of soda in co-existing nephelines and potash feldspar are plotted. In this case it is assumed that the distribution of the alkali metal atoms in the nepheline is statistically random. These data are plotted in Figure III-2 for the hybrid rock nephelines and co-existing potash feldspars, where it can be seen the results group consistently between the 700°C and 800°C isotherms with 50% of the points between 750°C and 800°C in good agreement with the Hamilton method. Perchuk and Ryabchikov (1968) offered an alternative solution that assumed the mixing is not totally random, with sodium and potassium randomly distributed over one quarter of the cation positions. Using this proposition, the temperature of crystallization falls to less than 600°C. These results are plotted in Figure III-3. The determinative curves do not have good resolution in this area with most values less than 700°C and some as low as 500°C. Since there is an inconsistent result here, perhaps it is due to the mixing mode adopted. Possibly for these minerals the random site distribution model may apply. In the case of the tinguaitite it was found that the potash feldspar had very low to absent soda and apparently not in equilibrium with the groundmass nepheline, and Perchuk and Ryabchikov model could not be used.

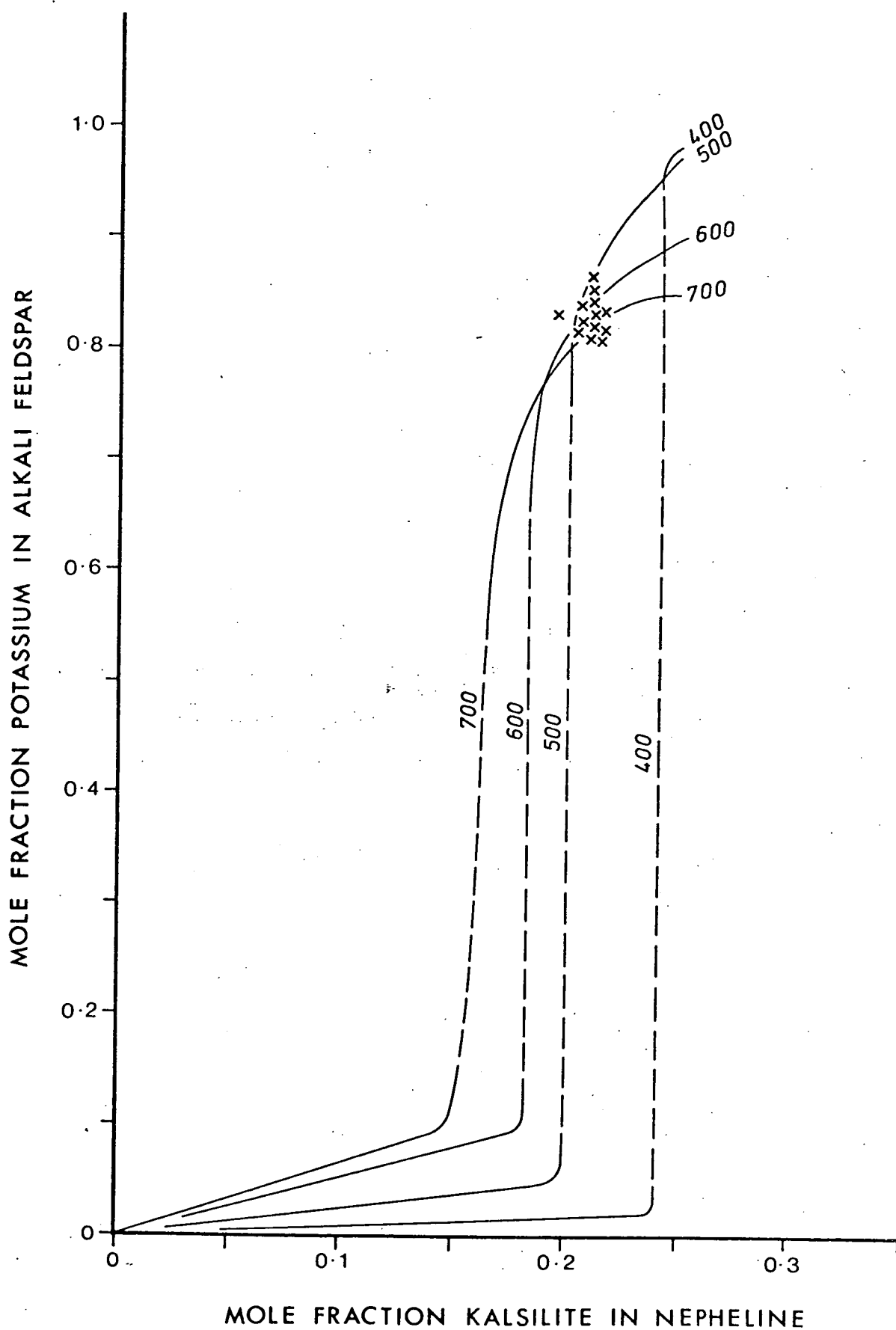


Figure III-3 Perchuk and Ryabchikov (1968) plot of distribution of K between co-existing nepheline and alkali feldspar for their ordered case.

TABLE III-1

Nepheline Geothermometer

Data for nephelines and co-existing alkali feldspars

Hybrid Rock CY29

Nepheline

	1	2	3	4	5	6	7	8	9	10	11	12	13	14	15
SiO ₂	43.72	44.49	44.01	44.13	44.57	44.22	45.41	44.76	44.60	43.96	44.18	43.79	43.40	43.59	43.54
Al ₂ O ₃	34.44	34.59	34.38	34.34	34.13	34.57	34.75	33.85	34.29	34.24	34.16	34.21	34.81	34.71	34.56
Na ₂ O	13.40	13.01	13.38	12.69	13.57	11.73	11.46	13.54	12.59	13.46	13.66	13.46	13.01	13.25	13.63
K ₂ O	6.52	6.36	6.33	6.00	6.07	5.17	5.31	6.04	5.66	6.33	6.13	6.34	6.25	6.15	6.24
CaO	1.41	1.56	1.56	2.60	1.43	4.00	2.78	1.44	2.61	1.58	1.49	1.63	2.18	1.95	1.66
FeO	0.51	0.00	0.33	0.24	0.23	0.31	0.30	0.36	0.26	0.43	0.39	0.56	0.36	0.36	0.37
Total	100.00	100.01	99.99	100.00	100.00	100.00	100.01	99.99	100.01	99.99	100.01	99.93	100.01	100.01	100.00

Atomic proportion on basis of 4 oxygen

Si	1.045	1.056	1.049	1.050	1.060	1.048	1.069	1.064	1.058	1.049	1.053	1.047	1.036	1.040	1.040
Al	0.970	0.968	0.966	0.963	0.957	0.966	0.964	0.949	0.959	0.963	0.960	0.964	0.980	0.976	0.973
Site Total	2.015	2.024	2.015	2.013	2.017	2.014	2.033	2.013	2.017	2.012	2.013	2.011	2.016	2.016	2.013
Na	0.621	0.599	0.619	0.585	0.625	0.539	0.523	0.624	0.579	0.623	0.631	0.624	0.602	0.613	0.631
K	0.199	0.193	0.193	0.182	0.184	0.156	0.159	0.183	0.170	0.193	0.186	0.194	0.190	0.187	0.190
Ca	0.036	0.040	0.040	0.066	0.036	0.102	0.070	0.037	0.055	0.040	0.038	0.042	0.055	0.050	0.043
Fe	0.010	0.000	0.007	0.005	0.005	0.006	0.006	0.007	0.005	0.009	0.008	0.012	0.007	0.007	0.008
Site Total	0.866	0.832	0.859	0.838	0.850	0.797	0.758	0.851	0.809	0.865	0.863	0.872	0.854	0.857	0.872

Co-existing alkali feldspar

SiO ₂	65.19	65.50	65.52	65.43	65.00	65.19	65.47	65.20	65.30	65.28	65.34	65.00	65.57	65.01	64.8
Al ₂ O ₃	18.47	17.99	18.00	18.12	18.19	18.03	17.88	17.94	18.24	18.05	18.10	18.11	18.18	18.09	18.39
Na ₂ O	1.74	1.52	1.37	1.53	1.11	1.52	1.56	1.22	1.41	1.62	1.46	1.60	1.51	1.47	1.63
K ₂ O	13.82	14.10	14.27	14.08	14.79	14.38	14.23	14.77	14.31	14.18	14.28	14.22	14.17	14.36	14.19

TABLE III-1 (continued)

CaO	0.78	0.89	0.84	0.83	0.90	0.87	0.87	0.86	0.74	0.87	0.83	0.95	0.92	0.91	0.99
BaO	0.00	0.00	0.00	0.00	0.00	0.00	0.00	0.00	0.00	0.00	0.00	0.00	0.00	0.00	0.00
Total	100.00	100.00	100.00	99.99	99.99	99.99	100.01	99.99	100.00	100.00	100.01	99.88	100.34	99.84	100.00

Atomic proportions on basis of 16 oxygen

Si	5.982	6.015	6.018	6.008	5.989	6.000	6.018	6.007	6.000	6.002	6.005	5.989	5.993	5.993	5.965
Al	1.998	1.948	1.949	1.961	1.976	1.956	1.938	1.948	1.975	1.956	1.960	1.967	1.971	1.965	1.995
Site Total	7.980	7.963	7.967	7.969	7.961	7.956	7.956	7.955	7.975	7.958	7.965	7.956	7.964	7.958	7.960
Na	0.310	0.271	0.245	0.273	0.199	0.272	0.277	0.219	0.252	0.289	0.261	0.286	0.270	0.263	0.291
K	1.617	1.652	1.672	1.649	1.739	1.688	1.668	1.737	1.677	1.663	1.674	1.672	1.662	1.689	1.667
Ca	0.076	0.087	0.083	0.082	0.089	0.086	0.085	0.085	0.073	0.087	0.081	0.094	0.091	0.090	0.097
Ba	0.000	0.000	0.000	0.000	0.000	0.000	0.000	0.000	0.000	0.000	0.000	0.000	0.000	0.000	0.000
Site Total	2.003	2.010	2.000	2.004	2.027	2.046	2.030	2.041	2.002	2.039	2.016	2.023	2.042	2.042	2.055

Tinguaite CY85

Nepheline

SiO ₂	44.36	44.98	44.02	44.89	44.71	45.46	44.09	43.62	45.81
Al ₂ O ₃	31.26	31.85	31.86	31.26	32.33	31.82	32.78	32.90	32.33
Na ₂ O	13.68	13.95	13.37	12.86	12.91	14.01	13.36	13.52	13.32
K ₂ O	7.26	6.85	7.33	7.76	8.08	6.54	7.20	7.26	6.35
CaO	0.68	0.32	0.65	0.82	0.45	0.32	0.39	0.41	0.33
FeO	2.77	2.04	2.66	2.40	1.53	1.85	2.18	2.29	1.86
Total	100.01	99.99	99.89	99.99	100.01	100.00	100.00	100.00	100.00

Atomic proportion on basis of 4 oxygen

Si	1.076	1.083	1.070	1.086	1.078	0.090	1.063	1.055	1.093
Al	0.894	0.984	0.911	0.892	0.918	0.849	0.931	0.937	0.909
Site Total	1.970	2.067	1.981	1.978	1.996	1.939	1.994	1.992	2.002

TABLE III-1 (continued)

Na	0.643	0.651	0.629	0.604	0.603	0.652	0.625	0.634	0.605
K	0.225	0.210	0.227	0.240	0.249	0.200	0.221	0.224	0.209
Ca	0.018	0.009	0.017	0.021	0.012	0.008	0.018	0.021	0.025
Fe	0.006	0.041	0.054	0.049	0.031	0.037	0.089	0.093	0.095
Site Total	0.892	0.911	0.927	0.914	0.895	0.897	0.953	0.972	0.934

Co-existing alkaline felspar

SiO ₂	64.27	64.10	61.67	64.09	64.55	62.29	63.99
Al ₂ O ₃	17.55	17.43	21.15	17.81	17.17	19.41	17.81
Na ₂ O	0.00	0.26	0.00	0.35	0.45	0.61	0.41
K ₂ O	16.72	15.98	15.72	16.25	15.73	14.06	16.60
CaO	0.96	1.11	1.02	1.00	1.01	0.77	0.90
BaO	0.00	0.00	0.00	0.60	0.00	2.86	0.00
FeO	0.50	1.11	0.44	0.51	1.10	0.00	0.29
Total	100.00	99.99	100.00	100.61	100.01	100.00	100.00

Atomic proportion on basis of 16 oxygen

Si	5.990	5.977	5.729	5.966	6.007	5.741	5.964
Al	1.928	1.915	2.316	1.955	1.884	2.108	1.956
Site Total	7.918	7.892	8.045	7.921	7.891	7.849	7.920
Na	0.000	0.047	0.000	0.062	0.081	0.110	0.075
K	1.987	1.901	1.863	1.931	1.867	1.653	1.973
Ca	0.096	0.111	0.102	0.099	0.101	0.076	0.090
Ba	0.000	0.000	0.000	0.000	0.000	0.198	0.000
Fe	0.039	0.087	0.034	0.039	0.085	0.00	0.023
Site Total	2.122	2.146	1.999	2.131	2.134	2.037	2.161

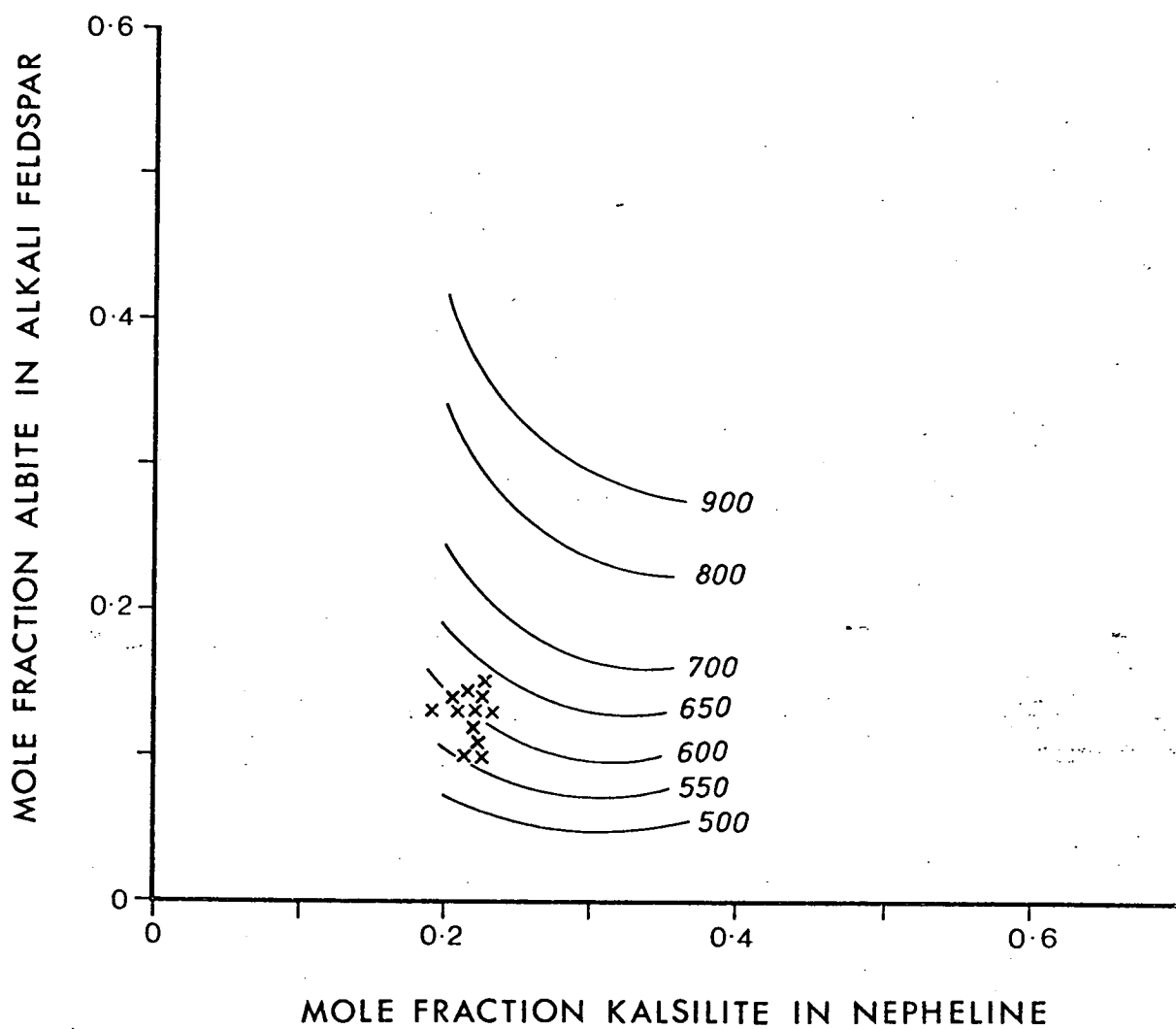


Figure III-4 Powell and Powell (1977) geothermometer for co-existing nepheline and alkali feldspar.

Powell and Powell (1977) proposed a nepheline geothermometer which differed from the Perchuk and Ryabchikov model in that two distinct sites were allocated to the sodium and potassium atoms and allowance was made for the presence of excess silica. Once again, nephelines from the tinguaita dyke do not give sensible results. For the hybrid rocks, the Powell and Powell method gives a result from about 550°C to 625°C (Figure III-4). This is a narrower range than the Perchuk and Ryabchikov ordered model. The Powell and Powell (1977) thermometer gives lower temperatures rather than higher temperatures as indicated by Powell and Powell (1977) in their paper.

THE TWO FELDSPAR GEOTHERMOMETER

Stormer (1975) developed a two-feldspar geothermometer using modern thermodynamic data based on the original model of Barth (1934) and subsequent modifications (Barth 1951, 1956, 1962). The thermometer is based on the equilibrium distribution of the albite molecule between co-existing plagioclase and alkali feldspar. The syenite porphyry contains phenocrysts of plagioclase with co-existing alkali feldspar. Although the sanidine porphyries have no co-existing plagioclase, the brown matrix rocks (CY92 and CY61) have co-existing plagioclase and sanidines, with potash feldspar overgrowths on some of the plagioclase phenocrysts.

Because of the porphyritic texture of the syenite it was realised that the feldspars may not constitute an equilibrium assemblage. For this reason analyses were performed only on the coarser grained rocks, where the groundmass crystal size approached that of the phenocrysts, in an attempt to see if the Stormer geothermometer could be successfully applied to these. Rim compositions were measured for adjacent crystals

TABLE III-2

Two Feldspar Geothermometer
Data for co-existing plagioclase and alkali feldspars

Syenite Porphyry

Plagioclase

CY70

SiO ₂	61.80	61.43	63.10	68.33	60.53	60.68	60.26	60.46	60.34	61.59
Al ₂ O ₃	24.54	24.74	23.63	20.70	25.12	24.76	25.31	25.11	25.54	24.50
Na ₂ O	6.49	6.53	7.01	8.93	6.48	6.59	6.64	6.65	6.57	6.87
K ₂ O	0.74	0.77	1.03	0.58	0.71	0.95	0.69	0.68	0.73	0.79
CaO	6.42	6.53	5.24	1.47	6.91	6.91	7.09	6.94	6.94	6.15
Total	99.99	100.00	100.01	100.01	99.75	99.89	99.99	99.84	100.12	99.90

Atomic proportion on basis of 16 oxygen

Si	5.474	5.448	5.577	5.946	5.392	5.407	5.364	5.385	5.376	5.467
Al	2.562	2.586	2.451	2.123	2.638	2.601	2.656	2.637	2.265	2.564
Total	8.036	8.034	8.028	8.069	8.030	8.008	8.020	8.022	7.641	8.031
Na	1.115	1.124	1.201	1.506	1.120	1.139	1.146	1.148	1.134	1.182
K	0.084	0.087	0.116	0.064	0.081	0.108	0.078	0.077	0.084	0.090
Ca	0.610	0.620	0.496	0.138	0.659	0.660	0.676	0.662	0.662	0.585
Total	1.809	1.831	1.813	1.708	1.860	1.907	1.900	1.887	1.880	1.857

Alkali feldspars

SiO ₂	65.28	64.95	64.54	64.66	64.91	64.04	66.25	64.49	64.38	64.62
Al ₂ O ₃	18.55	17.82	18.50	18.49	18.56	18.73	17.82	18.79	18.81	18.86
Na ₂ O	1.89	0.42	1.39	1.73	2.00	2.29	1.62	1.92	2.13	2.04
K ₂ O	13.11	15.85	13.91	13.52	13.28	13.08	12.96	13.05	12.95	13.00
CaO	0.88	0.96	0.99	0.94	0.89	0.92	0.79	0.83	0.83	0.74
BaO	0.29	0.00	0.67	0.66	0.35	0.94	0.56	0.96	0.90	0.73
Total	100.00	100.00	100.00	100.00	99.99	100.00	100.00	100.04	100.00	99.99

TABLE III-2(continued)

Atomic proportion on basis of 16 oxygen

Si	5.971	6.009	5.932	5.935	5.950	5.883	6.039	5.908	5.900	5.916
Al	1.999	1.943	2.004	2.000	2.006	2.028	1.915	2.025	2.032	2.035
Total	7.970	7.952	7.936	7.935	7.956	7.911	7.954	7.933	7.932	7.951
Na	0.335	0.076	0.247	0.309	0.356	0.409	0.286	0.341	0.379	0.363
K	1.530	1.871	1.631	1.584	1.553	1.533	1.507	1.525	1.514	1.519
Ca	0.087	0.095	0.097	0.092	0.088	0.091	0.077	0.081	0.081	0.073
Ba	0.020	0.000	0.047	0.045	0.024	0.065	0.038	0.066	0.062	0.050
Total	1.972	2.042	2.022	2.030	2.021	2.098	1.908	2.013	2.036	2.005

Plagioclase

CY8

SiO ₂	62.94	62.61	63.99	62.89	62.08	64.60	61.72	62.03	65.35	63.71
Al ₂ O ₃	23.84	24.15	23.35	24.01	24.57	22.80	24.77	24.13	22.29	23.16
Na ₂ O	7.11	7.00	7.61	7.31	7.12	7.96	7.07	7.22	8.60	7.31
K ₂ O	0.82	0.57	0.57	0.40	0.63	0.47	0.45	0.93	0.43	0.71
CaO	5.29	5.67	4.47	5.39	5.60	4.17	5.83	5.55	3.17	4.71
Total	100.00	100.00	99.99	100.00	100.00	100.00	99.84	99.86	99.84	99.60

Atomic proportion on basis of 16 oxygen

Si	5.560	5.530	5.632	5.548	5.491	5.679	5.467	5.506	5.741	5.624
Al	2.482	2.514	2.422	2.497	2.561	2.363	2.586	2.524	2.308	2.409
Total	8.042	8.044	8.054	8.045	8.052	8.042	8.053	8.030	8.049	8.033
Na	1.219	1.198	1.299	1.251	1.221	1.357	1.214	1.243	1.465	1.252
K	0.092	0.065	0.064	0.045	0.071	0.052	0.050	0.106	0.048	0.080
Ca	0.501	0.537	0.422	0.509	0.530	0.392	0.554	0.528	0.298	0.446
Total	1.812	1.800	1.785	1.805	1.822	1.801	1.818	1.877	1.811	1.778

TABLE III-2 (continued)

Alkali feldspar

SiO ₂	64.90	65.28	64.64	65.82	64.42	65.62	64.42	65.07	64.74	63.89
Al ₂ O ₃	17.78	18.15	18.03	18.37	18.78	18.95	19.11	18.94	18.35	19.03
Na ₂ O	0.57	1.74	0.00	2.85	2.63	4.07	3.10	2.87	1.70	1.84
K ₂ O	15.74	13.88	16.26	12.13	12.80	10.26	11.44	12.04	14.21	13.36
CaO	1.02	0.95	1.07	0.83	1.22	1.10	1.42	0.92	1.00	1.30
BaO	0.00	0.00	0.00	0.00	0.00	0.00	0.00	0.00	0.00	0.54
Total	100.01	100.00	100.00	100.00	99.85	100.00	99.49	99.84	100.00	99.96

Atomic proportion on basis of 16 oxygen

Si	6.005	5.996	5.989	6.001	5.921	5.951	5.894	5.946	5.963	5.877
Al	1.939	1.965	1.970	1.974	2.035	2.026	2.060	2.040	1.992	2.063
Total	7.944	7.961	7.959	7.975	7.956	7.977	7.954	7.986	7.955	7.940
Na	0.102	0.309	0.000	0.504	0.469	0.715	0.550	0.509	0.304	0.328
K	1.858	1.627	1.922	1.411	1.501	1.187	1.336	1.403	1.670	1.568
Ca	0.101	0.093	0.106	0.081	0.120	0.107	0.139	0.090	0.099	0.128
Ba	0.000	0.000	0.000	0.000	0.000	0.000	0.000	0.000	0.000	0.038
Total	2.061	2.029	2.028	1.996	2.090	2.009	2.025	2.002	2.073	2.062

Plagioclase

	CY45			CY64			CY120			
SiO ₂	64.22	63.71	64.33	59.94	62.26	62.87	65.39	60.44	63.56	64.09
Al ₂ O ₃	23.12	23.54	23.38	25.69	24.00	23.90	22.39	25.23	23.34	23.00
Na ₂ O	7.44	7.55	7.49	6.05	7.27	7.44	8.66	6.35	7.71	8.29
K ₂ O	0.84	0.69	0.58	0.81	0.53	0.40	0.32	0.62	0.43	0.46
CaO	4.37	4.51	4.22	7.54	5.62	5.27	3.17	7.21	4.72	4.16
Total	99.99	100.00	100.00	100.03	99.68	99.88	99.93	99.85	99.76	100.00

TABLE III-2 (continued)

Atomic proportion on basis of 16 oxygen

Si	5.654	5.612	5.651	5.335	5.523	5.554	5.737	5.380	5.612	5.646
Al	2.399	2.444	2.421	2.696	2.510	2.489	2.315	2.647	2.430	2.388
Total	8.053	8.056	8.072	8.031	8.033	8.043	8.052	8.027	8.042	8.034
Na	1.271	1.290	1.276	1.045	1.250	1.274	1.473	1.096	1.320	1.415
K	0.094	0.078	0.065	0.092	0.060	0.045	0.036	0.070	0.049	0.051
Ca	0.412	0.426	0.397	0.719	0.534	0.499	0.298	0.688	0.446	0.393
Total	1.777	1.794	1.738	1.856	1.844	1.818	1.807	1.854	1.815	1.859

Alkali feldspar

SiO ₂	64.58	64.60	64.22	64.72	64.82	64.98	64.49	64.28	63.97	63.38
Al ₂ O ₃	19.23	18.01	15.85	18.52	18.02	18.15	17.94	18.36	18.95	19.15
Na ₂ O	2.39	0.46	0.27	1.18	3.06	1.71	1.29	1.14	2.71	2.10
K ₂ O	12.04	15.99	15.85	14.30	12.28	14.25	15.02	15.01	12.01	12.89
CaO	1.29	0.94	1.01	0.91	1.65	0.92	1.26	0.93	0.90	0.92
BaO	0.47	0.00	0.00	0.37	0.00	0.00	0.00	0.28	1.45	1.55
FeO	0.00	0.00	0.93	0.00	0.00	0.00	0.00	0.00	0.00	0.00
Total	100.00	100.00	98.13	100.00	99.83	100.01	100.00	100.00	99.99	99.99

Atomic proportions on basis of 16 oxygen

Si	5.986	5.985	5.974	5.952	5.958	5.983	5.968	5.941	5.852	5.821
Al	2.069	1.967	1.944	2.008	1.952	1.969	1.955	2.000	2.044	2.074
Total	7.965	7.952	7.918	7.960	7.910	7.952	7.923	7.941	7.896	7.895
Na	0.424	0.083	0.049	0.210	0.545	0.306	0.187	0.204	0.481	0.375
K	1.402	1.891	1.880	1.678	1.441	1.674	1.844	1.770	1.402	1.510
Ca	0.126	0.093	0.101	0.089	0.163	0.090	0.116	0.092	0.088	0.091
Ba	0.033	0.000	0.000	0.025	0.000	0.000	0.000	0.020	0.100	0.107
FeO	0.000	0.000	0.072	0.000	0.000	0.000	0.000	0.000	0.000	0.000
Total	1.985	2.067	2.102	2.002	2.149	2.070	2.147	2.086	2.071	2.083

TABLE III-2 (continued)

Plagioclase

CY49

SiO ₂	63.22	62.73	62.60	63.48	63.49	62.47	63.80	63.64	63.14
Al ₂ O ₃	25.05	24.31	23.96	23.61	23.55	24.14	23.34	23.48	23.71
Na ₂ O	6.94	7.06	7.14	7.14	7.22	7.06	7.17	7.65	7.18
K ₂ O	0.40	0.36	0.79	0.73	0.74	0.73	0.98	0.44	0.73
CaO	4.39	5.54	5.51	5.03	5.00	5.59	4.71	4.80	5.23
Total	100.00	100.00	100.00	99.99	100.00	99.99	100.00	100.01	99.99

Atomic proportions on basis of 16 oxygen

Si	5.545	5.531	5.537	5.596	5.599	5.524	5.625	5.606	5.574
Al	2.590	2.527	2.498	2.454	2.448	2.516	2.425	2.438	2.467
Total	8.135	8.058	8.035	8.050	8.047	8.040	8.050	8.044	8.041
Na	1.180	1.207	1.225	1.221	1.234	1.211	1.225	1.307	1.230
K	0.045	0.041	0.089	0.082	0.083	0.083	0.110	0.049	0.082
Ca	0.413	0.523	0.522	0.475	0.473	0.530	0.445	0.453	0.495
Total	1.638	1.771	1.836	1.778	1.790	1.824	1.780	1.809	1.807

Alkali feldspar

SiO ₂	65.26	65.44	65.44	65.53	65.37	65.39	65.15	64.74	66.65
Al ₂ O ₃	18.01	18.10	18.19	17.95	17.99	17.93	17.99	18.79	17.95
Na ₂ O	1.44	1.11	1.75	0.96	1.63	1.85	1.23	1.66	2.05
K ₂ O	14.43	14.56	13.77	14.52	14.17	14.08	14.81	13.11	12.42
CaO	0.86	0.79	0.85	1.04	0.83	0.75	0.82	0.96	0.93
BaO	0.00	0.00	0.00	0.00	0.00	0.00	0.00	0.74	0.00
Total	100.00	100.00	100.00	100.00	99.99	100.00	100.00	100.00	100.00

Atomic proportions on basis of 16 oxygen

Si	6.005	6.014	6.003	6.022	6.009	6.011	6.004	5.926	6.061
Al	1.954	1.961	1.967	1.944	1.949	1.942	1.954	2.027	1.924
Total	7.959	7.975	7.970	7.966	7.958	7.953	7.958	7.953	7.985

TABLE III-2 (continued)

Na	0.257	0.197	0.311	0.171	0.291	0.331	0.221	0.295	0.362
K	1.693	1.707	1.611	1.702	1.662	1.651	1.741	1.531	1.441
Ca	0.084	0.078	0.083	0.102	0.082	0.073	0.081	0.094	0.090
Ba	0.000	0.000	0.000	0.000	0.000	0.000	0.000	0.051	0.000
Total	2.034	1.982	2.005	1.975	2.035	2.055	2.043	1.971	1.893

Plagioclase

CY92

SiO ₂	63.31	64.75	59.27	63.60	64.90	63.31	64.99
Al ₂ O ₃	22.76	22.28	26.10	23.23	22.14	23.28	22.16
Na ₂ O	7.42	7.57	6.01	7.07	7.60	7.14	7.47
K ₂ O	1.29	1.41	0.65	1.33	1.74	1.27	1.60
CaO	4.65	3.36	7.97	4.77	3.62	4.79	3.78
Total	99.43	99.37	100.00	100.00	100.00	99.79	100.00

Atomic proportions on basis of 16 oxygen

Si	5.609	5.711	5.284	5.619	5.727	5.598	5.730
Al	2.377	2.316	2.743	2.419	2.303	2.426	2.303
Total	7.986	8.027	8.027	8.038	8.030	8.024	8.033
Na	1.274	1.294	1.038	1.212	1.301	1.223	1.278
K	0.145	0.158	0.074	0.150	0.196	0.143	0.180
Ca	0.441	0.318	0.761	0.452	0.343	0.454	0.357
Total	1.860	1.770	1.873	1.814	1.840	1.820	1.815

Alkali feldspar

SiO ₂	65.77	66.06	66.54	66.21	66.73	66.50	66.00
Al ₂ O ₃	18.85	18.76	18.95	18.57	18.95	18.96	19.00
Na ₂ O	3.20	3.53	4.42	3.25	5.21	4.60	3.66
K ₂ O	11.20	10.70	9.15	11.16	8.14	8.88	10.24
CaO	0.98	0.95	0.94	0.80	0.98	1.05	1.10
BaO	0.00	0.00	0.00	0.00	0.00	0.00	0.00
Total	100.00	100.00	100.00	99.99	100.01	99.99	100.00

TABLE III-2 (continued)

Atomic proportions on the basis of 16 oxygen

Si	5.974	5.987	5.991	6.006	5.990	5.985	5.971
Al	2.018	2.004	2.011	1.986	2.005	2.012	2.026
Total	7.992	7.991	8.002	7.992	7.995	7.997	7.997
Na	0.564	0.621	0.772	0.572	0.906	0.802	0.641
K	1.298	1.237	1.051	1.292	0.093	1.020	1.181
Ca	0.095	0.092	0.091	0.078	0.094	0.101	0.107
Ba	0.000	0.000	0.000	0.000	0.000	0.000	0.000
Total	1.957	1.950	1.914	1.942	1.093	1.923	1.929

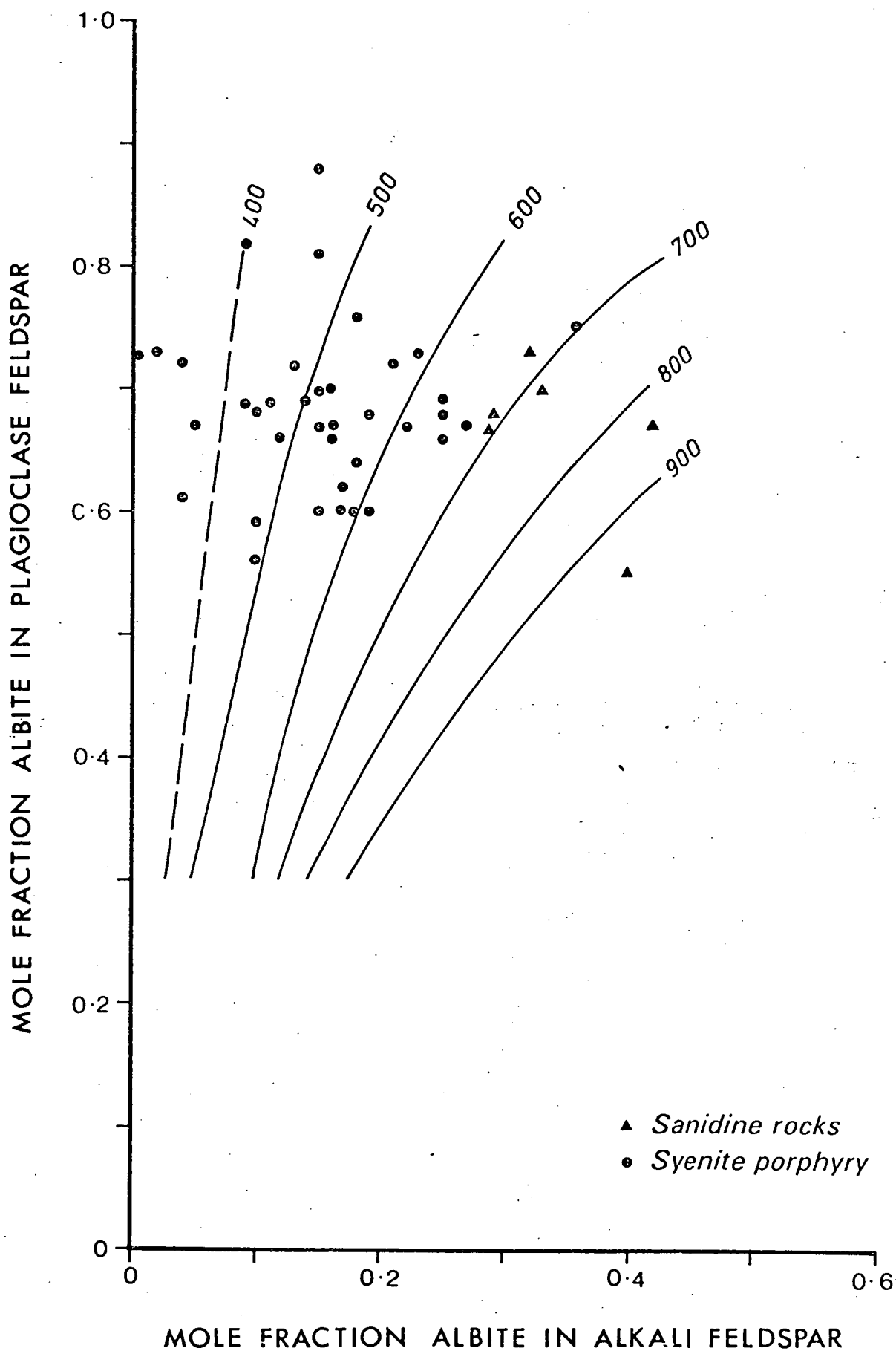


Figure III-5 Stromer geothermometer plot for Ab distribution between co-existing feldspars.

on the assumption that these were the most likely to have been in equilibrium with the last common liquid. There is no evidence of exsolution in the alkali feldspar phases in the syenite porphyries.

Electron probe analyses, for rim compositions of the co-existing feldspars in the above mentioned rocks, appear in Table III-2. These data are plotted in Figure III-5 on a Stormer diagram equivalent to five kilobars. The five kilobar isobar was taken as a probable maximum, assuming limitation by the crustal thickness available, for the pressure pertaining to the crystallization of the feldspars and also because variation due to pressure effects are of minor importance up to this value.

There is not a very great scatter of the mole fraction of albite in the plagioclase, compared with the scatter of the mole fractions of albite in the alkali feldspar. In the petrographic section it was reported that plagioclase crystals in the syenite porphyry are euhedral, with well-developed faces, but the alkali feldspars are subhedral to anhedral with a consequent poor development of crystal faces. These observations, together with the data on the plot, would suggest that these are not equilibrium assemblages.

The interpretation of the Stormer plot is of low temperature non-equilibrium crystallization with a possible maximum of 700°C for the syenite porphyries. The brown matrix rocks appear to have a higher temperature of crystallization than do the syenites, with a minimum of 700°C and a possible maximum over 900°C. However the spread of the data once again point to disequilibrium.

Powell and Powell (1977) modified the Stormer geothermometer by allowing a temperature correction proportional to the mole fraction of anorthite present. According to these authors, without this correction, the Stormer temperatures are too high. The above data have been

replotted on the Powell and Powell diagram (Fig. III-6) using the mole fraction of anorthite as 0.08, a good approximation for the present data. The influence of the anorthite molecule causes the estimate of the crystallization temperature to drop by about 100°C. Thus the maximum temperature for the syenite porphyry is now just below 600°C. The brown matrix rock is still above the syenite porphyry temperature with the range from 600°C to approximately 800°C. Once again the values are scattered and suggest disequilibrium.

The distribution of the data is not compatible with the Stormer Geothermometer. Repeated analysis of the feldspars confirm the distribution pattern for these minerals. Thus while the mole fraction of albite remains largely within the range 0.60-0.75 for the plagioclase and is consistent for crystallization over a small temperature interval, the wide range of Ab in the alkali feldspar distorts the Stormer plot (Fig. III-5) pointing to the alkali feldspar not being in equilibrium, which would follow from the porphyritic texture.

Probably the ideal rock type for which this thermometer could be applied would be one containing both plagioclase and alkali feldspar, but with a matrix containing abundant aegirine, in which case the system would have been buffered with sodium throughout its crystallization history and equilibrium distribution of soda between the feldspars would have been attained and maintained.

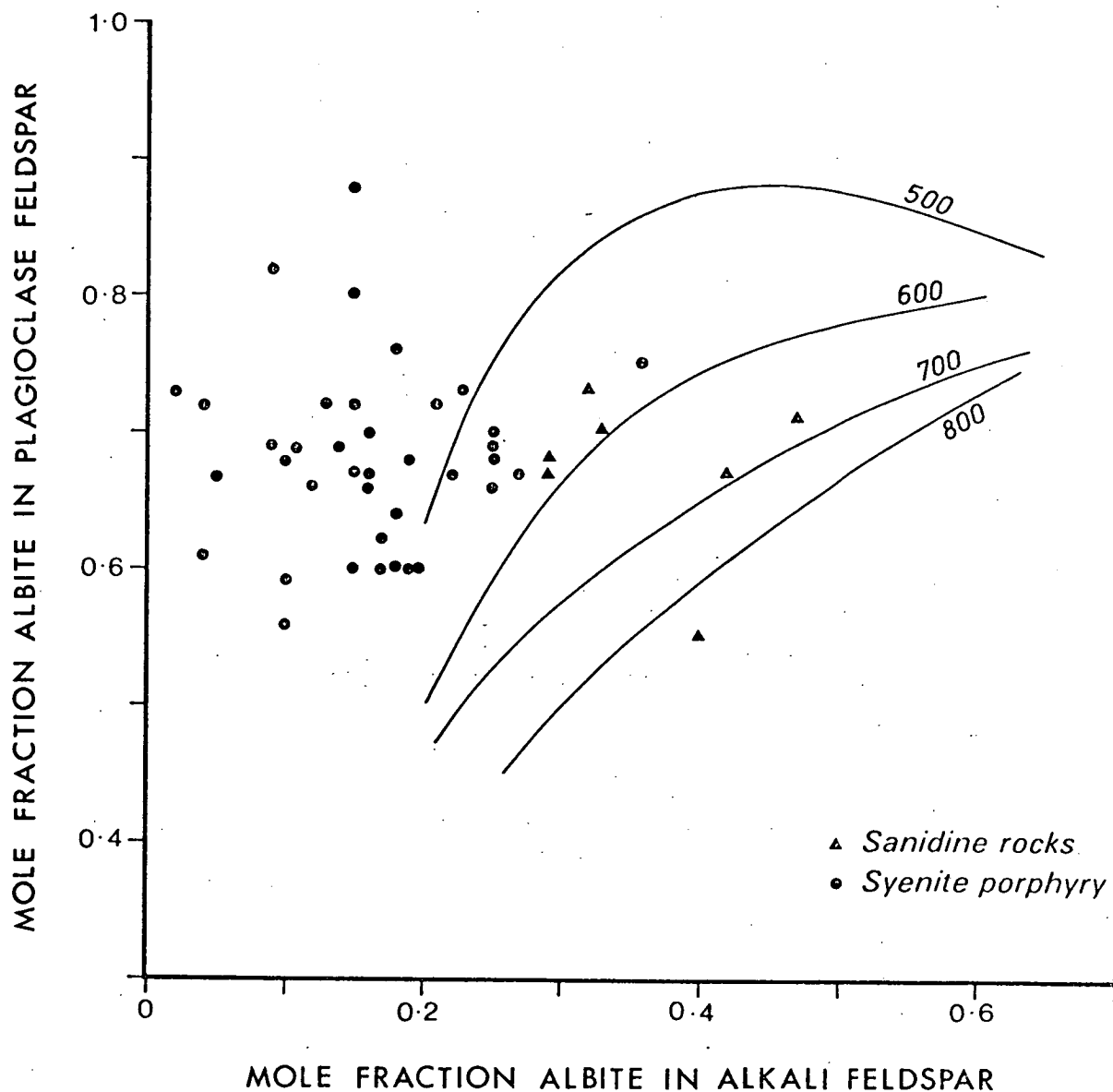


Figure III-6 Powell and Powell geothermometer plot of distribution of Ab between co-existing plagioclase and alkali feldspar.

TABLE III-3

Distribution data for the albite molecule from Table III-2.

CY70

Mole Fraction Ab in Plagioclase

0.62 0.61 0.66 0.88 0.60 0.60 0.60 0.60 0.60 0.64

average = 0.64

Mole Fraction Ab in Alkali Feldspar

0.17 0.04 0.12 0.15 0.18 0.19 0.15 0.17 0.19 0.18

average = 0.15

CY8

Mole Fraction Ab in Plagioclase Feldspar

0.67 0.67 0.73 0.69 0.67 0.75 0.67 0.66 0.81 0.70

average = 0.70

Mole Fraction Ab in Alkali Feldspar

0.05 0.15 0.00 0.25 0.22 0.36 0.27 0.25 0.15 0.16

average = 0.19

CY45B

Mole Fraction Ab in Plagioclase

0.72 0.72 0.73

average = 0.72

Mole Fraction Ab in Alkali Feldspar

0.21 0.04 0.02

average = 0.09

CY92

Mole Fraction Ab in Plagioclase

0.68 0.73 0.55 0.67 0.71 0.67 0.70

average = 0.67

CY64

Mole Fraction Ab in Plagioclase

0.56

average = 0.56

Mole Fraction Ab in Alkali Feldspar

0.29 0.32 0.40 0.29 0.47 0.42 0.33

average = 0.36

Mole Fraction Ab in Alkali Felspar

0.10

average = 0.10

CY120

Mole Fraction Ab in Plagioclase

0.68 0.70 0.82 0.59 0.73 0.76

average = 0.71

Mole Fraction Ab in Alkali Feldspar

0.25 0.15 0.09 0.10 0.23 0.18

average = 0.17

CY49

Mole Fraction Ab in Plagioclase

0.72 0.68 0.67 0.69 0.69 0.66 0.69 0.72 0.68

average = 0.69

Mole Fraction Ab in Alkali Feldspar

0.13 0.10 0.16 0.09 0.14 0.16 0.11 0.15 0.19

average = 0.14

THE BIOTITE THERMOMETER

Work by Wones and Eugster (1962), Wones and Eugster (1965) and Rutherford (1969) has defined limits of biotite stability and its composition with respect to sanidine and magnetite. As co-existing sanidine, magnetite and biotite exist in the hybrid rocks, then it may be possible to apply these equilibria to these rocks. Rutherford (1969) determined the effect of sodium on the equilibrium with respect to sodium-bearing micas and to the two feldspar scheme of Orville (1963), as a development of the Wones and Eugster model. As many of the granular hybrid rocks do not contain exsolved feldspars and the biotites do not contain any sodium in solid solution, the model of Wones and Eugster was used to try to determine the formation temperature and fO_2 .

Only biotites in contact with crystals of magnetite and sanidine were measured. The compositions of these minerals are summarized in Tables III-4 and III-5, and the data are plotted on the (Temperature)-(Fe/Fe+Mg)-(log fO_2) diagram of Wones and Eugster (op. cit.) (Fig. III-7). Since these rocks resulted from the alteration of pre-existing dolerite intruded into Permian sediments and because the maximum depth of burial of the Permian rocks has probably been about 2.5 km (M.R. Banks pers. comm.), the 1 kbar isobar of Wones and Eugster has been chosen as being the best applicable in this case, with their data recalculated to this pressure. The biotites range from 0.37 to 0.47 in the ratio

TABLE III-4

Electron-probe analyses of biotites from altered dolerites. Total cations based on O = 11. Deficiency in un-normalized total considered as OH. All iron as FeO.

Na ₂ O	0.61	0.57	0.27	0.23	0.38	0.00	0.41	0.36	0.33	0.21	0.25	0.22	0.56
MgO	13.01	14.06	13.58	13.49	11.13	14.48	14.60	14.35	13.90	13.26	14.02	14.54	15.50
Al ₂ O ₃	16.89	14.21	15.32	14.82	14.43	14.33	14.01	13.80	14.14	14.44	14.81	14.23	13.65
SiO ₂	38.25	38.01	37.43	36.67	36.30	38.48	38.59	38.30	38.36	37.22	37.76	38.32	38.65
K ₂ O	9.48	9.89	10.20	10.46	9.86	10.30	10.36	10.10	10.22	10.21	10.18	10.29	9.97
CaO	1.54	0.55	0.56	0.59	0.66	0.53	0.62	0.56	0.56	0.62	0.57	0.50	0.59
TiO ₂	2.07	2.81	1.10	2.67	2.56	2.25	1.44	2.52	1.96	2.37	1.28	2.92	3.17
MnO	0.59	0.49	0.64	0.73	0.70	0.62	0.54	0.60	0.62	0.74	0.68	0.58	0.21
FeO	17.55	19.41	20.89	20.34	23.97	19.01	19.42	19.41	19.91	20.92	20.47	18.38	17.69
Un-normalized Total	95.00	94.76	92.49	92.85	92.68	92.53	92.41	93.96	91.14	90.43	91.56	94.12	92.69

Cations on basis of 11 oxygen

[illegible]

TABLE III-4 (continued)

Na ₂ O	0.00	0.41	0.43	0.27	0.00	0.44	0.34	0.41	0.41	0.42
MgO	15.64	14.94	15.92	16.50	18.27	14.87	16.80	15.47	15.80	14.75
Al ₂ O ₃	13.64	13.44	13.75	13.55	11.88	13.19	13.98	14.16	13.89	14.09
SiO	38.86	38.58	38.67	39.03	41.07	38.50	38.79	38.30	38.52	38.05
K ₂ O	10.09	10.18	9.91	10.18	10.36	10.01	9.62	9.73	9.48	9.96
CaO	0.72	0.49	0.53	0.58	0.64	0.57	0.71	0.54	0.74	0.61
TiO ₂	3.39	3.59	3.18	2.61	1.32	2.05	1.27	1.96	1.65	2.66
MnO	0.37	0.39	0.24	0.28	0.24	0.22	0.37	0.45	0.37	0.39
FeO	17.31	17.98	17.38	16.99	16.21	20.17	18.12	18.99	19.03	19.07
Un-normalized Total	92.93	94.04	92.37	93.11	94.37	94.89	95.46	95.33	94.25	95.38
Cations on basis of 11 oxygen										
Na	0.000	0.057	0.060	0.038	0.000	0.062	0.048	0.058	0.072	0.059
K	0.929	0.944	0.914	0.938	0.947	0.936	0.888	0.904	0.880	0.927
Ca	0.056	0.038	0.041	0.045	0.049	0.045	0.055	0.042	0.057	0.048
Total	0.985	1.039	1.015	1.021	1.096	1.043	0.991	1.004	1.009	1.034
Mg	1.684	1.618	1.716	1.775	1.953	1.625	1.813	1.679	1.714	1.606
Fe	1.046	1.093	1.050	1.026	0.972	1.237	1.097	1.156	1.158	1.164
Ti	0.184	0.196	0.173	0.142	0.071	0.113	0.069	0.107	0.090	0.146
Mn	0.022	0.024	0.015	0.017	0.014	0.013	0.023	0.028	0.023	0.024
Al	0.000	0.000	0.000	0.000	0.000	0.000	0.001	0.004	0.000	0.000
Total	2.936	2.931	2.954	2.960	3.010	2.988	3.003	2.974	2.985	2.940
Al	1.162	1.151	1.171	1.153	1.004	1.140	1.192	1.211	1.191	1.212
Si	2.808	2.803	2.795	2.818	2.944	2.823	2.808	2.789	2.802	2.777
Total	3.970	3.954	3.966	3.971	3.948	3.963	4.000	4.000	3.993	3.989
O	11.000	11.000	11.000	11.000	11.000	11.000	11.000	11.000	11.000	11.000
$\frac{\text{Fe}}{\text{Fe}+\text{Mg}}$	0.383	0.403	0.582	0.366	0.332	0.432	0.377	0.408	0.403	0.420

TABLE III-5

Electron microprobe analyses of biotites from recrystallized hybrid rocks.

	CY97			CY29		CY33C		CY34		CY102			CY116	
MgO	12.80	13.07	11.87	14.91	14.19	16.22	18.29	11.97	16.13	16.55	16.35	17.24	13.96	14.58
Al ₂ O ₃	16.27	15.49	16.70	14.04	13.94	14.34	14.36	13.59	13.53	13.74	13.66	13.11	14.19	15.85
SiO ₂	36.82	36.99	35.92	38.31	38.01	40.13	40.60	38.48	39.19	38.87	39.08	39.49	38.91	39.94
K ₂ O	10.03	9.73	9.76	10.46	10.20	10.31	10.42	9.91	10.22	10.01	9.96	10.11	9.88	10.34
CaO	0.48	0.55	0.53	0.67	0.71	0.67	0.66	0.56	0.46	0.43	0.57	0.49	0.53	0.59
TiO ₂	4.09	4.34	4.50	2.62	3.52	1.62	1.05	2.27	2.92	1.57	2.07	1.83	0.60	0.00
MnO	0.76	0.88	0.97	0.61	0.58	1.01	0.39	0.67	0.00	0.41	0.37	0.34	0.96	0.00
FeO	18.74	18.98	19.75	18.59	19.10	15.74	14.23	22.53	17.56	18.41	17.92	17.38	20.96	18.72
Normalized Total	99.99	100.03	100.00	100.21	100.25	100.04	100.00	99.98	100.01	99.99	99.98	99.99	99.99	100.02
Cations on basis of 11 oxygen														
Na	0.000	0.000	0.000	0.000	0.000	0.000	0.000	0.000	0.000	0.000	0.000	0.000	0.000	0.000
K	0.933	0.906	0.915	0.973	0.952	0.943	0.943	0.936	0.941	0.926	0.919	0.930	0.925	0.951
Ca	0.037	0.043	0.042	0.053	0.056	0.052	0.050	0.044	0.036	0.034	0.044	0.038	0.042	0.045
Total	0.970	0.949	0.957	1.026	1.008	0.994	0.993	0.980	0.977	0.960	0.963	0.968	0.967	0.996
Mg	1.391	1.421	1.298	1.600	1.547	1.732	1.935	1.321	1.736	1.789	1.763	1.856	1.528	1.567
Fe	1.143	1.958	1.211	1.134	1.168	0.941	0.844	1.595	1.060	1.117	1.084	1.049	1.287	1.129
Ti	0.224	0.238	0.248	0.144	0.179	0.087	0.056	0.126	0.158	0.086	0.113	0.100	0.033	0.000
Mn	0.047	0.054	0.060	0.038	0.036	0.061	0.023	0.042	0.000	0.025	0.023	0.021	0.059	0.000
Al	0.082	0.032	0.079	0.002	0.000	0.086	0.082	0.034	0.000	0.000	0.000	0.000	0.085	0.229
Total	2.887	2.903	2.896	2.918	2.930	2.907	2.940	3.118	2.954	3.017	2.983	3.026	2.992	2.925
Al	1.316	1.301	1.365	1.205	1.202	1.125	1.119	1.151	1.151	1.174	1.165	1.115	1.143	1.119
Si	2.684	2.699	2.635	2.795	2.779	2.875	2.881	2.849	2.828	2.819	2.827	2.850	2.857	2.881
Total	4.000	4.000	4.000	4.000	3.981	4.000	4.000	4.000	3.979	3.993	3.992	3.965	4.000	4.000
O	11.000	11.000	11.000	11.000	11.000	11.000	11.000	11.000	11.000	11.000	11.000	11.000	11.000	11.000
Fe														
Fe+Mg	0.451	0.449	0.483	0.415	0.430	0.352	0.303	0.513	0.379	0.384	0.370	0.361	0.457	0.419

TABLE III-5 (continued)

MgO	15.45	14.97	15.97	15.32	15.21	13.55	13.61	14.86	15.16	18.03	17.02	16.21
Al O	13.96	13.79	14.36	14.28	14.25	13.64	14.15	13.81	14.11	12.04	12.09	12.58
SiO	38.85	38.95	39.08	39.15	39.98	38.16	37.80	38.70	39.13	41.33	40.49	39.80
K O	10.12	9.90	10.09	10.03	10.09	9.99	9.64	9.99	9.85	10.39	10.44	10.05
CaO	0.67	0.64	0.67	0.69	0.71	0.48	0.52	0.48	0.57	0.54	0.44	0.60
TiO	4.39	4.10	2.30	3.12	2.35	2.44	2.07	2.12	1.53	1.38	1.74	3.18
MnO	0.00	0.00	0.00	0.00	0.00	0.44	0.36	0.58	0.54	0.25	0.24	0.00
FeO	16.57	17.61	17.53	17.41	18.41	21.32	21.32	19.46	18.49	15.87	17.36	17.42
Normalized Total	100.01	99.96	100.00	100.00	100.00	100.02	99.47	100.00	99.38	99.83	99.82	99.84
Cations on basis of 11 oxygen												
Na	0.000	0.000	0.000	0.000	0.000	0.000	0.000	0.000	0.000	0.000	0.000	0.000
K	0.928	0.911	0.928	0.922	0.932	0.938	0.905	0.929	0.913	0.949	0.963	0.926
Ca	0.052	0.050	0.052	0.053	0.055	0.038	0.041	0.037	0.045	0.040	0.034	0.046
Total	0.980	0.961	0.980	0.975	0.987	0.976	0.946	0.966	0.958	0.989	0.997	0.972
Mg	1.656	1.609	1.716	1.645	1.641	1.487	1.494	1.615	1.640	1.925	1.834	1.745
Fe	0.996	1.062	1.057	1.048	1.115	1.313	1.313	1.187	1.122	0.951	1.049	1.051
Ti	0.237	0.223	0.125	0.169	0.128	0.135	0.115	0.116	0.084	0.074	0.095	0.172
Mn	0.000	0.000	0.000	0.000	0.000	0.027	0.023	0.036	0.033	0.015	0.015	0.000
Al	0.000	0.000	0.037	0.031	0.038	0.000	0.011	0.009	0.048	0.000	0.000	0.000
Total	2.889	2.894	2.935	2.893	2.922	2.962	2.956	2.963	2.927	2.965	2.993	2.968
Al	1.183	1.172	1.183	1.181	1.178	1.184	1.217	1.178	1.160	1.016	1.030	1.070
Si	2.792	2.809	2.817	2.819	2.822	2.810	2.783	2.822	2.840	2.960	2.926	2.872
Total	3.975	3.981	4.000	4.000	4.000	3.994	4.000	4.000	4.000	3.976	3.956	3.942
O	11.000	11.000	11.000	11.000	11.000	11.000	11.000	11.000	11.000	11.000	11.000	11.000
$\frac{\text{Fe}}{\text{Fe}+\text{Mg}}$	0.376	0.398	0.387	0.384	0.405	0.469	0.468	0.424	0.406	0.330	0.363	0.376

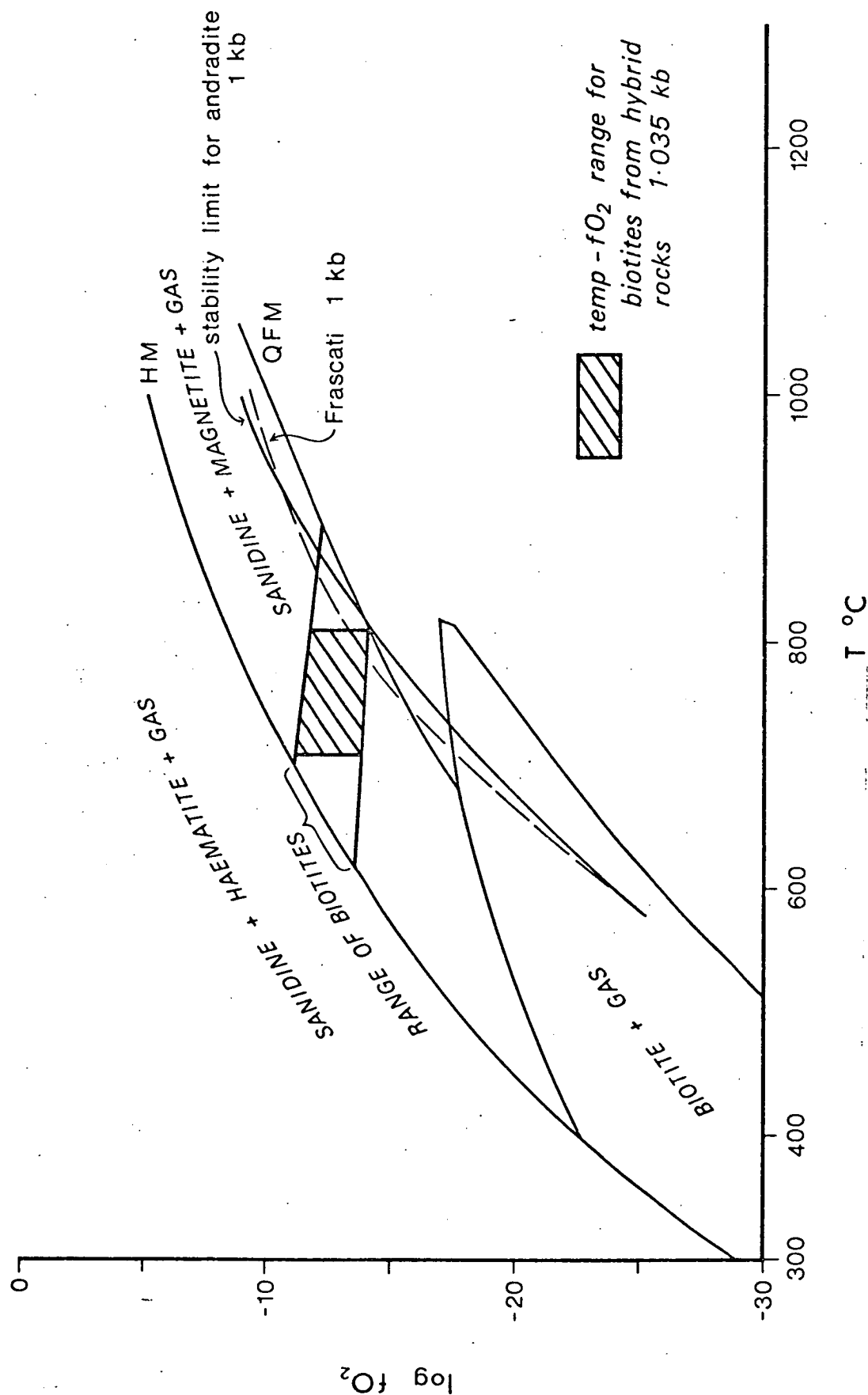


Figure III-7

Wones-Eugster log f_{O_2} -temperature plot for biotites from the hybrid rocks. Data recalculated to 1.035 kb. Stability limit for andradite at 1 kb calculated from the data of Gustafson (1974). Data for Frascati melanite from Huckenholz *et al.* (1976).

(Fe/Fe+Mg) and these have been plotted on the Eugster-Wones diagram for 1035 bars.

From this it can be seen that $\log fO_2$ is fixed within about 3 units and does not vary much due to the low slope of the isopleths in this area of the diagram. The median value for $\log fO_2$ is between -11 and -14.0. On the basis of the plot of the data the minimum temperature will be about 625°C where the 0.7 annite isopleth intersects the hematite-sanidine curve. As no hematite has been observed in the rocks then the formation temperature must lie on one of a series of curves parallel to the sanidine-hematite boundary; consequently the minimum formation temperature must be somewhere above 625°C. The highest possible temperature is limited by the breakdown of the biotites, with the formation of fayalite and quartz. Fayalite has not been observed in any of the rocks. The highest Mg-biotites are also those with highest temperature of formation and do not show any evidence of equilibrium with hematites hence these biotites would indicate a minimum temperature of formation of 710°C. As there is no evidence of biotite altering to fayalite for the high Fe biotites this would put a limiting maximum temperature of 810°C for the biotite.

There is no microscopic evidence of biotite breakdown in any of the rocks. Thus based on the evidence from the biotites, if the Wones and Eugster relationships holds here, then the formation temperature of the hybrid rocks must lie in the range between 710°C and 810°C, with $\log fO_2$ between -11 and -14.

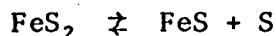
It can be seen that a consistent formation temperature from the models of Hamilton and Perchuk and Ryabchikov is indicated between 750°C and 800°C for the hybrid rocks. All these methods suggest a range from 710°C to 810°C.

From the pattern of alteration of the dolerite in the hybrid zone,

particularly the initial formation of biotite from magnetite, there has probably been a diffusive transfer of potassium from the alkaline rocks, in which case a feldspar exsolution curve of the Orville (1963) type is probably more applicable than that of Tuttle and Bowen (1958). The maximum temperature for a two feldspar field, in a diffusion system according to Orville's data is about 700°C. Some feldspars from the leucocratic rocks of the hybrid zone do show extensive exsolution with unexsolved cores (e.g. 71-311, Plate 55). These feldspars have enough soda to lie on the high part of Orville's solvus curve (see data 71-311, Vol. 2). They may have inherited the soda from breakdown of the plagioclase of the dolerite country rock. This is probably near their original crystallization temperature since heat losses would be high at the time of intrusion because of the small amount of material present, its consolidation at a relatively shallow depth and the presence of some unexsolved cores in the crystals suggesting a quenching process. It could therefore be expected that these feldspars exsolved at some temperature greater than the 660°C solvus maximum established by Tuttle and Bowen (1958) up to the maximum permitted by Orville's solvus.

A further indication of the temperature reached in the hybrid area of Port Cygnet is offered by the presence of pyrrhotite nodules in thermally metamorphosed Permian sediments which crop out on the eastern shore of Port Cygnet, approximately 500 metres away from the hybrid rocks, coupled with the evidence of Leaman (1977) that the hybrid zone extends into the Port Cygnet estuary. These nodules probably formed from the metamorphism of original sedimentary pyrite-marcasite nodules which elsewhere are abundant in certain horizons of the lower Permian rocks. Using the data from Barnes (1979) the minimum temperature for the formation of pyrrhotite from pyrite is 729°C.

For the reaction:



the Gibbs free energy change becomes positive below 729°C. Assuming only a small confining pressure this could be regarded as a minimum temperature for the processes operating in this area.

MELANITE MINERALOGY

Melanite garnet is a constituent of the hybrid rocks. Because its stability, among other factors, is also a function of $f\text{O}_2$ and temperature, it would be useful to see if the presence of melanite in the hybrid rocks is compatible with the conditions suggested by the Wones-Eugster (1962, 1965) model for biotites from the altered dolerite and hybrid rocks. Investigation of the stability of andradite was carried out by Gustafson (1974) as part of an investigation in the system Ca-Fe-Si-O-H. He found that andradite at 2000 bars was stable above $f\text{O}_2 = 10^{-15}$ at 800°C and above $f\text{O}_2 = 10^{-32}$ at 400°C. This stability limit just covers the area delineated by the biotites in the Wones-Eugster diagram outlined above (Fig. III-7), with Gustafson's data recalculated to 1 kbar. However, the melanites are titaniferous andradite garnets and the incorporation of TiO_2 into their structures could modify their fields of stability.

Huckenholz (1969) synthesized titaniferous andradites at a pressure of one atmosphere. Under these conditions pure andradite was stable below 1137°C and above this temperature contained Ti-garnet solid solution in equilibrium with para-wollastonite and hematite. In a further report on titaniferous garnets, Huckenholz, Holzl, Huggins and Virgo (1976) made a reconnaissance study of the stability of titaniferous garnets at defined oxygen fugacities, using artificially

TABLE III-6

Electron probe analyses of Melanites

Hybrid Rocks

					Core	Edge	Core	Edge	Core	Edge	CY73		CY10	Frascati
	1	2	3	4	5	6	7	8	9	10	11	12	13	
Na ₂ O	0.50	0.00	0.31	0.47	0.00	0.27	0.39	0.20	0.40	0.25	0.00	0.00	0.00	0.00
MgO	0.72	0.54	0.75	0.81	0.91	0.63	0.81	0.61	0.60	0.69	0.44	0.50	0.45	0.57
Al ₂ O ₃	1.09	1.40	2.87	1.21	1.50	1.01	2.16	2.38	0.95	2.27	4.29	2.36	7.64	6.57
SiO ₂	33.12	32.60	33.12	32.82	28.86	31.74	33.15	33.32	32.71	34.44	34.62	33.52	35.61	35.49
CaO	31.06	31.76	31.52	31.27	31.64	31.52	31.66	31.64	31.31	31.63	31.03	31.24	30.71	33.01
TiO ₂	5.30	5.29	4.45	5.36	11.83	7.93	4.72	3.83	5.96	2.58	3.46	4.84	2.48	2.53
Cr ₂ O ₃	0.00	0.21	0.00	0.00	0.00	0.20	0.00	0.00	0.00	0.00	0.00	0.00	0.00	0.00
MnO	0.43	0.53	0.52	0.39	0.23	0.36	0.50	0.42	0.41	0.46	1.03	0.87	1.09	0.28
Fe ₂ O ₃	28.59	28.46	27.18	28.46	25.66	27.05	27.35	28.37	28.44	28.47	25.75	27.42	22.48	20.62
Unnormalized Total	96.77	97.57	100.26	97.79	97.40	98.42	99.38	99.08	99.51	99.88	99.66	99.66	98.63	99.07

Atomic proportions on basis of 24 oxygen

														12 oxygen
Na	0.166	0.000	0.100	0.153	0.000	0.088	0.126	0.064	0.130	0.080	0.000	0.000	0.000	0.000
Mg	0.203	0.135	0.186	0.202	0.229	0.104	0.201	0.152	0.150	0.171	0.065	0.123	0.100	0.070
Mn	0.061	0.075	0.073	0.055	0.033	0.051	0.071	0.059	0.058	0.065	0.042	0.122	0.149	0.020
Ca	5.571	5.700	5.617	5.605	5.725	5.659	5.653	5.651	5.617	5.629	5.470	5.564	5.320	2.914
Site Total	6.001	5.910	5.975	6.015	5.987	5.902	6.051	5.925	5.955	5.945	5.577	5.809	5.569	3.004
Cr ³⁺	0.000	0.028	0.000	0.000	0.000	0.027	0.000	0.000	0.000	0.000	0.000	0.000	0.000	1.201
Fe ³⁺	3.60	3.587	3.402	3.583	3.261	3.411	3.430	3.559	3.584	3.559	3.188	3.430	2.737	0.077
Al	0.215	0.276	0.563	0.238	0.299	0.200	0.424	0.468	0.187	0.444	0.833	0.463	1.456	0.638
Ti ³⁺	0.210	0.127	0.065	0.165	0.376	0.318	0.117	0.034	0.227	0.043	0.125	0.174	0.065	0.015
Site Total	4.026	4.018	4.03	3.986	3.936	3.956	3.971	4.061	3.998	4.046	4.146	4.067	4.258	1.931
Ti ⁴⁺	0.457	0.539	0.492	0.509	1.126	0.681	0.475	0.445	0.523	0.279	0.303	0.431	0.237	0.015
Si ⁴⁺	5.543	5.46	5.508	5.491	4.874	5.319	5.525	5.554	5.477	5.721	5.697	5.569	5.763	2.924
Site Total	6.000	6.000	6.000	6.000	6.000	6.000	6.000	5.995	6.000	6.000	6.000	6.000	6.000	6.000
$\frac{\Sigma \text{Ti}^{4+} + \text{Fe}^{3+}}{\Sigma (\text{Ti} + \text{Fe})}$	0.951	0.970	0.984	0.961	0.921	0.928	0.971	0.992	0.947	0.989	0.965	0.957	0.971	0.936

crystallized minerals as standards and comparing these with natural specimens from various localities (Frascati and Kaiserstuhl).

At higher temperatures across the boundary curve these minerals break down to garnet solid solution, wollastonite, kirschsteinite and magnetite.

The artificial minerals were characterised by having the sum of $\text{Si} + \text{Ti} = 3.0$ based on an oxygen total of 12 which contrasts with a natural melanite from Frascati, Italy and a schorlomite from the Kaiserstuhl area, W. Germany which have $\text{Si} + \text{Ti} > 3.0$ per formula unit.

The stability field of these garnets were determined in terms of $f\text{O}_2$ and temperature. With $\text{Si} + \text{Ti} > 3.0$ there is an excess of oxygen which requires the presence of Ti^{3+} and Fe^{2+} for charge balance in the structure. The Cygnet melanite electron probe analyses confirm the observation of Huckenholz et al. that the titanium content always exceeds the silicon deficiency and that titanium must be present as Ti^{3+} and Ti^{4+} with electron-hopping between iron and titanium cations creating the dark colour so typical of these garnets. Since the Port Cygnet melanites exhibit oxidised characteristics (due to $\text{Si} + \text{Ti}$ exceeding the simple cation requirement) they could have stability characteristics similar to those studied by Huckenholz et al.

Table III-6 shows some compositions of melanites from Port Cygnet, and of Frascati melanite, for comparative purposes.

The measure of oxidation of the melanite may be gauged by the silicon deficiency. With a large deficiency the garnet is oxidised and has a larger unit cell parameter than for one saturated with silica. X-ray powder and analytical data are given in Table III-7 for a melanite segregation from the hybrid rocks, with a unit cell dimension of 12.050 A.U.

The unit cell dimension was measured using a Philips-Straumanis

TABLE III-7

X-ray Debye-Scherrer Pattern and X.R.F. analysis, Melanite garnet,
Hybrid rock, Port Cygnet

Camera: Philips-Straumanis type.

Diameter: 114.6 mm

Collimator: Fine

Radiation: $\text{FeK}\alpha = 1.9373 \text{ \AA.U.}$

β filter = Mn; X.R.F. tube = Rh - 2.7 kwatt side window.

Line	Intensity ⁺	d (obs.)	d (calc.)	h	k	l	Analysis	
1	VW	4.255	4.260	2	2	0	Fe_2O_3	22.85
2	S	3.013	3.013	4	0	0	FeO	2.47
3	VS	2.697	2.694	4	2	0	MnO	0.79
4	VW	2.569	2.569	3	3	2	TiO_2	3.10
5	S	2.464	2.460	4	2	2	CaO	31.97
6	W	2.367	2.363	5	1	1	K_2O	0.05
7	W	2.203	2.200	5	2	1	P_2O_5	0.00
8	S	1.958	1.955	6	1	1	SiO_2	36.13
9	W	1.909	1.905	6	2	0	Al_2O_3	2.19
10	VVW	1.778	1.777	6	3	1	MgO	0.23
11	W	1.743	1.739	4	4	4	Na_2O	0.00
12	S	1.674	1.671	6	4	0	loss	0.58
13	VS	1.612	1.610	6	4	2	Total	100.36
14	W	1.508	1.506	8	0	0		
15	VVW	1.484	1.483	8	1	1		
16	W	1.347	1.347	8	4	0	Formula on basis	
17	S	1.313	1.315	8	4	2	of 24 Oxygen:	
18	VVW	1.298	1.299	9	2	1		
19	S	1.283	1.285	6	6	4	Ca	5.710
20	VVW	1.269	1.270	9	3	0	Mn	0.111
21	W	1.216	1.217	9	4	1	R_6^{2+} Mg	0.058
22*	VS	1.1189	1.1188	10	4	0	Fe	0.030
23	VS	1.1000	1.1000	10	4	2	K	0.010
24	VS	1.0653	1.0651	8	8	0	TOTAL=	5.919
25	VS	1.0043	1.0042	8	8	4	Fe	3.18
26	Vs	0.99055	0.99050	12	2	0	R_4^{3+} Al	0.431
27	Vs	0.97737	0.97738	12	2	2	Ti	0.389
							TOTAL	4.000
							R_6^{4+} Si	6.020
							TOTAL=	6.020

+ estimated intensities: VW = very weak;

VS = very strong

* α_1 and α_2 doublets present

a = $12.050 \pm 0.001 \text{ \AA.U.}$ Density measured =

3.806 gm/c.c.; Density calculated =

3.793 gm/c.c.

Total cations =

15.939

O = 24.000

type powder camera and determining a value of "a" for a θ of 90° using the extrapolation function of Nelson-Riley and Taylor-Sinclair (Henry, Lipson and Wooster, 1951). This is about the middle of the range for titaniferous garnets which have smaller unit cells as they become less silica deficient. It is larger than the cell for Huckenholz's Frascati garnet and smaller than the cell size for pure andradite as measured by Huckenholz (1969) at $12.053 \text{ A.U.} \pm 0.003$. Huckenholz gives the increase in unit cell parameter as $0.038 \pm 0.002 \text{ A.U. per } 10\% \text{ wt. Ti garnet}$.

The X.R.F. analytical data for this mineral are significantly different from the electron probe data of Table III-6 in that this sample is saturated with silicon and only permits titanium in the R^{3+} position in the structure. This is consistent with the unit cell dimensions and there is good agreement between the calculated density of 3.793 gm/c.c. and the measured density of 3.806 gm/c.c. The reason for this difference is unknown, however the probe data differ most with respect to Fe_2O_3 and SiO_2 when compared with the X.R.F. analysis. As the probe standard contained 3.93% FeO and 51.90% SiO_2 and the correction program is greatly influenced by each in an inverse manner, the large amount of Fe_2O_3 in the melanite may have been responsible for the discrepancies particularly when coupled with the relatively low silica in the garnet with respect to the standard.

The differences in stability of the melanite garnets were related by Huckenholz et al. to the degree of silica undersaturation as indicated by the ratio:

$$\frac{\sum \text{Ti}^{4+} + \text{Fe}^{3+}}{\sum (\text{Ti} + \text{Fe})}$$

This ratio has been calculated for the melanites in Table III-6. The values of FeO and its consequent molecular proportions have not been

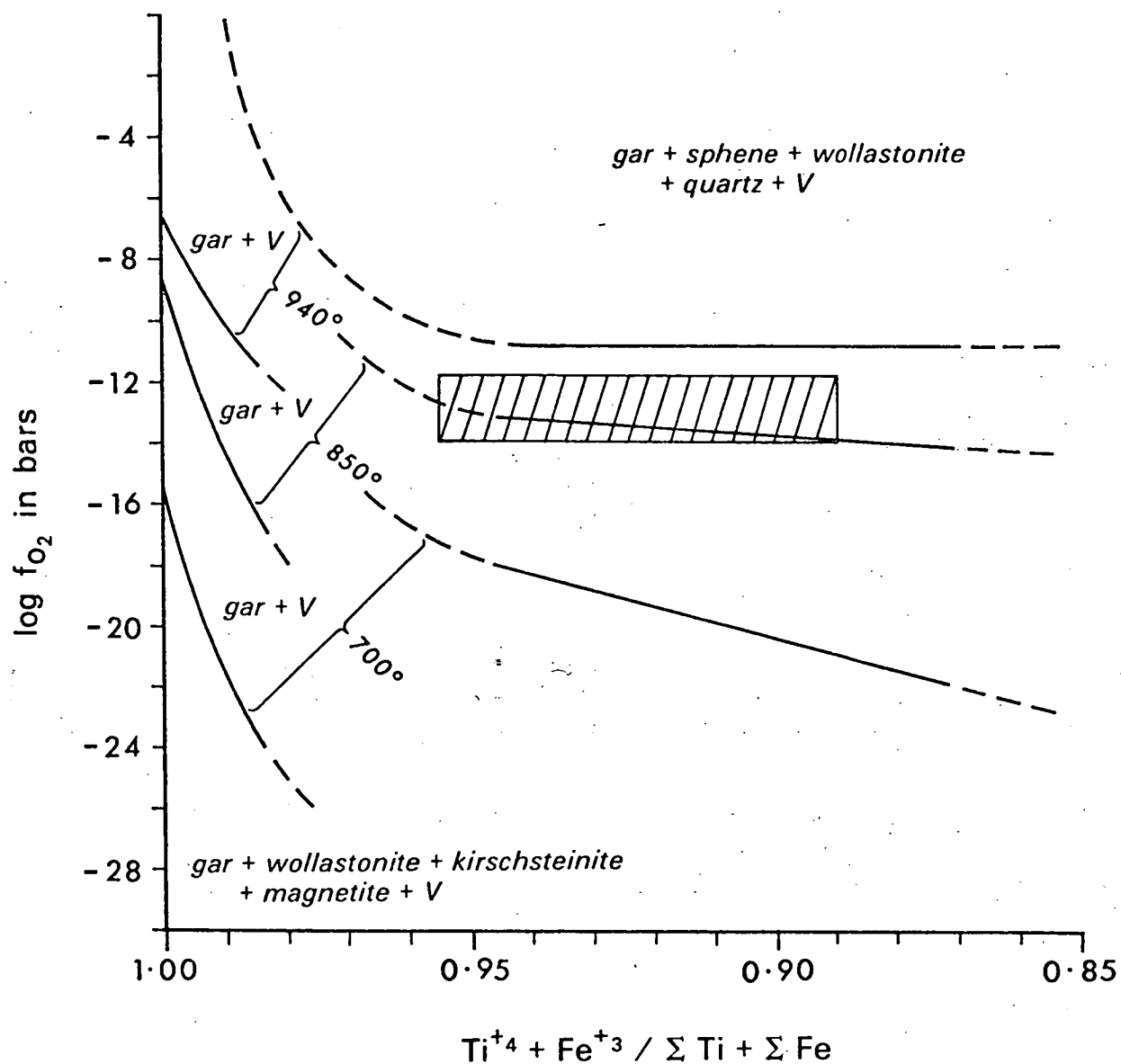


Figure III-8 Data (shaded area) for melanite garnets of hybrid rocks plotted on log f_{O_2} -silica undersaturation diagram of Huckenholz *et al.* (1976).

determined but an independent analysis of FeO on a massive melanite (Table III-7) accumulation from the hybrid rocks, gave a value of 2.57% FeO which would correspond to an atomic proportion of about 0.1 for Fe^{2+} , thus making a negative correction of about 0.03 necessary for the values indicated above, assuming this to be representative.

The lower temperature stability curve for the Frascati mineral as determined by Huckenholz et al. at 1 kb has been plotted on Fig. III-7. If this curve is applicable to the Cygnet data then this would place a very restricted range for the formation conditions at 800°C and $\log f\text{O}_2 = -14$.

Huckenholz et al. constructed a set of curves relating $f\text{O}_2$, temperature and silicon deficiency from their artificial melanites (Fig. III-8). Assuming the $f\text{O}_2$ range as determined from the Wones-Eugster plot (Fig. III-7) to be $10^{-11} - 10^{-14}$, then using the Huckenholz et al. curves within the range of

$$\frac{\sum \text{Ti}^{4+} + \text{Fe}^{3+}}{\sum (\text{Ti} + \text{Fe})} = 0.891 - 0.954$$

with the empirical -0.03 correction for Fe^{2+} , the Port Cygnet melanites would be stable over the approximate temperature range from over 700°C , but less than 850°C , up to a maximum of 940°C . Not enough information is available to locate the lower temperature precisely but it would probably be about 800°C . The experimental data of Gustafson (op. cit.) on andradite stability at 1 kb would place a maximum temperature constraint between 830°C and 870°C at a $\log f\text{O}_2 = -12$ to -14 . The data are summarised in Figure III-8, and suggest a temperature of formation somewhat higher ($800^\circ\text{C}+$) than that derived for the biotites and nephelines. At this stage the latter are preferred because of their better consistency and theoretical and practical foundations.

Because of the inconsistencies in the interpretation of the melanite garnet data it is inferred that more information will be required before this mineral will be useful for establishing conditions of formation of the hybrid rocks of Port Cygnet.

AMPHIBOLE MINERALOGY

Amphiboles are not very abundant in the Port Cygnet alkaline rocks, a consequence of the relatively low CaO, MgO and FeO contents. Amphiboles associated with the alkaline complex occur in four distinct associations which are: the hybrid rocks, syenite porphyries, hornblende porphyry and amphibolite inclusions within the syenite porphyry. The analytical data for minerals from the various associations are summarized in Table III-8. Although scarce most amphibole is found in the hornblende porphyries, CY91 and CY2 where phenocrysts of euhedral dark green crystals having dimensions up to 1 cm x 2 mm in CY91 and somewhat smaller at 0.5 cm x 1 mm in CY2.

TABLE III-8

Some electron microprobe analyses of amphiboles

* un-normalized totals 0 Fe^{2+} + X.R.F. analysis

Syenite porphyry

	CY6		CY8	CY17		CY18		CY47C		CY52				
Na ₂ O	1.93	1.55	1.98	2.33	2.31	2.49	2.29	2.31	2.87	1.93	2.12	2.10	1.86	1.75
MgO	12.78	7.81	8.49	6.55	9.70	11.16	8.01	10.26	6.86	4.15	8.59	8.01	8.87	6.98
Al ₂ O ₃	13.70	12.81	12.77	14.17	14.80	13.53	13.64	13.53	11.14	10.09	13.36	13.89	14.27	14.19
SiO ₂	41.27	40.26	39.68	37.20	38.46	40.09	39.25	39.34	40.26	40.71	39.19	37.97	39.87	38.81
K ₂ O	1.72	2.18	2.32	2.47	2.11	1.64	2.07	2.04	1.78	1.58	1.51	2.16	2.00	2.10
CaO	12.12	11.98	11.64	11.19	11.75	11.64	11.01	11.52	11.24	11.22	11.60	11.54	11.47	11.32
TiO ₂	1.87	2.65	2.05	1.95	2.55	2.60	1.62	2.14	1.55	-	2.27	2.30	1.78	1.50
MnO	-	0.59	0.68	0.72	0.39	-	0.66	-	2.43	1.20	0.35	0.35	0.57	0.80
FeO	14.60	20.04	20.36	23.40	17.93	16.85	21.41	18.85	21.83	29.14	21.12	21.66	19.30	22.55
*Total	96.90	97.13	103.60	97.37	95.70	98.21	93.84	97.62	103.89	100.74	95.46	96.10	94.50	96.90

Atomic Proportion on basis of 23 oxygen

Na	0.548	0.455	0.585	0.702	0.672	0.719	0.677	0.673	0.859	0.590	0.599	0.599	0.542	0.520
Ca	1.904	1.943	1.898	1.862	1.894	1.855	1.799	1.857	1.857	1.898	1.814	1.818	1.849	1.858
K	0.322	0.421	0.451	0.489	0.405	0.311	0.403	0.391	0.351	0.318	0.280	0.404	0.383	0.409
Total	2.774	2.819	2.934	3.053	2.971	2.885	2.879	2.921	3.067	2.806	2.693	2.821	2.774	2.787
Mg	2.795	1.762	1.925	1.516	2.175	2.474	1.820	2.303	1.578	0.975	1.868	1.755	1.989	1.594
Fe	1.791	2.538	2.591	3.039	2.256	2.096	2.730	2.373	2.816	3.847	2.319	2.396	2.427	2.890
Ti	0.208	0.302	0.235	0.228	0.289	0.291	0.186	0.242	0.180	-	0.249	0.254	0.201	0.173
Al	0.420	0.380	0.328	0.367	0.409	0.332	0.437	0.323	0.244	0.303	0.005	0.000	0.123	0.510
Mn	-	0.076	0.088	0.095	0.049	-	0.085	-	0.317	0.161	0.043	0.043	0.072	0.103
Total	5.214	5.058	5.167	5.244	5.178	5.193	5.258	5.241	5.135	5.286	4.484	4.448	4.812	5.270
Al	1.948	1.906	1.963	2.226	2.214	2.039	2.015	2.078	1.790	1.574	2.293	2.406	2.002	2.053
Si	6.052	6.094	6.037	5.774	5.786	5.961	5.985	5.922	6.210	6.426	5.707	5.582	5.998	5.947
Total	8.000	8.000	8.000	8.000	8.000	8.000	8.000	8.000	8.000	8.000	8.000	7.988	8.000	8.000
O	23.000	23.000	23.000	23.000	23.000	23.000	23.000	23.000	23.000	23.000	23.000	23.000	23.000	23.000

TABLE III-8 (continued)

Total cations	15.988	15.890	16.101	16.297	16.149	16.078	16.137	16.162	16.202	16.092	15.177	15.257	15.997	16.064		
Ca	29.34	31.12	29.59	29.02	29.94	28.87	28.34	28.42	29.71	28.24	30.23	30.00	30.00	29.00		
Mg	43.07	28.23	30.01	23.63	34.39	38.51	28.67	35.25	25.24	14.51	31.13	29.00	32.00	25.00		
Fe	27.60	40.65	40.40	47.35	35.67	32.62	43.00	36.32	45.05	57.25	38.64	41.00	38.00	46.00		
K/Na	0.588	0.925	0.771	0.697	0.603	0.433	0.545	0.581	0.409	0.539	0.467	0.674	0.707	0.787		
Syenite Porphyry								Hybrid Rocks								
	CY55		CY60		CY83		CY25	CY26	CY30		CY33		CY34	CY113a	70.216	CY3
													green	brown		
Na ₂ O	1.98	1.89	2.09	1.50	1.86	2.32	4.04	3.01	2.67	2.67	2.63	3.83	2.69	3.03	2.59	2.02
MgO	10.71	6.67	7.56	9.27	7.19	9.72	7.69	9.80	10.43	9.77	9.50	7.49	7.53	9.86	8.09	8.540
Al ₂ O ₃	13.38	13.13	14.34	13.83	12.35	15.12	11.11	12.19	12.15	12.81	12.62	11.87	12.78	10.40	13.53	14.13
SiO ₂	41.50	40.15	39.55	41.93	40.24	40.90	39.81	39.85	40.45	39.25	39.92	39.15	38.42	42.16	39.64	39.40
K ₂ O	2.13	1.99	1.69	1.76	1.71	1.05	1.76	2.11	1.92	2.22	1.98	1.58	2.08	1.59	1.82	2.12
CaO	11.89	11.25	11.54	11.33	11.25	11.10	10.05	11.03	11.61	11.43	11.56	10.37	10.80	10.47	11.75	12.10
TiO ₂	1.55	1.23	2.62	2.55	1.26	1.82	0.63	1.08	0.85	1.93	2.24	1.00	1.27	1.24	2.09	2.59
MnO	0.34	0.90	0.43	0.32	0.89	-	1.18	0.58	0.46	0.54	0.48	0.56	0.31	0.26	-	-
FeO	16.50	22.80	20.18	17.51	23.24	18.00	23.72	20.36	19.43	19.39	19.09	24.17	24.11	20.94	20.48	19.08
*Total	96.80	96.90	99.25	94.35	98.06	101.09	100.15	98.91	99.70	102.63	102.06	97.41	103.63	101.34	97.47	97.64

Atomic Proportion on basis of 23 oxygen

Na	0.569	0.561	0.611	0.429	0.552	0.665	1.216	0.887	0.782	0.786	0.770	1.150	0.808	0.886	0.760	0.591
Ca	1.890	1.950	1.867	1.795	1.848	1.758	1.669	1.799	1.881	1.859	1.871	1.721	1.792	1.696	1.908	1.954
K	0.403	0.389	0.325	0.332	0.335	0.198	0.348	0.409	0.369	0.429	0.381	0.312	0.412	0.307	0.352	0.407
Total	2.862	2.900	2.803	2.556	2.735	2.621	3.233	3.095	3.032	3.074	3.022	3.183	3.012	2.889	3.020	2.952
Mg	2.369	1.522	1.701	2.042	1.642	2.141	1.778	2.224	2.350	2.210	2.140	1.731	1.737	2.222	1.828	1.918
Fe	2.047	2.112	2.548	2.165	2.978	2.225	3.076	2.593	2.456	2.461	2.412	3.132	3.123	2.646	2.595	2.404
Ti	0.173	0.142	0.297	0.284	0.146	0.202	0.074	0.124	0.097	0.221	0.254	0.117	0.148	0.141	0.239	0.293
Al	0.495	0.513	0.522	0.608	0.398	0.681	0.204	0.255	0.280	0.251	0.279	0.232	0.284	0.225	0.422	0.446
Mn	0.043	0.117	0.054	0.040	0.116	-	0.154	0.075	0.060	0.070	0.061	0.073	0.041	0.034	-	-
Total	5.127	4.406	5.122	5.139	5.280	5.249	5.286	5.271	5.243	5.213	5.146	5.275	5.333	5.268	5.084	5.061

TABLE III-8 (continued)

Al	1.844	1.855	2.030	1.802	1.833	1.953	1.827	1.932	1.885	2.041	1.969	1.935	2.050	1.628	1.994	2.064
Si	6.156	6.145	5.970	6.198	6.167	6.047	6.173	6.068	6.115	5.959	6.031	6.065	5.950	6.372	6.006	5.936
O	23.000	23.000	23.000	23.000	23.000	23.000	23.000	23.000	23.000	23.000	23.000	23.000	23.000	23.000	23.000	23.000
Total cations	16.219	15.306	15.925	15.695	16.015	15.870	16.519	16.366	16.275	16.287	16.168	16.458	16.345	16.157	16.104	16.013
Ca	29.97	34.92	30.53	29.91	28.57	28.71	25.59	27.19	28.13	28.47	29.13	26.14	26.94	25.84	30.14	31.13
Mg	37.57	27.26	27.81	34.02	25.39	34.96	27.26	33.62	35.14	33.84	33.32	26.29	26.11	33.85	28.87	30.56
Fe	32.46	37.82	41.66	36.07	46.04	36.33	47.16	39.19	36.73	37.69	37.55	47.57	46.95	40.31	40.99	38.30
K/Na	0.708	0.693	0.532	0.774	0.607	0.286	0.461	0.472	0.546	0.495	0.208	0.510	0.347	0.463	0.463	0.689

Amphibolite Inclusions

	x54			x55			x60-core				x60-rim					
Na ₂ O	2.41	1.95	1.78	1.91	1.98	2.43	2.14	2.29	2.05	2.36	1.82	1.68	1.54	1.68	1.79	1.62
MgO	9.84	9.45	9.40	10.50	10.35	12.90	11.26	12.39	12.77	11.76	13.36	11.71	10.71	11.38	10.40	12.17
Al ₂ O ₃	13.81	14.11	13.55	12.28	12.74	13.64	13.06	13.74	12.53	14.42	11.07	14.42	13.57	13.43	14.63	12.74
SiO ₂	41.47	41.84	42.06	42.72	42.18	41.12	43.00	43.36	44.45	42.66	46.36	42.98	42.74	43.36	41.93	44.73
K ₂ O	1.17	1.60	1.45	1.48	1.63	1.58	1.36	0.87	1.12	1.12	0.71	1.60	1.64	1.31	1.39	0.88
CaO	11.50	11.56	11.60	11.53	11.50	11.56	11.66	11.80	11.87	11.77	12.15	12.16	11.85	11.87	11.89	11.95
TiO ₂	0.78	0.62	0.72	0.87	1.03	2.02	0.98	0.62	0.58	0.63	0.70	0.73	1.08	0.85	1.03	0.72
MnO	0.32	-	-	-	0.39	-	0.30	0.32	0.28	0.27	-	-	0.37	0.40	0.39	0.36
FeO	19.09	18.85	19.45	18.71	18.20	14.78	16.24	14.63	14.33	15.00	13.84	14.72	16.48	15.70	16.57	14.83
Total	92.15	97.51	97.92	96.23	95.31	96.30	97.59	96.65	96.79	97.64	93.57	93.56	95.89	94.17	94.19	93.47

Atomic Proportion on basis of 23 oxygen

Na	0.698	0.563	0.514	0.551	0.571	0.691	0.610	0.646	0.576	0.667	0.507	0.476	0.438	0.477	0.512	0.454
Ca	1.838	1.841	1.850	1.834	1.832	1.818	1.834	1.836	1.843	1.839	1.870	1.897	1.867	1.858	1.875	1.854
K	0.222	0.304	0.275	0.281	0.308	0.296	0.255	0.161	0.207	0.208	0.130	0.298	0.207	0.245	0.260	0.162
Total	2.758	2.708	2.639	2.666	2.711	2.805	2.699	2.643	2.626	2.714	2.50	2.671	2.612	2.580	2.647	2.470

TABLE III-8 (continued)

Mg	2.109	2.094	2.086	2.323	2.293	2.823	2.465	2.683	2.760	2.556	2.863	2.540	2.348	2.478	2.281	2.627
Fe	2.381	2.343	2.421	2.323	2.263	1.815	1.994	1.777	1.738	1.830	1.664	1.792	2.027	1.918	2.039	1.796
Ti	0.088	0.620	0.080	0.097	0.116	0.223	0.109	0.067	0.064	0.070	0.076	0.080	0.120	0.093	0.114	0.078
Al	0.605	0.692	0.637	0.492	0.504	0.395	0.574	0.652	0.586	0.701	0.536	0.730	0.636	0.650	0.707	0.651
Mn	0.041	-	-	-	0.049	-	0.037	0.040	0.035	0.034	-	-	0.047	0.050	0.048	0.044
Total	5.224	5.749	5.224	5.235	5.225	5.256	5.179	5.219	5.183	5.191	5.139	5.142	5.178	5.189	5.189	5.196
Al	1.823	1.781	1.740	1.657	1.728	1.965	1.686	1.700	1.555	1.778	1.339	1.744	1.715	1.646	1.830	1.523
Si	6.177	6.219	6.260	6.343	6.272	6.035	6.314	6.300	6.445	6.222	6.661	6.256	6.285	6.336	6.170	6.477
Total	8.000	8.000	8.000	8.000	8.000	8.000	8.000	8.000	8.000	8.000	8.000	8.000	7.982	8.000	8.000	8.000
O	23.000	23.000	23.000	23.000	23.000	23.000	23.000	23.000	23.000	23.000	23.000	23.000	23.000	23.000	23.000	23.000
Total cations	15.982	16.457	15.863	15.901	15.936	16.061	15.878	15.862	15.809	15.905	15.646	15.813	15.790	15.769	15.836	15.666
Ca	29.05	29.32	29.10	28.30	28.68	28.16	29.14	29.16	29.06	29.54	29.23	30.45	29.91	29.71	30.27	29.54
Mg	33.33	33.35	32.81	35.85	35.90	43.73	39.17	42.16	43.53	41.06	44.76	40.78	37.62	39.62	36.82	41.85
Fe	37.63	37.32	38.08	35.85	35.43	28.11	31.69	28.22	27.41	29.40	26.01	28.77	32.47	30.67	32.91	28.61
K/Na	0.318	0.540	0.535	0.521	0.539	0.428	0.418	0.249	0.359	0.312	0.256	0.626	0.701	0.514	0.508	0.357
Hornblende Porphyry							Experiment T541					x60+	CY5+	CY91+		
Na ₂ O	2.05	1.87	2.02	1.70	1.71	2.05	1.86	2.02	2.21	1.79	2.01	1.54	1.54	1.33		
MgO	7.59	7.25	7.49	6.68	5.97	12.02	12.93	12.73	11.31	6.58	9.85	10.79	8.75	6.91		
Al ₂ O ₃	14.34	14.38	14.36	14.66	15.02	13.45	12.17	12.75	15.32	16.93	15.91	12.70	12.46	13.91		
SiO ₂	37.56	36.88	37.03	37.07	36.34	43.90	47.02	46.60	42.21	53.80	46.21	43.26	34.90	36.76		
K ₂ O	2.92	3.05	3.02	2.98	3.10	1.40	0.84	1.04	0.95	1.26	1.16	1.35	1.84	3.04		
CaO	11.46	11.47	11.40	11.42	11.31	11.59	11.45	11.73	11.54	9.30	10.66	14.20	11.33	11.71		
TiO ₂	2.45	2.40	2.52	2.40	2.10	0.68	0.57	0.72	0.67	0.42	0.63	0.72	2.36	2.14		
MnO	0.41	0.46	0.41	0.45	0.37	-	-	0.30	0.28	-	-	0.37	0.34	0.52		
FeO	21.23	22.24	21.72	22.63	24.07	14.91	13.17	14.10	15.50	9.91	13.60	11.56	12.23	-		
Fe ₂ O ₃												3.54	10.96	23.09		
Total	97.03	97.80	96.94	97.10	96.39	93.09	93.40	97.17	96.49	96.66	94.11	100.03	98.58	101.53		

TABLE III-8 (continued)

Atomic Proportion on basis of 23 oxygen														
Na	0.610	0.562	0.605	0.509	0.518	0.577	0.514	0.567	0.625	0.474	0.554	0.436	0.470	0.403
Ca	1.887	1.902	1.885	1.892	1.889	1.804	1.749	1.817	1.804	1.359	1.626	2.219	1.911	1.959
K	0.571	0.602	0.595	0.587	0.616	0.259	0.153	0.191	0.177	0.220	0.210	0.251	0.370	0.606
Total	3.068	3.066	3.085	2.988	3.023	2.640	2.416	2.575	2.606	2.053	2.390	2.906	2.751	2.968
Mg	1.739	1.672	1.724	1.540	1.387	2.604	2.749	2.745	2.458	1.337	2.089	2.347	2.054	1.610
⁵⁶ Fe	2.728	2.879	2.802	2.926	3.139	1.812	1.571	1.705	1.890	1.129	1.618	1.410	1.610	3.354
Ti	0.283	0.280	0.292	0.279	0.246	0.075	0.061	0.078	0.073	0.043	0.068	0.079	0.279	0.251
Al	0.368	0.330	0.325	0.404	0.428	0.682	0.750	0.624	0.790	2.051	1.245	0.495	1.298	0.307
Mn	0.054	0.061	0.054	0.059	0.049	-	-	0.036	0.035	-	-	0.046	0.045	0.069
Total	5.172	5.222	5.197	5.208	5.249	5.173	5.131	5.188	5.246	4.560	5.020	4.377	3.983	5.591
Al	2.229	2.293	2.287	2.268	2.333	1.622	1.295	1.550	1.845	0.668	1.424	1.688	2.312	2.255
Si	5.771	5.707	5.713	5.732	5.667	6.378	6.705	6.450	6.155	7.332	6.576	6.312	5.495	5.745
Total	8.000	8.000	8.000	8.000	8.000	8.000	8.000	8.000	8.000	8.000	8.000	8.000	8.000	8.000
O	23.000	23.000	23.000	23.000	23.000	23.000	23.000	23.000	23.000	23.000	23.000	23.000	23.000	23.000
Total cations	16.240	16.288	16.282	16.196	16.272	15.813	15.547	15.763	15.852	14.613	15.410	15.283	15.844	16.559
Ca	29.70	29.47	29.40	29.76	29.45	29.00	28.82	28.99	29.32	35.33	30.49			
Mg	27.37	25.91	26.89	24.22	21.62	41.86	45.30	43.80	39.95	34.95	39.17			
Fe	42.93	44.61	43.71	46.02	48.93	29.13	25.89	27.21	30.72	29.52	30.34			
K/Na	0.94	1.071	0.983	1.153	1.189	0.449	0.298	0.337	0.283	0.464	0.379			

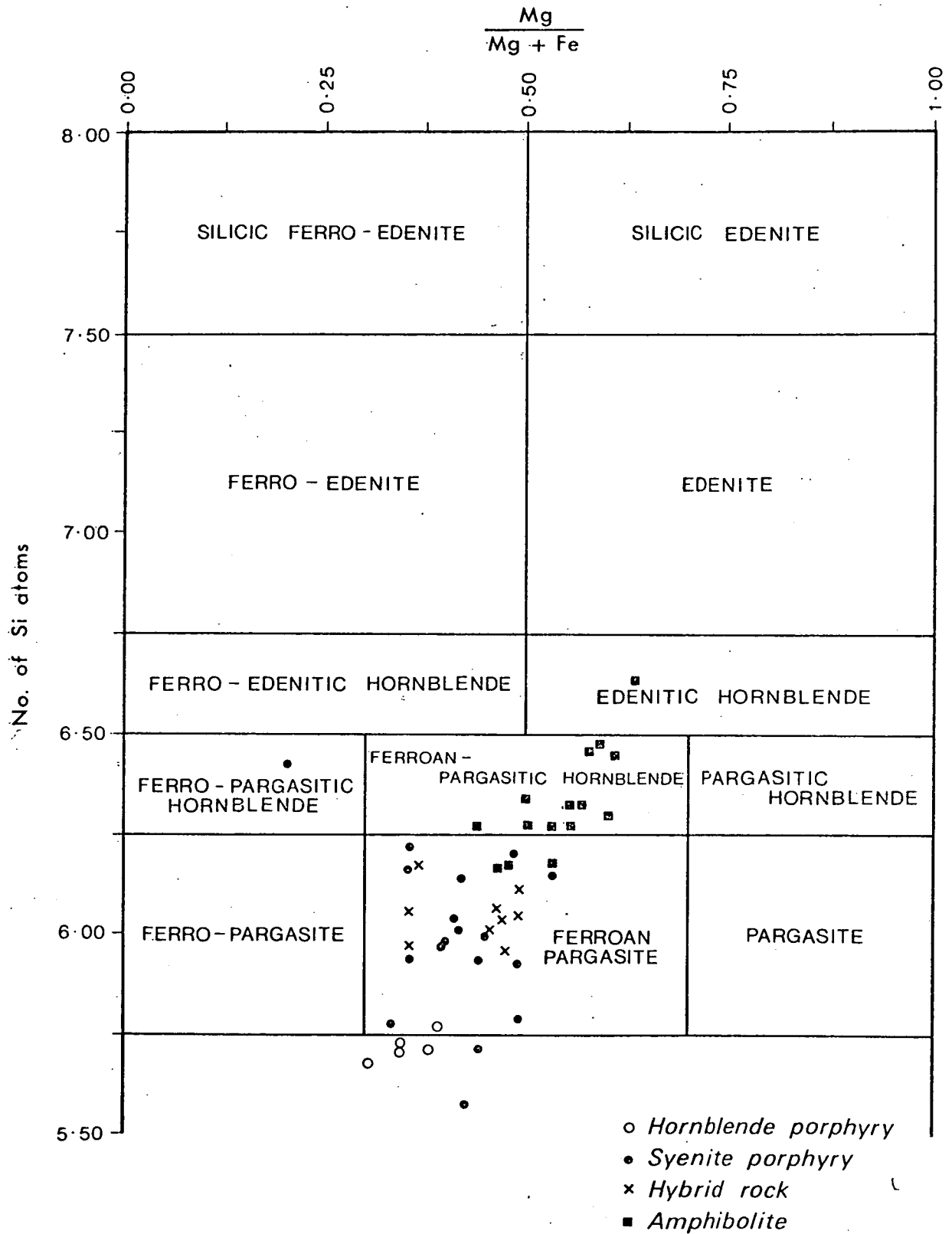


Figure III-9 Plot of amphibole compositions superimposed on nomenclature recommended by the International Mineralogical Association (from Leake, 1978).

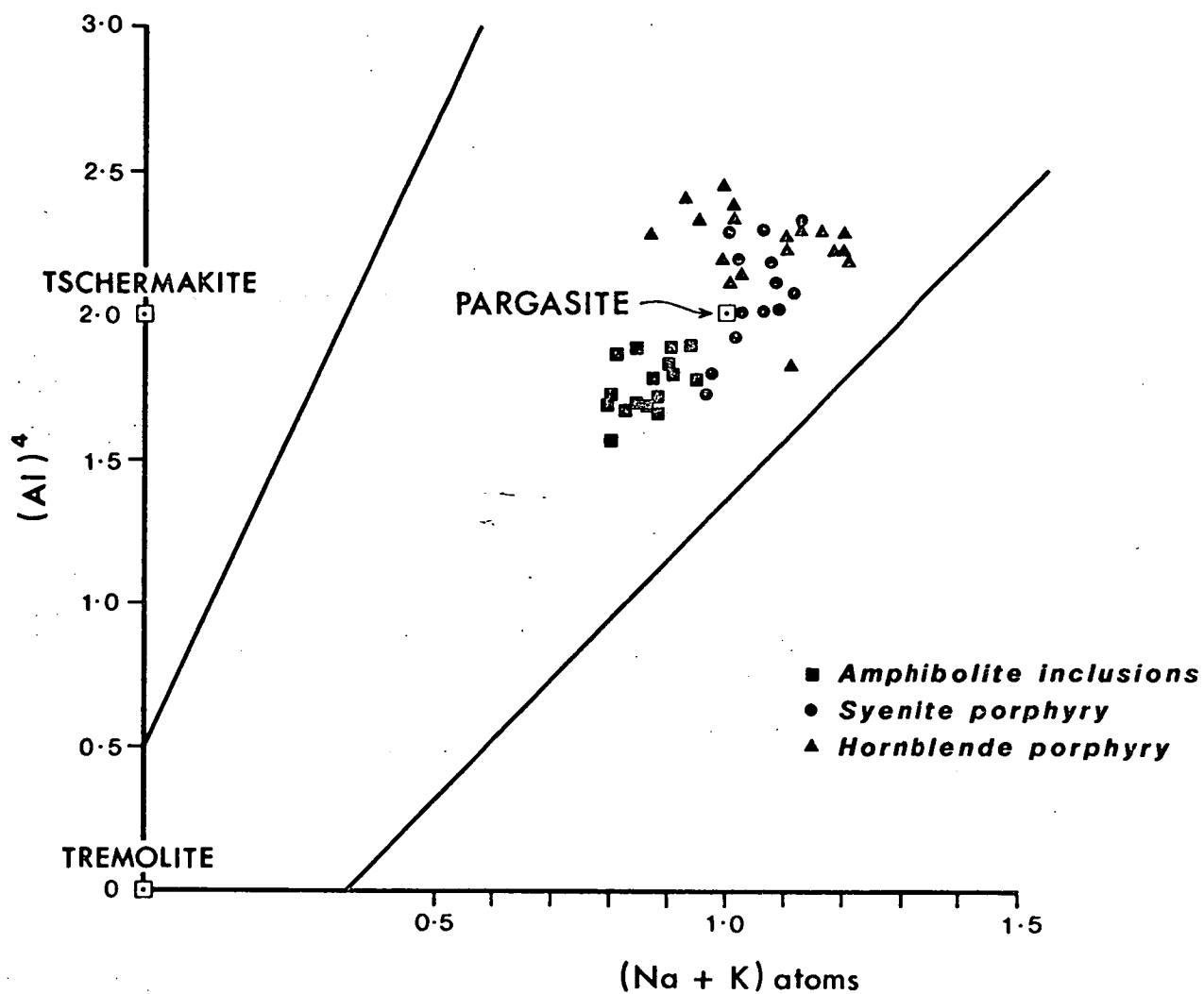
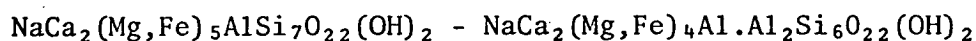


Figure III-10 Tetrahedral Al-alkali metal plot for amphiboles in amphibole-bearing rocks.

The most obvious features shown by the analyses are that all amphiboles are closely related to the pargasite molecule as defined by Leake (1977) and shown in Figure III-9 in terms of Mg-Fe-Si, and in Figure III-10 in terms of tetrahedral Al and alkali metal atoms. Except for some amphiboles within the hybrid zone of alteration the amphiboles from both the igneous rocks and metamorphic inclusions, with very few exceptions, are members of the calcic amphibole chemical group as defined by the International Mineralogical Association subcommittee on Amphiboles (Leake 1978). The main compositions are covered by the end member molecules from edenite-ferroedenite to pargasite-ferropargasite thus:



edenite-ferroedenite

pargasite-ferropargasite

with most lying in the ferropargasite field.

The oxidation state of the iron is not available for the probe results. However from the FeO values for the X.R.F. analyses of the amphibole (Table III-8) obtained independently using the method of Shapiro (1960) it is clear that should the $\left(\frac{\text{Mg}}{\text{Mg}+\text{Fe}}\right)$ ratio increase for most samples, they would still essentially lie within the ferroan pargasite field. The trend indicated by the analyses of the amphiboles is towards an increase in the amount of iron oxides (Fig. III-9) in the minerals and possibly also to an increased amount of oxidized iron (Fe_2O_3).

While all amphiboles are essentially pargasite there are some differences apparent within the group. The first is that the amphibolite minerals have less tetrahedral and more octahedral aluminium than the syenite porphyry consistent with Leake's (1965) observation that metamorphic amphiboles usually have greater octahedral aluminium than their

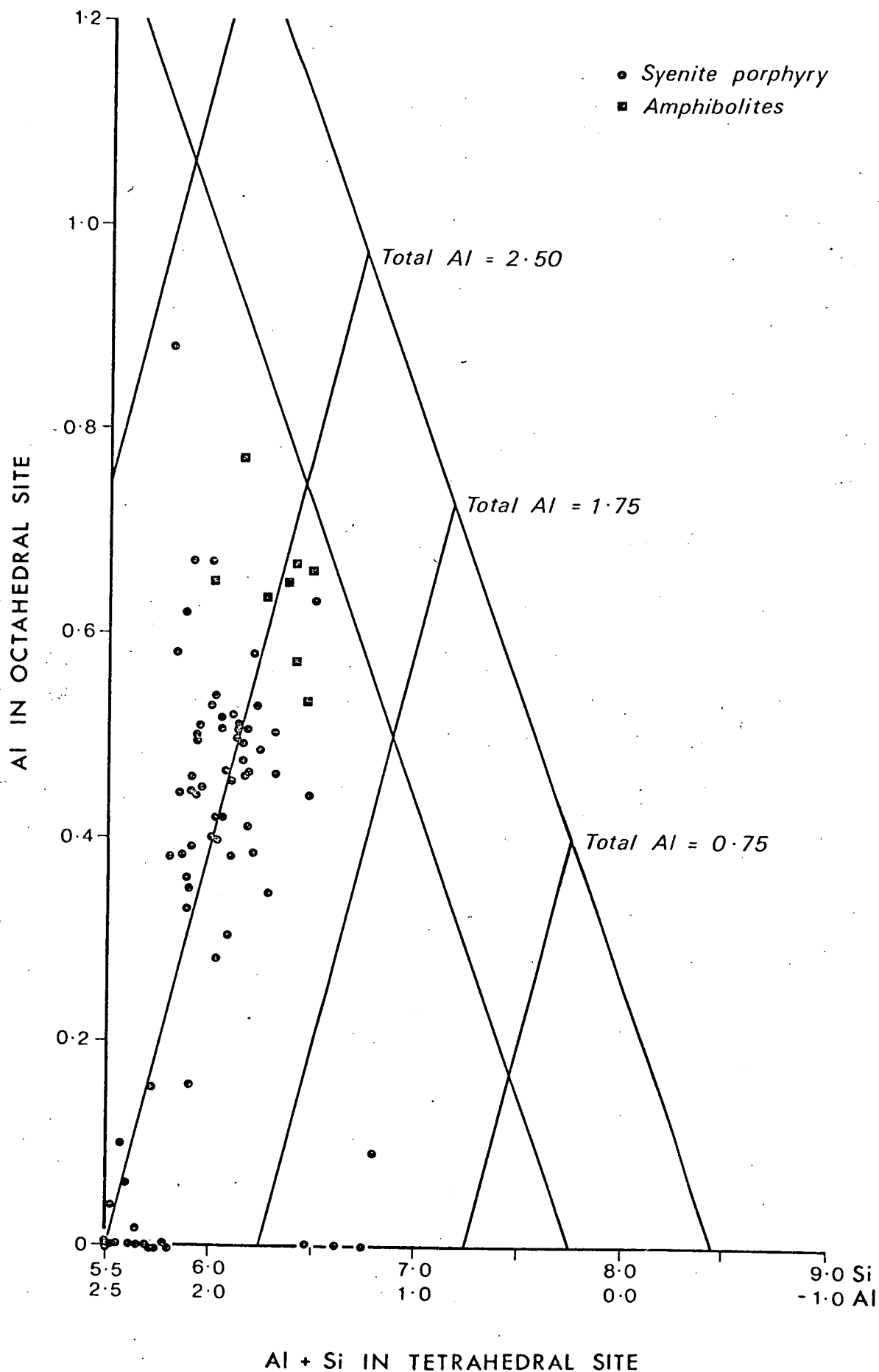


Figure III-11 Site occupancy of Al in the amphibolite amphiboles and syenite porphyry. After Leake (1964).

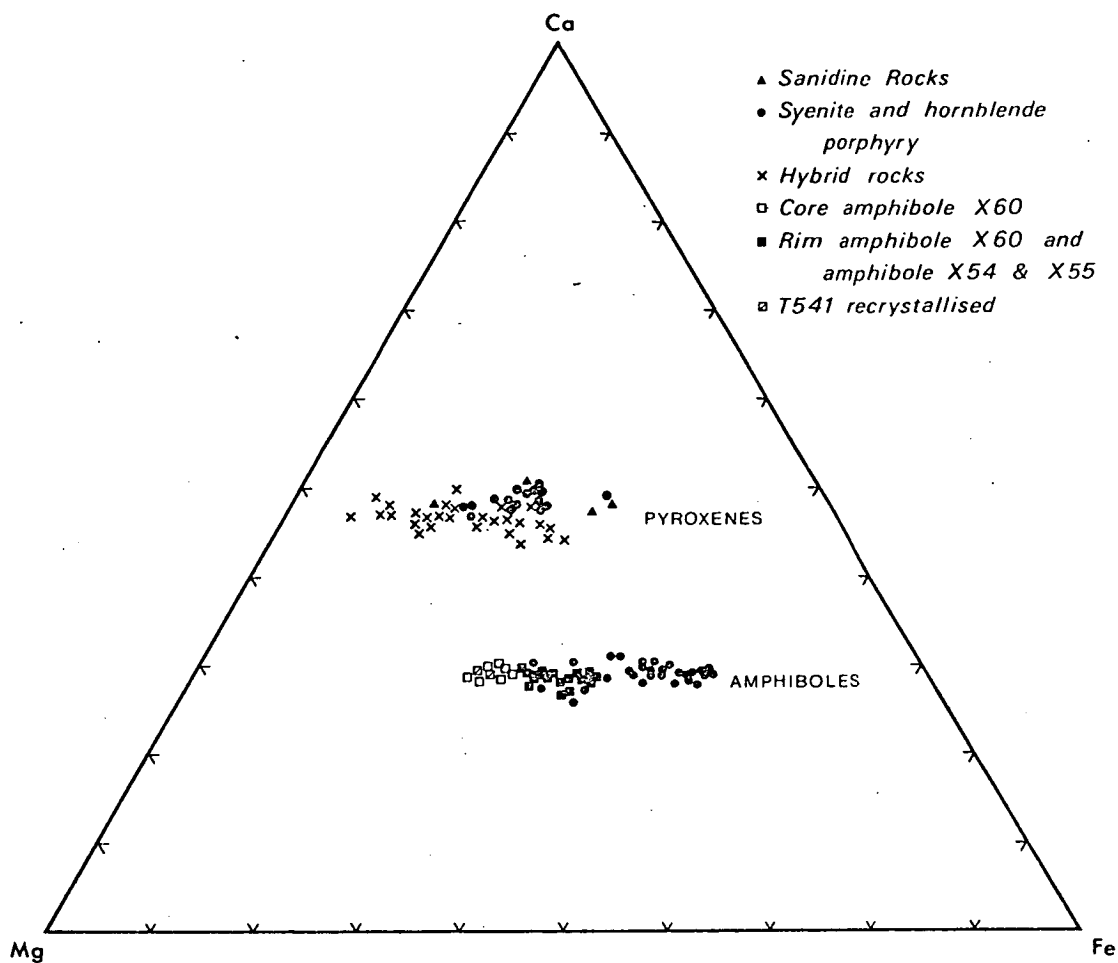


Figure III-12 Ca-Mg-Fe plot for amphiboles and pyroxenes of all rocks. Core and rim compositions are for minerals from amphibolite inclusions. T541 represents amphibole from an inclusion recrystallized at 8 kb p_{H_2O} and 800°C.

igneous counterparts. The distributions are shown on a Leake plot (Fig. III-11). This follows because the metamorphic minerals are more silica-saturated than their igneous counterparts. Nockolds and Mitchell (1948) suggested that amphiboles formed at higher temperatures have greater substitution of silicon by aluminium and this also appears to be the case for these minerals with the amphibolite minerals having least aluminium replacing silicon.

The recrystallized inclusions (X54, X55), and the recrystallized rim amphiboles (of X60) have a higher content of iron than the core amphiboles of the amphibolite inclusion (X60), Table III-8. They would have recrystallized and may have been in equilibrium with the molten feldspathic groundmass from the original amphibolite. The distribution for the inclusions is plotted in Figure III-12 where the iron enrichment can be observed and compared with the syenite and hornblende porphyry minerals.

From the information in Fig. III-12 there appears to be a trend of iron enrichment between the amphiboles of the amphibolite inclusions and those of the hornblende porphyry (described in Chapters I and II) via the intermediate syenite porphyry.

A further similar relationship is shown in Fig. III-13 where there is a trend in potassium enrichment from the amphibolite inclusion amphiboles, through those of the syenite porphyries to the hornblende porphyry phenocrysts. This suggests that the amphibolite amphiboles could have been incorporated in and modified by the alkaline melt. There is no reaction relationship between the inclusions and incoming magma, although as shown earlier there is recrystallization of the rim amphibole.

As part of the problem of determining the origin of the Port Cygnet alkaline rocks, an amphibolite inclusion from the Mt. Windsor outcrop was re-equilibrated at 8 kbars P_{H_2O} and 800°C in a Boyd-

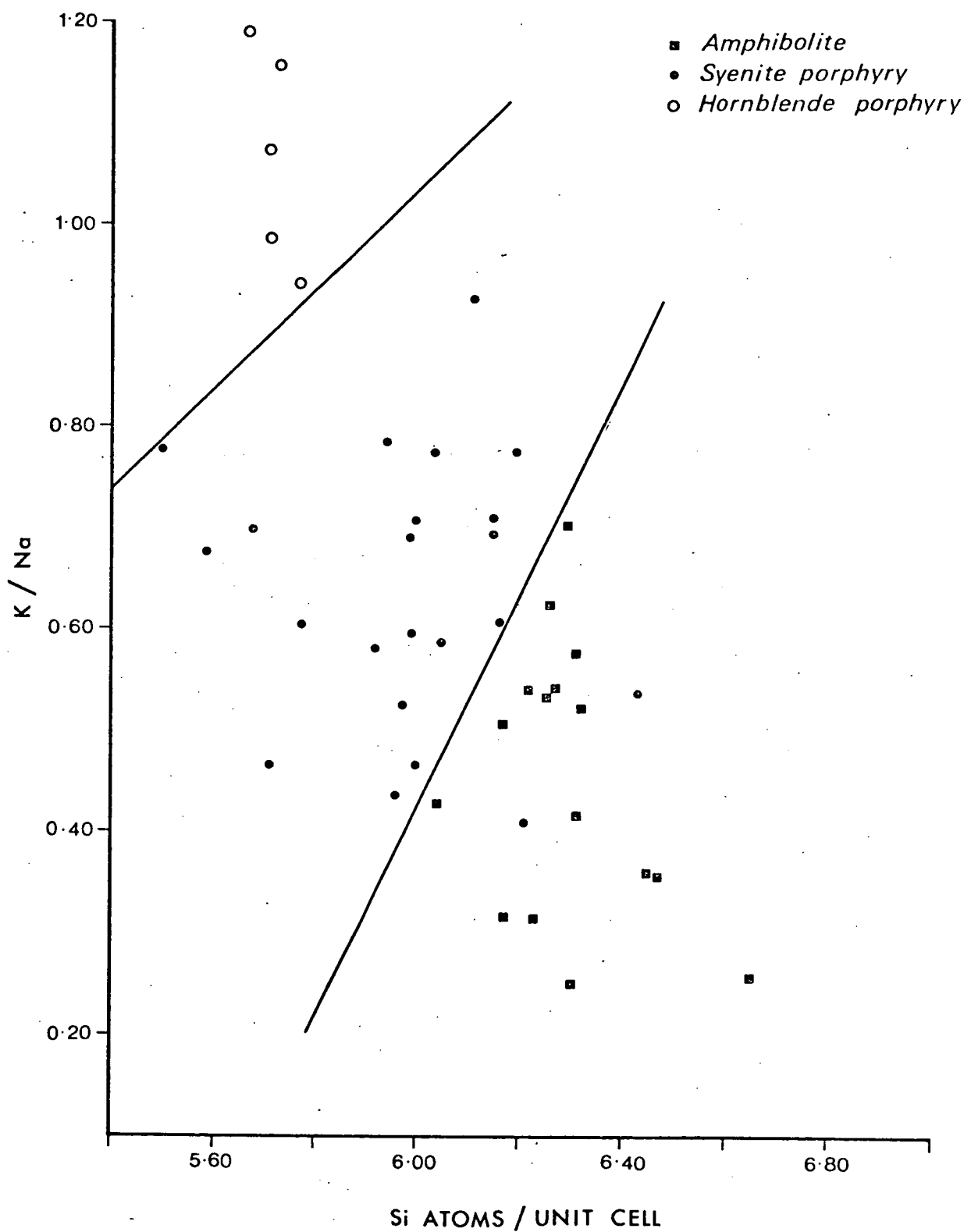


Figure III-13 The variation of K/Na and Si atoms for amphiboles from amphibolite inclusions, syenite porphyry and hornblende porphyry.

England high pressure apparatus. These conditions were considered the lowest P and T at which equilibrium would be reached within a few days. The composition of the recrystallized amphiboles are presented in Table III-8 for experiment No. T541, High Pressure Laboratory, University of Tasmania. These can then be compared with those of the original inclusion (X60, X54 and X55) and those of the hornblende-bearing rocks CY2 and CY91 in Fig. III-12.

The results (Figs. III-12 and III-13) suggest a relationship between the amphiboles of the amphibolite inclusions and those of the syenite porphyry and particularly the hornblende porphyry where the interpretation may be that amphiboles from the parent amphibolite were recrystallized and re-equilibrated to produce the phenocrysts in the latter rock leading to a progressive enrichment in iron and the K/Na ratio.

The amphiboles of the Port Cygnet rocks are ferroan pargasites (Fig. III-9) and as such represent a general association with many basaltic rocks. With higher temperatures of formation there is a greater substitution of Si by Al, and with the incorporation of sodium the thermal stability of the mineral increases. Thus tremolite with no included sodium has the lowest thermal stability of the Ca-amphiboles, but with increase in sodium thermal stability may increase to a maximum in richterite and potassium richterite (Gupta and Yagi, 1980).

Amphibole stability data have been summarised by Merrill and Wyllie (1975). They concluded that between 10 kb and 20 kb amphiboles are stable at higher temperature with greater TiO_2 but break down at lower temperatures with increasing SiO_2 and $\text{Na}_2\text{O}/(\text{Na}_2\text{O} + \text{K}_2\text{O})$ ratios.

Amphiboles show characteristic stability fields with a high pressure limit around 30 kb and a thermal maximum around 1100°C which are much

greater than probable conditions at Port Cygnet where a pressure of 7 kb is regarded as the limiting value and no evidence of thermal breakdown of the amphiboles in the rocks.

Gilbert (1969) established that pargasite was stable in the range 800°C-900°C at 20 kb. In the presence of CO₂ and H₂O, Holloway (1973) found the decomposition temperature of pargasite to be 1042°C at 4.5 kb and 1053°C at 7.5 kb. Oba (1980) has investigated the tremolite-pargasite join of the hornblende molecule. At 5 kb tremolite and pargasite form a continuous solution series above 800°C and at 1 kb exsolution occurs at 80 mol. percent pargasite at 850°C and expands to 90 mol. percent pargasite at temperatures below 800°C. With addition of Fe²⁺ the thermal stability is reduced. With $\text{Fe}^{2+}/(\text{Fe}^{2+} + \text{Mg}^{2+}) = 0.2$ there is a gap between actinolite 85 pargasite 15 and actinolite 45 pargasite 55 at 700°C and 1 kb-however at higher pressures and temperatures the miscibility gap appears to close but further data are required. The relationships of Fe/Mg and Fe³⁺ have still to be established experimentally. The Port Cygnet amphiboles lie well away from the tremolite end member (Fig. III-10) and close enough to pargasite to be clear of any exsolution field.

The experimental work of Holloway (op. cit.) would put a maximum stability temperature for pargasite from the Port Cygnet rocks. With an addition of iron, which is so with the rocks investigated, the stability will fall. It would be reasonable to assume that the amphiboles from the Port Cygnet alkaline rocks never exceeded 1000°C and formed at a somewhat lower figure which would be closely related to the amount of iron substitution and the fO₂ of the system during the amphibole crystallization.

The stability of ferropargasite has been summarized by Ernst (1968) and Gilbert (1966) who shows that fO₂ and water pressure are very important parameters in determining the formation of this mineral. Pure pargasite

has a maximum stability temperature of approximately 1050° at 1.5 kb. Pure ferroan pargasite is very fO_2 sensitive, but if the Wones-Eugster data for the hybrid rocks are applicable then the maximum temperature would be about 650°C at 2 kb. Thus a rough estimate for the maximum stability temperature for the Port Cygnet hornblendes might be about 850°C.

PYROXENE MINERALOGY

As with the amphiboles, and for similar reasons, pyroxenes are not abundant in the syenite porphyry. They are somewhat more common in the sanidine rocks, where the groundmass of the tinguaites contains abundant needles of aegirine having a minimal range of composition, and occasional larger crystals of sodium-bearing salitic pyroxenes. Inclusions of salitic pyroxenes occur in the hornblende porphyry rocks (CY2 and CY91). Diopsidic-salitic pyroxenes and aegirine-augites also occur in the hybrid rocks as derivatives from the alteration of the dolerite. All pyroxenes are clinopyroxene with no evidence of orthopyroxene.

The Ca-Mg-Fe compositions are shown in Figure III-12 where not all hybrid analyses have been shown for clarity of plotting. The feature of these is the very restricted range of composition for the syenite porphyries and the hybrid rocks; where the compositions fall almost exclusively into the salite field as defined by Poldervaart and Hess (1951) (Fig. III-14). It is not possible to determine if the pyroxenes of all the syenite porphyries are direct primary crystallates. In the case of CY2 the pyroxene occurs as an inclusion and has the same composition of pyroxenes in the mottled zones of CY91 where it appears to be part of a disrupted previously existing material (Pl. 25). The compositions of these can be compared in Table III-9. In these two rocks, at least the pyroxene has been derived from some other source,

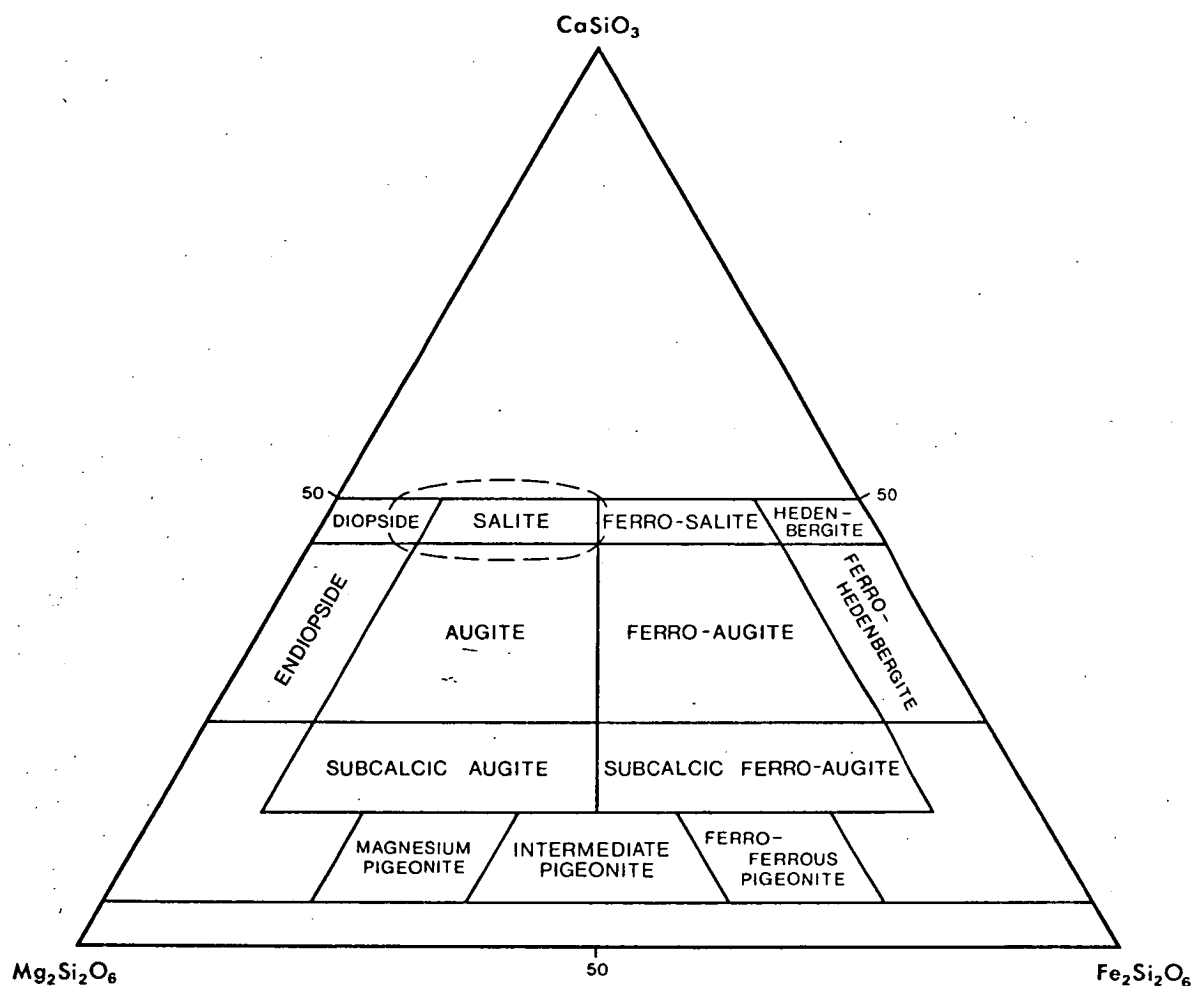


Figure III-14 The main compositional field of pyroxenes for all rocks superimposed on the pyroxene nomenclature scheme of Poldervaart & Hess (1951).

possibly related to the amphibolite inclusions noted elsewhere. These also have significantly greater alumina compositions than the other pyroxenes. In the other alkaline rocks the compositions are quite similar but still appear to be part of the normal crystallization sequence. Most of the pyroxenes have less than 5% Al_2O_3 content, those with higher contents may represent higher temperatures of formation

(Deer, Howie and Zussman, Vol. 2a, p.235), higher alumina in source melt or perhaps a higher pressure environment.

The occasional pyroxenes in the sanidine rocks are sodium-bearing salites. These have been included in Fig. III-11, where the effect of sodium, which replaces calcium in the M2 site is to cause the apparent composition in the standard pyroxenes quadrilateral to be pushed towards the ferrosalite field. For this exercise aegirine-augite is defined with a soda content greater than 2.00% Na_2O , distinct yellow-green pleochroism and has the smaller extinction angle between the 110 cleavage, on the 010 section, and the fast ray.

While most of the pyroxenes of the alkaline igneous rocks are dominated by the salite composition indicated on the appropriate diagram (Fig. III-14), there is always a significant amount of soda present, and some may approach an aegirine-augite composition. In order to show this, the pyroxene compositions have been replotted on a diopside (Di)-hedenbergite (Hd)-Acmite (Ac) triangle (Fig. III-16), where those from both the syenite porphyry and sanidine rocks are shown in the appropriate symbols. The relatively low pyroxenes in the syenite porphyry can be compared with the pyroxenes from a xenolith in CY2 and the clots of disseminated pyroxene fragments of CY91. As can be seen from Fig. III-16 there is overlap in the compositions of the pyroxenes in this system with perhaps a tendency for the minerals from the potash-rich rocks to contain a small extra amount of soda. This plot indicates that the pyroxenes for all of these rocks are very similar and probably had the same origin with those of CY91 probably representing fragmented pyroxenes brought in with the later potassium-rich magma. On the plot are also

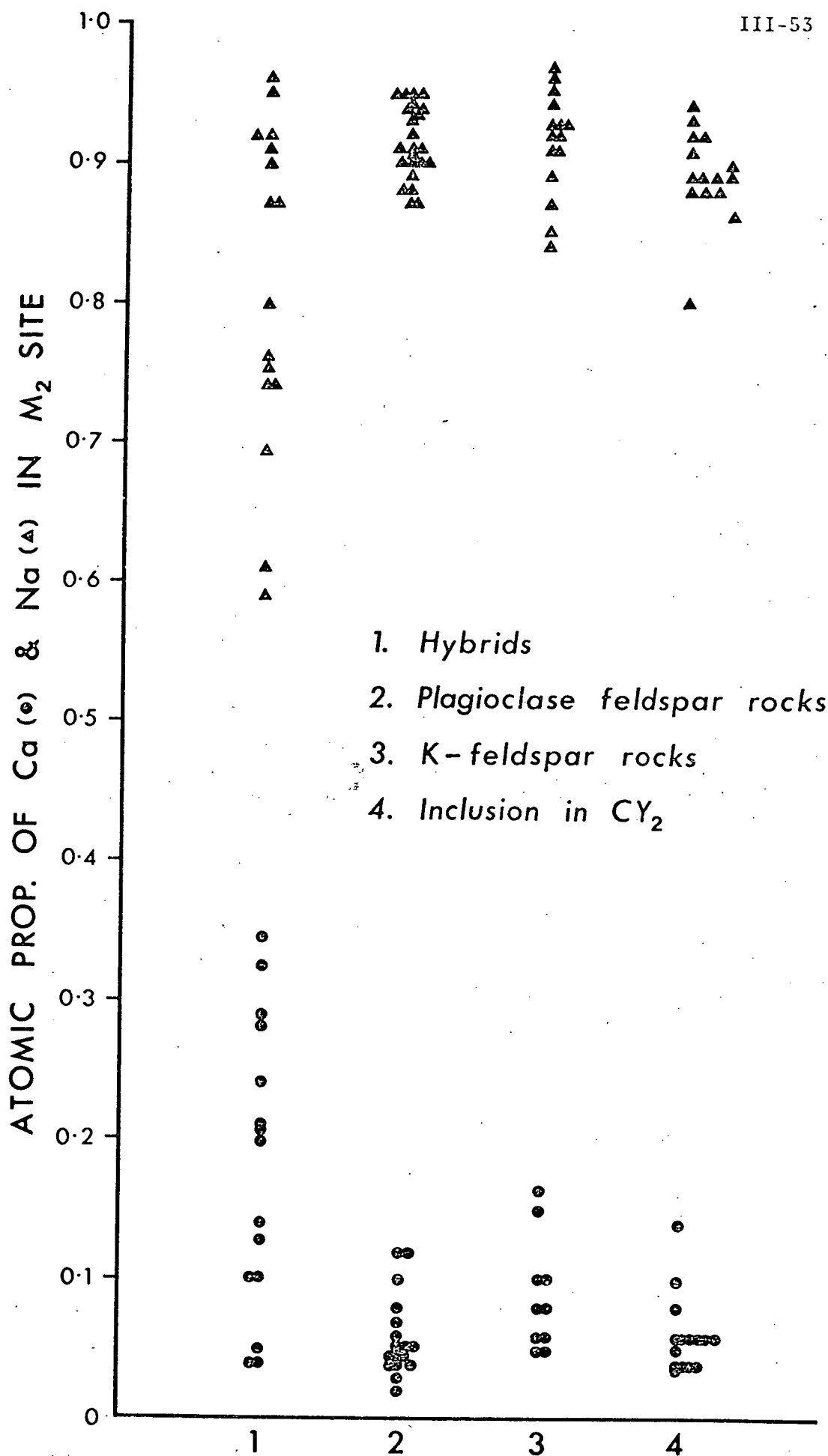


Figure III-15 Replacement of Ca by Na in pyroxenes, particularly in those from the hybrid rocks.

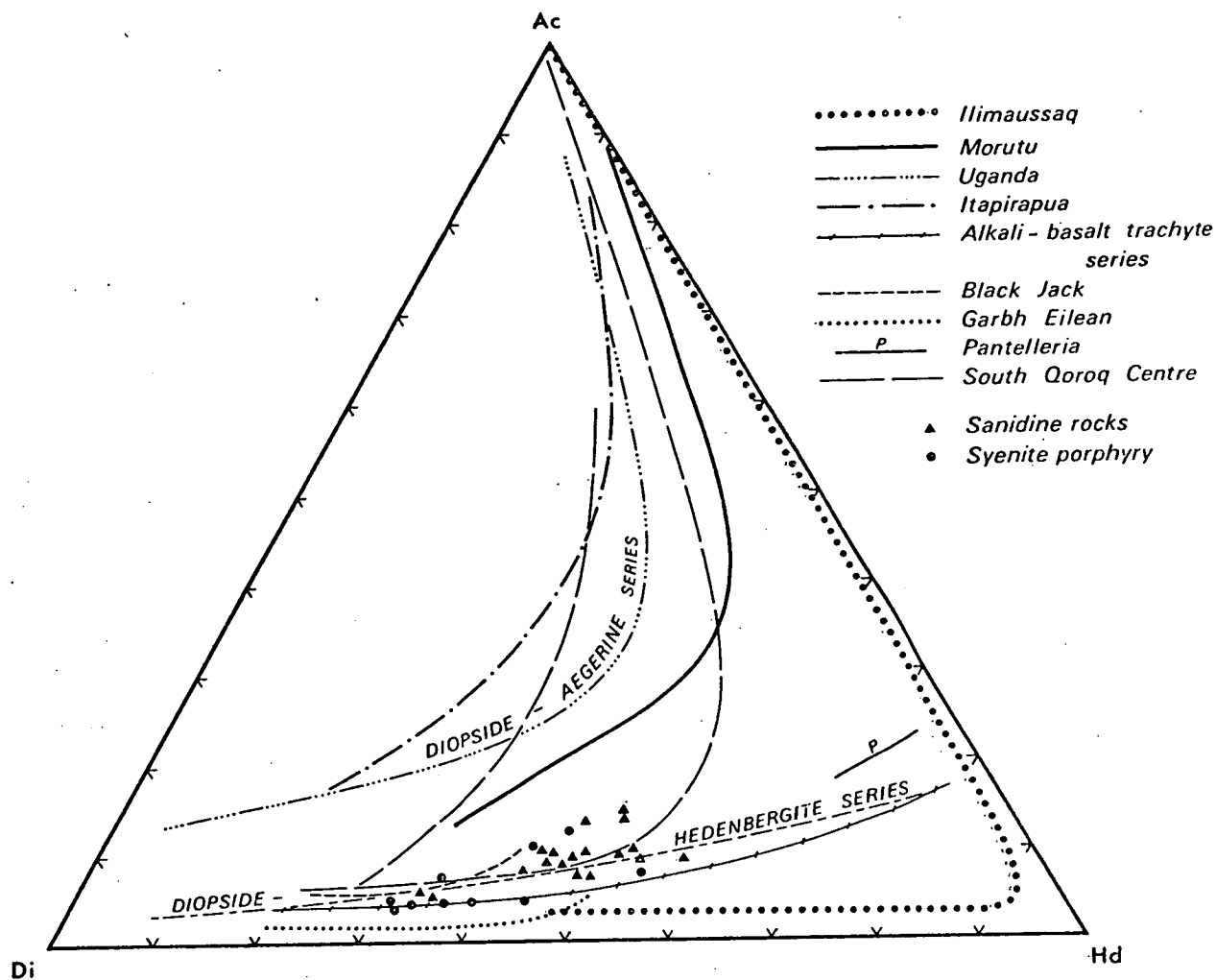


Figure III-16 Di-Hd-Ac molecular plot of pyroxenes from Port Cygnet rocks. The comparative trends have been taken from Tyler & King (1967), Stephenson (1972) and Larsen (1976).

TABLE III-9

Some electron microprobe analyses of pyroxenes

* un-normalized totals

+ X.R.F. analysis

Sanidine Porphyries - Green Groundmass

Na ₂ O	0.25	0.65	0.70	0.80	0.55	1.06	0.70	0.47	0.00	0.00	0.00	0.51
MgO	11.44	10.61	11.14	10.60	11.41	10.28	10.25	14.67	14.39	15.27	15.79	13.94
Al ₂ O ₃	0.42	0.96	0.57	0.45	1.10	1.87	1.19	1.47	2.46	1.11	1.85	4.33
SiO ₂	52.09	52.65	51.75	51.90	51.85	51.26	51.58	54.06	51.83	52.80	52.80	51.19
K ₂ O	-	-	-	-	-	-	-	-	-	-	-	0.43
CaO	23.19	21.31	22.15	21.98	22.15	21.38	21.62	23.69	22.78	28.83	22.77	11.97
TiO ₂	-	-	-	-	-	-	-	-	0.42	0.37	0.33	0.81
MnO	0.23	1.15	0.76	0.70	1.18	1.21	1.32	-	-	-	-	-
FeO	12.28	12.66	12.93	13.56	11.49	12.94	13.34	5.63	8.09	6.61	16.66	6.47
*Total	100.71	100.34	99.82	100.07	100.60	100.00	101.30	99.50	99.00	99.39	101.90	98.70

Atomic proportions on basis of 6 oxygen

Ca	0.946	0.868	0.907	0.902	0.902	0.875	0.887	0.933	0.907	0.946	0.899	0.482
Na	0.018	0.048	0.052	0.059	0.040	0.078	0.052	0.033	-	-	-	0.037
K	-	-	-	-	-	-	-	-	-	-	-	0.021
Total	0.964	0.916	0.959	0.961	0.942	0.953	0.939	0.966	0.907	0.946	0.899	0.540
Mg	0.650	0.601	0.635	0.605	0.646	0.585	0.585	0.804	0.797	0.843	0.867	0.781
Fe	0.391	0.402	0.413	0.434	0.365	0.413	0.427	0.173	0.251	0.205	0.199	0.524
Mn	0.007	0.037	0.025	0.023	0.037	0.039	0.043	-	-	-	-	-
Ti	-	-	-	-	-	-	-	-	0.011	0.010	0.009	0.023
Al	0.003	0.043	0.004	0.007	0.020	0.043	0.028	0.051	0.034	0.005	0.138	0.005
Total	1.051	1.083	1.077	1.069	1.068	1.080	1.083	1.028	1.093	1.063	1.213	1.333
Al	0.016	0.000	0.022	0.013	0.029	0.041	0.025	0.012	0.073	0.044	0.054	0.075
Si	1.984	2.001	1.978	1.987	1.971	1.959	1.975	1.988	1.927	1.956	1.946	1.925
Total	2.000	2.001	2.000	2.000	2.000	2.000	2.000	2.000	2.000	2.000	2.000	2.000
O	6.000	6.000	6.000	6.000	6.000	6.000	6.000	6.000	6.000	6.000	6.000	6.000

TABLE III-9 (continued)

Total cations	4.015	4.000	4.036	4.030	4.010	4.033	4.022	3.994	4.000	4.009	4.112	3.873
Ca	47.61	46.39	46.39	46.47	47.14	46.70	46.70	48.84	46.38	47.44	34.73	26.97
Mg	32.71	32.12	32.48	31.17	33.78	31.24	30.80	42.09	40.77	42.28	44.12	43.70
Fe	19.68	21.49	21.13	22.36	19.08	22.06	22.49	9.07	12.86	10.28	10.15	29.32
Na ₂ O	1.97	2.37	1.71	0.67	0.67							
MgO	7.46	6.88	6.72	10.48	11.36							
Al ₂ O ₃	4.06	3.10	4.46	2.97	1.89							
SiO ₂	48.32	48.56	46.74	48.52	49.97							
K ₂ O	-	-	-	-	-							
CaO	20.29	19.88	20.88	22.83	22.61							
TiO ₂	0.65	0.50	0.75	1.13	0.78							
MnO	0.71	0.79	0.90	0.31	0.44							
FeO	16.54	17.91	17.86	12.97	12.26							
Total	102.26	98.18	98.50	99.60	102.59							

Atomic proportion on basis of 6 oxygen

Ca	0.847	0.836	0.882	0.941	0.926
Na	0.149	0.181	0.131	0.050	0.050
K	0.000	0.000	0.000	0.000	0.000
Total	0.996	1.017	1.013	0.991	0.976
Mg	0.433	0.403	0.395	0.601	0.647
Fe	0.539	0.588	0.589	0.417	0.392
Mn	0.023	0.026	0.030	0.010	0.014
Ti	0.019	0.015	0.022	0.033	0.023
Al	0.070	0.049	0.500	0.001	0.000
Total	1.084	1.081	1.536	1.062	1.076
Al	0.117	0.094	0.157	0.134	0.085
Si	1.883	1.906	1.843	1.866	1.911
Total	2.000	2.000	2.000	2.000	1.996
O	6.000	6.000	6.000	6.000	6.000

TABLE III-9 (continued)

Total cations	4.080	4.098	4.099	4.057	4.048										
Ca	46.56	45.76	47.27	48.03	47.12										
Mg	23.81	22.06	21.17	30.68	32.93										
Fe	29.63	32.18	31.56	21.29	19.95										
Sanidine Porphyries - Grey Groundmass						Hornblende Phenocryst Rocks									
Na ₂ O	1.69	0.00	1.42	1.46	0.56	0.54	1.13	1.86	0.80	1.04	0.53	--	1.02	-	
MgO	8.33	13.20	7.74	6.49	13.18	13.41	12.19	8.46	9.25	6.68	8.82	13.18	10.79	11.76	
Al ₂ O ₃	3.35	4.04	2.47	5.68	1.81	1.55	1.88	2.17	6.50	7.48	6.93	2.25	1.23	4.80	
SiO ₂	48.18	49.42	49.33	45.72	51.57	52.21	52.68	49.86	45.78	44.37	45.74	51.00	52.41	47.92	
K ₂ O	-	-	-	-	-	-	0.08	-	-	-	-	-	-	-	
CaO	21.58	23.55	20.10	20.85	22.90	22.76	22.09	19.87	21.95	21.95	22.77	23.56	22.50	22.46	
TiO ₂	0.43	1.13	-	0.55	-	-	0.09	-	1.03	1.13	1.35	0.50	-	1.00	
MnO	0.60	-	1.48	0.76	0.32	0.35	0.71	0.43	0.34	0.54	0.27	-	0.39	-	
FeO	15.69	8.66	17.16	18.34	9.35	8.96	-	16.87	14.31	16.80	13.61	9.52	11.28	12.07	
Fe ₂ O ₃ +							10.53								
*Total	103.76	102.10	101.57	101.80	101.05	102.58	101.39	99.72	98.53	98.09	98.58	98.81	98.67	100.29	
Atomic proportions on basis of 6 oxygen															
Ca	0.902	0.947	0.844	0.884	0.925	0.911	0.865	0.803	0.887	0.924	0.942	0.949	0.913	0.897	
Na	0.128	0.000	0.108	0.112	0.041	0.039	0.080	0.136	0.058	0.079	0.039	0.000	0.075	0.000	
K	0.000	0.000	0.000	0.000	0.000	0.000	0.004	0.000	0.000	0.000	0.000	0.000	0.000	0.000	
Total	1.030	0.947	0.952	0.996	0.966	0.950	0.949	0.939	0.945	1.023	0.981	0.949	0.988	0.897	
Mg	0.485	0.738	0.452	0.383	0.741	0.750	0.664	0.476	0.520	0.391	0.508	0.739	0.610	0.653	
Fe	0.512	0.271	0.562	0.607	0.295	0.281	0.290	0.479	0.406	0.552	0.439	0.299	0.357	0.338	
Mn	0.020	0.000	0.049	0.025	0.010	0.011	0.022	0.030	0.011	0.018	0.009	0.000	0.012	0.000	
Ti	0.013	0.031	0.000	0.016	0.000	0.000	0.002	0.000	0.029	0.034	0.039	0.014	0.000	0.028	
Al	0.034	0.032	0.047	0.073	0.024	0.029	0.007	0.000	0.015	0.091	0.082	0.018	0.040	0.000	
Total	1.064	1.072	1.110	1.104	1.070	1.071	0.985	0.985	0.981	1.086	1.077	1.070	1.019	1.019	

TABLE III-9 (continued)

Al	0.120	0.146	0.067	0.192	0.056	0.040	0.074	0.097	0.274	0.256	0.234	0.082	0.015	0.211
Si	1.880	1.854	1.933	1.808	1.944	1.960	1.926	1.881	1.726	1.744	1.766	1.918	1.985	1.785
Total	2.000	2.000	2.000	2.000	2.000	2.000	2.000	1.978	2.000	2.000	2.000	2.000	2.000	1.996
O	6.000	6.000	6.000	6.000	6.000	6.000	6.000	6.000	6.000	6.000	6.000	6.000	6.000	6.000
Total cations	4.094	4.019	4.062	4.100	4.036	4.021	3.934	3.902	3.926	4.109	4.058	4.019	4.007	3.912
Ca	47.50	48.39	45.40	47.17	47.17	47.02	47.55	45.68	48.92	49.49	49.87	47.76	48.56	47.51
Mg	25.54	37.73	24.33	20.44	37.79	38.54	36.50	27.08	28.68	20.94	26.89	37.19	32.45	34.59
Fe	26.96	13.88	30.25	32.39	15.04	14.44	15.94	27.25	22.39	29.57	23.24	15.05	18.99	17.90

Dolerites

Pyroxene, contact skarn

Na ₂ O	0.00	0.00	0.00	0.00	0.49	0.68	0.27	0.74	0.00	0.39	0.00
MgO	16.70	18.32	13.38	17.89	13.95	14.84	17.31	15.06	19.22	16.33	9.09
Al ₂ O ₃	1.28	1.15	1.36	1.23	7.58	2.77	1.92	2.25	1.80	2.07	0.00
SiO ₂	52.50	53.39	50.72	53.44	56.92	52.84	54.28	48.27	56.84	55.30	51.51
K ₂ O	-	-	-	-	-	-	0.23	-	-	-	-
CaO	17.21	17.34	16.19	17.97	10.54	12.78	11.86	10.88	11.31	11.94	23.44
TiO ₂	0.28	-	0.58	-	-	0.54	0.41	5.38	-	-	-
MnO	-	-	0.31	-	-	-	0.25	0.29	0.28	-	0.30
FeO	12.03	9.79	17.46	9.47	10.52	15.21	13.42	16.87	10.55	13.47	15.42
*Total	99.06	98.66	99.92	98.42	101.89	101.69	99.03	102.75	99.06	98.17	101.35

Atomic proportions on basis of 6 oxygen

Ca	0.687	0.684	0.663	0.709	0.402	0.512	0.468	0.442	0.436	0.471	0.971
Na	0.000	0.000	0.000	0.000	0.033	0.050	0.019	0.054	0.000	0.028	0.000
K	0.000	0.000	0.000	0.000	0.000	0.000	0.011	0.000	0.000	0.000	0.000
Total	0.687	0.684	0.663	0.709	0.435	0.562	0.498	0.496	0.436	0.499	0.971
Mg	0.927	1.006	0.763	0.982	0.740	0.827	0.951	0.854	1.031	0.896	0.524
Fe	0.375	0.302	0.558	0.292	0.313	0.475	0.413	0.537	0.318	0.415	0.499

TABLE III-9 (continued)

Mn	0.000	0.000	0.000	0.000	0.000	0.000	0.008	0.009	0.000	0.000	0.000
Ti	0.008	0.000	0.017	0.000	0.000	0.015	0.011	0.154	0.000	0.000	0.000
Al	0.011	0.016	0.001	0.021	0.318	0.096	0.082	0.000	0.076	0.090	0.000
Total	1.321	1.324	1.339	1.295	1.371	1.413	1.457	1.554	1.425	1.401	1.023
Al	0.045	0.034	0.060	0.032	0.000	0.026	0.001	0.101	0.000	0.000	0.000
Si	1.955	1.966	1.940	1.968	2.026	1.974	1.999	1.836	2.046	2.035	1.993
Total	2.000	2.000	2.000	2.000	2.026	2.000	2.000	1.937	2.046	2.035	1.993
O	6.000	6.000	6.000	6.000	6.000	6.000	6.000	6.000	6.000	6.000	6.000
Total cations	4.008	4.008	4.012	4.004	3.832	3.975	3.955	3.987	3.907	3.935	3.987
Ca	34.54	34.34	33.42	35.75	27.63	28.22	25.55	24.11	24.43	26.43	48.70
Mg	46.61	50.50	38.46	49.53	50.86	45.59	51.91	46.59	57.76	50.28	26.28
Fe	18.85	15.16	28.12	14.73	21.51	26.19	22.54	29.30	17.82	23.29	25.03

Hybrid Zone Rocks

Na ₂ O	0.00	1.54	1.77	3.14	0.78	0.00	0.00	0.00	0.00	13.43	13.18	2.97	1.16	2.86
MgO	9.83	8.44	9.27	7.76	11.57	14.28	16.78	15.01	13.40	0.88	1.29	7.45	11.18	5.92
Al ₂ O ₃	3.55	3.53	1.95	1.22	3.27	1.68	0.94	1.40	2.82	0.83	0.40	1.10	1.13	0.91
SiO ₂	48.77	48.24	49.97	51.08	49.61	51.58	53.42	52.45	50.78	51.38	51.11	50.01	51.23	49.91
K ₂ O	-	-	-	-	-	-	-	-	-	-	-	-	-	-
CaO	23.31	20.93	20.92	17.81	22.39	23.53	24.51	23.72	23.42	2.80	3.55	19.64	22.26	19.03
TiO ₂	0.48	0.52	0.33	0.00	0.65	0.60	0.25	0.40	0.80	0.25	0.00	0.00	0.00	0.00
MnO	0.35	0.65	0.85	0.59	0.40	0.00	0.00	0.00	0.00	1.56	0.76	1.16	0.83	1.14
FeO	13.69	16.15	14.92	18.18	11.31	8.34	3.76	7.00	8.76	28.87	29.68	17.66	12.20	20.22
*Total	99.47	100.93	100.96	101.60	100.73	99.57	98.21	100.65	99.01	103.75	103.99	101.64	100.19	100.13

Atomic proportions on basis of 6 oxygen

Ca	0.961	0.873	0.867	0.745	0.912	0.943	0.963	0.943	0.940	0.122	0.155	0.827	0.911	0.809
Na	0.000	0.116	0.132	0.238	0.058	0.00	0.00	0.000	0.000	1.060	1.044	0.226	0.086	0.220

TABLE III-9 (continued)

K	0.000	0.000	0.000	0.000	0.000	0.000	0.000	0.000	0.000	0.000	0.000	0.000	0.000	0.000
Total	0.961	0.989	0.999	0.983	0.970	0.943	0.963	0.943	0.940	1.182	1.199	1.053	0.997	1.029
Mg	0.540	0.490	0.535	0.451	0.656	0.796	0.917	0.830	0.748	0.053	0.079	0.436	0.637	0.350
Fe	0.440	0.526	0.483	0.594	0.360	0.261	0.115	0.217	0.274	0.983	1.014	0.580	0.390	0.671
Mn	0.011	0.021	0.028	0.019	0.013	0.000	0.000	0.000	0.000	0.054	0.026	0.039	0.027	0.038
Ti	0.014	0.015	0.010	0.000	0.019	0.017	0.007	0.011	0.023	0.008	0.000	0.000	0.000	0.000
Al	0.037	0.041	0.023	0.050	0.032	0.002	0.000	0.008	0.026	0.040	0.019	0.015	0.009	0.021
Total	1.042	1.093	1.079	1.114	1.080	1.076	1.039	1.066	1.071	1.138	1.138	1.070	1.063	1.080
Al	0.124	0.121	0.066	0.006	0.114	0.072	0.041	0.053	0.098	0.000	0.000	0.036	0.042	0.021
Si	1.876	1.879	1.934	1.994	1.886	1.928	1.958	1.947	1.902	2.092	2.087	1.964	1.958	1.979
Total	2.000	2.000	2.000	2.000	2.000	2.000	1.999	2.000	2.000	2.092	2.087	2.000	2.000	2.000
O	6.000	6.000	6.000	6.000	6.000	6.000	6.000	6.000	6.000	6.000	6.000	6.000	6.000	6.000
Total cations	4.003	4.082	4.078	4.097	4.050	4.019	4.001	4.009	4.011	4.412	4.424	4.123	4.060	4.109
Ca	48.91	46.21	45.99	41.62	47.30	47.15	48.27	47.39	47.91	10.54	12.42	44.87	47.01	44.21
Mg	28.70	25.94	28.38	25.20	34.02	39.80	45.96	41.71	38.12	4.58	6.33	23.66	32.87	19.13
Fe	22.39	27.85	25.62	33.18	18.67	13.05	5.76	10.90	13.97	84.89	81.25	31.47	20.12	36.67
Na ₂ O	0.00	0.00	0.00	0.69	3.79	1.55	1.52	0.00	0.00	2.02	1.63	0.66	1.68	0.59
MgO	13.55	13.81	14.28	11.62	6.78	10.79	11.84	15.62	15.07	15.62	12.72	9.87	9.53	10.98
Al ₂ O ₃	2.15	2.48	1.87	4.19	1.25	1.00	0.64	1.15	1.19	4.14	-	0.98	0.87	0.70
SiO ₂	51.15	50.44	52.09	48.67	51.32	51.38	52.32	53.05	52.54	51.21	53.59	51.49	51.17	51.73
K ₂ O	-	-	-	-	-	-	-	-	-	0.60	-	-	-	-
CaO	23.90	23.94	23.32	23.37	17.67	21.24	21.60	24.46	24.46	11.68	21.27	21.49	21.03	22.40
TiO ₂	0.72	1.03	0.63	1.10	-	0.35	-	0.42	0.57	0.43	-	-	-	-
MnO	0.00	0.00	0.00	0.26	0.75	0.54	0.45	0.00	0.00	0.43	0.70	1.32	0.87	1.27
FeO	8.53	8.27	7.81	10.12	18.45	13.16	11.62	5.29	6.18	14.29	10.10	14.20	14.85	12.34
*Total	100.17	100.19	101.62	102.79	102.87	102.85	103.31	100.85	99.94	99.95	99.99	98.01	100.65	100.82

TABLE III-9 (continued)

Atomic proportions on basis of 6 oxygen

Ca	0.960	0.962	0.930	0.950	0.740	0.871	0.878	0.966	0.971	0.469	0.857	0.885	0.870	0.917
Na	0.000	0.000	0.000	0.051	0.287	0.115	0.112	0.000	0.000	0.147	0.119	0.049	0.126	0.044
K	0.000	0.000	0.000	0.000	0.000	0.000	0.000	0.000	0.000	0.029	0.000	0.000	0.000	0.000
Total	0.960	0.962	0.930	1.001	1.027	0.986	0.990	0.966	0.971	0.645	0.976	0.934	0.996	0.961
Mg	0.757	0.772	0.792	0.658	0.395	0.616	0.670	0.859	0.833	0.872	0.713	0.565	0.549	0.625
Fe	0.267	0.259	0.243	0.321	0.603	0.421	0.369	0.163	0.191	0.448	0.318	0.457	0.479	0.395
Mn	0.000	0.000	0.000	0.008	0.025	0.018	0.015	0.000	0.000	0.014	0.022	0.043	0.028	0.041
Ti	0.020	0.029	0.018	0.031	0.000	0.010	0.000	0.012	0.016	0.000	0.000	0.000	0.000	0.000
Al	0.012	0.000	0.020	0.035	0.057	0.010	0.014	0.006	0.000	0.001	0.000	0.024	0.016	0.008
Total	1.056	1.060	1.073	1.053	1.080	1.075	1.068	1.040	1.040	1.335	1.053	1.089	1.072	1.069
Al	0.083	0.109	0.062	0.153	0.000	0.035	0.015	0.044	0.052	0.082	0.000	0.021	0.024	0.023
Si	1.917	1.891	1.938	1.847	2.004	1.965	1.985	1.956	1.947	1.918	2.015	1.979	1.976	1.977
Total	2.000	2.000	2.000	2.000	2.004	2.000	2.000	2.000	1.999	2.000	2.015	2.000	2.000	2.000
O	6.000	6.000	6.000	6.000	6.000	6.000	6.000	6.000	6.000	6.000	6.000	6.000	6.000	6.000
Total cations	4.016	4.022	4.003	4.054	4.111	4.061	4.058	4.006	4.010	4.080	4.044	4.023	4.068	4.030
Ca	48.39	48.27	47.33	49.25	42.58	45.65	45.80	48.59	48.67	26.22	45.39	46.41	45.84	47.34
Mg	38.16	38.74	40.31	34.11	22.73	32.29	34.95	43.21	41.75	48.74	37.76	29.63	28.93	32.27
Fe	13.46	13.00	12.37	16.64	34.70	22.06	19.25	8.20	9.57	25.04	16.84	23.96	25.24	20.39
Na ₂ O	-	-	-	-	0.67	3.18	2.98	0.44	0.54	0.62				
MgO	14.54	15.97	17.08	14.26	12.55	9.02	8.72	15.57	14.05	13.94				
Al ₂ O ₃	1.53	1.06	0.76	0.98	1.59	1.19	1.17	0.40	1.97	1.56				
SiO ₂	53.33	53.20	54.12	53.42	52.09	52.50	52.13	53.99	52.48	52.32				
K ₂ O	-	-	-	-	-	-	-	-	-	-				
CaO	22.43	23.76	23.91	22.75	22.70	19.32	19.39	24.36	17.65	20.16				
TiO ₂	-	0.40	-	-	0.35	-	-	-	0.35	0.22				
MnO	-	-	-	-	0.53	-	-	-	0.38	0.26				
FeO	8.18	5.61	3.87	8.34	9.52	14.77	15.61	4.88	12.43	10.73				
*Total	102.17	101.65	101.36	99.73	100.92	101.93	101.15	100.36	98.62	103.44				

TABLE III-9 (continued)

Atomic proportions on basis of 6 oxygen

Ca	0.891	0.938	0.936	0.906	0.914	0.793	0.799	0.961	0.709	0.811
Na	0.000	0.000	0.000	0.000	0.049	0.236	0.222	0.032	0.039	0.045
K	0.000	0.000	0.000	0.000	0.000	0.000	0.000	0.000	0.000	0.000
Total	0.891	0.938	0.936	0.906	0.963	1.029	1.021	0.993	0.848	0.856
Mg	0.803	0.877	0.930	0.790	0.703	0.515	0.500	0.855	0.785	0.780
Fe	0.254	0.173	0.118	0.259	0.299	0.473	0.502	0.150	0.390	0.337
Mn	0.000	0.000	0.000	0.000	0.017	0.000	0.000	0.000	0.012	0.008
Ti	0.000	0.011	0.000	0.000	0.010	0.000	0.000	0.000	0.010	0.006
Al	0.043	0.006	0.011	0.028	0.028	0.000	0.053	0.005	0.054	0.032
Total	1.100	1.067	1.059	1.077	1.057	0.988	1.055	1.010	1.251	1.163
Al	0.024	0.040	0.022	0.015	0.042	0.000	0.000	0.012	0.033	0.037
Si	1.976	1.960	1.978	1.985	1.958	2.010	2.004	1.988	1.967	1.963
Total	2.000	2.000	2.000	2.000	2.000	2.010	2.004	2.000	2.000	2.000
O	6.000	6.000	6.000	6.000	6.000	6.000	6.000	6.000	6.000	6.000
Total cations	3.991	4.005	3.995	3.983	4.020	4.081	4.027	4.003	3.999	4.019

Ca	45.74	47.18	47.18	46.34	47.70	44.53	44.36	48.88	37.63	42.06
Mg	41.22	44.11	46.87	40.41	36.69	28.92	27.76	43.49	41.67	40.46
Fe	13.04	8.70	5.95	13.25	15.61	26.56	27.87	7.63	20.70	17.48

Na ₂ O	-	-	0.34	0.37	1.74	4.45	2.71	3.72	3.14	2.67	0.22	0.75
MgO	16.51	15.67	14.03	13.26	9.94	4.58	6.73	6.68	7.71	8.25	15.47	10.83
Al ₂ O ₃	1.03	1.72	1.30	0.82	1.55	1.23	1.05	1.02	0.63	0.41	1.46	5.96
SiO ₂	52.93	52.17	52.46	52.42	50.58	50.90	51.02	51.07	50.91	50.99	52.25	47.13
K ₂ O	-	-	-	-	-	0.23	0.59	-	-	-	-	-
CaO	24.62	24.19	23.68	22.29	21.01	14.38	17.99	16.42	17.63	18.91	23.79	22.97
TiO ₂	0.28	0.30	0.29	-	-	-	-	-	-	-	0.45	1.28
MnO	-	-	-	0.37	0.71	0.56	0.37	0.47	0.40	0.35	-	0.24
FeO	4.44	5.89	7.52	10.29	14.24	23.61	19.43	20.35	19.48	18.26	6.19	11.54
Total	99.61	100.03	103.77	103.70	101.64	99.87	99.69	101.87	101.95	101.91	102.93	104.24

TABLE III-9 (continued)

Atomic proportions on basis 6 oxygen

Ca	0.972	0.960	0.947	0.900	0.869	0.613	0.757	0.692	0.741	0.792	0.946	0.942
Na	0.000	0.000	0.025	0.027	0.130	0.343	0.207	0.284	0.238	0.202	0.016	0.056
K	0.000	0.000	0.000	0.000	0.000	0.012	0.030	0.000	0.000	0.000	0.000	0.000
Total	0.972	0.960	0.972	0.927	0.999	0.968	0.994	0.976	0.979	0.994	0.962	0.998
Mg	0.907	0.865	0.780	0.745	0.572	0.271	0.394	0.392	0.451	0.481	0.856	0.619
Fe	0.137	0.182	0.235	0.324	0.460	0.785	0.638	0.669	0.639	0.597	0.192	0.370
Mn	0.000	0.000	0.000	0.012	0.023	0.019	0.012	0.016	0.013	0.012	0.000	0.008
Ti	0.008	0.008	0.008	0.000	0.000	0.000	0.000	0.000	0.000	0.000	0.013	0.037
Al	0.000	0.007	0.014	0.032	0.023	0.057	0.049	0.047	0.026	0.013	0.003	0.038
Total	1.052	1.062	1.037	1.113	1.078	1.132	1.093	1.124	1.129	1.103	1.064	1.072
Al	0.045	0.068	0.043	0.025	0.047	0.000	0.000	0.000	0.003	0.006	0.061	0.195
Si	1.950	1.932	1.957	1.975	1.953	2.024	2.004	2.009	1.997	1.994	1.939	1.805
Total	1.995	2.000	2.000	2.000	2.000	2.024	2.004	2.009	2.000	2.000	2.000	2.000
O	6.000	6.000	6.000	6.000	6.000	6.000	6.000	6.000	6.000	6.000	6.000	6.000
Total cations	4.019	4.022	4.009	4.040	4.077	4.124	4.090	4.109	4.108	4.097	4.026	4.070
Ca	48.21	47.83	48.27	45.71	45.71	46.73	42.31	39.48	40.47	42.35	47.44	48.78
Mg	44.99	43.10	39.76	37.84	30.09	16.24	22.02	22.36	24.63	25.72	42.93	32.06
Fe	6.80	9.07	11.98	16.46	24.20	47.03	35.66	38.16	34.90	31.93	9.63	19.16

shown the trends for pyroxenes from the eastern Uganda alkaline complexes from Tyler and King (1967) and the crystallization trends for clinopyroxenes of the diopside-hedenbergite series of Aoki (1964). The Tasmanian rocks have an affinity to the diopside-hedenbergite trend rather than to the diopside-aegirine series.

The plot of the pyroxenes from the alkaline rocks in Fig. III-16 suggests an association with the alkali basalt-trachyte trend with the addition of sodium causing a slight divergence of the sanidine porphyry towards the more soda-rich types. It can also be noted that this divergence has a tendency to follow the South Qoroq trend.

When compared with the other pyroxene trends shown in Fig. III-16, the pyroxenes from Port Cygnet do not represent a highly differentiated sequence. They do not show a high degree of sodium enrichment nor do they contain significant amounts of exotic elements such as zirconium, exemplified by extreme differentiation as shown by the pyroxenes from the Ilimaussaq complex (Larsen, 1976). Larsen has also commented on the variation of calcium and its association with silica activity. While the pyroxenes of the Port Cygnet syenite porphyries and sanidine rocks do not show significant differences, notwithstanding their oversaturated-undersaturated character.

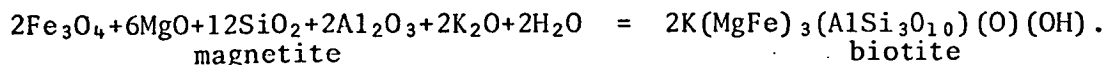
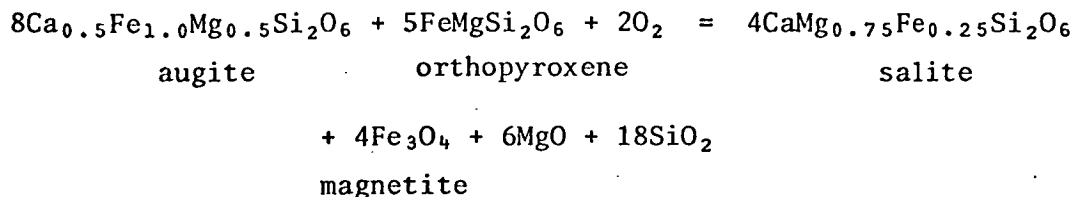
PYROXENES IN THE HYBRID ROCKS

The pyroxenes from the unaltered dolerite are co-existing augites and pigeonites. They fall into three distinct groups:

pigeonites, ranging from intermediate to magnesium pigeonite; and augites of two distinct types: one relatively calcium-rich and the other relatively calcium-poor. When compared with the pyroxenes from the hybrid rocks, it is clear that there has been a direct addition of calcium to the pyroxene, or the removal of equivalent amounts of iron and magnesium oxides. As pigeonite and magnesium-iron rich pyroxenes are also absent from the hybrid rocks, then this suggests removal of iron and magnesium. This process can be accomplished by reaction with potash, forming biotite as observed previously and proposed by Edwards (1947).

Under the influence of the invading alkaline material, the exsolved pyroxenes of the dolerite re-equilibrate, with the less stable Mg-pyroxenes decomposing to produce magnetite and releasing magnesia, which react with incoming potash, alumina, silica and water to produce biotite. The augite recrystallizes to produce a molecule richer in calcium thus moving its composition into the salite field. It may also receive lime and alumina from the breakdown of the plagioclase of the dolerite. These are largely sub-solidus reactions.

The following idealized reactions are proposed for producing the above changes. For purposes of balancing the equations, the small amounts of alumina present in all of the pyroxenes have been omitted and it is necessary to add oxygen to partially oxidise iron for the magnetite. It is to be noted that $\text{Fe}_2\text{O}_3/\text{FeO}$ is greater than unity for most of the alkaline rocks, although the work of Huckenholz et al. (1976) suggests that oxidation states may also be related to charge transfer processes between ions in the magma rather than as a direct consequence of the activity of oxygen.



The reactions generate excess silica for biotite formation, assuming this is related to MgO production. Thus silica and iron (also in excess) are available for the formation of other minerals such as melanite and salitic pyroxene. Exsolution lamellae, defined by lines of magnetite, in the pyroxenes (Pl. 46) indicate the breakdown of exsolved iron-rich pyroxene from original pyroxene to form magnetite with magnesia-rich material released for formation of biotite.

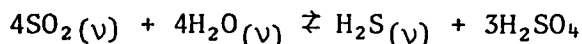
Aegirine-augite also occurs in the hybrid rocks, although the soda content is rarely greater than 3.0%. Originally Edwards (1947) considered all the pyroxenes to be aegirine-augites on the basis of their green colour, and pleochroism, however the salite pyroxenes also have a deep green colour and as such are superficially indistinguishable from aegirine-augite. Aegirine and soda-bearing salite pyroxenes occur as primary phases in the potash rich rocks and can be directly contributed to the hybrids by the alkaline magma. It is also possible for soda from the breakdown of plagioclase, to contribute to the formation of the soda-pyroxene as originally proposed by Edwards. This addition of soda to the Ca site is shown from the analyses of Fig. III-15. Most of the soda in the hybrid zone contributes to the formation of albitic feldspars and nepheline.

FELDSPATHOID MINERALOGY

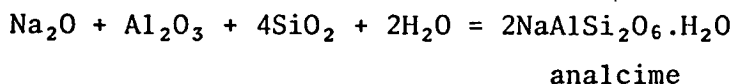
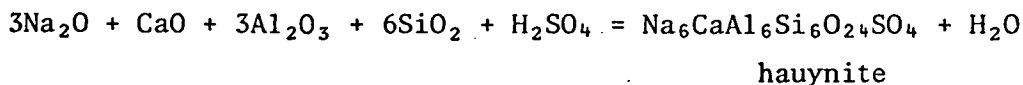
Feldspathoids present in the rocks are nepheline, hauynite and analcime. The characteristics and relationships of the nephelines have already been discussed. Hauynite is isotropic and lacks an

interference figure and has lower silica content in microprobe analyses while analcime is distinguished by its relatively high soda and silica. The best development of hauynite and analcime occurs in the tinguaitite CY73. The hauynite occurs as euhedral phenocrysts, but analcime occurs as irregular anhedral grains and masses in the groundmass where it is intergrown with aegirine laths and is a late stage phase. A small amount of sulphur must have been present to contribute to the formation of hauynite. This process fixed the sulphur in the system. The remaining soda and a hydrous late stage fluid phase led to the formation of the analcime (Pl. 37).

The microprobe analyses of the hauynite suggest an idealized proportion of Na/Ca = 6/1 for the mineral. Sulphur is apparently oxidized to sulphate because the mineral is not coloured blue, which a preponderance of sulphur as sulphide would indicate (cf. lazurite). Thus oxidizing conditions are required for the formation of hauynite which on textural grounds (euhedral phenocrysts and no intergrowths) has crystallized, as a primary phase, well before the analcime. The most likely species for sulphur in the system is SO₂ (see discussion concerning scapolite). This would hydrolyse with water thus:



The formation of hauynite could then be specified:



Both equations could be combined to give:

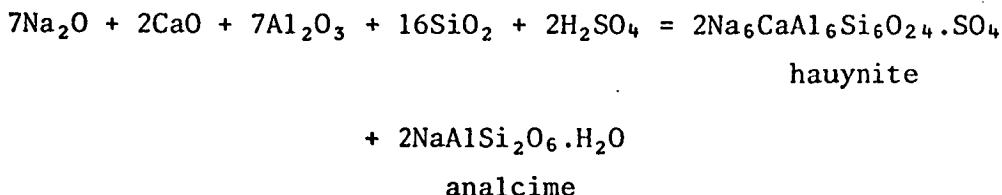


TABLE III-10

Electron microprobe partial analyses of hauynite and analcime#

Hauynite					Analcime				
Na ₂ O	15.28	14.49	13.46	15.06	13.43*	14.62*	13.78*	13.69*	14.33*
Al ₂ O ₃	26.62	25.35	23.52	26.72	24.53	24.26	24.32	24.35	24.91
SiO ₂	32.63	31.27	26.48	32.81	52.37	52.47	52.41	52.48	54.91
K ₂ O	5.32	5.04	5.34	5.91	0.21	0.16	0.17	0.21	0.00
CaO	4.48	7.87	12.33	4.00	0.00	0.00	0.00	0.00	0.00
+S									
Unnormal- ized total	84.33	84.03	83.25	84.49	90.54	91.51	90.68	90.74	94.17
Cations on basis of 24 Oxygen ~					Cations on basis of 6 Oxygen				
Na	5.255	5.070	4.886	5.172	0.969	1.049	0.994	0.987	0.994
K	1.203	1.160	1.227	1.337	0.010	0.008	0.008	0.010	0.000
Ca	0.851	1.522	2.473	0.759	0.000	0.000	0.000	0.000	0.000
Al	5.564	5.390	5.190	5.579	1.077	1.058	1.066	1.067	1.050
Si	5.787	5.639	5.331	5.809	1.948	1.942	1.950	1.951	1.964
Total	18.660	18.781	19.107	18.656	4.003	4.057	4.018	4.025	4.008
O	24.000	24.000	24.000	24.000	6.000	6.000	6.000	6.000	6.000

analyses taken from specimen
CY73.* If repeated analyses of analcime
are performed beginning with
large area scans and ending with
spot analyses, the sodium concen-
trations increase slightly due to
loss of H₂O from the sample.

It is apparent that the two minerals did not form concurrently because of their textural relationships in the rocks. The sequence could have begun by hydrolysis of SO_2 and subsequent fixing of the sulphate by hauynite, at an early stage, with H_2S escaping from the system. The H_2S would normally be fixed by iron if in high concentrations, but iron sulphides are rare in the sanidine bearing rocks. With fixing and removal of excess sulphur, H_2O dominates and analcime is formed as a very late stage mineral. This assumes hydrolysis of SO_2 as the prime cause of these minerals. Obviously the relative fugacities of SO_2 and H_2O are important in determining the particular mineral which may crystallize. As hauynite formed, sulphur was removed from the system so that the fugacity of H_2O reached the point at which analcime formed as the last phase as grains and intergrowths in the groundmass.

As discussed earlier (Chapter II) the analcime is in a reaction relationship with sanidine phenocrysts and groundmass. According to Roux and Hamilton (1976) this places a maximum restraint of 8 kb and 800°C for the equilibrium association of analcime and sanidine, which is outside the range for these rocks because the analcime is a groundmass phase. On the other hand the reaction of nepheline + albite + H_2O to form analcime is at subsolidus equilibrium between 500°C and 600°C over most of the likely pressure range (Greenwood, 1961) for these rocks. As albite does not appear in these rocks and the analcime is fresh then the maximum temperature at which it formed would be below 600°C . This would be consistent with the late stage interstitial appearance of the analcime in the tinguaites and the work of Edgar (1978) (see Chapter IV).

FELDSPAR MINERALOGY

The feldspar mineralogy of the Port Cygnet rocks is comparatively simple with the syenite porphyries containing mainly oligoclase with

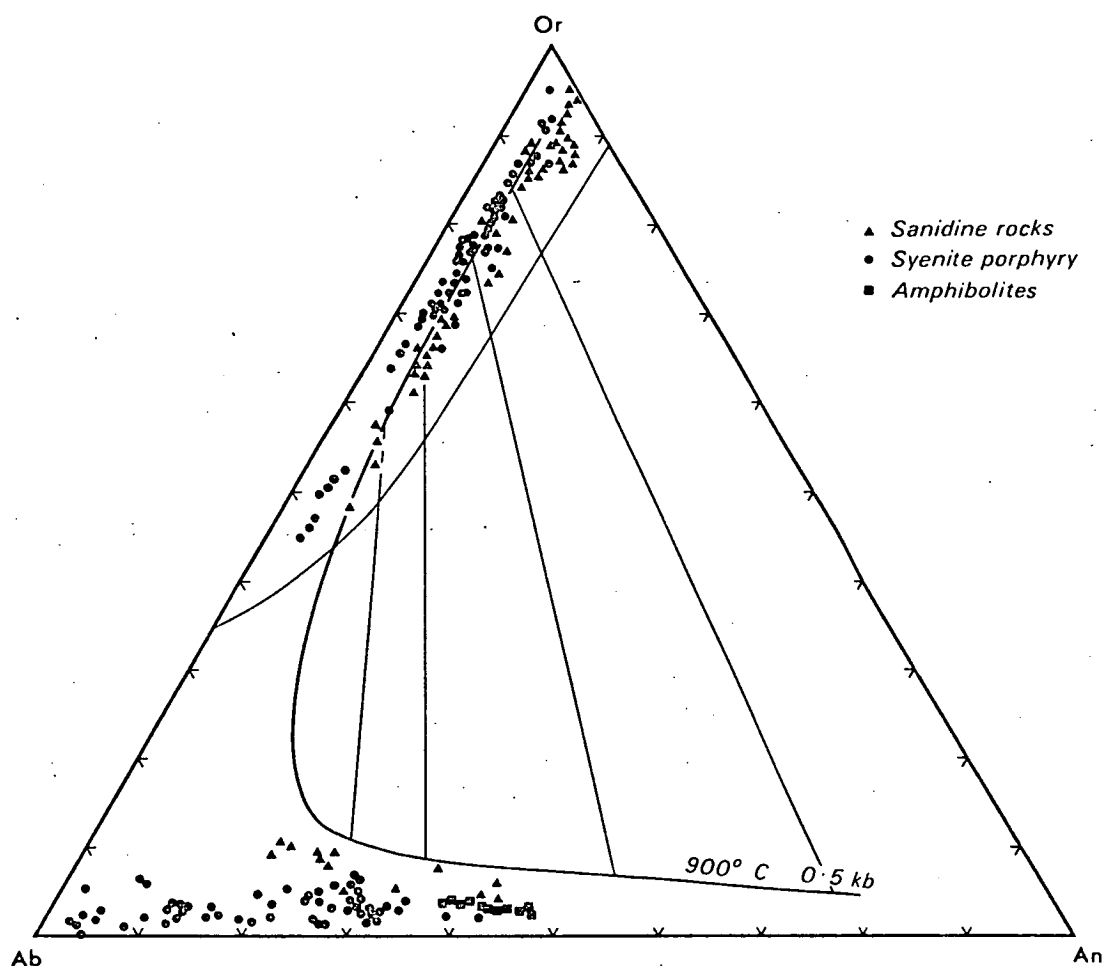


Figure III-17 Ternary feldspar plot for feldspars from all the alkaline rocks with the solvus for the 900°C isotherm and 0.5 kb p_{H_2O} . Curve in figure represents the approximate locus of compositions of liquids with which two feldspars may co-exist in equilibrium with leucite omitted.

some compositional spread into the adjacent andesine and albite fields. Some crystals have andesine cores of which many represent original grains onto which oligoclase has subsequently crystallized (Pl. 16). The rocks with flow textures have sanidines with co-existing oligoclase and andesine only in specimens CY61 and CY92 where overgrowths of potash feldspar armour plagioclase phenocrysts. Both the syenites and the trachytic rocks have groundmasses composed essentially of potash feldspars. Some larger potash feldspars occur in the syenites but these are not euhedral phenocrysts as are the plagioclases. The total feldspar compositions for all alkaline rocks are plotted in the ternary Ab-Or-An diagram (Fig. III-17).

Data are also presented in ternary feldspar plots of core-rim plagioclase compositions and co-existing potash feldspar compositions for various representative alkaline rocks (Figs. III-18, III-21). Plagioclase compositions from the amphibolite inclusions on Mt. Windsor have also been added for comparison. These feldspars do not show twinning under the microscope.

The potash feldspars from both groups of alkaline rocks show an interesting trend with most compositions outside the field of anorthoclase as defined by Wright and Stewart (1968). Using the data of Seck (1971) the solvus for 900°C at 0.5 kb H_2O pressure has been added to Fig. III-17. The plagioclases for the sanidine rocks in this figure are contributed by CY61 and CY92 (also Fig. III-20) which appear to have a more complicated origin by virtue of the potash feldspar overgrowths on the plagioclase crystal. By virtue of their normative plots near the equilibrium line, and the observation that the tie-lines for feldspar pairs are incompatible with those of Seck (1971) (Figs. III-17 and III-22), the sanidine crystals in the brown matrix rocks have a reaction hence non-equilibrium relationship to the oligoclase phenocrysts. The other rocks have only sanidine as the feldspar phenocryst. From the figure it can be seen that the feldspars from the sanidine rocks plot towards the inner part of the field relative to the feldspars of the syenite porphyries. The two possible interpretations of this distribution are that:

(a) the syenite porphyry was formed at a higher pressure than the sanidine rocks, since for a specific temperature an increase in P_{H_2O} causes the solubility field to contract,

(b) the sanidine rocks formed at a higher temperature than the syenites because an increase in temperature will increase the solubility field of the feldspars.

It would be unlikely that there would be a great pressure difference during the formation of these rocks hence it is more probable that the relative distributions are due to temperature differences. It should also be noted that because the sanidine rocks contain euhedral feldspar phenocrysts they were more likely in equilibrium with melt at the time of their formation whereas the potash feldspars of the syenites occur mainly as anhedral crystals formed after the plagioclase and in the groundmass and therefore at a lower temperature not in equilibrium with the plagioclase phenocrysts. This problem has been noted in other chapters. The data would indicate a minimum temperature of formation of 900°C for the sanidine rocks at a pressure of 0.5 kb. As the real pressure was probably higher, as suggested by the absence of leucite, then the temperature of formation would have been somewhat greater. The extremely potash-rich varieties do show a tendency towards a higher formation temperature, if the pressure is assumed to be uniform for all rocks. This probably represents crystallization in a deeper magma chamber with the subsequent quick injection of the later dykes freezing the equilibrium. While the co-existing feldspar geothermometers do not apply to these rocks, the sanidine rocks probably have a higher formation temperature than do the syenite porphyries.

An apparent anomaly exists for the feldspars of CY92 and CY61 where potash feldspar phenocrysts occur with/and mantle plagioclase phenocrysts which do not appear to plot on the same isotherm but on one of a lower temperature value which relate them to the syenite porphyries.

Euhedral crystals of oligoclase-andesine in the rocks frequently have overgrowths of potash feldspar with some crystals showing resorption phenomena (Pl. 9). Normatively these are low in the anorthite molecule with about six weight percent the calculated maximum.

If the final consolidation temperature was about 900°C or greater then the potash feldspars would have the high sanidine structure. The optical studies of the sanidine crystals indicates their optical axial planes are perpendicular to 010 with low 2V and places them in the partially ordered sanidines as stated by Marfunin (1966). The euhedral crystals with tabloid development of (010) show the classical sanidine form. Because of their gross development these are regarded as having high temperature structures because metastable low temperature disordered structures are usually associated with small crystals.

The structural states of the potash feldspar phenocrysts were determined by using the three peak method of Wright (1968) in which the 2θ values of $\text{CuK}\alpha_1$ for the diffraction peaks 060, $\bar{2}04$ and $\bar{2}01$ were obtained. These were measured using a Philips PW1025 vertical goniometer, equipped with a lithium fluoride monochromator aligned for $\text{CuK}\alpha_1$. The diffractometer was calibrated using silicon and potash alum standards. The data obtained are listed in Table III-11.

No splitting of the 130 peak (McKenzie, 1954) was observed for any of the specimens measured, thus indicating the monoclinic symmetry of these. The above data are plotted in Figure III-22 following the procedure of Wright (op. cit.). All feldspars plot towards the high sanidine part of the diagram but only CY73 and CY74 would be regarded as within the high sanidine structure of Wright (op. cit.) whereas the other specimens are anomalous with respect to cell volume. If the final consolidation temperature for the sanidine crystals was about 900°C then the anomalous character could well be explained by partial ordering between high and partially ordered sanidine following Laves (in Marfunin, 1966) or possibly ordered orthoclase phases (Martin, 1974 in Feldspars: McKenzie - Zussman). This would be compatible with the optical orientations observed earlier for the sanidine.

TABLE III-11
Structural state data for sanidine phenocrysts

Specimen	060	$2\theta\text{CuK}\alpha_1$		$\bar{2}01$ -Wright (1968)	$\Delta 2\theta$
		$\bar{2}04$	$\bar{2}01$		
CY13	41.74	51.02	21.31	21.60 ± 0.10	-0.29
CY32	41.80	51.00	21.23	21.70 ± 0.10	-0.47
CY40	41.75	50.87	21.27	21.50 ± 0.10	-0.23
CY73	41.70	50.96	21.34	21.50 ± 0.10	-0.16
CY74	41.65	50.88	21.26	21.30 ± 0.10	-0.04
CY77	41.75	50.90	21.20	21.60 ± 0.10	-0.40
CY93	41.73	50.91	21.21	21.50 ± 0.10	-0.29
X44	41.72	50.82	21.17	21.40 ± 0.10	-0.23

TABLE III-12

Compositions for feldspars with structural state data

	CY13			CY32			CY40			CY73			CY74	
Na ₂ O	1.41	1.62	3.46	2.38	1.170	0.72	0.56	0.83	2.86	2.48	1.35	1.30	1.28	
Al ₂ O ₃	18.96	18.87	18.89	18.38	18.950	18.86	18.31	18.39	18.85	18.63	19.25	19.33	19.28	
SiO ₂	64.82	64.77	66.05	66.24	64.18	62.33	64.68	64.64	65.92	65.47	63.77	64.00	64.00	
K ₂ O	13.58	13.53	10.39	12.29	13.92	14.20	15.25	15.21	11.58	12.35	13.34	13.63	13.43	
CaO	0.84	0.85	0.56	0.71	0.75	0.88	0.96	0.96	0.79	0.87	0.82	0.79	0.87	
BaO	0.39	0.37	0.00	0.00	1.03	2.35	0.00	0.00	0.00	0.00	1.23	0.96	1.14	
FeO	0.00	0.00	0.31	0.00	0.00	0.66	0.24	0.24	0.00	0.21	0.24	0.00	0.00	
Total	100.33	100.44	99.27	101.46	99.68	99.03	99.10	101.21	99.44	100.09	98.35	100.02	100.00	
Cations on basis of 16 oxygen														
Na	0.251	0.287	0.608	0.420	0.208	0.129	0.100	0.148	0.503	0.439	0.240	0.230	0.228	
K	1.586	1.582	1.200	1.427	1.631	1.678	1.797	1.791	1.341	1.438	1.562	1.595	1.571	
Ca	0.082	0.083	0.055	0.070	0.073	0.087	0.095	0.093	0.077	0.085	0.081	0.078	0.086	
Ba	0.027	0.026	0.000	0.000	0.071	0.164	0.000	0.000	0.000	0.000	0.085	0.066	0.078	
Fe	0.000	0.000	0.024	0.000	0.000	0.000	0.000	0.000	0.000	0.016	0.018	0.000	0.000	
Site Total	1.946	1.978	1.887	1.917	1.983	2.058	1.992	2.032	1.921	1.978	1.986	1.969	1.963	
Al	2.047	2.038	2.014	1.970	2.051	2.058	1.993	2.001	2.018	2.004	2.083	2.090	2.083	
Si	5.937	5.937	5.976	6.026	5.894	5.772	5.974	5.968	5.987	5.977	5.853	5.872	5.867	
Site Total	7.984	7.975	7.990	7.996	7.945	7.830	7.967	7.969	8.005	7.981	7.936	7.962	7.950	
O	16.000	16.000	16.000	16.000	16.000	16.000	16.000	16.000	16.000	16.000	16.000	16.000	16.000	

TABLE III-12 (continued)

	CY77				CY93				X44	
Na ₂ O	2.82	2.50	3.03	1.77	0.35	0.93	2.55	1.03	0.33	0.00
Al ₂ O ₃	19.53	19.24	19.10	18.79	18.25	18.59	18.88	18.61	17.99	18.27
SiO ₂	64.90	65.21	64.97	62.24	64.01	64.79	65.46	64.21	64.20	64.38
K ₂ O	11.29	11.63	11.23	13.64	15.41	14.79	12.15	14.14	16.09	16.01
CaO	1.24	1.18	1.18	0.93	0.82	0.89	0.96	0.89	0.95	0.95
BaO	0.00	0.25	0.23	0.00	0.00	0.00	0.00	0.87	0.46	0.39
FeO	0.22	0.00	0.25	0.63	1.16	0.00	0.00	0.25	0.00	0.00
Total	99.42	98.50	98.87	100.45	99.95	101.21	102.28	96.89	98.23	97.50

Cations on basis of 16 oxygen

Na	0.497	0.441	0.536	0.316	0.063	0.165	0.451	0.184	0.059	0.000
K	1.311	1.349	1.306	1.604	1.826	1.738	1.412	1.661	1.904	1.890
Ca	0.121	0.115	0.115	0.092	0.082	0.088	0.094	0.088	0.094	
Ba	0.000	0.017	0.016	0.000	0.000	0.000	0.000	0.060	0.032	0.027
Fe	0.016	0.000	0.019	0.049	0.090	0.000	0.000	0.019	0.000	0.000
Site Total	1.945	1.922	1.992	2.061	2.061	1.991	1.957	2.012	2.089	2.011
Al	2.096	2.062	2.051	2.041	1.997	2.018	2.028	2.019	1.967	1.993
Si	5.907	5.931	5.918	5.919	5.944	5.966	5.966	5.911	5.955	5.958
Site Total	8.003	7.993	7.969	7.960	7.941	7.984	7.994	7.930	7.922	7.951
O	16.000	16.000	16.000	16.000	16.000	16.000	16.000	16.000	16.000	16.000

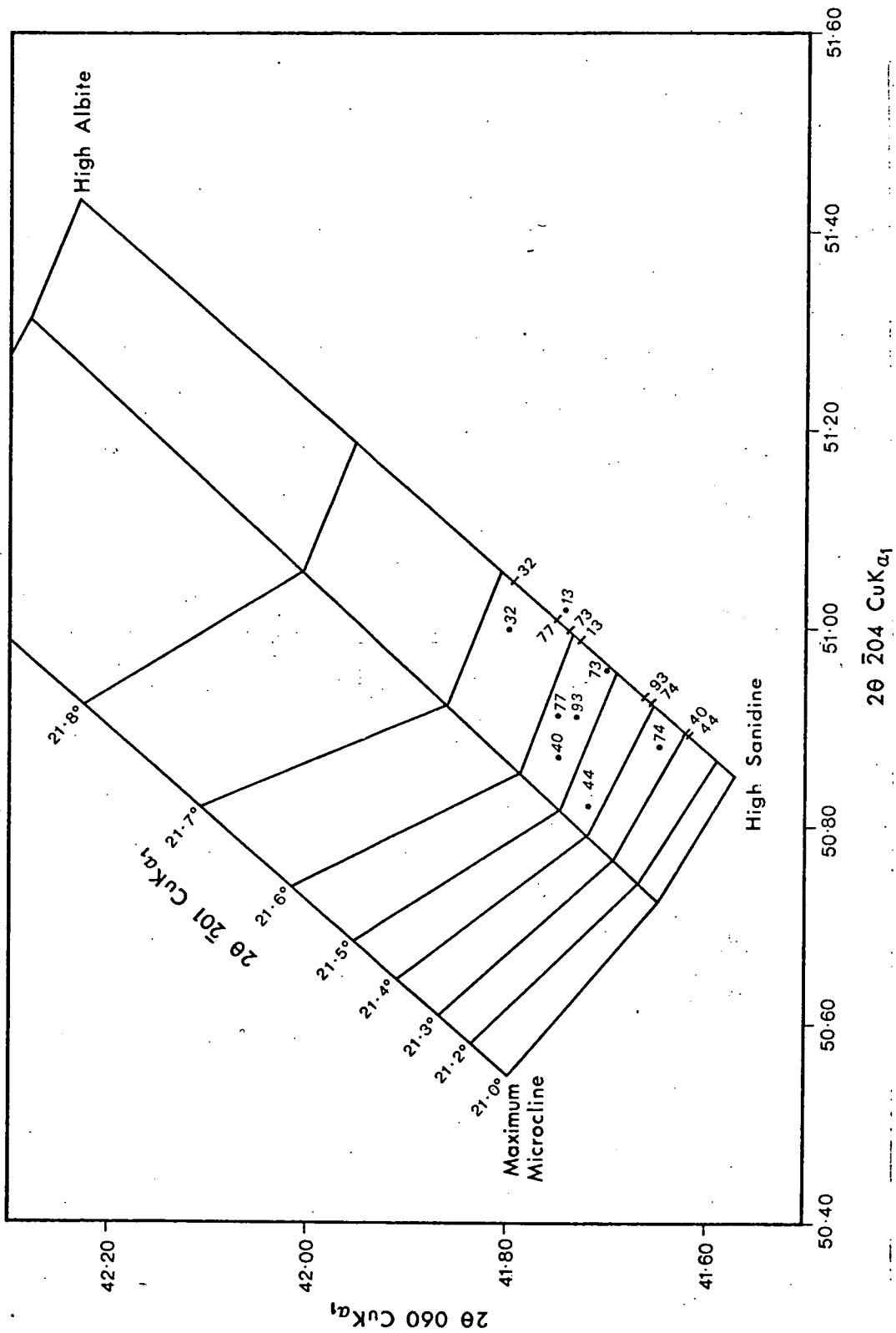


Figure III-18 Structural states of alkali feldspars from sanidine porphyries after Wright (1968). Compositions of samples are plotted as bars along the high sanidine-high albite edge.

While distinct exsolution patches are not obvious under the microscope, the electron microprobe analyses indicate the inhomogeneity of the crystal compositions which no doubt contributes to the scatter of the structural results. However, it can be seen from Figure III-18 that the structural and compositional data scatter covers the same area of the diagram so that while they may differ in detail, the results are in general, compatible. Clear evidence for unmixing is shown by soda and potash-rich patches in sanidine from specimen X44.

The compositions of the ternary feldspars for the hybrid rocks have been plotted in Figure III-19. Here the compositions of the original dolerite plagioclases (andesine and labradorite) appear, together with the potash feldspars produced by the alkaline magma. The outstanding feature here is the presence of anomalously high anorthite component in these feldspars, which may represent a degree of disequilibrium in the reaction between the introduced potash and the original dolerite feldspars. The range of the feldspar compositions here could also be due to the release of the albite component from the dolerite plagioclase together with a contribution from the alkaline magma.

In the case of the syenite porphyries, there are euhedral phenocrysts of plagioclase with either fine grained altered groundmass or with a better crystallized coarse groundmass containing subhedral alkali feldspar crystals and some interstitial quartz. Once again with these rocks the empirical plot of the data indicates that the plagioclase crystals have formed at a lower temperature than have the subhedral alkali feldspars.

Associated with these there is evidence of two periods of growth of the plagioclase phenocrysts. This apparent reversed process would suggest that the alkali feldspar was a later addition rather than evolution from a single parent magma. However, there is a significant anorthite component in the CIPW normative values for the host rock (Appendix No. 3). This is mainly related to feldspar composition as calcic ferromagnesian minerals are not abundant in most rocks and are absent in many.

From the work of von Platten (1965) and also that of James and Hamilton (1969) it can be seen that with a significant amount of anorthite present, the crystallization of alkali potash feldspar is suppressed and with an anorthite content of about 12%, alkali feldspar is suppressed completely and only a plagioclase will form and eventually crystallize with quartz and alkali feldspar in the matrix. James and Hamilton presented their results for 1 kb pressure. When compared with the simpler system of Bowen and Tuttle (1958) it can be shown empirically that an increase in pressure should drive the equilibrium boundary towards the albite apex of the triangle. Thus for the higher values of anorthite it is not likely that an equilibrium potash feldspar can form. Many of the plagioclase crystals show evidence of at least two stages of growth and some occasionally have irregular core grains of andesine, while with some crystals there is evidence of fracturing and re-cementing processes having taken place (Pl. 15). Referring to Fig. III-17 where the compositions of feldspars from all rocks have been plotted, there is no evidence from the syenite porphyries of plagioclase compositions tending to approach the alkali feldspar field. This indicates a discontinuity between the two sets of minerals and evidence at least of disequilibrium within these rocks.

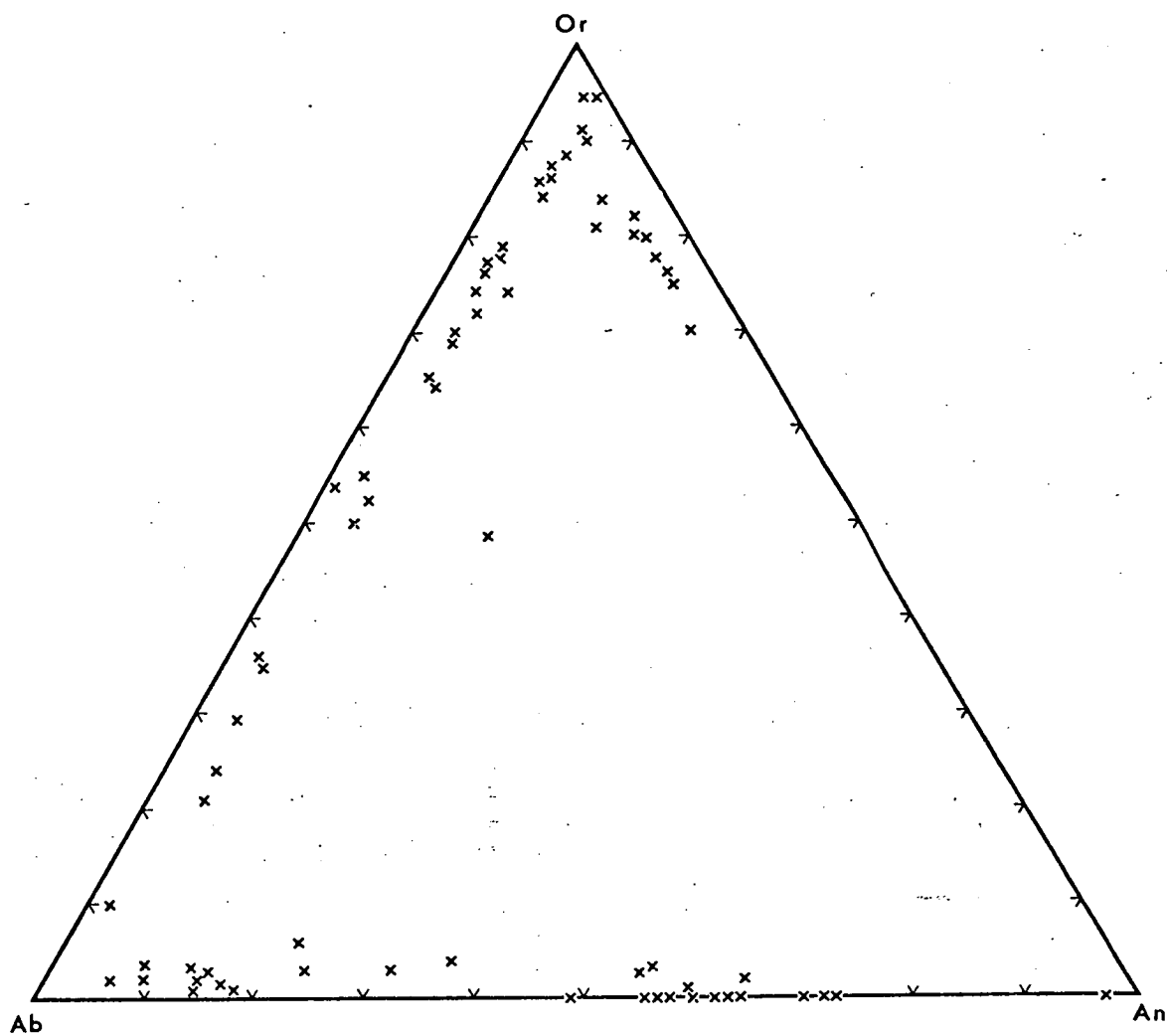


Figure III-19 Ternary feldspar plot for feldspars from the hybrid rocks.

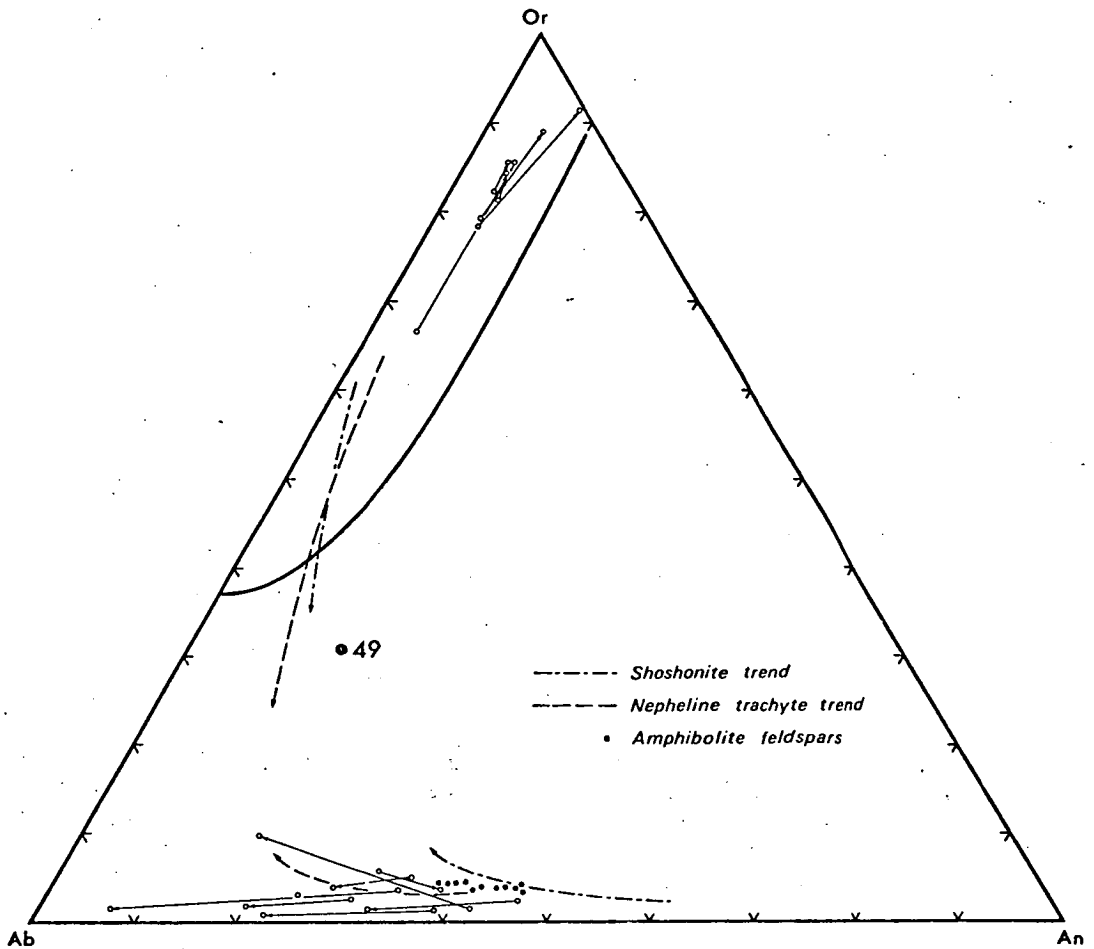


Figure III-20 Core-rim compositions for co-existing feldspars in syenite porphyry CY49. Compositions of amphibolite feldspars and shoshonite and nepheline trachyte trends (Carmichael et al., 1974) have also been added together with normative composition of CY49. Curve in figure represents the approximate locus of compositions of liquids with which two feldspars may co-exist in equilibrium with leucite omitted.

The potash feldspars in particular, do not follow the crystallization trends observed by Nichols and Carmichael (1974) and the plagioclase phenocrysts follow an apparent trend parallel to the Ab-An edge whereas for an equilibrium crystallization trend they should trend towards the alkali feldspar apex of the triangle (Or-Ab-An).

The compositions for the cores and rims of feldspar crystals from the syenite porphyries (CY49 and CY70) are featured in Figures III-20 and III-21. On these diagrams are also plotted the expected equilibrium crystallization trends of Carmichael et al. (1974) for nepheline trachyte and shoshonite trends. The trends shown seem to be non-equilibrium. For CY70 there is apparently a simple crystallization trend largely independent of the potash feldspars and parallel to the Ab-An edge with some reversals. Texturally, the plagioclases are usually euhedral, and precede the potash feldspars in their formation. For CY49, once again there is no obvious dependence of the plagioclase trend, upon the potash feldspars. There is more evidence of a reversal of trend for some of the plagioclase crystals in this rock.

Perhaps the most interesting feature of these rocks is the consistent trend to potassium enrichment from core to rim in the alkali feldspar crystals. This indicates that these crystals were not in equilibrium with the associated liquid which apparently was being progressively enriched in potassium, whereas in a normal crystallization sequence, the liquid should become progressively enriched in soda as potash rich feldspars and/or plagioclase are removed from the system. This together with the earlier observations leads to the conclusion that equilibrium crystallization was not operative for the Cygnet porphyries. For comparison, the compositions of the plagioclases from the amphibolite inclusions are also plotted in the above figures.

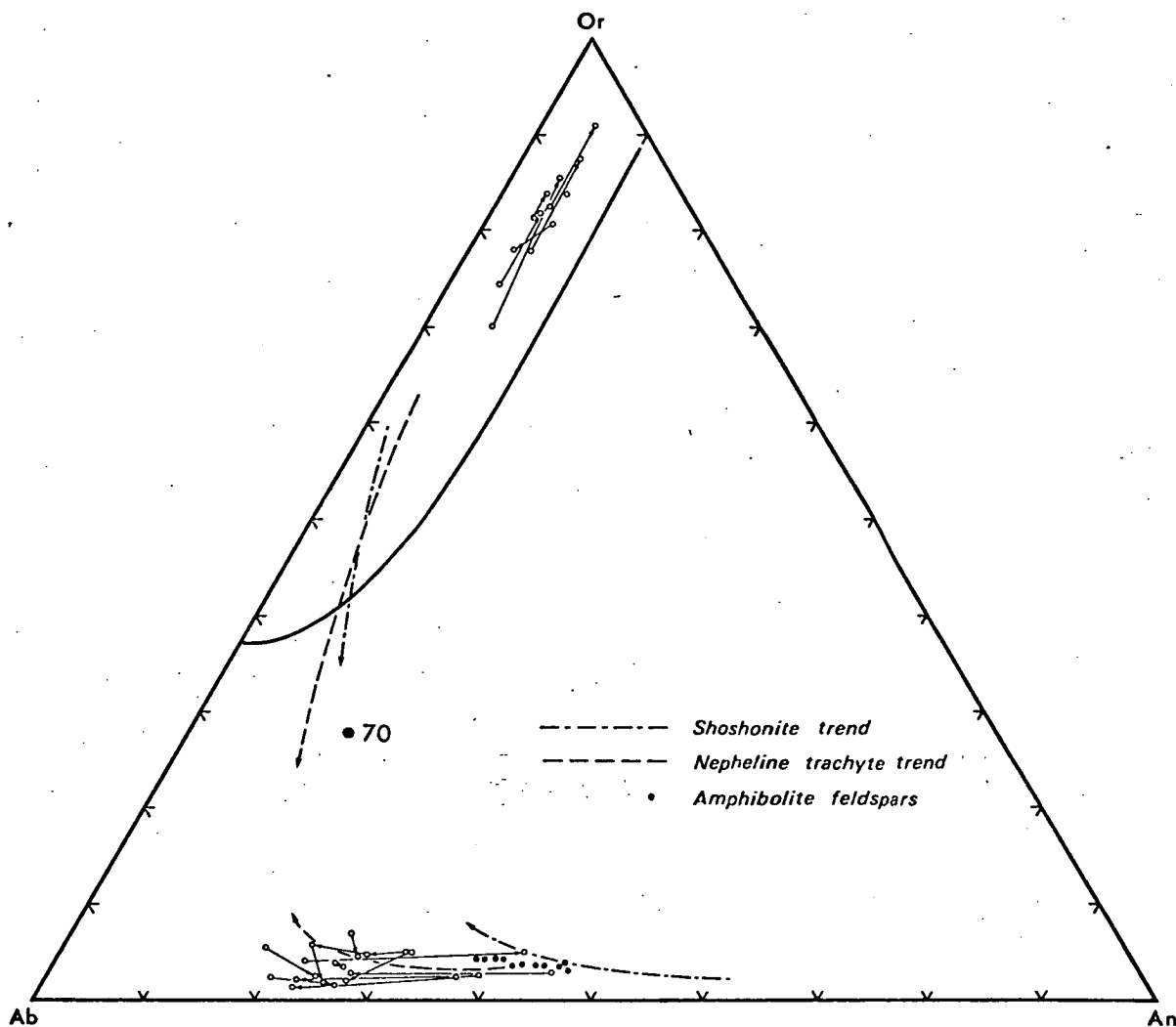


Figure III-21 Core-rim compositions for co-existing feldspars in syenite porphyry CY70. Compositions of amphibolite feldspars and shoshonite and nepheline trachyte trends (Carmichael et al., 1974) have also been added together with normative composition of CY70. Curve in figure represents the approximate locus of compositions of liquids with which two feldspars may co-exist in equilibrium with leucite omitted.

For the dykes where there is a mixed phenocryst assemblage present (CY61 and CY92) the relationships show a better correlation than for those described above. The compositions for centres and rims of phenocrysts from these rocks are plotted in Fig. III-22. In these rocks the trends for the plagioclase rocks are more like an equilibrium trend. Some potash feldspars show the expected trend towards sodium rich rims but there are still many reversals. This, together with the armouring of the pre-existing plagioclase by a later superposition of potash feldspar (Pl. 9), suggests the addition of a later stage liquid richer in potash, or that crystallization of plagioclase had pushed the melt to the co-tectic line with the consequent precipitation of the co-existing potash feldspar or that the plagioclase had reached a resorption point with the remaining melt. The tie lines in Fig. III-22 represent associations of rim composition for the plagioclase and the armouring potash feldspar. Where measurable a core value for the potash feldspar has also been given.

Empirically it can be seen that the normative plots of CY61 and CY92 are close to the cotectic trough on the Ab-Or-An triangle (Carmichael et al., 1974) whereas the syenite porphyries CY49 and CY70 do not plot near this (Figs. III-20 and III-21).

From this it would appear that the most likely cause of the potash feldspar armouring the plagioclase is due to resorption of the plagioclase by the magma and precipitation of the potash feldspar as outlined by Stewart and Rosenboom (1962), Rahman and MacKenzie (1969), Carmichael et al. (1974) although co-precipitation near the system minimum is still a possibility.

Neglecting the detail of the relationships of the feldspars, it is sufficient to recognise that the brown matrix rocks have crystallized near the minimum for the system and thus may represent a late stage,

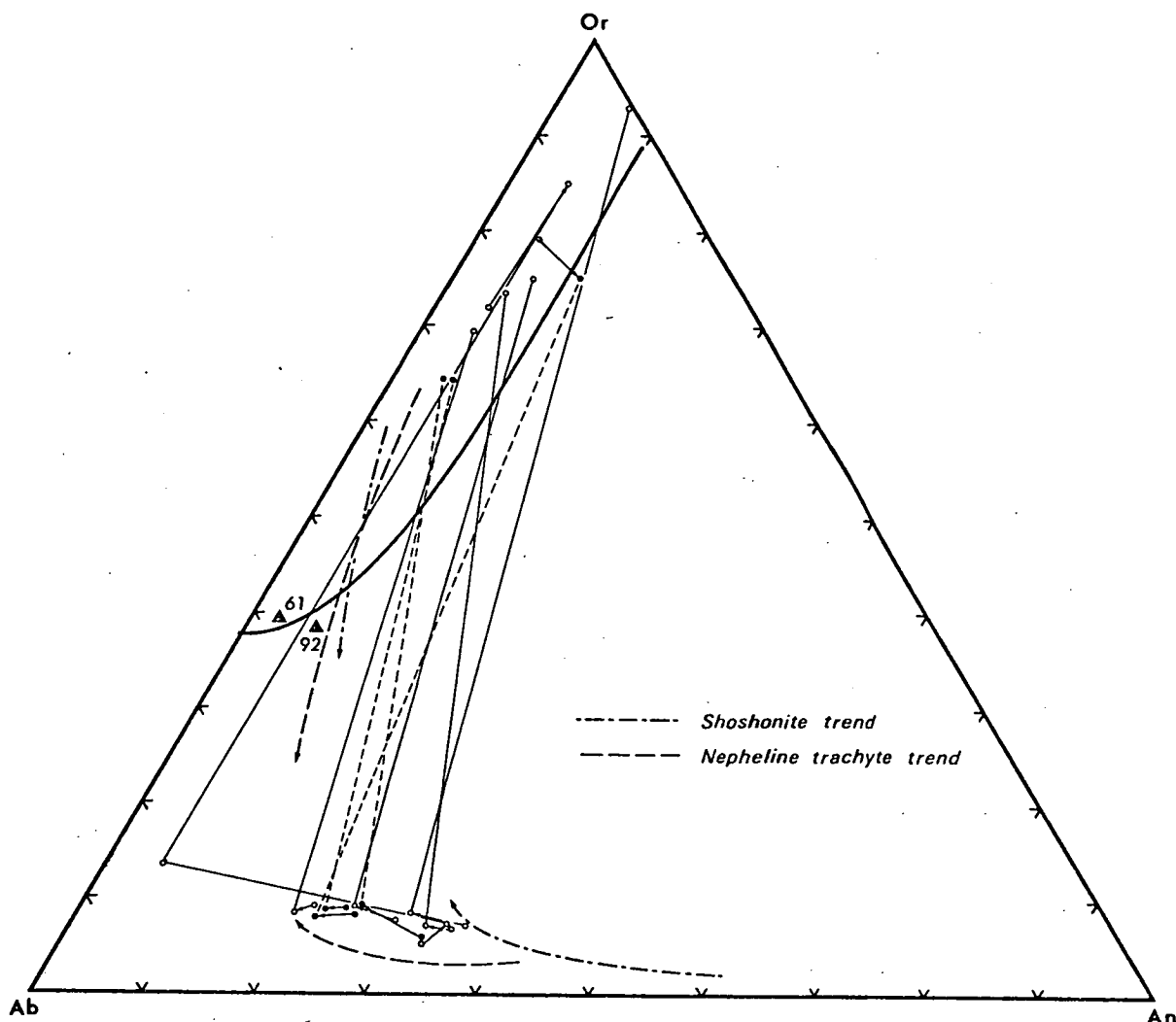


Figure III-22 Core-rim compositions for co-existing phenocrysts in CY61 (open circle) and CY92 (closed circle). Tie lines connect crystals with K-feldspar overgrowths. Shoshonite and nepheline trachyte trends (Carmichael et al., 1974) have been added together with normative compositions of CY61 and CY92. Solid lines for CY61 and dashed tie lines for CY92. Curve in figure represents the approximate locus of compositions of liquids with which two feldspars may co-exist in equilibrium with leucite omitted.

TABLE III-13

Electron microprobe analyses of cores and rims of feldspar phenocrysts and crystals. c = core; e = edge; o = overgrowth;
G.M. = groundmass crystal.

Syenite Porphyries

CY49

	c	e	c	e	c	e	c	e	c	e	c	e	c	e
Na ₂ O	7.33	7.34	1.83	0.83	7.08	7.11	1.35	0.46	5.49	7.36	2.30	1.38	1.61	1.28
Al ₂ O ₃	23.59	23.56	18.78	18.10	23.22	23.55	18.34	17.82	26.74	23.66	18.92	18.29	18.24	18.22
SiO ₂	63.21	63.10	64.62	65.03	63.34	62.97	65.22	65.31	58.44	62.88	64.85	65.46	65.45	65.44
K ₂ O	0.55	0.61	12.92	15.01	1.10	0.76	13.89	15.43	0.48	0.53	12.44	13.95	13.80	14.12
CaO	4.77	4.84	1.09	1.03	4.74	5.01	0.97	0.98	8.61	5.08	0.84	0.92	0.90	0.93
BaO	0.00	0.00	0.77	0.00	0.00	0.00	0.23	0.00	0.00	0.00	0.64	0.00	0.00	0.00
Total	99.45	99.45	100.01	100.00	89.48	89.40	100.00	100.00	99.76	99.51	89.79	100.00	100.00	99.99
Ca	25.54	25.65	5.52	5.01	25.11	26.69	4.84	4.86	45.07	26.67	4.28	4.28	4.42	4.66
Na	70.95	70.48	16.70	7.39	67.94	68.52	12.28	4.11	51.97	70.00	21.03	21.03	14.42	11.60
K	3.51	3.87	27.78	87.59	6.94	4.79	82.87	91.02	2.96	3.33	74.69	74.69	81.16	83.74
	c	e	c	e	c	e	c	e	c	e	c	e	c	e
Na ₂ O	6.75	5.62	6.70	7.43	2.59	1.17	6.40	8.07	1.31	1.52	6.19	7.77	6.56	6.19
Al ₂ O ₃	24.51	25.92	24.28	23.75	19.36	18.11	25.24	22.97	18.51	18.27	25.52	23.13	24.19	25.52
SiO ₂	61.53	59.60	61.96	63.28	64.42	65.15	60.57	63.89	64.10	65.10	60.11	64.07	62.15	60.11
K ₂ O	0.68	0.82	0.82	0.33	11.35	14.63	0.40	0.28	14.21	14.19	0.45	0.35	0.80	0.45
CaO	6.13	7.82	5.84	4.87	1.16	0.94	6.92	4.26	1.13	0.92	7.41	4.25	5.87	7.41
BaO	0.00	0.00	0.00	0.00	1.13	0.00	0.00	0.00	0.73	0.00	0.00	0.00	0.00	0.00
Total	99.60	99.73	99.60	99.66	100.01	100.00	99.93	99.47	99.99	100.10	99.68	99.57	99.57	98.68
Ca	32.00	41.24	30.83	26.02	5.99	4.55	36.47	22.20	5.55	5.59	38.69	22.68	31.43	38.69
Na	63.77	53.57	64.00	71.88	24.21	10.39	61.03	76.04	11.65	13.33	58.51	75.11	63.49	58.51
K	4.23	5.20	5.18	2.10	69.81	85.06	2.49	1.77	82.80	82.18	2.80	2.21	5.08	2.80

TABLE III-13 (continued)

Syenite Porphyries

CY49 continued ...

	c	o	c	e	c	e	o	o
Na ₂ O	7.21	7.72	1.15	1.96	7.90	7.35	1.61	1.29
Al ₂ O ₃	23.47	23.28	18.15	18.25	22.57	23.55	18.36	18.05
SiO ₂	63.10	63.20	65.51	65.77	65.03	63.47	65.25	65.54
K ₂ O	0.85	0.40	14.13	13.14	0.33	0.32	13.83	14.22
CaO	4.96	4.74	1.06	0.88	3.78	4.81	0.95	0.89
BaO	0.00	0.00	0.00	0.00	0.00	0.00	0.00	0.00
Total	99.59	99.34	100.00	100.10	99.61	99.30	100.00	99.99
Ca	26.08	24.70	5.30	4.37	20.46	26.00	4.70	4.44
Na	68.63	72.82	10.40	17.65	77.41	71.99	14.31	11.59
K	5.28	2.48	84.30	77.98	2.13	2.01	80.99	83.97

CY70

	c	e	c	e	c	e	c	e	o	c	e	c	e
Na ₂ O	5.86	7.59	6.77	6.09	1.50	1.24	6.57	6.69	9.31	1.81	-	6.29	7.31
Al ₂ O ₃	26.12	23.75	24.04	25.20	18.98	18.31	24.54	24.76	18.88	19.17	17.46	24.97	23.9
SiO ₂	59.53	62.89	61.82	60.70	63.86	65.13	61.52	61.12	69.74	63.59	64.20	61.09	62.44
K ₂ O	0.26	1.54	0.87	0.62	13.40	14.20	0.57	0.51	0.29	12.72	16.57	0.77	0.49
CaO	7.90	3.30	6.03	7.14	0.95	0.87	6.43	6.55	1.21	0.85	1.77	6.56	5.44
BaO	0.00	0.00	0.00	0.00	1.32	0.25	0.00	0.00	0.00	1.86	0.00	0.00	0.00
Total	99.67	99.07	99.53	99.75	99.01	100.00	99.63	99.63	99.43	100.00	100.00	99.68	99.58

TABLE III-13 (continued)

Syenite Porphyries

CY70 continued ...

	c	e	c	e	c	e	o	c	e	o	c	e	c
Ca	41.96	17.48	31.19	37.79	4.82	4.31	33.85	34.01	6.55	4.39	8.20	34.77	28.29
Na	56.36	72.81	63.42	58.32	13.80	11.22	62.60	62.83	91.58	16.98	0.00	60.38	68.70
K	1.67	9.72	5.39	3.90	81.38	84.47	3.55	3.17	1.87	78.64	91.80	4.85	3.02
	c	e	c	e	c	e	c	e	c	e	c	e	c
Na ₂ O	1.76	0.52	5.53	6.98	3.11	1.12	7.08	8.14	1.43	1.11	6.34	8.04	1.37
Al ₂ O ₃	18.75	17.83	26.86	24.37	19.05	17.87	24.24	22.33	18.73	18.43	25.09	22.64	19.04
SiO ₂	64.92	65.12	58.06	62.02	64.90	65.47	62.13	65.00	64.20	64.87	60.67	64.75	63.80
K ₂ O	12.81	15.38	0.36	0.25	10.84	14.57	0.40	0.32	13.60	14.06	0.32	0.30	13.40
CaO	0.86	1.15	8.89	6.02	0.83	0.95	5.64	3.71	0.89	0.90	7.12	3.86	0.86
BaO	0.90	0.00	0.00	0.00	1.26	0.00	0.00	0.00	1.16	0.64	0.00	0.00	1.53
Total	100.00	99.00	99.70	99.64	99.89	99.98	99.49	99.50	100.01	100.02	99.54	99.59	100.00
	c	e	c	e	c	e	c	e	c	e	c	e	c
Ca	4.45	5.60	46.00	31.75	4.30	4.69	29.77	19.72	4.50	4.61	37.53	20.55	4.48
Na	16.52	4.61	51.78	66.63	29.07	9.97	67.67	78.25	13.14	10.20	60.48	77.52	12.82
K	79.04	89.79	2.22	1.62	66.63	85.34	2.56	2.03	82.36	85.20	2.00	1.93	82.70

TABLE III-13 (continued)

Mixed Phenocryst Sanidine Rocks

CY61

	c	e	c	e	c	e	o	c	e	c	e	c	e	c	e
Na ₂ O	2.78	0.97	3.35	3.22	6.12	7.07	1.97	6.83	6.91	7.43	8.34	2.35	8.71	2.39	2.15
Al ₂ O ₃	18.62	18.78	18.61	18.30	24.43	23.12	18.75	23.42	23.13	21.77	21.89	18.47	19.65	18.90	18.26
SiO ₂	65.13	64.32	65.61	65.11	61.82	62.87	64.50	62.70	62.92	65.36	65.66	65.15	68.44	65.76	65.09
K ₂ O	12.15	14.47	11.18	12.00	1.11	1.44	12.81	1.44	1.52	1.81	0.50	12.76	1.97	11.89	13.34
CaO	1.03	0.95	0.89	0.78	4.99	4.75	1.44	4.89	4.78	3.14	3.03	1.03	0.00	1.07	0.92
BaO	0.00	0.51	0.00	0.00	0.00	0.00	0.00	0.00	0.00	0.00	0.00	0.00	0.00	0.00	0.00
Total	99.68	100.00	99.64	99.41	98.47	99.25	99.47	99.28	99.28	99.51	99.42	99.76	98.77	100.01	99.76
Ca	5.03	4.78	4.36	3.71	28.69	24.70	7.08	25.76	25.01	16.74	16.16	5.03	0	5.46	4.42
Na	24.49	8.8	29.90	27.89	63.68	66.39	17.62	65.19	65.51	71.78	80.65	20.78	87.05	22.11	18.82
K	70.48	86.43	65.74	68.39	7.63	8.91	75.30	9.05	9.48	11.48	3.19	74.19	12.95	72.43	76.76
	c	e	c	e	c	e	o	c	e	o	c	e	c	e	c
Na ₂ O	1.82	2.47	2.03	0.65	6.24	6.38	2.35	7.26	7.7	2.93	2.81	2.97	2.49	2.88	2.32
Al ₂ O ₃	18.66	18.58	18.43	18.17	24.89	24.27	18.66	22.55	22.49	18.58	18.33	18.71	18.33	18.48	18.76
SiO ₂	64.59	65.66	64.87	64.42	60.38	61.33	64.87	64.02	63.43	65.79	65.22	65.77	65.41	65.80	65.38
K ₂ O	12.91	12.25	13.31	15.76	1.11	1.14	12.57	1.43	1.37	1.81	12.00	12.60	11.77	12.33	12.19
CaO	0.92	1.04	1.06	1.01	6.53	6.04	1.08	3.98	3.81	0.89	0.93	0.91	0.90	0.84	0.97
BaO	0.00	0.00	0.00	0.00	0.00	0.00	0.00	0.00	0.00	0.00	0.00	0.00	0.00	0.00	0.00
Total	98.90	100.00	99.70	100.01	99.05	99.16	99.53	99.24	98.80	100.00	99.29	100.96	98.90	100.33	99.62
Ca	4.72	5.15	5.19	4.81	34.12	31.89	5.32	21.16	19.66	4.41	4.58	4.53	4.45	4.19	4.89
Na	16.80	22.26	17.84	5.58	58.98	60.95	20.93	69.81	71.95	26.18	25.05	26.73	22.06	25.97	21.17
K	78.49	72.59	76.98	89.61	6.90	7.15	73.74	9.03	8.39	69.42	70.37	68.74	73.49	69.84	73.93

TABLE III-13 (continued)

Mixed Phenocryst Sanidine Rocks

CY61 continued ...

	e	c	e	o	c	e	c	e	c	e	c	e	o	c	e
Na ₂ O	7.42	6.04	6.33	0.00	6.56	6.19	2.59	1.13	3.02	5.34	6.85	7.17	1.07	2.57	1.27
Al ₂ O ₃	19.31	24.82	24.45	18.55	24.72	24.96	18.70	18.23	18.94	19.27	24.08	23.34	18.08	19.07	18.26
SiO ₂	67.11	60.74	61.65	63.88	61.30	60.50	65.17	65.09	65.32	66.82	61.99	62.72	64.99	65.17	64.87
K ₂ O	4.46	1.14	1.27	15.57	1.02	1.15	12.24	14.55	11.38	7.21	1.01	1.18	15.07	11.77	14.42
CaO	0.29	6.67	5.67	1.33	6.00	6.42	0.96	1.00	1.01	1.03	5.34	4.81	0.80	0.94	0.91
BaO	0.00	0.00	0.00	0.00	0.00	0.00	0.00	0.00	0.00	0.00	0.00	0.00	0.00	0.25	0.00
Total	98.59	99.41	99.37	99.33	99.60	99.22	99.66	100.00	99.67	99.67	99.27	99.22	100.01	99.77	99.73
Ca	1.55	35.2	30.40	6.73	31.46	33.79	4.75	4.88	5.02	5.36	28.20	25.03	3.87	4.81	4.48
Na	70.55	57.61	61.48	0	62.15	58.99	23.15	10.01	27.32	50.11	65.46	67.62	9.35	23.69	11.29
K	27.90	7.19	8.12	93.27	6.39	7.22	72.09	85.11	67.66	44.53	6.34	7.35	86.78	71.50	84.23

CY92

	c	e	o	c	e	o	c	e	c	3	o	G.M. Crystal	c	e	c
Na ₂ O	6.74	7.15	3.44	7.20	7.31	3.30	7.15	7.61	6.92	7.32	4.50	7.61	7.07	7.58	4.26
Al ₂ O ₃	24.50	23.01	18.72	22.91	22.73	18.65	23.04	22.52	23.18	23.00	18.98	20.28	23.08	22.21	18.98
SiO ₂	61.01	62.90	65.92	63.20	63.68	65.88	63.30	64.46	63.15	63.34	65.90	66.61	63.31	64.47	65.93
K ₂ O	0.96	1.53	10.81	1.37	1.40	10.91	1.30	0.98	1.28	1.28	9.19	2.93	1.38	1.65	9.26
CaO	6.10	4.89	0.91	4.77	4.33	0.94	4.67	2.34	4.92	4.53	1.02	1.68	4.65	3.61	1.20
Total	99.31	99.48	99.80	99.45	99.45	99.68	99.46	97.91	99.45	99.47	99.59	99.11	99.49	99.52	99.63
Ca	31.35	24.89	4.58	24.57	22.50	4.71	24.39	13.56	25.93	23.47	5.09	8.87	24.34	18.72	6.02
Na	62.76	65.79	31.11	62.03	68.83	29.99	67.57	79.69	66.05	68.65	40.48	72.71	67.09	71.10	38.69
K	5.89	9.31	64.32	8.41	8.67	65.31	8.04	6.75	8.01	7.88	54.42	18.42	8.57	10.18	55.29

TABLE III-13 (continued)

Mixed Phenocryst Sanidine Rocks

CY92 continued ...

	e	c	e	G.M. Crystal	c	e	o	c	e	c	e	c	e
Na ₂ O	4.38	7.35	7.58	4.01	7.35	7.51	3.63	7.02	7.48	2.79	2.78	7.18	7.39
Al ₂ O ₃	18.90	23.02	22.45	18.49	22.69	22.27	18.66	22.87	22.60	18.57	18.22	22.91	22.35
SiO ₂	66.07	63.42	63.99	66.03	63.74	64.45	64.17	63.59	63.88	65.96	64.74	63.49	64.17
K ₂ O	9.35	1.29	1.41	10.25	1.47	1.49	10.05	1.35	1.35	11.68	11.86	1.54	1.44
CaO	0.96	4.52	3.97	0.79	4.26	3.68	3.48	4.71	4.14	1.00	2.40	4.24	4.03
Total	100.68	99.60	99.39	99.57	99.51	99.40	99.99	99.54	99.45	100.00	99.00	99.36	99.38
Ca	4.80	23.32	20.50	3.92	22.06	19.33	15.81	24.70	21.50	5.10	11.20	22.30	21.10
Na	39.62	68.72	70.83	35.83	68.87	71.33	29.81	66.80	70.20	25.20	23.30	68.14	70.00
K	55.58	7.96	8.67	60.25	9.07	9.33	54.38	8.40	8.30	69.70	65.50	9.60	8.90

Sanidine Phenocryst Rocks

CY19

CY60

CY77

	c	e	c	e	c	e	c	e	c	e	c	e	c	e
Na ₂ O	2.22	2.11	2.36	2.24	2.29	2.12	2.17	2.15	1.16	0.98	0.83	0.97	2.64	2.63
Al ₂ O ₃	19.92	19.18	18.97	19.38	18.53	19.02	19.24	19.24	19.12	19.04	19.21	19.28	18.98	18.97
SiO ₂	63.58	65.10	65.15	65.01	65.32	65.17	64.54	64.61	62.81	63.67	63.20	62.80	65.48	65.14
K ₂ O	11.37	12.28	11.98	11.59	12.38	12.27	12.05	12.15	13.40	13.72	13.40	13.32	11.65	11.59
CaO	1.00	1.00	1.01	1.12	1.19	1.04	1.01	0.98	0.81	0.83	0.78	0.94	0.98	1.05
BaO	1.64	0.00	0.21	0.45	-	0.38	0.98	0.53	2.49	1.76	2.57	2.40	-	0.25
Total	99.73	99.67	99.68	99.79	99.71	100.00	99.99	99.66	99.79	99.01	98.99	99.71	99.73	99.62
Ca	5.36	5.16	5.14	5.90	5.91	5.31	5.20	5.08	4.31	4.4	4.24	5.04	5.02	5.38
Na	21.66	19.67	21.83	21.37	20.67	19.71	20.38	20.11	11.14	9.39	8.26	9.42	24.35	24.26
K	72.98	85.17	73.03	72.73	73.42	74.99	74.42	74.81	84.55	86.21	87.5	85.53	70.64	70.36

TABLE III-13 (continued)

Sanidine Phenocryst Rocks

CY84		CY40						CY74						
	c	e	c	e	c	e	c	e	c	e	c	e	c	e
Na ₂ O	2.06	1.48	2.56	1.54	1.44	1.35	1.08	0.62	0.93	0.87	1.18	1.35	1.16	1.48
Al ₂ O ₃	18.44	18.65	18.75	18.65	17.97	18.75	18.35	17.76	18.48	18.72	19.38	19.14	18.73	18.82
SiO ₂	65.55	64.96	65.30	64.92	65.20	64.66	64.07	65.40	63.75	63.70	64.02	63.91	64.48	65.08
K ₂ O	12.94	13.53	11.57	13.65	14.25	13.69	14.27	15.39	14.35	14.25	13.09	13.15	13.71	13.29
CaO	0.77	0.77	0.71	0.78	0.82	0.77	0.84	0.82	0.85	0.75	0.84	0.81	0.79	0.92
BaO	0.00	0.62	0.22	0.47	0.00	0.78	1.15	0.00	1.42	1.48	1.50	1.36	1.11	0.41
Total	99.76	100.01	99.11	100.01	99.68	100.00	99.76	99.99	99.78	99.74	100.01	99.72	99.98	100.00
Ca	3.90	3.91	3.70	3.91	3.99	3.91	4.25	4.04	4.28	3.89	4.51	4.26	4.13	4.73
Na	18.73	13.66	24.28	14.04	12.76	12.57	9.84	5.59	8.57	8.20	11.50	12.88	10.96	13.81
K	77.37	82.43	72.03	82.06	93.26	83.52	85.90	90.36	87.15	87.91	83.99	82.86	84.91	81.46

CY85		c	e	c	e	c	e	c	e
Na ₂ O	0.56	0.76	0.54	0.91	0.84	0.76	0.74	0.33	
Al ₂ O ₃	19.22	19.28	19.09	19.24	19.10	18.99	19.07	19.47	
SiO ₂	62.31	62.57	62.90	62.82	62.86	63.61	63.07	62.33	
K ₂ O	14.09	13.58	14.08	13.85	13.99	14.06	13.06	14.02	
CaO	0.81	0.70	0.87	0.84	0.90	0.76	0.78	0.82	
BaO	2.79	3.11	2.52	2.13	2.31	1.83	2.48	3.03	
Total	99.78	100.00	100.20	99.79	100.00	99.01	99.20	100.00	
Ca	4.36	3.84	4.68	4.43	4.73	4.03	4.19	4.48	
Na	5.39	7.51	5.23	8.35	7.92	7.26	7.24	3.30	
K	90.25	88.65	90.09	86.91	91.55	87.35	88.70	88.56	

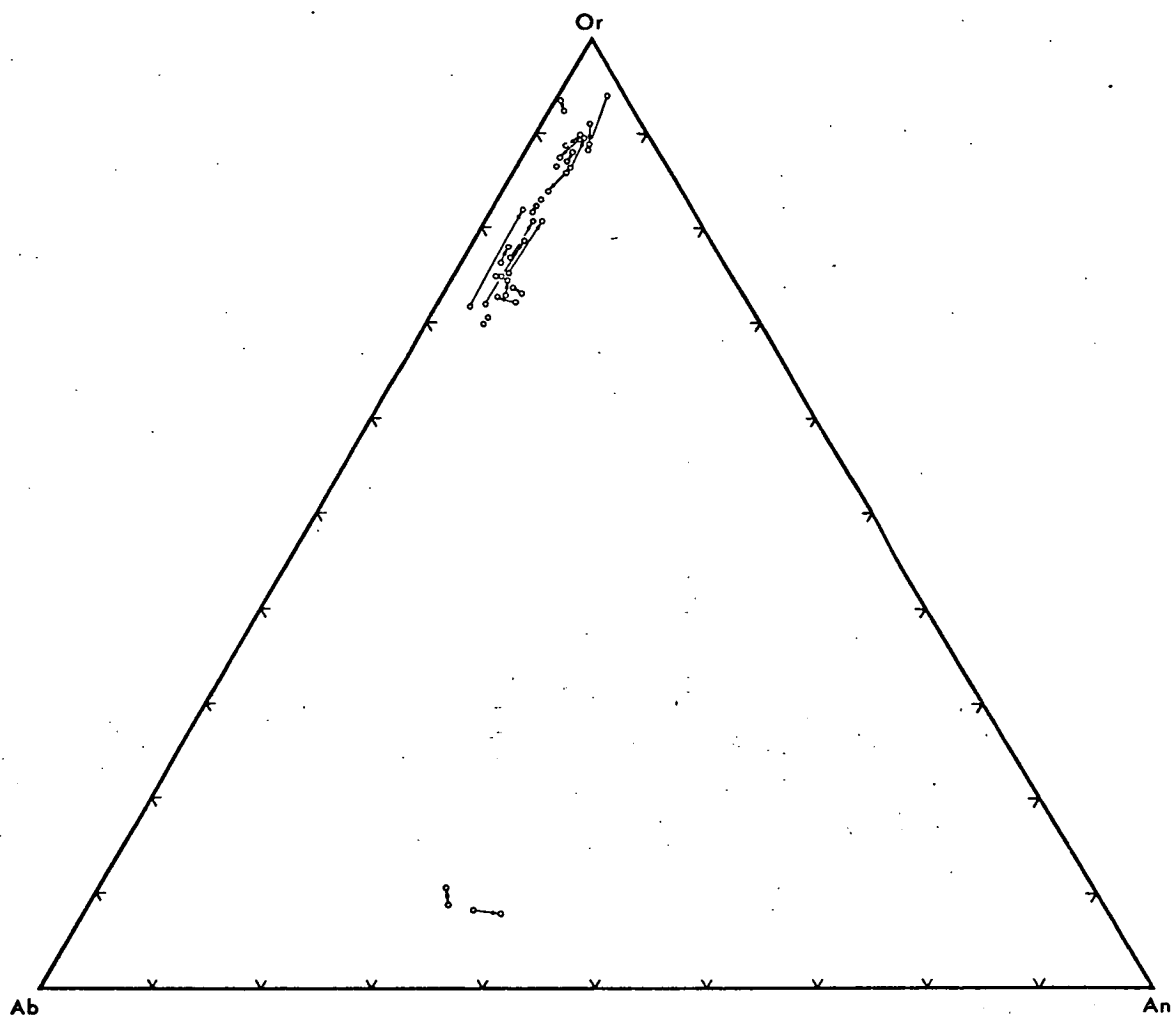


Figure III-23 Core-rim compositions for feldspar phenocrysts from the sanidine porphyry rocks.

near-equilibrium, fractionation of the syenite porphyries. When compared with the plagioclase compositions for the syenite porphyries, CY49 and CY70 (Figs. III-20 and III-21), the plagioclase of CY61 and CY92 are slightly more evolved if the scheme of Carmichael et al. (1974) is followed.

To complete the sequence Fig. III-23 summarizes the data for the rim and core compositions from the sanidine phenocryst rocks. In this plot the phenocryst trends are closer to normal with smaller variations, but still with some significant reversals. As field relations suggest these rocks were intruded towards the last part of the active period it can be visualized that these phenocrysts formed under conditions conducive to equilibrium euhedral crystal growth in some type of small magma chamber.

The trends recorded above may explain the failure of the feldspar thermometers reported earlier, which depend for their interpretation on the attainment of equilibrium. In the case of the rocks where sanidine forms the only phenocryst feldspar the lack of a coexisting plagioclase negated the application of the two feldspar geothermometer.

The trends in Fig. III-24, apart from the Californian rhyolite and the syenite porphyry trends, are comparable with the feldspar equilibria demonstrated by Seck (1971) (Fig. III-17) but the former two and in particular the syenite porphyry trend transgress Seck's tie lines and on this basis must be considered to be not in equilibrium although many authors have commented on the divergent trends for over-saturated and undersaturated rocks (Carmichael 1965, Sobolev 1959).

In making comparisons with the feldspar equilibrium compositions determined by Seck (1971), there may be a discrepancy due to non-saturation with water of the melts when compared with Seck's results, but so far the evidence favours water saturation.

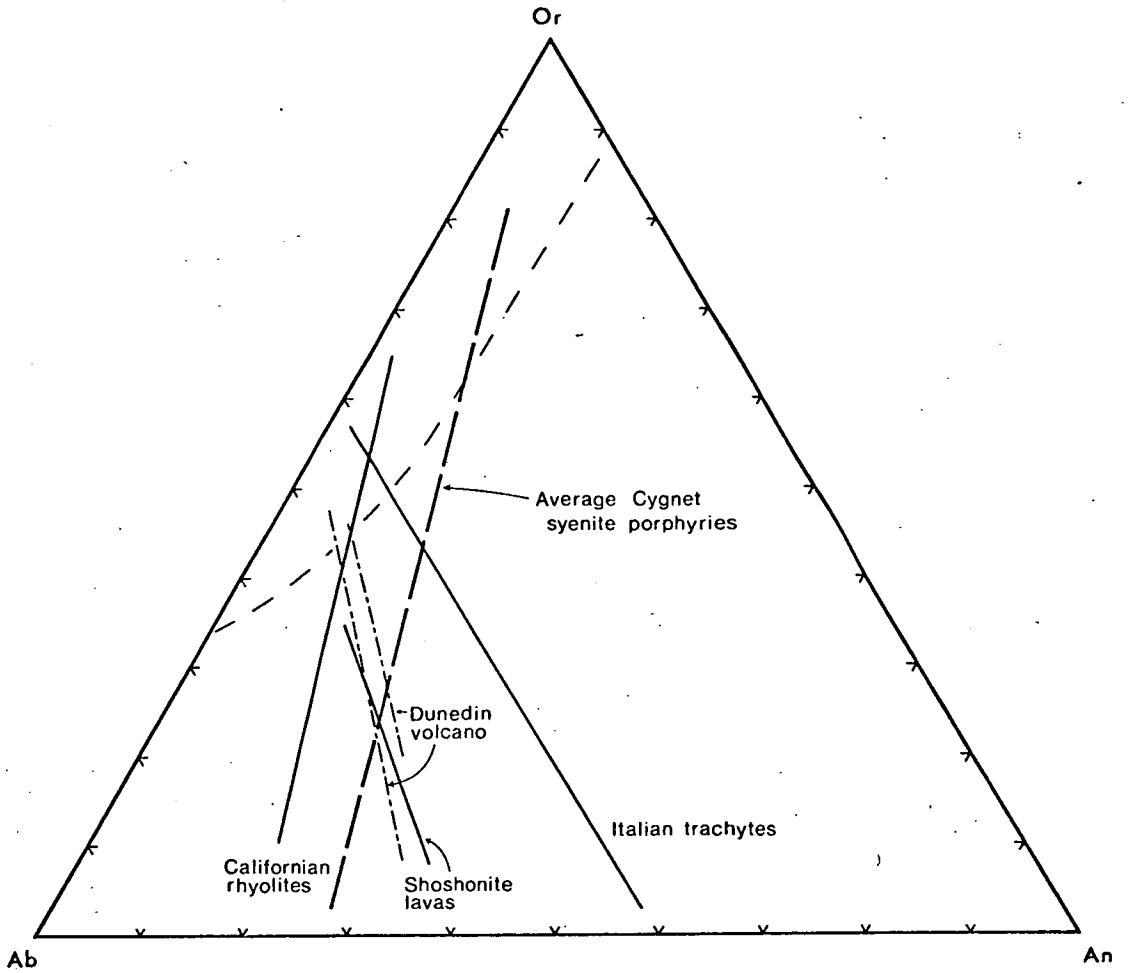


Figure III-24 Averaged values of co-existing feldspars from the syenite porphyry plotted on Ternary feldspar triangle. Other groups have been added for comparison (from Carmichael, Turner & Verhoogen, 1974).

SCAPOLITE MINERALOGY

Scapolite occurs only in dyke CY44 where it is relatively abundant and related to melanite garnet by a reaction relationship (Pl. 38). In the more normal associations of scapolite and garnet in metamorphic rocks the conditions favour the formation of garnet from scapolite, e.g. White (1959). Shaw (1960), Newton and Goldsmith (1975) and Goldsmith (1976) summarized the main parageneses of scapolite which virtually encompass the realms of high temperature metamorphism with hydrothermal or pneumatolytic alteration of pre-existing rocks. Von Knorring and Kennedy (1958) described a sulphate rich mizzonite occurring in a garnet-hornblende-pyroxene-scapolite gneiss of the Mampong Inselberg, Shai Hills, Ghana, and suggested that the scapolite had formed from the interaction of sulphide with other minerals present in an originally basic igneous rock.

In the case of CY44, because of the higher fugacity of sulphur species causing reaction with the melanite phenocrysts, there is the possibility that this increase was due to contamination from an alternative source. In the other potash dykes melanite is stable in the presence of hauynite which is a primary mineral. Where the melanite of CY44 has reacted it is surrounded by a rim of clear garnet with small crystals of highly birefringent sphene and a scattering of pyrite grains. There is then a further rim of strongly birefringent scapolite which may have included pyrite grains (Pl. 38). Pyrite may also show alteration to biotite and scapolite. Electron probe analysis of the scapolite shows it to be a sodium rich variety containing sulphur. A summary of the mineral compositions is given in Table III-14.

TABLE III-14

Electron microprobe analyses of phases from CY44

	Fresh melanite	Altered zone about fresh melanite	Scapolite	Biotite	Sphene
Na ₂ O	0.42	0.00	8.26	0.32	0.00
MgO	0.60	0.00	0.00	4.64	0.23
Al ₂ O ₃	6.81	10.91	19.87	18.07	6.26
SiO ₂	35.12	36.24	50.19	32.31	32.47
K ₂ O	0.00	0.00	2.32	9.09	0.00
CaO	31.65	32.41	1.38	0.50	29.03
TiO ₂	3.51	5.57	0.00	1.77	24.92
MnO	0.99	1.74	0.00	2.13	0.92
FeO	20.63	12.58	0.00	25.97	5.91
Unnormalized Total	103.09	101.24	82.12*	94.81	95.34

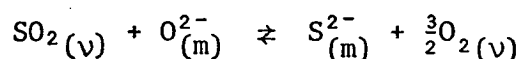
Cations on basis of equivalent oxygens

	Fresh melanite	Altered Zone	Scapolite	Biotite	Sphene
Na	0.138	0.000	Na 2.630	Na 0.051	Ca 2.064
Mg	0.151	0.000	K 0.480	K 0.936	Mg 0.023
Ca	5.778	5.676	Ca 0.240	Ca 0.043	
Mn	0.099	0.241			
Total	6.166	5.917	Total 3.350	Total 1.030	Total 2.087
Ti	0.450	0.685		Fe 1.752	Ti 1.244
Fe	2.940	1.719		Mg 0.558	Al 0.490
Al	1.352	2.022		Al 0.325	Fe 0.328
				Mn 0.146	Mn 0.052
				Ti 0.107	
Total	4.742	4.426		Total 2.888	Total 2.114
Al	0.016	0.079	Al 3.840	Al 1.393	
Si	5.984	5.921	Si 8.220	Si 2.607	Si 2.155
Total	6.000	6.000	Total 12.060	Total 4.000	Total 2.155
Oxygen	24.000	24.000	Oxygen 24.000	Oxygen 11.000	Oxygen 10.000

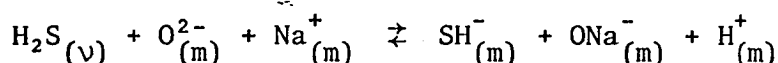
* Sulphur not analysed.

Initial fixing of sodium leads to potassium later reacting with the pyrite to form biotite. The following reactions are suggested as expressing the mineralogical changes involved. As sodium activity is lowered, potassium activity increases and later alteration of pyrite to biotite occurs. There must also be a balance between the activity of water and sulphur species. The clear pink garnet formed in the reaction is anisotropic hence it may be partially hydrated.

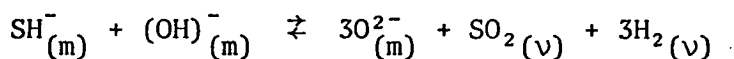
The physical chemistry of sulphur in magmatic melts has been summarised by C.W. Burnham in Barnes (1979). According to Burnham the solubility of sulphur in an aluminosilicate melt is related to the non-bridging oxygen O^{2-} , thus:



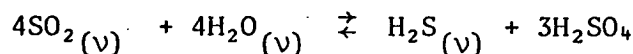
In the presence of H_2O the SO_2 will hydrolyse to the more soluble H_2S which may dissolve in the magma in the manner:



Under the fO_2 conditions of typical acid rocks, about $\log fO_2 = -14$ (Carmichael et al., 1974) most of the sulphur exsolved from a magma may form SO_2 via such reactions as:



At sub-solidus temperatures and higher than normal fO_2 , SO_2 may undergo hydrolysis according to the scheme:



For CY44, which crops out within 400 m of the hybrid rocks of Regatta Point, the conditions established there could be applied to the former locality. Thus $\log fO_2$ would be about -13 and the maximum pressure at 1 kb. Because pyrite is produced the temperature probably did not greatly exceed 742°C.

Eastoe (1979) has developed equations describing likely sulphur

species at varying values of f_{O_2} . The equation applicable here is:

$$\log k = \log f_{H_2O} + \log f_{SO_2} - \frac{3}{2} \log f_{O_2} - \log f_{H_2S}$$

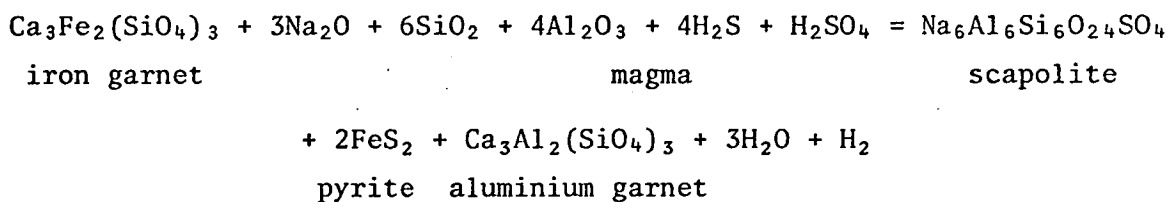
For 1 kb and 727°C, that is 1000°K, and using the appropriate value of f_{H_2O} then:

$$\begin{aligned} \frac{\log f_{SO_2}}{\log f_{H_2S}} &= \log k - \log f_{H_2O} + \frac{3}{2} \log f_{O_2} \\ &= 23 - (2.8) + \frac{3}{2} (-13) = 0.7 \end{aligned}$$

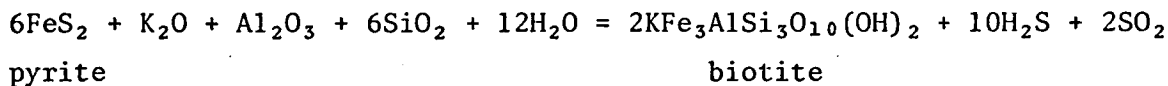
Hence $\frac{f_{SO_2}}{f_{H_2S}} = 5.01$

The data have been taken from Eastoe (op. cit.) who based his equation on the H-M buffer data of Haas and Robey (1973) and Newton (1935).

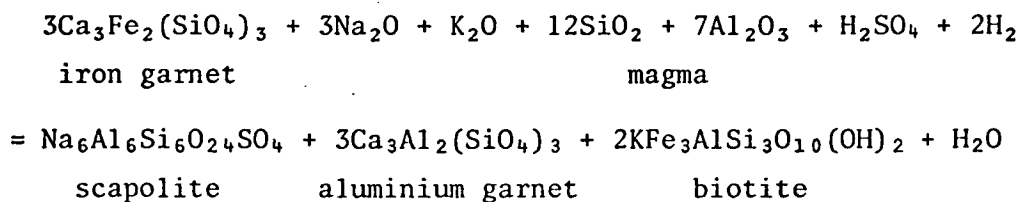
Thus the sulphur species in the magma are probably dominated by SO_2 and in the presence of excess water would hydrolyse as outlined above with production of H_2SO_4 favoured. The formation of scapolite could then be formulated as follows:



Reaction of pyrite with potash gives:



Occasionally an outer rim of biotite can be seen with no obvious pyrite cubes, which would suggest both of the above equations could be amalgamated to give the following:



Any titanium released by stoichiometric adjustments of the garnets

crystallizes as sphene. The fugacities of the sulphur species and water components are very important in the above equilibria and are related in a complex way. In this particular dyke sulphur activity was the highest of all the Port Cygnet rocks as similar reactions have not been seen in other rocks. In CY74, also a grey groundmass rock, there has been formation of calcite reaction rims around some of the melanites (Pl. 29) indicating a high f_{CO_2} but in the other dykes the melanites are unaltered and co-exist with feldspathoids.

CHAPTER IV

THE MAJOR ELEMENT CHEMISTRY OF THE ROCKS

Approximately 138 analyses of major elements on selected specimens from the area were determined by x-ray fluorescence analysis. They were analysed using a Philips PW1410 spectrometer, following the method of Norrish and Hutton (1969), with rock-standards set up at the University of Tasmania and calibrated against various International Standards. As all iron is reported as Fe_2O_3 by X.R.F. techniques, FeO was determined independently on most samples using the method of Shapiro (1960). The full analytical results are tabulated in Appendix II. From the data, the C.I.P.W. norms were calculated and these (together with the original data) were used to prepare appropriate variation diagrams. The data were also subjected to a factor analysis program, Statistical Package for the Social Sciences, written for the Burroughs B6700 computer, to test any correlations which might have been present, but were initially not obvious.

A convenient method of distinguishing syenites uses the concept of agpaitic co-efficient or index which was originally defined by Ussing (1912) as the molecular ratio $\frac{\text{Na}_2\text{O} + \text{K}_2\text{O}}{\text{Al}_2\text{O}_3}$ and referring only to nepheline bearing syenites: equivalent to the sanidine-bearing rocks at Port Cygnet. Later authors, Goldschmidt (1930) and Polanski (1949) also included oversaturated rocks in their definitions, which may be conveniently used here. When the agpaitic coefficient is greater than unity, syenites are defined as agpaitic and those with the coefficient less than unity are known as miaskitic syenites. Thus the Port Cygnet alkaline rocks are miaskitic with low values of Zr, Nb and R.E.E. Zircon, apatite and sphene are typical accessory minerals whereas agpaitic syenites contain higher values of Zr, Nb, Zn and R.E.E. Typical accessory minerals include

Table IV-1

Chemical analyses of some syenite porphyries from
Port Cygnet.

	CY5	CY8	CY16	CY18	CY49	CY67	CY70	CY120
SiO ₂	59.82	62.90	66.35	62.22	65.05	64.91	65.89	65.31
TiO ₂	0.59	0.43	0.37	0.51	0.28	0.42	0.34	0.39
Al ₂ O ₃	16.82	17.77	19.24	17.05	17.36	17.45	17.56	18.00
Fe ₂ O ₃	3.13	2.22	0.59	2.95	1.16	2.07	2.14	1.53
FeO	2.48	1.17	0.00	2.31	0.91	1.32	1.48	1.17
MnO	0.22	0.18	0.00	0.17	0.05	0.04	0.02	0.06
MgO	1.85	0.66	0.00	1.80	0.44	0.73	0.59	0.94
CaO	4.88	4.49	2.26	4.41	3.64	3.82	2.49	4.37
Na ₂ O	5.01	5.11	4.49	3.81	4.69	4.20	4.82	4.62
K ₂ O	3.68	3.98	4.35	3.25	4.23	4.14	3.71	3.42
P ₂ O ₅	0.09	0.04	0.01	0.21	0.05	0.15	0.11	0.18
loss	0.98	0.87	1.30	2.32	0.61	1.32	1.83	0.00
Total	99.55	99.82	98.96	101.01	98.47	100.57	100.98	99.99

CIPW norms

Q	5.70	9.29	18.77	15.64	13.95	16.05	17.55	15.41
C	-	-	3.06	-	-	-	1.35	-
or	21.75	23.52	25.71	19.21	25.00	24.47	21.93	20.21
ab	42.39	43.24	37.99	32.24	39.68	35.54	40.78	39.09
an	12.54	13.80	11.15	19.83	13.83	16.54	11.63	18.28
di	7.71	3.55	-	0.54	3.01	1.12	-	1.76
wo	-	1.39	-	-	0.06	-	-	-
hy	2.32	-	-	5.50	-	1.39	1.89	1.86
mt	4.54	3.11	-	4.28	1.68	3.00	3.10	2.22
hm	-	0.07	0.59	-	-	-	-	-
il	1.12	0.82	-	0.97	0.53	0.80	0.65	0.74
ap	0.73	0.21	0.02	0.50	0.12	0.35	0.26	0.42

Trace elements (ppm)

Rb	100	119	104	81	80	111	139
Sr	2026	2171	2384	1517	2113	1559	1755
Cs	<1	<1	<1	<1	<1	<1	<1
Ba	991	1071	1475	1125	1058	1173	1108
Sc	13	5	7	14	3	7	8
Y	18	27	11	45	22	41	58
Zr	157	217	200	160	142	142	153
Nb	1	13	1	8	9	10	6
Ni	<1	2	3	12	<1	29	4
Cu	45	<1	10	<1	<1	23	3
Zn	61	47	19	95	11	133	34
Pb	<3	<3	67	<3	<3	<3	<3
Ga	23	23	21	20	20	19	22

not determined
for this rock

Table IV-2

Chemical analyses of some sanidine porphyries from Port Cygnet.

	CY13	CY19	CY40	CY74	CY44	CY85A	CY73	CY46
SiO ₂	56.63	58.95	56.54	55.78	60.04	55.78	57.04	55.73
TiO ₂	0.66	0.29	0.95	0.57	0.30	0.35	0.33	0.61
Al ₂ O ₃	17.45	18.92	17.41	17.95	17.73	20.15	19.76	18.94
Fe ₂ O ₃	4.45	2.33	3.65	4.35	2.89	3.75	3.15	3.98
FeO	1.10	0.71	3.99	1.27	0.28	0.74	0.50	0.60
MnO	0.16	0.15	0.15	0.21	0.15	0.16	0.13	0.19
MgO	0.85	0.13	0.86	0.54	0.46	0.20	0.24	0.42
CaO	2.43	3.59	3.11	4.70	1.50	1.51	2.75	3.41
Na ₂ O	4.49	4.71	1.20	6.52	6.83	6.31	7.08	4.88
K ₂ O	8.06	7.88	9.18	7.36	7.90	10.31	7.93	8.52
P ₂ O ₅	0.16	0.02	0.22	0.09	0.06	0.02	0.05	0.08
loss	3.03	2.52	1.63	3.65	1.09	0.92	2.60	1.82
Total	99.47	100.20	98.89	102.99	99.23	100.20	101.56	99.18

CIPW Norms

Q	-	-	5.72	-	-	-	-	-
or	47.64	46.57	54.26	43.50	46.69	60.94	46.87	50.36
ab	27.57	30.73	10.15	18.28	26.54	1.21	20.01	18.53
an	3.66	7.21	13.99	-	-	-	-	4.62
ne	5.64	4.94	-	17.92	11.20	24.40	20.30	12.33
ac	-	-	-	3.35	8.36	6.29	2.12	-
di	4.57	0.70	-	2.90	3.03	1.07	1.29	2.26
wo	0.62	4.00	-	7.94	1.36	2.50	4.87	3.71
hy	-	-	5.16	-	-	-	-	-
mt	2.15	1.94	5.29	3.12	-	1.89	1.08	0.79
hm	2.96	0.99	-	1.03	-	0.27	1.67	3.44
il	1.25	0.55	1.80	1.08	0.57	0.66	0.63	1.16
ap	0.38	0.05	0.52	0.21	0.14	0.05	0.12	0.19

Trace Elements (ppm)

Rb	234	213	287	220	135	238	239	278
Sr	1922	3097	2373	3240	4637	4279	2740	3626
Cs	14	4	<1	8	11	4	7	10
Ba	2338	2288	3190	3240	3457	2825	1843	2220
Sc	<1	2	7	4	3	3	3	5
Y	19	4	36	11	24	0	4	22
Zr	187	245	192	273	342	150	253	233
Nb	15	18	20	24	37	23	20	16
Ni	11	1	6	3	<1	1	2	13
Cu	26	<1	59	2	<1	<1	<1	6
Zn	100	85	106	113	89	178	98	110
Pb	6	14	<3	<3	62	30	28	8
Ga	26	23	27	27	28	31	29	32

Table IV-3

Average alkaline igneous rock chemical compositions
from Le Maitre (1976).

	Nepheline syenite	Monzonite	Tinguaite	Phonolite	Syenite	Trachyte
SiO ₂	54.99	62.60	54.08	56.19	58.58	61.21
TiO ₂	0.60	0.78	0.54	0.62	0.84	0.70
Al ₂ O ₃	20.96	15.65	18.65	19.04	16.64	16.96
Fe ₂ O ₃	2.25	1.92	3.92	2.79	1.04	2.99
FeO	2.05	3.08	2.28	2.03	3.13	2.29
MnO	0.15	0.10	0.22	0.17	0.13	0.15
MgO	0.77	2.02	1.07	1.07	1.87	0.93
CaO	2.31	4.17	2.77	2.72	3.53	2.34
Na ₂ O	8.23	3.73	8.10	7.79	5.24	5.47
K ₂ O	5.58	4.06	5.52	5.24	4.95	4.98
H ₂ O ⁺	1.30	0.90	2.10	1.57	0.99	1.15
H ₂ O ⁻	0.17	0.19	0.23	0.37	0.23	0.47
P ₂ O ₅	0.13	0.25	0.20	0.18	0.29	0.21
CO ₂	0.20	0.08	0.06	0.08	0.28	0.09
Total	99.69	99.53	99.74	99.86	99.74	99.94

CIPW norms

Q	-	14.02	-	-	0.83	5.00
C	-	-	-	-	-	-
or	32.98	24.00	32.63	30.96	29.29	29.41
ab	29.45	31.56	26.03	35.48	44.34	46.26
an	3.78	11.97	-	1.50	7.24	7.05
lc	-	-	-	-	-	-
ne	21.77	-	21.22	16.50	-	-
ac	-	-	2.90	-	-	-
ns	-	-	-	-	-	-
di	4.53	3.78	7.24	6.89	5.35	2.14
wo	-	-	1.26	0.73	-	-
hy	-	6.01	-	-	4.16	2.06
ol	0.28	-	-	-	-	-
hm	-	-	-	-	-	-
mt	3.27	2.78	4.22	4.05	4.41	4.33
il	1.13	1.48	1.03	1.18	1.60	1.34
ap	0.30	0.60	0.48	0.41	0.70	0.49
cc	0.45	0.17	0.13	0.15	0.64	0.20

Table IV-4

Average alkaline igneous rock chemical compositions from Nockolds (1954), plus T541, the felsic matrix of amphibolite inclusions from Port Cygnet.

	Nepheline syenite (Juvet type)	Alkali syenite	Alkali trachyte	T541 glass
SiO ₂	55.38	61.86	61.95	69.59
TiO ₂	0.66	0.58	0.73	0.00
Al ₂ O ₃	21.30	16.91	18.03	18.48
Fe ₂ O ₃	2.42	2.32	2.33	0.00
FeO	2.00	2.63	1.51	2.73
MnO	0.19	0.11	0.13	0.00
MgO	0.57	0.96	0.63	0.43
CaO	1.98	2.54	1.89	5.11
Na ₂ O	8.84	5.46	6.55	1.51
K ₂ O	5.34	5.91	5.53	2.13
H ₂ O ⁺	0.96	0.53	0.54	0.00
P ₂ O ₅	0.19	0.19	0.18	0.00
Total	99.83	100.00	100.00	99.99
Q	-	1.71	-	38.78
C	-	-	-	4.40
or	31.56	34.93	32.69	12.59
ab	31.19	46.20	53.73	12.78
an	2.68	4.18	3.47	25.35
ne	23.62	-	0.92	-
di	4.82	5.92	3.38	-
wo	-	0	0.16	-
hy	-	1.63	-	6.08
mt	3.51	3.36	3.17	-
hm	-	-	0.14	-
il	1.25	1.10	1.39	-

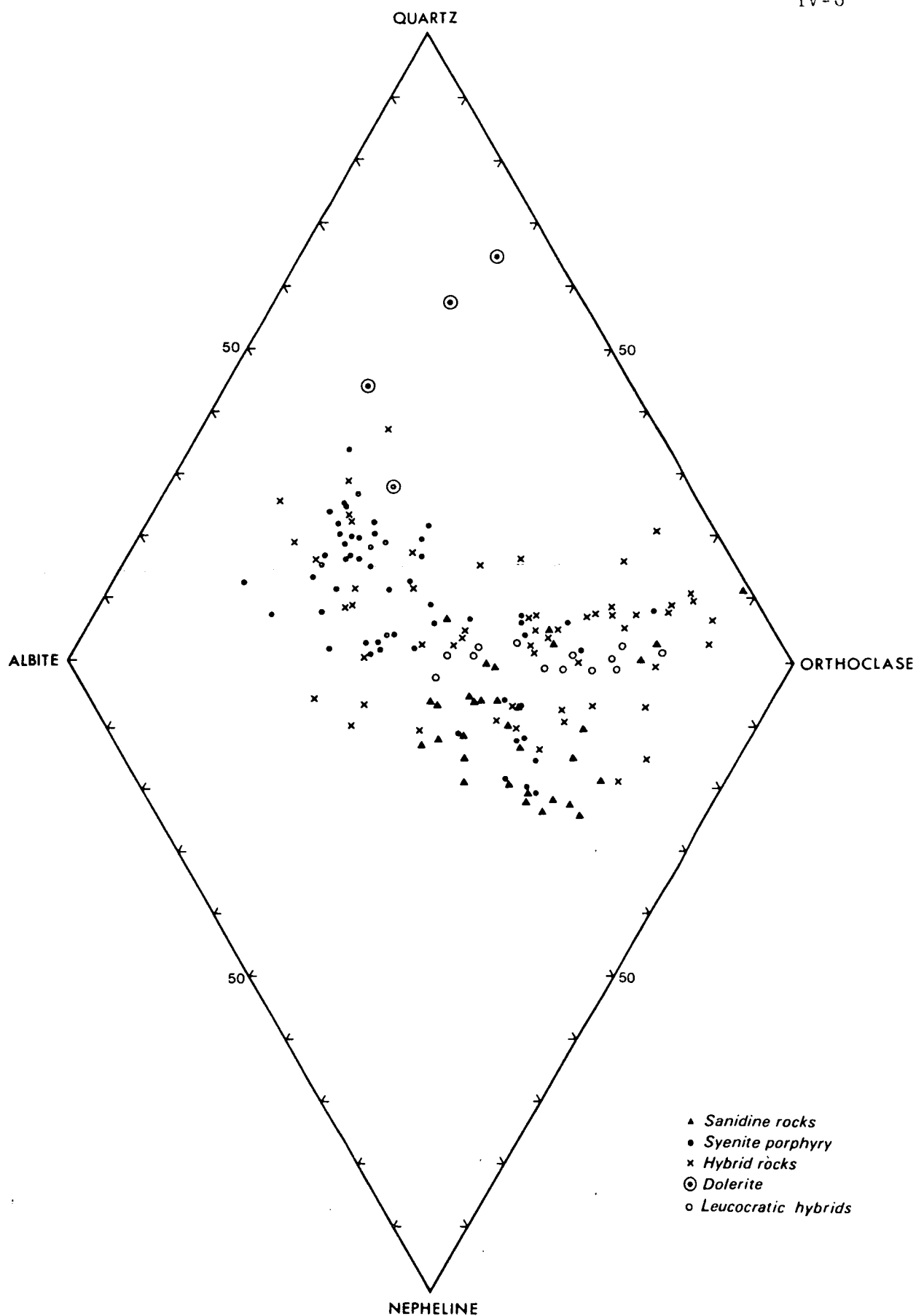


Figure IV-1 Albite-quartz-orthoclase-nepheline normative plot for all rock types.

eudialyte, Fe-arfvedsonite, villiaumite and chkalovite. It may be noted here that grains of eudialyte occur sporadically in some of the green groundmass (tinguaite) rocks at Port Cygnet otherwise their characteristics are clearly miaskitic.

For convenience in plotting on the variation diagrams, these data have been divided into three groups, namely syenite porphyry (plagioclase-bearing), sanidine rocks (sanidine-bearing) and hybrid rocks (including unaltered dolerite and alkaline dykes associated with the hybrid rocks).

The normative data are shown plotted on combined quartz-albite-orthoclase-nepheline triangles (Fig. IV-1). Because leucite does not appear in the normative compositions this field has been omitted for ease of plotting. Tables IV-1 to IV-4 show a comparison of average syenite porphyry analyses and sanidine rocks from this complex with the average values for syenite and trachyte given by Nockolds (1954) and Le Maitre (1976).

THE ALKALINE INTRUSIVE ROCKS

The data for these rocks have been plotted on several variation diagrams in the following section. A feature of the plots, is that they usually demonstrate the presence of two distinct groups.

The normative plot in Fig. IV-2 shows that the syenite porphyries are Q-normative, reflecting the groundmass quartz grains and occasionally larger grains that are present in many thin sections. The sanidine-bearing rocks are generally undersaturated with only a few specimens being slightly saturated. Modal feldspathoid is present in the undersaturated rocks. Hybrid rocks have also been added to this plot and it is evident there are saturated and undersaturated members in these.

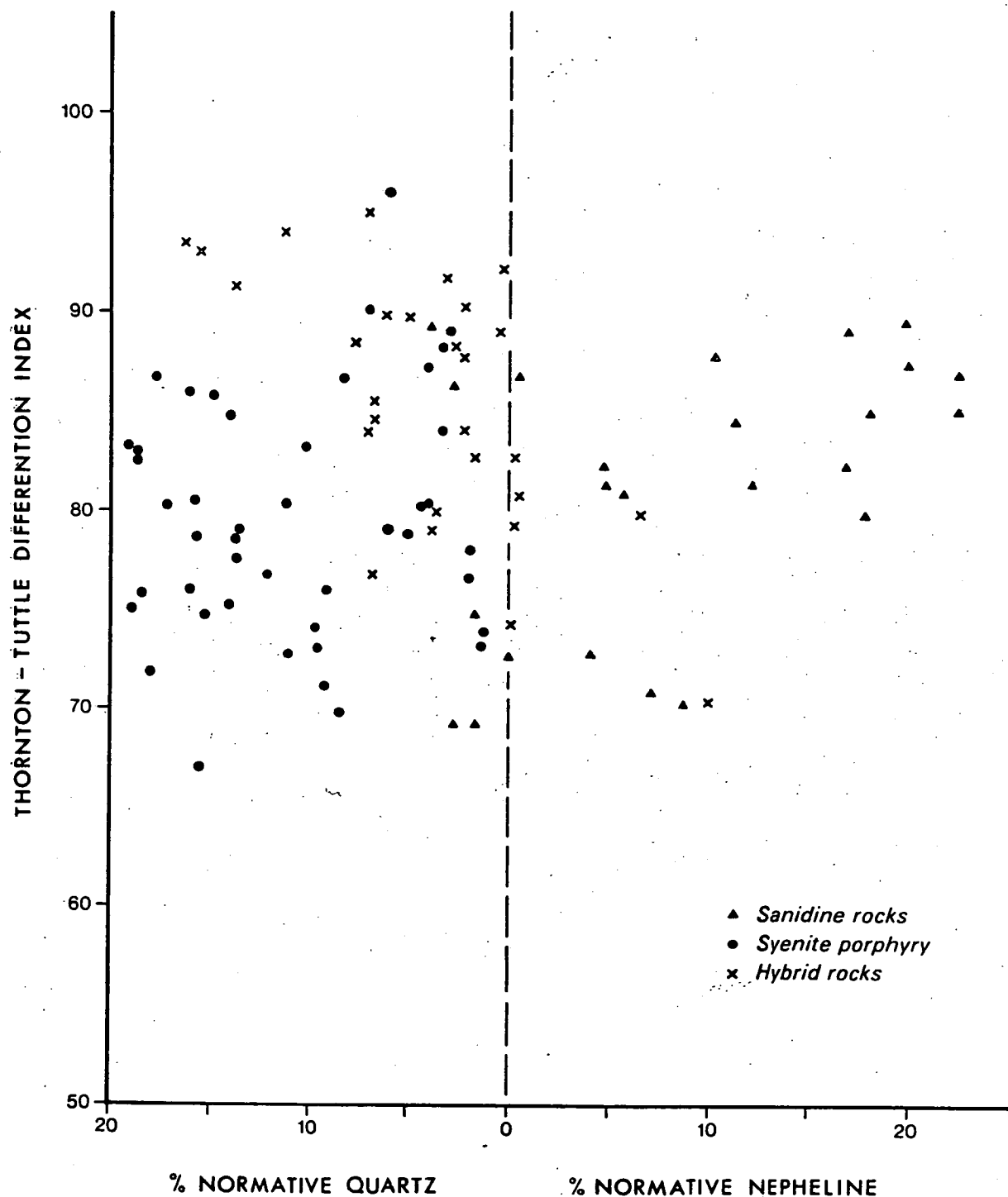


Figure IV-2 Plot of Thornton-Tuttle differentiation index against normative quartz or nepheline for all rocks.

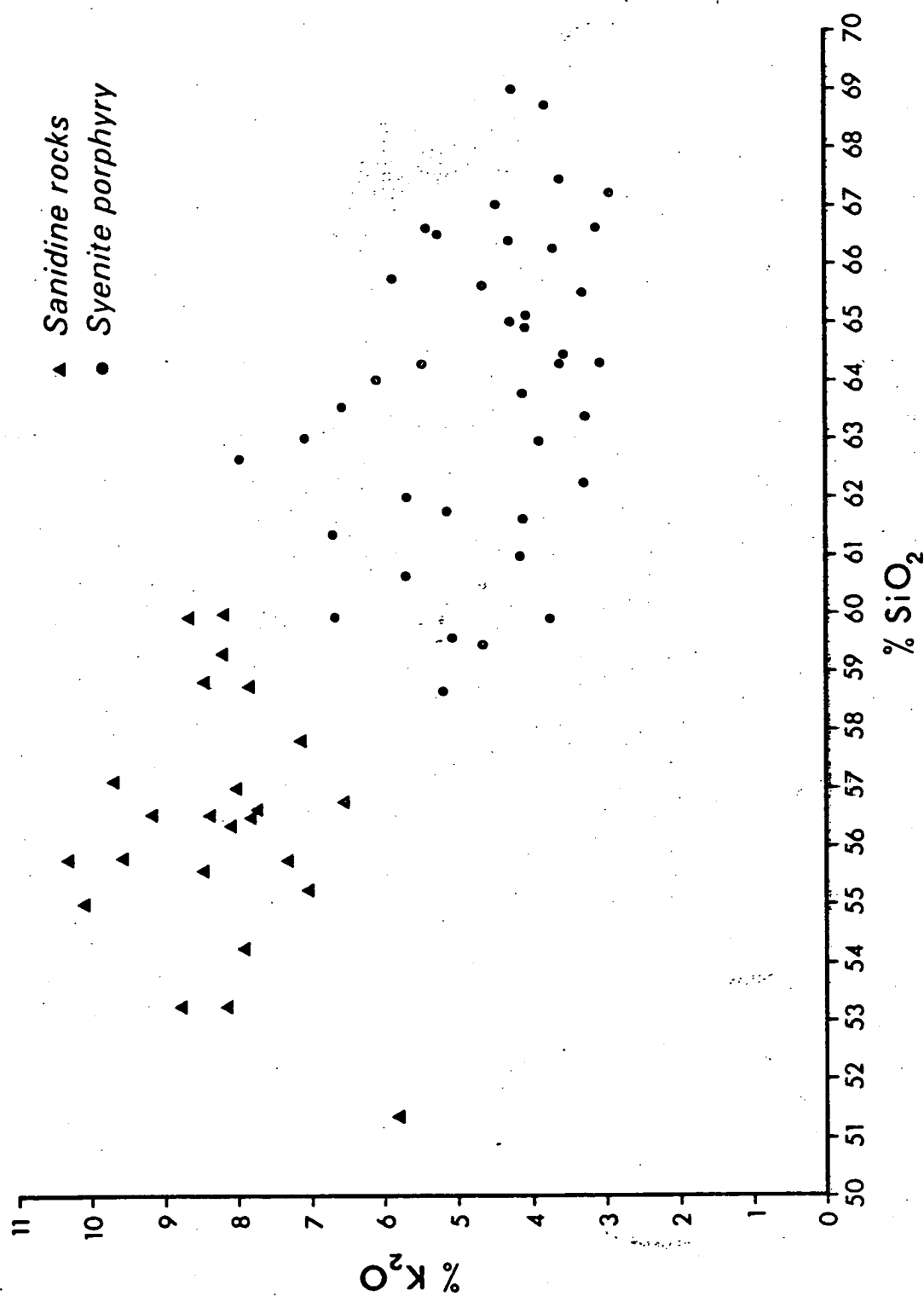


Figure IV-3 Potash-silica plot for the alkaline rocks.

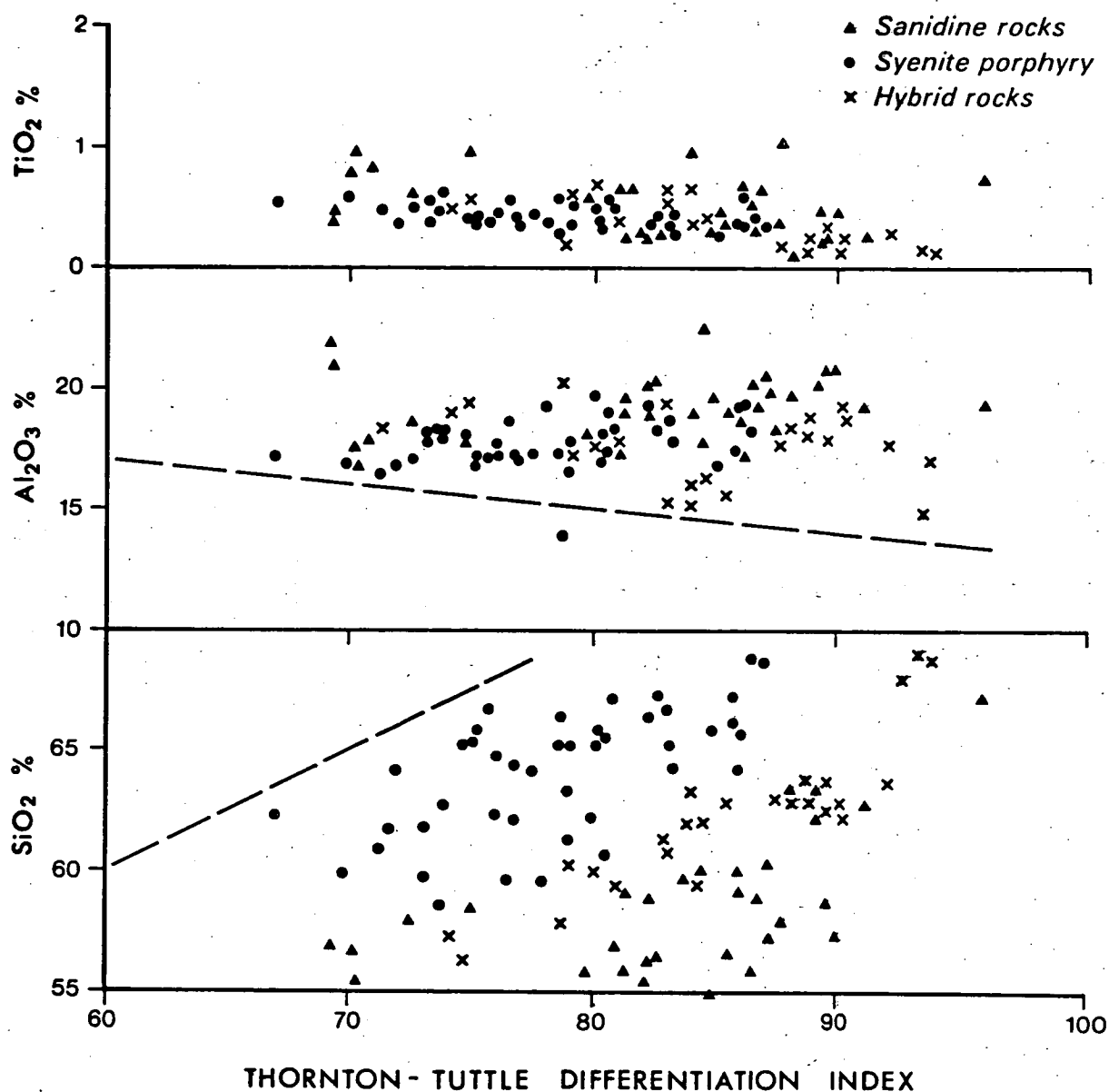


Figure IV-4 Thornton-Tuttle differentiation index plot of SiO_2 , Al_2O_3 , and TiO_2 for all rocks. The most common trend is shown by the dashed line.

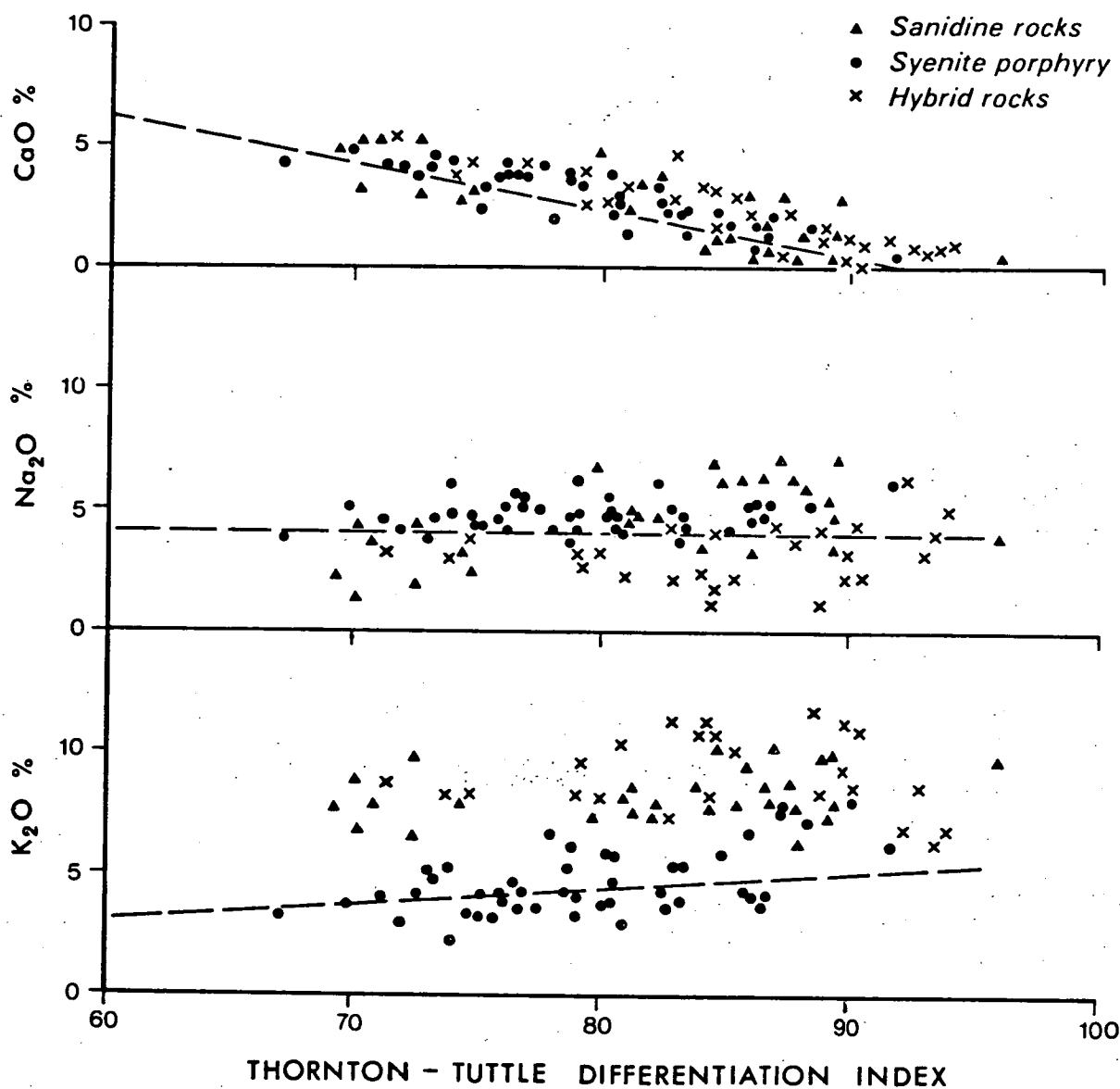


Figure IV-5 Thornton-Tuttle differentiation index plot of K₂O, Na₂O and CaO for all rocks. The most common trend is shown by the dashed line.

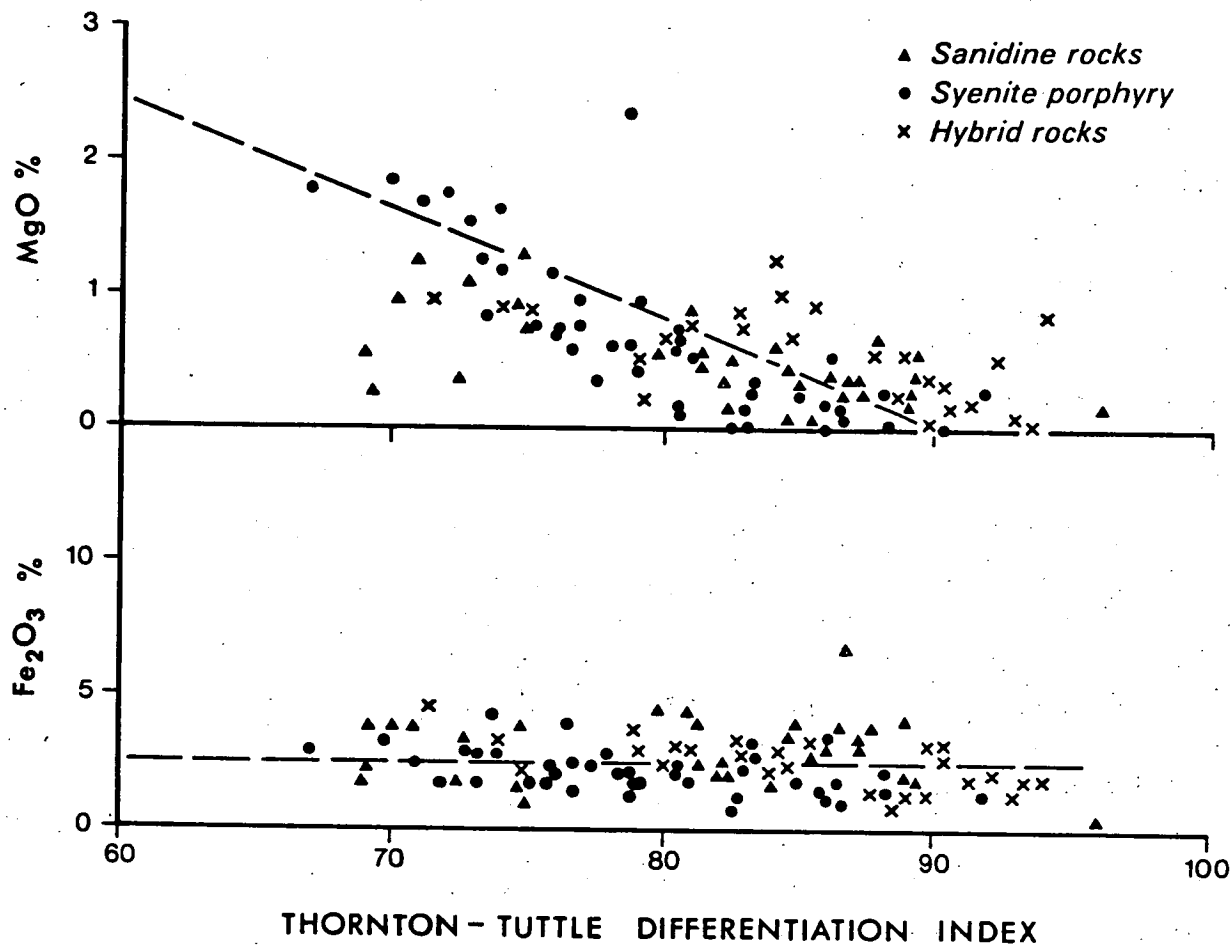


Figure IV-6 Thornton-Tuttle differentiation index plot of Fe₂O₃ and MgO for all rocks. The most common trend is shown by the dashed line.

Harker Plot

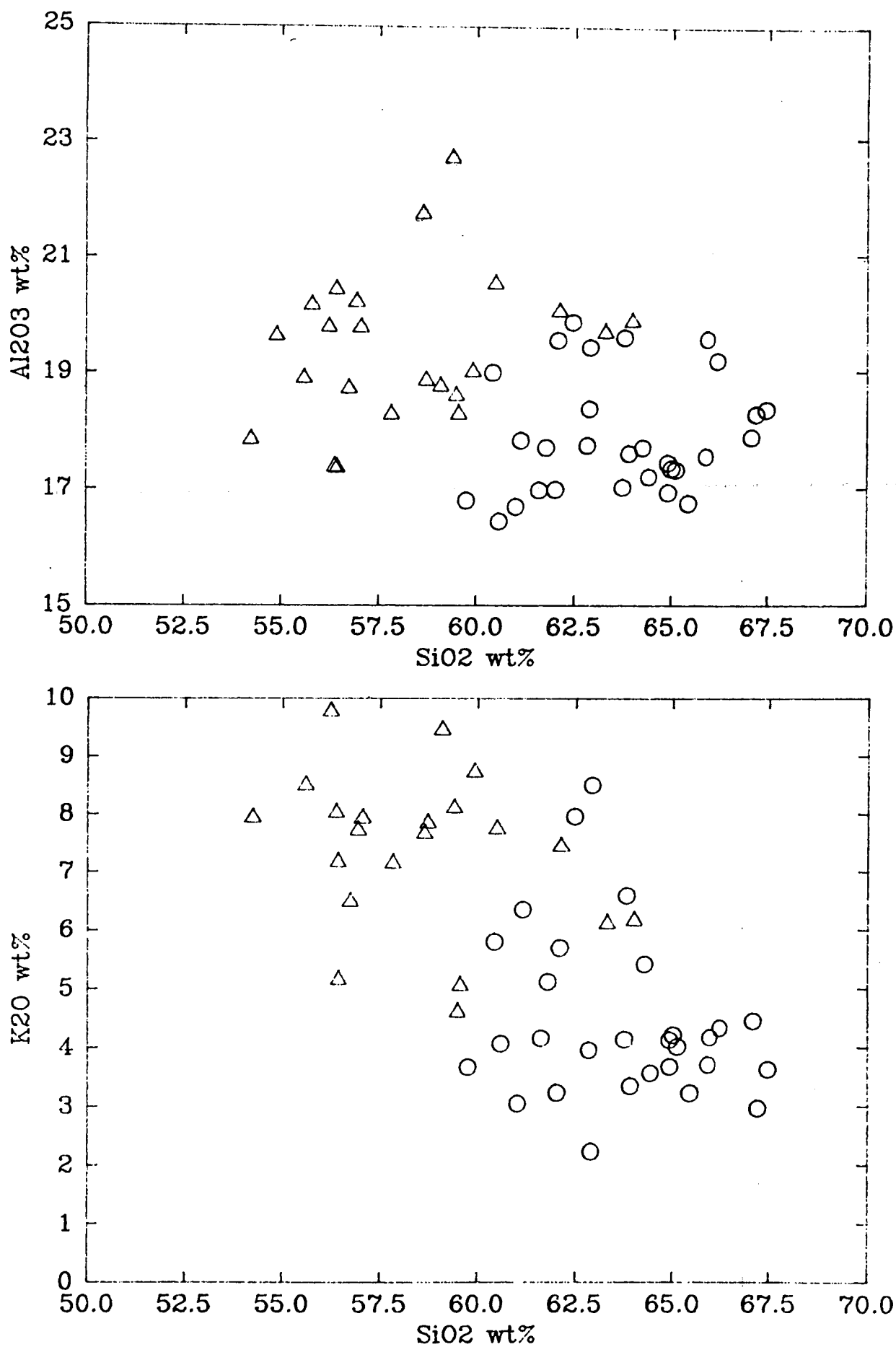


Figure IV-6a Plot for Al_2O_3 and K_2O . Triangles for sanidine rocks and circles for syenite porphyries.

Harker Plot

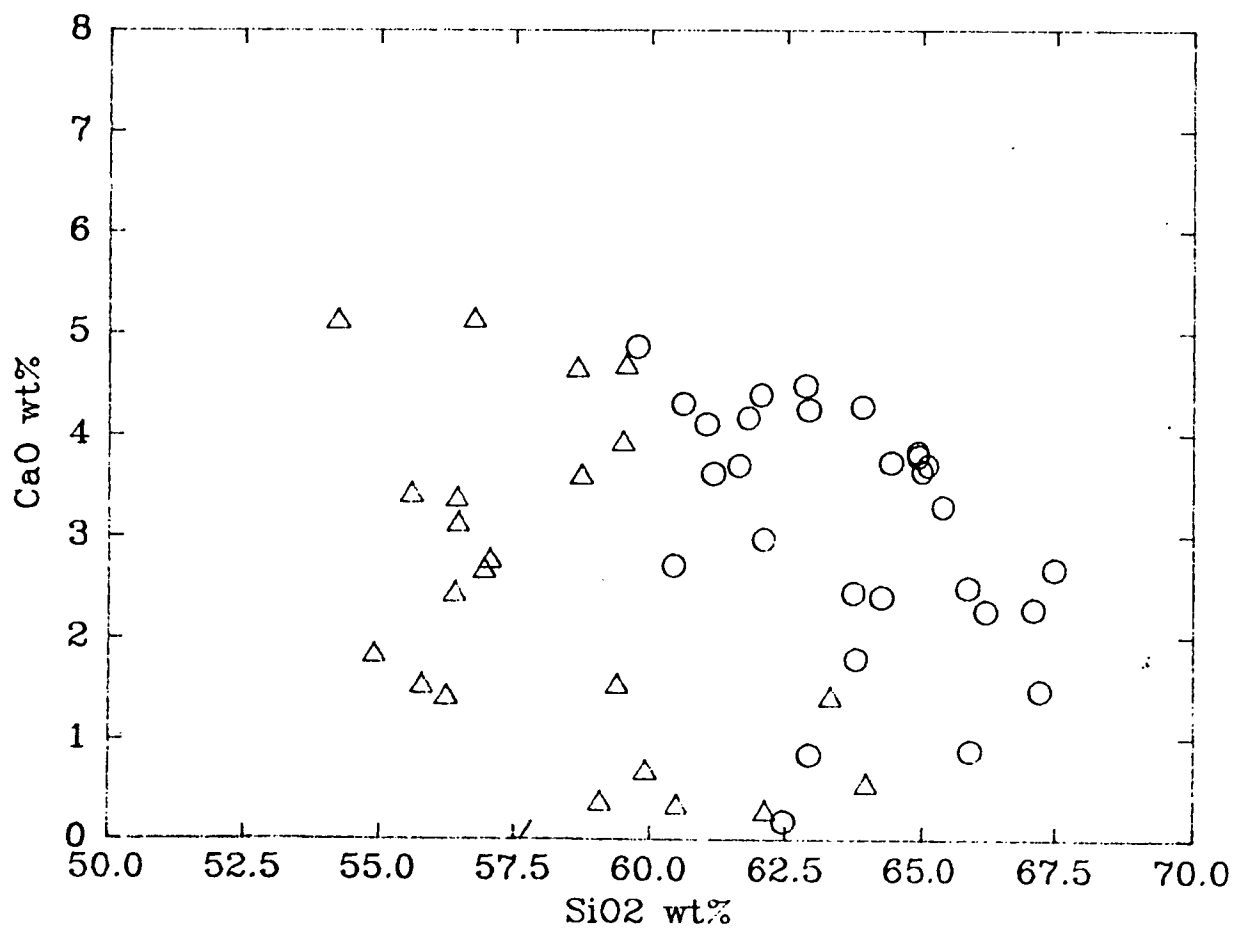
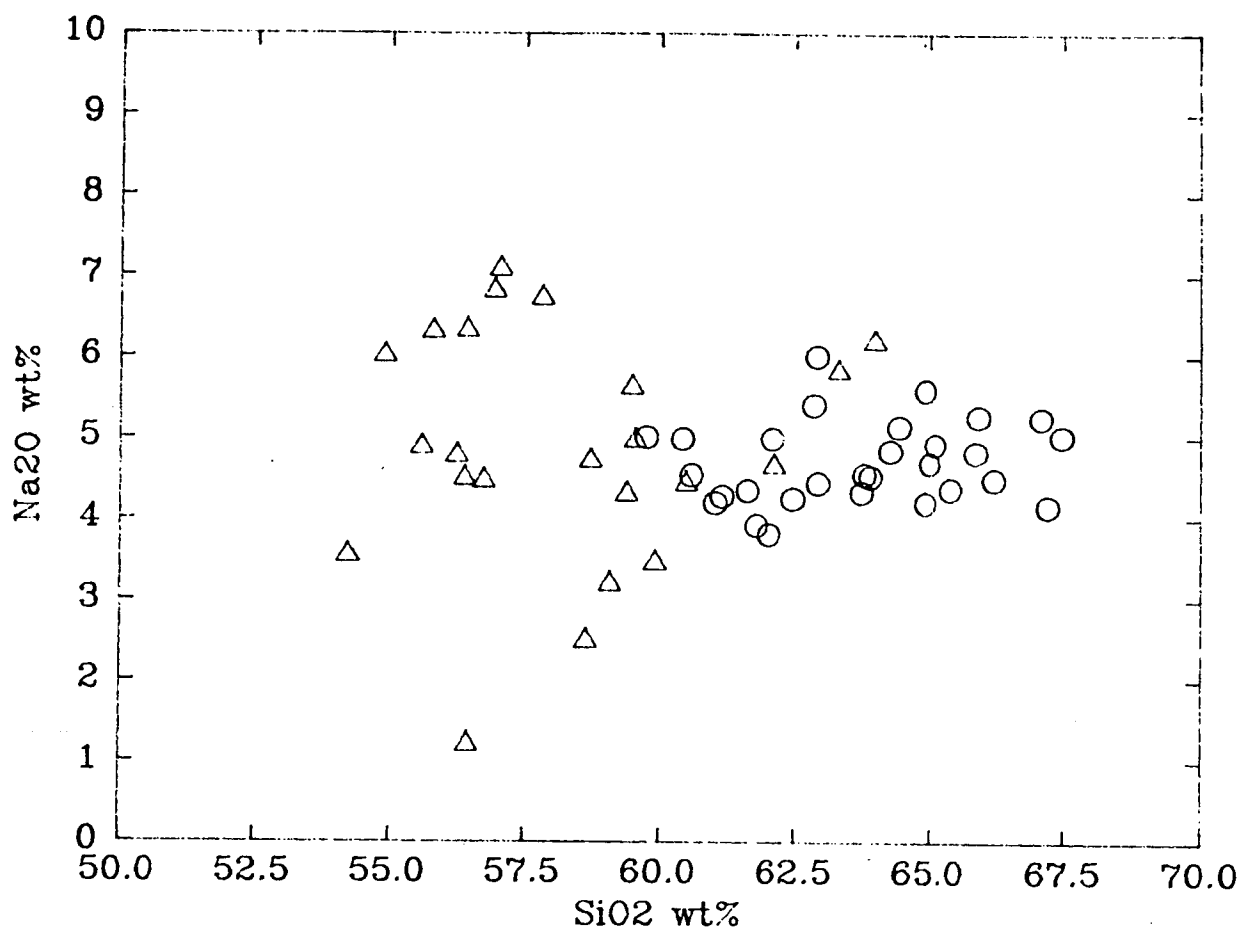


Figure IV-6b Plot for Na_2O and CaO . Triangles for sanidine rocks and circles for syenite porphyries.

Harker Plot

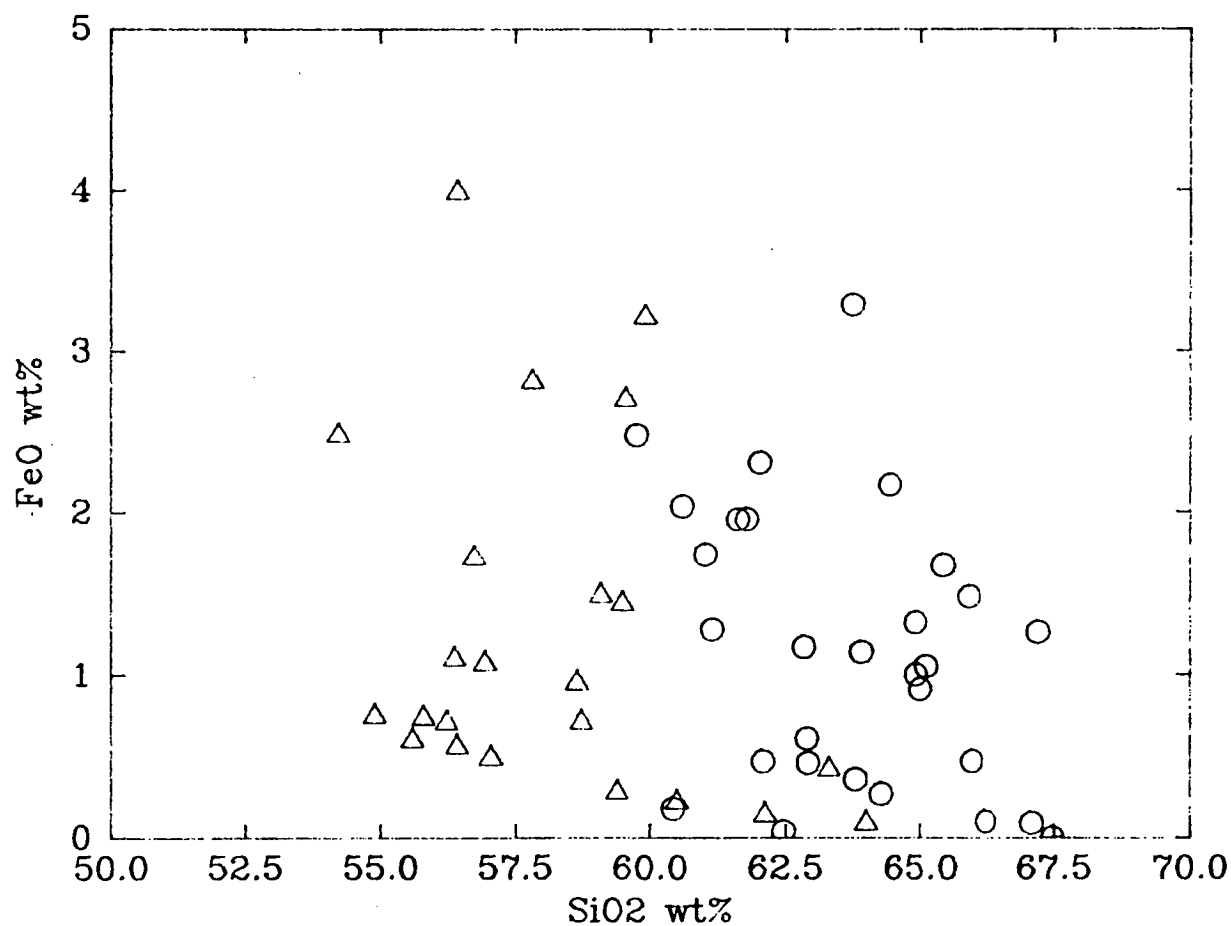
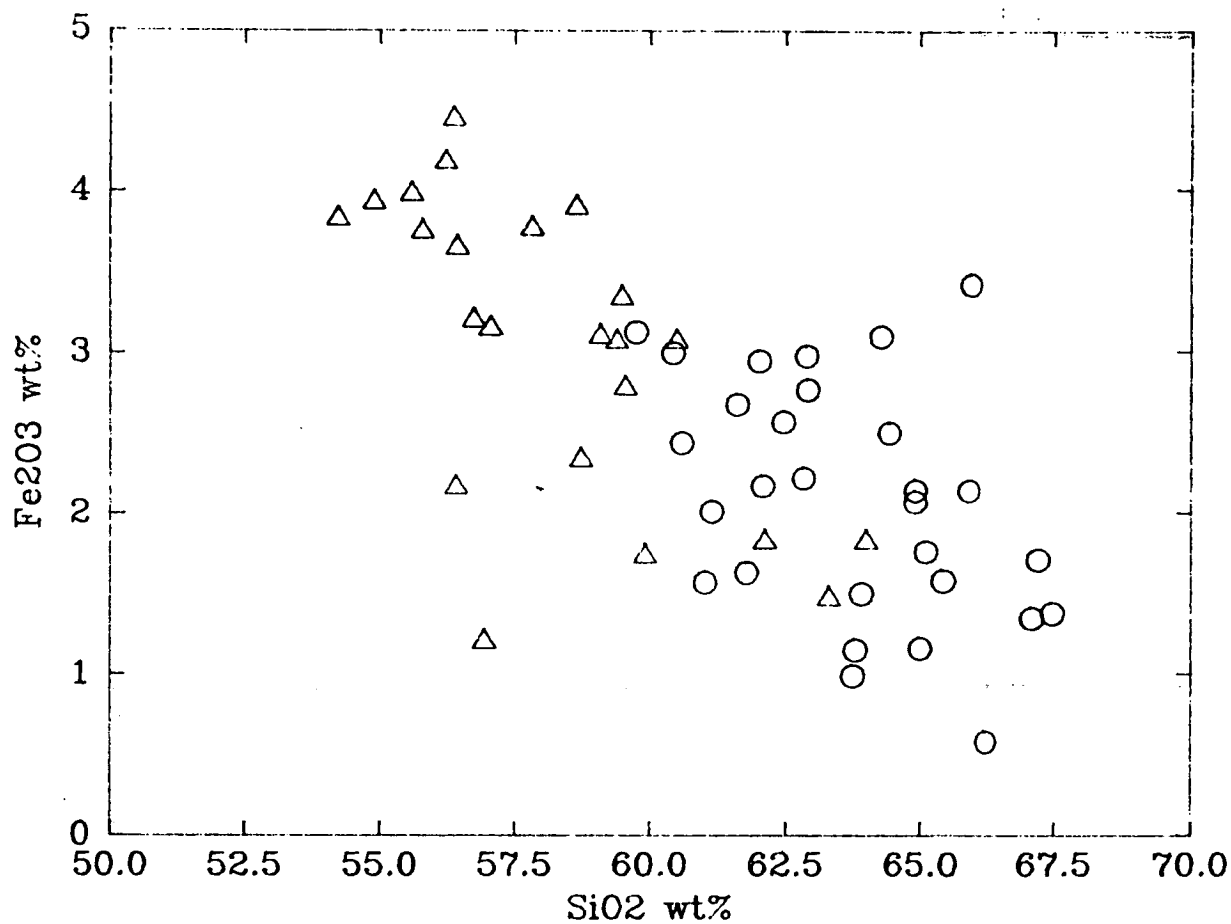


Figure IV-6c Plot for Fe_2O_3 and FeO . Triangles for sanidine rocks and circles for syenite porphyries.

Harker Plot

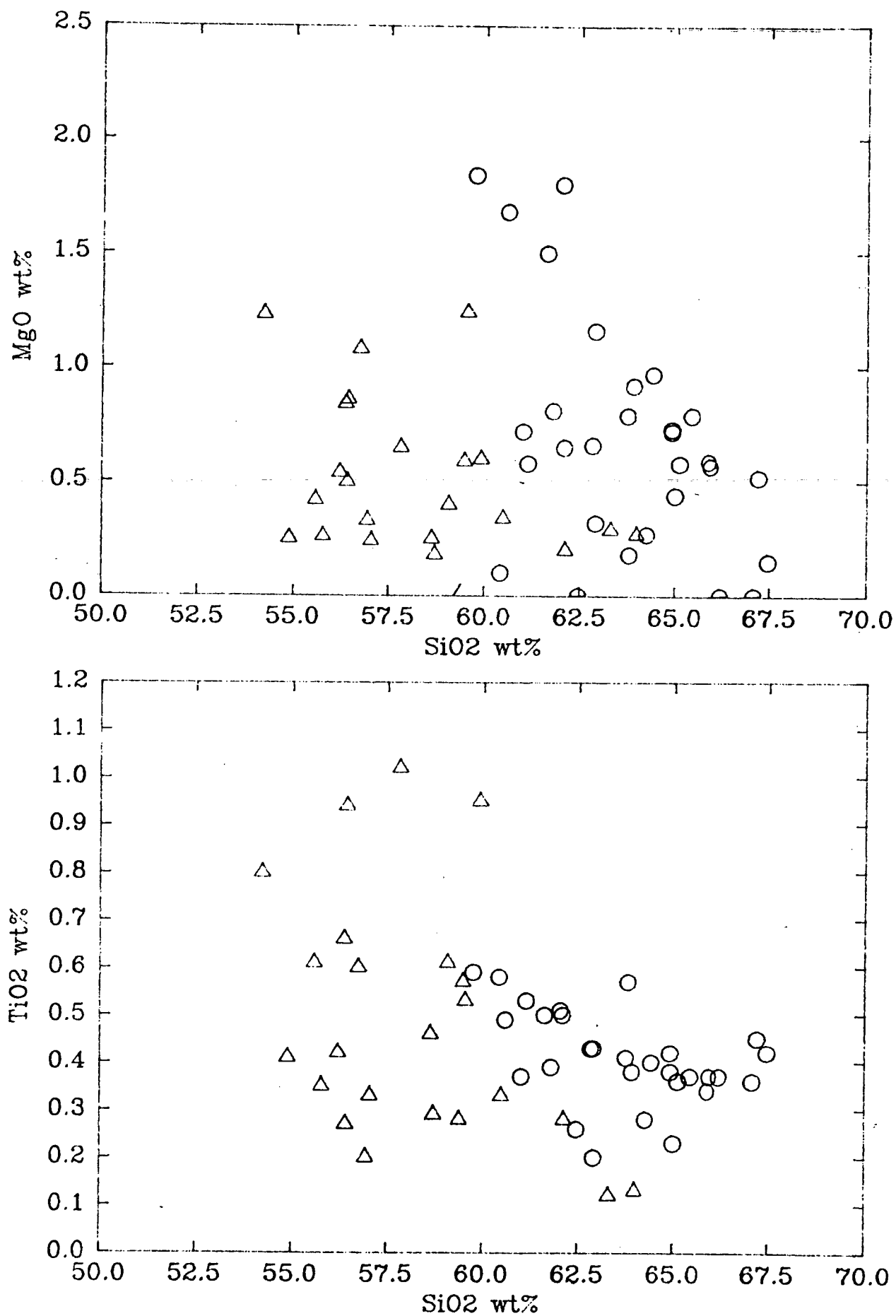


Figure IV-6d Plot for MgO and TiO_2 . Triangles for sanidine rocks and circles for syenite porphyries.

Fig. IV-3 shows the variation of potash and silica for the alkaline rocks. There is a reverse trend here with the sanidine rocks showing the higher potash values and the lower concentrations in the syenite porphyry, represented by subhedral orthoclase phenocrysts and groundmass grains.

The data for eight of the major element oxides have been plotted against the Thornton-Tuttle differentiation indices for all the analysed rocks (Figs. IV-4 to IV-6). The dashed lines on the diagrams show the most common trends for the data used by Thornton and Tuttle (1960) in defining their model which is based on superior chemical analyses from Washington's compilation. The aim of the Differentiation Series is to reveal differentiation trends in magma series. In a normal differentiation sequence for a magma series it would be expected that all analyses would lie within some general trend defined by the differentiation index and have a consecutive trend.

The trends for the hybrid rocks have been commented on elsewhere, hence the rocks to be considered here are the syenite porphyries and the sanidine rocks. If the Port Cygnet alkaline rocks are part of a differentiated stock as suggested by Edwards (1947), then the Thornton-Tuttle model should reveal this. From Figs. IV-4 to IV-6 it can be seen that the Cygnet alkaline rocks do not follow the most common trend of Thornton and Tuttle. The most important feature, particularly well displayed for the oxides SiO_2 , K_2O and Na_2O and to a lesser extent for the oxides Al_2O_3 and Fe_2O_3 , is the development of parallel trends for the syenite porphyry and the sanidine rocks. These parallel trends are particularly apparent for K_2O (Fig. IV-5) where the syenite porphyries closely follow the main trend but the sanidine rocks (and hybrids) form a distinct and parallel trend. For SiO_2 (Fig. IV-4) the trend also reflects the difference between the oversaturated and under-saturated rocks.

The existence of parallel trends does not favour a simple differentiation mechanism as a means of deriving either group. If the Differentiation Indices are accepted then there may be two differentiation trends with the potash-rich rocks as part of one trend and the syenite porphyries part of another, which may be related to each other by a fractionation process. If this is true then other representatives of the two trends should appear, but there is no evidence of these. The Thornton-Tuttle plot, with regard to silica, potash, soda and ferric oxide indicates there may be two sources for the alkaline rocks.

Harker Plots of syenite porphyries and sanidine rocks have been prepared in Figures IV-6a - IV-6d. In these plots, the presence of two groups is more clearly shown than by the Thornton-Tuttle indices. The only possible trend occurs on the Fe_2O_3 plot where it probably reflects the presence of melanite and aegirine in the sanidine rocks.

Because the alkaline rocks are dominated by feldspars, to the exclusion of ferromagnesian minerals, in large amounts, normative plots of the data via Q-Ab-An-Or-Ne should be useful in its interpretation. Although Steiner et al. (1975) suggest that normative interpretation of simple experimental systems may not truly represent the conditions of formation, Abbott and Clarke (1979) claim that with two feldspars the liquids should approximate the conditions of Tuttle and Bowen (1958). Bowen and Tuttle (1950) considered that in the granite system Q-Ab-Or normative plots approximated equilibrium conditions for the coarse grained plutonic rocks.

Since the syenite porphyry is quartz normative then it may be interpreted using the Q-Ab-Or triangle or if comparison with the under-saturated rocks is made then the Q-Ne-Ks triangle would be more appropriate. However because of the porphyritic nature of the rocks they may not represent an equilibrium assemblage. If this is so it

may be that due to the small amount of melt involved, disequilibrium might not be very large.

The Syenite Porphyries

As a preliminary the syenite porphyry compositions were plotted on a Ab+An-Q-Or triangle (Fig. IV-7) to determine the presence of any trends. On this diagram the syenite porphyries plot as a group with no trends apparent. The basic Ab-Q-Or triangle for the syenite porphyries is also plotted in Fig. IV-10) with the minima for the system shown up to 10 kb total water pressure (after Luth et al., 1964). The distribution is quite similar to Fig. IV-7 with the syenite porphyries forming a group towards the higher pressure minima.

Because the compositions of the rocks are dominated by feldspars with only minor quartz or feldspathoid, a test of their equilibrium state would be to check their plots on various equilibria diagrams involving feldspars and feldspathoids. On the Ab-Q-Or plot (Fig. IV-10) for various pressures of water saturated liquids the data for the syenite porphyries do not fall directly on any particular minimum although the closest minimum point is about 5 kb. However most of the analyses do not plot about any minimum nor do they appear to fall within the usual common trends (Luth et al., 1964). On this plot there is no support for the attainment of equilibrium, hence this would favour the deductions made from the porphyritic texture of the syenite porphyries. To allow comparison with the sanidine bearing rocks the data for both groups have been recalculated and are presented in the Ne-Q-Ks diagrams of Figs. IV-8 and IV-9.

The use of the Ne-Ks-Q plot is justified because all rocks are feldspar rich with both quartz and feldspathoid not being major phases in either group. They are not peralkaline, being miaskitic rather than agpaitic (see Fig. IV-10) and while some rocks have modal ground-

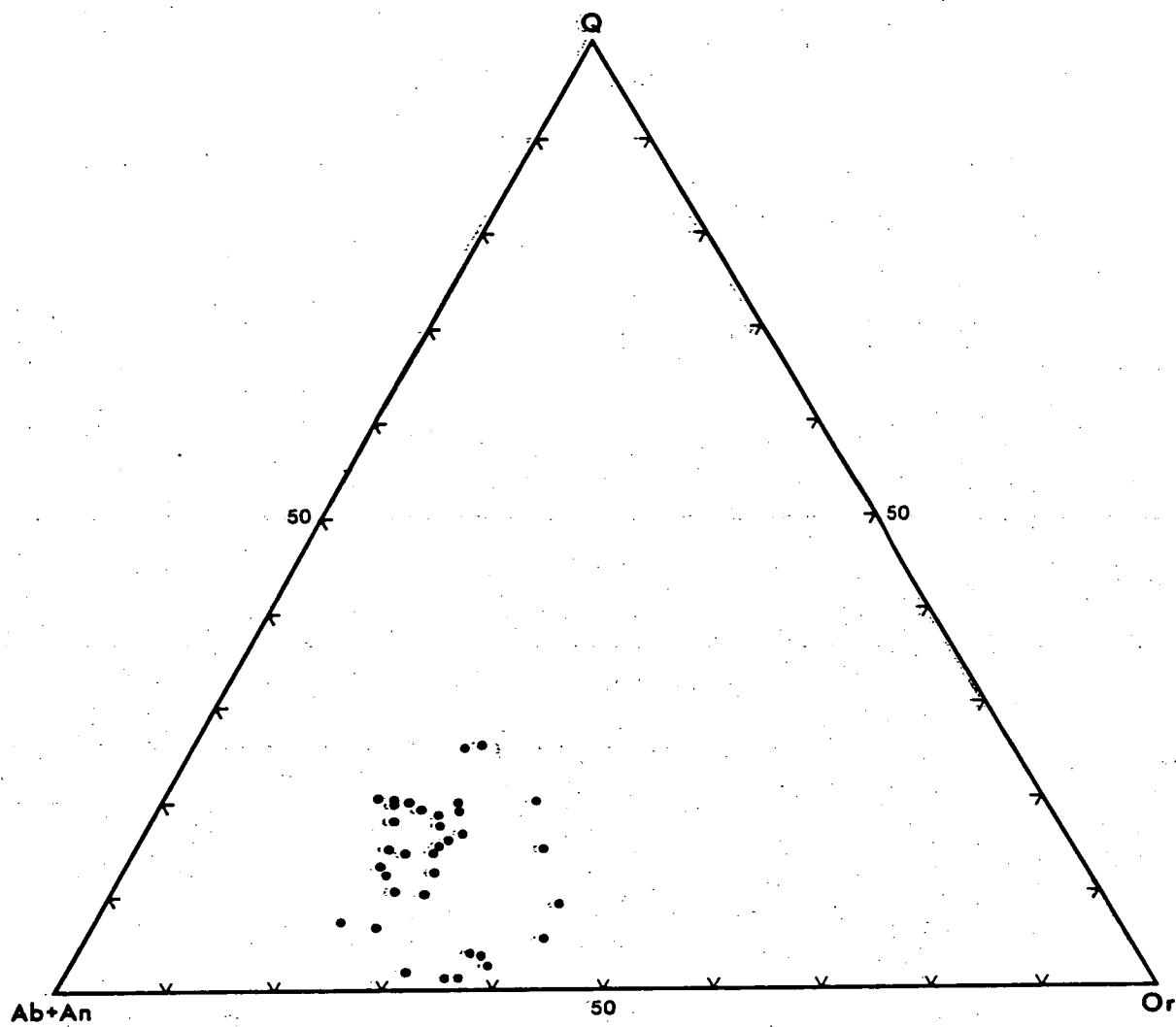


Figure IV-7 Normative plagioclase-quartz-orthoclase plot for syenite porphyries.

mass aegirine this does not appear in the normative calculation.

The normative components recalculated and plotted on a silica-nepheline-kalsilite triangle are shown for the syenite porphyries and the sanidine rocks in Fig. IV-8 . In Fig. IV-9 the liquidus base-projected plots for 1 atmosphere (Bowen, 1937), 1 kb (Hamilton and Mackenzie, 1965) and 5 kb (Morse, 1969) ($p_{H_2O}=p_{total}$) have been added for comparison.

Some of the syenite porphyries follow the surface of the saturated-undersaturated thermal divide along the albite-orthoclase join, and others tend to plot along the 5 kb cotectic line towards the ternary eutectic. While no firm conclusions can be made, the data plot nearer the 5 kb minimum than for the 1 kb cotectic. These would indicate crystallization at water pressures greater than 1 kb, and possibly approaching 5 kb for an equilibrium situation.

In order to see any indication of fractionation and what the final melt compositions might have been, Figure IV-9a has been constructed. In this figure some of the rocks of Fig. IV-9 have been replotted with the equivalent compositions of their feldspar phenocrysts removed after determination by point counting. As the diagram does not show the anorthite component of the oligoclase phenocrysts, from the syenite porphyries, they have been calculated as equivalent albite (reduced to nepheline and quartz) for accuracy of plotting. In this way the composition of the groundmass (= final melt phase) can be calculated and the relationship to minimum melt trends established.

The groundmass composition is indicated by an arrow from its whole rock conjugate. As the proportion of phenocrysts increases, the groundmass composition will lie further from the whole rock plot along a line having an origin near $NaAlSi_3O_8$ or $KAlSi_3O_8$, depending on the precise compositions of the phenocrysts.

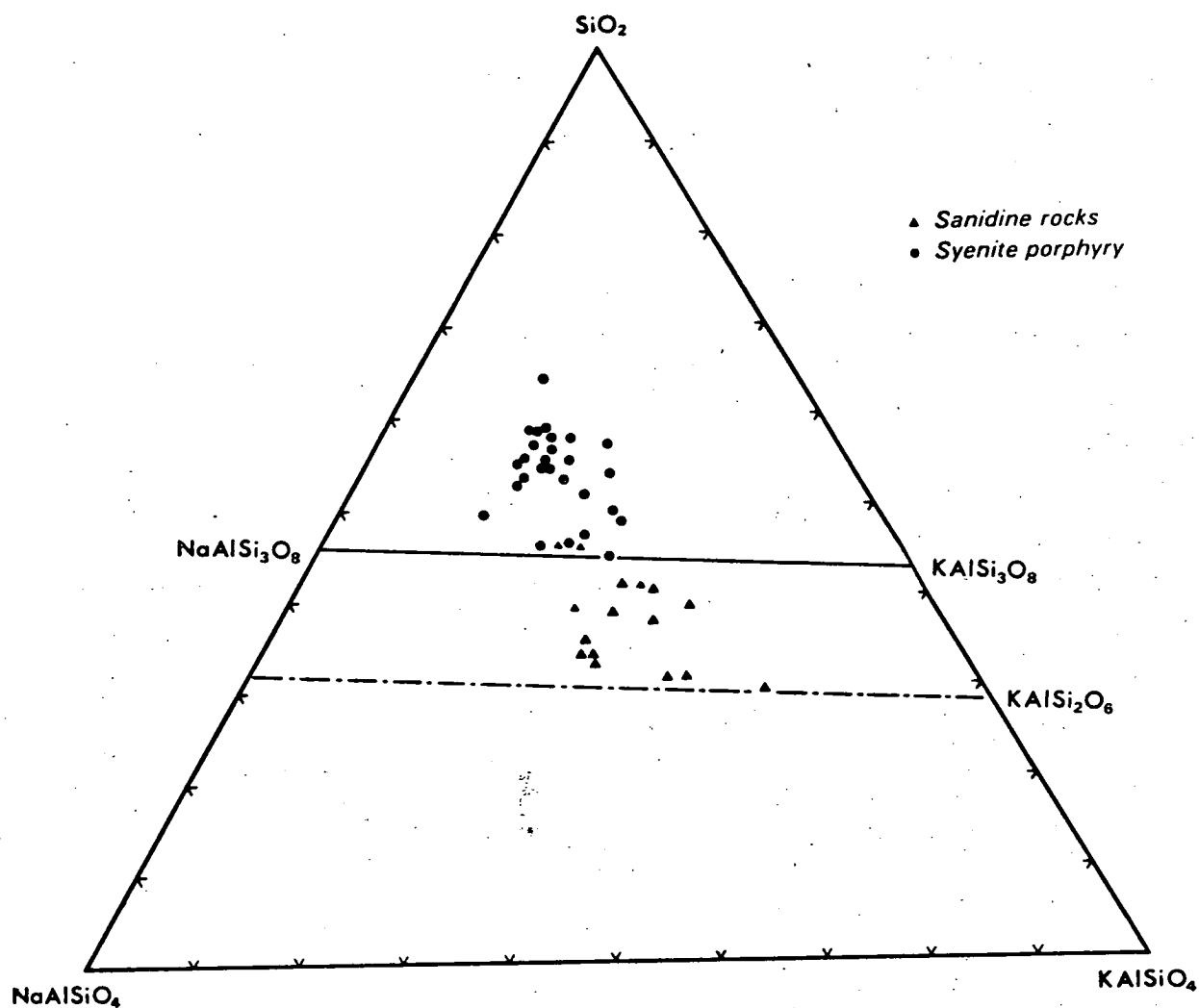


Figure IV-8 Nepheline-quartz-kalsilite plot for syenite porphyries and sanidine porphyries.

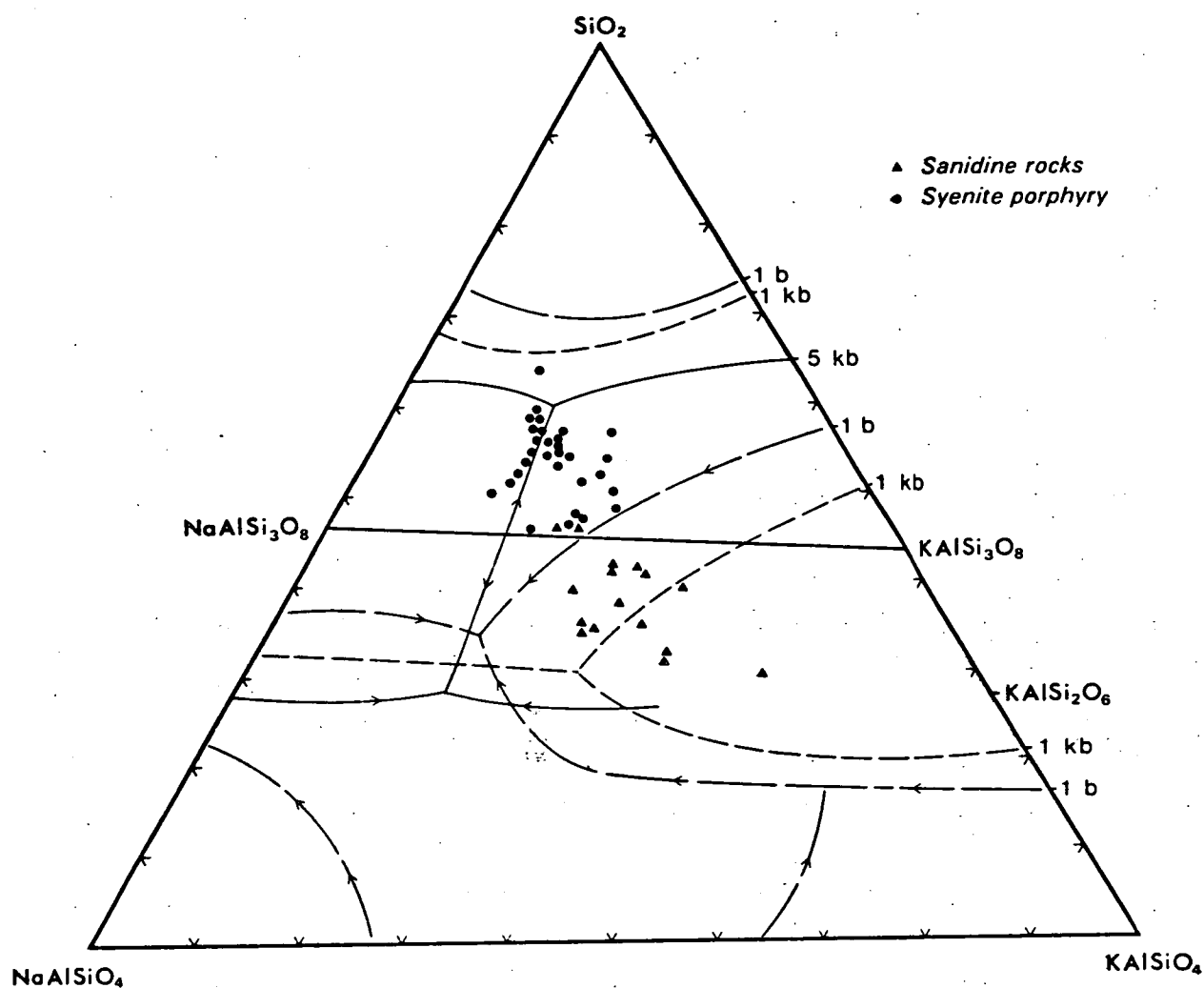


Figure IV-9 NaAlSiO₄-SiO₂-KAlSiO₄ plot for syenite porphyries and sanidine porphyries. Main phase boundaries for 1 bar, 1 kbar and 5 kbar are shown. ($P_{H_2O} = P_{total}$).

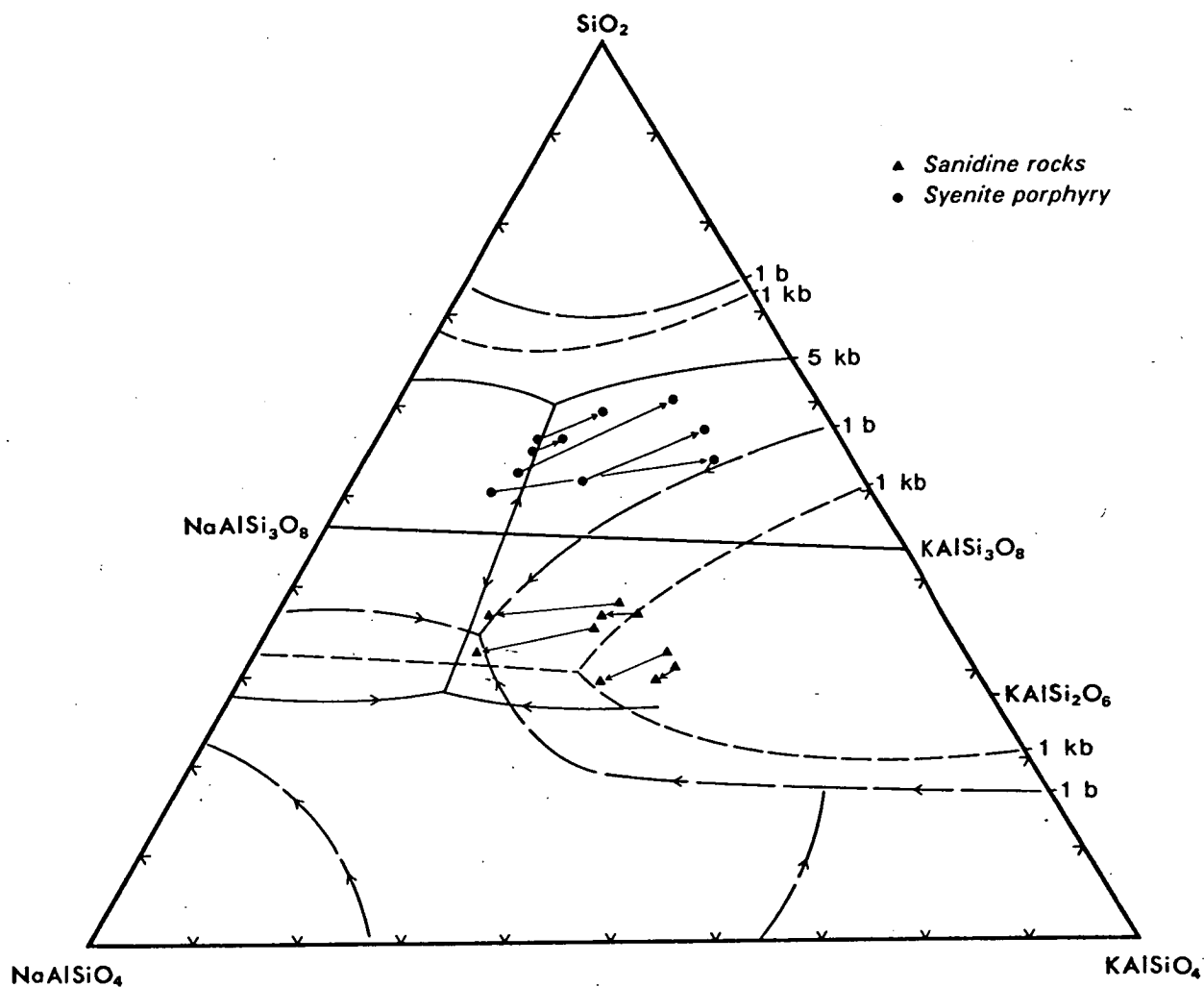


Figure IV-9a Fractionation trends for selected rocks of Fig. IV-9 established by subtracting total phenocryst composition from whole rock normative composition.

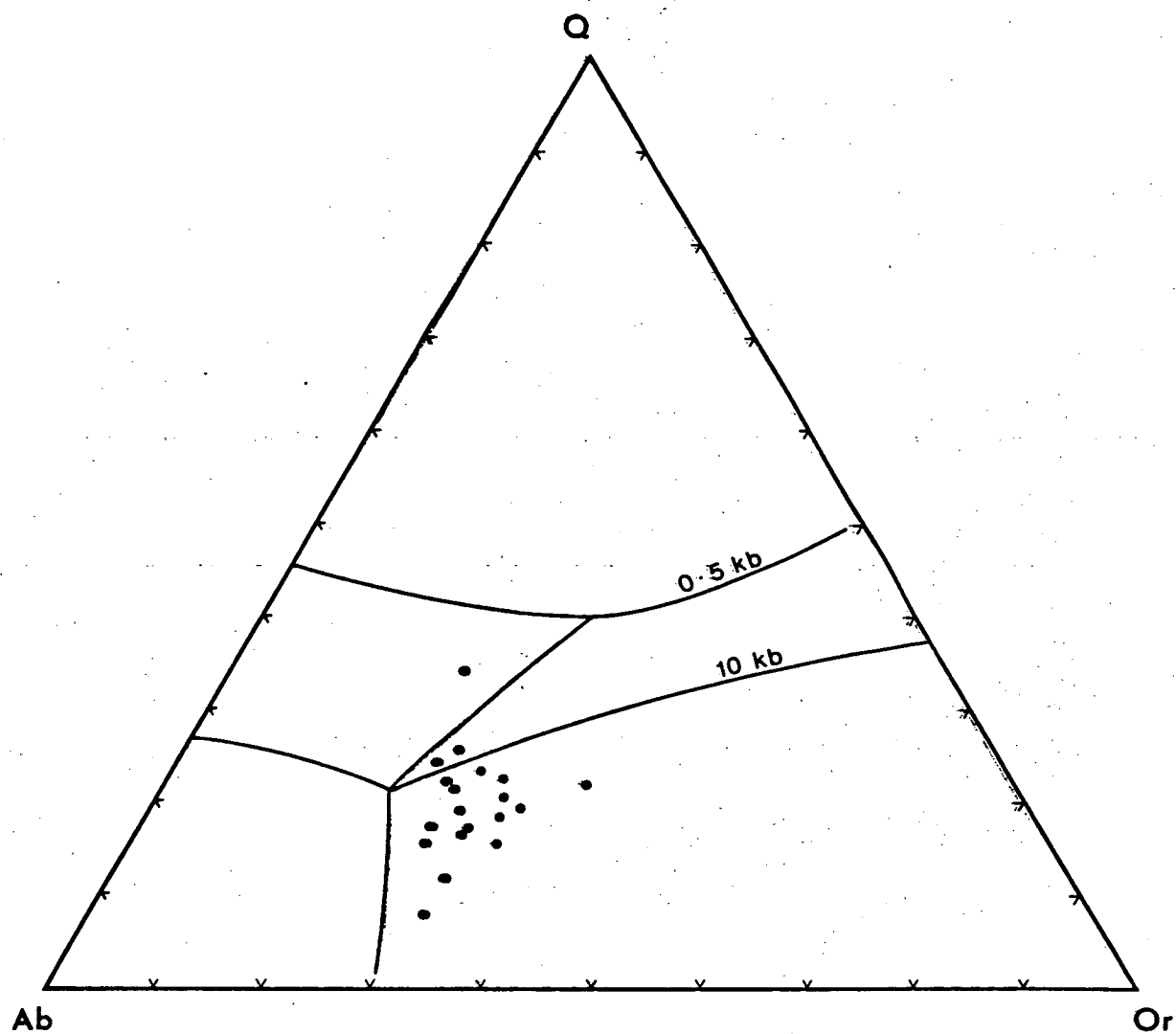


Figure IV-10 Ab-Q-Or normative plot of syenite porphyries with minima, in the system Ab-Q-Or from 0.5 kb to 10 kb, added. ($P_{H_2O} = P_{total}$).

For the syenite porphyries the minima obtained in this way lie away from the 5 kb feldspar cotectic and parallel with the silica cotectic. This suggests, if the assemblage is at equilibrium, that the system crystallised at some pressure less than 5 kb but no accurate value can be found.

Similarly for the sanidine porphyries, when the phenocryst compositions are removed the remaining groundmass composition moves towards the albite-silica side of the triangle and the 5 kb minimum.

While no firm conclusions can be reached an empirical observation suggests that the sanidine porphyries could have crystallised at a higher pressure than the syenite porphyries.

According to von Platen (1959), James and Hamilton (1969), Presnal and Bateman (1973), Winkler (1965, 1967, 1974), Carmichael et al. (1974), and Winkler et al. (1975) it is unwise to plot such data without allowing for the anorthite component which forces the apparent eutectic/ternary minimum towards the quartz-albite-anorthite face of the quartz-albite-anorthite-orthoclase tetrahedron. If the method of Winkler et al. (1975) is followed, then Fig. IV-11 may be constructed.

Three components are plotted in the conventional manner and the fourth is plotted as a series of spot heights to the intersection of the isotherms with the cotectic surface for the fourth component. The values for the spots represent the weight percent of the fourth component in the melt in equilibrium with crystal of composition defined by the other three components. Thus one may plot An-Q-Or with spot heights for anorthite or alternatively, Ab-Or-An with quartz as the fourth component. From the earlier data using Ab-Q-Ks it appeared that the syenite porphyries clustered near the 5 kb minimum. In order to allow for the anorthite component, data of Winkler et al. (op. cit.) were taken for the 5 kb (total water pressure) isobar and the data for the syenite porphyries were plotted on Fig. IV-11. These authors

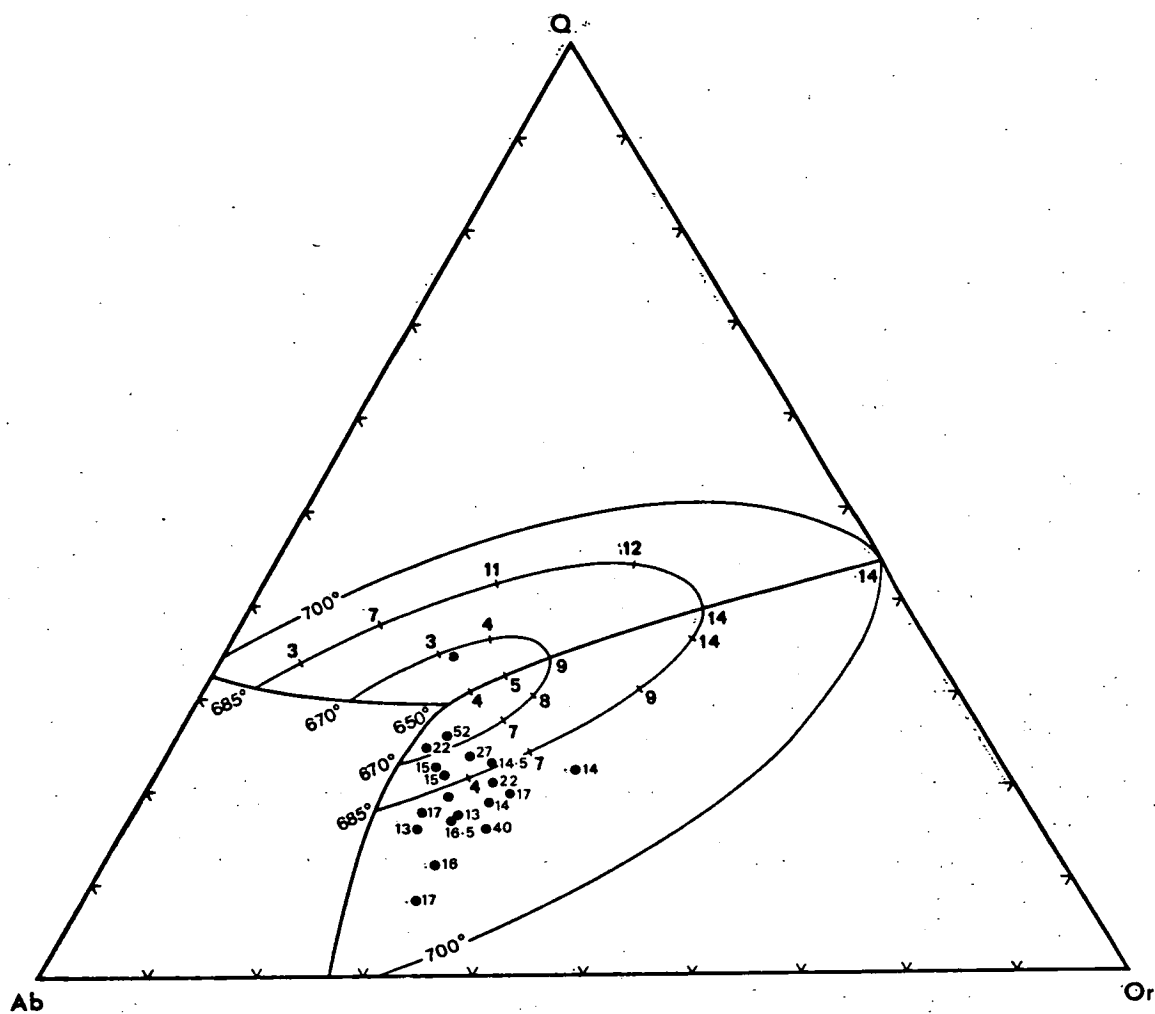


Figure IV-11 Winkler plot for normative Quaternary Ab-Or-Q-An.

also state that the 5 kb form of the equilibrium diagram does not change much over the pressure range of 3 kb to 7 kb hence it is likely to be applicable to the syenite porphyry system because the maximum crustal thickness at Port Cygnet was about 26 km (Leaman et al., 1980) corresponding to a load of 7 kb giving a maximum limit to the system. At 3 kb the depth equivalent is about 10 km which is regarded as too shallow for the maintenance of a magma chamber in which phenocrysts began to grow. For an equilibrium situation the anorthite content of the syenite porphyry shown in spot numbers on the Winkler diagram, should equal the anorthite contour value. This proposition is valid if the sum of quartz plus albite plus orthoclase plus anorthite is normalized to 100. Since microscopic examination of the syenite porphyry shows that many specimens may have some alteration, only the samples of syenite porphyry showing fresh unaltered groundmass have been plotted. The normalized anorthite contents of these range from 11% to 20%, but for equilibrium they should be about 4% to 5%. For the anorthite values of the syenite to be in equilibrium the values projected on to the quartz-albite-orthoclase base of the tetrahedron should lie much closer to the quartz-orthoclase side of the triangle. Once again it would appear that the syenite porphyry is not an equilibrium assemblage even though its texture demonstrates crystallization from an initial liquid.

James and Hamilton (1969) have demonstrated that at 1 kb total water pressure with increasing amounts of the anorthite component in the system, the crystallization of potash feldspar tends to be suppressed with the minimum valley being pushed to the potash feldspar apex if the Q-Ab-Or plot is used. This would explain the greater abundance of plagioclase phenocrysts in the syenite porphyries. Because anorthite is not a major molecule in these rocks, if added to the normative plots, it only changes their positions marginally as a comparison of Figs. IV-7 and IV-10 will show.

While the 5 kb minimum for the syenite porphyry initial crystallization is by no means firmly established, reference to Fig. VIII-1 shows that for a high heat flow environment 5 kb ($p_{H_2O}=p_{total}$) would be close to the maximum possible for crystallization of the syenite porphyry, with melting occurring at higher pressures. This diagram would also put a lower limit of approximately 2.5 kb or about 8 km depth for the formation of the phenocrysts of the syenite porphyry, if the system approximates the minimum melt curve for granite. This then gives a depth range from about 20 km maximum to about 8 km minimum for initial crystallization of phenocrysts.

If the syenite porphyries and sanidine rocks are considered to be an integral part of the system Ne-Q-Ks outlined in Fig. IV-9 the interpretation would be one of initial crystallization of the potash feldspar rocks with a progressive evolution via the syenite porphyry towards the Ab-Q-Or minimum. The field evidence (Plate 2) shows however that the sanidine porphyries have intruded the syenite porphyries, thus the sequence is reversed and the rocks cannot be regarded in toto as part of a simple crystallization scheme. The only rocks which might be directly related to the syenite porphyries are the brown matrix rocks CY61 and CY92, which are represented by the two triangles on the saturated side of the Ab-Or line in Fig. IV-9 and lie near the feldspar cotectic at one bar.

Also the sanidine rocks plot on the undersaturated side of the thermal divide which suggests that if a single magma source was involved, it would have divided across this barrier and then followed the appropriate crystallization paths, thus requiring a particular composition for such an initial melt.

Bailey and Schairer (1966) have discussed the importance of acmite and Fe_2O_3 in establishing piercing points between oversaturated and undersaturated systems. Apart from aegirine needles in the (late

stage) groundmass of the green matrix rocks there is no evidence of such processes operating for the Port Cygnet rocks.

The Sanidine Rocks

The rocks are nearer to the kalsilite parameter on the normative plot of the data (Fig. IV-8 and IV-9). The relatively high soda content that leads to the appearance of modal aegirine, nepheline, hauynite and analcime appears as nepheline in the norm, resulting in the rocks plotting as a group on the undersaturated side of the Ab-Or join of Fig. IV-9.

Fig. IV-9 shows that the sanidine rocks fall within the projection of the leucite field with many values lying between the 1 bar and 1 kb boundaries for leucite. In spite of this, there is no evidence of the prior existence of leucite phenocrysts or their relicts. The phenocryst assemblage comprises sanidine crystals in the classical form of (010) tablets with 3 cm maximum dimension.

The results of Goranson (1938) show that in a water saturated system leucite is eliminated at pressures greater than 2.6 kb but Lindsley (1966) has established that leucite may persist at greater confining pressures up to 19 ± 1 kb in the anhydrous system, related to the melting of potash feldspar.

The implication of these results is that the field of leucite plus liquid will have a high pressure limit, in a natural system, somewhere between 2.6 kb (Goranson, 1938) and 19 kb when P_{H_2O} is not equal to the total pressure of the system. It is not possible to determine the relation of P_{H_2O} to P_{total} for the Port Cygnet rocks but in the absence of suitable evidence it has been assumed the $P_{H_2O} = P_{total}$.

On the basis of the plots of the sanidine rocks in Fig. IV-9 an estimate of approximately 1.5 kb would exclude the leucite field. Many similar rocks have no leucite present. As there is no evidence as to precise water pressure the simplest interpretation would be that the

system was water saturated at some pressure greater than about 1.5 kb with an equivalent depth of about 5-6 km, as a minimum value, subject to the partial pressure of H_2O which if less than P_{total} would lead to an equivalent increase in the above values.

The presence of analcime in the groundmass together with its reaction with pre-existing sanidine phenocrysts, pectolite in the groundmass and the generation of large amounts of biotite in the formation of the hybrid rocks show that water had a high activity at least in the late stages of crystallization. Because of the narrowness of the sanidine bearing dykes (usually less than 1 metre) and their consequent rapid cooling, with absence of glass but with fine-grained unaltered crystals in the groundmass, it is considered that the hydrous minerals in the groundmass are of late stage magmatic origin than due to post-magmatic hydrothermal alteration which might also be expected to produce sericitisation of the feldspars. The very nature of the flow structures in the dykes (e.g. Plate 5) is indicative of large amounts of volatiles of which water must have been a major component to lower the viscosity of the magma sufficiently to allow turbulent flow and preserve the integrity of the phenocrysts.

Within the groundmass of the tinguaitite dyke (CY85) there are both altered and unaltered small anhedral nepheline grains whose compositions indicate the presence of larger quantities of silica and potash than is usually present in nepheline. While it is impossible to resolve the altered grains with the electron probe, the analytical results would suggest the presence of a hydrous phase and that the grains are intimate intergrowths of nepheline, analcime? and potash feldspar.

Initially it was thought that these might have been pseudoleucite and that perhaps some of the mechanisms proposed for its formation could be responsible for the alteration of the nepheline.

Pseudoleucite formation has been discussed extensively by Knight (1906), Bowen and Ellestad (1937), Bowen (1937), Larsen and Buie (1938), Fudali (1963), Templeman-Kluit (1968), Davidson (1970), Taylor and MacKenzie (1975), and Edgar (1978). The analcime present in the Cygnet rocks contains no potash, but it is clear from the experiments of Barrer and Hinds (1953) and Taylor and MacKenzie (1975) that considerable ion exchange is possible: and an environment with nepheline, potash feldspar and liquid could lead to intimate intergrowth of nepheline, analcime and potash feldspar, as well as later subsolidus reactions.

A further analysis of the pseudoleucite problem has been given by Gittins et al. (1980) who, in a study of the alkali ultramafic Batbjerg intrusion of east Greenland, found that pseudoleucite from this complex consisted of a vermicular or dactylitic intergrowth of nepheline and potash feldspar, and suggest that the term pseudoleucite be restricted to those examples where there is clear evidence of the icositetrahedral form of the parent leucite crystal. Other intergrowths may have no recognizable crystal outlines and may have albite instead of potash feldspar in the intergrowths.

The "grains" from the groundmass of CY85 are rounded, but many do have the hexagonal shape of nepheline (Plate 32). These consist of intimate reticulate intergrowths of nepheline and potash feldspar which are extremely difficult to resolve with the electron probe. There are also intergrowths of aegirine laths, suggesting that the nepheline crystals in this dyke have grown within the groundmass and enclosed pre-existing minerals. There is no evidence of micaceous alteration of nepheline in this rock. The origin of these would then be compatible with the work of Edgar (1978) who showed that at temperatures between about 550°C and 370°C at 1 kb P_{H_2O} there is an extensive subsolidus field in which analcime, nepheline and feldspar can co-exist.

Since nepheline and its associates occur only in the groundmass it is more likely that these formed under relatively low pressure conditions, as co-crystallized intergrowths in the matrix surrounding the coarser sanidine phenocrysts, with no crystallographic evidence of the prior existence of leucite.

Apart from the problem of leucite in the crystallization sequence the subsequent evolution of the system after the formation of the sanidine phenocrysts followed a path avoiding soda feldspar to the cotectic with nepheline, because the nepheline in the groundmass is intergrown with potash feldspar and occasional aegirine crystals rather than soda feldspar. It is unlikely that there was equilibrium crystallization of the groundmass phases. This can be supported by applying the alternative method of Hamilton (1961) for determining the temperature of formation of nephelines. In this method three points relating nepheline composition, melt composition and feldspar composition should form a triangle from which the formation temperature may be estimated. For the sanidine rocks a suitable triangle cannot be constructed.

With reference to Fig. IV-8 one composition (CY85) plots in the $\text{NaAlSi}_2\text{O}_6$ - KAlSi_2O_6 join. This plane of the diagram was investigated by Edgar (1978) and appears in Fig. IV-12 with the plot of CY85 superimposed. In a low pressure or anhydrous system, according to this plot, leucite should have crystallized, but for this rock (and all the others) it is absent. From Edgar's data and knowing from the textural relationship (Plate 37) that analcime is a late-stage phase, then from the position of CY85 the maximum formation temperature of analcime was about 450°C. However with the initial removal of sanidine the composition of the remaining liquid would be pushed to the sodium-rich part of the system which leads to a higher temperature of formation for analcime, the maximum for which, from Edgar's work, would be at

550°C. There is a complication because the natural system has three components hence crystallization of sanidine would move the liquid away from the two component join. As the paths in the solidus surface are approximately parallel to Edgar's plane then the results should not be too different. Thus crystallization of CY85 was probably completed by analcime formation at a maximum temperature between 450°C and 550°C at a relatively low pressure (e.g. 1 kb), since this is a groundmass phase and must have formed near the end of the emplacement process. Assuming the amount of overburden removed is about 2.5 km (see page III-22), the pressure regime of the experiments cited above would be appropriate. However if the actual pressure differs from this then the equilibria will also be different but pressure and temperature cannot be increased indefinitely for analcime whose dehydration curve is of similar form to that of amphiboles and reaches a maximum of 800°C at 8 kb in equilibrium with K-feldspar.

COMPARISONS

The major element data have also been used to prepare several variation diagrams to compare the relationships of the Port Cygnet alkaline rocks with other sequences. The most useful of these are the following: Al_2O_3 - SiO_2 -($\text{Na}_2\text{O}+\text{K}_2\text{O}$) of Bailey and Macdonald (1969) $\text{A}(\text{Na}_2\text{O}+\text{K}_2\text{O})$ - $\text{F}(\text{FeO}+\text{Fe}_2\text{O}_3)$ - $\text{M}(\text{MgO})$, total alkali ($\text{Na}_2\text{O}+\text{K}_2\text{O}+\text{CaO}$), and the Q(quartz)-L(leucocratic minerals)-M(melanocratic minerals) of Niggli (1954).

In Fig. IV-13 the data have been plotted on a Bailey-Macdonald diagram [Al_2O_3 - SiO_2 -($\text{Na}_2\text{O}+\text{K}_2\text{O}$)] (Bailey and Macdonald, 1969). The Bailey-Macdonald diagrams were developed to show trends in strongly peralkaline liquids which cannot be plotted on the usual Q-Ne-Ks diagram without introducing distortion of the $\text{Na}_2\text{O}/\text{K}_2\text{O}$ ratios and feldspar/liquid relationships. The plots are based on the molecular

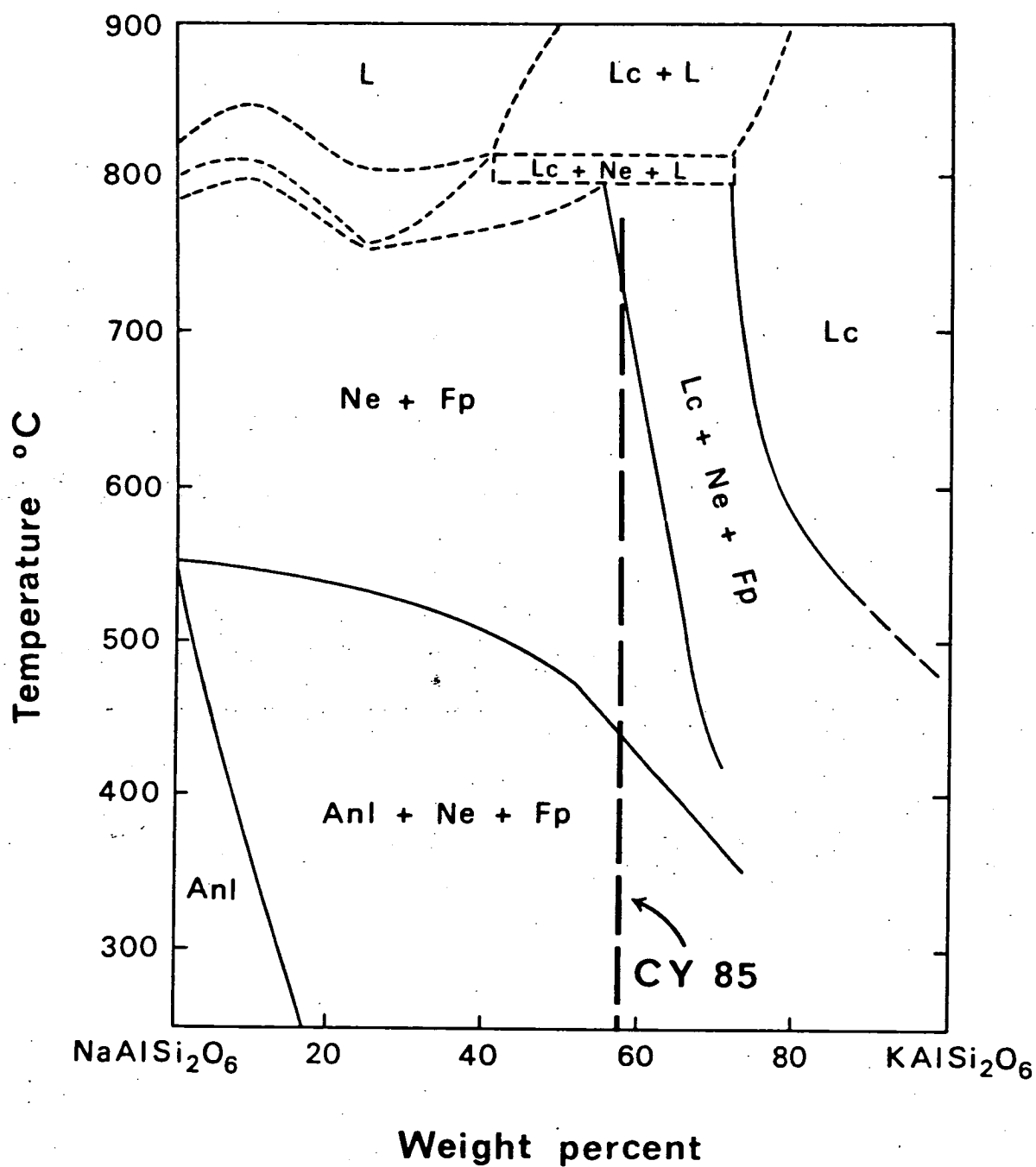


Figure IV-12 Position of CY85 on the $\text{NaAlSi}_2\text{O}_6$ - KAlSi_2O_6 join at one kbar (from Edgar, 1978). $P_{\text{H}_2\text{O}} = P_{\text{total}}$.

proportions of SiO_2 , Al_2O_3 , Na_2O and K_2O . Added to the plot are the average alkali syenite and Juvet-type nepheline syenite from Nockolds (1954). These have been preferred to Le Maitre's values (1976) which are not as closely defined as those of the former author. In accordance with the Bailey-Macdonald method, the data have been replotted with the plane of feldspar compositions defined in Fig. IV-15 being projected on to the SiO_2 - Na_2O - K_2O face of the fundamental Al_2O_3 - SiO_2 - Na_2O - K_2O tetrahedron (Fig. IV-14). According to Bailey and Macdonald (op. cit.) this method of presentation of data should show if there was fractionation of feldspar during the period of formation of the rocks.

The model pre supposes that alkaline-peralkaline assemblages have formed in suites of rocks where feldspar is fractionating. Fractionation trends where both feldspars and feldspathoids are crystallizing, may distort the projection. However in the case of the Port Cygnet rocks where the phenocryst assemblage is dominated by sanidine in the undersaturated rocks and feldspathoid is absent from the slightly oversaturated syenite porphyry, there should be little distortion of the final plots.

The albite-orthoclase saturation plane in the Al_2O_3 - SiO_2 - Na_2O - K_2O tetrahedron (vertical line in Fig. IV-13) is not parallel to the plane defined by undersaturated rocks and the Port Cygnet rocks which lie in a plane passing through the edge at 90SiO_2 - $10\text{Al}_2\text{O}_3$. As the two planes do not diverge greatly, particularly in the field of the potassium-rich rocks it is considered that there is no large distortion in the plot of Fig. IV-14 which follows the procedure of Gill (1972), for undersaturated rocks. The nepheline cotectic passes along the bottom of the figure.

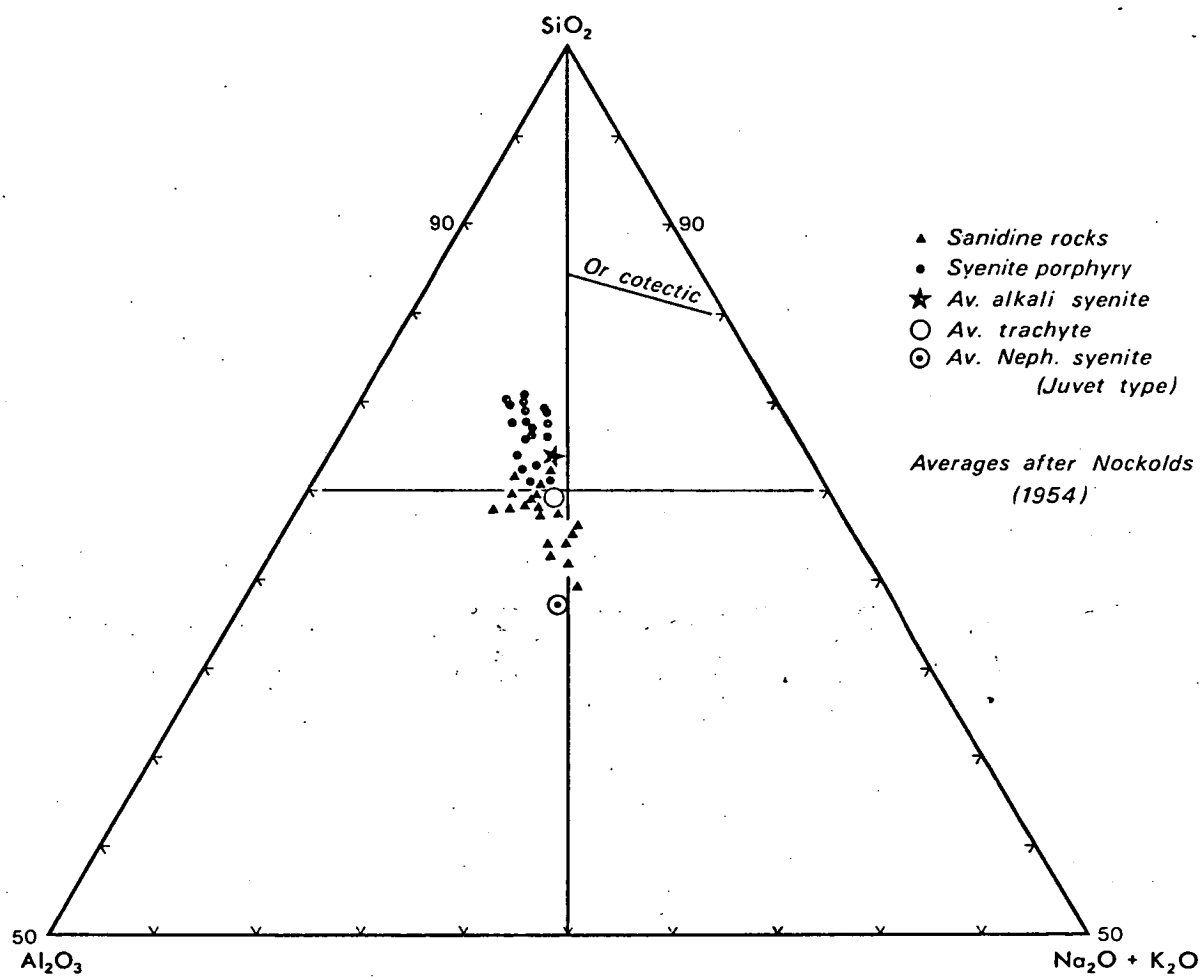


Figure IV-13 Bailey-McDonald Al_2O_3 - SiO_2 - $\text{K}_2\text{O}, \text{Na}_2\text{O}$ plot of Port Cygnet alkaline rocks.

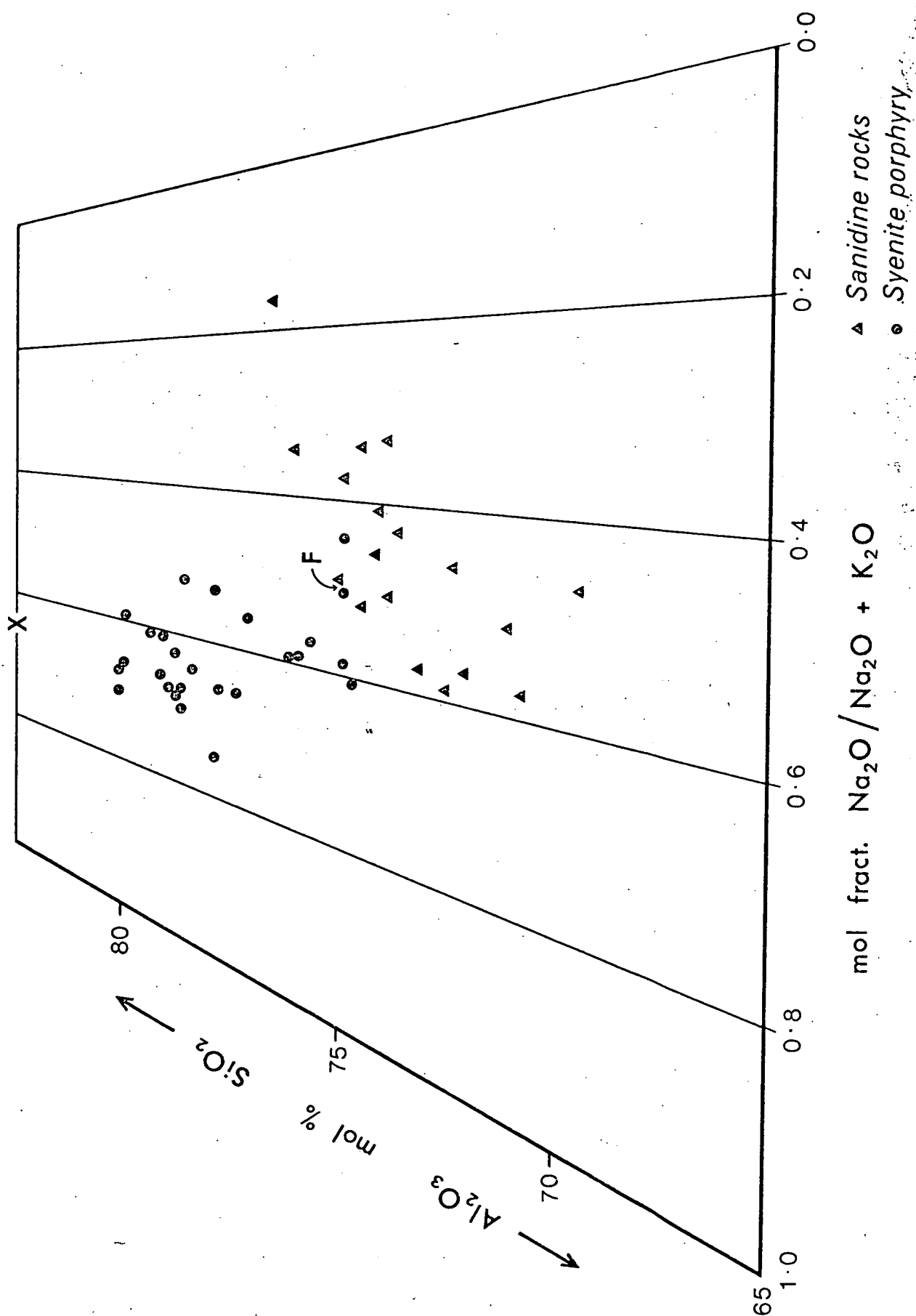


Figure IV-14 Section across Al_2O_3 - SiO_2 - Na_2O - K_2O tetrahedron corresponding to the general trend of the alkaline rocks of Figure IV-13 with the alkali mole fraction superimposed. F is 1:1 feldspar and X is the plot of the 5 kb feldspar minimum. $P_{\text{H}_2\text{O}} = P_{\text{total}}$.

Fig. IV-14 shows the rocks plotting as two groups with the sanidine rocks closer to the base because of their having normative nepheline. There is no strong feldspar fractionation trend for either group.

In Fig. IV-15 are plotted the AFM variation data for Port Cygnet. Fig. IV-16 shows the comparison of the Port Cygnet data with the AFM trends for other complexes. The most obvious features of Fig. IV-15 is the clustering of the rocks towards the alkali apex of the triangle with no extended differentiation trend. The other important feature is the appearance of a dual and divergent trend with a dichotomy between the syenite porphyries and the sanidine-bearing rocks with the latter having a relatively lower and less variable magnesia content. The curve across Fig. IV-15 has been drawn on the basis of the relationship exhibited by the amphiboles in Figs. III-10 and III-13. This reflects the relationships noted earlier with regard to the trends (Figs. IV-4 and IV-5) shown in the Thornton-Tuttle differentiation index variation diagrams. The rocks plot in a relatively restricted area, and like other similar rocks the Port Cygnet alkaline rocks tend to lie at the termination of many trends. The sanidine rocks fall along the liquid line of descent for the Klokken (Gardar Province, Greenland) intrusion described by Parsons (1979) and the St. Helena trend (Baker, 1968), but differences in Na_2O and K_2O are not revealed in this plot.

In Fig. IV-17 a detailed comparison has been made with the Finmark and east Ontario rocks (Appleyard, 1974), where the Cygnet potassium-rich rocks could be regarded as part of a more extensive trend, of a sequence similar to the east Ontario rocks. But it must be remembered

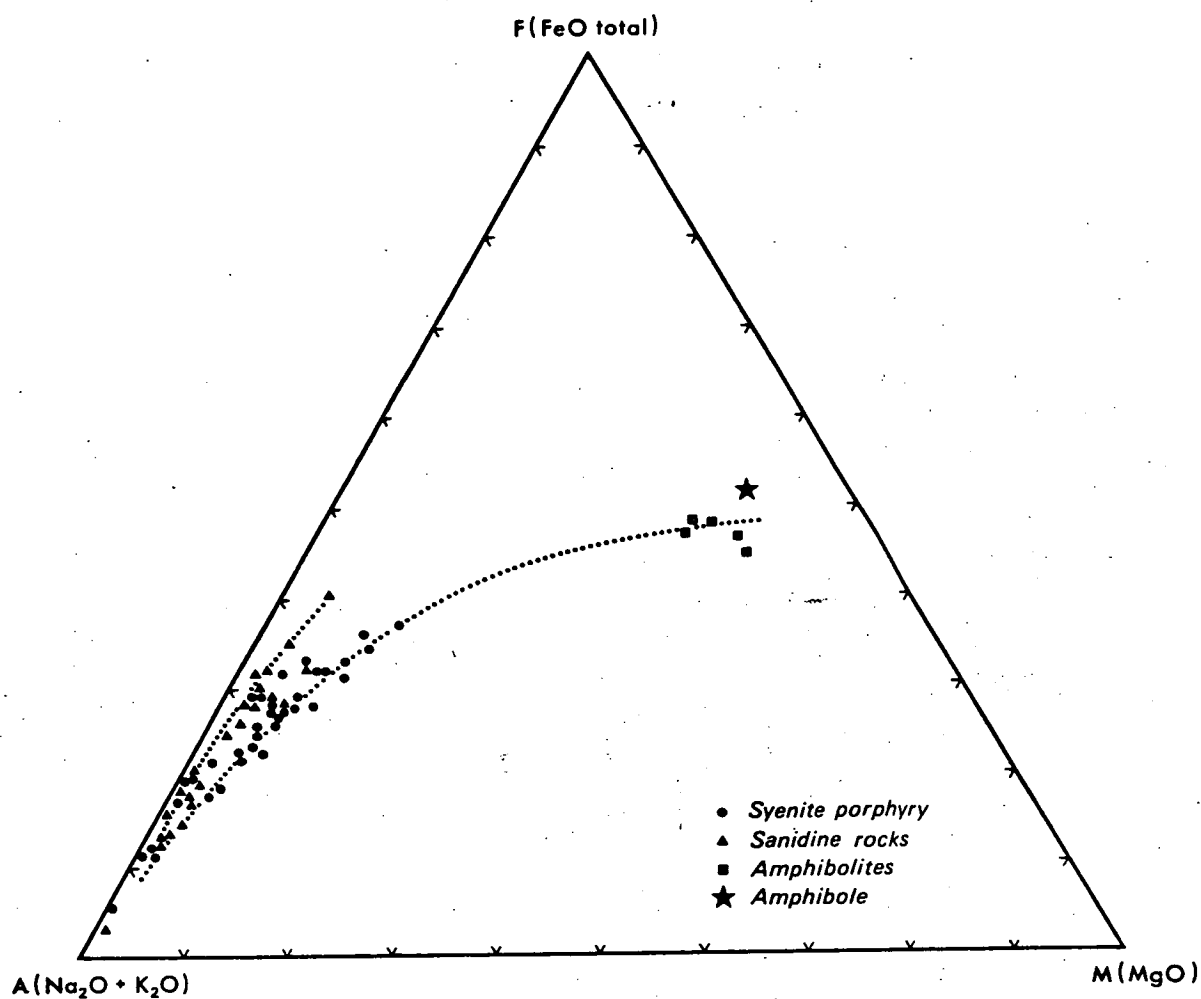


Figure IV-15 AFM plot for the Port Cygnet alkaline rocks with amphibolite inclusions and their amphibole added.

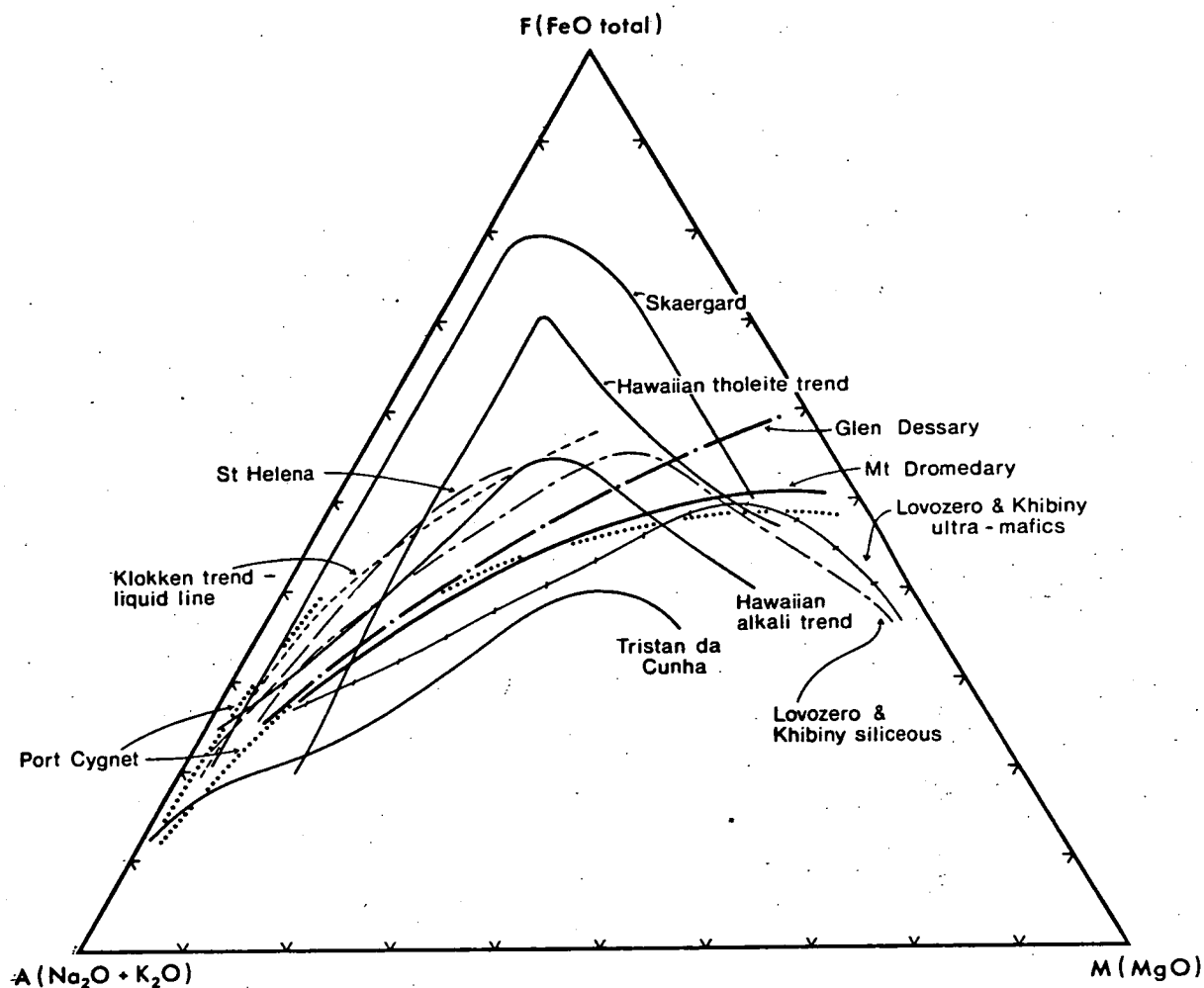


Figure IV-16 Comparative AFM plots for other areas with Port Cygnet plot added. Note the similarity of Port Cygnet (syenite porphyry) to Glen Dessary and Mt. Dromedary.

that because of the restricted range of compositions of the former group, they would plot near any alkali-rich system on such a diagram.

This evidence could therefore suggest that these rocks might be the final phase of a differentiation sequence but are different from the sequence shown by the syenite porphyries. There is no field evidence of any rock types from such a sequence in the area.

The syenite porphyry trend has been extended through the compositions of the amphibolite inclusions from Mt. Windsor and their constituent amphibole. This trend is very similar to those of Mt. Dromedary and Glen Dessary. In these latter two examples there are associations with pyroxenite at Mt. Dromedary and amphibolite at Glen Dessary and comparison of these with the Port Cygnet trend suggests that the syenite porphyries may have a similar association with their associated amphibolite inclusions. The characteristic downturn towards the MgO apex, evident in most of the other trends is not present in those discussed above.

Use may be made of the total alkali plot ($\text{Na}_2\text{O}-\text{K}_2\text{O}-\text{CaO}$) (Fig. IV-18) where the Port Cygnet data have been compared with other complexes. Whereas there are distinctive trends for other localities, the Port Cygnet rocks plot as two distinct groups with their boundary largely controlled by the proportion of potash present. In this plot there is no evidence of any trend, however the syenite porphyry group plots at soda-potash-rich ends of the comparative trends. The sanidine rocks appear to have little relationship to the other complexes cited.

Another comparison has been made in Fig. IV-19 where the sanidine rocks have been superimposed on the total alkali plot of the Finmark and east Ontario rocks (Appleyard, 1974). When presented in this way the Port Cygnet rocks are similar to those of Finmark which also plot as a group but with a somewhat higher soda content than in the former rocks. The eastern Ontario rocks show a distinct trend on this plot.

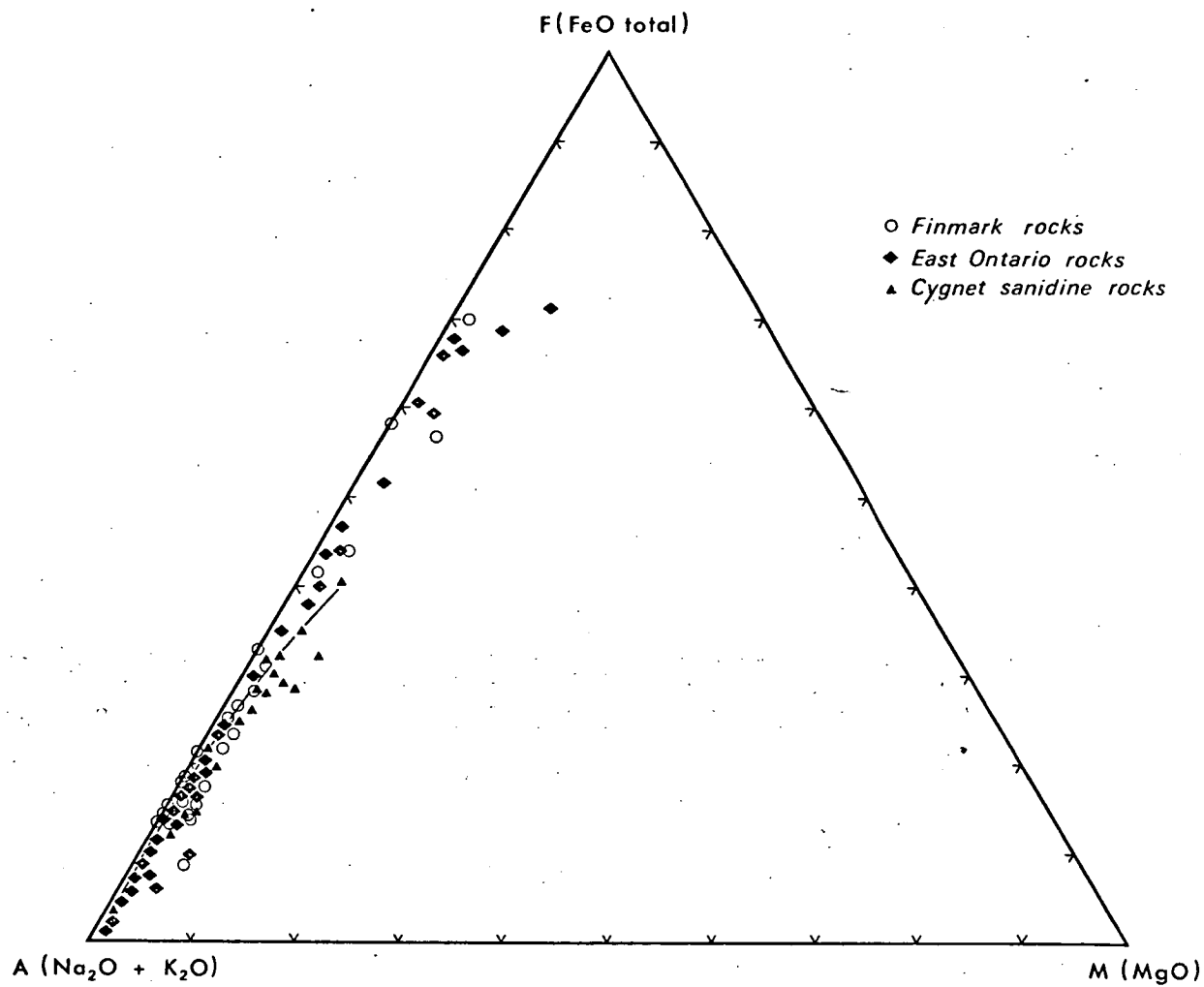


Figure IV-17 AFM plot comparing the Port Cygnet potassium-rich rocks with those of Finmark and eastern Ontario (after Appleyard, 1974).

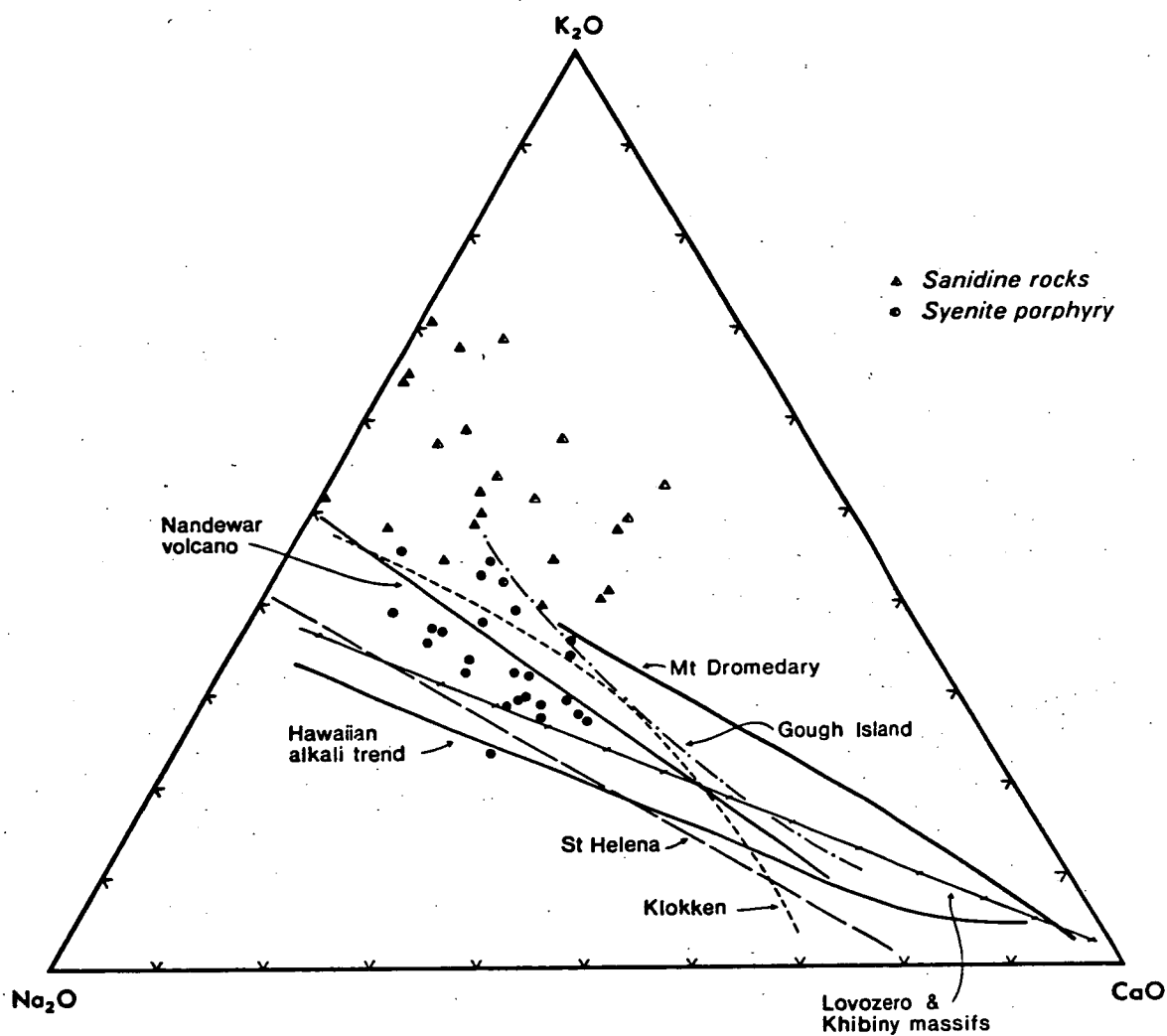


Figure IV-18 Total alkali plot for all rocks with trends for other areas added.

Thus in the total alkali plot the sanidine rocks plot as a group distinct from the syenite porphyries and could have an origin different from these and from those with which they are compared.

The major element data for the alkaline rocks of Port Cygnet are plotted on the Q (quartz) - L (leucocratic minerals) - M (melanocratic minerals) triangle from Niggli (1954). Fig. IV-20 shows this plot together with the compositions of the amphibolite inclusions, amphibole from the inclusions, matrix of the inclusions and the phengitic inclusions from the dyke X50. The amphibolite matrix represents the oversaturated limit of the sequence while the undersaturated limit occurs at the phengitic end of the spread.

The extra details have been included to see if it is possible to relate them to the origin of the alkaline rocks. The trachyte and phonolite trends of King and Sutherland (1960) have also been added.

On this plot the data for the Cygnet rocks again fall into two groups but there is now more evidence of a trend. The petrography indicated that the amphibolite inclusions have been recrystallized and their feldspathic matrices melted out. The plot for the matrix glass composition as determined by experiment T541 (Table IV-4) is shown in Fig. IV-20 and could well represent a limiting value for the syenite porphyry composition on this plot. The phengite inclusions from X50 have been added to the diagram, but because of their high K_2O content they plot near the L apex of the triangle and may not necessarily represent a source of the sanidine rocks.

The hornblende porphyry, which is a unique rock in the complex, and has petrographic characteristics (pyroxene aggregates) suggesting a mixed source origin, from its position on the Q-L-M diagram could be interpreted as a mix of the more potash rich rocks and amphibole from the recrystallized amphibolite.

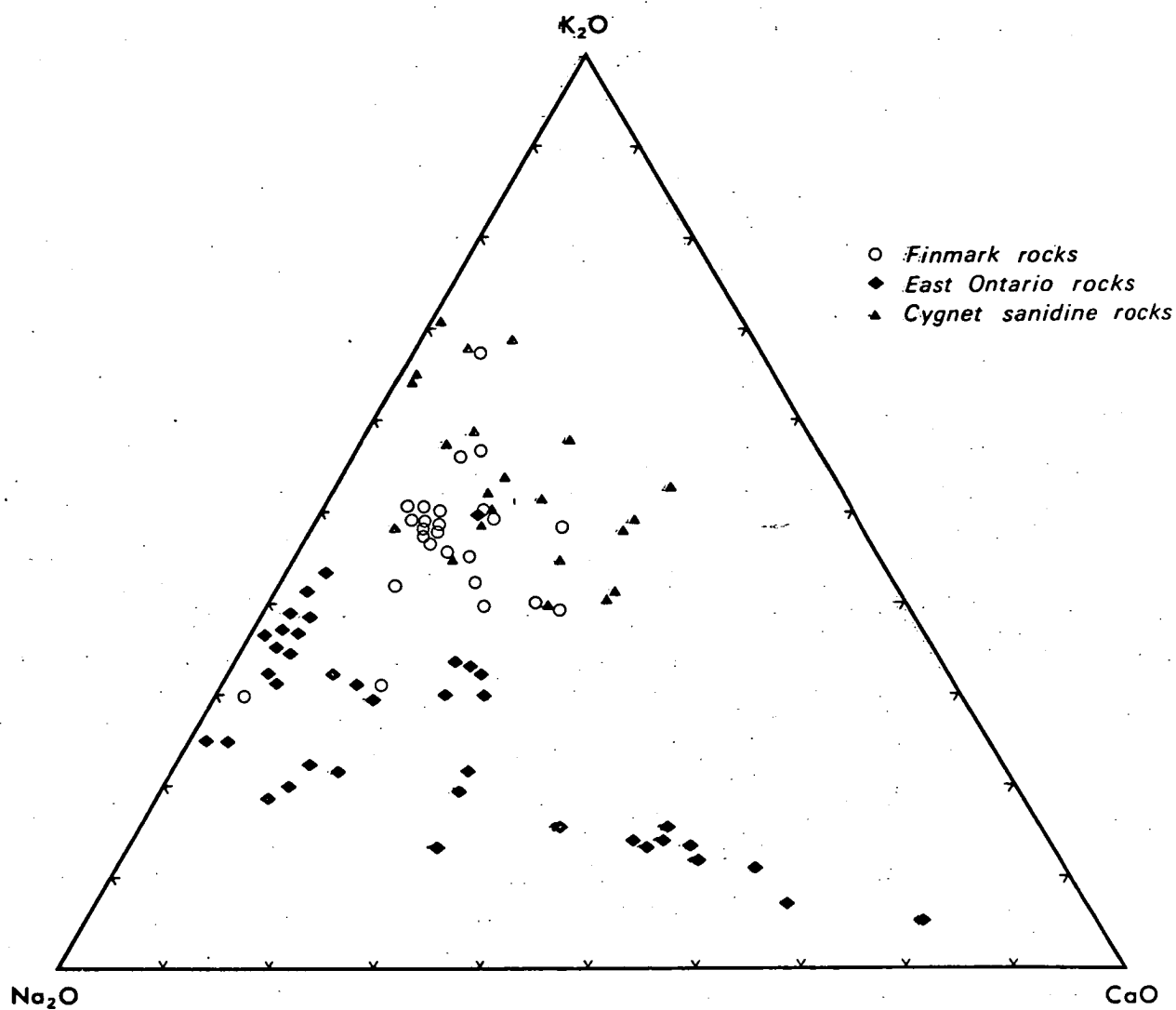


Figure IV-19 Total alkali plot comparing the Port Cygnet potassium-rich rocks with those of Finmark and eastern Ontario (after Appleyard, 1974).

SUMMARY OF MAJOR ELEMENT DATA FOR THE ALKALINE ROCKS

When plotted on the variation diagrams already referred to the rocks from the Port Cygnet alkaline complex tend to fall into two groups. Because of the relatively restricted compositional range strong fractionation trends would not be demonstrated by the major element data. Thus the Thornton-Tuttle differentiation index plot shows two parallel rather than consecutive trends, the Ne-Ks-Q shows saturated and undersaturated groups, the total alkali plot favours two groups and the A.F.M. plot indicates two diverging trends. The Bailey-McDonald diagrams also indicate two groups of rocks with no evidence of fractionation of feldspar within them.

Harker Plots of the rocks also indicate that two groups are present. The A.F.M. diagram with the compositions of the amphibolite inclusions added defines trends similar to those of Mt. Dromedary (New South Wales) and Glen Dessary (Scotland).

The Q-L-M plot shows a trend for the alkaline rocks between one extreme that corresponds to the quartz-feldspathic matrix of the amphibolite inclusions and another corresponding to the phengite inclusions of X50. The hornblende porphyry appears as a mix of amphibole (from the inclusions) with the more potassic alkaline rocks. This association can be compared with the Q-L-M plot of the Phalaborwa complex, East Transvaal (Frick, 1975) where there is a close association of syenites with feldspathic pyroxenite and pyroxenite (Fig. IV-21).

The data, apart from those for the brown matrix rocks, suggest that the rocks do not have equilibrium phenocryst assemblages.

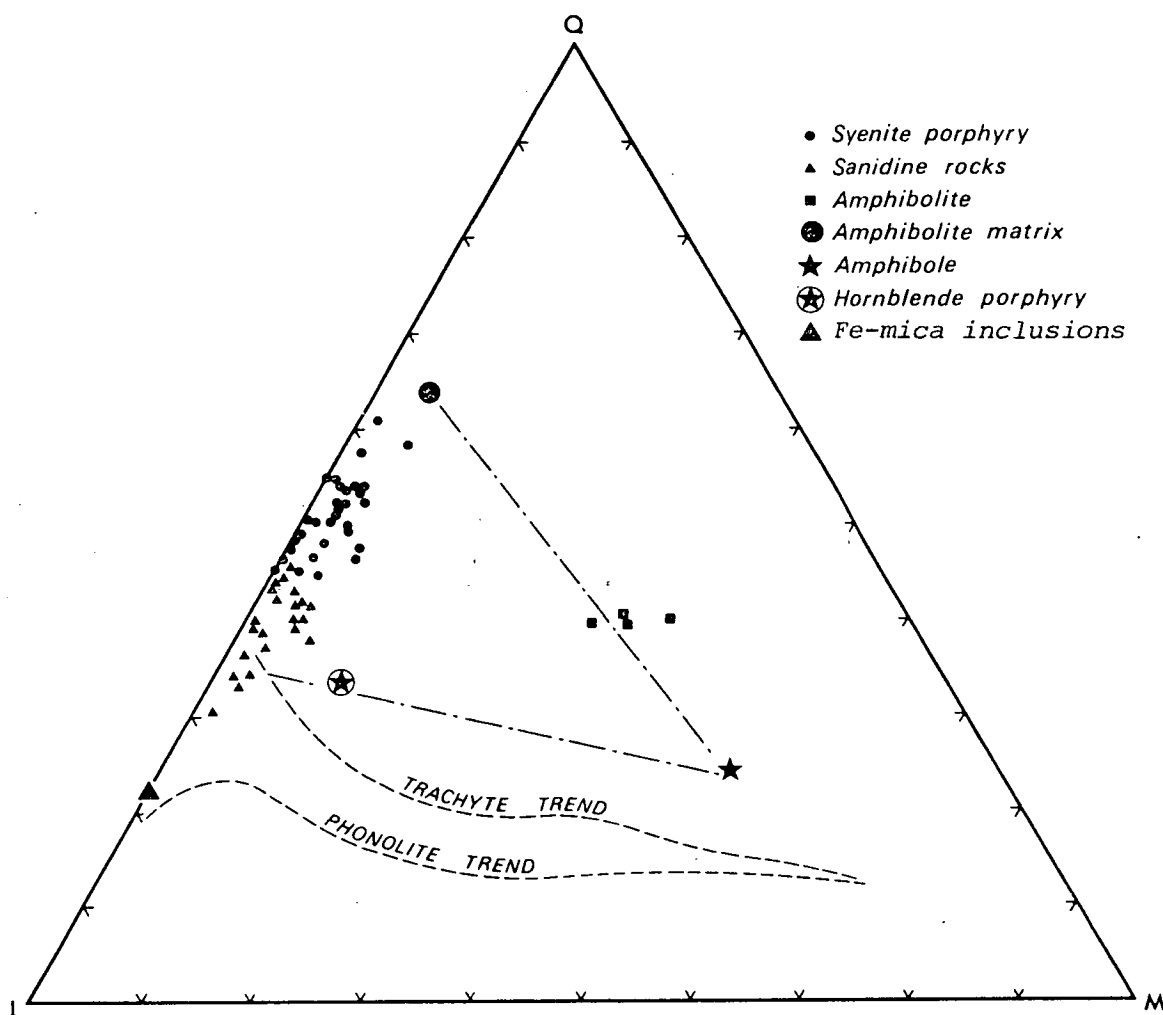


Figure IV-20 Niggli QLM plot for alkaline rocks and their inclusions. Trachyte and phonolite trends from King & Sutherland (1960) have been added.

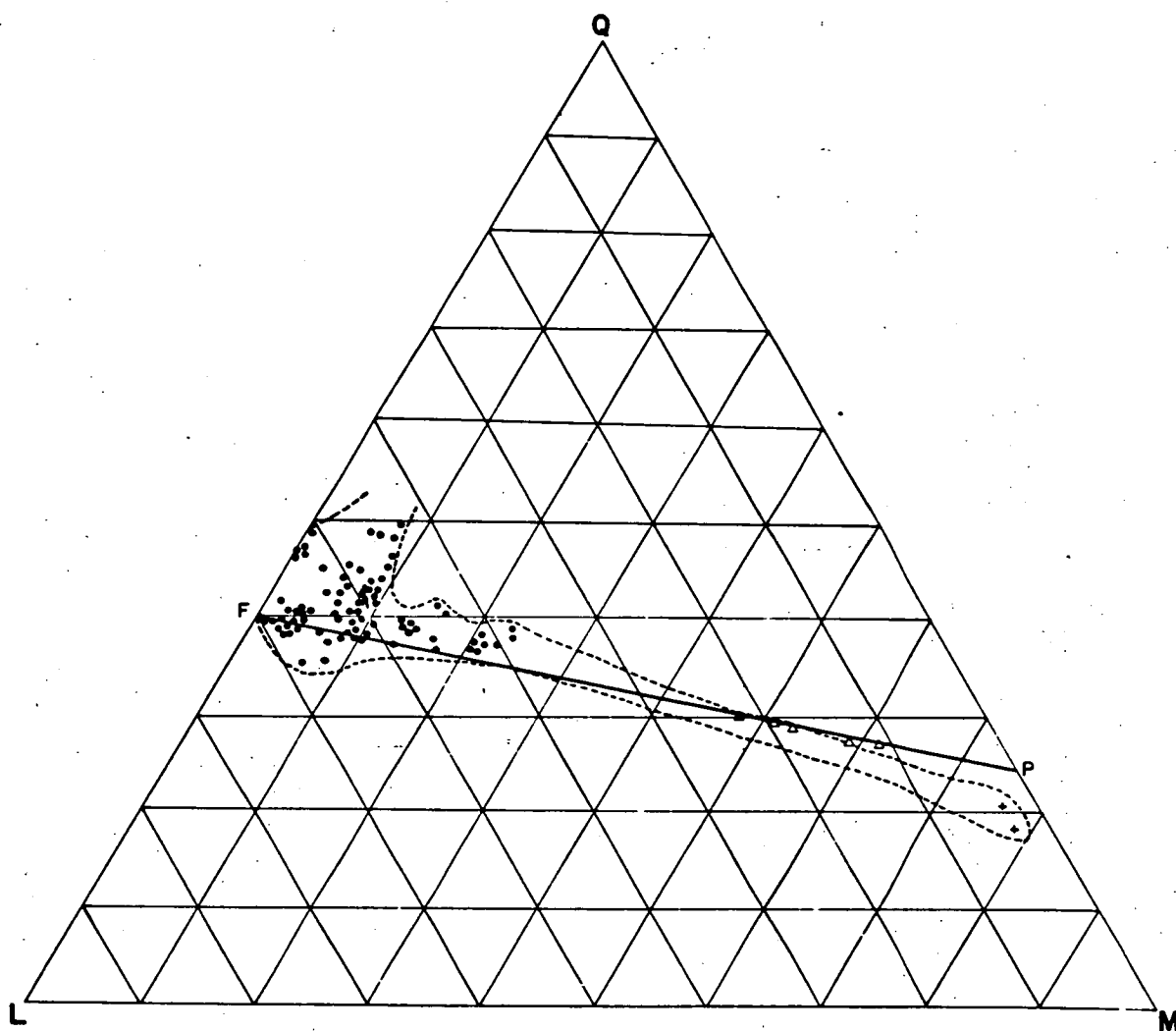


Figure IV-21 Niggli QLM plot for the Phalaborwa Complex showing the relation between syenite (o), feldspathic pyroxenite (Δ) and pyroxenite (+) (from Frick, 1975).

The syenite porphyries probably began crystallizing at depths between 20 km and 8 km.

The mixed phenocryst, brown matrix rocks plot near the feldspar minimum and are apparently associated with the syenite porphyries.

The absence of leucite in the presence of volatiles places a lower pressure limit of 2.6 kbars (= 10 km) on the pressure = depth of crystallization conditions for the phenocryst assemblage. If $P_{H_2O} < P_{total}$ then this limit may go as high as 19 kbar for the case where H_2O is absent.

HYBRID ROCKS

The hybrid rocks are the crystallized product of the reaction of the potassic alkaline magma and associated fluids with pre-existing Jurassic dolerite.

Considering the hybrid rocks, it can be seen that these plot virtually as a band about the equator of Fig. IV-1 with a strong bias towards the orthoclase apex resulting from the addition of potash to these rocks. Even though albite-rich feldspars may occur these do not have a great influence on the overall chemistry. Many of the potash-rich dykes also plot in this band. The general trend of the uncontaminated alkaline rocks is concentrated around the centre of the figure. Analyses of hybrid zone rocks appear in Table IV-5.

The petrography (Chapter II) shows that the first evidence of chemical interaction of the dolerite and alkaline rocks leads to the formation of biotite reaction rims on iron-bearing minerals. The sequence of alteration is then primarily one of metasomatism of the dolerite by potassium.

An empirical relationship should then be apparent between potassium, being the dominant characteristic element of the alkaline

rocks, and iron and magnesium which are elements characteristic of dolerite. In Fig. IV-22 are plotted the molecular proportions of Fe_2O_3 against the ratios of the molecular proportion of K_2O to MgO . This method has been used to enable the three most typical components to be plotted on a biaxial diagram. Thus dolerites with high iron and magnesium and low potassium plot as a group distinct from the alkaline rocks with high potassium and low magnesium. The melanocratic hybrid rocks fall into a group between these with the resulting distribution for all rocks being dominated by the potassium variation.

The hybrid rock compositions may also be plotted on a K_2O - Fe_2O_3 - MgO triangle (Fig. IV-23) where the influence of potassium in the reaction process becomes evident, with the melanocratic rocks not showing large variations in their iron-magnesium ratios. Other chemical differences appear in the Thornton-Tuttle differentiation indices plot (Figs. IV-4 to IV-6) where the relationship to the high potassium sanidine-bearing rocks rather than the syenite porphyry, is evident. In addition to potash it can be seen that soda (Fig. IV-5) is also overall lower in the hybrids than the alkali rocks in spite of the appearance of albite in some of these rocks.

The hybrid rocks cannot be represented by simple mixes of two end members because of the selectivity of the reactions involved and the recrystallization and breakdown of the original minerals of the dolerite.

The main process has been the addition of potash to the pre-existing dolerite with consequent formation of biotite and potash feldspar and re-equilibration of the ferromagnesian minerals and feldspars to produce aegirine-augite, melanite, albite-andesine, nepheline and zeolites.

The major element data may be summarised thus: there is a

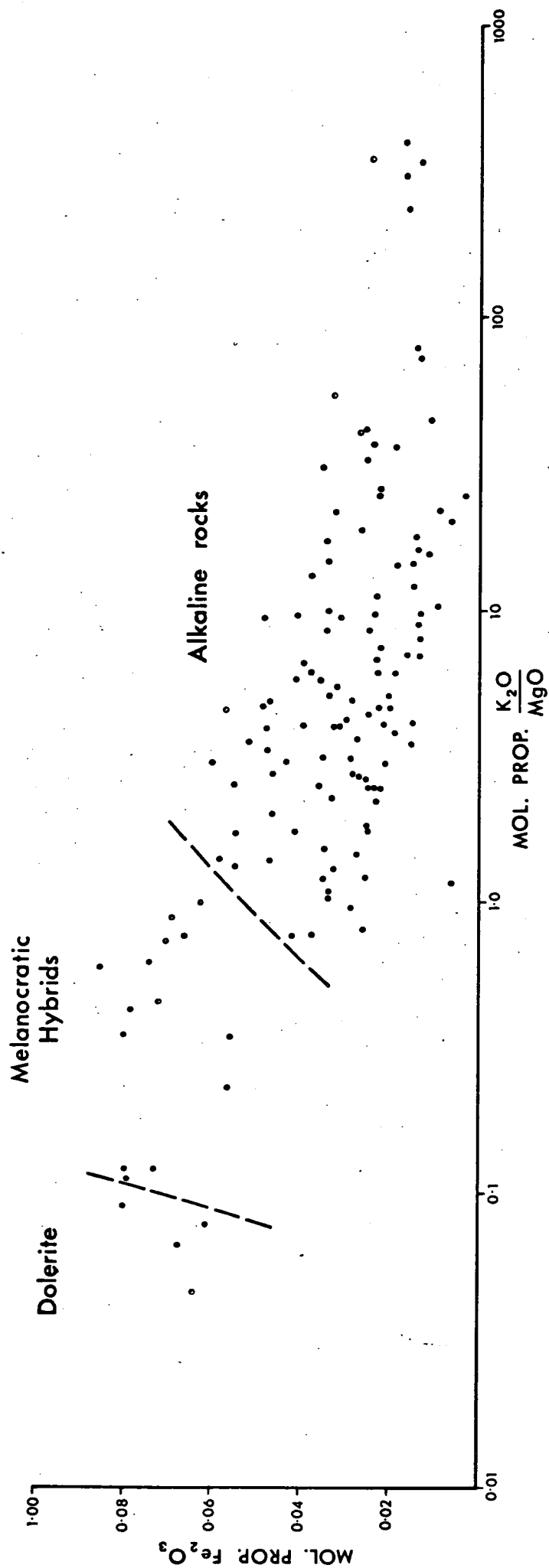


Figure IV-22 Fe_2O_3 - $\text{K}_2\text{O}/\text{MgO}$ plot for all rocks showing relationship of dolerites, melanocratic hybrids and alkaline rocks including leucocratic hybrids.

Table IV-5

Chemical analyses of some hybrid rocks from Port Cygnet.

	CY97	CY98A	CY29	CY31	CY33B	CY36	CY118	CY114	CY108
SiO ₂	62.91	55.32	53.30	63.57	55.30	51.23	55.92	61.31	48.84
TiO ₂	0.20	0.90	1.01	0.31	1.23	1.08	0.75	0.41	1.13
Al ₂ O ₃	19.43	18.02	18.25	17.47	15.26	12.13	14.20	13.12	12.62
Fe ₂ O ₃	2.77	4.44	4.61	1.41	5.72	4.90	2.40	3.39	6.59
FeO	0.46	2.07	1.90	0.16	1.79	5.10	7.05	2.47	3.97
MnO	0.05	0.12	0.18	0.06	0.12	0.23	0.19	0.35	0.21
MgO	0.32	1.17	0.95	0.33	2.27	5.40	5.01	1.41	4.80
CaO	0.84	1.46	5.42	1.36	6.41	10.33	10.05	4.62	11.06
Na ₂ O	4.44	2.61	3.32	2.15	2.31	0.39	2.66	2.69	2.18
K ₂ O	8.51	9.05	8.77	11.26	7.00	5.80	1.42	9.94	4.88
P ₂ O ₅	0.05	0.19	0.20	0.04	0.48	1.16	0.14	0.30	0.82
loss	0.54	3.63	1.59	0.38	1.11	1.52	1.52	0.43	1.44
Total	100.52	98.98	99.50	98.50	99.00	99.27	101.31	100.44	98.54

CIPW norms

Q	2.37	1.16	0.00	5.04	3.20	4.40	7.50	1.42	0.00
C	1.51	1.73	-	-	-	-	-	-	-
or	50.30	53.40	51.84	66.55	41.37	34.28	8.39	58.75	28.84
ab	37.57	22.08	9.62	18.19	19.54	3.30	22.51	12.14	12.45
an	3.84	6.00	9.00	4.76	10.60	14.22	22.62	-	10.24
ne	-	-	10.01	-	-	-	-	-	3.25
ac	-	-	-	-	-	-	-	9.35	-
di	-	-	5.10	1.17	12.19	23.54	21.63	15.81	26.48
wo	-	-	4.19	-	1.00	-	-	0.83	2.24
hy	0.80	2.91	-	0.28	-	6.17	11.92	-	-
mt	1.07	4.45	3.78	-	2.60	7.10	3.48	0.23	9.55
hm	2.03	1.37	2.00	1.41	3.93	-	-	-	-
il	0.38	1.71	1.92	0.47	2.34	2.05	1.42	0.78	2.15
ap	0.12	0.45	0.47	0.09	1.13	2.74	0.33	0.71	1.92
sph	-	-	-	0.16	-	-	-	-	-

Trace elements (ppm)

Rb	126	241	191	305	202	165	72	211	110
Sr	1552	872	2552	1293	2260	1746	48	580	2706
Cs	<1	28	1	2	<1	1	6	1	31
Ba	815	6423	3863	1106	2465	1221	324	802	1943
Sc	3	5	3	3	13	22	42	12	25
Y	nd	109	10	nd	30	31	34	5	nd
Zr	255	129	86	104	142	94	71	38	20
Nb	10	24	12	8	19	5	4	57	8
Ni	<1	1	<1	2	6	19	36	<1	<1
Cu	72	171	61	140	0	141	119	<3	113
Zn	36	173	60	37	78	134	77	228	126
Pb	6	16	<3	1	<3	<3	<3	<3	<3
Ga	29	24	24	25	21	18	17	95	19

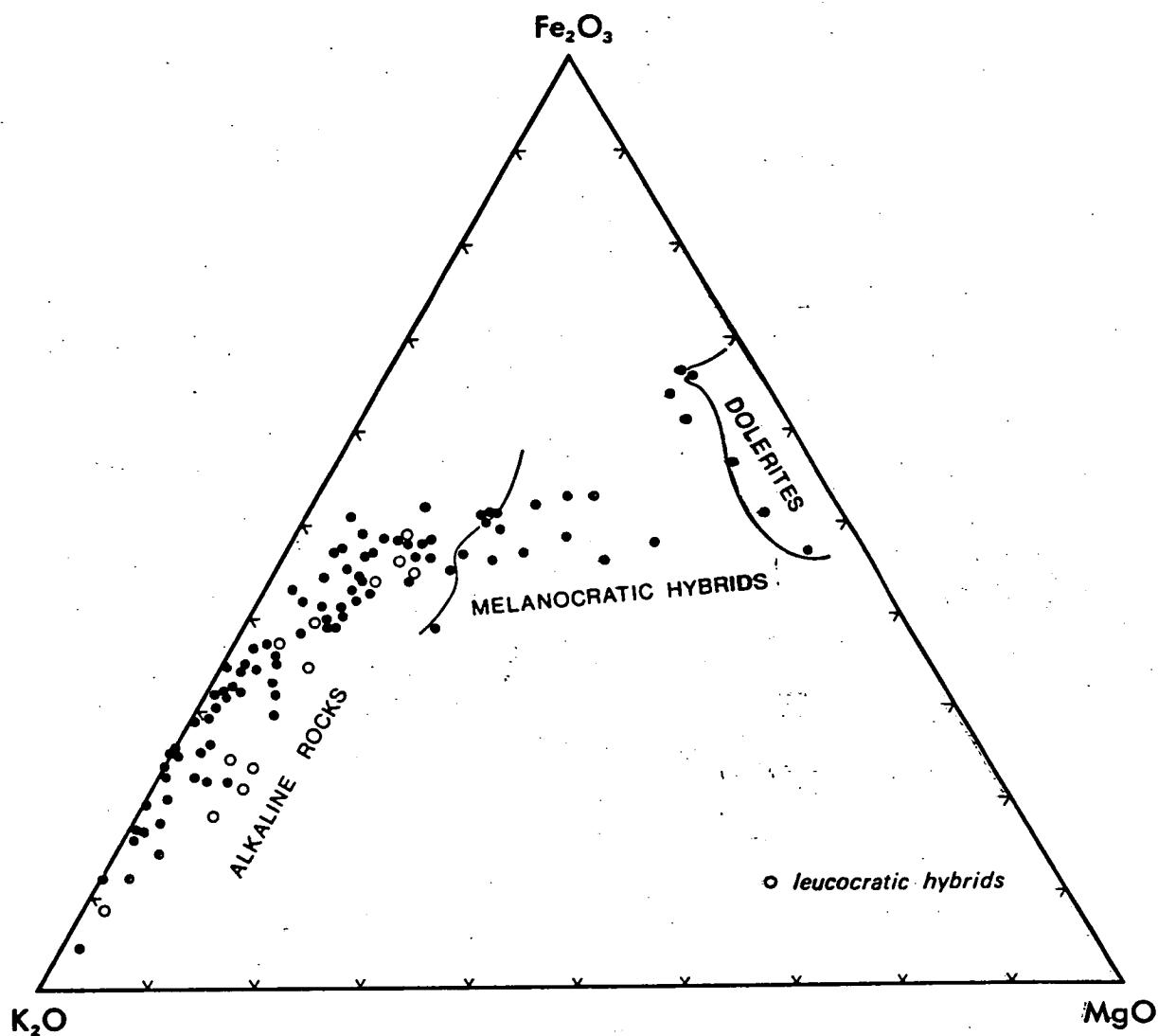


Figure IV-23. K₂O-Fe₂O₃-MgO molar plot for the alkaline and hybrid rocks.

variation between the alkaline rocks and Jurassic dolerite which is reflected by the addition of potash to the dolerite, with formation of biotite from magnesia and iron oxides, and recrystallization of pyroxenes and alkali feldspars to produce the hybrid rocks.

CHAPTER V

MINOR ELEMENT CHEMISTRY

Specimens were prepared by fine grinding in a Siebtechnik tungsten carbide mill after a preliminary crushing in a Sturtevant jaw crusher. Minor elements were determined in all rocks by X.R.F. methods using standards prepared from pressed powders with boric acid backing following the methods of Norrish and Hutton (1969). Standards and specimens were pressed at 12500 p.s.i. Mass absorption corrections were made knowing the compositions of the matrices of the standards and the total major element composition of the rocks. The analyses are detailed in Appendix II. The minor elements which have been determined are Rb, Cs, Sr, Ba, Sc, Y, Zr, Nb, Ni, Cu, Zn and Ga. The results will be discussed in the above order which approximates their association in the Periodic Table of the Elements. All rocks will be covered but specific characteristics of the hybrid rocks will be discussed in a later section.

THE ALKALINE ROCKS

Rubidium

The rubidium concentration of the alkaline rocks varies from 70 ppm to 290 ppm with the syenite porphyry averaging 125 ppm. The sanidine rocks contain somewhat higher values averaging 225 ppm (Fig. V-1) reflecting the geochemical association of potassium and rubidium. These represent some enrichment over the crustal average of about 37 ppm.

The values may be compared with the early phases of Lovozero nepheline syenites (130 ppm) and Ilimaussaq augite syenite (200 ppm)

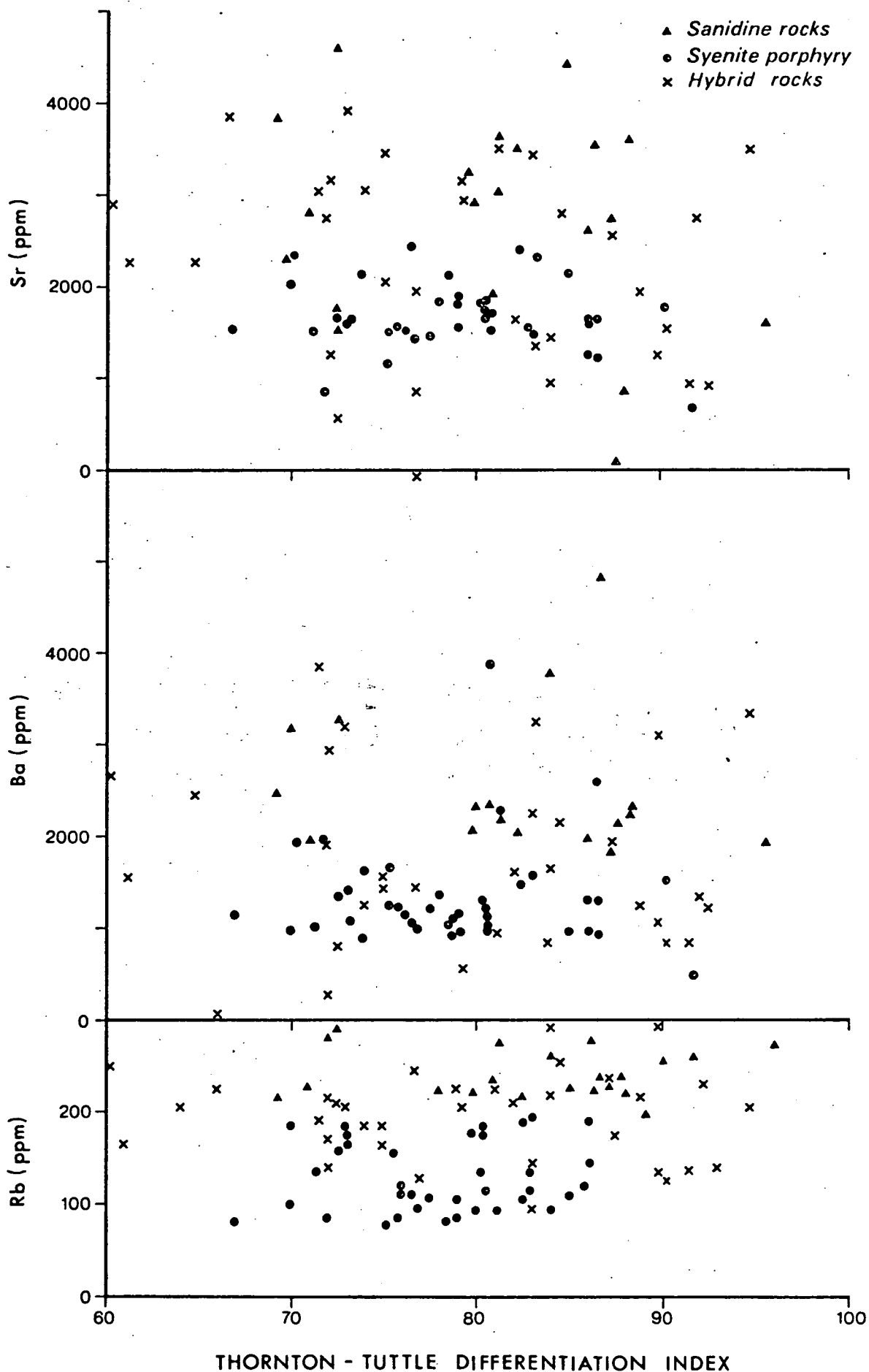


Figure V-1 Thornton-Tuttle differentiation index plot for Sr, Ba and Rb.

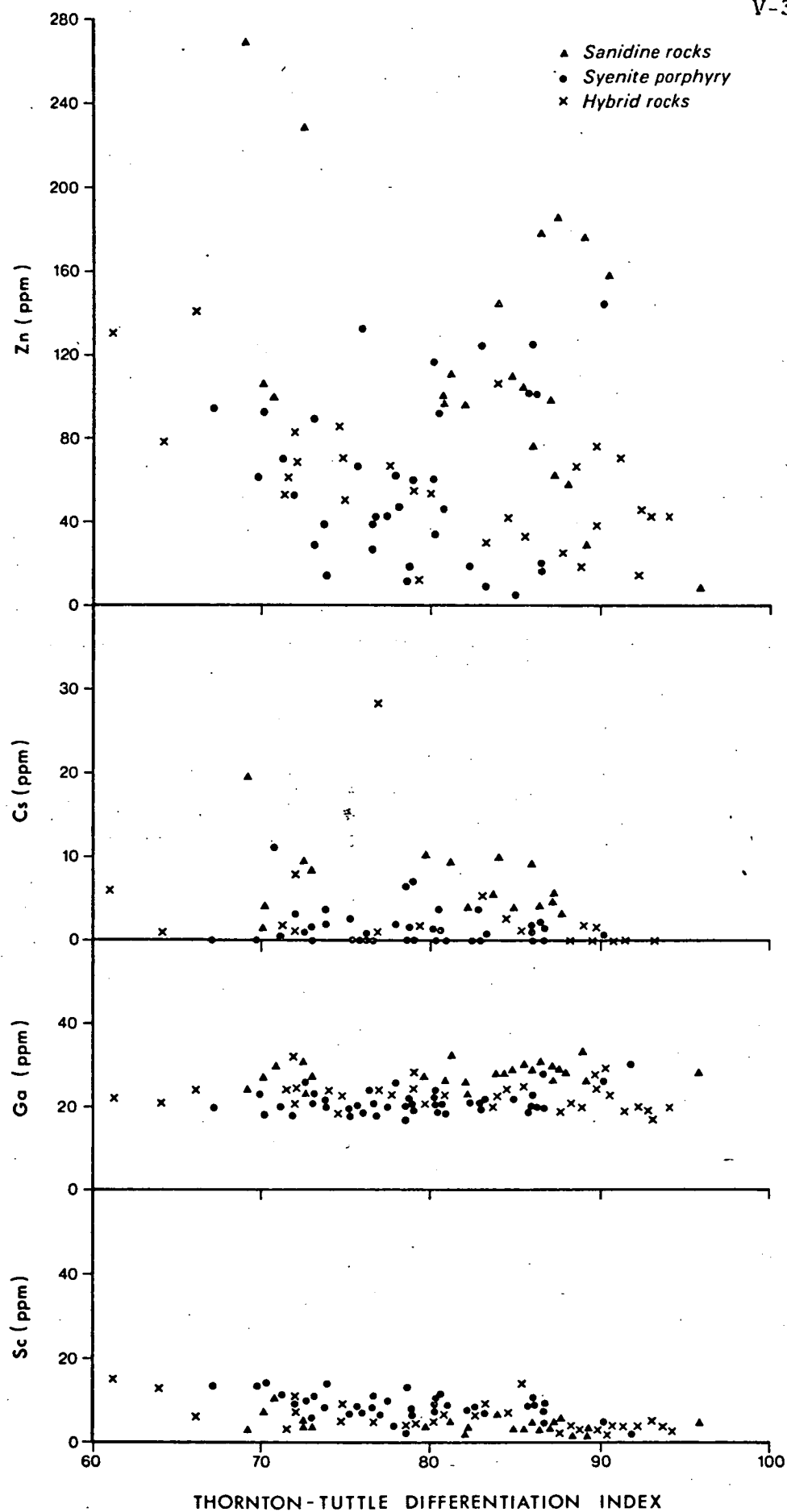


Figure V-2 Thornton-Tuttle differentiation index plot for Sc, Ga, Cs and Zn.

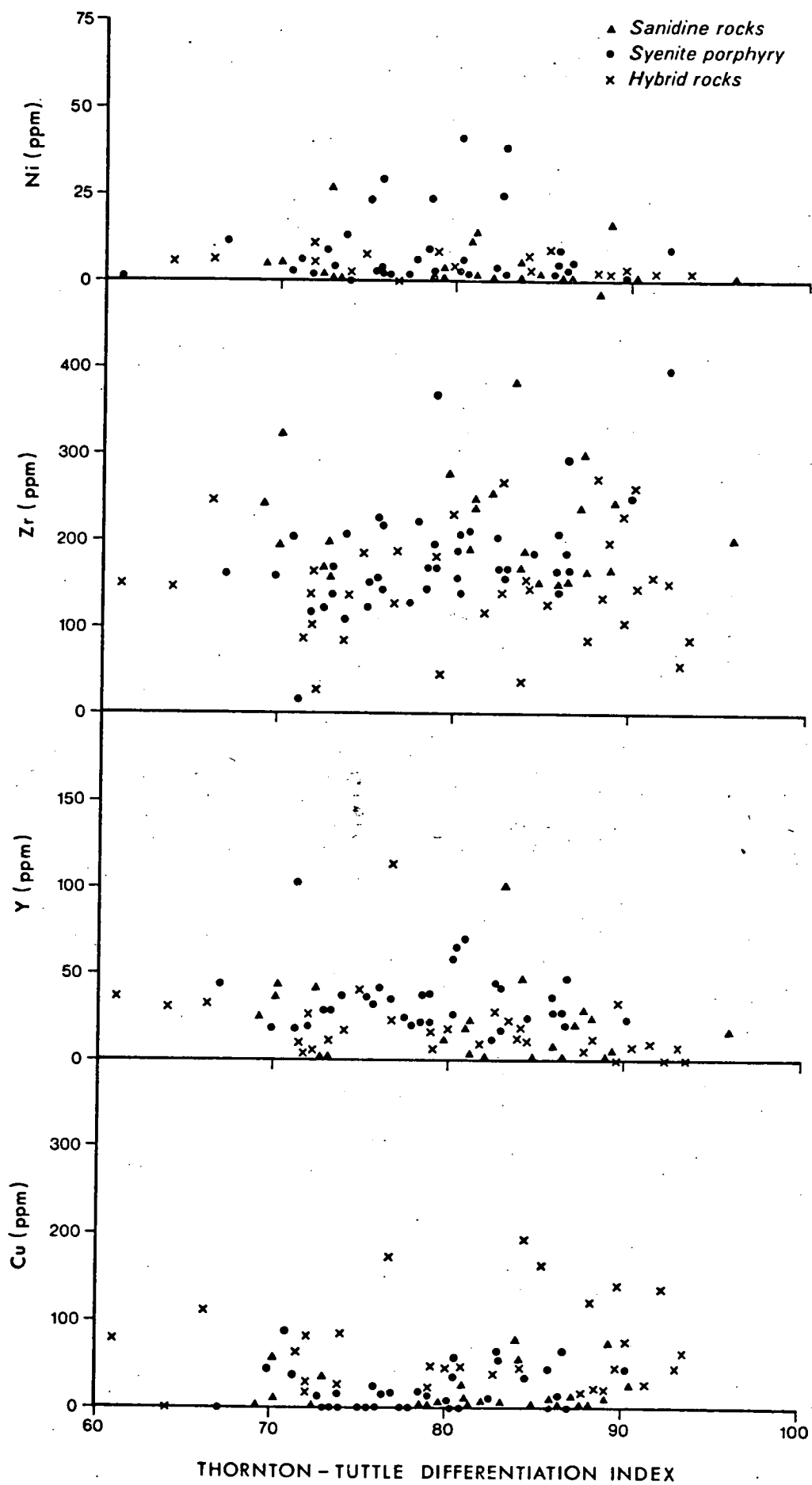


Figure V-3. Thornton-Tuttle differentiation index plot for Cu, Y, Zr and Ni.

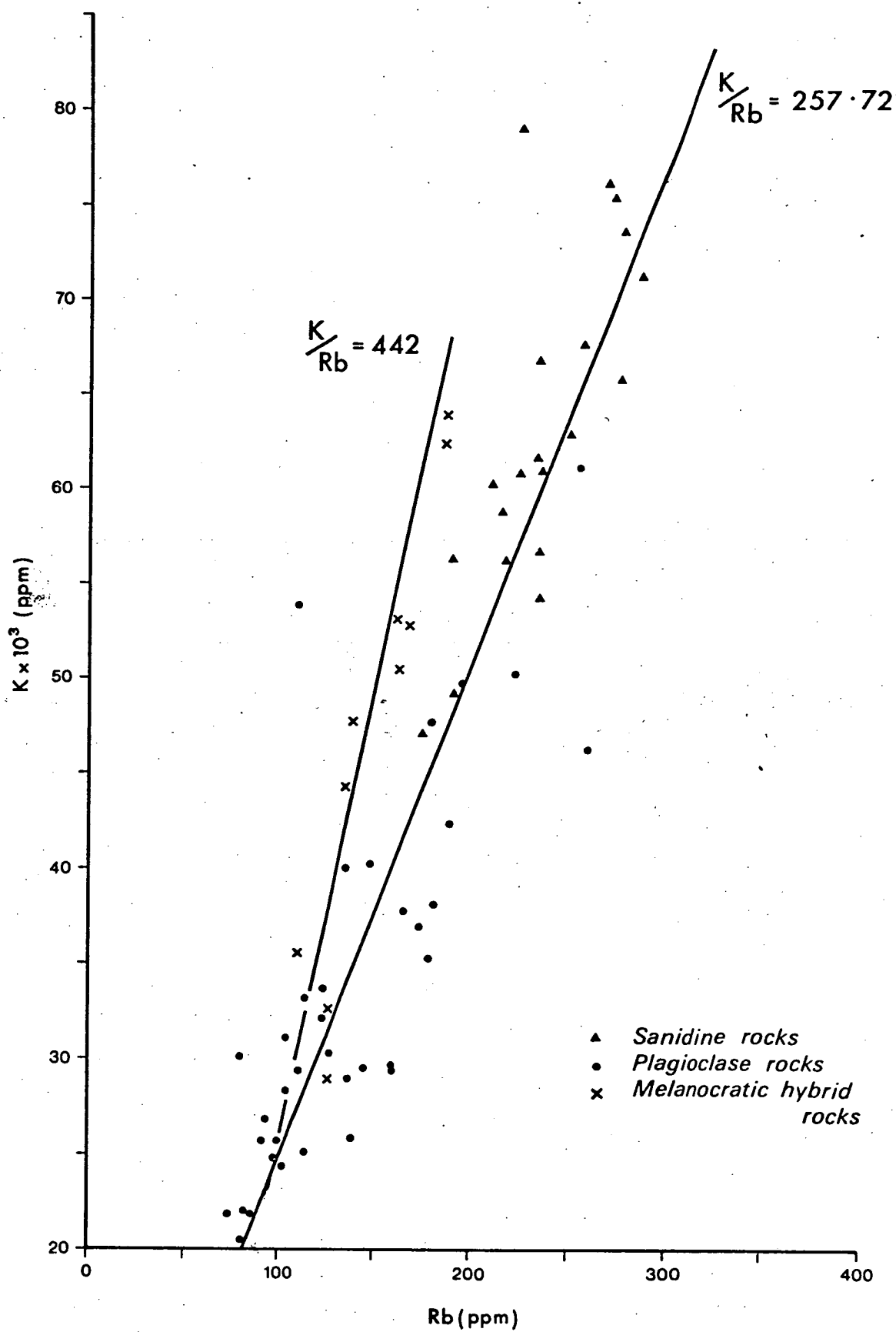


Figure V-4 K-Rb plots for melanocratic hybrids, syenite porphyries and sanidine rocks.

however for the depleted Stjernøy nepheline syenite it is 115 ppm (Heier, 1964) and nepheline syenite gneisses from Bancroft Ontario (40-60 ppm) (Appleyard, 1969). These figures would suggest that the source materials for the Port Cygnet rocks have not been depleted in rubidium.

The significance of K/Rb ratios was first described by Ahrens, Pinson and Kearns (1952) and it has since been generally accepted that K/Rb increases from the crust down into the mantle due to the depletion of rubidium in the lower rocks (as a function of crustal evolution). Thus rocks with lower ratios of K/Rb could be modelled as of crustal rather than sub-crustal or lower origin (Heier and Adams, 1964; Taylor, 1965). However there may be many inconsistencies (Taubeneck, 1965; Shaw, 1968) and later work (e.g. summaries by Carmichael et al., 1974) has shown that care must be taken in the interpretation of K/Rb ratios.

The relationship of potassium to rubidium is shown in Figure V-4, with rubidium ranging from 80 to 305 ppm, and may be expressed as $K \text{ (ppm)} = 257.72 \text{ Rb} + 3311.10$ with a correlation coefficient of 0.77. Because the graph does not pass through the origin as indicated by the constant in the equation, it suggests that potassium may have been added to the system or rubidium removed.

The K/Rb ratio of 258, a reasonable approximation, follows the main trend of Shaw (1968) (Fig. V-5). If these rocks were part of a differentiated sequence, as proposed by Edwards (1947), the evidence shows that the process had little influence on the K/Rb ratio (Carman et al., 1975). Some of the larger alkaline complexes which have been derived from a parent basic source also retain higher K/Rb ratios indicative of their original source (Nyambok, 1980). Variation in the K/Rb ratios may be due to extreme fractionation involving alkali feldspar (see Price and Chappell, 1975). Many of the

ultra-potassic rocks which appear to have had a deep seated origin (e.g. Leucite Hills, Kuehner et al., 1981) have unusually low K/Rb ratios (Carmichael et al., 1974) as does the Tasmanian Jurassic dolerite (Heier et al., 1965) but many of these rocks also have strontium isotope ratios (especially the Tasmanian dolerite) which suggest an interaction with the earth's crust.

The values of K/Rb appear consistent for both the sanidine porphyries and the syenite porphyries. In the case of the Port Cygnet rocks two questions may be asked concerning the modification (if any) of the K/Rb ratio.

The first of these asks if there is any evidence of feldspar fractionation which might have modified the ratio. The evidence from the Bailey-McDonald plots (Figs. IV-13 and 14) is that there is no such fractionation and the R.E.E. patterns (see later) are also not indicative of strong feldspar fractionation.

The other asks if there is any evidence of interaction with crustal materials. The form of the K/Rb graph could suggest a depletion of Rb which might preserve the low initial strontium isotope ratio (see Chapter VI). However the observations on Tasmanian dolerite indicate that addition of rubidium and an increase of initial strontium isotope ratio was more likely.

The K/Rb ratio for the Port Cygnet rocks is not definitive but tends to favour a shallower rather than a deep-seated source for the rocks. For comparison it can also be noted that amphibolite facies rocks may have K/Rb values of 150-250 (Lambert and Heier, 1968).

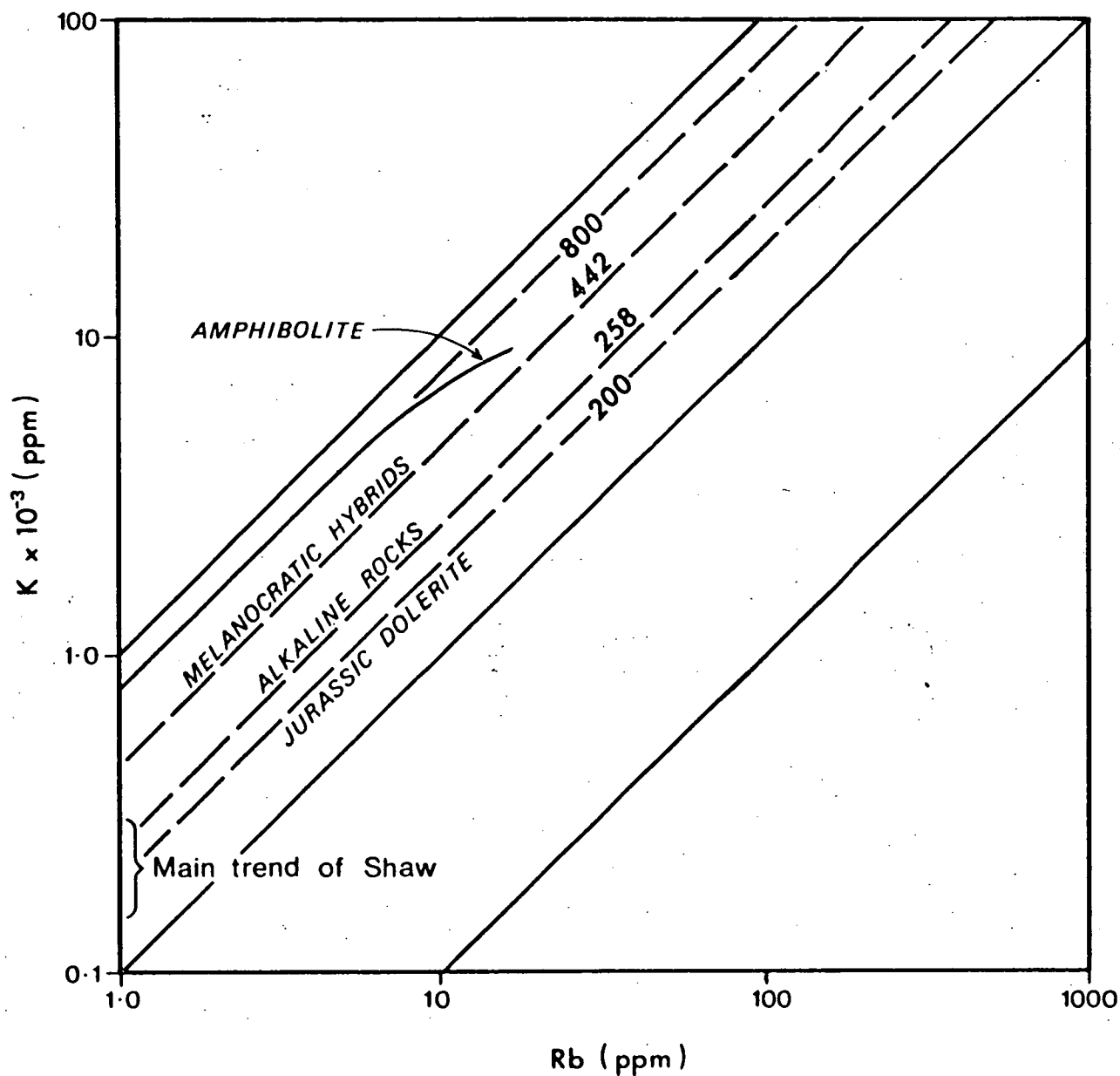


Figure V-5 Shaw plot of K/Rb for the main rock types of Port Cygnet. Note the variability of the amphibolite inclusions while the others follow the main trend.

Cesium

The cesium values (Fig. V-2) are greater for the sanidine porphyries which average about 5 ppm with one extreme value of 56 ppm for CY92 which is a mixed feldspar dyke rock. The detailed geochemistry of cesium is not well known because of its low abundance and the dispersed nature of the element away from its concentration in late stage pegmatitic dykes. The crustal value has been estimated at about 3 ppm (Heier and Billings, 1969). Gerasimovsky (1966) indicates that miaskitic nepheline syenites have higher values than agpaitic types. The Cygnet rocks are miaskitic (see Fig. V-10).

While Heier and Billings query Gerasimovsky's figures which may be inaccurate because the analyses are relatively old, the values from Pt. Cygnet would tend to support Gerasimovsky. It is considered by Heier and Billings (1969) that all cesium is confined to the crust of the earth, with the upper mantle value at an estimated 0.01 ppm. If this model is accurate the relatively high values would favour a crustal origin for the rocks, particularly if these are compared with those from the Kola Peninsula (0.4 ppm) (Kukharensko et al., 1965) where there is an association with parent mafic rocks. It is also useful to note that the cesium values for the sanidine rocks are comparable with the values for the phonolitic rocks from Dunedin volcano (Price and Chappell, 1975) which are regarded as the final fraction of a fractional crystallization sequence from a basaltic parent.

Gulson and Godber (1979) found that they could distinguish the I and S type granites of Chappell and White (1977) on their cesium contents with the higher cesium related to the S types. For other rocks of eastern Australia the division was not so clear.

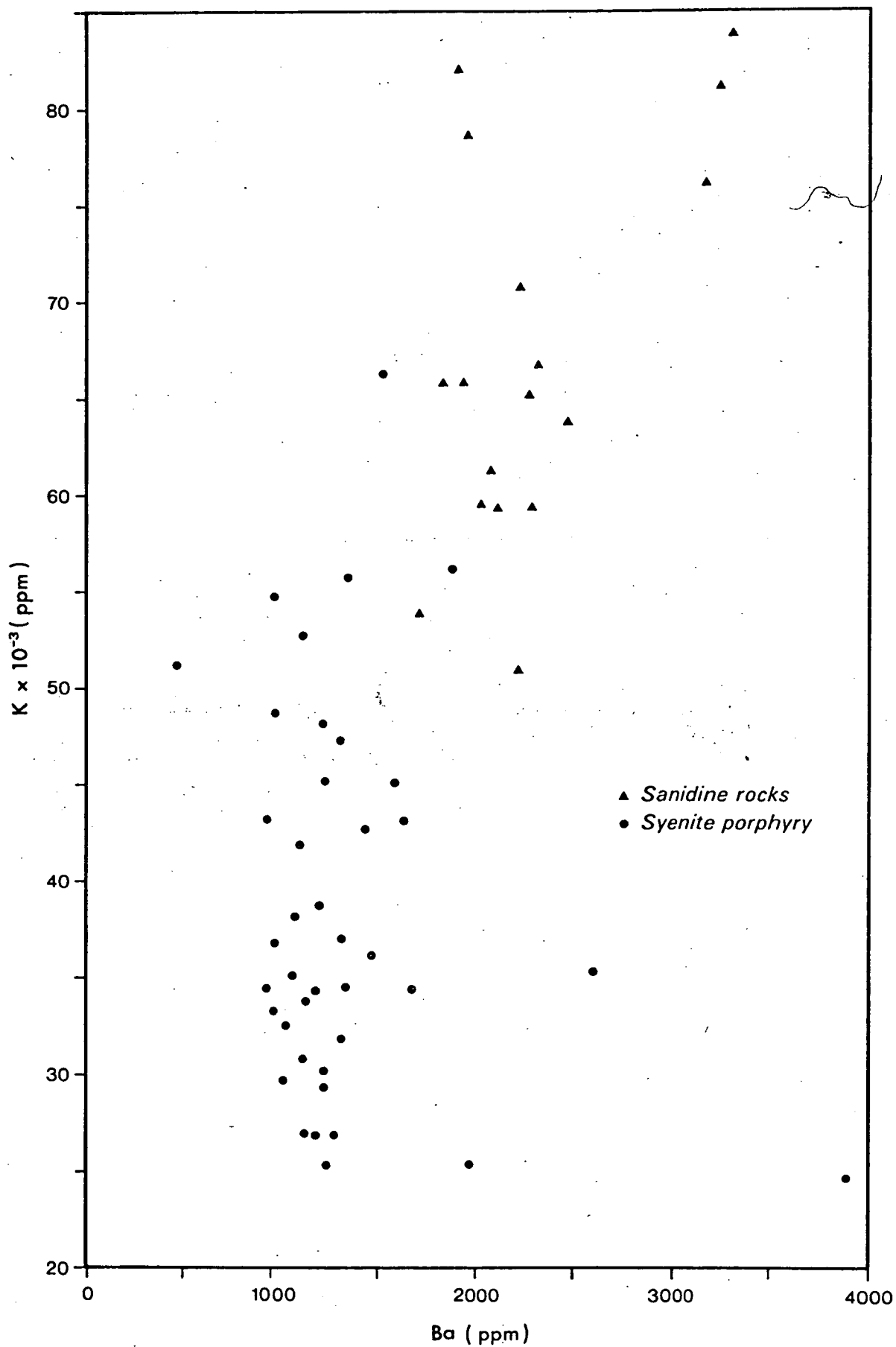


Figure V-6 K-Ba plot for syenite porphyries and sanidine porphyries.

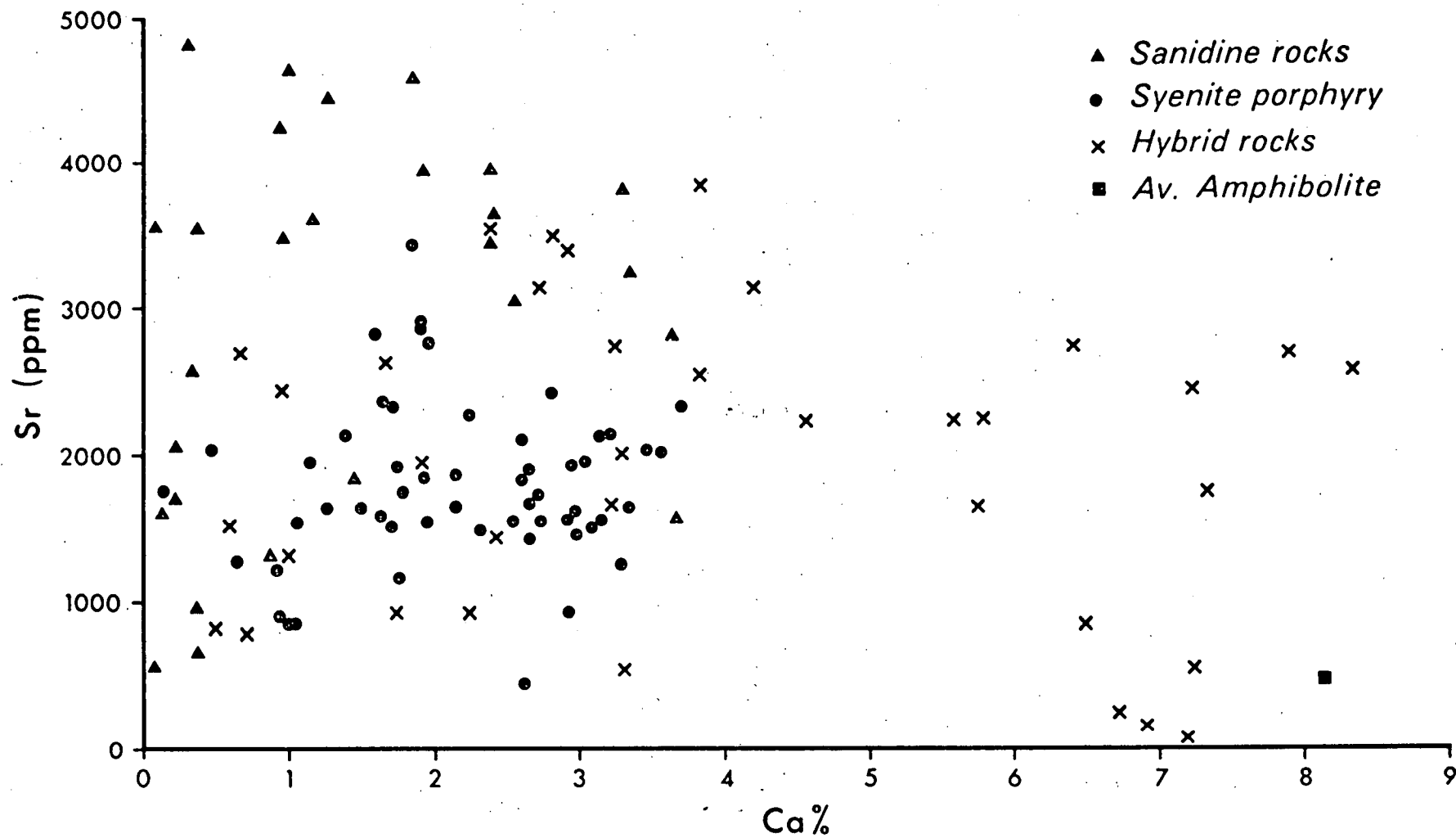


Figure V-7 Sr-Ca plot for all rocks.

Strontium

Strontium concentrations in the alkaline rocks vary from 670 ppm up to 5000 ppm with the mean value being about 2500 ppm (Fig. V-1). The strontium contents of alkaline rocks are extremely variable. Heier (1962) and Turekian (1978) show that strontium is preferentially accommodated in soda-rich plagioclases with labradorite being about the most calcium rich plagioclase to accept appreciable strontium. High values may also be associated with potash feldspars. With plagioclase fractionation the values tend to fall. For trachytes these range from 3 to 1750 ppm (Peterman and Hedge, 1974). The syenite porphyry from Port Cygnet averages about 1550 ppm and the sanidine rocks 3000 ppm (Fig. V-7). The crustal average for strontium is about 140 ppm (Peterman and Hedge, op. cit.). The concentration is greater than those of the Lovozero and Ilimaussaq massifs but are quite comparable with the Stjernøy complex at 3500 ppm Sr (Heier, 1964, op. cit.). As late stage differentiates of basaltic melts are usually depleted in strontium the high values present in the Port Cygnet rocks may show that there has been little plagioclase fractionation of the melts associated with these rocks.

High values of strontium may also occur in alkaline rocks associated with carbonatites (Peterman and Hedge, 1974). However, this association does not occur at Port Cygnet. The relation between strontium and calcium shows a cluster for the alkaline rocks and hybrid rocks with the latter differentiated by virtue of the higher calcium content of the melanocratic types.

Barium

The average value of barium for the syenite porphyry is 1250 ppm with the range from 475 to 2600 ppm but most values lie between 1000 and 1500 ppm. For the potassium rich rocks the average is 2300 ppm.

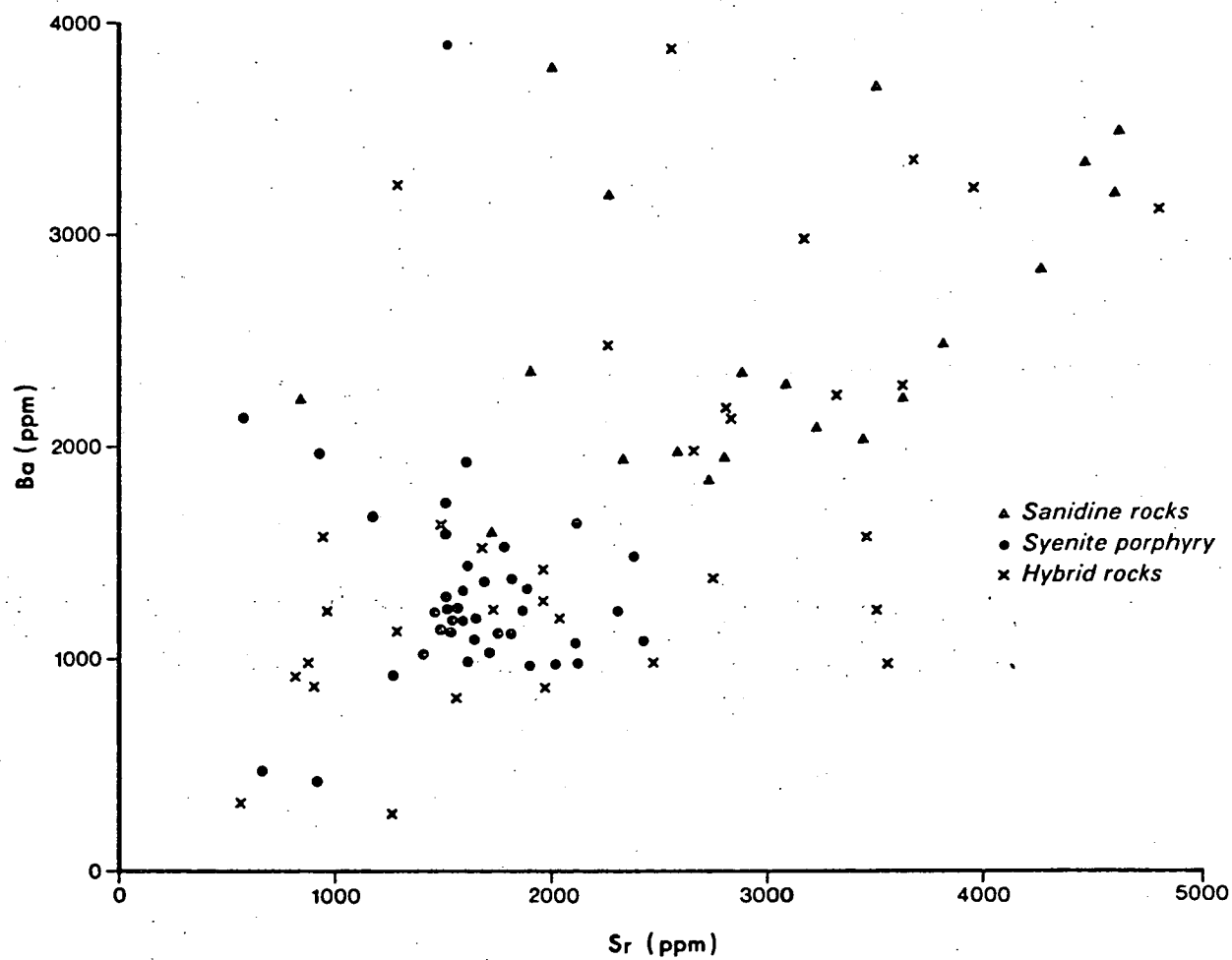


Figure V-8 Ba-Sr plots for alkaline and hybrid rocks.

Figure V-1 shows the relation between the rock types. The syenites show a much narrower spread than for the sanidine porphyries. The crustal average for barium is about 700-800 ppm.

The barium concentrations are greater than the syenites in differentiated massifs like Lovozero and Ilimaussaq and quite similar to the Stjernøy complex (Heier, op. cit.) but are much different from those of Blue Mountain, Canada (Payne, 1968). The barium values at Port Cygnet fall into two groups which are related to the concentration of potassium (Fig. V-6). The high barium concentrations suggest these rocks are not highly differentiated when the tendency is for values to fall for such rocks, e.g. oceanic trachytes (Baker, 1969).

The relation of potassium to barium is frequently useful in the interpretation of geochemical data. Figure V-6 shows the data for these rocks with a K-Ba plot. The syenite porphyry and sanidine rocks have been differentiated on the plot. There is not a simple relation as with K/Rb. The values for the syenite porphyries show no great variation with potassium content while the sanidine rocks are higher and have a greater scatter. Barium-strontium for all rocks is plotted in Figure V-8 which shows overall values greater for the sanidine rocks than for the syenite porphyry with a range through all values for the hybrid rocks.

Scandium

Scandium is a dispersed element and occurs as such in the Port Cygnet rocks. All concentrations are less than 20 ppm, ranging from 2 to 14 ppm. The potassium rich rocks tend to have the lower values. As these are the undersaturated rocks this result tends to confirm the low values for nepheline syenites found by Russian workers (Handbook of Geochemistry 1974). The range overall is similar to the figures

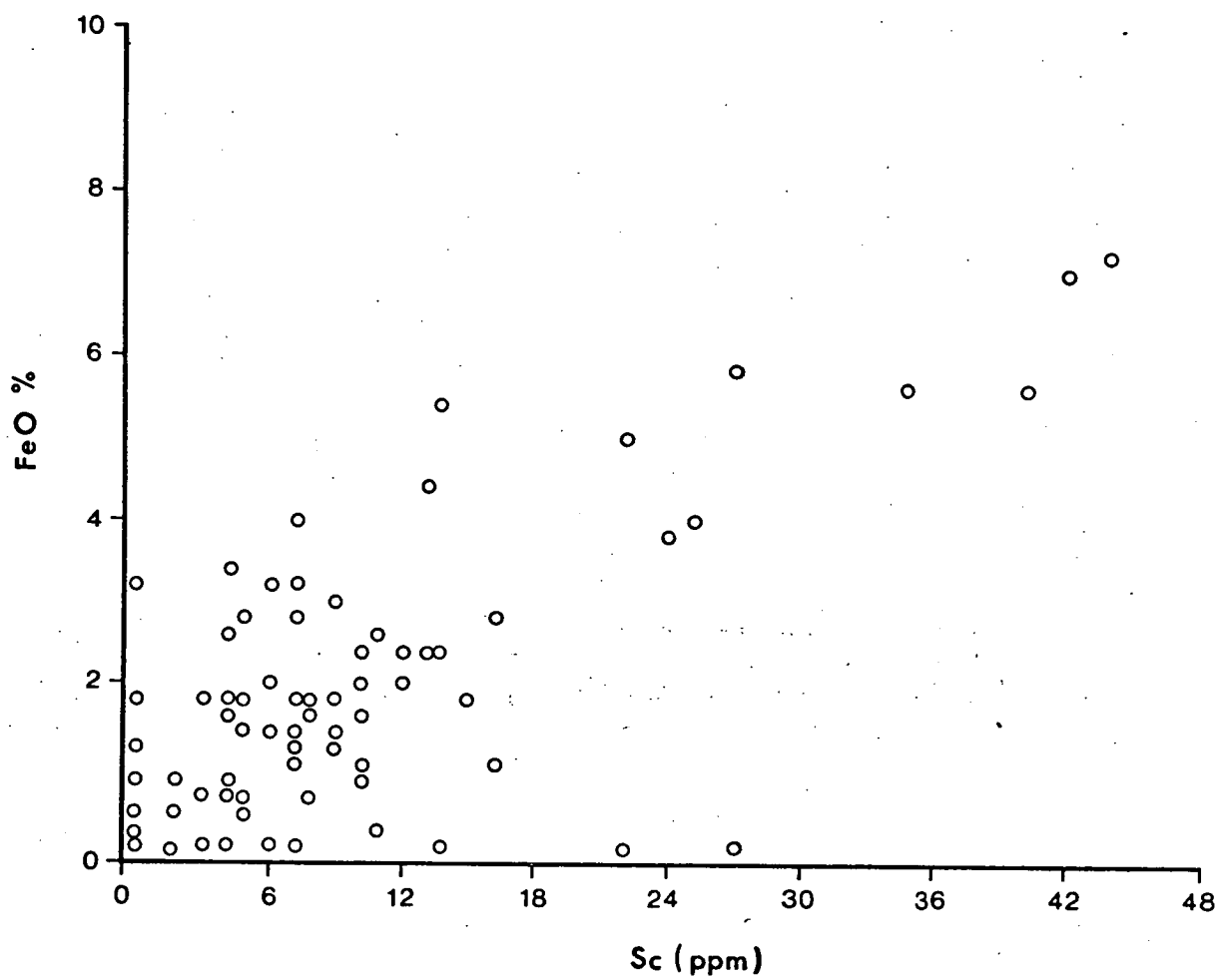


Figure V-9. The relationship of Sc and FeO for all rocks.

of Norman and Haskin (1968). There is a positive correlation between scandium, and FeO (Fig. V-9). Data are not abundant for scandium, however agpaitic syenites also appear to have greater concentrations of scandium particularly when occurring as differentiation-derived rocks. Scandium in syenites varies from 1 to 8 ppm. The correlation of scandium with ferrous oxide suggests its possible association with ferromagnesian minerals.

This correlation has been observed in many rocks but the precise nature of this relationship has not been determined (Norman and Haskin, 1968; Frondel, 1970). The average crustal value for scandium has been given by Frycklund and Fleischer (1963) at 30 ppm. The Port Cygnet rocks are less than this figure, but there is not enough information about scandium to draw any conclusions. Scandium is more abundant in the syenite porphyries than in the sanidine rocks.

Yttrium

The yttrium values for the alkaline rocks vary from <3 to about 65 ppm with two "rogue" values greater than 100 ppm. Most values are less than 50 ppm with an average of 25 ppm. Thus these rocks are among some of the lowest for syenites and trachytes. There is no distinction between abundances in the syenites and the sanidine porphyries but tend to fall into two groups when related to the agpaitic index (Fig. V-10) or to Ti % (Fig. V-11). The crustal average for yttrium is about 35 ppm (Herman, 1969).

The port Cygnet values for yttrium compare with 210 ppm for Lovozero Massif average and 76 ppm for early stage nepheline syenites of this massif. Nepheline syenites from the Turpi Massif, Aloi Range have one of the lowest values reported, of 36 ppm (Balashov, 1963). Although data for yttrium in alkaline rocks are scarce,

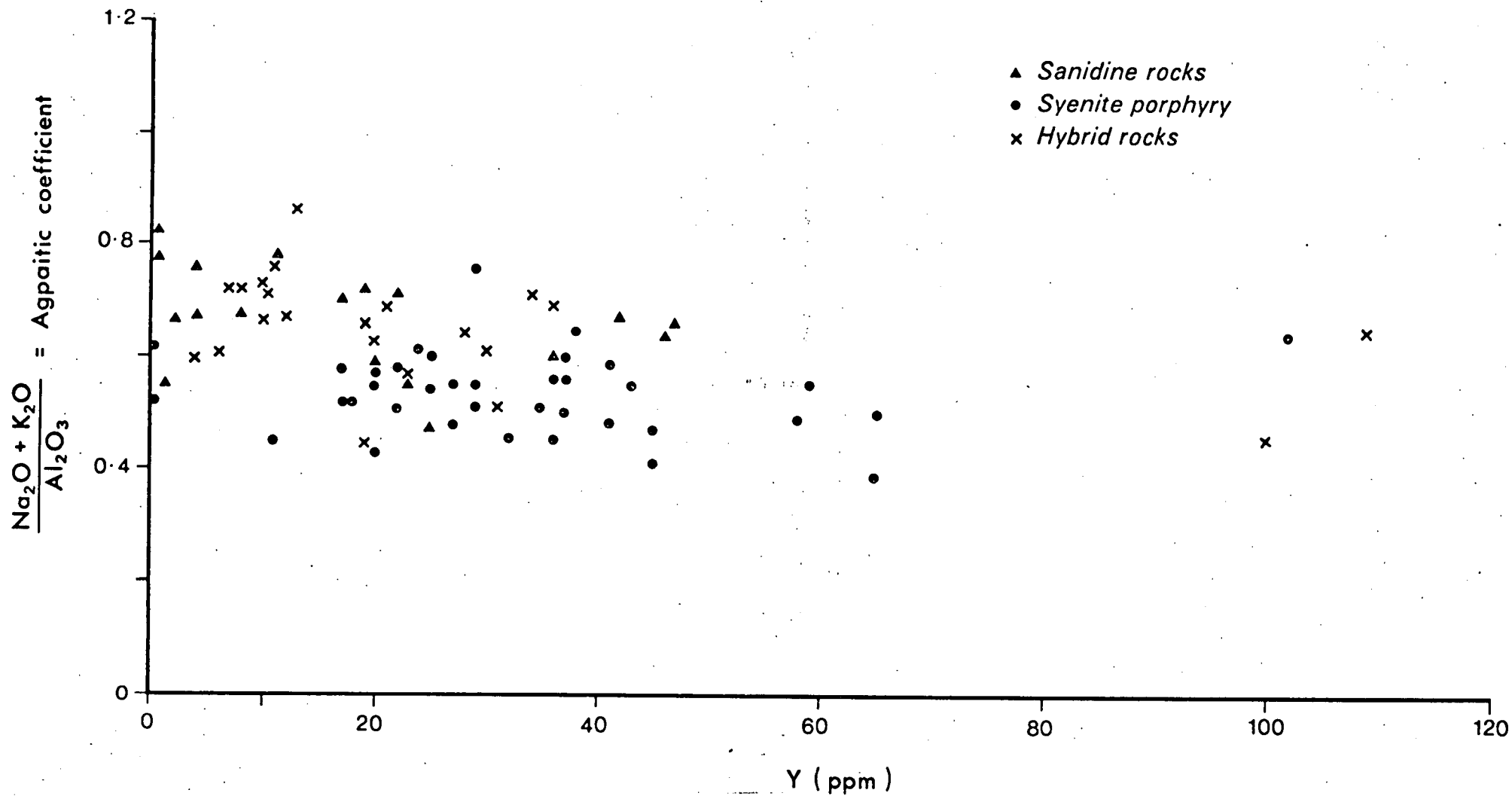


Figure V-10 Agpaite coefficient-Y plot for all rocks.

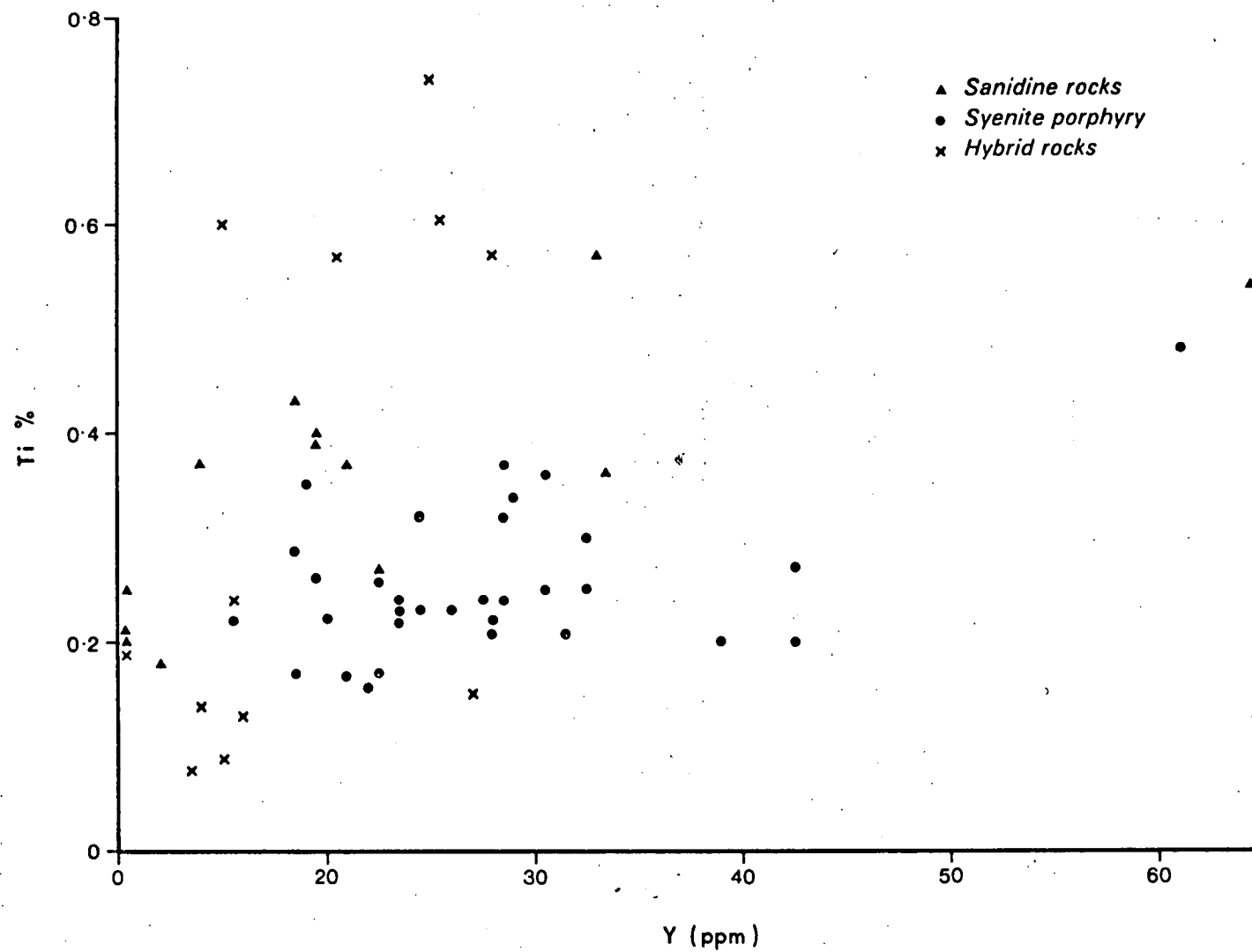


Figure V-11 Ti-Y plot for all rocks.

nevertheless it is apparent that the values reported here are rather low for alkaline rocks of a differentiated sequence. The source of these rocks may have been depleted in yttrium.

Zirconium

The zirconium concentrations range from 100 ppm to 483 ppm. The more potassic rocks tend to have higher values but there is no clear distinction between them. The mean value for these rocks is 175 ppm. The values are consistent with those for miaskitic syenites which tend to be impoverished in most trace elements when compared with agpaitic rocks. The crustal abundance of zirconium for igneous rocks has been variously estimated at 156 ppm (Degenhardt, 1957), 170 ppm (Vinogradov, 1962), and 165 ppm (Taylor, 1964). Oceanic trachytes range from 369 ppm - 1800 ppm. Most syenites have values greater than 175 ppm particularly Lovozero and Ilimaussaq. A notable exception is a maximum 80 ppm for the nepheline syenite from Stjernøy, Norway (Heier, 1964). The Blue Mountain complex, Ontario, has only 47 ppm Zr. The zirconium abundance in the Port Cygnet rocks would negate a high degree of concentration and suggests that the source was probably depleted in zirconium. Zirconium and yttrium are compared in Figure V-12 and show no correlation.

Niobium

All niobium values with one exception are less than 30 ppm with an average of 10 ppm. They show no correlation with TiO_2 (Fig. V-13) but the syenite porphyries average 10 ppm and the sanidine rocks about 20 ppm. The lower concentration of niobium is consistent with the miaskitic character of the rocks, but these are among the lowest values ever recorded for these rock types. Some similar values occur

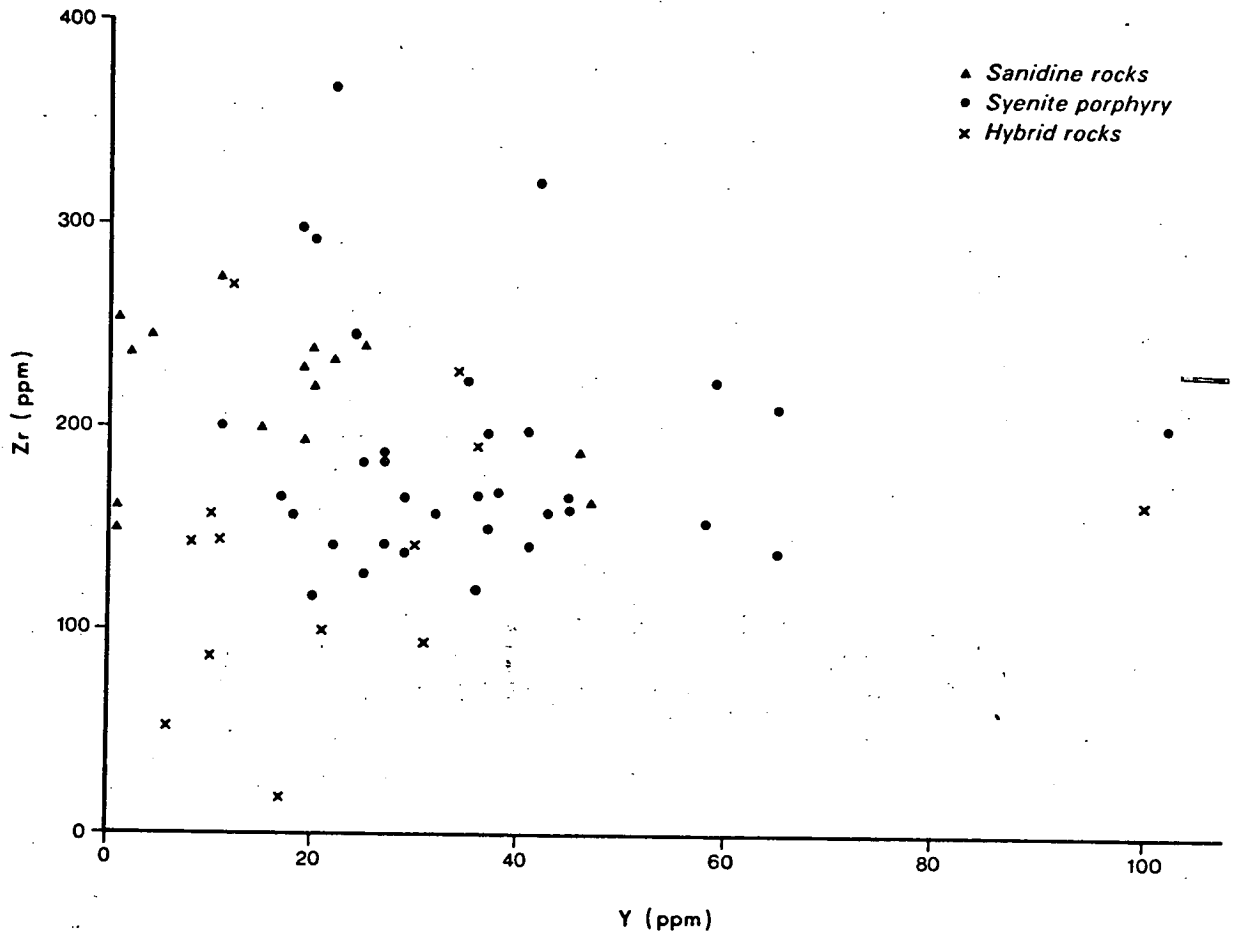


Figure V-12 Zr-Y plot for all rocks..

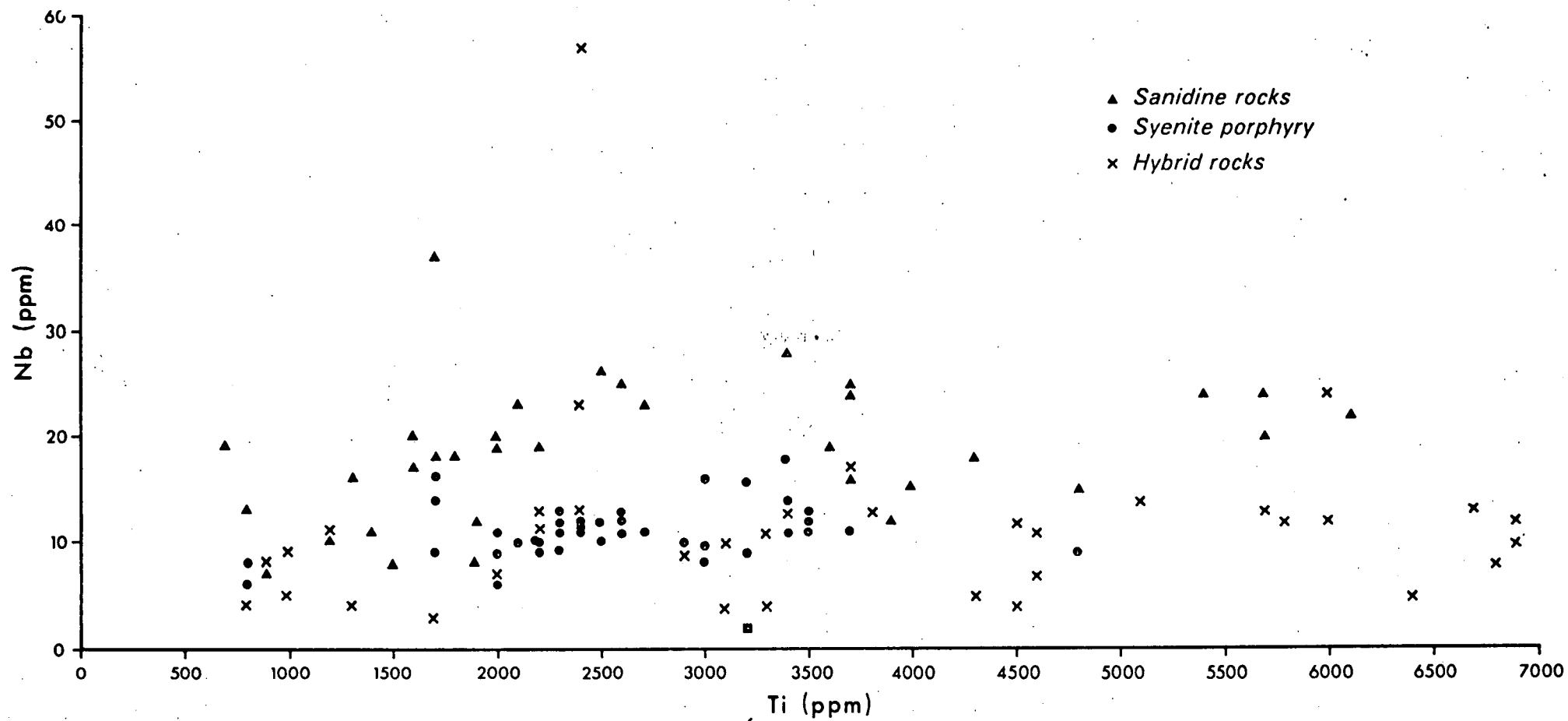


Figure V-13. Nb-Ti plot for all rocks.

in some trachytes associated with the Magnet Cove alkali complex, Arkansas, U.S.A. (Erickson and Blade, 1963), but other members of that complex have much higher concentrations up to 400 ppm. Niobium values for oceanic trachytes from Easter Island (150 ppm) and Guadalupe Island (120-140 ppm) have been reported by Baker and Buckley (1974) and Engel, Engel and Havens (1965) respectively. The low abundance of niobium might be compared with the average for syenites and related rocks of 100 ppm (Wedepohl, 1978). The source of Cygnet rocks was probably depleted in niobium.

Nickel

The rocks are low in nickel. Most values are less than 5 ppm (Fig. V-3) with two greater than 25 ppm; the reason for which is unknown at this stage. These concentrations are expected for these rocks and no differentiation trend is apparent. They are lower than Lovozero and Ilimaussaq and are comparable to Blue Mountain (Payne, op. cit.). Gerasimovsky and Belyayev (1963) showed that nickel values increased with differentiation for Lovozero rocks and agpaitic syenites usually had higher nickel than miaskitic types. Their values are generally less than 10 ppm for miaskitic syenites which agree with the Cygnet rocks.

Copper

Copper values range widely from <3 ppm to 90 ppm with most being below 20 ppm (Fig. V-3). These concentrations are not unusual for syenitic rocks and a similar scatter and values have been observed by Gerasimovsky and Belyayev (op. cit.) for syenitic rocks of various Russian alkaline complexes and also for the Ilimaussaq complex from Greenland.

Zinc

The values for zinc are much more scattered for the Port Cygnet rocks than for any of the aforementioned elements. The common range is from 5 ppm to 453 ppm (Fig. V-3) with two exceptional values of 2030 and 3320 ppm which will be discussed later. The average is about 70 ppm with the potassium rich rocks having higher values than the syenite porphyries. Again, even with the greater scatter the concentrations are much lower than for Ilimaussaq or Lovozero and close to the crustal average of 70 ppm (Wedepohl, 1974). For syenites generally there is a wide scatter of reported values. Trachytes have values greater than the crustal average where once again there is apparently an increase with differentiation. As the average is about the same as crustal values with a scattered range zinc is of little value in determining the origin of the alkaline rocks but the very high values give an important clue to the origin of the garnet trachyte.

Gallium

Gallium is a dispersed element, usually related to aluminium. The gallium range over all rocks is very low, with the values falling between 17 and 33 ppm with the sanidine rocks having slightly higher values than the syenite porphyry (Fig. V-1). There is a relationship to Al_2O_3 (Fig. V-14) but the values still plot into two distinct groups. These concentrations are generally equivalent to the lower parts of ranges for syenites. Miaskitic syenites are lower than nepheline syenites where in general, as the agpaitic coefficient decreases so does the gallium concentration (Gerasimovsky in Sørensen, 1974, p.402-404). The values are similar to those of amphibolite

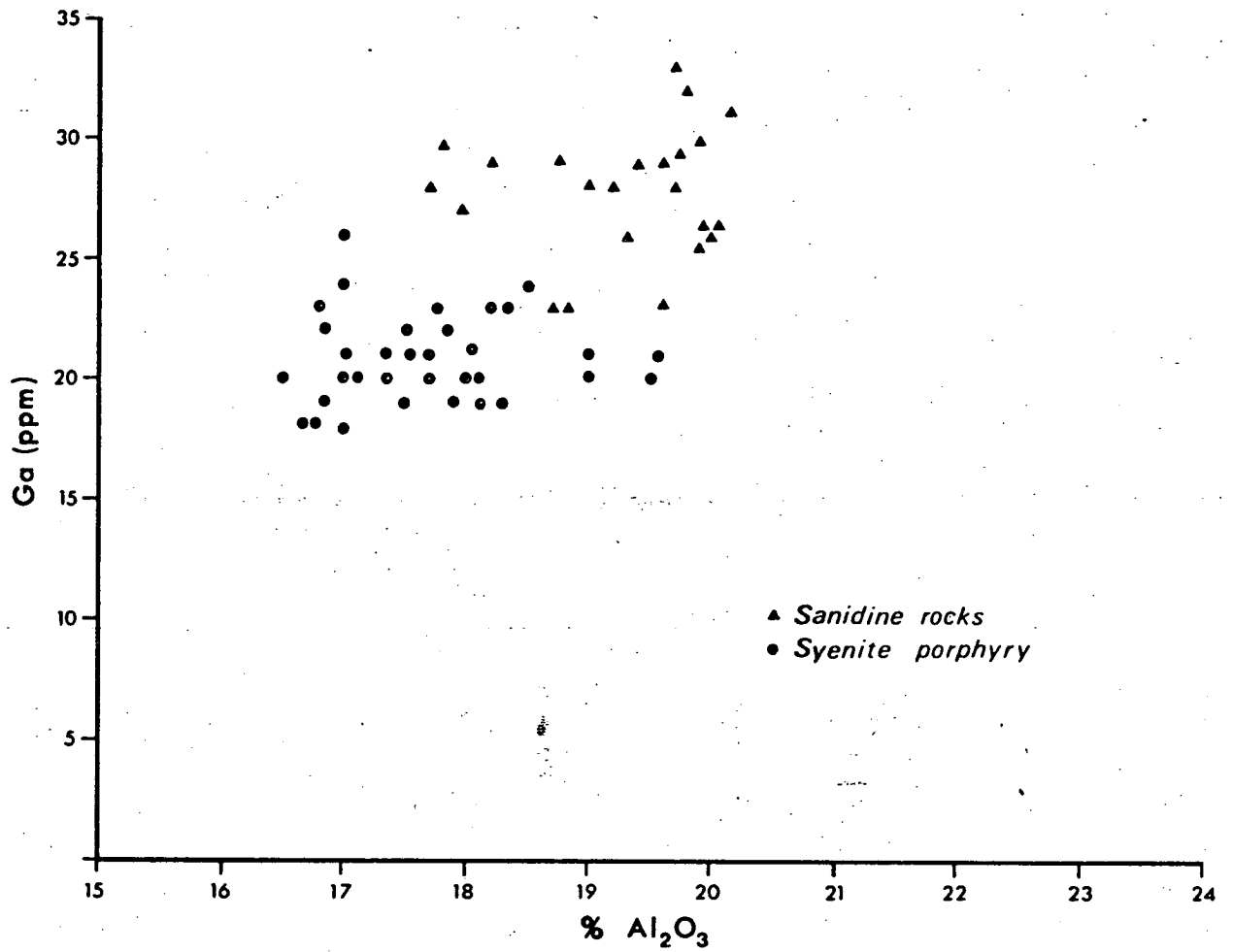


Figure V-14 Ga-Al₂O₃ plot for the alkaline rocks.

(Burton and Culkin, 1970). They might also be compared with those for Ilimaussaq (110 ppm), Lovozero (60 ppm) and Blue Mountain, Canada (17.7 ppm) (Gerasimovsky, op. cit.). The crustal average for gallium is estimated at 18 ppm (Burton and Culkin, 1972). The syenite porphyries contain an average of 20 ppm gallium with the sanidine rocks having a slightly higher average of about 26 ppm. This limited variation is typical of gallium and only becomes larger with extreme differentiation (Nockolds, Mitchell, 1948; Nockolds and Allen, 1953; Douglas, 1964).

Rare Earth Elements

Samples from the main rock types represented at Port Cygnet were submitted to the Australian Atomic Energy Commission Research Establishment at Lucas Heights, N.S.W., for analysis of their rare earth element content. The determinations were made in the Chemical Technology Division by the method of Spark Source Mass Spectrometry (Project S47CT001). The results are estimated to be within $\pm 20\%$ of the true value for the heavy R.E.E. with the relatively large amount of barium present in most samples being the major factor affecting the precision of the results, which are listed in Table V-1. The data have been normalised against average chondrite, R.E.E. (Taylor and Gorton, 1977) and are plotted in Figs. V-15, V-16, V-17 and V-18.

The plots for the sanidine-rocks and syenite porphyries appear in Figs. V-15 and V-16 respectively. The features of these are the moderate enrichment of the light R.E.E. with the sanidine rocks having about double the enrichment of the syenite porphyries, and the absence of any significant europium anomalies in spite of their being feldspar-rich. The results usually show positive anomalies

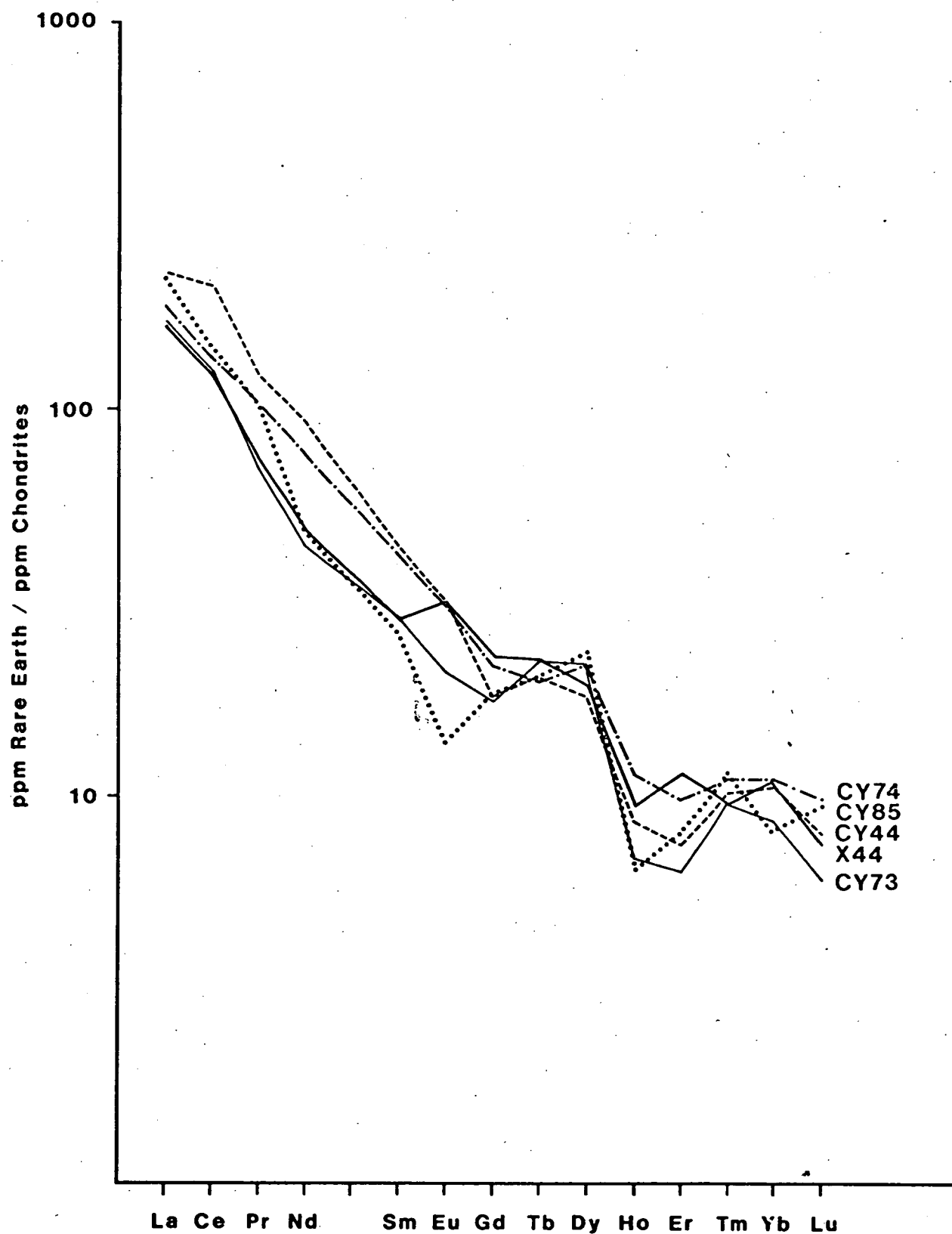


Figure V-15 Chondrite normalised rare earth element plots for the sanidine rocks. The data have been normalised to the values of Taylor and Gorton (1977).

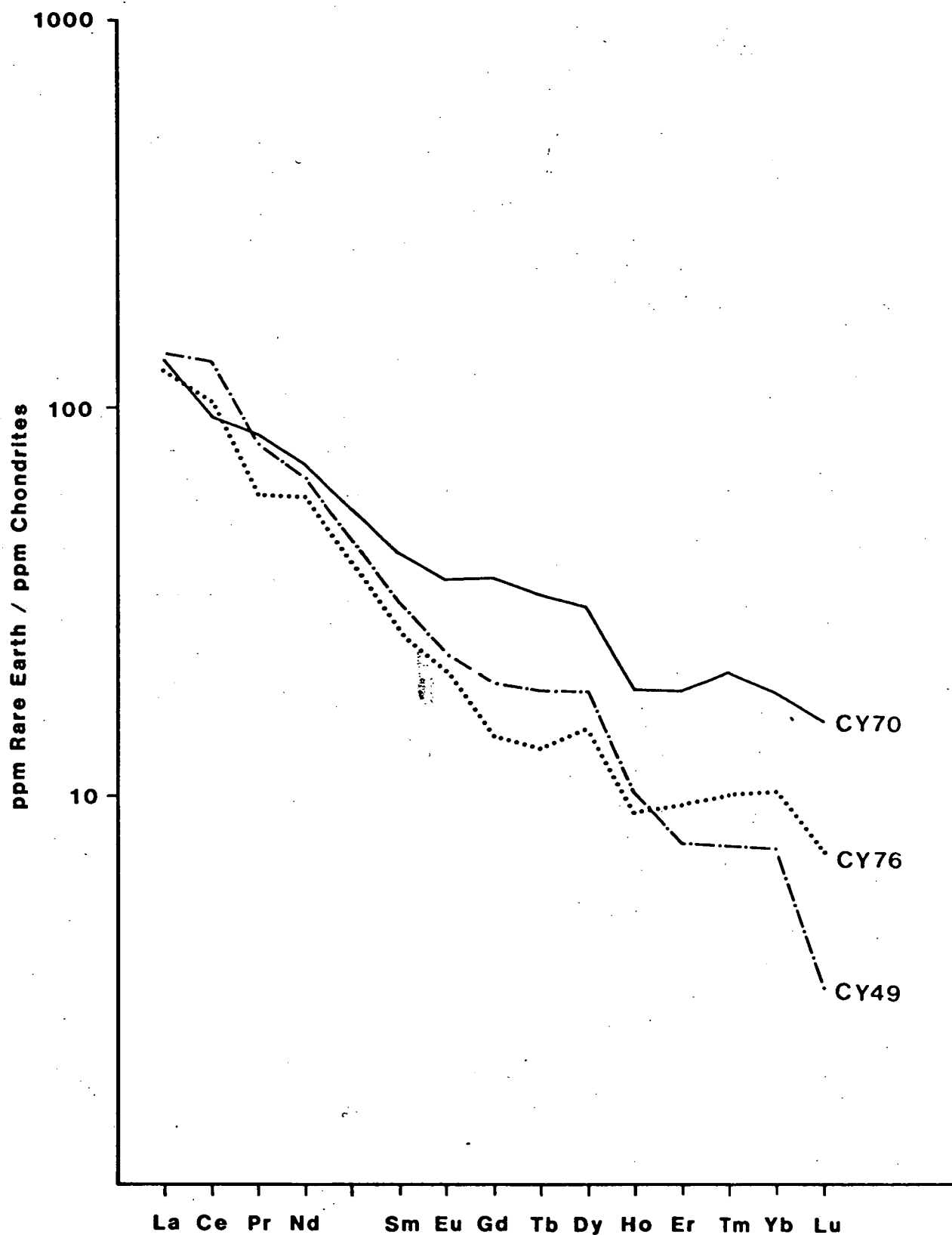


Figure V-16 Chondrite normalised rare earth element plots for the syenite porphyries. The data have been normalised to the values of Taylor and Gorton (1977).

TABLE V-1

Rare-earth values (ppm) for Port Cygnet rocks

Sanidine porphyries

	La	Ce	Pr	Nd	Sm	Eu	Gd	Tb	Dy	Ho	Er	Tm	Yb	Lu
CY44	71	170	14	55	8.5	2.3	4.7	0.99	5.9	0.63	1.6	0.31	2.2	0.26
CY73	53	100	8.2	27	5.6	1.5	4.6	1.1	7.2	0.51	1.4	0.29	1.8	0.20
CY74	58	110	12	46	8.2	2.3	5.9	0.97	7.1	0.82	2.1	0.33	2.3	0.32
CY85	69	120	12	29	5.1	1.0	4.8	1.0	7.7	0.48	1.7	0.35	1.7	0.30

Syenite porphyries

CY49	44	110	9.4	38	6.3	1.9	5.1	0.92	6.10	0.74	1.60	0.22	1.5	0.10
CY70	42	77	10	43	8.0	2.6	9.4	1.60	9.80	1.40	4.0	0.64	3.90	0.49
CY89	29	60	7.2	32	7.4	2.1	4.8	0.46	4.0	1.0	2.4	0.36	2.70	0.35

Hybrid rocks

CY29	38	90	12	49	9.3	2.1	5.6	0.76	4.0	0.61	1.3	0.27	1.8	0.19
CY32	23	88	8.0	33	5.6	1.8	2.8	0.56	3.6	0.61	1.2	0.19	1.7	0.17
CY96	66	170	13	46	8.2	2.4	6.5	1.30	7.60	0.66	1.5	0.23	2.6	0.30
CY119	17	35	4.1	19	4.2	1.1	4.8	0.84	5.8	1.1	3.7	0.65	3.5	0.41

Other rocks

Amphibolite	1.7	3.9	0.62	3.6	1.6	0.57	2.7	0.46	2.7	0.70	2.2	0.30	2.1	0.29
Amph. Matrix	8.7	15	2.0	9.6	2.5	0.87	3.1	0.69	3.8	0.87	2.1	0.27	1.8	0.22
Garnet-trachyte	29	69	6.1	18	3.7	1.4	2.8	0.53	2.6	0.27	0.67	0.19	0.86	0.28
CY61*	9.5	27.60	3.3	11.9	1.65	0.23	0.96	-	0.60	-	0.43	-	0.58	-
CY92*	41	77	12.8	47	11	1.81	6.73	-	5.36	-	2.58	-	2.18	-

* ion exchange, X.R.F. by N. Higgins.

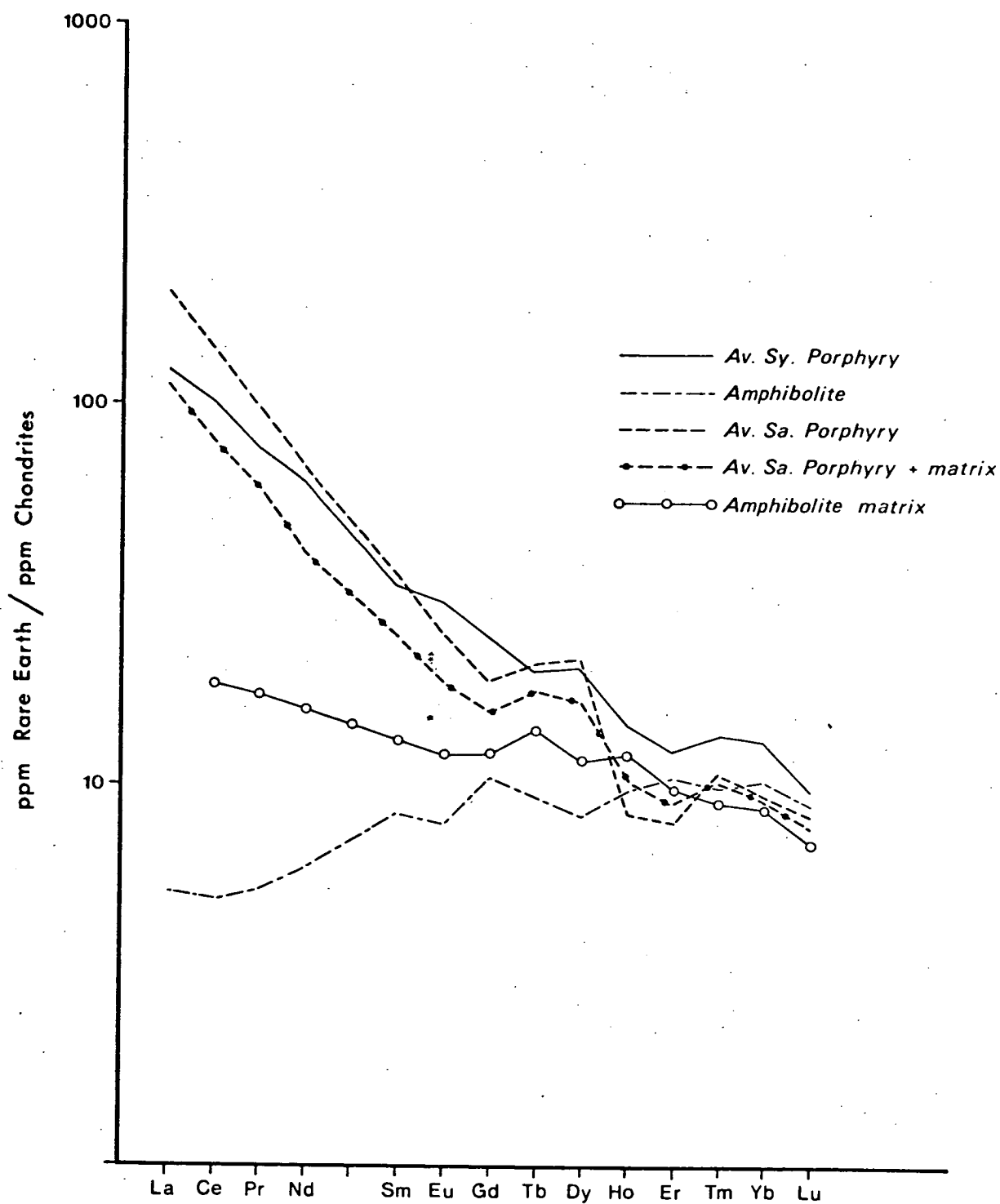


Figure V-17 Chondrite normalised rare earth element plots for syenite porphyry, sanidine porphyry and amphibolite inclusions. The data have been normalised to the chondrite values of Taylor and Gorton (1977).

about terbium, dysprosium, and ytterbium. The reason for this is unknown at this stage. It may be due to interference or to some instrumental parameters, however the interpretation is based on the light rare earth range up to gadolinium where the curves appear to be consistent.

A possible model, stemming from the strontium isotope results, discussed later, is that the syenite porphyry may have been produced by the mixing of a partial melt of a source rock similar to the amphibolite inclusions, with a potassium-rich melt representing a melt parental to the sanidine rocks. The amphibolite pattern is typical of light rare earth depleted oceanic tholeiites (Frey et al., 1968). On the other hand the feldspathic matrix of the amphibolite is significantly enriched in the light rare earths as the ferro-magnesian minerals in the amphibolite are depleted in these. A small europium anomaly in the total amphibolite pattern has disappeared from the matrix pattern.

To test this proposal a mixture of the averaged values for the sanidine rocks and the feldspathic matrix of the amphibolite inclusions has been plotted in Figure V-17 and can be compared with the syenite porphyry pattern in that figure. It can be seen that the resulting patterns are similar and would be consistent with the mixing model proposed.

Fig. V-18 has the chondrite normalised plots for the mixed feldspar phenocryst brown matrix rocks. These are significantly different from the other alkaline rocks in possessing distinct europium anomalies in their patterns. This has been interpreted as showing some feldspar fractionation and will be related to other observations when discussing the origin of these particular rocks.

Haskin and Paster (1976) and Hanson (1978) have considered the

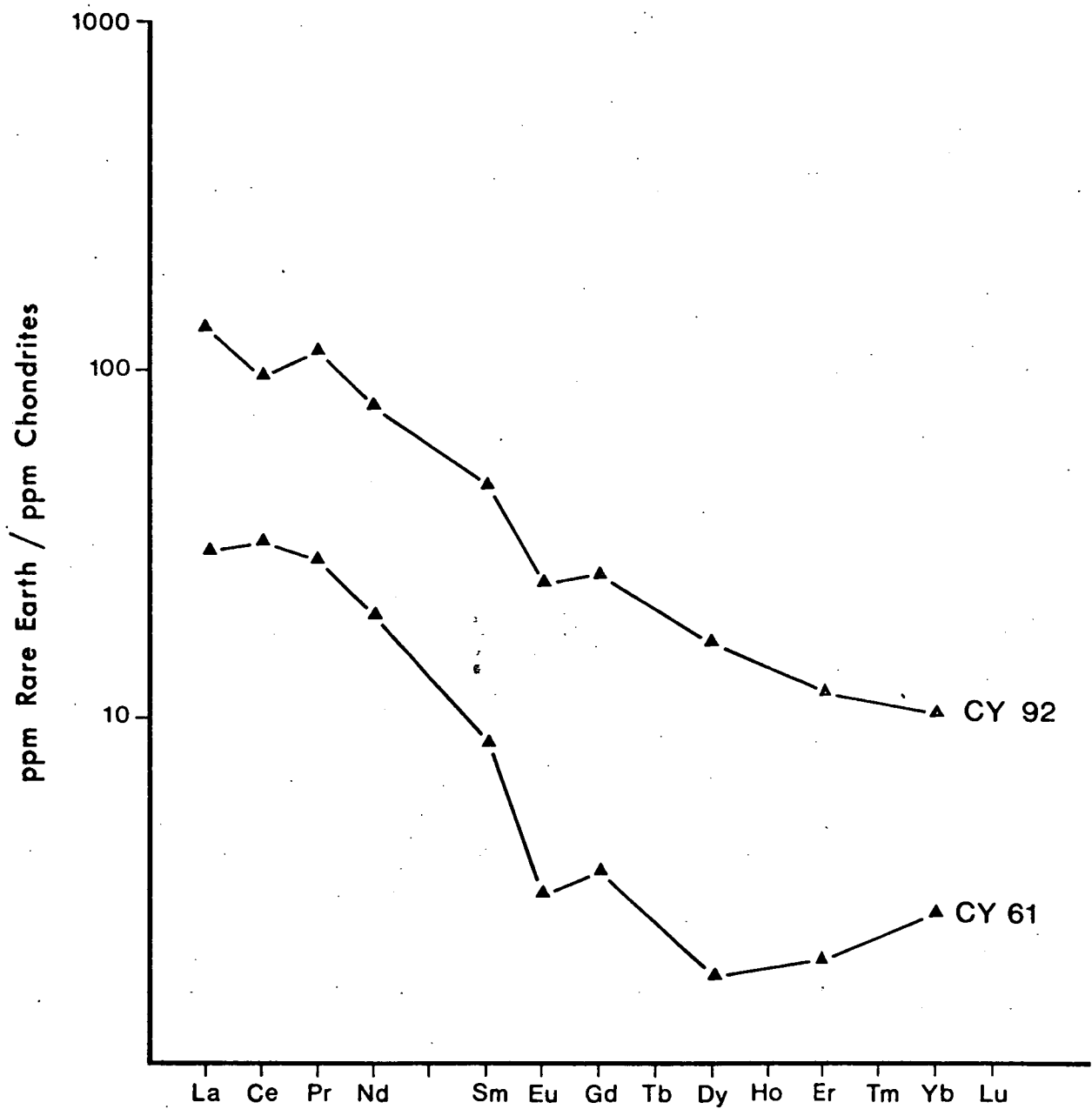


Figure V-18 Chondrite normalised plots of the rare earth element values for the brown matrix rocks, CY61 and CY92.

interpretation of rare earth element patterns and the following conclusions may be drawn from their work, with regard to the significance of europium anomalies. When europium is reduced to the Eu^{2+} state it is preferentially incorporated into feldspar structures, thus depending on the way europium partitions in a melt-solid system there may be enhancement or depletion in relation to the other rare earth elements:

1. Europium anomalies in feldspars are related to decreasing $f\text{O}_2$ and temperature.
2. A europium anomaly will be produced if feldspar occurs in the residue of a partial melt.
3. An anomaly may not be produced if the melt was produced from a non-feldspar bearing source.
4. If the whole feldspar bearing component of the source was melted an anomaly may not necessarily be formed.
5. According to Hanson (op. cit.) a europium anomaly could be suppressed by a residual consisting of equal amounts of plagioclase and clinopyroxene or with twice as much plagioclase as hornblende.

Of the above possibilities the first option may not be favoured on the grounds that $\text{Fe}_2\text{O}_3/\text{FeO}$ ratio for most of the rocks is greater than unity which suggests the $f\text{O}_2$ was relatively high and thus not favouring the formation of Eu^{2+} .

The other options will be discussed later when dealing with the origin of the sanidine-bearing rocks.

At this stage, it can be noted that the chondrite-normalised R.E.E. patterns for the Port Cygnet alkaline rocks are very similar to those of alkali basalts and 'intermediate' basalts (Frey, Green and Roy, 1978; Haskin and Paster, 1979).

They are not typical of those for alkaline rocks derived from differentiated sequences such as ocean island trachytes (Zielinski, 1975), Ilimaussaq (Larsen, 1976) and Dunedin volcano (Price and Taylor, 1973).

THE HYBRID ROCKS

The most useful trace element data for the hybrid rocks are obtained from rubidium, strontium and barium.

Other trace elements do not show any significant trends for these rocks and have values generally similar to the alkaline rocks with the possible exception of copper where some hybrids may have values ranging up to 20 ppm with the average value about 10 ppm for the alkaline rocks.

In most geochemical environments, correlations between potassium-barium and calcium-strontium are usually found. This situation does not exist with the hybrid rocks of Port Cygnet.

The potassium-barium and calcium-strontium data for the hybrid rocks are scattered (Figs. V-19 and V-7) with no clearly defined trends apparent. The relationship of barium and strontium for the melanocratic (i.e. dolerite derived) hybrids, does show an interesting trend (Fig. V-20). The curve is of the form: $y = 215.72 e^{(0.000856)x}$ with concentration units in parts per million. For the rocks whose alteration is restricted to alteration of magnetite to biotite and preliminary break down of the pyroxene crystals, the barium content does not vary from the range 250-400 ppm while the strontium values may rise up to 1250 ppm. With increasing alteration particularly with formation of potash feldspars, the barium concentration increases at a

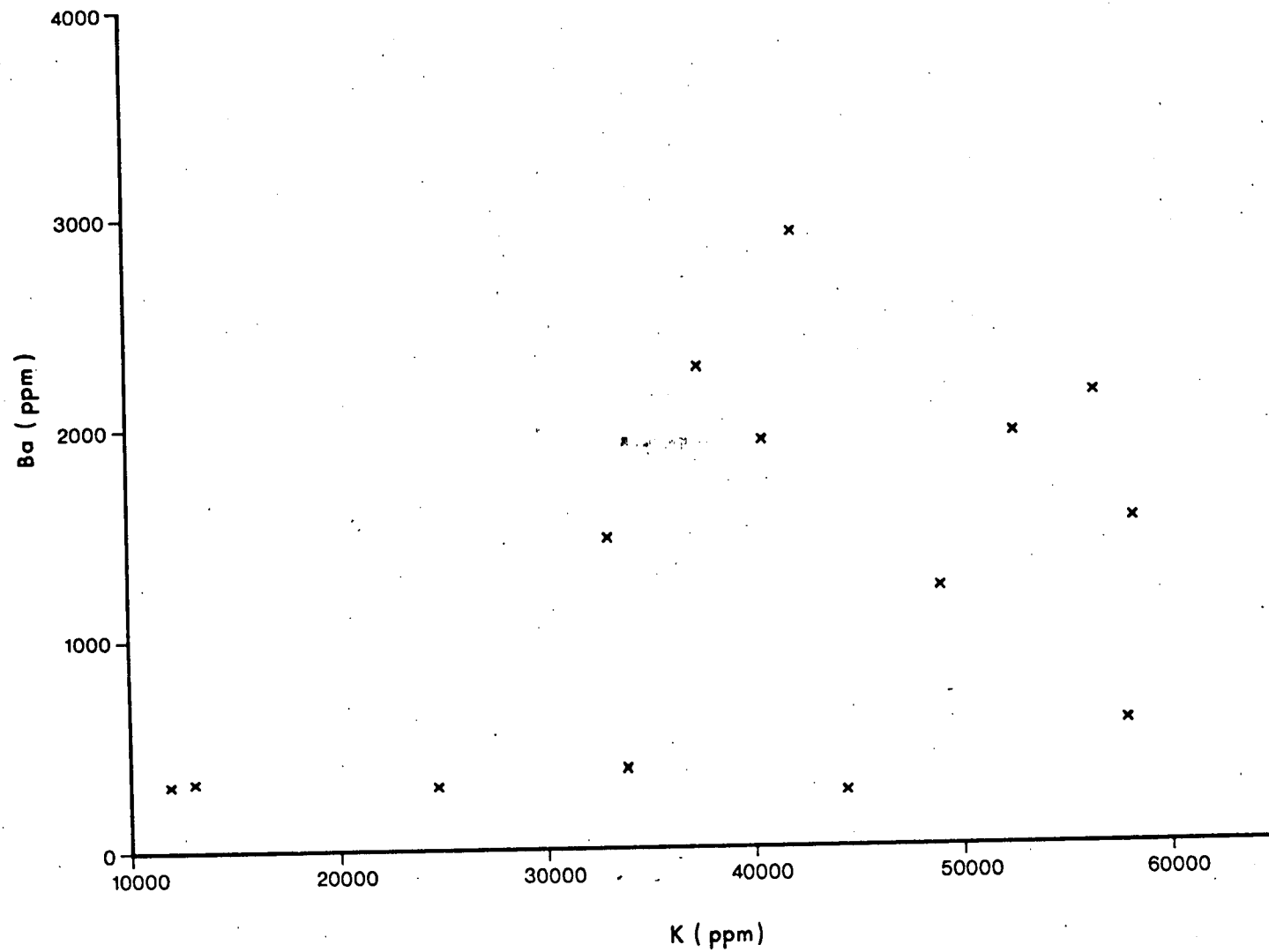


Figure V-19 Ba-K plot for the melanocratic hybrid rocks.

rate only slightly less than that of strontium. As biotite is the main new mineral forming in the initial stages of reaction then strontium must enter this mineral in preference to barium, and also the subsequent ferromagnesian minerals as they form. Thus as complete recrystallization takes place, barium and strontium are added in approximately equal amounts from the alkaline magma. The differential movement of strontium and barium during the alteration of the dolerite is indicative of a diffusion process which favours the application of the Orville model of alkali feldspar exsolution over the Bowen-Tuttle model as referred to in Chapter III. The amounts of barium and strontium present in the hybrids can be compared to those of 200-222 ppm of barium and 121-163 ppm of strontium as ranges for unaltered Jurassic dolerite from the area, and the average value of 130 ppm for Sr for Tasmanian Jurassic dolerite (Compston et al., 1968). These trace elements show the additive process involved in the production of the hybrid rocks. The concentrations of these elements in the leucocratic rocks is also scattered as found for the other alkaline rocks.

The rubidium values of the melanocratic hybrid rocks are about 150 ppm. However the potassium-rubidium ratio is more instructive and gives further evidence of the mixing process involved in the production of these rocks. The plot of these values appears in Figure V-4 with a value of 442 for the slope and hence K/Rb ratio, for the melanocratic hybrid rocks. This value can be compared with 258 for the alkaline rocks and 200 for Tasmanian Jurassic dolerite (Compston et al., 1968). These slopes have been replotted on a log-log scale in Figure V-5.

Since the ratio has changed between the hybrids and original dolerite, then potassium/rubidium has partitioned from the alkaline

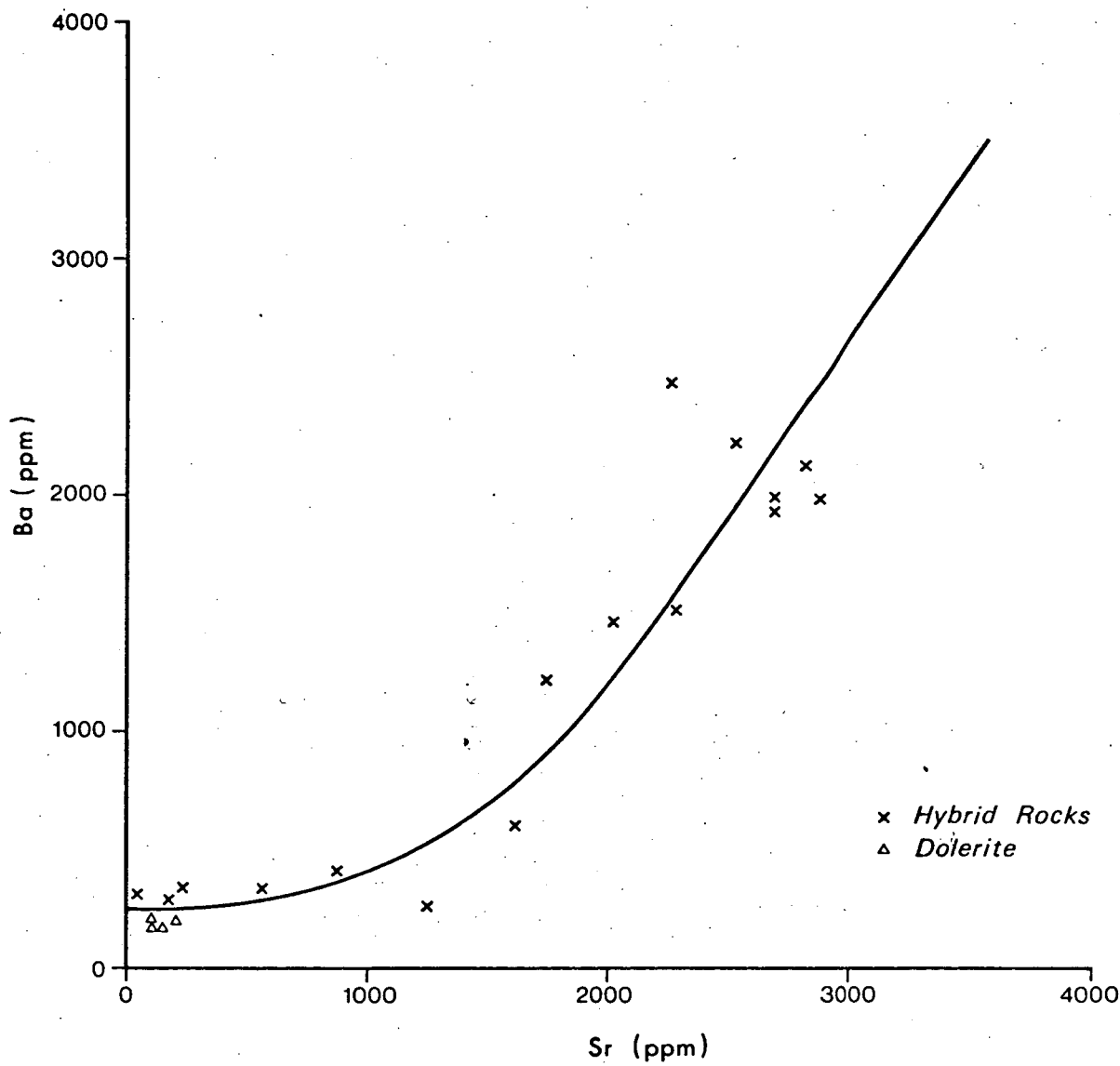


Figure V-20 Ba-Sr plot for the melanocratic hybrid rocks showing their relationship to unaltered dolerite.

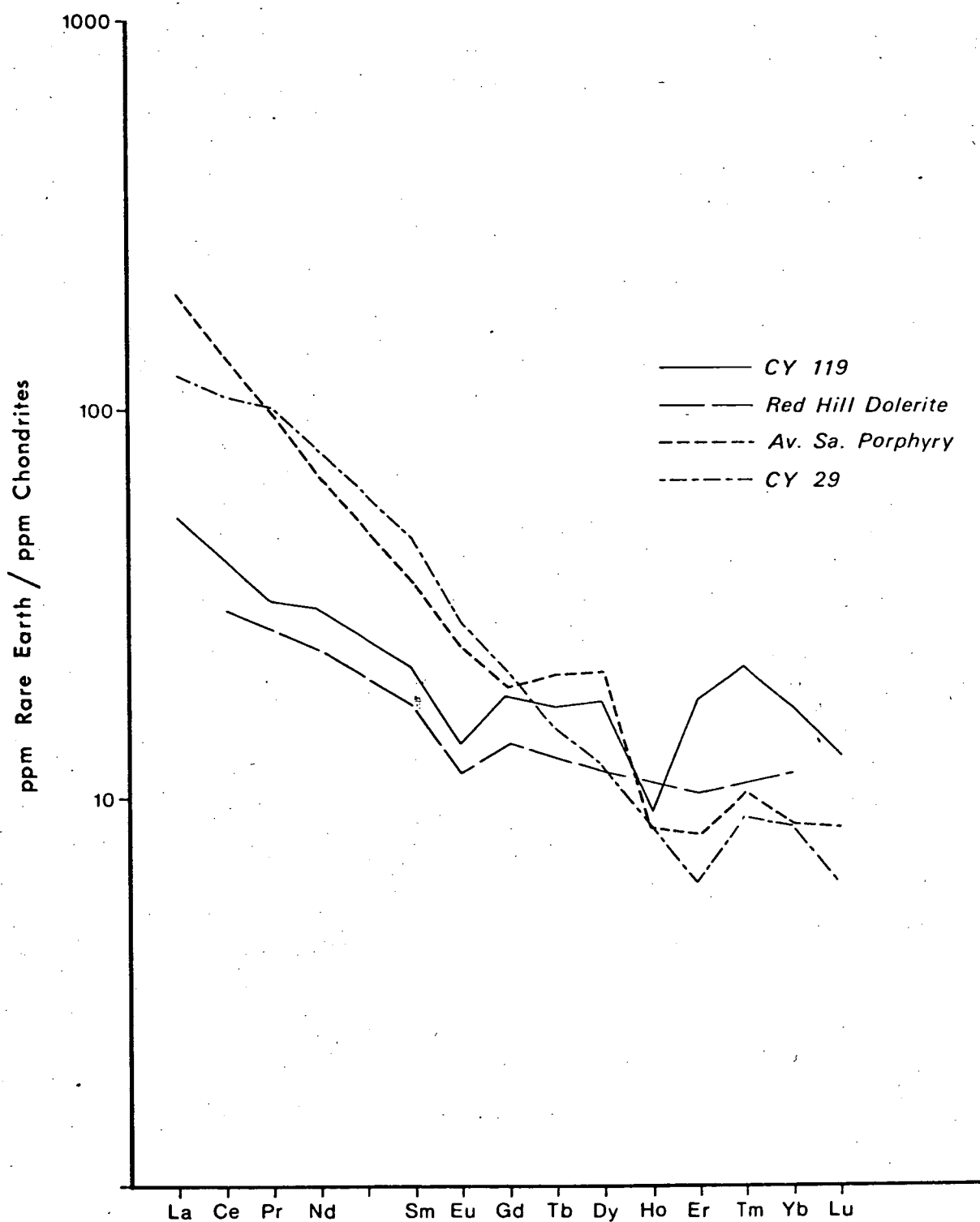


Figure V-21 Chondrite normalised rare earth element plot for sanidine porphyry, hybrid (CY29) and altered dolerite (CY119). Red Hill dolerite from Philpotts & Schnetzler (1968). Data normalised to values of Taylor & Gorton (1977).

magma with a coefficient of about 2.21. This would be expected from the data of Gast (1968) and Shaw (1968) where partition of potassium and rubidium into mafic minerals will favour potassium. The main minerals involved here are clinopyroxene and biotite. While precise values of distribution coefficients are unknown the above figure may be compared with 1.5 for clinopyroxene from Gast (op. cit.) and also knowing that potassium is preferred in biotite which is abundant in the hybrid rocks. The other minerals are mainly potash feldspars where no significant fractionation would be expected.

In the plot of titanium against yttrium (Fig. V-11) the hybrids show two distinct groups related to their titanium content. Those with the higher value correspond to the melanocratic rocks, reflecting the presence of titanomagnetite and melanite, while the other group is due to the leucocratic rocks where titanomagnetite is absent and melanite relatively rare.

For rare earth elements in the hybrid rocks, a comparison has been made (Fig. V-21) between a relatively unaltered dolerite (CY119); CY29, which is a nepheline-bearing hybrid and represents the greatest amount of recrystallization in the hybrid zone at Port Cygnet; and the averaged sanidine porphyries which probably most closely represent the original potassium-rich magma. Also shown on the plot is the REE pattern for a dolerite from Red Hill (McDougall, 1962; Philpotts & Schnitzler, 1968) which is situated near the north-east limit of the area of alkaline rock outcrop. The partially altered dolerite pattern is very similar to that from Red Hill and probably reflects the absence of any significant amounts of added potash feldspar, with the alteration consisting of altered pyroxene and secondary biotite. The rare-earth pattern for the hybrid rock shows it is dominated by the alkaline contribution rather than by the dolerite component, which follows from

TABLE V-2

Determination of Trace Elements in Standard Rocks

<u>Element</u>	<u>Standard</u>	<u>Found</u>	<u>Recommended</u>	<u>Reference</u>
Zr	AGV1	224	220	Abbey (1977)
	BR	258	250	" "
	G2	290	300	" "
	GA	127	150	" "
	JG1	104	110?	" "
	GH	136	150	" "
	JB1	134	155	" "
	ZGITB	176	175	" "
Sr	AGV1	643	660	" "
	BR	1324	1320	" "
	G2	458	480	" "
	GA	295	310	" "
	GH	7	10	" "
	JB1	447	440	" "
	ZGITB	163	155	" "
	JG1	186	185	" "
Ni	AGV1	18	17	" "
	BR	272	260	" "
	ZGIBM	62	57	" "
	GA	5	7	" "
	BCR1	8	13	" "
	ZGITB	40	40	" "
	G2	4	6	" "
	GH	5	3	" "
Sc	BCR1	31	34	" "
	JB1	25	27?	" "
	T1	12	12	" "
	G2	5	4	" "
	AGV1	16	12	" "
Ga	BR	18	20	" "
Cs	ZGITB	7	6.8	" "
Y	G2	8	12	" "
	GA	18	21	" "
	BR	32	30	" "
	AGV1	23	26	" "
Rb	G2	172	170	" "
	GA	175	175	" "
	AGV1	70	67	" "
	BR	46	47	" "
Zn	BR	145	150	" "
	GA	78	80	" "
	GH	76	85	" "

<u>Element</u>	<u>Standard</u>	<u>Found</u>	<u>Recommended</u>	<u>Reference</u>
Ba	BCR1	722	680	Abbey (1977)
	AGV1	1197	1200	" "
	G2	1831	1850	" "
	GA	820	850	" "
	GH	18	22	" "
	BR	1119	1050	" "
	JG1	459	460	" "
	GSP1	1263	1300	" "
Nb	BR	96	100?	" "
	GSP1	22	29	" "
	BCR1	14	14	" "
	G2	9	14	" "
	AGV1	14	15	" "
	GA	10	10	" "
Pb	G2	28	29	" "
	GSP1	51	53	" "
	BCR1	21	15	" "
	GA	35	30	" "
	GH	41	45	" "
	BR	8	8	" "
	AGV1	36	36	" "
Cu	G2	9	11	" "
	GH	11	14	" "
	BR	73	72	" "
	BCR1	20	19	" "
	JB1	53	56	" "
	AGV	61	63	" "
	GA	15	16	" "

the greater abundance of R.E.E. in the former. Trace element analytical accuracies may be estimated from Table V-2.

THE AMPHIBOLITE INCLUSIONS IN THE SYENITE PORPHYRY

The average values of five fresh specimens of amphibolite were analysed. The range of values of these are shown in Table V-3. For comparison the values for an average tholeiitic basalt and gabbro (Nockolds, 1954) are included.

Figure III-11 shows the distribution of aluminium between the tetrahedral and octahedral sites of the amphibole in the amphibolite after Leake (1965). These amphiboles are of a higher pressure origin than those of the alkaline rocks, but do not belong to the high pressure regime defined by Leake (op. cit.).

If the "immobile" element discriminant diagrams of Floyd and Winchester (1975) and Winchester and Floyd (1977) are used (Fig. V-22) the amphibolite inclusions are shown to be related to tholeiitic basalts. These results are a consequence particularly of low TiO_2 , P_2O_5 , Zr and Nb present in these inclusions. As stated by Floyd and Winchester (1977) that provided one is dealing with volcanic rocks the preceding model should be applicable. On these grounds it is then possible to suggest that the amphibolite inclusions could represent an original tholeiitic basalt. Figure V-23 shows values of TiO_2 and chromium plotted according to the scheme of Leake (1964) for the differentiation of ortho-amphibolites of igneous origin from para-amphibolite of sedimentary origin. The high chromium contents place most of the specimens in the igneous origin field.

The potassium-rubidium ratio for the amphibolite inclusions varies from about 500 to 800. These are shown on the Shaw plot (Fig. V-5) where they may be compared with the main trend of this author. Their trend traverses the main trend somewhat like the

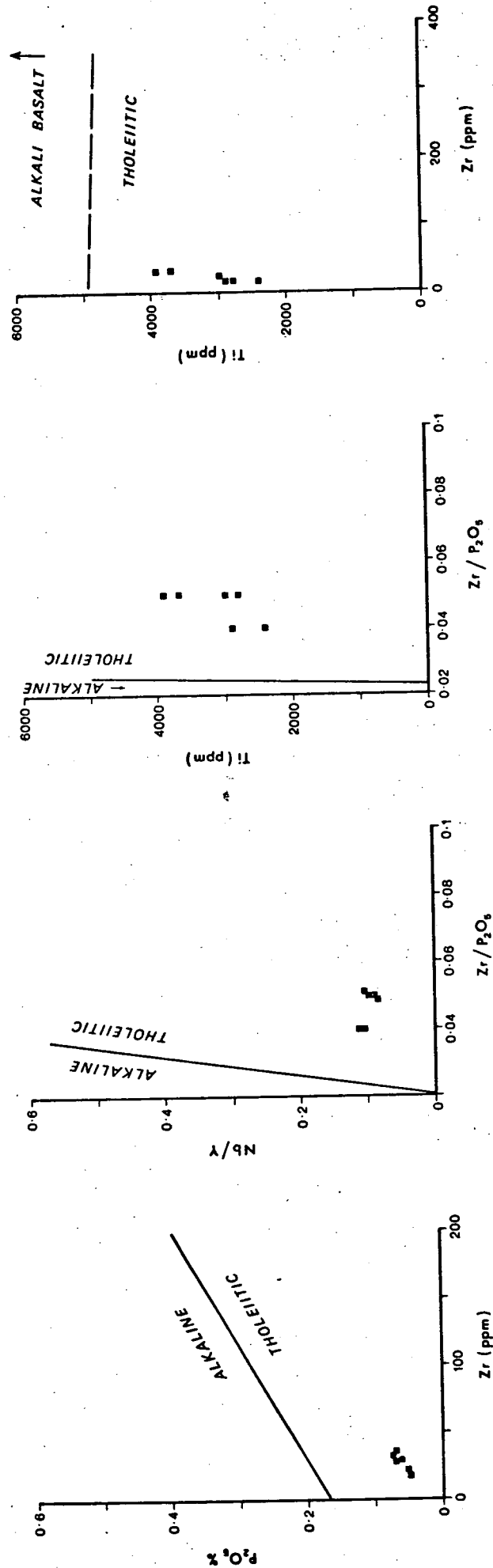


Figure V-22 Plot of immobile discriminate elements for amphibolite inclusions after Floyd & Winchester (1975).

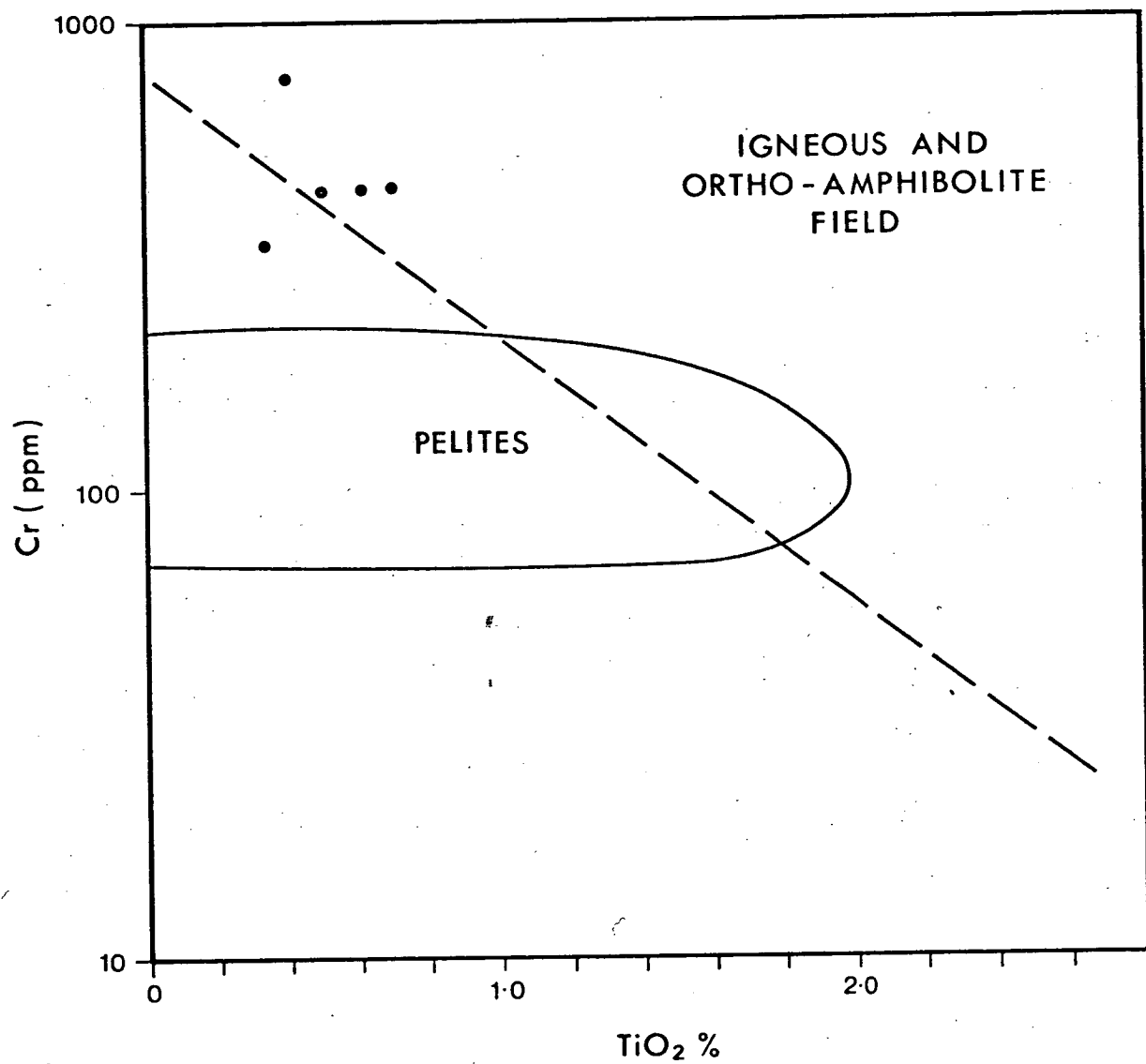


Figure V-23 Leake plot for the differentiation of igneous and sedimentary derived amphibolites.

TABLE V-3

ANALYTICAL AND COMPARATIVE DATA FOR AMPHIBOLITE INCLUSIONS

Major Elements	Amph. 2	Amph. 3	Amph. 5	Amph. 6	Amph. 7	Amph. Range	Gabbro Nockolds 1954	Tholeiite 1954	Tholeiite Le Maitre 1976	Gabbro 1976
SiO ₂	49.41	49.58	48.92	49.42	47.90	47.90-49.9	48.36	50.83	49.58	50.14
TiO ₂	0.48	0.49	0.61	0.40	0.65	0.40-0.65	1.32	2.03	1.98	1.12
Al ₂ O ₃	14.53	15.03	15.47	14.07	14.73	14.07-15.47	16.84	14.07	14.79	15.48
Fe ₂ O ₃	3.23	3.34	3.50	3.65	3.50	3.23-3.65	2.55	2.88	3.38	3.01
FeO	7.45	7.59	7.93	6.57	7.93	6.57-7.93	7.92	9.00	8.03	7.62
MnO	0.29	0.21	0.35	0.23	0.36	0.23-0.36	0.18	0.18	0.18	0.12
MgO	8.37	9.36	8.79	9.30	8.47	8.37-9.36	8.06	6.34	7.30	7.59
CaO	11.79	11.91	10.11	12.96	10.13	10.11-12.96	11.07	10.42	10.36	9.58
Na ₂ O	2.54	2.24	2.55	2.44	2.71	2.24-2.71	2.26	2.23	2.37	2.39
K ₂ O	0.86	0.58	1.17	0.46	1.23	0.46-1.23	0.56	0.82	0.43	0.93
P ₂ O ₅	0.07	0.05	0.07	0.05	0.07	0.05-0.07	0.24	0.23	0.24	0.24
loss	2.03	1.95	1.68	2.01	1.70	1.08-2.03			1.68	1.17
Total	101.05	102.34	101.15	101.56	99.38	99.38-102.34	99.36	99.03	100.08	99.15
C.I.P.W. Norms										
Q	-	-	-	-	-	-	-	3.75	2.39	6.71
Or	5.06	3.43	6.92	2.72	7.27	2.72-7.27	3.31	4.85	2.55	5.49
Ab	21.49	18.43	21.56	20.34	22.45	18.43-22.45	19.12	18.87	20.02	20.26
An	25.71	29.30	27.31	26.18	24.40	24.4-29.30	34.16	25.96	28.47	28.60
Ne	-	-	-	-	0.26	0-0.26	-	-	-	-
Di	26.19	23.80	18.14	30.48	20.60	18.14-26.19	15.57	19.82	17.15	13.70
Hy	3.95	9.78	5.26	3.30	-	3.30-9.78	13.40	17.22	18.68	22.13
Ol	10.01	9.25	13.93	10.31	16.23	9.25-16.23	7.05	-	-	-
Mt	4.75	4.30	5.07	4.86	5.07	4.30-5.07	3.70	4.18	4.90	4.36
Il	0.91	0.93	1.16	0.76	1.23	0.76-1.16	2.51	3.86	3.76	2.13
Ap	-	-	-	-	-	-	-	-	0.56	0.56
Cc	-	-	-	-	-	-	-	-	0.07	0.17
Minor Elements (ppm)										
Ni	76	115	98	101	94	76-115		Amph. 2	Amph. 3	Amph. 5
Y	19	22	34	19	21	19-34				Amph. 6
Rb	11	6	17	5	22	5-22				Amph. 7
Sr	545	227	692	343	609	227-692				
Nb	2	2	3	<1.5	4	<1.5-4				
Zr	29	23	34	19	32	19-34				
Ga	16	14	16	15	15	14-16				
Sc	59	53	57	57	59	53-59				
Cr	349	455	466	760	437	349-760				

oceanic tholeiites shown by Shaw (op. cit.) however these differ by virtue of their curvature being reversed and their K/Rb ratio covers the lower part of the range for oceanic tholeiites (700-1700). These data would then suggest that the amphibolite inclusions may represent an original rock related in composition to a tholeiitic basalt.

SUMMARY OF MINOR ELEMENT DATA

As with many of the major element data there is the distinct division into two groups for much of the minor element data. Thus the values for scandium, gallium, cesium, zinc, rubidium, barium, strontium and niobium are divided while those of copper, yttrium, zirconium and nickel cannot be differentiated from either rock type. The hybrid rocks have scattered values covering those of the other rocks.

The diadochy of potassium, barium and rubidium is well known and needs no amplification here beyond the observation of their enrichment in the sanidine rocks.

Cesium probably has a similar relationship fundamentally due to its very large ionic radius and its concentration is also likely to be as a result of volatiles in the system. It may reflect a crustal source because of its apparent depletion in mantle rocks (Heier & Billings 1969) but it can be noted that Price & Chappell (1975) found similar values in the basalts from the Dunedin volcano.

The greater enrichment of strontium in the sanidine rocks rather than in the syenite porphyry is significant and important in assessing the origin of that rock. The field evidence shows the syenite porphyry intruded by the sanidine porphyry hence if these rocks had a common single magmatic parent which fractionated and formed the syenite porphyry first, then because of its crystallizing sodium rich plagioclase feldspars, this rock should have extracted most of the

strontium (Heier, 1962) leaving the potash rocks depleted. This process can only be demonstrated for CY61 and CY92 which probably represent the final phase of crystallization of the syenite porphyry.

On this basis the strontium distribution points to dual sources for the rocks.

Nickel is apparently not preferred by either group of rocks with most values being below 20 ppm and consistent with concentrations in granites. About 7 analyses of syenite porphyry have concentrations between 25 ppm and 50 ppm which is rather high and may suggest nickel in the source material.

Yttrium is not biased to any group, is about crustal average and may have come from a depleted source but could also be lowered by partitioning into a ferromagnesian remnant of a partial melt. Copper does not have any preference and with values somewhat scattered, but overall less than 50 ppm, is typical of alkaline rocks (Wedepohl, 1974). Some of the hybrid rocks have higher values probably due to contributions from the dolerite.

Zirconium has some scattered values with most lying between 100 and 300 ppm and having no preference for either syenite or sanidine porphyries. However when compared with other alkaline rocks the values are rather low. This would suggest a depleted source for the zirconium. Partitioning into remnant ferromagnesian minerals and oxides could also have caused this phenomenon.

Niobium values are extremely low when compared with other alkaline rocks, reflecting a depleted source. Residual ferro-magnesian minerals with magnetite and ilmenite could lead to the production of a melt depleted in niobium. The low concentration is not consistent with a liquid differentiation origin where it would be expected to accumulate, being an incompatible element. The low values of niobium for all rocks, prompted the testing of a trace element mixing model (cf. Sr

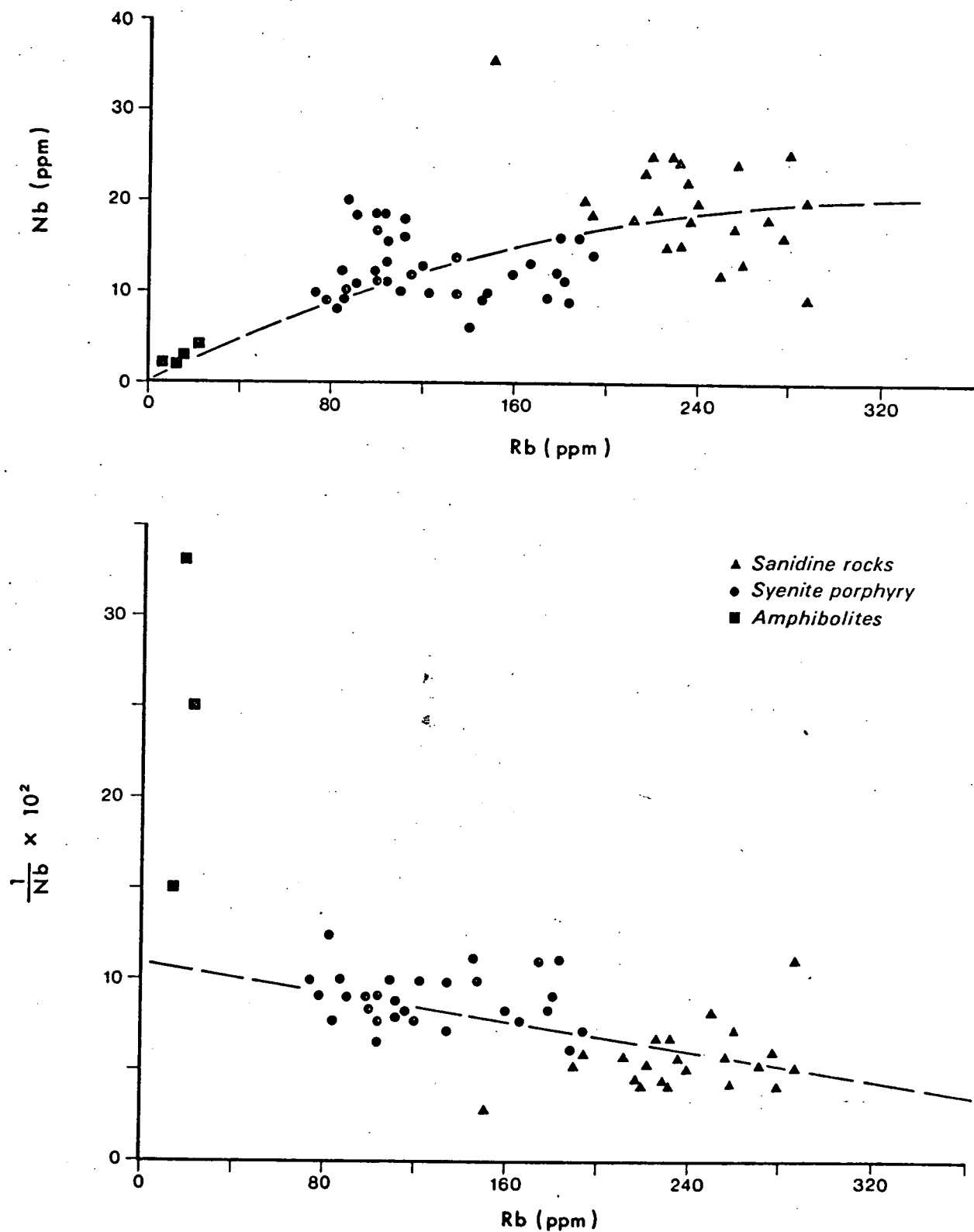


Figure V-24 Plot of Nb-Rb for the alkaline rocks and amphibolite inclusions together with the reciprocal plot.

isotopes (relating sanidine rocks, syenite porphyries and amphibolite inclusions. Figure V-24 shows the plot of Nb-Rb for all rocks with the associated reciprocal plot. The reciprocal plot does not favour the amphibolite, in toto, as a mixing component, and data could not be obtained about niobium in the matrix, and the reciprocal curve is inconclusive, possibly indicating non-equilibrium mixing. The fact that the sanidine rocks have more niobium than the syenite porphyries is consistent with a liquid differentiation and accumulate model but the magnitude of the concentration is not great enough, unless there is extreme depletion of niobium in the source material.

In a normal liquid line of descent whereby fractionation of a mafic parent by removal of plagioclase, gives rise to alkaline rocks, the latter tend to become enriched in zirconium and niobium and depleted in strontium (Carmichael et al., 1974). The trends in the Port Cygnet alkaline rocks for these elements are not consistent with such a model.

Scandium is divided between the syenite porphyry and sanidine rocks, being more abundant in the former. This is not related to Fe_2O_3 which is more abundant in the sanidine rocks (Fig. IV-6) although an overall relationship exists with FeO (Fig. V-9). Because of its dispersed nature it may indicate a dual source for the rocks.

Gallium is more concentrated in the sanidine rocks than the syenite porphyry. It has a relationship to Al_2O_3 (Fig V-14) but there is a strong tendency for parallelism in the plot which would point to two sources for the rocks.

Empirically the concentrations of niobium, gallium, scandium, rubidium, strontium and barium in the syenite porphyries are bracketed by the values in the amphibolite inclusions (Table V-3) and the

sanidine rocks which may suggest a mixing process for the production of the syenite porphyries.

Zinc has a wide range of values but two groups are present with the greater concentrations in the sanidine rocks. Ferromagnesian minerals were probably not important in the original melt which was apparently not greatly depleted in zinc.

The chondrite-normalised R.E.E. patterns indicate that the syenite porphyries and the sanidine rocks have not fractionated from a common source magma because of the suppression of any europium anomalies (Fig. V-15 and Fig. V-16). If such a magma had fractionated into a primary plagioclase bearing part ultimately forming the syenite porphyries, followed by a later potash rich fraction then a distinct positive europium anomaly should characterise the syenite porphyry and the converse, i.e. a negative europium anomaly should be the feature of the sanidine rocks. That their patterns are relatively flat with no significant europium anomaly shows no fractionation taking place between these two intrusive types.

The patterns show a moderate degree of enrichment of the lighter elements, with a greater enrichment shown by the sanidine rocks over the syenite porphyries. The patterns characteristically have no pronounced europium anomalies with indication of anomalies in the tinguaites cancelling out. The inference is that the source was not greatly enriched in R.E.E. and that feldspar fractionation was not an important process in their generation. Superficially the patterns are similar to those of alkali basalts or moderately enriched granites. They are also similar to some East African alkaline lavas (Haskin and Paster, 1979).

The R.E.E. patterns for the mixed feldspar rocks CY61 and CY92 are depleted and have europium anomalies consistent with fractionation

of plagioclase, also indicated by the relative depletion of strontium in these rocks.

Apart from the relatively high concentration of strontium, barium and cesium the trace element assemblage of the Port Cygnet complex is one of low concentration suggesting a small degree, if any, of fractionation and does not represent a late stage differentiation accumulate.

There is evidence of two melts but no fractionation between these.

CHAPTER VI

ISOTOPE GEOLOGY

As part of the investigations of the origin of the Port Cygnet Alkaline rocks, some measurements were made of sulphur and strontium isotopic compositions for selected minerals and rocks.

SULPHUR ISOTOPES

Associated with the alkaline rocks, there is a weak mineralization which led to the production of some 3,000 ozs of gold, mainly from alluvials, during the latter part of the nineteenth century (Twelvetrees, 1907). The gold was spatially associated with the alkaline rocks and has been positively identified in the tinguaita from the dyke (X44) 100 metres north of the old Lymington deep water jetty at Langdon's Point (Pl. 6). Minor sulphides occur in the syenite porphyry and the garnet trachyte, mostly as pyrite but small amounts of pyrrhotite, arsenopyrite, and galena are also associated with the latter rock. In the syenites the pyrite occurs as sporadic cubic crystals and grains. It shows its greatest development in CY70, east of Holland's Quarry. The pyrite in the garnet trachyte is in close association with the spessartite garnet, often forming a partial coating on the surfaces of the crystals.

Thermal metamorphism of Permian sediments in contact with the garnet trachyte has produced a siliceous hornfels in which there is a significant amount of pyrite. The Permian rocks mapped as Basal tillite by Leaman and Naqvi (1967) contain pyrite nodules. At Wilson's shipyard on the eastern shore of Port Cygnet opposite Regatta Point these rocks have been thermally metamorphosed to a dark

siliceous hornfels, in which erratics are still visible, and the original pyrite of the nodules has been converted to pyrrhotite. This has already been mentioned in connection with the hybrid rocks which crop out on the opposite shore about 500 metres to the west. Samples of sulphides were collected from specimens where sulphides were more abundant and submitted to the D.S.R. laboratories, Lower Hutt, New Zealand for sulphur isotope analysis through the courtesy of Dr. D.C. Green of the Tasmanian Department of Mines. It is well known that the isotopes of sulphur may be fractionated during geological processes and that various isotopic ratios may be indicative of specific sources for the sulphur (e.g. Rankama, 1954; Barnes, 1979).

The aim of the investigation was to prove the origin of the sulphur in the sulphides with the aim of establishing the following possibilities:

- (a) the sulphur is of primary origin and hence brought in by the alkaline magmas,
- (b) the sulphur had its origin in the pyrite nodules of Permian sediments and was remobilized by the heat of the intrusion,
- (c) the sulphur may have had some other source.

Natural sulphur is composed of four isotopes whose mass numbers are 32, 33, 34 and 36 with respective abundances of 95.02%, 0.75%, 4.2% and 0.01% (MacNamara and Thode, 1950). The best isotopes to measure, with respect to fractionation are the 32-34 mass numbers because their mass differences are almost the maximum possible for this element, and they are relatively more abundant.

Fractionation factors for various sulphide reactions have been determined by Sakai (1968) and Ohmoto (1972). The fractionation of sulphur between co-existing sulphide minerals has been studied by

several authors, Grootenboer and Schwarz (1969), Kajiwarra and Krouse (1971), Cyzamanske and Rye (1974) and their results have established that $\delta^{34}\text{S}$ values for mineral pairs follow the form of:

$$\Delta^{34}\text{S} = \frac{A \times 10^6}{T^2}$$

where $\Delta^{34}\text{S}$ is the difference between $\delta^{34}\text{S}_1$ and $\delta^{34}\text{S}_2$ for a mineral pair 1 and 2, T is the absolute temperature, and A is a constant characteristic of the particular exchange reaction. $\delta^{34}\text{S}$ is defined as:

$$\delta^{34}\text{S} = \frac{\left(\frac{^{34}\text{S}}{^{32}\text{S}}\right)_{\text{sample}} - \left(\frac{^{34}\text{S}}{^{32}\text{S}}\right)_{\text{standard}}}{\left(\frac{^{34}\text{S}}{^{32}\text{S}}\right)_{\text{standard}}} \times 10^3\text{‰}$$

The standard used is sulphur from troilite of the Canyon Diablo meteorite. Fractionation factors for sulphides become negligible at temperatures in the region of 800°C and higher (Sakai, 1968; Barnes, 1979) so that in the temperature regime of the Port Cygnet rocks which would appear to range from about 750°C to 900°C there should be very little fractionation of sulphur even if there had been development of equilibrium mineral pairs. Thus any differences may be due to the source of the sulphur rather than to mineral exchange reactions which would have negligible influence under the probable conditions of formation of the rocks.

The values for the syenites and sanidine rocks (Table VI-1) confirm the observation that igneous rocks show little fractionation of sulphur isotopes. Ohmoto and Rye (1979) give the range of $\delta^{34}\text{S}$ values of mafic and ultramafic igneous rocks ranging from -1 to +2‰ and for crust and acidic igneous rocks the $\delta^{34}\text{S} = 0 \pm 3\text{‰}$.

The value for the pyrrhotite with its large negative value is in keeping with the large negative $\delta^{34}\text{S}$ values usually found in sediments, Vinogradov et al. (1962), Kaplan et al. (1963), Thode

TABLE VI-1

 $\delta^{34}\text{S}$ values relative to Canyon Diablo Troilite

<u>Specimen</u>	<u>Mineral</u>	$\frac{\delta^{34}\text{S}}{(\text{CDT})}$	<u>Specimen Type</u>
CY5	Pyrite	-0.1‰	Pyrite included in amphibole nodule in syenite porphyry
CY70	Pyrite	+1.4‰	Pyrite cubes in syenite porphyry
X50	Pyrite	-0.2‰	Pyrite from sanidine dyke with phengitic inclusions
J.R. (Garnet trachyte)	Pyrite	+2.9‰	Pyrite associated with spessartite in garnet trachyte
Contact pyrite	Pyrite	-11.0‰	Pyrite from hornfels near garnet trachyte
Pyrrhotite nodule	Pyrrhotite	-13.3‰	Pyrrhotite from thermally metamorphosed pyrite nodule

Standard deviation for all values = $\pm 0.3\%$

(1970), Barnes (1979). The large negative value for pyrite from the contact rocks would suggest that this sulphide has formed largely from sulphur mobilized from the Permian sediments by breakdown of the pre-existing pyrite nodules with a 14% addition from the alkaline rocks.

The garnet trachyte is very interesting in that it has double the positive value of the nearest syenite porphyry even though it might be still considered to have a typical igneous sulphide ratio (Ohmoto and Rye, 1979). On the basis of its high manganese and anomalous lead and zinc values it is proposed that this dyke may have assimilated a mineralised carbonate pod of similar composition to those associated with the sulphide ore deposits at Zeehan, western Tasmania (Solomon, 1981). Since the pyrite in the garnet trachyte is usually a co-crystallizate of the spessartite garnet, it is postulated that the sulphur had part of its origin in such a pod. Hydrothermal sulphides invariably have positive $\delta^{34}\text{S}$ values (Sakai 1968, op. cit.) so that if any sulphur from these minerals was incorporated into the igneous rock it would tend to push the isotopic ratio of the resulting sulphur mixture to a more positive value. Both et al. (1969) have reported $\delta^{34}\text{S}$ values for sulphides from the Zeehan field, although ranging from -3.6 to +12.08 $\delta^{34}\text{S}\%$, 90% of the values are positive. Thus it would be possible for assimilation of a similar assemblage to produce the more positive $\delta^{34}\text{S}$ of the garnet trachyte relative to the other rocks although it is recognized that the measured ratio is not of sufficient magnitude to be definitive.

STRONTIUM ISOTOPES

Because of the relatively large amounts of strontium and rubidium present in the alkaline rocks it was decided to have some

initial $^{87}\text{Sr}/^{86}\text{Sr}$ ratios determined in order to gain some information concerning the origin of the alkaline rocks, particularly as some of the chemical compositional data imply that the rocks could have been generated by melting of crustal rocks.

It has been well established that there is an overall world-wide increase in the initial ratios of $^{87}\text{Sr}/^{86}\text{Sr}$ from a primordial initial value close to 0.699 (Papanastassiou and Wasserburg, 1969; Allegre et al., 1975). Due to the early formation and addition to it of granitic rocks enriched in rubidium, the continental crust has become relatively enriched in radiogenic strontium. This enrichment is in contrast to the much lesser growth rate of ^{87}Sr in the upper mantle due to depletion of rubidium in this region. Thus rocks which have been derived from a crustal source should have initial ratios of $^{87}\text{Sr}/^{86}\text{Sr}$ showing a significant increase over those rocks derived from an upper mantle source. This in many ways parallels the use of K/Rb ratio as an indicator for the sources of rocks.

Initial strontium isotope ratios (Faure, 1977) that would be expected for tholeiites in the following environments are:

$^{87}\text{Sr}/^{86}\text{Sr} = 0.70290$ - oceanic tholeiites from mid-oceanic ridges

$^{87}\text{Sr}/^{86}\text{Sr} = 0.70386$ - tholeiites from oceanic islands

$^{87}\text{Sr}/^{86}\text{Sr} = 0.70437$ - tholeiites from island arcs

$^{87}\text{Sr}/^{86}\text{Sr} = 0.70577$ - tholeiites from continental areas.

These values may be regarded as mean values which may be subject to contamination by various processes which usually lead to an increase in the ratios. For example, tholeiites from continental sources show a pronounced range to higher values, biased in fact by Tasmanian dolerite.

While it is arguable as to what might be the ratios for the average mantle or even for parts of it, mechanisms have been proposed

by various authors e.g. Long (1964), Krogh and Hurley (1968), and Heier and Compston (1969) to account for variations of isotopic ratios. These variations may be summarized as being due to:

1. Strontium isotope mixing between rocks of differing Rb/Sr ratio with variable results.
2. Total loss of radiogenic strontium from the system with a consequent increase of $\text{Rb}^{87}/\text{Sr}^{87}$.
3. Dilution by the introduction of large amounts of common strontium with a consequent decrease in the $\text{Rb}^{87}/\text{Sr}^{87}$ ratio.

It is to be noted that the last great event in the geological history of Tasmania before the formation of the Cretaceous alkaline rocks of Cygnet was the injection of the Jurassic dolerites approximately 75 million years earlier. These intrusives feature an unusually high initial strontium isotope ratio of 0.71 (Heier, Compston and MacDougall, 1965).

Samples were prepared from representative rocks of the Port Cygnet area for strontium isotope analysis by the Australian Mineral Development Laboratories, Adelaide, South Australia. The rocks chosen consisted of four amphibolite inclusions from Mt. Windsor, two syenite porphyries CY49 and CY70, and two specimens of the sanidine rocks CY74 and X44. The aim of this investigation was to test the indication of the geochemical data that the alkaline rocks were of crustal, rather than sub-crustal origin and the relationship, if any, between the amphibolite and the alkaline rocks. The results are shown in Table VI-2, corrected to initial ratios using the K-Ar data as their relatively young age (95 m.yr. - Evernden and Richards, 1962) makes the construction of a reliable Rb-Sr isochron difficult.

For the amphibolite the above results are virtually the present day ratios because of the low rubidium abundance. An independent

TABLE VI-2

Specimen	Initial $\frac{^{87}\text{Sr}}{^{86}\text{Sr}}$ (error 2σ of population) (Corrected to $T=95 \times 10^6$ yr B.P.)	St concentration (ppm)	Rb concentration (ppm)
Amphibolite 2	0.70492 ± 0.00033	545	11
Amphibolite 3	0.70475 ± 0.00036	227	6
Amphibolite 5	0.70502 ± 0.00039	692	17
Amphibolite 7	0.70492 ± 0.00036	609	22
CY49	0.7044 ± 0.00025	1784	89
CY70	0.7048 ± 0.00046	1692	153
X44	0.7049 ± 0.00022		
CY74	0.7036 ± 0.00032	3750	155
	0.7039 ± 0.00033	2992	229
Amphibolite matrix		1284	
E.A.SrCO ₃ SRM987	0.70791 ± 0.00041		
	0.71027 ± 0.00037		

age determination is not available for the amphibolite, however, if an age of 600 m.yr. is assumed (Cambrian) then the initial ratio would have been within the range 0.7040-0.7045. No amphibolites of age younger than Cambrian are known, at the present time, from Tasmania.

The value of the ratios from the above table have been plotted in Figure VI-1 where it can be seen that there seems to be a mixing curve. To test this the reciprocals of the strontium values have also been plotted against the initial ratios (Fig. VI-1) from the models of Boger and Faure (1974). This confirms the mixing curve with respect to the alkaline rocks but the amphibolites do not lie on the line. However from the microscopic and chemical evidence it is not envisaged that the amphibolite *in toto* contributed to the syenite porphyry, but that at least the major mixing component was the matrix of the amphibolite, that is, the predominantly feldspathic part. Because of the difficulty of obtaining a clean matrix fraction, this was not analysed directly for its initial strontium isotope ratios. It is assumed that the initial ratios for the matrix were the same as for the whole rock ratios. A small amount of the amphibolite matrix was separated using an electromagnetic separator and this was analysed for strontium using the absorption flame photometry technique. The result gave $Sr = 1284 \text{ ppm} \pm 43 \text{ ppm}$. At the same time the value for AGV1, which has a recommended value of 660 ppm (Abbey, 1980), was determined at $688 \text{ ppm} \pm 17$, as a check on the accuracy of the analysis. If this value is plotted it can be seen to be consistent with the other values for the reciprocal-Sr curve and indicates that a component dominated by the feldspathic matrix of the amphibolite is compatible with the syenite porphyry end of the mixing curve. The reciprocal curve is described by the relation: $\frac{^{87}\text{Sr}}{^{86}\text{Sr}} \text{ initial} = 0.000275 \left(\frac{1}{S_r} \times 10^4 \right) + 0.702983$. The correlation coefficient (R) = 0.933.

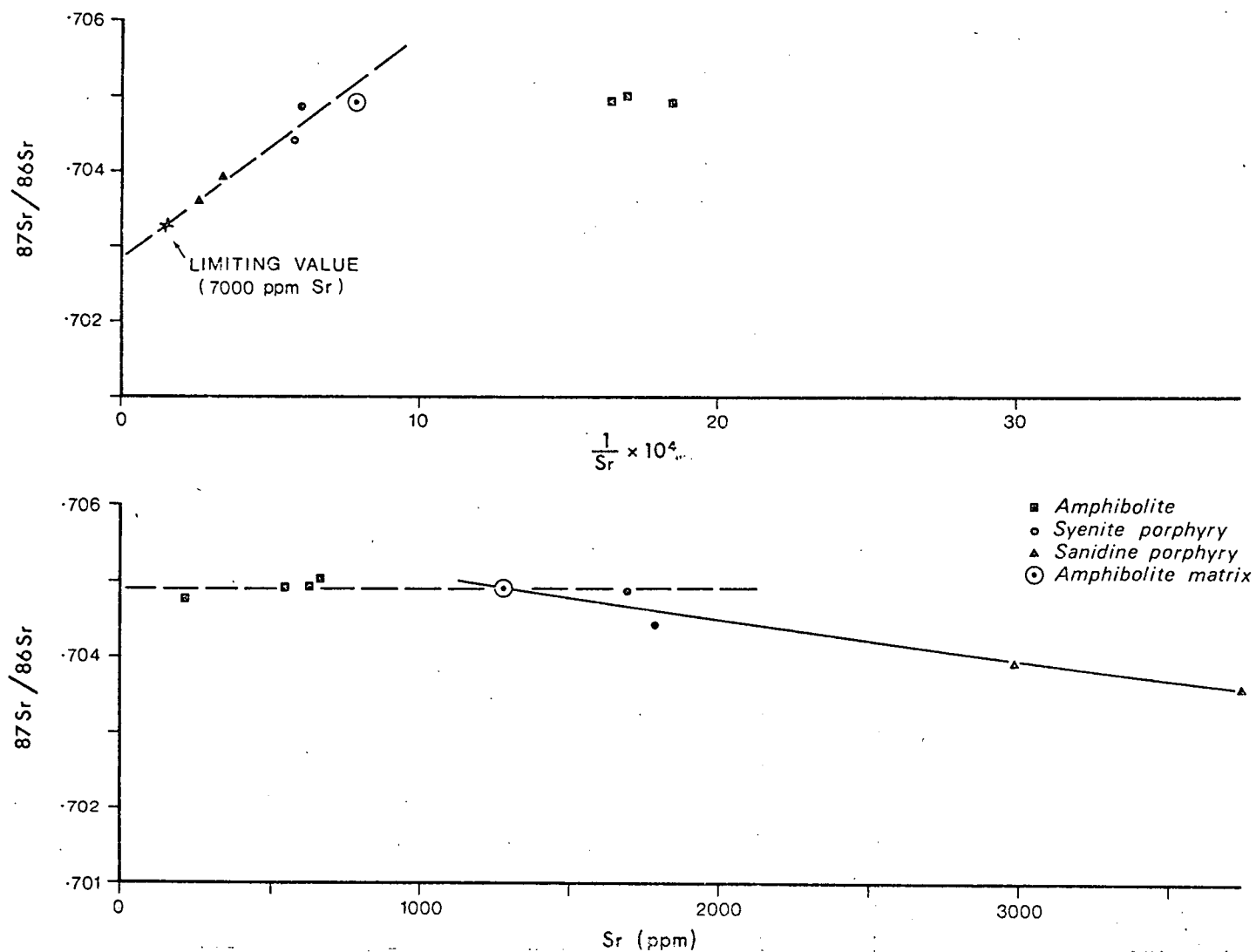


Figure VI-1 Upper: Reciprocal Sr plot against initial ratios with chosen limiting value of 7000 ppm Sr added.
Lower: Sr isotope mixing curve for syenite porphyries, sanidine porphyries and amphibolites with initial ratio plotted against Sr concentration.

These results then demonstrate, on the basis of initial strontium isotope ratios, that the Port Cygnet alkaline rocks could have been formed by mixing of a partial melt of the quartzo-feldspathic matrix of the amphibolite inclusions with a potassium, strontium rich material having an initial $^{87}\text{Sr}/^{86}\text{Sr}$ ratio of about 0.702, if the graph is extrapolated to $\frac{1}{\text{Sr}} = 0$. However this ratio implies a source rock with an infinite amount of strontium which is an unrealistic situation. The highest recorded concentrations of strontium occur in some of the alkaline rocks of the east African rift system (Powell and Bell, 1974). These reach at least 7000 ppm Sr. Using this as a limiting value for the amount of strontium likely to have been present in the original material and substituting this into the mixing curve of Fig. VI-1, an initial ratio of 0.7033 for $^{87}\text{Sr}/^{86}\text{Sr}$ is the likely extreme for the other mixing component of these rocks.

While the Port Cygnet values are much less than the high values for the Tasmanian Jurassic dolerites, they are closer to those of some Tasmanian Tertiary basalts (Compston, McDougall and Heier, 1968). Apart from one apparently anomalous ratio of 0.7078 the values for these rocks vary from 0.7026 to 0.7039 which would be regarded as upper mantle ratios.

A conventional interpretation of the initial strontium isotope ratios suggests an upper mantle, rather than a crustal origin for the potassium rich sanidine rocks.

It can be noted here that, ⁱⁿ their study of the strontium isotope geochemistry of the Dunedin volcano, Price and Compston (1973) found that the basalt, intermediate and phonolitic rocks had initial ratios about 0.703 while the quartz normative trachytes have values about 0.704 which is somewhat similar to the undersaturated-saturated rock association at Port Cygnet. Price and Compston came to the

conclusion that the trachytes of the Dunedin volcano had formed by the partial melting of an alkali feldspar rich portion of older igneous rocks (compare with feldspathic matrix of the amphibolite inclusions as a parent component for the Port Cygnet syenite porphyries).

SUMMARY

Sulphur isotope studies do not reveal any formation temperature because the temperature was probably too high for fractionation of isotopes and suitable mineral pairs are absent.

Sulphides in the hornfels near Langdon's Point contain a component of remobilized local sulphur of sedimentary origin.

The garnet trachyte has sulphur isotope ratios slightly more positive than the other alkaline rocks whose ratios are within the normal igneous range.

The initial strontium isotope ratios show two sources for the alkaline rocks and these lie on an apparent mixing curve linking the green matrix rocks (X44), grey matrix (CY74), syenite porphyries (CY49 and CY70) and the quartzo-feldspathic matrix of the Mt. Windsor amphibolite inclusions.

CHAPTER VII

THE ORIGIN OF THE PORT CYGNET ALKALINE ROCKS

The origins of alkaline rocks, particularly those of high potash content, have posed many questions, only some of which have been answered. The diversity of the alkaline syenitic rocks reported in Appendix 1 seems to demand equally diverse origins. Many of these rocks form part of an association that also includes more mafic rocks, and may be differentiates. Other rocks usually of minor occurrence have formed by assimilation processes. There are also syenitic rocks which have crystallized from a magma, of small outcrop and with no obvious parent or residual rocks. In many of these there is an association with mafic rocks and their metamorphic equivalents.

As a result of the observations of many investigators it has been recognized that alkaline rocks cannot be related to a single universal magma and that there is a variety of processes by means of which alkaline igneous rocks may be derived and appear in many petrological associations. These processes have been summarised by various authors in Sorenson (1974).

The proposed mechanisms capable of generating alkaline rocks are: Anatexis, Fractional Crystallization, Limestone Assimilation, Volatiles, Liquid Fractionation, Resorption of Silicate Minerals and Metasomatic Processes.

Using the evidence gathered from the Port Cygnet rocks an attempt can now be made to see which of the aforementioned mechanisms could have produced these rocks.

Using the data and conclusions reached in earlier chapters a model will be proposed to explain the origin of the syenite porphyries and sanidine rocks which constitute the great bulk of the Port Cygnet alkaline complex. On account of its unique nature the proposed

origin of the garnet trachyte will be outlined separately. Other variants of the rock types will also be modelled. A summary of the relationships of the various rock types is outlined in Fig. VIII-2.

The following important points emerge from the field relationships and analytical studies of the Port Cygnet rocks:

(a) The Port Cygnet alkaline rocks are spatially dispersed with the largest bodies appearing near Mt. Windsor and Farewell Hill.

(b) There was a small amount of melt intruded into the district. A maximum of 75 km^3 for the volume of the alkaline rocks can be computed, assuming a source at the base of the crust, by simply extrapolating the maximum surface area (approximately 3 km^2) to this depth (25 km) thus arriving at the computed value. This is almost certainly an overestimate since the gravity data do not indicate such a simple structure. A modification may be incorporated by assuming a point source at the crustal base with an overall inverted pyramidal or conical form which reduces the maximum volume by 50% to 37.5 km^3 . The latter is a more realistic figure which could be reduced by assuring a pipe-like structure from depth to a higher level magma chamber in the crust (suggested by inclusion in the syenite porphyries). Supposing the syenite magma chamber occurred at 15 km depth (from the aeromagnetic traverse) and a conical dispersion from this source is considered a volume of 22.5 km^3 is derived, which could be considered a minimum value.

Thus the most likely volume of alkaline magma lies somewhere between 22.5 km^3 and 37.5 km^3 . It was emplaced as a host of small irregular dykes and occasional sills.

(c) The major element differentiation index plots show some parallel trends (Chapter IV) for the alkaline rocks suggesting that these may not have had a simple origin. Harker Diagrams do not show any significant fractionation trends but rather plot as two groups.

(d) Many of the minor element differentiation plots also show parallel trends (Chapter V).

(e) The sanidine-bearing dykes post-date the emplacement of the syenite porphyry.

(f) The presence of amphibolite and phengitic inclusions, whose plots on the Q-L-M diagram of Niggli bracket the compositions of the alkaline rocks, suggest that these might be related to the source of these rocks (Fig. IV-20).

(g) The flow and swirl structures of the sanidine-bearing dyke rocks and presence of some broken and reconstructed crystals together with the occurrence of minerals such as analcime, pectolite, hauynite, scapolite, cancrinite, and small calcite reaction rims on melanite demonstrate the presence of volatiles and the probable emplacement of the dykes as volatile-rich systems.

(h) The high concentrations of strontium and barium coupled with the low concentrations of niobium and zirconium suggest that crystal fractionation was probably not an important process in their formation but partial melting is possible. A depleted source for the latter two elements is also a possibility.

(i) Strontium concentration is higher in the sanidine rocks than in the syenite porphyries, although calcium does not show much variation, indicating that they have not fractionated from a common magma source.

(j) The K/Rb ratio favours a crustal source.

(k) There is a relationship between the K/Na ratio and Si atoms/unit cell linking the amphiboles from the amphibolite inclusions through the syenite porphyries to the hornblendeⁿ porphyry.

(l) Europium anomalies in the rare earth patterns are either absent or minor implying that feldspar fractionation has only occurred if the Eu was unoxidised.

(m) This lack of europium anomalies suggests that the syenite porphyries and sanidine rocks are not fractionates of a more mafic magma.

(n) The feldspar mineralogy indicates non-equilibrium conditions of growth for these minerals, with a general indication of higher temperatures of formation for the sanidine-bearing dyke rocks than for the syenite porphyries.

(o) The Bailey-McDonald diagrams (Figs. IV-13 and IV-14) also indicate the absence of feldspar fractionation.

(p) The mineralogy indicates a saturated quartz-bearing group (syenite porphyry) and a feldspathoid-bearing group (sanidine porphyry).

(q) The relationship of niobium to rubidium tends to define a mixing curve.

(r) The initial strontium isotopes may fit a mixing curve relating the sanidine porphyries, syenite porphyries and feldspathic matrix of the amphibolite inclusions.

On the basis of the major and minor element chemistry, mineralogy and initial strontium isotope values it is proposed that there are two main rock groups, represented here by the syenite porphyries and sanidine rocks. The syenite porphyry may have been formed by contamination of the magma parental to the sanidine rocks.

SUMMARY OF MECHANISMS CAPABLE OF GENERATING ALKALINE ROCKS

Metasomatic Processes

These are usually related to regional metamorphism and are recognized by various types of zoning in the field and appropriate metamorphic and replacement textures within the rocks. The Port Cygnet rocks are spatially restricted and have typical igneous textures; having gone through a melt stage which has obliterated any textural

evidence of the traces of any initial metasomatic period and would have been related to anatectic melting in this model.

Resorption of Silicate Minerals

A summary by Luth (1974) suggested that production of silica-undersaturated assemblages by resorption of muscovite and similar peraluminous minerals by a granitic magma as first suggested by Bowen, was an inefficient mechanism of generating alkaline rocks, particularly because a large amount of peraluminous material is required. Biotite is also a possible source of potash rich undersaturated magma, however the process is still inefficient and if resorption of ferro-magnesian phases occurred it would lead to associated ferro-magnesian minerals of which there is no evidence in the rocks which have a low range for $\frac{\text{Mg}}{\text{Mg}+\text{Fe}}$. This process is therefore not regarded as important for the generation of the Port Cygnet rocks.

Liquid Fractionation and the Role of Volatiles

Kogarko, Ryabchikov, and Sorensen (1974) have summarised the role of liquid fractionation in producing the alkaline rocks. They recognized two distinct processes: the first a pneumatolytic differentiation with migration of volatiles to the apical parts of magma reservoirs; and the second process one of liquid immiscibility leading to splitting of the magma during or before crystallization into two or more fractions.

The first process may lead to production of excess hydrous minerals such as zeolites, and loss of potassium with the derived alkaline rock having a close field relationship to the parent body (finitization?). Metasomatic processes involving alkalies, volatiles and alteration of country rocks produces fenites via a process known as finitization. Following the scheme of Borodin and Paulenko (1974), three main processes of finitization can be recognised. These are regional metasomatism

preceding anatexis, metasomatism at contacts of alkaline intrusions and postmagmatic alkaline metasomatism.

Small intrusions of alkaline rocks in dykes and stocks are not regarded as forming directly from metasomatic processes but might represent differentiates of alkaline magmas with accumulation of niobium, zirconium and strontium. Niobium and zirconium are not concentrated in the Port Cygnet alkaline rocks.

Fenitization of mafic-ultramafic rocks may lead to the formation of minerals such as nepheline, phlogopite and biotite which with ultimate development can lead to remnants of olivine and pyroxene with schorlomite, perovskite, melilite, magnetite and titanomagnetite as accessory phases.

Fenitization of country rocks such as granites and related rocks leads to the formation of alkali amphiboles, pyroxenes, soda plagioclase and potash feldspar.

As well as exotic minerals the absence of quantities of alkali amphibole and pyroxene and the small amounts of magnesia in the rocks, suggest these have not been formed by metasomatic processes. With regard to the second process (liquid immiscibility) the authors regard this as important only for late stage crystallization leading to the production of exotic rocks such as carbonatites and others enriched in apatite, sodalite, analcime and villiaumite. Such rocks have not been found at Port Cygnet nor is there a close association with any parent rock types or evidence of fenitization.

The role of volatiles has been summed up by Kogarko (1974) who pointed out that crystallization of miaskitic alkaline rocks (agpaitic index <1) must have proceeded with the separation of an aqueous vapour phase. The main role of volatiles according to Kogarko (op. cit.) is their influence on viscosity and mineral growth; features well exhibited by the Port Cygnet sanidine porphyries with their turbulent flow textures. Kogarko (op. cit.) concluded that high concentrations of

volatiles might lead to immiscible liquids as above, but there is no evidence of the expected exotic mineralogy. She also states that with high concentrations of volatiles the ratio $\text{Fe}^{2+}/\text{Fe}^{3+}$ tends to rise, but as this ratio at Port Cygnet is less than unity then volatiles were probably not a dominating factor to the extent of creating an immiscible liquid fraction or a reduced environment. The $\text{Fe}^{2+}/\text{Fe}^{3+}$ ratio is also related to the types of volatiles and to their source. For example, Perchuk (1977) has concluded that mantle fluids are reduced gases derived by decomposition of parent alkali metal compounds. It is only within the crust in the pressure range of 8 to 3 kb that reduced pore fluids become enriched in H_2O and CO_2 by oxidation processes.

The role of volatiles in magmatic systems has been summarised by Wyllie (1979). Of these H_2O and CO_2 are the most important but sulphur and fluorine may also be important in specific situations. A feature of CO_2 is its influence in the generation of alkalic subsilicic magmas from peridotite beneath continental shields.

When compared with anhydrous melts the addition of H_2O will produce a water-saturated melting curve having a negative slope up to high pressures. This has the effect that melts generated at or near their water-saturated liquidus curves may not rise to the surface (or near surface) without crystallization. However if liquids are undersaturated with respect to water at their depth of origin then they may move to the surface without crystallization until they intersect the water-saturated liquidus at shallow depths. The general effect of H_2O is to considerably reduce liquidus temperatures (Wyllie op. cit.) and particularly to promote the growth of amphibole in a ferromagnesian dominated system. For magmas from the continental crust where the deep crustal rocks are most likely related to the calc-alkaline series in the presence of aqueous pore fluids, melting begins at moderate temperatures with migmatitic products in rocks of amphibolite grade.

The influence of HF is to act as a flux, depressing melting points a little but contributing to the production of water-bearing melt. The presence of HCl acts to destroy feldspars and transfer alkalies into the vapour phase.

Wyllie and Tuttle (1959) found that CO_2 under pressure had little effect on the rates of melting or crystallisation of granite or feldspars and was less soluble than H_2O in granitic melts. Solution of CO_2 in these melts is probably a function of the presence of suitable cations not structurally bound into the silicate network.

Mysen (1976) found that CO_2 solubility in silicate melts is about one half to one order less than that of H_2O . With increasing pressure and basicity of the melt the solubility increases. At 5 kb the maximum relative solubility of CO_2 is approximately 5 mol. percent.

In considering fluids in the evolution of granitic magmas, Holloway (1976) found that the small amount of CO_2 in granitic magma could influence the activity of water in the system. If the mass ratio $\text{CO}_2/\text{H}_2\text{O}$ is ≥ 0.4 and the initial ratio of total volatiles to silicate magma is ≥ 0.5 then little or no loss of fluid phase occurs and the activity of H_2O remains nearly constant for the magmatic evolution. In all other cases the activity of H_2O increases rapidly with decreasing pressure and/or anhydrous phase crystallisation. The presence of fluid bubbles would also change the physical characteristics of the magma. At 5 kb and 5 wt.percent CO_2 the liquidus temperature could be lowered by about 100°C .

By lowering the $P_{\text{H}_2\text{O}}$ to less than P_{total} (in this case with $P_{\text{CO}_2} = 0.4$ and $P_{\text{H}_2\text{O}} = 0.6$). Holloway and Burnham (1972) demonstrated that liquidus temperatures in a basaltic system could be increased, however, the amount of CO_2 present was much greater than in the experiments cited above.

The available data for SO_2 have been summarised by Burnham (in Barnes, ed., 1979) and discussed in Chapter III.

Limestone Assimilation

This model for deriving alkaline rocks by desilification of a sub-alkaline magma by assimilation of limestone was first proposed by Daly in 1910 and subsequently developed by Shand (1930, 1943, 1945). Indeed, Cygnet was cited as an example of the alleged close field associations of limestones with alkaline rocks. In his summary (Wyllie, 1974) came to the conclusion that the field evidence is inconclusive and there is considerable experimental evidence against the hypothesis. Wyllie observes that there should be some sign of primary calc-silicate minerals which do not appear in the alkaline rocks although an inclusion of marble was noted in one syenite porphyry (Pl. 19) and there is evidence of appreciable CO_2 in the system (Pl. 29). However in the case of the garnet trachyte variant where a carbonate assimilation model is proposed (see later), an exotic calc-silicate (epidote) does crystallize. A feature of the analytical data for the Cygnet alkaline rocks is their low lime content. There is no evidence from inclusions of a parent sub-alkalic magma from which to draw the alkali magma. There is no firm evidence from the Port Cygnet alkaline rocks favouring the limestone assimilation model for their formation.

Fractional Crystallization

This process is believed to have been responsible for the production of many alkaline rocks. This can be demonstrated as a possibility from the experimental work of Bowen (1937) and the common association of alkaline rocks with more basic rocks (e.g. Coombs, 1963; Kuno, 1968; Coombs and Wilkinson, 1969). In a simple fractional crystallization system with removal of ferromagnesian minerals to concentrate a felsic residue, minor elements such as niobium and zirconium should also

accumulate with the felsic component. The zirconium concentrations are somewhat low and the niobium values extremely low when compared with probable differentiates of more mafic melts such as oceanic trachytes.

The niobium values for the sanidine rocks (Chapter V) are greater than for the syenite porphyries which may suggest fractionation relating these two groups because field evidence (Pl. 2) shows that the sanidine porphyry was intruded later than the syenite porphyry. The Bailey-McDonald plots (Chapter IV) do not suggest that these rocks are related by feldspar fractionation. If the syenite porphyries were an initial fractionate of a single magma crystallizing sodium rich plagioclase, then these should have concentrated strontium (Heier, 1962). However, most of the strontium is in the later sanidine rocks. This evidence together with that of the strontium isotopes (Chapter VI) and the presence of oversaturated and undersaturated rocks indicate dual sources rather than a fractionated single source. The high strontium values show that plagioclase fractionation was not related to the formation of the sanidine rocks.

On the basis of the above observations it is doubtful if the alkaline rocks have been derived from fractional crystallization although the evidence of armouring of plagioclase phenocrysts (Mueller and Saxena, 1977), the low strontium values and the europium anomalies in the chondrite normalised rare earth element patterns (Fig. V-18) shows that the brown matrix rocks are probably a fractionated product of the syenite porphyry.

Anatexis

This leaves anatexis as the remaining option for derivation of the alkaline rocks. This could be of either lower crustal or sub-crustal origin on the basis of the initial strontium isotope values (Chapter

VI) and also it seems likely that two sources for the rocks may have to be evoked. On the basis of the amount of magma involved in the Port Cygnet complex and the high concentrations of barium, strontium and rubidium it is most likely that partial melts were responsible and that these melts could represent secondary melting of original sub-crustal material that had been emplaced in the crust. The presence of amphibolite, quartzite and marble inclusions together with the epidote xenocrysts of CY76 show that the syenite porphyries crystallized in a crustal environment and the formation of sanidine phenocrysts about the phengite inclusions of the dyke X50 suggests that this dyke also started to crystallize in the crust.

It is proposed to develop an anatectic model for the formation of the Port Cygnet alkaline rocks based on the indication of separate sources for the syenite porphyries and sanidine rocks as outlined above.

SYENITE PORPHYRIES

The proposal for the origin of these rocks is based on the observation that the amphibolite inclusions from the Mt. Windsor locality appear to have lost their feldspathic matrices with recrystallization of the remaining amphibole (Pl. 26 and Pl. 27) and that there is a well defined initial strontium isotope mixing curve extending from the sanidine porphyries, at one extreme, through the syenite porphyries to the feldspathic amphibolite matrix at the other limit (Fig. VI-1).

An experimental investigation has been made of the proposition that the matrix was melted from the amphibolite. A sample of fresh powdered amphibolite from an inclusion was taken and 15 mg of powder was sealed in a platinum capsule and subjected to 800°C at 8 kbar ($P_{H_2O} = P_{total}$) for 24 hours in a Boyd-England high pressure apparatus.

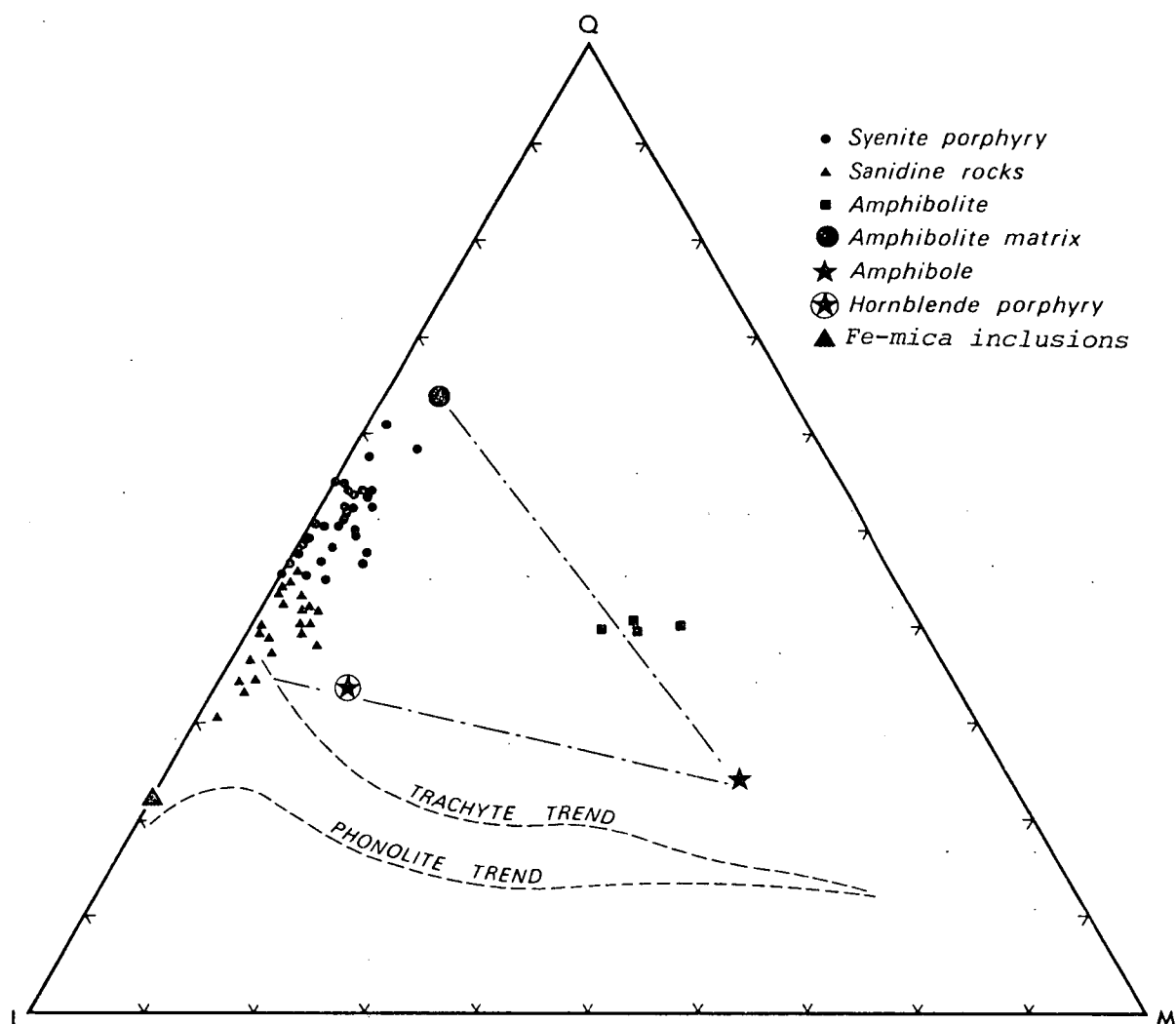


Figure VII-1 Niggli QLM plot for alkaline rocks and their inclusions. Trachyte and phonolite trends from King & Sutherland (1960) have been added.

These were considered to be the minimum necessary to establish equilibrium in the above apparatus, and are not inappropriate. The experiment caused melting of the matrix to a glass in which were embedded recrystallized amphiboles. The experiment is listed as number T541 of the high pressure laboratory, Geology Department, University of Tasmania and the analysis of the matrix glass is reported in Table IV-4, where compositions are given for other rocks that are typical of the Port Cygnet Complex. The position of this glass is shown on the variation diagrams of Figs. VII-1 to VII-3. From these plots it can be seen that the matrix of the amphibolite inclusions lies in a position which is commensurate with its forming one component (plus the potassium rich component) of a simple mix producing the syenite porphyries.

Referring to Figs. VII-2 and VII-3 showing the partial melt compositions derived from Helz's work (1976), it can be seen that T541 is similar to the partial melt of the 1921 Kilauea olivine tholeiite at 5 kb. Helz also points out in her paper that the melt compositions produced in this way do not show much variation in composition until the ferromagnesian minerals commence melting at which stage the iron and magnesium concentrations in the melt rise rapidly. The low iron and magnesium in the syenite porphyries reflects the low abundances of ferromagnesian mineral present.

T541 is a composition similar to that of the 1921 Kilauea tholeiite and could produce the syenite porphyries by mixing with the more potassic component (see below). Helz's values (Table VII-3) are less siliceous. From the Niggli Q-L-M diagram (Fig. VII-3) the range from T541 to the potassic CY73 covers most of the rocks.

It is noteworthy that CY91, the hornblende porphyry, could be regarded as formed from large recrystallized amphiboles from the residual amphibolite mixed with a component from the more potassic rocks.

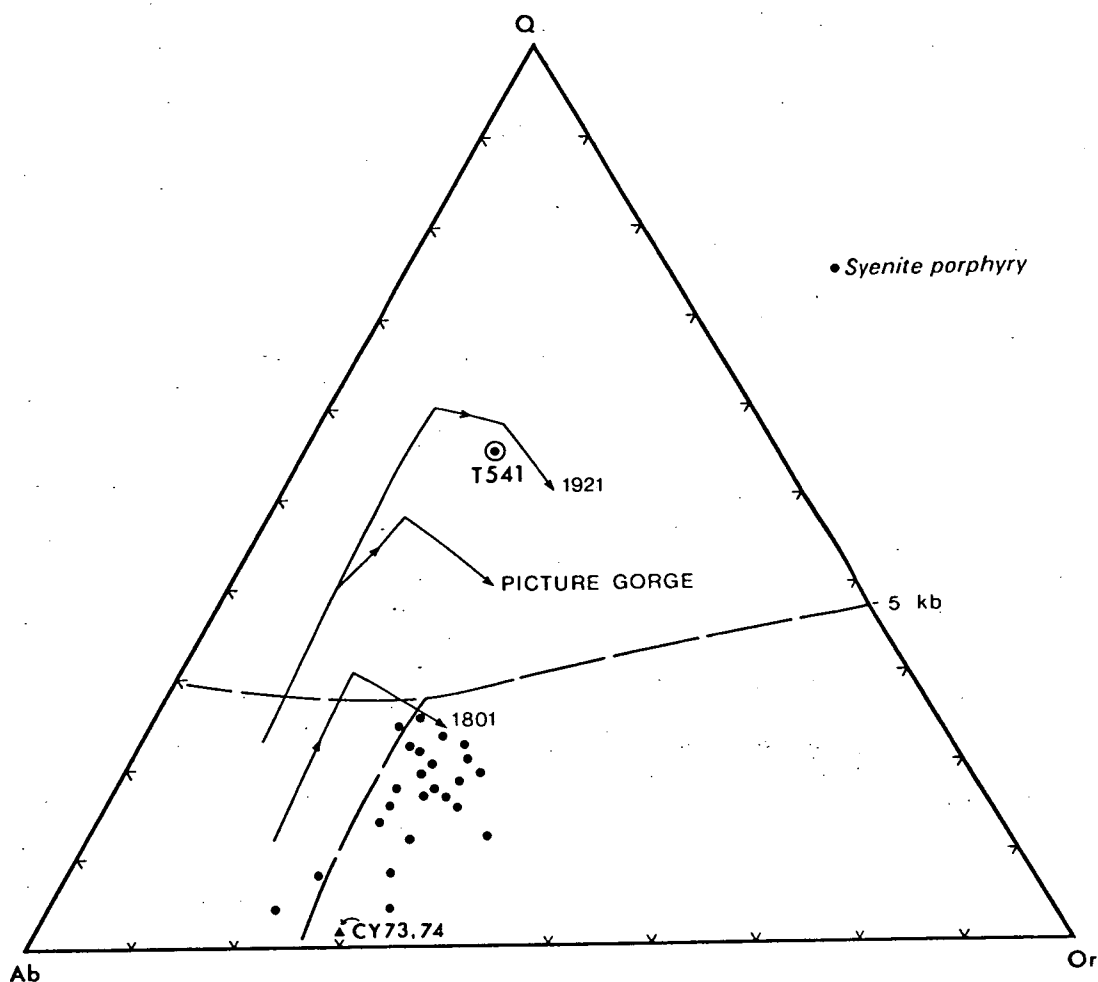


Figure VII-2 Ab-Q-Or plot of partial melts at 5 kbar of 1801 Hualalai alkali basalt, Picture Gorge tholeiite and 1921 Kilauea olivine tholeiite (after Helz, 1976) with syenite porphyries and sanidine rocks CY73 and CY74 added together with the partial melt of amphibolite inclusions at 8 kbar and 800°C (T541). $P_{H_2O} = P_{total}$.

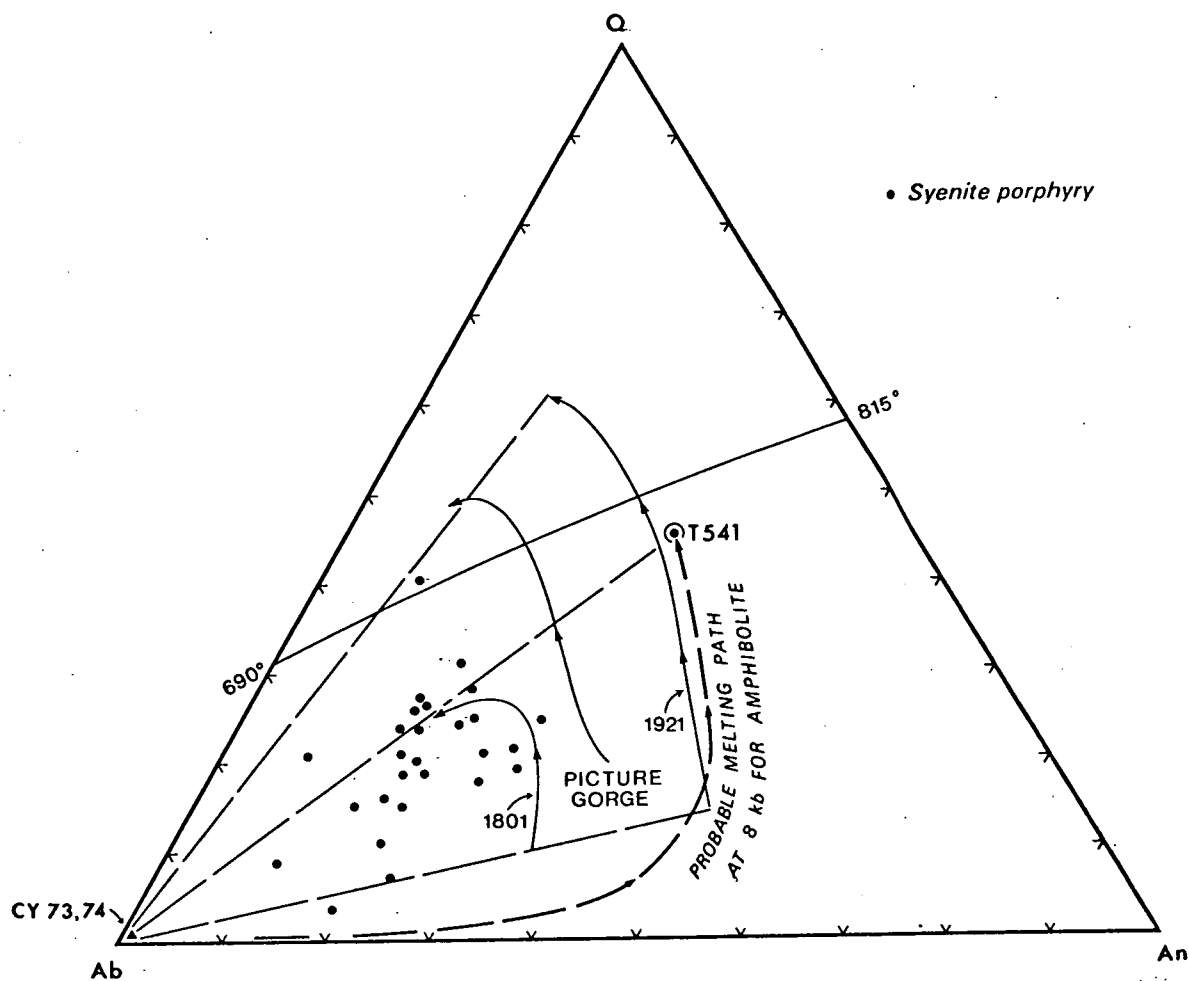


Figure VII-3 Ab-Q-An plot of partial melts at 5 kbar of 1801 Hualalai alkali basalt, Picture Gorge tholeiite and 1921 Kilauea olivine tholeiite (after Helz, 1976) with syenite porphyries and sanidine rocks CY73 and CY74 added together with the partial melt of amphibolite inclusions at 8 kbar and 800°C (T541). $P_{H_2O} = P_{total}$.

TABLE VII-1

COMPARISON OF CHEMICAL COMPOSITIONS OF TYPICAL PORT CYGNET ALKALINE ROCKS WITH MIXES OF AMPHIBOLITE MATRIX (T541), TINGUAITE, AMPHIBOLE AND SYENITE PORPHYRY

	MATRIX T541	SYENITE PORPHYRIES			TINGUAITE CY73	AMPHIBOLE FROM AMPHIBOLITE
		CY70	CY120	CY8		
SiO ₂	69.59	65.89	65.31	62.90	57.04	43.55
TiO ₂	0.00	0.34	0.39	0.43	0.33	0.73
Al ₂ O ₃	18.48	17.56	18.00	17.77	19.76	12.26
Fe ₂ O ₃	-	2.14	1.53	2.22	3.15	3.28
FeO	2.73+	1.48	1.17	1.17	0.50	11.56
MnO	0.00	0.02	0.06	0.18	0.13	0.34
MgO	0.43	0.59	0.94	0.66	0.24	11.12
CaO	5.11	2.49	4.37	4.49	2.75	11.70
Na ₂ O	1.51	4.82	4.62	5.11	7.08	1.70
K ₂ O	2.13	3.71	3.42	3.98	7.93	1.22
P ₂ O ₅	-	0.11	0.18	0.09	0.05	0.00
loss	-	1.83	0.18	0.87	2.66	3.20
	<u>99.98</u>	<u>100.98</u>	<u>100.17</u>	<u>99.87</u>	<u>101.62</u>	<u>100.65</u>

	1:1 MIX T541+CY73	SYENITE CY26	APLITE CY26+AMPHIBOLE	2:1 MIX CY26+AMPHIBOLE	HORNBLLENDE PORPHYRY CY91
SiO ₂	63.32	62.95		56.48	55.27
TiO ₂	0.16	0.21		0.38	0.80
Al ₂ O ₃	19.12	18.43		16.37	16.66
Fe ₂ O ₃	3.12*	2.14		2.52	3.28
FeO	-	0.18		3.97	5.34
MnO	0.07	0.08		0.17	0.19
MgO	0.51	0.01		3.71	2.04
CaO	3.93	1.66		5.01	5.15
Na ₂ O	4.30	5.13		3.99	4.47
K ₂ O	5.03	7.14		5.17	6.75
P ₂ O ₅	0.02	0.00		0.00	0.49
loss	1.33	0.29		1.26	0.91
	<u>100.91</u>	<u>98.25</u>		<u>99.03</u>	<u>100.93</u>

* all iron as Fe₂O₃

+ all iron as FeO

TABLE VII-2

Parental compositions from Helz (1976) compared with Port Cygnet amphibolite.

	1921 Kilauea olivine tholeiite	Picture Gorge tholeiite	Typical amphibolite from Cygnet
SiO ₂	49.11	50.71	49.58
TiO ₂	2.51	1.70	0.49
Al ₂ O ₃	12.74	14.48	15.05
Fe ₂ O ₃	3.23	4.89	3.35
FeO	8.40	9.07	7.59
MnO	0.17	0.22	0.21
MgO	10.31	4.68	9.36
CaO	10.73	8.83	11.91
Na ₂ O	1.97	3.16	2.24
K ₂ O	0.49	0.77	0.58
P ₂ O ₅	0.27	0.36	0.05
	<hr/> 99.93	<hr/> 98.87	<hr/> 100.41
Q	-	0.73	-
Or	2.90	4.55	3.43
Ne	-	-	-
Ab	16.67	26.74	18.95
An	24.67	23.05	29.30
Ol	7.30	-	9.25
Di	21.96	15.44	23.80
Hy	19.77	20.90	9.78
Mt	1.16	3.13	4.86
Il	4.77	3.23	0.93
Ap	0.63	0.83	-
	<hr/>		
	1801 Hualalai alkali basalt	1801 Hualalai alkali basalt	
SiO ₂	46.53	Q	-
TiO ₂	2.41	Or	5.73
Al ₂ O ₃	14.91	Ne	3.07
Fe ₂ O ₃	3.69	Ab	19.55
FeO	9.09	An	24.44
MnO	0.19	Ol	21.32
MgO	8.69	Di	18.43
CaO	9.86	Hy	-
Na ₂ O	2.98	Mt	1.54
K ₂ O	0.97	Il	4.58
P ₂ O ₅	0.31	Ap	0.72
	<hr/> 99.63		

TABLE VII-3

Partial melt compositions and CIPW norms at 875°C from Helz (1976)
at 5 kbar water pressure.

	1921 Kilauea olivine tholeiite	Picture Gorge tholeiite	1801 Hualalai alkali basalt
SiO ₂	68.60	67.3	66.10
TiO ₂	0.38	0.2	0.37
Al ₂ O ₃	19.00	19.5	19.30
FeO	1.78	2.18	1.45
MnO	-	-	0.06
MgO	0.40	0.46	0.32
CaO	6.02	4.95	5.08
Na ₂ O	2.60	4.20	5.20
K ₂ O	1.00	1.10	2.00
P ₂ O ₅	0.18	0.12	0.16
	<hr/> 99.16 <hr/>	<hr/> 100.01 <hr/>	<hr/> 100.04 <hr/>
Q	5.9	6.5	11.8
Ab	22.0	35.5	44.0
An	28.7	23.8	23.4
Ol	35.4	26.0	16.5
Hy	3.6	4.8	2.6
Di	-	-	0.6
Ap	0.4	0.3	0.4
Il	0.7	0.4	0.7
C	3.2	2.6	-

Because the field evidence shows that there are only small and very dispersed intrusions, it is considered that only small amounts of melt were formed and mixed with ultimate complete crystallization and no significant amounts of residual liquids. The paucity of pyroxenes and the chloritic alteration of these suggest a high P_{H_2O} . Also the evidence of non-equilibrium crystallization of the feldspars (Figs. III-19 and III-21) would support a mixing model rather than a single source for the syenite porphyry. With potassium increasing on the rims of the potash feldspars it could mean that potassium was being added during crystallization for those rocks not close to the equilibrium curve (e.g. CY49 and CY70).

The major element compositions for typical rocks are presented in Tables IV-1 and IV-2.

Thus from the data and mixes of Table VII-1 assuming simple disequilibrium mixing, the matrix composition may be mixed with a sanidine porphyry composition represented by CY73 to give the typical syenite porphyry composition while the addition of the amphibole composition of the amphibolite gives a close approximation to the composition of CY91 when added to the syenite aplite.

The light rare earth element data plotted in Fig. V-17 are compatible with a simple disequilibrium mix of the sanidine porphyry pattern with the amphibolite matrix pattern. As stated in Chapter V the analyses for the heavier rare earths may be subject to error.

The concentrations of the trace element strontium, rubidium and barium and perhaps niobium can be accounted for by such an explanation. It was not possible to determine other trace elements on the amphibolite matrix due to the lack of enough material for analysis by X.R.F.

THE SANIDINE ROCKS

The chemical, mineralogical and strontium isotope data point to a different source for the sanidine-bearing rocks which appear to represent the primary magma at Port Cygnet.

The minor element concentrations, particularly cesium and including the potassium-rubidium ratio are not inconsistent with a crustal source for these rocks but with an initial strontium isotope ratio of 0.7036 for CY73 there is some difficulty in producing a crustal source with this ratio, especially when most evidence shows contamination by crustal strontium or the presence of a heterogeneous source invariably leads to ratios greater than the value measured above.

Le Maitre's work at Mt. Elephant (1974) showed that on a minor scale it is possible to produce a syenitic material by partial fusion of granite hence a crustal source might be a source of the sanidine rocks.

Crustal Source for the Sanidine Rocks

It would appear that likely source materials for potash rich melts are potash mica-, potash feldspar-, plagioclase rocks. Partial melts of these could generate a liquid with high potash, soda, alumina and a significant volatile component. Such a source could explain the high strontium, barium, cesium and low niobium values found in the Port Cygnet rocks. It does not explain the low initial strontium isotope ratios, and under complete melting conditions would give rise to a liquid which would contain more alumina than observed in the present rocks.

Steuhl (1962) and Winkler (1966) have investigated the anatexis of gneisses with free water available. Two main gneiss types were considered by these workers, one composed of alkali feldspar-, plagioclase-, quartz and the other lacking the alkali feldspar.

For rocks containing alkali feldspar, plagioclase and quartz, Steuhl (1962) showed that in the melting of a high grade gneiss at 2 kb water pressure, melting began at 675°C. When 84% of the gneiss had melted the composition tended not to follow a simple path. Residual minerals present in these melts were cordierite, garnet, ore-minerals and sillimanite.

For rocks with K-feldspar absent and containing muscovite, plagioclase and quartz at $P_{H_2O} = 5$ kb and 680°C, an anatectic melt will begin to appear. Thus muscovite - quartz - plagioclase \rightarrow K-feldspar - plagioclase - quartz in the melt with an anorthite richer plagioclase and sillimanite and H_2O .

At a limiting value of 5-7 kb derived from geophysical estimates of the thickness of crust in the Cygnet area (Leaman et al., 1980) and a temperature greater than 750°C, the equilibrium involves muscovite + quartz = orthoclase + sillimanite + liquid (Winkler, 1976).

Winkler also shows that it is possible to produce an anatectic melt consisting of the components of potash feldspar, albite rich plagioclase and quartz from the reaction of muscovite + quartz + plagioclase + H_2O .

According to Winkler in general terms it is possible to produce a potassic melt at 5-7 kbar from a metamorphic assemblage, which could be the parent for the potassic magmas.

Green (1976) in testing the proposal that some S-type granites (Chappell and White, 1974) were derived by partial melting of pelitic rocks, found that fusion of these containing 2% and 5% water at pressures of 4, 7 and 10 kbar produced granitic liquids similar to those of tonalite-granodiorite composition.

Thompson and Tracey (1979) have shown that it is also possible to generate the most calcic plagioclase compositions observed in high grade pelitic rocks in the range of 650°-750° at 5 kbars and that in the

pressure range of 4 to 6 kbars there is maximum overlap between muscovite dehydration and initial melting reactions which could generate an anatectic melt.

From the experimental data summarized by Wyllie (1977), the early stages of fusion in the system $\text{Na}_2\text{O}-\text{K}_2\text{O}-\text{SiO}_2-\text{Al}_2\text{O}_3$ are dominated by the minerals quartz, alkali feldspar and the sodic component of plagioclase. These give rise to quartz-normative liquids.

Since Winkler's work suggests alumina-rich liquids and Wyllie (1977) came to the conclusion that most crustal melts are quartz-normative it appears that the formation of the sanidine rocks from quartz-bearing crustal material, is unlikely.

It is also difficult to imagine a low initial strontium isotope ratio of the source which would require some sort of isolation mechanism leading to a complicated model.

A Sub-Crustal Source for the Sanidine Rocks

An upper mantle source for these rocks must now be considered. This is compatible with the initial strontium isotope ratios. It has been shown that volatiles were present at the time of emplacement of the sanidine-bearing dykes and it is possible to produce potassium-rich liquids in the upper mantle by the breakdown of phlogopite according to the reaction:



That potassium-rich sanidine-bearing rocks may be derived from upper mantle sources has been demonstrated experimentally by Wendlandt and Egglar (1980) and by applying their data convincing evidence has been presented by Kuehner, Edgar and Arima (1980) for the origin of the Leucite Hills, Wyoming (Cross, 1897) and, as an extension of their model, the origin of similar suites from Birunga, Central Equatorial

Africa (Holmes and Harwood, 1937), West Kimberley, Western Australia (Wade and Prider, 1940; Prider, 1960), Jumilla, Spain (Fuster et al., 1967) and the Toro-Ankole region, Southwestern Uganda (Bell and Powell, 1969). Many of these rocks are ultra potassic, ranging up to 11% K_2O , with leucite and sanidine as well as magnesium minerals being typical and a trace element assemblage, characterised by high Cr (~400 ppm), Ba (3000-12000 ppm), Ni (149-428 ppm), Nb (42-137 ppm), Zr (1150-1300 ppm), Sr (1650-4900 ppm) and Rb (156-1274 ppm).

The only rocks at Port Cygnet with high potash and low soda are the orthoclasites, which are nearly pure sanidine, and the garnet trachyte which can be modelled in another fashion.

The orthoclasites from the Regatta Point hybrid zone could represent a small amount of potash-rich material with volatiles released from the upper mantle. In summarizing various authors' estimates of potash abundance Wendlandt and Eggler (1980) arrived at a value of 0.15 wt.% as a realistic value for the upper mantle. For H_2O a similar compilation revealed an estimate of 0.1 to 0.2% which is well in excess of the amount required (0.06%) for the above value of K_2O , assuming it is restricted to phlogopite. Their relatively high soda contents, low magnesia and the trace element assemblages suggest that the Port Cygnet sanidine rocks are not directly related to the ultra potassic rocks, and must have had their origin elsewhere.

A basaltic source would be a sufficient source of soda for these rocks. Green and Ringwood (1968) and especially Helz (1976) have shown that partial melting of basic rocks can give rise to derivative feldspathic and silicic liquids which may crystallize or mix with other liquids producing various alkaline and/or calcalkaline rocks. Wilkinson (1966) has also shown the undersaturated character of residual glasses from some alkali basaltic rocks.

From Helz's (1976) data the partial melts of several basaltic types at 5 kb are always quartz normative, however as the temperature increases the amount of quartz (and total silica) decreases. FeO and

MgO always remain relatively low until hornblende begins to melt.

Lower temperature melts favour the release of K_2O as Na_2/K_2O tends to increase with the temperature of the partial melt. The findings of Presnall et al. (1978) suggest that K_2O may increase with a pressure increase.

The values of $\frac{100 \text{ Mg}}{\text{Mg}+\text{Fe}}$ range from 9 to 21 over the temperature range 725-1000°C for the Hualalai alkali basalt and cover a similar range for the Port Cygnet sanidine rocks, i.e. 9-29.4. On this basis there is some similarity but the melts, as noted earlier are quartz normative and lose alkalies at higher temperatures. If this is the source of the potash rocks a different process must have occurred as alkalies and alkaline earth trace elements have to be further concentrated. A parent alkali basaltic rock with greater normative feldspathoid would have suitable chemical characteristics for the partial melt.

A Basaltic Source of the Rocks

It seems empirically that a basaltic source for these rocks is feasible and because of the low $\frac{\text{Mg}}{\text{Mg}+\text{Fe}}$ partial melting took place with no significant contribution from the mafic minerals. In alkali basalts the following range of concentrations of minor elements occurs: barium averages about 600 ppm, strontium 80-2400 ppm, zirconium 200-300 ppm, niobium 60-113 ppm and cesium <1 ppm.

Frey, Green and Roy (1978) have published data on alkali basalts from Victoria; in particular an alkali olivine basalt from Mt. Frazer and a basanite from Mt. Porndon, both of which are nepheline normative. The composition of these are given in Table VII-4.

It could be expected that Ba, Sr, and Rb would be concentrated in the feldspathic phases and that zirconium not in zircon, sphene and oxides would be in pyroxenes.

TABLE VII-4

Compositions of typical alkaline rocks, alkali olivine basalt
and basanite, and Port Cygnet tinguaitite.

	Nepheline syenite*	Tinguaitite*	Syenite*	Trachyte*	Mt Frazer alkali olivine basalt**	Mt Porndon basanite**	Port Cygnet tinguaitite CY85C
SiO ₂	54.99	54.08	58.58	61.21	48.00	46.21	57.12
TiO ₂	0.60	0.54	0.84	0.70	2.14	2.51	0.43
Al ₂ O ₃	20.96	18.65	16.64	16.96	13.91	12.38	20.96
Fe ₂ O ₃	2.25	3.92	3.04	2.99	1.85	2.00	4.05
FeO	2.05	2.28	3.13	2.29	9.27	9.98	0.71
MnO	0.15	0.22	0.13	0.15	0.16	0.18	0.12
MgO	0.77	1.07	1.87	0.93	11.39	11.71	0.28
CaO	2.31	2.77	3.53	2.34	8.35	8.56	1.39
Na ₂ O	8.23	8.10	5.24	5.47	3.23	3.54	5.45
K ₂ O	5.58	5.52	4.95	4.98	1.18	2.01	9.68
H ₂ O ⁺	1.30	2.10	0.99	1.13			
H ₂ O ⁻	0.12	0.23	0.23	0.47			
P ₂ O ₅	0.13	0.20	0.29	0.21	0.51	0.90	0.03
CO ₂	0.20	0.06	0.28	0.09			
Total	99.64	99.74	99.74	99.92	99.99	99.98	100.22

CIPW Norms:

Q	-	-	0.83	5.00	-	-	-
Or	32.98	32.63	29.29	29.41	7.00	11.90	57.21
Ab	29.45	26.03	44.34	46.26	24.90	14.90	14.71
An	3.78	-	7.24	7.04	19.90	11.90	4.14
Ne	21.77	21.22	-	-	1.30	8.20	17.01
Ac	-	2.90	-	-	-	-	-
Di	4.53	7.24	5.35	2.14	14.60	19.90	1.50
Wo	-	1.26	-	-	-	-	-
Hg	-	-	4.16	2.06			
Ol	0.28				24.20	23.40	-

TABLE VII-4 (continued)

Mt	1.27	4.22	4.41	4.33	2.70	2.90	1.43
Il	1.13	1.03	1.60	1.34	4.10	4.80	-
Ap	0.30	0.48	0.70	0.49	1.20	2.10	-
Cc	0.45	0.13	0.64	0.20	-	-	-

Minor elements (ppm):

Sc	23	19.4	2
Ni	364	375	3
Cu	-	-	12
Zn	-	-	175
Rb	24	40	197
Sr	543	862	3508
Ba	350	510	3688
Y	27	28	0
Zr	152	298	164
Nb	-	-	24

* from Le Maitre (1976)

** from Frey and Green (1974).

Using the Mt. Porndon data from Frey et al. (1978) and following Gast's (1968) scheme, presented by Cox et al. (1979) the partitioning of the important trace elements in partial melting of this rock was calculated. For the purpose of the exercise, the minor oxide components were neglected and only the major silicate phases were considered. Distribution coefficients used were taken from Cox et al. (op. cit.).

Mt. Porndon		Mineral K_D = crystal/intermediate melt		
recalculated to major phases		Rb	Sr	Ba
Orthoclase	13.20	0.40	4.0	6.0
Albite	16.50	0.07	2.2	0.2
Nepheline	9.10			
Anorthite	13.20			
Diopside	22.06	0.03	0.5	0.13
Olivine	25.90			
	<u>100.00</u>			

Bulk rock K_D = rock/intermediate melt

$$K_{DRb} = 0.074$$

$$K_{DSr} = 2.346$$

$$K_{DBa} = 0.937$$

Using the partial melt curves for simple batch melting, given by Cox et al. (op. cit.), rubidium could be concentrated sufficiently to satisfy the alkaline rock concentration by a partial melt of about 10%, but not so for strontium and barium. Because of the high bulk rock K_D , for strontium and barium, a melt enriched in these elements cannot be produced while feldspars, in the parent rock, remain in equilibrium with it. Any partial melt in equilibrium with feldspars would be relatively impoverished in barium and strontium and consequently in its turn would crystallize feldspars with relatively lowered concentrations of these elements whereas for the Port Cygnet rocks a high degree of enrichment of strontium and barium is required to account for the observed values.

With regard to the other important minor elements, niobium and zirconium, these elements are concentrated in titaniferous oxides (e.g. ilmenite) and titanium bearing minerals. . Niobium and zirconium are also accommodated in ferromagnesian minerals, hence if a basaltic component is associated with the source of the sanidine-bearing rocks, then a depletion of niobium and zirconium could be expected. The role of cesium is not clear but because of its incompatibility it will be taken up by any melt formed. This may be further enhanced by volatiles from below, possibly from dehydrated phlogopite, which could concentrate the elements. As stated earlier (Chapter V), the basalts from the Dunedin volcano do contain appreciable amounts of cesium (Price and Chappell, 1975) so that an association with basaltic rocks can be established even though the concentration mechanism is not clear.

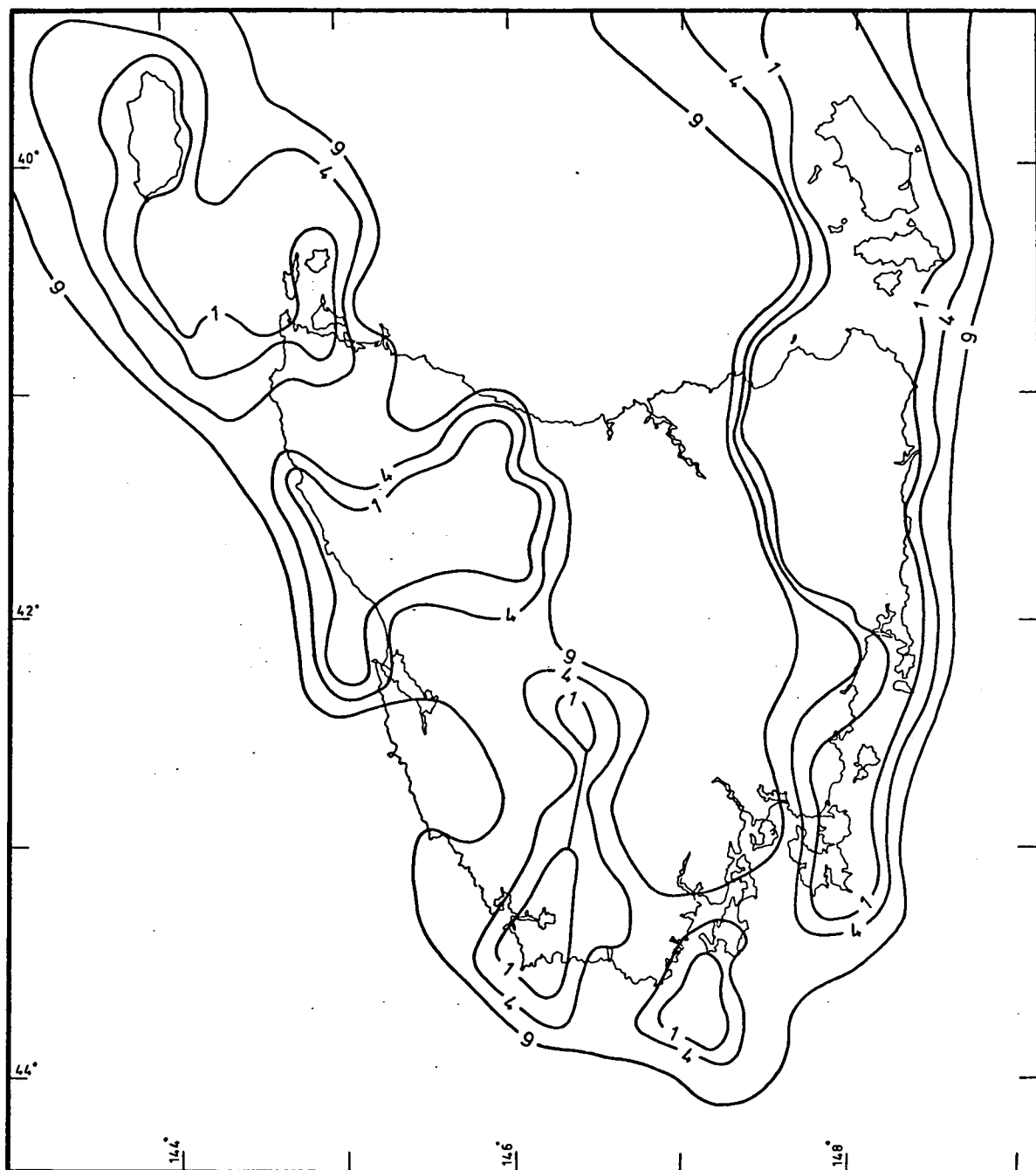
Could the sanidine rocks have formed from a melt which itself represented complete melting of the feldspathic component of the source? For a source like Mt. Porndon, this would represent about 50% partial melting. Because of the small amount of melt represented by the Port Cygnet rocks then this could mean 50% melt of a small amount of a parent similar to Mt. Porndon or a partial melt of a similar source in which the feldspathic component was much less. Any excess calcium component of the parent plagioclase could be accommodated as calcic pyroxene in the residuum and as melanite and sphene in the alkaline rocks.

The chondrite-normalized rare-earth patterns of the sanidine rocks have been given in Chapter V. These show only moderate enrichment of light rare earth elements and europium anomalies are not prominent. The patterns are similar to those of unfractionated granites or unfractionated alkali basalts (Haskin and Paster, 1979), with the suppression of the europium anomalies negating any large scale feldspar fractionation. Most chondrite-normalized R.E.E. patterns for Tasmanian

granitoids have prominent europium anomalies related to their degree of fractionation (Higgins et al., submitted for publication). The question might be asked if the sanidine rocks could have derived their rare-earth patterns by fractionation from these granitoids, with the separation of hornblende and plagioclase to depress any europium anomaly. While this could give a compatible R.E.E. pattern, other evidence is against this derivation. The lowest initial strontium isotope ratio for the granitoids is 0.706 (Cocker, 1978) any fractionation of these rocks would produce a quartz-normative melt, and gravity surveys indicate no granitoids under the Port Cygnet area (Leaman et al., 1980) (Fig. VII-4).

Miller (1977, 1978) has offered a R.E.E. model for saturated and slightly undersaturated feldspathic rocks. In discussing the origin of monzonite plutons in California, he came to the conclusion that these could have been derived by the partial melting of a garnet-bearing, virtually feldspar free source which was rich in LIL elements. Miller did not define his monzonites precisely but claims his model could apply to silica-saturated rocks such as monzonites, syenites, latites and trachytes. Slightly undersaturated rocks may also be included with the chief chemical characteristics being high $\text{Na}_2\text{O} + \text{K}_2\text{O}$, (about 10 wt.%), Sr 1000-2000 ppm, moderate SiO_2 (53-63 wt.%) and negatively sloping R.E.E. patterns from >100 to $<10\times$ chondritic abundance. A moderate initial ratio of $^{87}\text{Sr}/^{86}\text{Sr}$ ranging from 0.705 - 0.707 is also postulated.

To explain the lack of the europium anomaly, Miller suggests that the sodium is derived from eclogitic minerals such as omphacite or jadeite replacing the feldspar in an original alkali basalt. Ringwood (1975) states that any eclogitic bodies would be most likely of small dimensions and this would be consistent with the small amount of melt involved with the Port Cygnet rocks. Ringwood also points out (p. 99) that eclogites of undoubted mantle origin are associated with diamond pipes and some types of alkali basalts although Binns (1967) has



MODEL OF CRUST — GRANITE SURFACE

Figure VII-4 Contours show depth (km) to granite.
Granite density = 2.62 t/m^3
Crustal density = 2.73 t/m^3 .
From the gravity data of Leaman et al.
(1980).

presented evidence for a primary eclogite at Naustdal in Norway.

O'Hara and Yoder (1967) have also observed that partial melts of omphacite-bearing rocks are undersaturated and nepheline normative at 30 kbar. If the Naustdal eclogite is used as an example, this eclogite has the important trace elements strontium, barium and zirconium less than 10 ppm and potassium oxide at 200 ppm and sodium oxide at 2.7%. This composition would not produce potash-rich rocks with a suitable trace element component and would be sodium-rich.

In other eclogite models, Green and Ringwood (1968) investigated a sanidine-bearing quartz eclogite and found that progressive fusion of this rock led to andesitic compositions. Arth and Hanson (1972) derived quartz diorites by partial melting of eclogite or amphibolite at depths greater than thirty kilometres. The oversaturated nature of these derivatives is not compatible with the Port Cygnet sanidine porphyries.

Many authors (e.g. Bailey in Bailey and McDonald, (eds) 1976) have noted the difficulty of deriving potash rich rocks from an eclogitic parent and that the melts are quartz normative unless derived at high pressures and substantially greater depths.

Anhydrous eclogites are considered to have a minimum pressure stability limit of 5 kb (Green and Ringwood, 1968) but in the presence of water, amphibole bearing (so-called metamorphosed) eclogites are produced having stability limits down to 300°C at one atmosphere.

On the basis of their mineralogy the following eclogites may be recognized, namely: omphacite and garnet, hornblende and zoisite or glaucophane and epidote eclogites.

Whatever the mineralogy of the potential parent eclogite from which to derive the Port Cygnet magma, which has comparable amounts of soda and potash, the latter molecules are misbalanced particularly the potash fraction.

An outstanding feature of the potassic rocks from Port Cygnet, is their very low magnesia content which according to Helz's experiments (op. cit.) can be explained by partial melting, not involving a magnesium bearing phase.

But in an eclogitic model, sodium required for the alkaline rocks has to be obtained by the breakdown (melting) of a magnesian mineral which must cause a significant amount of magnesia to partition into the melt and eventually crystallise in a suitable phase.

There is no evidence of increased magnesia at Port Cygnet and this is taken to further demonstrate the unlikely role of eclogite as a parent of the Port Cygnet.

As this model is based on an initial alkali basalt it seems that an unnecessary step (i.e. eclogite formation) is involved and leads to a more complicated model.

There seems little evidence favouring Miller's R.E.E. model for the Port Cygnet alkaline rocks, on the basis of no direct evidence of an eclogitic parent, low initial strontium isotope ratio, higher (>2000 ppm) of trace strontium, rather greater relative amount of potash and the small complex relative to those quoted by Miller. The rocks may also be too undersaturated. Thus a granitic or eclogitic source for the Port Cygnet rocks is not favoured and leads to a model based on an alkali basalt equivalent with an undersaturated feldspathic component as a source of the alkaline rocks. The chondrite normalized R.E.E. pattern for the sanidine rocks is similar to alkali basaltic patterns (Haskin and Paster, 1976).

If the feldspathic part of this was completely melted then no significant europium anomaly would be produced (Hanson, 1978). With separation of a calcic plagioclase and pyroxene the light R.E.E. group would be enhanced, the europium anomaly suppressed (Hanson, 1978; Larsen, 1979), strontium accumulated and niobium and zirconium depressed which would empirically satisfy most of the requirements of the sanidine rocks from Port Cygnet.

In addition, according to the work of McCallum and Charette (1978), a residue containing aluminium and titanium would lead to a depletion of niobium in the parent melt fraction.

The melting of the alkali feldspathic fraction of a rock similar to the Mt. Porndon basanite, but with greater undersaturation and with the removal of a calcium-rich plagioclase, would be compatible with the requirements for the formation of the sanidine rocks.

Evidence of a Parent Material in the Port Cygnet Area

If the syenites have been derived from some parent material, there should be a more mafic associated feature at Port Cygnet by virtue of the relatively low concentration of iron oxides and very low amount of magnesia present in all rocks except for those in which amphibole is present. If the proposal that the Port Cygnet syenite porphyries have had, in part, an origin from partial melting of the quartzo-feldspathic components of an amphibolite now represented by the inclusions from Mt. Windsor, then there should also be a mafic hornblendite with a relative enrichment of iron and magnesium and impoverished, particularly in feldspathic component, as a complementary rock beneath Port Cygnet.

Surface gravity and magnetic surveys have been conducted over the Cygnet area (Leaman and Naqvi, 1967) and have not revealed any large anomalies which might be ascribed to an underlying body. The magnetic survey detected localized surface features associated with the hybrid rocks at Regatta Point and another feature of surface occurrence in the estuary of Port Cygnet (Leaman, 1967, 1977). While these are very intense, up to 1500 gammas, it is not considered that these would be detected on a high level aerial survey. However there is a general magnetic high over Port Cygnet with a maximum surface anomaly of approximately 2800 gammas. Leaman and Naqvi (1967) suggested

an anomaly due to altered dolerite at a shallow depth but were not very confident as to how deep it might be. Leaman (1977) also found evidence that there may be a deep seated magnetic anomaly beneath Port Cygnet.

An aeromagnetic survey of Tasmania by the Australian Bureau of Mineral Resources (Finney and Shelley, 1966) included one traverse (no. 18) at 3000 metres which crossed the Port Cygnet complex and also covered Tasman Peninsula to the east where gravity indicates large dolerite feeder channels with 300 metres of dolerite exposed on Tasman Island (Fig. VII-5).

The traverse showed a large anomaly of 250 gammas over Port Cygnet, but no significant anomaly over Tasman Peninsula. This is one of the largest anomalies observed throughout Tasmania. Dolerite also occurs abundantly in areas around Port Cygnet (see attached geological map of Tasmania), thus there is some suggestion of a body containing a significantly greater amount of magnetic minerals than does dolerite in the area. Gabbros and basalts could be expected to have a similar pattern to that of dolerite. An iron-rich amphibolite or hornblendite beneath Port Cygnet could provide a magnetic signature similar to the one observed. A magnetite body or a magnetite-bearing ultramafic body could also cause the same characteristics. The anomaly represents the maximum part of an anomaly bearing approximately southwest-northeast with areal dimensions at least 50 km x 20 km, and of adequate volume to supply the melt fraction proposed to contribute to the formation of the syenite porphyry.

The survey of Finney and Shelley (op. cit.) also showed another anomaly similar to the Port Cygnet feature but occurring in the Savage River area, North West Tasmania, where there is an ore deposit of magnetite associated with amphibolite (Coleman, 1976), bordering an ultramafic bearing Cambrian ophiolite complex (Brown et al., 1980). The source of the Port Cygnet anomaly could represent a similar association.

While the surface geology of Tasmania shows no amphibolite younger than Cambrian, another possibility is that fractionation of the Tasmanian Upper Devonian granitoids could have led to the derivation of a concealed hornblende-plagioclase restite acting as a parent for the Port Cygnet alkaline rocks. The Cambrian amphibolite is preferred on the grounds of its metamorphic texture, low rubidium value, and the initial strontium isotope ratios which for a granitic derivation would have 0.706 as their lowest value (Cocker, 1977). The precise interpretation of the Port Cygnet anomaly is difficult but could represent a body somewhere between 7 km to 15 km below the surface.

A gravity survey conducted by Leaman and Naqvi at Port Cygnet was aimed at determining the structure of dolerite intrusions in the area; however these authors point out (p.77) that the residual Bouguer gravity of 4-5 mgals might also be due to a basic or ultrabasic intrusion in the basement rock. Furthermore they point out that the magnetic and gravity anomalies are quite probably related.

Thus the evidence is that a concealed mafic-ultramafic body, not dolerite, which could be associated with the formation of the alkaline rocks, may exist at depth beneath the Port Cygnet area. The amphibolite inclusions have been suggested as one parent component of the syenite porphyries with the parent of the sanidine rocks as the other. For similar reasons the residual material from the formation of the sanidine rocks, must also be mafic-ultramafic but whether it is now present in the crust or sub-crustal cannot be determined.

The Depth of Formation of the Alkaline Rocks

Assuming that the alkaline rocks formed by some two stage process, and have been derived from mafic parental rocks, under conditions of water saturation ($P_{H_2O} = P_{total}$) (e.g. Bailey in Bailey and Macdonald, eds. 1976, p.88) on the basis of the simple mineralogy and flow textures,

an estimate of their depth of formation may be made. In a water saturated environment with the melt on a negative sloping curve there may be difficulty in the melt rising to higher levels in the crust. This restriction can be overcome if the system is heated beyond the temperature required for the equilibrium curve at a particular pressure. This can lead to a relative undersaturation of the system but allows it to rise to higher levels before intersecting the crystallization curve.

Similarly, for the Port Cygnet rocks there has probably been a degree of superheating which has allowed their intrusion relatively high into the crust. A consequence of their saturation and negative slope melting curve however is that they are emplaced as intrusives with no evidence of lava flows or surface activity in the area because loss of vapour at lower pressures leads to a higher melting point for the system.

As the evidence from the grey matrix rock (CY74) shows calcite reaction rims on melanite garnet the $f\text{CO}_2$ was low at the time of formation of the primary alkali melt with this phenomenon showing a change in $f\text{CO}_2$ at a later stage possibly due to minor contamination since the initial strontium isotope ratios indicate this to be a mixed rock.

While the presence of other vapour phases (e.g. CO_2) will reduce $P_{\text{H}_2\text{O}} < P_{\text{total}}$ and consequently alter phase boundaries, no CO_2 bearing fluid inclusions have been identified.

Most inclusions occur in the syenite porphyries and are represented by amphibolite (most abundant) with quartzite, some epidote, and rarely marble. This group is representative of the crustal environment. The size and degree of development of the syenite porphyry phenocrysts is not as great as those of the sanidine porphyry where the evidence

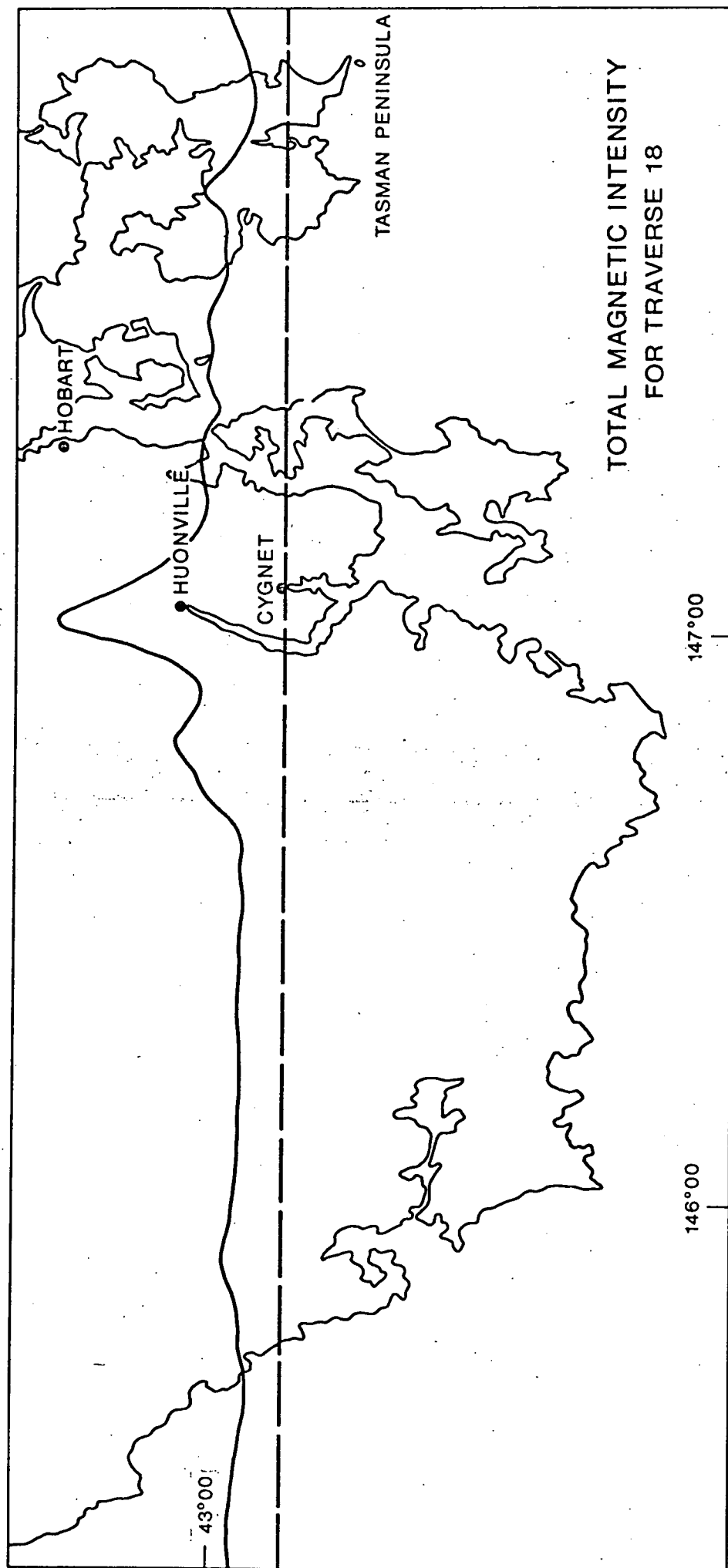


Figure VII-5 Aeromagnetic survey traverse line 18 with its magnetic profile from Finney & Shelley (1966). Total magnetic intensity of the anomaly is 280 gammas.

is of a deeper magma chamber where euhedral sanidine crystals grew with time such that successive intrusions of the sanidine bearing rocks contain larger phenocrysts (e.g. the increasing phenocryst size as shown at Holland's Quarry, Pl. 2).

The sanidine porphyries lack inclusions with the allanite inclusion (Pl. 31) the only one observed occurring in these rocks. The iron-muscovite inclusions in X50 suggest a crustal environment, and as this dyke does not have a well developed porphyritic texture the few phenocrysts in this rock have developed somewhat higher in the crust.

The inclusion of epidote with its reaction rim and feldspar overgrowth, in CY76, presumably represents epidote taken from the country rocks. Liou (1973) has determined the stability of epidote, with fO_2 defined by the hematite-magnetite buffer, to 748°C at 5 kbar. Bird et al. (1980) find similar results with the possibility of extrapolation to about 800°C at 6 kb corresponding to a depth of 22 km which could be regarded as the maximum depth at which the syenite porphyry began to crystallize. This would be on the high heat flow geotherm (Fig. VIII-1) at 800°C and above the alkali syenite minimum melt assuming a smooth curve. The minimum depth of crystallization would then be about 6 km (Fig. VIII-1) and the true depth of formation somewhere between these extremes, with the coarser syenite porphyries (which include the epidote bearing CY76) possibly forming at the greater depth or simply remaining longer in the magma chamber.

As the micaceous inclusions in X50 are closer to muscovite in their compositions their maximum stability temperature would be approximately 700°C (Velde, 1965) which would place the maximum depth at 20 km on the high heat flow geotherm. Since it is unlikely that the inclusions (both epidote and iron-muscovite) were derived from source rocks near the base of the crust, they would have been incorporated at some lesser depth with the enclosing sanidine in X50 growing over these at a later stage.

The only inclusion recorded in the sanidine porphyries is of allanite which is a crustal rather than subcrustal mineral. The optical and structural data for the sanidine phenocrysts suggest they were formed or annealed at a temperature near 900°C (Marfunin, 1966) which if extrapolated down the high heat flow geotherm (Fig. VIII-1) gives a depth close to 26 km. At this depth Mg-bearing phases are almost certainly present and from Helz's experiments (op. cit.) temperatures should not greatly exceed 1000°C otherwise significant amounts of magnesium would partition into the melt. This temperature could be regarded as maximum because the presence of other vapour phases (e.g. CO₂, HF) would reduce the temperature stability of sanidine. The evidence at this stage does not indicate a significant fCO₂ in the system, and the maximum temperature drop may have been around 100°C (Holloway, 1976). A reliable independent pressure indicator is not available.

The above data indicate that the parent melt was generated near the crust-upper mantle boundary. Presumably the finer grained dykes represent early formed material, some of which mixed with country rocks to form the garnet trachyte, iron-muscovite bearing rock and syenite porphyry, after being derived directly from the primary source and intruded without having gone through a static stage of crystallisation of sanidine phenocrysts.

Precisely where the sanidine phenocrysts were generated cannot be determined. They probably developed in a separate magma chamber (based on the lack of inclusions when compared with the syenite porphyries) however there is the possibility, because of their later intrusion that they may have crystallised in the chamber originally occupied by the syenite porphyry magma. This would then explain the grey groundmass rocks as an intermediate mixed rock as indicated by the strontium isotope data.

The non-appearance of leucite in the feldspathoidal rocks may place a minimum depth limit in the range of 5-6 km assuming water saturated conditions.

On the basis of the above and the low initial strontium isotope values it is proposed that the sanidine porphyries have been derived from partial melting of an undersaturated alkali mafic parent which occurs near the base of the crust at Port Cygnet. This may also constitute the deep seated source of the gravity anomaly suggested by Leaman and Naqvi (1967).

The Heat Source

In a summary of heat flow data for Australia, Sass and Lachenbruch (1979) delineated three main heat flow provinces. They came to the conclusion that heat flow from the mantle is uniform across the continent with variations in surface heat flow due to variations in the distribution of radioactivity for the western two-thirds of the continent, however in the eastern third of the continent where the natural radio-activity is not high enough, and the crust (≈ 40 km) is too thick for massive melting, high heat flows have been attributed to upper crustal intrusions more widespread than suggested by observed vulcanism.

At the present time Tasmania is part of a high heat flow (>1.5 hfu) band extending from the southeast part of the continent to Arnhem Land (Northern Territory). These conditions have probably existed throughout the Cenozoic era, and the Port Cygnet rocks could well have been associated with the precursor of the present situation.

The palaeomagnetic data for Ordovician limestones from the Ida Bay area, approximately 50 km southwest of Port Cygnet, give a pole position which falls close to the Late Cretaceous-Early Tertiary parts of the Australian apparent polar wander path (Sharples and Klootwijk, 1981).

These authors considered this to be a magnetic overprint reflecting "an increased geothermal heat flow during initial rift forming processes preceding opening of the Tasman Sea", as part of the break-up of Gondwana Land. This evidence would favour the extension into the Cretaceous of the molten substrate proposed by Sass Lachenbruch (op. cit.) and provides a tectonic association, so common with continental alkaline rocks.

Embleton (1981) also comments on a Cretaceous palaeomagnetic overprint pole for rocks in the Sydney Basin which he considered was related to initial rifting heralding sea floor spreading leading to the formation of the Tasman Sea. The removal of overburden associated with this, produced uplift thereby reducing temperatures in the upper crust of Eastern Australia in mid-Cretaceous times. If applied in the Tasmanian region this mechanism would explain the small amounts of melt generated in the Port Cygnet complex, the very similar Mt. Dromedary complex, N.S.W. (Boesen, 1964 - see appendix I) and also in the smaller Cape Portland complex (see later).

The evidence of widespread Tertiary basaltic lavas throughout southeast Australia and Tasmania is direct evidence of melting in the upper mantle, and the emplacement of the Port Cygnet rocks (and also the Cape Portland rocks) probably a consequence of an initial heating event that led ultimately to the Tertiary basaltic flows.

Note on Cape Portland Rocks

A very small complex of lamprophyric dyke rocks occurring near Cape Portland, at the northeastern tip of Tasmania, is about the same age as the Port Cygnet rocks (Jennings and Sutherland, 1969). Analyses of two of the more siliceous rocks of this complex, recalculated anhydrously, are compared with Helz's (1976) partial melt for an olivine tholeiite at 5 kbar pH_2O and 1045°C (Table VII-5). These are generally similar to the olivine tholeiite partial melts with the

major exception again being potash, markedly enriched in the lamprophyres, and TiO_2 , enriched in Helz's partial melt. It may be that in the natural environment with a relatively open system as opposed to an experimental one, particularly in the presence of volatiles, potassium may be preferentially concentrated. Of all the common rock forming elements, potassium has by far the largest ion and would be expected to be parted from its initial environment more readily than the other elements. The composition of the melt has been recalculated assuming potassium has been added as potash. Empirically the addition of potash to a melt derived in a similar manner to Helz's experiments may give rise to liquids comparable to those of the Cape Portland rocks. These may have formed from mixing of a potash rich liquid, having an upper mantle derivation, with a partially melted olivine tholeiite. The potash rich source may have been related to the Port Cygnet source, but much more detailed investigation is required to establish the truth of this proposition. It could also happen that partial melting of an olivine basalt at higher pressures than those applied by Helz (op. cit.) caused a greater amount of potash to become incorporated in the partial melt to improve the similarity noted above. No trace element or isotope data are available for these rocks which also may not represent the freshest specimens from this complex.

THE ORIGIN OF THE GARNET TRACHYTE

The most unusual rock from the Port Cygnet alkaline complex is the garnet trachyte originally described by Macleod and White (1898), and now in Chapter II above. The characteristic features of this rock are the presence of apparent rounded crystals of green epidote and brown spessartite with narrow rims of white potash feldspar, embedded in a dense dark grey aphanitic groundmass. Because of its unique character (Plate 12), and undoubted igneous origin, a model for its formation will be proposed.

TABLE VII-5

COMPARISON OF CAPE PORTLAND ROCKS WITH EXPERIMENTAL PARTIAL MELT

SiO ₂	57.85	54.84	55.50	54.27
Al ₂ O ₃	16.59	15.56	17.30	16.92
Fe ₂ O ₃	2.66	3.40	-	-
FeO	5.63	6.70	8.46	8.27
MnO	0.18	0.20	0.14	0.14
TiO ₂	0.68	1.13	2.21	2.16
CaO	6.35	7.94	9.25	9.04
MgO	3.07	4.12	3.36	3.29
Na ₂ O	3.58	2.99	2.80	2.74
K ₂ O	3.17	2.89	0.71	2.91
P ₂ O ₅	0.38	0.72	0.28	0.27
	<u>100.14</u>	<u>100.49</u>	<u>100.01</u>	<u>100.01</u>
<div style="display: flex; justify-content: space-between;"> <div style="width: 20%;"> Sphene-augite- hornblende spessartite (anhydrous from Jennings & Sutherland 1969) </div> <div style="width: 20%;"> Hornblende- porphyrite </div> <div style="width: 20%;"> Olivine tholeiite pH₂O = 5 kb temp. = 1045°C (from Helz 1976) (partial melt) </div> <div style="width: 20%;"> +2.25% K₂O </div> </div>				

The origin of the epidote and to a lesser extent that of the spessartite is a problem, which has to be solved if the origin of the garnet trachyte is to be established. The major and minor element composition of this rock is given in Table VII-7. The notable features of the analysis are the large amount of MnO, small amount of Na₂O and the unusually high concentrations of lead (2552 ppm) and zinc (2030 ppm). The high concentration of MnO can only mean contamination of the original magma by manganiferous material or partial melting of a manganese-rich source. There is no other known process whereby a high MnO concentration can be built up in a melt. The question still arises as to whether the spessartite is a xenocryst or a true phenocryst.

Spessartite can be a primary constituent of alkaline rocks.

Epidote may be a constituent of alkaline rocks but it usually occurs as a late stage hydrothermal mineral or as an alteration product of earlier formed minerals. In referring to epidote-rich rocks as epidosites, Johannsen (1937) implied that these were derivative rocks formed by alteration rather than being of primary igneous origin and this is a generally accepted implication.

Other similar occurrences include the Kamloops garnet syenite which from the description is a melanite-bearing rock [Kwak (1964), quoted by Currie (1976, pp.141-143)], and hence not very different from the sanidine porphyries and the Galore Creek body described by Kerr (1948) as representing at least five intrusive phases. Brecciated phases of the Galore Creek syenites contain lenses and pods of intensely metamorphosed biotite-orthoclase-garnet-epidote rocks which are assumed to have been derived from surrounding volcanic rocks. Some of the latter rocks contain pseudo-leucite phenocrysts. Brown garnets and colourless garnets are present, but their compositions have not been determined. The epidote occurs associated with the alteration of the orthoclase.

The epidotes and spessartites of the garnet trachyte, apart from the feldspar rims, are isolated crystals with no evidence that they are alteration products of other minerals. If these are xenocrysts then it would be expected that other signs of their parent environment would appear in the rock. The evidence from syenite porphyry CY76, for example (Pl. 22), shows epidote as a xenocryst phase reacting with the magma to produce a protective rim of amphibole. In the case of the garnet trachyte the rim of potash feldspar could also act as a protecting layer to stabilize the mineral. The spessartites are commonly coated with a layer or accompanied by a crystal of pyrite which places a limit of about 742°C for this mineral in a low

pressure - low sulphur environment. Epidote may enclose spessartite and pyrite, but never the reverse (Pl. 12).

From the data of Bocke (1914) quoted by Winchell (1951) there would appear to be a miscibility gap between the pyralspite and ugrandite groups of garnets. Winchell suggests (op. cit.) that this gap could be bridged by manganese garnets because of the better size compatibility of manganese and calcium atoms. If the garnet molecular proportions are plotted on Bocke's diagram they fall well within the miscibility gap (Fig. VII-6). Smith and Albee (1967) have also drawn attention to this gap and have a spessartite garnet plotting within it.

Brown (1967) found spessartite garnets of metamorphic origin, in greenschist facies rock, from Eastern Otago, New Zealand, which also plot in this gap, but his minerals had a much smaller range in spessartite component (15-17 with one anomalous value at 70 mol.%), and probably did not represent an equilibrium situation on a small scale although overall the system was regarded as approximating equilibrium.

Although the garnets and epidotes apparently crystallized simultaneously, manganese is favoured by the garnet with little in the epidote. With so much MnO in the system the presence of the piemontite molecule in the epidote would have been expected. The mineral analyses are given in Table VII-6. From these data the following points emerge:

(a) the garnet cores are invariably richer in the spessartite molecule and poorer in grossular than the rims, suggesting crystallization from a melt which was being progressively depleted in manganese.

(b) manganese is a minor component in the epidote crystals whose Al/Fe^{3+} ratio varies from about 2.230 to 2.912.

(c) the iron prefers the epidote structure to that of the garnet with the partition coefficient being about 3.

Smith and Albee (1967) in describing the petrology of a piemontite-bearing gneiss at San Geronio Pass, California, found that in an

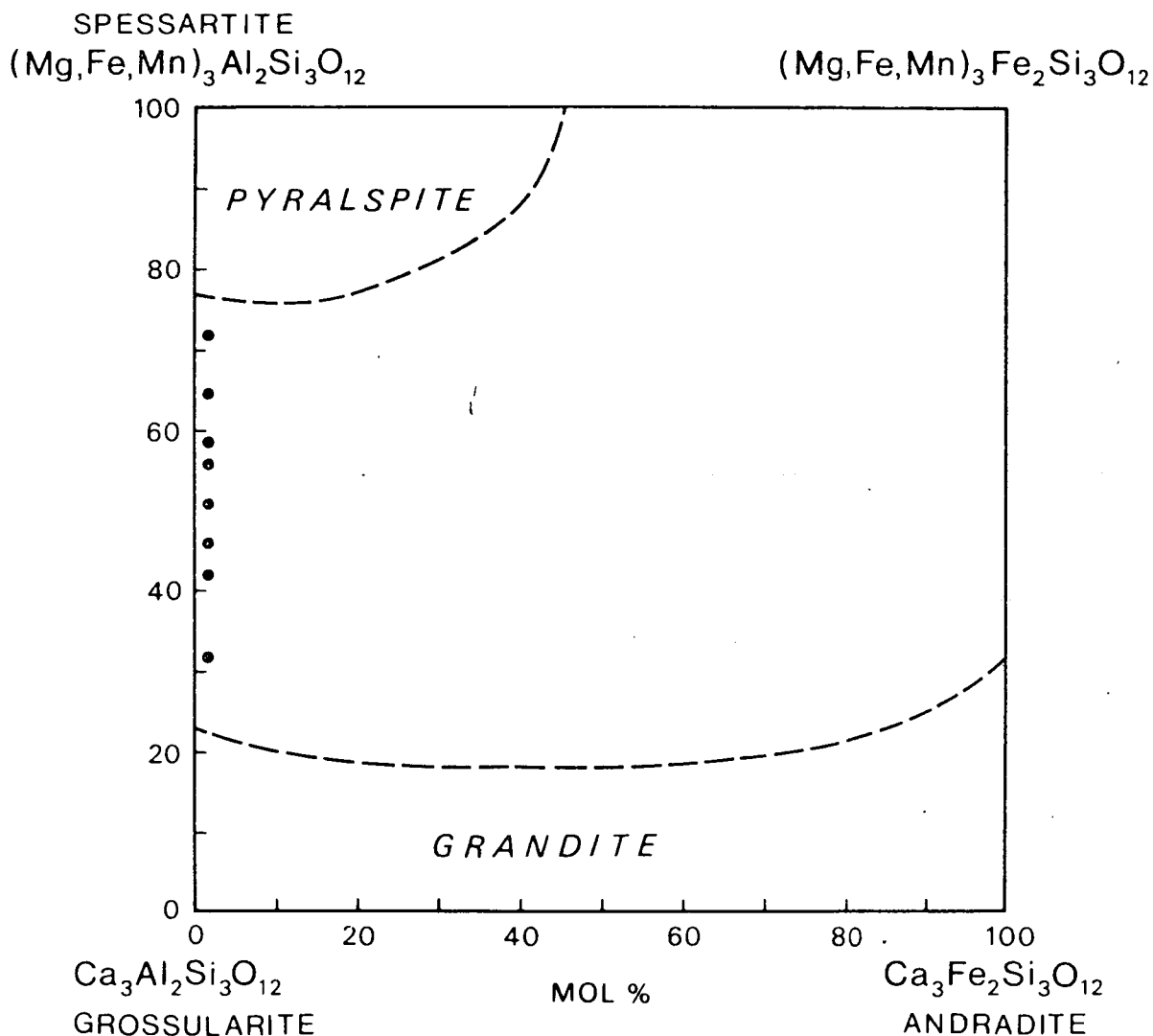
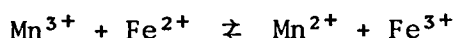


Figure VII-6 Compositions of spessartite garnets from garnet trachyte, plotted on the variation diagram from Winchell (1951).

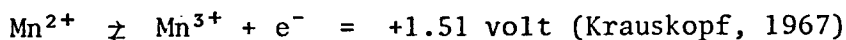
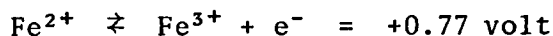
environment where conditions were less oxidising, epidote, rather than piemontite, crystallized together with a manganese-rich garnet. In less oxidised zones, trivalent manganese (necessary for piemontite to form) is absent. Iron and manganese with different valencies have been sharply partitioned in these rocks. By analogy the relatively large amount of manganese in the garnet trachyte melt would have

oxidised the iron present, which conversely keeps the manganese reduced, thus forcing iron into the epidote structure in preference to divalent manganese.

Under the conditions of formation of the garnet trachyte the partition of the elements would have reached equilibrium more rapidly than in the metamorphic environment. Smith and Albee report 1.30% MnO in epidote associated with spessartite containing 24.1% MnO, 11.5% CaO and 18.3% Al_2O_3 which may be compared with the analyses in Table VII-6. The buffering of the system by iron (indicated by iron chlorite in the unaltered groundmass) has kept the epidote relatively free of manganese which has almost exclusively formed the spessartite garnet. The influence of manganese on the iron in the melt would have been of the following type:



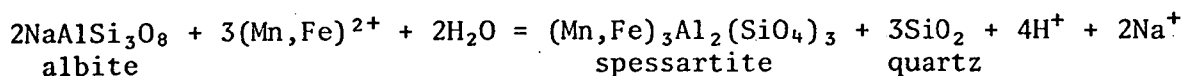
This equilibrium can be compared with the standard oxidation potentials in acid solution, e.g.



from which it follows that manganese would act as an oxidising agent in the above simple equilibrium. Thus with an excess of Fe^{2+} all the manganese would be reduced and this would have suppressed the piemontite molecule and favoured the formation of epidote and spessartite. The remaining iron is contained in the chlorite in the groundmass.

In offering an explanation of this rock it is useful to first consider the observations of Plimer (1974) who described metasomatic alteration of a roof zone from the Bega granite, N.S.W. Here a leucocratic soda syenite is surrounded by concentric spessartitic and sericitic alteration zones, with a range from spessartitized soda syenite to a rock composed entirely of spessartite garnets. The spessartite replaces the albite-rich plagioclase in the syenite.

Plimer envisaged the metasomatic spessartitization of the pre-existing rock by the reaction of Mn^{2+} and Fe^{2+} with albite to form spessartite with the removal of sodium. Plimer's proposed reaction is:



He considers that the potash feldspars take no part in the reaction.

An important implication of Plimer's model is that associated with the development of the spessartite there should be a concomittant decrease in soda which is significant when applying this model to the Port Cygnet garnet trachyte, where the low amount of soda has already been noted.

This deficiency of soda implies a mode of formation which may be similar to Plimer's mechanism. The anomalous character of this rock also extends to the trace elements where the high lead and zinc values are unique for the Port Cygnet rocks. While occasional sulphides, in addition to the pyrite associated with the spessartite, occur in the rock the fact that the feldspars in the matrix have a weak blue fluorescence strongly suggests that lead is incorporated in their structures. Also the high concentrations of these elements are greater than can be accounted for by the sulphides in the rock.

As stated earlier in Chapter VI, the unusual chemistry of the garnet trachyte may have been due to assimilation of a mineralized carbonate pod, e.g. Zeehan type (Solomon et al., 1981). The main feature of these carbonates is the high concentration of manganese with manganosiderite being a major component as well as sulphides of iron, zinc and lead. The Zeehan deposits occur in rocks which are underlain by Cambrian volcanics to the east. A deep drill hole at Glenorchy, a Hobart suburb about 60 km north of Port Cygnet, has shown the presence of similar volcanics (Leaman, 1975). It therefore seems

TABLE VII-6

Electron microprobe analyses of garnet and epidote from garnet trachyte.

	core	medial	rim	core	edge	core	edge	core	edge	core
Spessartites:										
Na ₂ O	0.33	0.32	0.34	0.50	0.51	0.47	0.25	0.41	0.00	0.32
MgO	0.42	0.32	0.42	0.38	0.31	0.38	0.23	0.34	0.22	0.00
Al ₂ O ₃	21.31	21.53	20.30	22.05	21.62	21.48	20.70	21.18	20.49	21.78
SiO ₂	38.00	37.85	38.37	38.04	38.27	38.18	38.42	38.07	38.02	38.34
CaO	11.72	14.72	20.95	12.52	14.29	17.89	19.77	16.77	24.65	13.94
TiO ₂	0.24	0.47	0.00	0.00	0.31	0.00	0.62	0.00	0.81	0.00
MnO	24.50	20.87	13.80	22.68	21.01	17.81	15.05	19.59	11.99	22.23
FeO	3.48	3.69	5.81	3.88	3.68	3.79	4.96	3.64	3.82	3.39
Total	100.03	97.17	103.60	102.96	99.23	101.36	101.15	102.32	101.66	99.91
Atomic proportions on basis of 24 oxygen:										
Na	0.101	0.098	0.105	0.152	0.157	0.143	0.077	0.126	0.000	0.099
Mg	0.099	0.075	0.098	0.090	0.072	0.089	0.054	0.079	0.052	0.000
Ca	1.993	2.489	3.531	2.119	2.412	3.012	3.322	2.835	4.127	2.357
Mn	3.295	2.789	1.839	3.027	2.804	2.370	1.999	2.618	1.587	2.971
Fe ²⁺	0.462	0.488	0.528	0.513	0.485	0.472	0.751	0.421	0.314	0.447
Total	5.930	5.939	6.101	5.901	5.930	6.086	6.103	6.079	6.080	5.874
Fe ³⁺	0.000	0.000	0.237	0.000	0.000	0.026	0.101	0.060	0.185	0.000
Ti	0.028	0.056	0.000	0.000	0.037	0.000	0.073	0.000	0.095	0.000
Al	3.986	3.979	3.763	4.106	4.014	3.974	3.826	3.940	3.716	4.051
Total	4.014	4.035	4.000	4.106	4.051	4.000	4.000	4.000	4.000	4.051
Al	0.000	0.026	0.000	0.000	0.000	0.003	0.000	0.000	0.058	0.000
Si	6.032	5.974	6.035	6.008	6.027	5.997	6.025	6.007	5.942	6.049
Total	6.032	6.000	6.035	6.008	6.027	6.000	6.025	6.007	6.000	6.049

TABLE VII-6 (continued)

O	24.000	24.000	24.000	24.000	24.000	24.000	24.000	24.000	24.000	24.000
Sp	56.33	47.75	30.67	52.65	48.57	39.71	33.29	47.15	26.45	51.45
Gr	34.07	42.61	58.82	36.86	41.78	50.46	55.32	43.54	68.67	40.81
Al	7.90	8.35	12.38	8.92	8.40	8.34	10.82	8.00	4.07	7.74
Py	2.00	1.20	1.63	1.57	1.25	1.49	0.90	1.31	0.87	0.00

Epidotes:

	1	2	3	4	5	6**
Na ₂ O	0.27	0.26	0.28	0.00	0.25	
MgO	0.00	0.00	0.31	0.00	0.00	0.10
Al ₂ O ₃	25.59	23.98	24.49	23.81	24.19	21.80
SiO ₂	39.47	38.99	39.35	39.44	39.25	
CaO	22.82	22.51	23.28	23.13	23.55	22.20
MnO	0.72	0.41	0.00	0.35	0.38	1.30
FeO*	11.14	13.64	12.30	13.06	12.38	15.10 (Fe ₂ O ₃)
Total	96.90	95.32	96.42	95.69	93.92	

Atomic proportions on basis of 25 oxygen:

Ca	3.849	3.847	3.947	3.940	4.008
Na	0.082	0.079	0.087	0.000	0.077
Mn	0.096	0.055	0.000	0.047	0.051
Mg	0.000	0.000	0.073	0.000	0.000
Total	4.027	3.981	4.107	3.987	4.136
Fe	1.467	1.819	1.628	1.737	1.644
Al	4.748	4.507	4.569	4.463	4.528
Total	6.215	6.326	6.197	6.200	6.172
Al	0.000	0.000	0.000	0.000	0.000
Si	6.213	6.219	6.228	6.271	6.234
Total	6.213	6.219	6.228	6.271	6.234

TABLE VII-6 (continued)

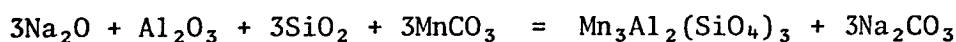
O	25.000	25.000	25.000	25.000	25.000
Al/Fe	2.912	2.230	2.525	2.312	2.478

* All iron as Fe^{2+} . Deficiency equal to $[(\text{Fe}_2\text{O}_3 \equiv \text{FeO}) + \text{OH}]$.

** Partial analysis of epidote from San Gorgonio Pass (Smith and Albee, 1967).

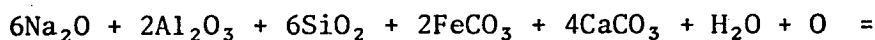
not unreasonable to assume that Zeehan-type carbonate pods may exist somewhere beneath the superficial Permian rocks at Cygnet. It can also be noted from Chapter VI that the ΔS^{34} value for the garnet trachyte is slightly greater than the other igneous rocks and could be consistent with assimilation of a hydrothermal sulphide such as Zeehan type sulphides (Both et al., 1969).

In deriving the exotic minerals by carbonate assimilation the following reactions can be postulated:

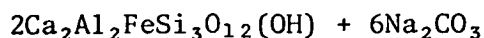


magma

spessartite



magma



epidote

Assuming, following Plimer (op. cit.), that the potash feldspar takes no part, then the above reactions, especially in the presence of water, will eliminate soda from the system in the form of soluble and stable sodium carbonate, leaving a rock ultimately deficient in soda. The addition of oxygen is necessary to oxidise iron as a requirement for epidote.

Because the strontium isotope data from Chapter VI indicate that the tinguaitite rocks could be representative of primary magma, the compositions of two of these (X44 and CY85A) have been compared with the garnet trachyte in Table VII-7. All iron has been calculated as Fe_2O_3 . If a potash magma assimilated carbonates equivalent to the following: 1.75% MnO , 1.10% CaO and 0.50% Fe_2O_3 , the garnet trachyte analysis may be recalculated as shown in the remaining columns of Table VII-7, assuming soda to have been displaced as postulated above. It can be seen that a reasonable agreement can be obtained and that the garnet

trachyte composition can be derived from the tinguaitite composition. The absence of large potash feldspar phenocrysts comparable with the tinguaitite, from the garnet trachyte implies that the melt was an early phase of the alkaline intrusion.

Experimental Test of the Model

To test the proposition that the garnet trachyte may have formed from assimilation of carbonates by a melt equivalent to X44 or CY85A, experiment (No. T860) was performed in the High Pressure Laboratory of the University of Tasmania. CY85A after having been fused to a glass by a preliminary melting, was crushed and mixed with the appropriate amounts of carbonate as specified above. An aliquot was sealed in a platinum capsule with an excess of water and then sealed within another capsule filled with ferric oxide to maintain an oxidising environment. The charge was held in a Boyd-England type solid-medium high pressure piston-cylinder apparatus at a temperature of 800°C and pressure of 6 kilobars for 72 hours after which the charge was quenched and examined by means of electron microprobe analysis. 800°C was regarded as the lowest temperature at which equilibrium could have been attained in this apparatus and 6 kb was taken as a probable pressure needed to stabilize epidote at such a temperature, although this apparatus is not regarded as being appropriate to carrying out buffered experiments where fO_2 and H_2O are critical parameters.

The experiment produced euhedral spessartitic garnet crystals and glass, implying formation above the solidus, whose compositions are reported in Table VII-8. No epidote was apparent. Other minerals that occur in the charge are potash feldspars and biotite which probably represent quench phases. Some of the feldspars contained a significant proportion of sodium in contrast to the low soda content

of those in the garnet trachyte. However, this was probably a consequence of the necessarily closed system of the apparatus rather than the open system which probably operated during the formation of the garnet trachyte.

The synthetic garnets are richer in the andradite molecule than the natural garnets which have more grossular molecule. Thus the experimental garnet has taken up the iron rather than aluminium and has also left the groundmass glass relatively richer in lime. If aluminium could be persuaded to enter the garnet in preference to iron then conditions for the formation of epidote would be more favourable with the large amount of lime in the glass. The presence of potassium, sodium and the apparent excess of silica in the analyses suggests there may be some included glass present, although this was not observed. There may also be a degree of hydration present, particularly as a result of the high proportion of andradite and grossular molecules present. With the entry of ferric iron into the garnet the cell size would have been increased and this may also have favoured the introduction of titanium which is somewhat higher in the synthetic than in the natural garnet. Addition of material to act as a sodium sink would improve the experiment.

Green (1977) has observed the formation of spessartite garnet as a residual phase in melting experiments on model pelitic compositions at pressures greater than 7 kb.

A summary of data on spessartite synthesis by Deer, Howie and Zussman (1962) suggests the mineral may be stable down to 500 bars and 500°C (for the aluminium-rich molecule). Thus the evidence is that, once formed, spessartite is stable over a wide range of physical conditions and in the particular rock from Port Cygnet might well be stable in the lower pressure, temperature regime which would probably favour epidote formation.

TABLE VII-7 Comparison of garnet trachyte and tinguaita analyses

Garnet trachyte	Recalculation assuming addition of MnO=1.75%, CaO=1.10%, Fe ₂ O ₃ =0.50%	Recalculation with Na ₂ O equivalent to Fe ₂ O ₃ +MnO+CaO	Tinguaite
			X44 CY85A
SiO ₂	57.42	55.55	59.39 55.78
Al ₂ O ₃	21.01	20.32	22.70 20.15
Fe ₂ O ₃ *	4.23	4.09	3.38 4.57
MnO	0.14	0.14	0.16 0.16
TiO ₂	0.39	0.38	0.28 0.35
CaO	1.58	1.53	1.51 1.51
MgO	0.35	0.34	0.01 0.20
Na ₂ O**	1.81	4.97	4.30 6.31
K ₂ O	10.10	9.77	8.11 10.31
P ₂ O ₅	0.09	0.09	0.00 0.00
Loss	1.55	1.50	0.90 0.84
Total***	98.70	98.68	100.75 100.20

* all iron as Fe₂O₃ ** Na₂O = (MnO x 0.874) + (CaO x 1.105) + (Fe₂O₃ x 1.164)
*** +(Sr+Ba+Pb+Zn) = 1.24% for trachyte.

Trace elements (ppm):

Zr	107	381	150
Sr	4636	4637	4279
Rb	307	135	238
Zn	2030	89	178
Ba	3059	3457	2825
Pb	2552	62	30

Hsu (1968) found that hydration of spessartite to form hydro-spessartite with OH replacing SiO_4 began at about 600°C , with OH being increasingly accepted as the temperature decreased. A total analysis of the spessartite garnet from the trachyte (Ford, 1967) shows (Table VII-9) negligible H_2O^+ thus indicating a crystallization temperature above 600°C . According to Hsu (op. cit.) spessartite is not very sensitive to fO_2 variations and in his experiments it was stable up to 930°C at 500 bars fluid pressure.

The presence of anhydrous spessartite garnets in low temperature greenschist facies rocks (Hutton, 1957) appears to contradict the experimental results of Hsu (1968), however, it must be remembered that spessartite is structurally related to the small-ion - small-cell garnets, having Mg, Fe and Mn as their characteristic cations, rather than to the larger-ion - large-cell group represented by the Ca-bearing garnets.

The small-cell garnets do not hydrate but with the larger Mn ion and consequent unit cell increase some small degree of hydration might be possible for spessartite. However, in a low temperature regime where pressure may or may not be a significant factor the formation of a hydro-spessartite is not favoured.

It is of value to note that of all garnet molecules, spessartite has the highest coefficient of thermal expansion and that the extension curve changes slope to a lower rate at about 500°C , i.e. the rate of extension is at a maximum near this temperature and falls gradually for higher temperatures. It is more than co-incidental that Hsu's experimental garnets hydrated near this temperature.

Thus the experimental results could demonstrate a hydrous phase stable around 500°C - 600°C which would be below the temperature of crystallization in the garnet trachyte due its quick cooling, e.g. fine grained groundmass, which is approximately 40 cm at maximum thickness. Hence the inference is that Hsu's experiments still apply here.

The above summary would then place the formation temperature for the spessartite from Port Cygnet somewhere in the range from 742°C to 930°C .

It may be possible, with other apparatus, to operate at a lower temperature and pressure and produce epidote as well as garnet.

TABLE VII-8

Electron probe microanalyses of synthetic garnets and a feldspar from experiment T860.

	Synthetic garnets					K-feldspar
Na ₂ O	0.00	0.00	0.00	0.61	0.00	2.29
MgO	0.31	0.32	0.37	0.51	0.31	0.00
Al ₂ O ₃	14.03	12.73	13.37	15.82	11.69	18.88
SiO ₂	36.75	36.64	36.51	37.30	37.02	63.28
K ₂ O	0.24	0.29	0.20	0.38	0.29	12.42
CaO	17.91	18.30	18.62	17.29	21.70	0.96
TiO ₂	1.97	2.01	2.02	1.08	1.35	0.48
MnO	16.30	16.33	15.52	15.94	12.81	0.33
FeO	12.50	13.40	13.39	11.07	14.83	1.36
Total	99.40	99.57	101.06	98.91	100.03	101.34

Atomic proportions on basis of 24 oxygen

K	0.000	0.060	0.044	0.078	0.061	1.463
Na	0.000	0.000	0.000	0.194	0.000	0.410
Mg	0.076	0.078	0.092	0.124	0.077	0.000
Ca	3.168	3.266	3.310	3.024	3.879	0.095
Mn	2.176	2.304	2.180	2.204	1.810	0.026
Fe ²⁺ *	0.480	0.285	0.374	0.376	0.073	0.105
Total	5.900	5.993	6.000	6.000	5.900	2.099
Al	2.732	2.500	2.614	3.042	2.298	2.056
Ti	0.244	0.252	0.252	0.132	0.170	0.033
Fe ³⁺ *	0.831	1.109	0.989	0.681	1.331	
Total	3.807	3.861	3.855	3.855	3.856	2.089
Si	6.068	6.102	6.040	6.086	6.174	5.844
O	24.000	24.000	24.000	24.000	24.000	16.000

* Fe²⁺-Fe³⁺ arbitrarily divided between sites

And.	21.14	28.04	24.91	17.84	34.20
Py.	1.29	1.31	1.54	2.17	1.32
Sp.	36.88	38.83	36.60	38.47	30.99
Gr.	23.17	18.25	21.44	31.49	25.48
Al.	13.02	4.80	6.28	6.56	1.25
Sch.	9.40	8.76	9.23	3.46	6.76

TABLE VII-9

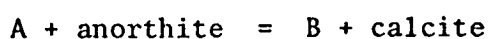
ANALYSIS OF SPESSARTITE GARNET-COMPOSITE FROM FORD (1967)

SiO ₂	36.60
TiO ₂	0.34
Al ₂ O ₃	20.50
Fe ₂ O ₃	0.70
FeO	2.70
MnO	26.00
CaO	13.10
Na ₂ O	0.00
K ₂ O	0.00
P ₂ O ₅	<u>0.14</u>
Total	<u>100.08</u>

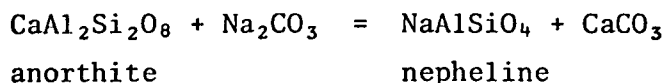
However, although the precise formation of epidote must still be conjectural at this stage, it would appear that the model proposed for the formation of the spessartitic garnet is feasible for this particular rock.

Formation of the Epidote

With the depletion of the magma in sodium, an albite-rich plagioclase cannot form and the composition is pushed to the anorthite molecule which is less stable in the presence of water and CO₂. The water present in the magma is not readily accepted into the garnet structure because of its relatively small cell size of 11.690 A.U. (Ford, 1967) due to the spessartite molecule. Rock (1976) has suggested that calcic plagioclase may be present in alkaline rocks associated with gabbroic rocks but absent from those associated with carbonatites, and these differences are a function of partial pressure of CO₂ with the involvement of equilibria of the form:



For example the spilite reaction of Eskola, Vuoristo and Rankama (1937):



The influence of water and carbon dioxide does not favour calcic plagioclase. Alumina has also been removed in the spessartite formation thus suppressing zoisite. These factors would be empirically expected to favour epidote formation.

TABLE VII-10

Microprobe analyses of core plagioclase and zeolite alteration in garnet trachyte

Plagioclase core (Labradorite)		Zeolite rim (Chabazite)
Na ₂ O	5.72	3.40
Al ₂ O ₃	28.11	20.35
SiO ₂	56.78	49.85
CaO	9.40	6.68
K ₂ O	0.00	1.12
H ₂ O*	0.00	18.60
Total	<u>100.01</u>	<u>81.40+</u>

Cations on basis of 16 Oxygen

Na	0.992
Ca	0.901
Al	2.964
Si	5.079
O	16.000

Cations on basis of 72 Oxygen

Na	3.233
Ca	3.510
K	0.702
Al	11.759
Si	24.427
O	72.000

*H₂O by difference, + Total less H₂O

The stability of epidote has been studied extensively by Holdaway (1972), Liou (1973), Helgeson et al. (1978) and Bird and Helgeson (1980). Although these studies have been in hydrothermal systems at conditions designed to model the formation of epidote during metamorphism, it is obvious that $f\text{O}_2$, pressure, temperature, and co-existing garnet phases

are important. With fO_2 defined by the hematite-magnetite buffer under the conditions used by Liou, epidote is stable up to 748°C at 5 kb ($P_{H_2O} = P_{total}$) and drops to 635°C at 2 kb, with grandite garnet and anorthite as equilibrium silicate phases. From the summary of data given by Helgeson et al. (1978) it is possible for epidote to exist up to about 800°C and 6 kb where $P_{H_2O} = P_{total}$. These conditions are equivalent to a depth of 23 km which is approaching the base of the crust at Port Cygnet, but is too deep for the occurrence of a carbonate ore deposit.

If the original primary alkaline magma was contaminated with a Zeehan-type carbonate, the stratigraphic column for Tasmania would place it at a maximum allowable depth of 7 km which is approximately equivalent to 2.5 kb. At this pressure the maximum temperature for epidote according to Liou (1973) is close to 700°C . This is consistent with the textural sequence of crystallization of epidote after pyrite which would have a maximum stability temperature close to 770°C at this pressure. According to Bird and Helgeson (1980) provided there is sufficient iron present, an increase in fCO_2 will favour epidote formation. Thus growth of epidote phenocrysts (which are not as abundant as the spessartite) at a temperature around 700°C is thus possible with the addition of CO_2 to the volatile component also assisting in the emplacement of the dyke. Increasing fO_2 is important in enlarging the epidote stability field. For the hydrothermal system Liou states (p.409) that "introduction of albite component into the equilibrium ... would drastically displace the equilibrium boundary toward lower temperatures". Thus in the case of the garnet trachyte it is deduced that the removal of sodium would have encouraged a higher temperature for the stability of epidote. When compared with Liou's results the epidotes from the garnet trachyte tend to be relatively alumina-rich with Al varying from 4.46 to 4.75 and Fe^{3+} from 1.47 to 1.82 on the basis of 25 oxygen.

The latest work on epidote stability is by Bird and Helgeson (1980) who calculated the stability of epidote in a hydrothermal system involving, among others, grandite and plagioclase solid solutions. They have established that epidote may be in equilibrium with plagioclase *inter alia* only at low activities of CO_2 hence carbonate assimilation by the magma would not favour crystallization of an anorthite rich plagioclase. This is consistent with the observation of a zeolitized labradorite rim (Pl. 44), described in Chapter II now representing an original alteration of the mineral. The presence of the relict supports the proposal that elimination of sodium would initially favour the formation of a calcium-rich plagioclase, with the replacement of the feldspar by zeolite further supporting the model by demonstrating the instability of the labradorite in this environment (Table VII-10). In their work, Bird and Helgeson (op. cit.) found that epidotes with greater iron contents have wider stability fields at higher temperatures but in the hydrous system involving equilibria with grossularite and anorthite the maximum temperature for epidote stability is just over 600°C .

From the data presented above it can be seen that the stability ranges of spessartite and epidote do overlap but increasing temperature of formation requires a higher confining pressure for epidote because of its hydrous nature. If assimilation of a carbonate pod in Palaeozoic rocks by tinguaitic magma is the *raison d'etre* for this rock, the melt must have been static in the crust for a period of time sufficient to growth the phenocrysts. Many of the spessartite crystals are associated with crystals of pyrite, some of which occur as overgrowths and in turn may be enclosed by epidote (Pl. 12). In a low pressure environment pyrite will lose sulphur at 742°C (Arnold, 1962) with an increase of $14^\circ/\text{kbar}$ (Kullerud and Yoder, 1959). Thus the spessartite would have substantially finished crystallizing by this temperature which is just below the maximum temperature for epidote stability at 5 kb (Liou, op. cit.). If the epidotes formed from the same magma that had produced the

spessartites, it would be expected that there would be a small partitioning of manganese between these two phases. From the data of Table VII-6 it is apparent that there has been a partitioning of manganese between these suggesting that they are phenocrysts in the same magma. With the spessartite forming before the epidote the potential for anorthite formation would have been depressed by the removal of aluminium in the garnet and the presence of volatiles including CO_2 in the magma which ultimately favour crystallization of epidote.

The conclusion is that the garnet trachyte contains primary phenocrysts of spessartite and epidote with the latter forming at a later stage. The garnet trachyte has then crystallized a primary igneous epidote which is most unusual for this mineral which normally occurs as a late stage alteration product in this environment. A feature of the model requires that the melt was static for enough time in which to grow two sets of phenocrysts.

ORIGINS OF OTHER ROCKS

The Brown Matrix Rocks

These rocks, described previously in Chapter II, are found at only two small outcrops at Port Cygnet, and contain subhedral oligoclase-andesine crystals with potash feldspar overgrowths, together with discrete sanidine crystals. Because of their relatively high potash content, and the presence of sanidine, these rocks have been plotted with the sanidine rocks in the general chemical diagrams. As already outlined in Chapter II the interpretation is that they represent a late stage fractionation of the syenite porphyries, with potash feldspar overgrowths probably representing a resorption of the earlier plagioclase and at least representing crystallization along the cotectic line near the feldspar minimum. Their Ab-Or-An normative compositions are distinctly

different from the syenite porphyries. In addition they are markedly impoverished in strontium and enriched in cesium relative to the syenite porphyries, and their chondrite-normalized rare earth element patterns have negative europium anomalies as distinct from the more uniform pattern of the syenite porphyries (Fig. V-18). These observations would be consistent with fractionation of the syenite porphyry melt with crystallization of plagioclase leaving a strontium-depleted residue with a chondrite-normalized negative europium anomaly (compare oceanic trachytes). The barium values show no trend to suggest that fractionation of potash feldspar has occurred. This may have been the last material in the magma chamber leading to intrusion as dykes with flow textures similar to the sanidine-only phenocryst dykes, rather than the granular textured groundmass of the syenite porphyries.

The Hornblende Porphyry

This rock type is best represented in CY91 from Petchey's Bay but also occurs as finer grained varieties from the eastern part of the Port Cygnet Complex (e.g. CY2). Because of the relationships demonstrated in Figs. III-10 - III-13, the hornblende is considered to be recrystallized from a source related to the amphibolite inclusions from Mt. Windsor. The source of the pyroxene is not easy to determine but its occurrence as disaggregated patches and inclusions in the rock is indicative of an alternative source. The hornblende and pyroxene probably have a common source but this cannot be unequivocally established at this stage.

CHAPTER VIII

SUMMARY AND CONCLUSIONS

A summary of the data and discussions of the earlier chapters is given in the following paragraphs.

ALKALINE ROCKS

The alkaline rocks of Port Cygnet were intruded into Permian and Jurassic country rocks during the late Cretaceous as numerous small dykes and sills.

Many of the alkaline rocks are slightly oversaturated syenite porphyries with oligoclase-andesine as the main phenocryst phase. Others are undersaturated and sanidine-bearing, varying from fine-grained non-porphyritic varieties to rocks with large euhedral sanidine phenocrysts exhibiting pronounced flow textures.

Direct intrusion of the feldspathic melt without a static period for phenocryst formation produced fine-grained dykes lacking phenocrysts and carrying sanidine crystals only in the groundmass.

The porphyritic and pseudo-cumulate texture of some of the syenite porphyries shows initial slow crystallization in a magma chamber followed by injection into the present day intrusive forms.

Field evidence shows the sanidine porphyries intruded after the syenite porphyries, with the phenocryst size being larger for later intrusions.

The sanidine porphyries may be divided into green groundmass and grey groundmass groups correlated with presence or absence of aegirine. Variants of these include iron-mica inclusion-bearing and scapolite-bearing rocks and a unique garnet epidote trachyte.

Other unusual rocks are those with a brown matrix and mixed feldspar phenocryst assemblage, and the rocks with phenocrysts of euhedral hornblende (hornblende porphyry).

Major Element Data

The agpaitic index for the alkaline rocks is less than unity hence they are miaskitic rather than agpaitic syenites.

The major element chemistry is dominated by potassium in the sanidine porphyries but less so in the syenite porphyries.

The major element compositions of the syenite porphyries are close to the average alkali syenite of Nockolds (1954), but not the average syenite of Le Maitre (1976).

The major element compositions of the sanidine porphyries are close to the Juvet-type syenite of Nockolds (1954) and nepheline syenite of Le Maitre (1976).

Major element compositions for the main rock types can be matched by simple mixes of amphibolite matrix, tinguaite (green matrix rocks), syenite aplite, and amphiboles from the amphibolite.

Plots of potash, silica, ferric oxide and to a lesser extent soda against the Thornton-Tuttle D.I. show parallel rather than common trends suggesting two groups of rocks with no simple differentiation mechanism relating them. Trace elements also show parallel trends for the syenite porphyries and sanidine porphyries with regard to rubidium, cesium, strontium, barium, scandium, gallium and zinc. Harker plots do not show fractionation trends but rather two rock groups.

The Bailey-Macdonald plots show the alkaline rocks plotting as two adjacent groups and imply no feldspar fractionation.

On the nepheline-quartz-kalsilite triangle the syenite porphyries and the sanidine porphyries plot as two groups straddling the feldspar thermal divide.

The normative albite-orthoclase-quartz triangle and the nepheline-kalsilite-quartz triangles show the syenite porphyries tending to plot nearer the higher pressure minima but the core-rim compositions of the feldspar phenocrysts are not consistent with an equilibrium system.

The above normative plots for the syenite porphyries tend towards a high pressure minimum, in a water-saturated system of 5 kb.

This could represent a maximum depth of crystallization of 20 km, near the upper limit of plagioclase stability (Fig. VIII-1) but it is more likely crystallisation occurred somewhat higher in the crust.

Minor Element Data

Concentrations of the trace elements rubidium, strontium, barium, scandium, gallium and niobium in the syenite would also be consistent with mixes of amphibolite and tinguaitite compositions.

The light rare earth chondrite-normalised patterns of the syenite porphyries would be consistent with a mix of the amphibolite matrix and sanidine porphyry patterns.

The chondrite normalised rare earth element patterns for the alkaline rocks have negligible europium anomalies, also suggesting no feldspar fractionation to produce syenite porphyries and sanidine rocks from a common parent magma.

The brown matrix rocks do have chondrite normalised rare earth patterns with significant europium anomalies indicating feldspar fractionation. Reinforcing this conclusion, the trace concentrations of strontium and barium are typical of non-plagioclase fractionated sequences with the exception of the abnormally low strontium concentrations of the brown matrix rocks, apparently a result of fractionation.

The high concentrations of cesium (6 ppm in CY61 and 56 ppm in CY92) are also consistent with a fractionation process for the origin of these rocks. These are very high values for syenite porphyry derivatives.

The trace element and major element concentrations of the sanidine rocks are empirically similar to the felsic fractions of undersaturated alkali basaltic rocks.

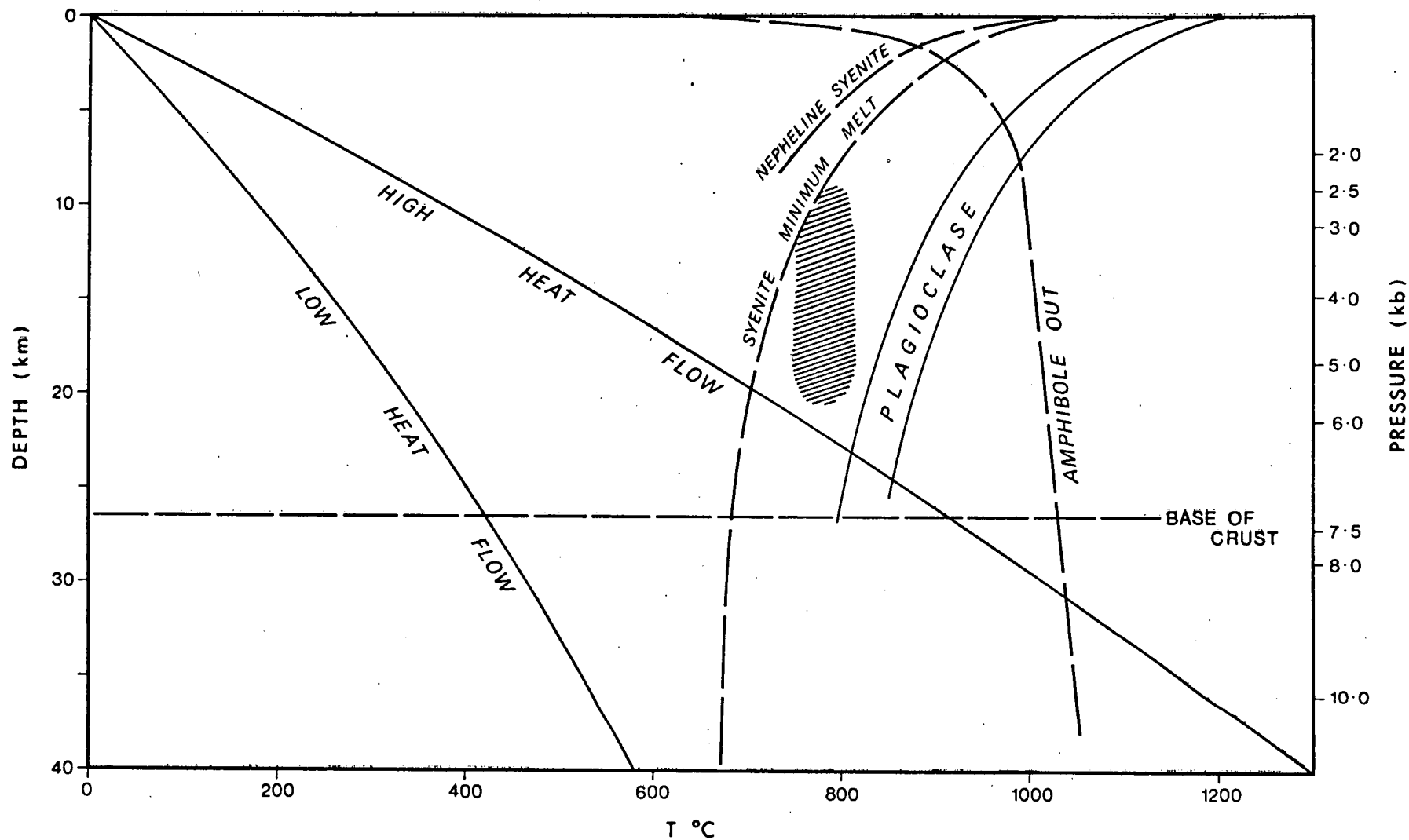


Figure VIII-1 Possible zone of initial formation of syenite porphyry. Zone of plagioclase melting is shown for $P_{H_2O} = P_{total}$. The high heat flow boundary is drawn for a thermal gradient of $35^\circ\text{C}/\text{km}$.

Whilst most high cesium values are regarded as of crustal origin, the concentration of this element in the sanidine rocks is most likely due to vapour phase concentration.

The source of the potassium-rich rocks was depleted in niobium and zirconium which would be consistent with a basaltic source if these elements were partially incorporated into ferromagnesian minerals, magnetite and ilmenite of the parent rock.

Mineralogical Data

The feldspar data are not consistent with the co-existing feldspar geothermometers of Stormer and Powell & Powell and do not demonstrate equilibrium systems, nor does the distribution of feldspar compositions on the Seck plot, however they do indicate empirically, a higher crystallization temperature for the sanidine porphyries than for the syenite porphyries.

The compositions of sanidines on the Seck plot suggest 900°C as a minimum formation temperature for these minerals, consistent with the structural states and optical properties of the sanidine crystals which also suggest a crystallization temperature of 900°C.

If the temperature of crystallization of the sanidine phenocrysts was 900°C, this gives a source at a depth of 25 km on the high geotherm provided there was no superheating of the system.

The compositional variation with respect to iron, potassium and sodium of the amphiboles shows an evolutionary relationship between the amphiboles of the amphibolite inclusions, syenite porphyry and the hornblende porphyry.

Isotopic Data

The initial strontium isotope ratios show the presence of rocks of

two distinct sources but linked by a mixing curve.

The mixing curve has the green matrix rocks (tinguaite) at one limit with the other defined by the feldspathic matrix of the amphibolite inclusions.

The low initial strontium isotope ratio for the sanidine rocks suggests these to be of upper mantle or lower crustal origin. It is considered that models to produce a low initial ratio by other means are unnecessarily complicated.

The green matrix, sanidine-bearing rocks (tinguaite) are considered the parent compositions of the alkaline rocks on the basis of the initial strontium isotope ratio, mixing curve and the simple chemical mixes.

The Niggli Q-L-M plot shows a relationship trend between the rocks which is consistent with the strontium isotope ratios.

The temperature of this intrusion was sufficient to alter pyrite nodules in the Permian country rock to pyrrhotite nodules with the released sulphur contributing to the formation of pyrite, at a later stage, in the hornfelses on the western shore of Port Cygnet.

The sulphur isotope data show that the sulphides in the hornfelsed country rocks at Langdon's Point have formed from remobilized sulphur predominantly of sedimentary origin but that of the igneous rocks is of primary origin.

The released sulphur may have also contributed to the scapolitization of dyke CY44.

Origin of the Sanidine Rocks

The work of Helz (1976) has shown that it is possible to produce low ferromagnesian melts from basaltic rocks provided the ferromagnesian minerals do not melt.

The alkaline rocks of the Port Cygnet complex have been derived from a dual source with the sanidine rocks formed from an upper mantle-lower crust partial melt which has mixed with a partial melt of an amphibolite to produce the syenite porphyry.

The sanidine rocks have been formed from a small scale partial melt because of their small volume, deep seated origin as indicated by the strontium isotope ratios, poorly evolved nature with regard to their trace element compositions, lack of feldspar fractionation, and low ferro-magnesian mineral abundance.

The Mg/Mg+Fe ratio for the sanidine rocks is more consistent with their being derived from an alkali basaltic component than for an ultramafic source.

Water may have been derived from a deeper source by dehydration of phlogopite.

The derivation of some of the potash from breakdown of a phlogopite source with subsequent separation of olivine is entirely possible but is not supported by the Mg/Mg+Fe ratio.

Origin of Other Rocks

The fine grained sanidine intrusive gave rise to the garnet trachyte. The model favoured to account for this rock is one in which a parent magma similar to a tinguaite in composition has assimilated a mineralized, manganese-bearing carbonate pod similar to the carbonate-bearing ore deposits of Zeehan, western Tasmania.

The evidence for this arises from: (a) the presence of high manganese and anomalous trace concentrations of zinc and lead; (b) sulphur isotopes with a slightly larger ΔS^{34} than the other igneous rocks; (c) epidote and spessartite crystals which are most likely phenocrysts with white rims of potash feldspar crystallized onto them, suggesting

the crystals were suspended in the melt. The association of pyrite with spessartite suggests that the latter had formed above 742°C. Some of the spessartite phenocrysts have overgrowths of epidote showing the post-spessartite formation of the epidote. No spessartite grows over the epidote. The epidote formed below the formation temperature of pyrite in this environment, which would be near 770°C as a maximum. Reduction of manganese by iron has prevented the formation of piemontite and favoured the epidote as alumina was first removed from the melt by growth of spessartite. The spessartite and epidote crystals probably grew at a rapid rate in a hydrous environment.

The presence of excess sulphur incorporated into dyke CY44 produced the scapolitic alteration of the melanite. Because this appears to be an isolated occurrence at Port Cygnet, suggesting incorporation of sulphur, the most likely origin for this is mobilization of the Permian sedimentary sulphur, or assimilation of sulphur from a mineralized source similar to the model proposed for the garnet trachyte, which occurs about 300 m away. No isotopic data are available for this sulphur.

The dyke X50 was produced with inclusions of iron-muscovite from a metamorphic source within the crust. There was excess sulphur associated with this rock which produced pyrite accumulations. The isotopic composition of this sulphur suggests a primary origin.

On the basis of the trend of amphibole compositions, the hornblende porphyry has formed from recrystallized amphibole of the parent amphibolite being incorporated into the syenite porphyry and potash-rich melts.

The brown matrix rocks with primary phenocrysts of oligoclase-andesine and later sanidine, are interpreted as fractionates from the syenite porphyry magma chamber, because of their low strontium, high-

cesium, europium-anomaly rare-earth patterns, armouring of plagioclase by sanidine and falling near the equilibrium trough on the feldspar normative plot.

The preceding points have been summarized in a flow sheet form in Fig. VIII-2.

A specific heat source cannot be identified but there is strong evidence (Sass and Lachenbruck, 1979) of a high geothermal regime in eastern Australia extending back at least as far as the beginning of the Tertiary, with many concealed intrusions. The evidence of palaeomagnetic overprinting of Ordovician limestones approximately 50 km south of Port Cygnet with an apparent Late Cretaceous-Early Tertiary pole was probably related to increased geothermal heat flow during the rift forming processes preceding the opening of the Tasman Sea. It is likely that the origin and intrusion of the Port Cygnet alkaline rocks was related to these processes.

The modes of formation of the Port Cygnet rocks outlined above require mafic residues. There is positive indication of these from the aeromagnetic survey of Finney and Shelley (1966) (Fig. VII-5) which probably shows the syenite porphyry complement rather than that of the sanidine rocks which might be hinted at from the gravity work of Leaman and Naqvi (1967).

HYBRID ROCKS

The fine grained and partially crystallized sanidine-bearing magma and associated volatiles was intruded into the Jurassic dolerite at Regatta Point.

Potassium-rich components of the alkaline magma reacted with the dolerite to produce hybrid rocks as shown by the Differentiation Index - potash plot.

The process began with thermal metamorphism and strontium and potassium metasomatism of the dolerite as demonstrated by the increased K/Rb ratio and the Ba-Sr plot for the melanocratic hybrids.

The mixing process producing the hybrid rocks is shown in the Fe_2O_3 - K_2O - MgO variation diagrams.

Hybrid rocks dominated by original dolerite constituents (darker) are known as the melanocratic group while those with a dominant alkaline component (lighter) are referred to as leucocratic rocks.

The temperature of formation of the hybrid rocks lies within the range of 710°C to 810°C with consistent results from the excess silica in nepheline method of Hamilton (1965), random structure nepheline of Perchuk and Ryabchikov (1968), sanidine, biotite, magnetite of Wones and Eugster (1965), exsolution of feldspars of Orville (1963), and breakdown of pyrite of Arnold (1962).

Inconsistent results were obtained from the ordered nepheline model of Perchuk and Ryabchikov (1968), equilibrium nepheline feldspar model of Hamilton (1965), and melanite garnet model of Huckenholz et al. (1976).

Log $f\text{O}_2$ for this alteration, according to the method of Wones and Eugster (1965) ranges from -11 to -14.

CONCLUSIONS

The hybrid rocks have formed by thermal metamorphism, metasomatism and recrystallisation between 710°C and 810°C.

The Port Cygnet alkaline rocks have a mixed source.

The syenite porphyries have formed by mixing of partial melts from two sources.

The partial melts have probably been derived from alkali-mafic and amphibolitic parent materials.

The garnet trachyte is an example of an alkaline magma modified by assimilation of carbonates.

The minimum depth at which phenocrysts formed was approximately 6 km.

Miaskitic syenites with relatively high strontium and barium coupled with low niobium and zirconium could be derived by partial melting of a mafic-alkali mafic parent.

FURTHER INVESTIGATIONS

Further isotope work would be useful particularly for strontium, sulphur from CY44 and for oxygen, where a comparative study for the amphibolite inclusions, syenite porphyry and sanidine porphyries should provide further evidence concerning their origins and relationships. Measurement of D/H ratios of the sanidine rocks may confirm their proposed lower crust - upper mantle origin.

Detailed experimental work is required to establish the conditions of formation for the garnet trachyte, particularly with respect to the epidote phenocrysts.

More sophisticated geophysical investigations could establish the nature and extent of the proposed residual features at Port Cygnet.

Fresher specimens and trace element and isotope studies of the Cape Portland rocks, mentioned earlier, would be useful to more clearly define their relationship to the Port Cygnet alkaline rocks and also to a possible basaltic parent.

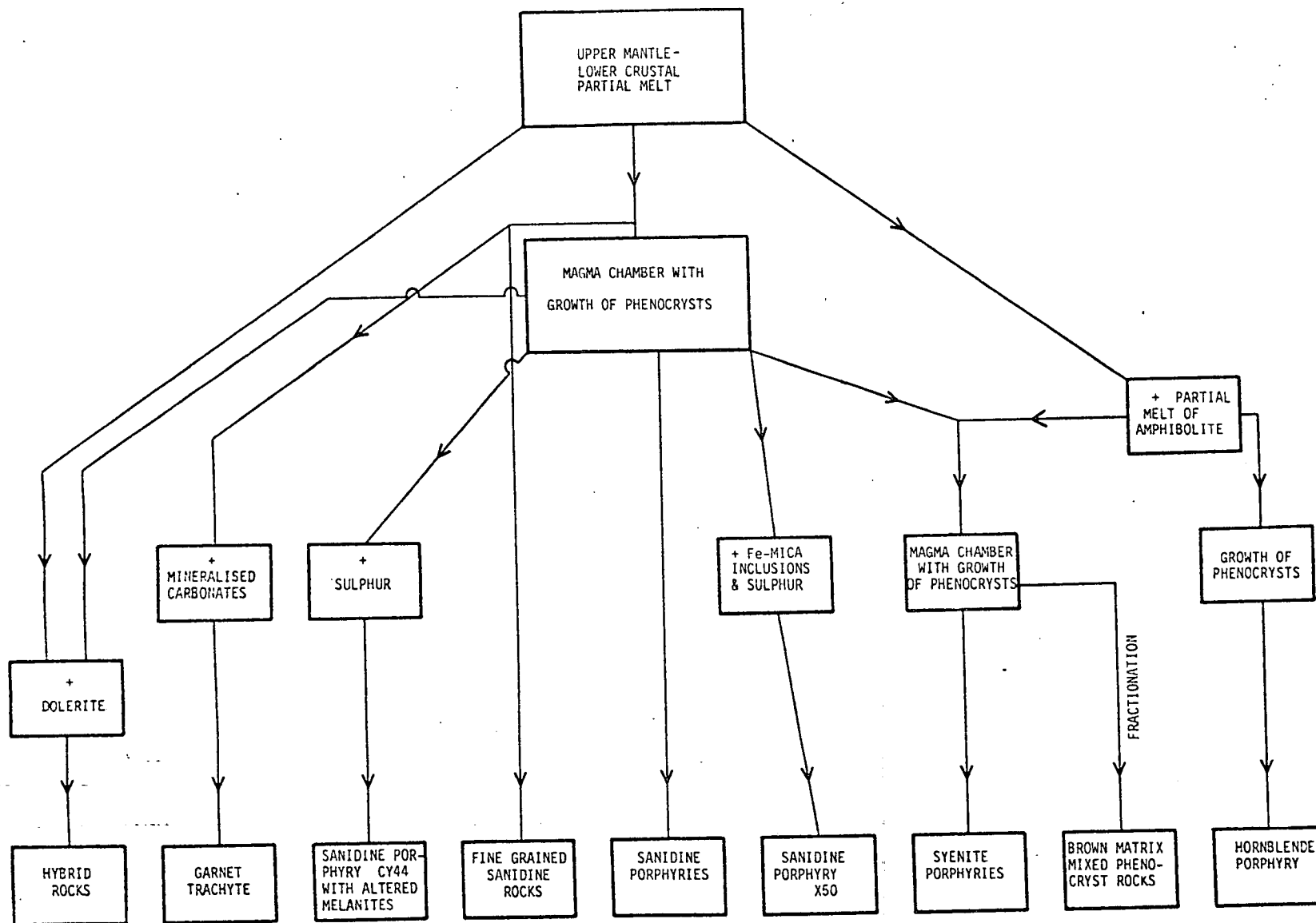


Fig. VIII-2 EVOLUTIONARY CHART OF PORT CYGNET ALKALINE ROCKS.

REFERENCES

- Abbott, R.N., 1978: Peritectic reactions in the system An-Ab-Or-Qz-H₂O. *Can. Min.*, 16: 245-256.
- Abbott, R.N., & Clarke, D.B., 1979: Hypothetical liquidus relationships in the subsystem Al₂O₃-FeO-MgO projected quartz alkali feldspar, and plagioclase for a(H₂O)<1. *Can. Min.*, 17: 549-560.
- Ahrens, L.H., Pinson, W.H., & Keams, M.M., 1952: Association of rubidium and potassium and their abundance in igneous rocks and meteorites. *Geochim. Cosmochim. Acta*, 2: 229-242.
- Allegre, C.J., Birck, J.L., Fourcade, S., & Semet, M.P., 1975: Rb⁸⁷/Sr⁸⁷ age of Jurinas basaltic achondrite and early igneous activity in the solar system. *Science*, 187: 436-438.
- Althaus, E., Karotke, E., Nitsch, K.H., & Winkler, H.G.F., 1970: An experimental re-examination of the upper stability limit of muscovite plus quartz. *N. Jb. Min. Mon.* 1: 325-336.
- Aoki, K., 1964: Clinopyroxenes from alkaline rocks of Japan. *Am. Min.*, 49: 1199-1221.
- Appleyard, E.C., 1967: Nepheline gneisses of the Wolfe belt, Lyndoch township, Ontario. I. Structure, stratigraphy and petrography. *Can. Jour. Earth Sci.*, 4: 371-395.
- Appleyard, E.C., 1969: Nepheline gneisses of the Wolfe belt, Lyndoch township, Ontario. II. Textures and mineral paragenesis. *Can. Jour. Earth Sci.*, 689-711.
- Appleyard, E.C., 1974: Syn-orogenic igneous alkaline rocks of Eastern Ontario and Northern Norway. *Lithos*, 7: 147-169.
- Appleyard, E.C., 1975: Silica-poor Hastingsitic amphiboles from metasomatic alkaline gneisses at Wolfe, Eastern Ontario. *Can. Min.*, 342-351.
- Arnold, R.G., 1962: Equilibrium relations between pyrrhotite and pyrite from 325°C to 743°C. *Econ. Geol.*, 57: 72-90.
- Bailey, D.K., 1969: The stability of acmite in the presence of H₂O. *Am. Jour. Sci.*, 267-A: 1-16.
- Bailey, D.K., 1976: Applications of experiments to alkaline rocks. In Bailey, D.K. & MacDonald, R. (eds), *The Evolution of the Crystalline Rocks*: 484. Academic Press.
- Bailey, D.K., & MacDonald, R., 1969: Alkali-feldspar fractionation trends and the derivation of peralkaline liquids. *Am. Jour. Sci.*, 267: 242-248.
- Bailey, D.K., & MacDonald, R., 1970: Petrochemical variations among mildly peralkaline (comendite) obsidians from the oceans and continents. *Contrib. Mineral. Petrol.*, 28: 340-351.

- Bailey, D.K., & Schairer, J.F., 1966: The systems $\text{Na}_2\text{O}-\text{Al}_2\text{O}_3-\text{Fe}_2\text{O}_3-\text{SiO}_2$ at 1 atmosphere, and the petrogenesis of alkaline rocks. *Jour. Petrol.*, 7: 114-170.
- Baker, I., 1968: Compositional variation of minor intrusions and the form of a volcano magma chamber. *Q. Jour. Geol. Soc. London*, 124: 67-79.
- Baker, P.E., Buckley, F., & Holland, J.G., 1974: Petrology and geochemistry of Easter Island. *Contrib. Mineral. Petrol.*, 44: 85-100.
- Bard, J.P., 1970: Composition of hornblendes formed during the Hercynian metamorphism of the Aracena Metamorphic Belt (S.W. Spain). *Contrib. Mineral. Petrol.*, 28: 117-134.
- Barker, D.S., 1970: North American feldspathoidal rocks in space and time: Reply. *Bull. Geol. Soc. Am.*, 81: 3501-3502.
- Barker, D.S., & Long, L.E., 1969: Feldspathoidal syenite in a quartz diabase sill, Brookville, New Jersey. *Jour. Petrol.*, 10: 202-221.
- Barker, D.S., Long, L.E., Hoops, G., & Hodges, F.N., 1977: Petrology and Rb-Sr isotope geochemistry of intrusions in the Diablo Plateau, northern Trans-Pecos magmatic province, Texas and New Mexico. *Bull. Geol. Soc. Am.*, 88: 1437-1446.
- Barnes, H.L., 1979: *Geochemistry of Hydrothermal Ore Deposits*. 2nd edition: 798. John Wiley.
- Barrer, R.M., & Hinds, P., 1953: Ion exchange in crystals of analcite and leucite. *J. Chem. Soc.*: 1879.
- Barth, T.F.W., 1934: Polymorphic phenomena and crystal structure. *Am. Jour. Sci.*, 5: 273.
- Barth, T.F.W., 1951: The feldspar geological thermometers. *N. Jb. Min. Abt.*, 82: 143-154.
- Barth, T.F.W., 1956: Studies in gneiss and granite. *Norske Vidensk. Acad. Oslo, I Mat.-Naturv. Klasse 1*: 263-274.
- Barth, T.F.W., 1962: The feldspar geologic thermometer. *Norks. Geol. Tidsskr.*, 42: 330-339.
- Barton, P.B., 1969: Thermochemical study of the system: Fe-As-S. *Geochim. Cosmochim. Acta*, 33: 841-857.
- Bass, M.N., 1970: North American feldspathoidal rocks in space and time: discussion. *Bull. Geol. Soc. Am.*, 81: 3493-3500.
- Bell, K., & Powell, J.L., 1969: Strontium isotope studies of alkaline rocks: the potassium-rich lavas of the Birunga and Toro-Ankole regions, east and central Equatorial Africa. *Jour. Petrol.*, 10: 536-572.

- Bell, K., & Powell, J.L., 1970: Strontium isotopic studies of alkalic rocks: the alkali complexes of Eastern Uganda. *Bull. Geol. Soc. Am.*, 81: 3481-3490.
- Bence, A.E., Grove, T.L., & Papike, J.J., 1980: Basalts as probes of planetary interiors: constraints on the chemistry and mineralogy of their source regions. *Precamb. Res.*, 10: 249-279.
- Best, M.G., Henage, L.F., & Adams, J.A.S., 1968: Mica peridotite, wyomingite and associated potassic igneous rocks in northeastern Utah. *Am. Min.*, 53: 1041-1049.
- Bikerman, M., Bowes, D.R., & van Breeman, O., 1975: Rb-Sr whole rock isotopic studies of Lewisian metasediments and gneisses in the Loch Marce region, Ross-shire. *Jour. Geol. Soc. London*, 131: 237-254.
- Binns, R.A., 1967: Barroisite-bearing eclogite from Naustdal, Sogn og Fjordane, Norway. *Jour. Petrol.*, 8: 349-371.
- Bird, D.K., & Helgeson, H.C., 1980: Chemical interaction of aqueous solutions with epidote-feldspar mineral assemblages in geologic systems. I. Thermo-dynamic analysis of phase relations in the system $\text{CaO-FeO-Fe}_2\text{O}_3\text{-Al}_2\text{O}_3\text{-SiO}_2\text{-H}_2\text{O-CO}_2$. *Am. Jour. Sci.*, 280: 907-941.
- Bird, D.K., & Helgeson, H.C., 1981: Chemical interaction of aqueous solutions with epidote-feldspar mineral assemblages in geologic systems. II. Equilibrium constraints in metamorphic/geothermal processes. *Am. Jour. Sci.*, 281: 576-614.
- Boesen, R., 1964: A re-examination of the monzonitic complex at Mt. Dromedary, N.S.W. Unpub. Ph.D. thesis, Australian National University, Canberra.
- Boettcher, A.L., 1967: The Rainy Creek alkaline-ultramafic igneous complex near Libby, Montana. I. Ultramafic rocks and ferite. *Jour. Geol.*, 75: 526-553.
- Boettcher, A.L., 1970: The system $\text{CaO-Al}_2\text{O}_3\text{-SiO}_2\text{-H}_2\text{O}$ at high pressures and temperatures. *Jour. Petrol.*, 11: 337-379.
- Boger, P.D., & Faure, G., 1974: Strontium isotope stratigraphy of a Red Sea core. *Geol.*, 2: 181-183.
- Both, R.A., Rafter, T.A., Solomon, M., & Jensen, M.L., 1969: Sulphur isotopes and zoning of the Zeehan Mineral Field. *Econ. Geol.*, 64: 618-628.
- Bowler, C.M.L., 1959: The distribution of the five alkali elements and fluorine in some granites and associated aureoles from south west of England. *Abst. Hbk Geochem.*, 1978: 37M1.

- Bridgewater, D., 1967: Feldspathic inclusions in the Gardar igneous rocks of South Greenland and their relevance to the formation of major anorthosite in the Canadian Shield. *Can. Jour. Earth Sci.*, 4: 995-1014.
- Bridgewater, D., & Harry, W.T., 1968: Anorthosite xenoliths and plagioclase megacrysts in Precambrian intrusions of South Greenland. *Meddr. Gronland*, 185, 2: 1-66.
- Brock, P.W.G., 1968: Metasomatic and intrusive nepheline-bearing rocks from the Mbozi syenite-gabbro complex, southwestern Tanzania. *Can. Jour. Earth Sci.*, 5: 387-419.
- Brown, A.V., Rubenach, M.J., & Varne, R., 1980: Geological environment, petrology and tectonic significance of the Tasmanian ophiolitic and ultramafic-mafic complexes. *Proc. Int. Ophiolite Symposium, Cyprus 1979*: 649-659.
- Brown, E.H., 1968: The Si^{4+} content of natural phengites: a discussion. *Contrib. Mineral. Petrol.*, 17: 78-81.
- Brown, P.E., Brown, R.D., Chambers, A.D., & Soper, N.J., 1978: Fractionation and assimilation in the Borginderne syenite, East Greenland. *Contrib. Mineral. Petrol.*, 67: 25-34.
- Brown, G.C., & Fyffe, W.S., 1970: The production of granitic melts during ultrametamorphism. *Contrib. Mineral. Petrol.*, 28: 310-318.
- Brown, I.A., 1925: Geology of the Milton district, N.S.W. *Proc. Linn. Soc. N.S.W.*, 50: 448-465.
- Brown, I.A., 1930a: The geology of the south coast of New South Wales. Part II. Devonian and older Palaeozoic rocks. *Proc. Linn. Soc. N.S.W.*, 55: 145-158.
- Brown, I.A., 1930b: The geology of the south coast of New South Wales. Part III. The monzonitic complex of the Mt. Dromedary district. *Proc. Linn. Soc. N.S.W.*, 55: 637-698.
- Buddington, A.F., & Leonard, B.F., 1953: Chemical petrology and mineralogy of hornblendes in northwest Adirondack granitic rocks. *Am. Min.*, 38: 891-902.
- Buerger, M.J., 1954: The stuffed derivatives of the silica structures. *Am. Min.*, 39: 600-614.
- Buie, B.F., 1941: Igneous rocks of the Highwood Mountains, Montana. Part III. Dikes and related intrusives. *Bull. Geol. Soc. Am.*, 52: 1753-1808.
- Burgess, C.H., 1941: Igneous rocks of the Highwood Mountains, Montana. Part IV. The stocks. *Bull. Geol. Soc. Am.*, 1809-1828.

- Burnham, C.W., 1979: Hydrothermal fluids at the magmatic stage.
In Barnes, H.L. (ed.): *Geochemistry of Hydrothermal Ore Deposits*.
2nd ed.: 798. John Wiley.
- Burnham, C.W., & Johns, R.H., 1962: A method for determining the solubility of water in silicate melts. *Am. Jour. Sci.*, 260: 721-745.
- Burton, J., & Culkin, F., 1972: Gallium. *Handbook of Geochemistry*.
II-3: 31E1-3101. Springer-Verlag.
- Carman, M.F., Cameron, M., Gunn, B., Camneron, K., & Butler, J.C., 1975: Petrology of Rattlesnake Mountain sill, Big Bend National Park, Texas. *Bull. Geol. Soc. Am.*, 86: 177-193.
- Carmichael, I.S.E., 1965: Trachytes and their feldspar phenocrysts. *Min. Mag.*, 34: 107-125.
- Carmichael, I.S.E., 1967: Volcanic rocks from the Leucite Hills, Wyoming. *Contrib. Mineral. Petrol.*, 15: 24-66.
- Carmichael, I.S.E., Turner, F.J., & Verhoogen, J., 1974: *Igneous Petrology*. 739 p. McGraw-Hill.
- Chappell, B.W., & White, A.J.R., 1974: Two contrasting granite types. *Pacific Geol.*, 8: 173-174.
- Cocker, J.D., 1977: Petrogenesis of the Tasmanian granitoids. Unpub. Ph.D. thesis, University of Tasmania.
- Coleman, R.J., 1976: Savage River magnetite deposits. In Knight, C.L. (ed.): *Economic Geology of Australia and Papua New Guinea*, 6: 600-604. Australas. Inst. Min. Metall., Melbourne.
- Compston, W., McDougall, I., & Heier, K.S., 1968: Geochemical comparison of Mesozoic basaltic rocks of Antarctica, South Africa, South America and Tasmania. *Geochim. Cosmochim. Acta*, 32: 129-149.
- Coombs, D.S., & Wilkinson, J.F.G., 1969: Lineages and fractionation trends in undersaturated volcanic rocks from the East Otago Volcanic Province (New Zealand) and related rocks. *Jour. Petrol.*, 10: 440-501.
- Cox, K.G., Gass, I.G., & Mallick, D.I.J., 1970: The peralkaline volcanic suite of Aden and Little Aden, South Arabia. *Jour. Petrol.*, 11: 433-461.
- Cox, K.G., Bell, J.D., & Pankhurst, R.J., 1979: *The Interpretation of Igneous Rocks*: 450. Allen & Unwin.
- Craig, G.Y., 1965: *The Geology of Scotland*: 566. Oliver & Boyd.
- Cross, W., 1987: Igneous rocks of the Leucite Hills and Pilot Butte, Wyoming. *Am. Jour. Sci.*, 4: 115-141.

- Currie, K.L., 1976: The alkaline rocks of Canada. *Bull. Geol. Surv. Can.*, 239: 228.
- Czamanske, G.K., & Mihalik, P., 1972: Oxidation during magmatic differentiation, Finmark Complex, Olso area, Norway. Part I. The opaque oxides. *Jour. Petrol.*, 13: 492-509.
- Daly, R.A., 1910: Origin of alkaline rocks. *Bull. Geol. Soc. Am.*, 21: 87-118.
- Daly, R.A., 1914: *Igneous Rocks and their Origins*: 563. McGraw-Hill.
- Day, A.A., 1969: Geology of New South Wales. *Jour. Geol. Soc. Aust.*, 16, 1: 15-17.
- Deer, W.A., Howie, R.A. & Zussman, J., 1962: *The Rock Forming Minerals*. 5 vols. Longmans.
- Deer, W.A., Howie, R.A., & Zussman, J., 1978: Single chain silicates. In *Rock-Forming Minerals 2A*: 668. 2nd edition. Longmans.
- De Vore, G.W., 1975: The role of partial melting of metasediments in the formation of the anorthosite-norite-syenite complex, Laramie Range, Wyoming. *Jour. Geol.*, 83: 749-762.
- Donnay, G., & Donnay, J.D.H., 1952: The symmetry change in the high-temperature alkali-feldspar series. *Am. Jour. Sci.*, Bowen Volume: 115-132.
- Eastoe, C.J., 1979: The formation of the Panguna porphyry copper deposit, Bougainville, Papua New Guinea. Unpub. Ph.D. thesis, University of Tasmania.
- Edgar, A.D., 1978: Subsolidus phase relations in the system $\text{NaAlSi}_3\text{O}_8$ - KAlSi_3O_8 at 1 kb PH_2O and their bearing on the origin of pseudo-leucites and analcimes in igneous rocks. *N. Jb. Min. Mh.*, 5: 210-222.
- Edwards, A.B., 1947: Alkali hybrid rocks of Port Cygnet, Tasmania. *Proc. Roy. Soc. Vic.*, 58 (n.s.), I-II: 81-115.
- Embleton, B.J.J., 1981: A review of the paleomagnetism of Australia and Antarctica. In McElhinny, M.W., & Valencio, D.A. (eds): *Geodynamics Series Vol. 2*. Am. Geophys. Union.
- Engel, A.E.J., Engel, C.G., & Havens, R.G., 1965: Chemical characteristics of oceanic basalts and the upper mantle. *Bull. Geol. Soc. Am.*, 76: 719-733.
- Erickson, R.L., & Blade, L.V., 1963: Geochemistry and petrology of the alkalic igneous complex at Magnet Cove, Arkansas. *U.S. Geol. Surv. Prof. Pap.* 425: 93.

- Ernst, W.G., 1968: *The Amphiboles*: 125. Springer-Verlag.
- Eskola, P., Vuoristo, U., & Rankama, K., 1937: An experimental illustration of the spilite reaction. *Compt. Rend. Soc. geol. Finlande*, 119: 61-68.
- Eugster, H.P., Albee, H.L., Bence, H.F., Thompson, J.B., & Waldbaum, D.R., 1972: The two-phase region and excess mixing properties of paragonite-muscovite crystalline solutions. *Jour. Petrol.*, 13: 147-179.
- Evans, B., 1965: Application of a reaction-rate method to the breakdown equilibria of muscovite and muscovite plus quartz. *Am. Jour. Sci.*, 263: 647-667.
- Evernden, J.F., & Richards, J.R., 1962: Potassium-argon ages in Eastern Australia. *Jour. Geol. Soc. Aust.*, 9: 1-37.
- Ewart, A., Baxter, K., & Ross, J.A., 1980: The petrology and petrogenesis of the Tertiary anorogenic mafic lavas of southern and central Queensland, Australia - possible implications for crustal thickening. *Contrib. Mineral. Petrol.*, 75: 129-152.
- Faure, G., 1977: *Principles of Isotope Geology*: 464. John Wiley.
- Ferguson, A.K., 1978: The crystallization of pyroxenes and amphiboles in some alkaline rocks and the presence of a pyroxene compositional gap. *Contrib. Mineral. Petrol.*, 67: 11-15.
- Ferguson, A.K., & Cundari, A., 1975: Petrological aspects and evolution of the leucite bearing lavas from Bufumbria, S.W. Uganda. *Contrib. Mineral. Petrol.*, 50: 25-46.
- Field, D., & Clough, P.W.L., 1976: K/Rb ratios and metasomatism in metabasites from a Precambrian amphibolite-granulite transition zone. *J. Geol. Soc. London*, 132: 277-288.
- Finney, W.A., & Shelley, E.P., 1966: Tasmanian aeromagnetic survey 1966. *B.M.R., Geol. & Geophys. Record* 1966/139.
- Florensov, N.A., 1969: Rifts of the Baikal Mountain region. *Tectonophysics*, 8: 443-456.
- Floyd, P.A., & Winchester, J.A., 1975: Magma type and tectonic setting discrimination using immobile elements. *Earth Planet. Sci. Letters*, 27: 211-218.
- Ford, R.J., 1967: Re-appraisal of johnstonotite. *Pap. Proc. Roy. Soc. Tasm.*, 101: 11-12.
- Ford, R.J., 1982: A.W.H. Humphrey - His Majesty's Mineralogist in N.S.W. - a comment. *Proc. Linn. Soc. N.S.W.*, in press.
- Frey, F.A., Green, D.H., & Roy, S.D., 1978: Integrated models of basalt petrogenesis: a study of quartz tholeiites to olivine melilitites from south eastern Australia utilizing geochemical and experimental data. *Jour. Petrol.*, 19: 463-513.

- Frey, F.A., Haskin, M.A., Poetz, J.A., & Haskin, L.A., 1968: Rare earth abundances in some basic rocks. *J. Geophys. Res.*, 73: 6085-6098.
- Frick, C., 1975: The Phalaborwa syenite intrusions. *Trans. Geol. Soc. S. Afr.*, 78: 201-213.
- Fronzel, C., 1970: Scandium. In *Handbook of Geochemistry*. II-2, 21A-F. Springer-Verlag.
- Fudali, R.F., 1963: Experimental studies nearing on the origin of pseudoleucite and associated problems of alkalic rock systems. *Bull. Geol. Soc. Am.*, 74: 1101-1125.
- Fuster, J.M., Gestesi, P., Sagredo, J., & Fermojo, M.L., 1967: Las rocas lamproiticas del S.W. de Espana. *Estud. Geol.*, 23: 35-69.
- Gerasimovsky, V.I., 1966: Geochemical features of agpaitic nepheline syenites. In Vinogradov, A.P. (ed): *Chemistry of the Earth's Crust*. Vol. I. Israel Prog. Sci. translations.
- Gerasimovsky, V.I., & Kuznetsova, S.Ya., 1967: On the petrochemistry of the Ilimaussaq intrusion, south Greenland. *Geokhimiya*, 1967: 274-283.
- Gilbert, M.C., 1966: Synthesis and stability relations of the hornblende ferropargasite. *Am. Jour. Sci.*, 264: 698-742.
- Gill, R.C.O., 1972: Chemistry of peralkaline phonolite dykes from the Gromedal-Ika area, S. Greenland. *Contrib. Mineral. Petrol.*, 34: 87-100.
- Gittins, J., 1961: Nephelinization in the Haliburton-Bancroft district, Ontario, Canada. *Jour. Geol.*, 69: 291-308.
- Gittins, J., Fawcett, J.J., Brooks, C.K., & Rucklidge, J.C., 1980: Intergrowths of nepheline-potassium feldspar and kalsilite-potassium feldspar: a re-examination of the 'pseudoleucite problem'. *Contrib. Mineral. Petrol.*, 73: 119-126.
- Goldsmith, J.R., 1976: Scapolites, granulites and volatiles in the lower crust. *Bull. Geol. Soc. Am.*, 87: 161-168.
- Goranson, C., 1938: Silicate-water systems: phase equilibria in the $\text{NaAlSi}_3\text{O}_8\text{-H}_2\text{O}$ and $\text{KAlSi}_3\text{O}_8\text{-H}_2\text{O}$ systems at high temperatures and pressures. *Am. Jour. Sci.*, 35A: 71-91.
- Grapes, R., Yagi, K., & Okumura, K., 1979: Aenigmatite, sodic pyroxene, arfvedsonite and associated minerals in syenites from Morotu, Sakhalin. *Contrib. Mineral. Petrol.*, 69: 97-103.
- Green, D.H., & Lambert, I.B., 1965: Experimental crystallization of anhydrous granite at high pressures and temperatures. *J. Geophys. Res.*, 70: 5259-5268.

- Green, T.H., 1976: Experimental generation of cordierite or garnet-bearing granitic liquid from a pelitic composition. *Geology* 4, 85-88.
- Green, T.H., 1977: Garnet in silica liquids and its possible use as a P-T indicator. *Contr. Mineral. Petrol.*, 65: 59-67.
- Green, T.H., & Ringwood, A.E., 1968: Genesis of the calc-alkaline igneous rock suite. *Contr. Mineral. Petrol.*, 18: 105-162.
- Greenwood, H.J., 1961: The system $\text{NaAlSi}_2\text{O}_6\text{-H}_2\text{O-Argon}$: Total pressure and water pressure in metamorphism. *Jour. Geophys. Res.*, 66: 3923-3946.
- Griffin, B.J., 1979: Energy dispersive analysis system calibration and operation with Tas-sueds, an advanced interactive data-reduction package. *Uni. of Tas. Geol. Dept. Publ.*, 343.
- Grootenboer, J., & Schwarz, H.P., 1969: Experimentally determined sulphur isotope fractionations between sulphide minerals. *Earth Planet. Sci. Letters*, 7: 162-166.
- Gulson, B.L., & Godber, W., 1979: Caesium as a possible discriminant between felsic rocks of different origins from eastern Australia. *Jour. Geol. Soc. Aus.*, 26: 11-16.
- Gustafson, W.I., 1974: The stability of andradite, hedenbergite and related minerals in the system Ca-Fe-Si-O-H . *Jour. Pet.*, 15: 455-496.
- Haas, J.L., Jr., & Robie, R.A., 1973: Thermodynamic data for wustite, $\text{Fe}_{0.947}\text{O}$, magnetite, Fe_3O_4 and hematite Fe_2O_3 (Abstract). *Amer. Geophys. Union Trans.*, 54: 483.
- Hall, A., 1967: The distribution of some major and trace elements in feldspars from the Rosses and Ardara granite complexes, Donegal, Ireland. *Geochem. et Cosmochim. Acta*, 31: 835-847.
- Hamilton, D.L., 1961: Nephelines as crystallization temperature indicators. *Jour. Geol.*, 69: 321-329.
- Hamilton, D.L., & Mackenzie, W.S., 1965: Phase equilibrium studies in the system $\text{NaAlSiO}_4\text{-KAlSiO}_4\text{-SiO}_2\text{-H}_2\text{O}$. *Min. Mag.*, 34: 214-231.
- Hansen, G.N., 1978: The application of trace elements to the petrogenesis of igneous rocks of granitic composition. *Earth. Planet. Sci. Letters*, 38: 26-43.
- Harper, L.F., 1915: Geology and mineral resources of the Southern Coalfield. Part I: The South Coastal Portion. *Mem. Geol. Surv. N.S.W.*, 7.
- Haskin, L.A., 1979: On rare earth element behaviour in igneous rocks. In Ahrens, L.H. (Ed.): *Phys. & Chem. Earth*: 11. Pergamon, 175-189.
- Haskin, L.A., & Paster, T.P., 1979: The geochemistry and mineralogy of the rare earths. In Gschneider, K.A. & Eyring, L. (Eds): *Handbook on the Physics and Chemistry of Rare Earths*, 3(21). North Holland Pub. Co.

- Hearn, B.C., Pecora, W.T., & Swadley, W.C., 1964: Geology of the Rattlesnake quadrangle, Bearpaw Mountains, Blaine County, Montana. *Bull. U.S. Geol. Surv.*, 1181-B: 66.
- Heier, K.S., 1961: Layered gabbro, hornblende, carbonatite, and nepheline syenite on Stjernøy, North Norway. *Norsk Geol. Tidsskrift*, 41: 109-155.
- Heier, K.S., 1962: Trace elements in feldspars - a review. *Norsk Geol. Tidsskrift*, 42: 415.
- Heier, K.S., 1964: Geochemistry of the nepheline syenite on Stjernøy, North Norway. *Norsk Geol. Tidsskrift*, 44: 205-215.
- Heier, K.S., & Adams, J.A.S., 1964: The geochemistry of the alkali metals. *Phys. Chem. Earth*, 5: 253-381.
- Heier, K.S., & Billings, G.K., 1969: Cesium. In *Handbook of Geochemistry*. II-5, 55: D1-01. Springer-Verlag.
- Heier, K.S., & Billings, G.K., 1978: Rubidium. In *Handbook of Geochemistry*. II-4, 37: D1-N1. Springer-Verlag.
- Heier, K.S., & Compston, W., 1969: Rb-Sr isotopic studies on the plutonic rocks of the Oslo region. *Lithos*, 2: 133-156.
- Heier, K.S., Compston, W., & McDougall, I., 1965: Thorium and uranium concentrations, and the isotopic composition of strontium in the differentiated Tasmanian dolerites. *Geochim. Cosmochim. Acta*, 29: 643-659.
- Helgeson, H.C., Delany, J.M., Nesbitt, H.W., & Bird, D.K., 1978: Summary and critique of the thermodynamic properties of the rock-forming minerals. *Am. Jour. Sci.*, 278A: 227.
- Helz, R.T., 1976: Phase relations of basalts in their melting ranges of $P_{H_2O} = 5$ kb. Part II - melt compositions. *Jour. Petrol.*, 17: 139-193.
- Henderson, C.M.B., & Gibb, F.G.F., 1977: Formation of analcime in the Dippin sill, Isle of Arran. *Min. Mag.*, 41: 534-537.
- Henry, N.F.M., Lipson, H., & Wooster, W.A., 1951: *The Interpretation of X-ray Diffraction Photographs*: 258. Macmillan.
- Hermann, A.G., 1969: Rare earths. In *Handbook of Geochemistry*. II-5, 57-71: D1-01. Springer-Verlag.
- Hermann, A.G., Potts, M.J., & Krake, D., 1974: Geochemistry of the rare earth elements in spilites from the oceanic and continental crust. *Contrib. Mineral. Petrol.*, 44: 1-16.
- Hodge, D.S., Smith, B.D., & Smithson, S.B., 1970: Qualitative geophysical study of petrogenesis of syenites related to Laramie anorthosite, Wyoming. *Lithos*, 3: 237-250.
- Holdaway, M.J., 1972: Thermal stability of Al-Fe epidote as a function of fO_2 and Fe content. *Contrib. Mineral. Petrol.*, 37: 307-340.

- Hsu, L.C., 1968: Selected phase relationships in the system Al-Mn-Fe-Si-O: a model for garnet equilibria. *Jour. Petrol.*, 9: 40-83.
- Huang, W.L., & Wyllie, P., 1973: Melting relations of muscovite-granite to 35 kbars as a model for fusion of metamorphosed subducted oceanic sediments. *Contrib. Mineral. Petrol.*, 42: 1-14.
- Huang, W.L., & Wyllie, P., 1973: Muscovite de-hydration and melting in deep crust and subducted oceanic sediments. *Earth Planet. Sci. Letters*, 18: 133-136.
- Huang, W.L., & Wyllie, P., 1974: Melting relations of muscovite with quartz and sanidine in the $K_2O-Al_2O_3-SiO_2-H_2O$ system to 30 kbars and an outline of paragonite melting relations. *Am. Jour. Sci.*, 274: 378-395.
- Huckenholz, H.G., 1969: Synthesis and stability of Ti-andradite. *Am. Jour. Sci.*, 267: 209-232.
- Huckenholz, H., Holzl, E., Huggins, F.E., & Virgo, D., 1976: A reconnaissance study of the Ti-garnet stability field at defined oxygen fugacities. *Carnegie Inst. Washington Yearbook*, 75: 711-720.
- Ivanova, G.F., 1963: Content of tin, tungsten and molybdenum in granites enclosing tin-tungsten deposits. *Geochem.*, 5: 492-500.
- Jakes, P.J., 1970: High potassium calc-alkaline rocks from Cape Nelson, Eastern Papua. *Contrib. Mineral. Petrol.*, 28: 259-271.
- James, R.S., & Hamilton, D.L., 1969: Phase relations in the system $NaAlSi_3O_8-KAlSi_3O_8-CaAl_2Si_2O_8-SiO_2$ at 1 kilobar water vapour pressure. *Contrib. Mineral. Petrol.*, 21: 111-141.
- Jennings, D.J., & Sutherland, F.L., 1969: Geology of the Cape Portland area, with special reference to the Mesozoic (?) appinitic rocks. *Tasm. Dept Mines Technical Report* 13: 45-81.
- Johnston, R.M., 1888: *Systematic Account of the Geology of Tasmania*. Tasmanian Government Printer.
- Joplin, G.A., 1964: *A Petrography of Australian Igneous Rocks*: 253. Angus and Robertson.
- Joplin, G.A., 1965: The problem of the potash-rich basaltic rocks. *Min. Mag.*, 34: 266-275.
- Joplin, G.A., 1968: The shoshonite association - a review. *Jour. Geol. Soc. Aust.*, 15: 275-294.
- Kajiwara, Y., & Krouse, H.R., 1971: Sulphur isotope partitioning in metallic sulphide systems. *Can. Jour. Earth Sci.*, 8: 1397-1408.
- Kaplan, I.R., Emery, K.O., & Rittenberg, S.C., 1963: The distribution and isotopic abundance of sulphur in recent marine sediments off southern California. *Geochim. Cosmochim. Acta*, 27: 297-331.

- Kelley, V.C., 1968: Geology of the alkaline Precambrian rocks at Pajarito Mountain, Otero County, New Mexico. *Bull. Geol. Soc. Am.*, 79: 1565-1572.
- Kempe, D.R.C., 1968: The Kilonwa syenite, Tanzania. *Q. Jour. Geol. Soc. London*, 124: 91-100.
- Kerr, F.A., 1948: Lower Stikine and western Iskut River areas, British Columbia. *Geol. Surv. Can. Mem.*, 246: 49-53.
- Kesson, S., & Price, R.C., 1972: The major and trace element chemistry of kaersutite and its bearing on the petrogenesis of alkaline rocks. *Contrib. Mineral. Petrol.*, 35: 119-124.
- Kesson, S.E., 1973: The primary geochemistry of the Monaro alkaline volcanics, southeastern Australia - evidence for upper mantle heterogeneity. *Contrib. Mineral. Petrol.*, 42: 93-105.
- King, B.C., & Sutherland, D.S., 1960: *Recent Advances in Science: Geology*. Sci. Progress.
- Kogarko, L.N., 1977: General regularities of differentiation of magmas oversaturated with alkalis. *Geochem. Int.*, 14: 9-25.
- Kramers, J.D., 1977: Lead and strontium isotopes in Cretaceous kimberlites and mantle-derived xenoliths from Southern Africa. *Earth Planet. Sci. Lett.*, 34: 419-431.
- Krauskopf, K.B., 1967: *Introduction to Geochemistry*: 721. McGraw-Hill.
- Krogh, T.E., & Hurley, P.M., 1968: Strontium isotope variation and whole-rock isochron studies, Grenville Province, Ontario. *Jour. Geophys. Res.*, 73: 7107-7125.
- Kudo, A.M., & Weill, D.F., 1970: An igneous plagioclase thermometer. *Contrib. Mineral. Petrol.*, 25: 52-65.
- Kuehner, S., Edgar, A.D., & Arima, M., 1981: Petrogenesis of the ultramafic rocks from the Leucite Hills, Wyoming. *Am. Mineral.*, 66: 663-677.
- Kullerud, G., & Yoder, H.S., 1959: Pyrite stability relations in the Fe-S system. *Econ. Geol.*, 54: 533-572.
- Kushiro, I., 1968: Composition of magmas formed by partial zone melting of the earth's upper mantle. *Jour. Geophys. Res.*, 73: 619-634.
- Kwak, T.A.P., 1964: A garnet-bearing syenite near Kamloops, B.C. Unpub. M.Sc. thesis, University of British Columbia.
- Kyle, P.R., Adams, J., & Rankin, P.C., 1979: Geology and petrology of the McMurdo volcanic group at Rainbow Ridge, Brown Peninsula, Antarctica. *Bull. Geol. Soc. Am.*, 90: 676-688.
- Lambert, I.B., & Heier, K.S., 1968: Geochemical investigations of deep-seated rocks in the Australian shield. *Lithos*, 1: 30-53.

- Langworthy, A.P., & Black, L.P., 1978: The Mordor Complex: a highly differentiated potassic intrusion with kimberlitic affinities in central Australia. *Contrib. Mineral. Petrol.*, 67: 51-62.
- Larsen, E.S., 1941: Igneous rocks of the Highwood Mountains, Montana. Part II - The extrusive rocks. *Bull. Geol. Soc. Am.*, 52: 1733-1752.
- Larsen, E.S., & Buie, B.F., 1938: Potash analcime and pseudoleucite from the Highwood Mountains of Montana. *Am. Mineral.*, 23: 837.
- Larsen, E.S., Hurlbut, C.S., Burgess, C.H., & Buie, B.F., 1941: Igneous rocks of the Highwood Mountains, Montana. Part VII - Petrology. *Bull. Geol. Soc. Am.*, 52: 1857-1868.
- Larsen, L.M., 1976: Clinopyroxene and co-existing mafic minerals from the alkaline Ilimaussaq Intrusion, South Greenland. *Jour. Petrol.*, 17: 258-290.
- Larsen, L.M., 1979: Distribution of R.E.E. and other trace elements between phenocrysts and peralkaline undersaturated magmas, exemplified by rocks from the Gardar igneous province, south Greenland. *Lithos*, 12: 303-315.
- Leake, B.E., 1964: The chemical distinction between ortho- and para-amphibolite. *Jour. Petrol.*, 5: 238-254.
- Leake, B.E., 1965: The relationship between tetrahedral aluminium and the maximum possible octahedral aluminium in natural calciferous and sub-calciferous amphiboles. *Am. Mineral.*, 50: 843-847.
- Leake, B.E., 1978: Nomenclature of amphiboles. *Min. Mag.*, 42: 533-563.
- Leaman, D.E., 1975: Structural re-interpretation of the Glenorchy-Collinsvale region. Tas. Mines Dept Unpub. Rept 1975/13.
- Leaman, D.E., 1977: Magnetic survey, Port Cygnet. *Tasm. Dept Mines Technical Report* 20: 134-135.
- Leaman, D.E. & Naqvi, I.H., 1967: Geology and geophysics of the Cygnet district. *Bull. Tasm. Geol. Surv.* 49.
- Leaman, D.E., Richardson, R.G., & Shirley, J.E., 1980: Tasmania - the gravity and its interpretation. Tasm. Dept Mines Unpub. Rept 36.
- Le Maitre, R.W., 1962: Petrology of volcanic rocks, Gough Island, South Atlantic. *Bull. Geol. Soc. Am.*, 73: 1309-1340.
- Le Maitre, R.W., 1974: Partially fused granite blocks from Mt. Elephant, Victoria, Australia. *Jour. Petrol.*, 15: 403-412.
- Le Maitre, R.W., 1976: The chemical variability of some common igneous rocks. *Jour. Petrol.*, 17: 589-637.
- Lindh, A., 1978: Aspects of plagioclase-epidote thermometry. *N. Jb. Min. Abh.*, 133, 2: 113-131.

- Lindsley, D.H., 1966: Melting relations of KAlSi_3O_8 . *Am. Mineral.*, 51: 1793-1799.
- Liou, J.G., 1971: Analcime equilibria. *Lithos*, 4: 389-402.
- Liou, J.G., 1973: Synthesis and stability relations of epidote, $\text{Ca}_2\text{Al}_2\text{FeSi}_3\text{O}_{12}(\text{OH})$. *Jour. Petrol.*, 14: 381-413.
- Lovering, J.F., & White, A.J.R., 1969: Granulitic and eclogitic inclusions from basic pipes at Delegate, Australia. *Contrib. Mineral. Petrol.*, 21: 9-52.
- Luth, W.C., 1974: Resorption of silicate minerals. In Sorenson, H. (Ed.): *The Alkaline Rocks*: 622. John Wiley.
- Luth, W.C., Jahns, R.H., & Tuttle, O.F., 1964: The granite system at pressures of 4 to 10 kilobars. *Jour. Geophys. Res.*, 69: 759-773.
- Luth, W.C., & Tuttle, O.F., 1969: The hydrous vapour phase in equilibria with granite and granite magmas. In Larsen, L.H. (Ed.): *Poldervaart Memorial Volume. Geol. Soc. Am. Mem.* 115: 513-548.
- McCallum, I.S., & Charette, M.P., 1978: Zr and Nb partition coefficients: implication for the genesis of mare basalts, KREEP and sea-floor basalts. *Geochem. Cosmochim. Acta*, 42: 859-869.
- McDougall, I., 1962: Differentiation of the Tasmanian dolerites: Red Hill dolerite-granophyre association. *Bull. Geol. Soc. Am.*, 73: 279-316.
- McDowell, S.D., & Wyllie, P.J., 1971: Experimental studies of igneous rock series: the Kugnut syenite complex of south-west Greenland. *Jour. Geol.*, 79: 173-194.
- MacKenzie, W.S., 1952: The effect of temperature on the symmetry of high temperature soda-rich feldspars. *Am. Jour. Sci., Bowen Volume*, 2: 319-342.
- MacKenzie, W.S., & Smith, J.V., 1956: The alkali feldspars III: An optical and X-ray study of high temperature feldspars. *Am. Mineral.*, 41: 405-427.
- MacKenzie, W.S., & Zussman, J., 1972: *The Feldspars*: 717. NATO Advanced Study Institute in Feldspars, Manchester.
- MacLeod, W.A., & White, O.E., 1898: On the occurrence of a new species of garnet at Port Cygnet. *Pap. Proc. Roy. Soc. Tasm.*, 1898-1899: 74-76.
- MacNamara, J., & Thode, H.G., 1950: Comparison of the isotopic constitution of terrestrial and meteoric sulphur. *Phys. Rev.*, 78: 307-308.
- Marfunin, A.S., 1966: *Feldspars: Phase Relations, Optical Properties, Geological Distribution*: 317. Translated from Russian 1962 ed. Israel Prog. Sci. Translations.
- Miller, C.F., 1977: Early alkalic plutonism in the calc-alkaline batholithic belt of California. *Geology*, 5: 685-688.

- Miller, C.F., 1978: Monzonite plutons, California, and a model for generation of alkali-rich near silica-saturated magmas. *Contrib. Mineral. Petrol.*, 67: 349-355.
- Millhollen, G.L., Wyllie, P.J., & Burnham, C.W., 1971: Melting relations of $\text{NaAlSi}_3\text{O}_8$ to 30 kbar in the presence of $\text{H}_2\text{O}:\text{CO}_2=50:50$ vapor. *Am. Jour. Sci.*, 271: 481-489.
- Milligan, J., 1852: Proceedings 9th July 1851. *Pap. Proc. Roy. Soc. V.D.L.*, II, 1: 151.
- Milligan, J., 1855: Proceedings 10th May 1854. *Pap. Proc. Roy. Soc. V.D.L.*, III, 1: 173.
- Mitchell, R.H., & Crocket, J.H., 1972: Isotopic composition of strontium in rocks of the Fen alkaline complex, South Norway. *Jour. Petrol.*, 13: 83-97.
- Mitchell, R.H., & Bell, K., 1976: Rare earth element geochemistry of potassic lavas from the Birunga and Toro-Ankole regions of Uganda, Africa. *Contrib. Mineral. Petrol.*, 58: 293-303.
- Miyashiro, A., 1978: Nature of alkalic volcanic rock series. *Contrib. Mineral. Petrol.*, 66: 91-104.
- Morey, G.W., & Hesselgesser, J.M., 1952: The system $\text{H}_2\text{O}-\text{Na}_2\text{O}-\text{SiO}_2$ at 400°C . *Am. Jour. Sci., Bowen Volume*, 2: 343-371.
- Morteani, G., 1978: High alumina amphiboles from the penninic rocks of the western Tauern (Tyrol, Austria). *N. Jb. Min. Abh.*, 133: 132-148.
- Mueller, R.F., & Saxena, S.K., 1977: *Chemical Petrology*: 394. Springer-Verlag.
- Mukherjee, A., 1967: Role of fractional crystallization in the descent: basalt \rightarrow trachyte. *Contrib. Mineral. Petrol.*, 10: 139-148.
- Nance, W.B., & Taylor, S.R., 1976: Rare-earth element patterns and crustal evolution - I - Australian post-Archaeon sedimentary rocks. *Geochim. Cosmochim. Acta*, 40: 1539-1552.
- Nash, W.P., Carmichael, I.S.E., & Johnson, R.W., 1969: The mineralogy and petrology of Mt. Suswa, Kenya. *Jour. Petrol.*, 10: 409-439.
- Nemee, D., 1967: Determination of the character of oriented potash feldspar overgrowth on plagioclase crystals in igneous rocks. *Contrib. Mineral. Petrol.*, 10: 149-155.
- Newton, R.C., & Goldsmith, J.R., 1975: Stability of the scapolite meionite ($3\text{CaAl}_2\text{Si}_2\text{O}_8\cdot\text{CaCO}_3$) at high pressures and storage of CO_2 in the deep crust. *Contrib. Mineral. Petrol.*, 49: 49-62.
- Newton, R.H., 1935: Activity coefficients of gases. *Ind. Eng. Chem.*, 27: 302-306.
- Niggli, P., 1954: *Rocks and Mineral Deposits*: 559. (English translation by R.C. Parker.) Freeman.

- Niyogi, D., 1966: Petrology of the alkalic rocks of Kishangarth, Rajasthan, India. *Bull. Geol. Soc. Am.*, 77: 65-82.
- Nockolds, S.R., 1954: Average chemical compositions of some igneous rocks. *Bull. Geol. Soc. Am.*, 65: 1007-1032.
- Nolan, J., 1966: Melting-relations in the system $\text{NaAlSi}_3\text{O}_8$ - NaAlSiO_4 - $\text{NaFeSi}_2\text{O}_6$ - $\text{CaMgSi}_2\text{O}_6$ - H_2O , and their bearing on the genesis of alkaline, undersaturated rocks. *Quart. Jour. Geol. Soc. London*, 122: 119-157.
- Norman, J.C., & Haskin, L.A., 1968: The geochemistry of scandium: a comparison to the rare earths and Fe. *Geochim. Cosmochim. Acta*, 32: 93-108.
- Nyambok, I.O., 1980: Petrology and geochemistry of the alkaline intrusion, Jombo Hill, Kenya. *Geol. Mag.*, 117: 327-338.
- O'hara, M.J., & Yoder, H.S., 1967: Formation and fractionation of basic magmas at high pressures. *Scott. Jour. Geol.*, 3: 67-117.
- Ohashi, Y., & Finger, L.W., 1978: The role of octahedral cations in pyroxenoid crystal chemistry. I. Bustmatite, wollastonite and the pectolite-schizolite-serandite series. *Am. Mineral.*, 63: 274-288.
- Ohmoto, H., 1972: Systematics of sulphur and carbon isotopes in hydrothermal ore deposits. *Econ. Geol.*, 67: 551-578.
- Ohmoto, H., & Rye, R.O., 1979: Isotopes of sulphur and carbon. In Barnes, H.L. (Ed.): *Geochemistry of Hydrothermal Ore Deposits*: 798. 2nd edition. John Wiley.
- O'nions, R.K., & Pankhurst, R.J., 1974: Petrogenetic significance of isotope and trace element variations in volcanic rocks from the mid-Atlantic. *Jour. Petrol.*, 15: 603-634.
- Orville, P.M., 1963: Alkali ion exchange between vapor and feldspar phases. *Am. Jour. Sci.*, 261: 201-236.
- Orville, P.M., 1975: Stability of scapolite in the system Ab-An-NaCl-CaCO_2 at 4 kb and 750°C. *Geochim. Cosmochim. Acta*, 39: 1091-1105.
- Oyawoye, M.O., 1967: The petrology of a potassic syenite and its associated biotite pyroxenite at Shaki, Western Nigeria. *Contrib. Mineral. Petrol.*, 16: 115-158.
- Papanastassiou, D.A., & Wasserberg, G.J., 1969: Initial strontium isotopic abundances and the resolution of small time differences in the formation of planetary objects. *Earth Planet. Sci. Letters*, 8: 269-278.
- Parsons, I., 1979: The Klokken gabbro-syenite complex, South Greenland: cryptic variation and origin of inversely graded layering. *Jour. Petrol.*, 20: 653-694.

- Paul, D.K., Potts, P.J., Rex, D.C., & Beckinsale, R.D., 1977: Geochemical and petrogenic study of the Girnar igneous complex, Deccan volcanic province, India. *Bull. Geol. Soc. Am.*, 88: 227-234.
- Paul, F.P., 1906: Foyaitisch-Theralitische Gesteine aus Tasmanien. *Min. Petr. Mitt.*, 25 (n.f.): 269-318.
- Payne, J.G., 1968: Geology and geochemistry of the Blue Mountain nepheline syenite. *Can. Jour. Earth Sci.*, 5: 259-272.
- Pearce, J.A., & Cann, J.R., 1973: Tectonic setting of basic volcanic rocks, determined using trace element analyses. *Earth Planet. Sci. Letters*, 19: 290-300.
- Pearce, J.A., & Norry, M.J., 1979: Petrogenic implications of Ti, Zr, Y and Nb variations in volcanic rocks. *Contrib. Mineral. Petrol.*, 69: 33-47.
- Perchuk, L.L., & Ryabchikov, I.D., 1968: Mineral equilibria in the system nepheline-alkali feldspar-plagioclase and their petrological significance. *Jour. Petrol.*, 9: 123-167.
- Peron, F., 1807: *Voyage de Decouvertes aux Terres Australes*. 2 vols. Imperial Press, Paris.
- Philpotts, A.R., 1968: Igneous structures and mechanism of emplacement of Mount Johnson, a monteregean intrusion, Quebec. *Can. Jour. Earth Sci.*, 5: 1130-1137.
- Philpotts, J.A., & Schnetzler, C.C., 1968: Genesis of continental diabases and oceanic tholeiites considered in light of rare-earth and barium abundances and partition coefficients. In Ahrens, L.H. (Ed.): *Origin and Distribution of the Elements*: 939-947. Pergamon.
- Pidgeon, R.T., & Compston, W., 1965: The age and origin of the Cooma granite and its associated metamorphic zones, New South Wales. *Jour. Petrol.*, 6: 193-222.
- Piguenit, W.C., 1857: Anon. *Hobart Town Advertiser*, March 13, 1857.
- Plimer, I.R., 1974: A spessartite-rich alteration assemblage from the Bega Granite. N.S.W., Australia. *Lithos*, 7: 43-51.
- Poldervaart, A., & Hess, H.H., 1951: Pyroxenes in the crystallization of basaltic magma. *Jour. Geol.*, 59: 472-489.
- Powell, J.L., & Bell, K., 1970: Strontium isotopic studies of alkalic rocks: localities from Australia, Spain and the western United States. *Contrib. Mineral. Petrol.*, 27: 1-10.
- Powell, M., 1978: The crystallization history of the Igdlarfigssalik nepheline syenite intrusion, Greenland. *Lithos*, 11: 99-120.
- Powell, M., & Powell, R., 1977: A nepheline-alkali feldspar geothermometer. *Contrib. Mineral. Petrol.*, 62: 193-204.

- Powell, M., & Powell, R., 1977: Plagioclase-alkali-feldspar geothermometry revisited. *Min. Mag.*, 41: 253-256.
- Presnall, D.C., 1969: The geometrical analysis of partial fusion. *Am. Jour. Sci.*, 267: 1178-1194.
- Presnall, D.C., & Bateman, P.C., 1973: Fusion relations in the system $\text{NaAlSi}_3\text{O}_8\text{-CaAl}_2\text{Si}_2\text{O}_8\text{-KAlSi}_3\text{O}_8\text{-SiO}_2\text{-H}_2\text{O}$ and generation of granitic magmas in the Sierra Nevada Batholith. *Bull. Geol. Soc. Am.*, 84: 3181-3202.
- Presnall, D.C., Dixon, S.A., Dixon, J.R., O'Donnell, T.H., Brenner, N.L., Shrock, R.L., & Dycus, D.W., 1978: Liquidus phase relations on the join diopside-forsterite-anorthite from 1 atm to 20 kbar: their bearing on the generation and crystallization of basaltic magma. *Contrib. Mineral. Petrol.*, 66: 203-220.
- Price, R.C., & Compston, W., 1973: The geochemistry of the Dunedin Volcano: strontium isotope chemistry. *Contrib. Mineral. Petrol.*, 42: 55-61.
- Price, R.C., & Chappell, B.W., 1975: Fractional crystallization and the petrology of Dunedin Volcano. *Contrib. Mineral. Petrol.*, 44: 157-180.
- Price, R.C., & Taylor, S.R., 1973: The geochemistry of the Dunedin volcano, East Otago, New Zealand: rare earth elements. *Contrib. Mineral. Petrol.*, 40: 195-205.
- Prider, R.T., 1960: The leucite lamproites of the Fitzroy Basin, Western Australia. *J. Geol. Soc. Aust.*, 6: 71-118.
- Rahman, S., & MacKenzie, W.S., 1969: The crystallization of Ternary feldspars: a study from natural rocks. *Am. Jour. Sci.*, 267A: 391-406.
- Rankama, K., 1954: *Isotope Geology*: 477. Pergamon.
- Richardson, S.W., 1968: The petrology of the metamorphosed syenite in Glen Desarry, Inverness-shire. *Quart. Jour. Geol. Soc. London*, 124: 9-51.
- Rickwood, P.C., 1968: On recasting analyses of garnet into end-member molecules. *Contrib. Mineral. Petrol.*, 18: 175-194.
- Ringwood, A.E., 1975: *Composition and Petrology of the Earth's Mantle*: 618. McGraw-Hill.
- Robertson, J.K., & Wyllie, P.J., 1971: Experimental studies on rocks from the Deboullie stock, northern Maine, including melting relations in the water deficient environment. *Jour. Geol.*, 79: 549-571.
- Rock, N.M.S., 1976: The comparative strontium isotopic composition of alkaline rocks: new data from southern Portugal and east Africa. *Contrib. Mineral. Petrol.*, 56: 205-228.
- Rock, N.M.S., 1976: The role of CO_2 in alkali rock genesis. *Geol. Mag.*, 113: 97-113.

- Roedder, P.L., 1974: Paths of crystallization and fusion in systems showing ternary solid solutions. *Am. Jour. Sci.*, 274: 48-60.
- Rosenweig, A., & Watson, E.H., 1954: Some hornblendes from southeastern Pennsylvania and Delaware. *Am. Mineral.*, 39: 581-599.
- Roux, J., & Hamilton, D.L., 1976: Primary igneous analcite - an experimental study. *Jour. Petrol.*, 17: 244-257.
- Rutherford, M.J., 1969: An experimental determination of iron biotite-alkali feldspar equilibria. *Jour. Petrol.*, 10: 381-408.
- Sakai, H., 1968: Isotopic properties of sulphur compounds in hydrothermal processes. *Geochem. Jour.*, 2: 29-49.
- Sass, J.H., & Lachenbruch, A.H., 1979: Thermal regime of the Australian continental crust. In McElhinny, M. (Ed.): *The Earth: Its Origin, Structure and Evolution*. Academic Press.
- Seck, H.A., 1971: Koexistierende Alkalifeldspate und Plagioklase im System $\text{NaAlSi}_3\text{O}_8$ - KAlSi_3O_8 - $\text{CaAl}_2\text{Si}_2\text{O}_8$ - H_2O bei Temperaturen von 650°C bis 900°C . *N. Jb. Min. Abh.*, 115: 315-345.
- Seck, H.A., 1971: Alkali feldspar-liquid and alkali feldspar-liquid vapour relations at pressures of 5 and 10 kbar. *N. Jb. Min. Abh.*, 115: 91-92.
- Schairer, J.F., & Bowen, N.L., 1955: The system K_2O - Al_2O_3 - SiO_2 . *Am. Jour. Sci.*, 253, 681-716.
- Schairer, J.F., & Yoder, H.S., 1960: The nature of residual liquids from crystallization: with data on the system nepheline-diopside-silica. *Am. Jour. Sci.*, 258A: 273-283.
- Shand, S.J., 1949: *Eruptive Rocks*: 488. 3rd ed. revised. Thomas Murby.
- Shapiro, L., 1960: A spectrometric method for the determination of FeO in rocks. *Geol. Surv. Res. - Short Papers in the Geological Sciences B*: 496-497.
- Shapiro, L., & Brannock, W.W., 1962: Rapid analysis of silicate, carbonate and phosphate rocks. *Bull. U.S. Geol. Surv.*, 1144A: 56.
- Sharples, C., & Klootwijk, C., 1981: Palaeomagnetic results from the Gordon Subgroup of Tasmania: further evidence for a late Cretaceous magnetic overprint in south-eastern Australia. *Pap. Proc. Roy. Soc. Tasm.*, 115: 85-91.
- Shaw, D.M., 1954: Trace elements in pelitic rocks. Part I: Variation during metamorphism. *Bull. Geol. Soc. Am.*, 65: 1151-1166.
- Shaw, D.M., 1956: Geochemistry of pelitic rocks. Part III: Major elements and general geochemistry. *Bull. Geol. Soc. Am.*, 67: 919-934.
- Shaw, D.M., 1970: Trace element fractionation during anatexis. *Geochim. Cosmochim. Acta*, 34: 237-243.

- Shaw, H.R., 1963: The four-phase curve sanidine-quartz liquid-gas between 500 and 4000 bars. *Am. Mineral.*, 48: 883-896.
- Skeats, E.W., 1917: On the age of the alkali rocks of Port Cygnet and the D'Entrecasteaux Channel in S.W. Tasmania. *Proc. Roy. Soc. Vic.*, 29 (n.s.), II: 154-164.
- Smith, D., & Albee, A.L., 1967: Petrology of a piemontite-bearing gneiss, San Gorgonio Pass, California. *Contrib. Mineral. Petrol.*, 16: 189-203.
- Smith, J.V., 1974: *Feldspar Minerals*. 3 vols. Springer-Verlag.
- Sobolev, V.S., 1959: On the phase correlation in the system nepheline-kalsilite-anorthite-silica. *Lvov Geol. Obsch. Mineralog. Sbornik.*, 13: 126-138.
- Solomon, M., 1981: An introduction to the geology and metallic ore deposits of Tasmania. *Econ. Geol.*, 76: 194-208.
- Sørensen, H., (Ed.), 1974: *The Alkaline Rocks*; 622. John Wiley.
- Spencer, A.B., 1969: Alkalic igneous rocks of the Balcones Province, Texas. *Jour. Petrol.*, 10: 272-306.
- Steiner, J.C., Jahns, R.H., & Luth, W.C., 1975: Crystallization of alkali feldspar and quartz in the haplogranite system $\text{NaAlSi}_3\text{O}_8$ - KAlSi_3O_8 - SiO_2 - H_2O at 4 kb. *Bull. Geol. Soc. Am.*, 86: 83-98.
- Stephenson, D., 1972: Alkali clinopyroxenes from nepheline syenites of the South Qoroq Centre, south Greenland. *Lithos*, 5: 187-201.
- Stephenson, D., 1974: Mn and Ca enriched olivines from nepheline syenites of the South Qoroq Centre, South Greenland. *Lithos*, 7: 35-41.
- Stewart, D.B., & Rosenboom, E.H., 1962: Lower temperature terminations of the three phase region plagioclase-alkali feldspar-liquid. *Jour. Petrol.*, 3: 280-315.
- Stormer, J.C., 1975: A practical two-feldspar geothermometer. *Am. Mineral.*, 60: 667-674.
- Stormer, J.C., & Carmichael, I.S.E., 1970: The Kudo-Weill plagioclase geothermometer and porphyritic acid glasses. *Contrib. Mineral. Petrol.*, 28: 306-309.
- Stout, J.H., 1972: Phase petrology and mineral chemistry of co-existing amphiboles from Telemark, Norway. *Jour. Petrol.*, 13: 99-145.
- Streckeisen, A.L., 1967: Classification and nomenclature of igneous rocks. *N. Jb. Min. Abh.*, 107: 144-240.
- Streckeisen, A.L., 1976: To each plutonic rock, its proper name. *Earth Sci. Rev.*, 12: 1-33.
- Sturt, B.A., & Ramsay, D.M., 1965: The alkaline complex of the Breivikbotn area, Sørøya, northern Norway. *Nor. Geol. Unders.*, 231.

- Subbarao, K.V., 1971: The Kunavaram series - a group of alkaline rocks, Khammam district, Andhra Pradesh, India. *Jour. Petrol.*, 12: 621-641.
- Sutherland, D.S., 1967: Potassium-rich trachytes in the Kaiserstuhl carbonatite complex, W. Germany. *Min. Mag.*, 36: 334-341.
- Taubeneck, W.H., 1965: An appraisal of some potassium-rubidium ratios in igneous rocks. *Jour. Geophys. Res.*, 70: 475-478.
- Taylor, D., 1967: The sodalite group of minerals. *Contrib. Mineral. Petrol.*, 16: 172-188.
- Taylor, D., & Mackenzie, W.S., 1975: A contribution to the pseudoleucite problem. *Contrib. Mineral. Petrol.*, 49: 321-333.
- Taylor, S.R., 1965: The application of trace element data to problems in petrology. *Phys. Chem. of the Earth*, 6: 133-214.
- Taylor, S.W., Ewart, A., & Capp, A., 1968: Leucogranites and rhyolites: trace element evidence for fractional crystallization and partial melting. *Lithos*, 1: 179-186.
- Taylor, S.R., & Gorton, M.P., 1977: Geochemical application of spark source mass spectrography - III. Element sensitivity, precision and accuracy. *Geochim. Cosmochim. Acta*, 41: 1375-1380.
- Templeman-Kluit, P.J., 1969: A re-examination of pseudoleucite from Spotted Fawn Creek, west-central Yukon. *Can. Jour. Earth Sci.*, 6: 55-62.
- Thode, H.G., 1970: Sulphur isotope geochemistry and fractionation between co-existing minerals. *Min. Soc. Am. Spec. Pap.*, 3: 133-144.
- Thompson, A.B., & Tracy, R.J., 1979: Model systems for anatexis of pelitic rocks. *Contrib. Mineral. Petrol.*, 70: 429-438.
- Thornton, C.P., & Tuttle, O.F., 1960: The chemistry of igneous rocks. I: differentiation index. *Am. Jour. Sci.*, 258: 664-684.
- Tilley, C.E., 1958: Problems of alkali rock genesis. *Quart. Jour. Geol. Soc.*, 113: 323-360.
- Turekian, K.K., 1978: Strontium. In *Handbook of Geochemistry*. II-4, 38: D1-K13. Springer-Verlag.
- Turner, D.C., 1968: Volcanic and intrusive structures in the Kila-Warjic ring complex, northern Nigeria. *Quart. Jour. Geol. Soc. London*, 124: 81-89.
- Tuttle, O.F., 1952: Optical studies on alkali feldspars. *Am. Jour. Sci.*, Bowen Volume: 553-567.
- Tuttle, O.F., 1952: Origin of the contrasting mineralogy of extrusives and plutonic rocks. *Jour. Geol.*, 60: 107-124.

- Tuttle, O.F., & Bowen, N.L., 1958: Origin of granite in the light of experimental studies in the system $\text{NaAlSi}_3\text{O}_8$ - KAlSi_3O_8 - SiO_2 - H_2O . *Geol. Soc. Am. Mem.* 74.
- Twelvetrees, W.H., & Petterd, W.F., 1898: On the hauyne-trachyte and allied rocks in the district of Port Cygnet and Oyster Cove. *Pap. Proc. Roy. Soc. Tasm.*, 1898-1899: 3-26.
- Twelvetrees, W.H., 1903: A geological excursion to Port Cygnet in connection with the Australasian Association for the Advancement of Science 1902. *Pap. Proc. Roy. Soc. Tasm.*, 1903-1905: 42-48.
- Twelvetrees, W.H., 1903: Note on jacupirangite in Tasmania. *Pap. Proc. Roy. Soc. Tasm.*, 1903-1905: 73-74.
- Twelvetrees, W.H., 1907: Report on gold at Port Cygnet and Wheatleys Bay, Huon River. *Ann. Rept Sec. Mines Tasm.* 1907.
- Tyler, R., & King, B.C., 1967: The pyroxenes of the alkaline igneous complexes of eastern Uganda. *Min. Mag.*, 36: 5-21.
- Upton, B.G.J., Thomas, J.E., & McDonald, R., 1971: Chemical variation within three alkaline complexes in south Greenland. *Lithos*, 4: 163-184.
- Vallance, T.G., 1981: The start of Government science in Australia: A.W.H. Humphrey, His Majesty's Mineralogist in New South Wales, 1803-1812. *Proc. Linn. Soc. N.S.W.*, 105: 107-146.
- Van Groos, A.F.K., 1975: The effect of high CO_2 pressures on alkalic rocks and its bearing on the formation of alkalic ultrabasic rocks and the associated carbonatites. *Am. Jour. Sci.*, 275: 163-185.
- Veevers, J.J., & McElhinny, M.W., 1976: The separation of Australia from other continents. *Earth Sci. Rev.*, 12: 139-159.
- Velde, B., 1967: Si^{4+} content of natural phengites. *Contrib. Mineral. Petrol.*, 14: 250-258.
- Vidal, P., Dosso, L., Bowden, P., & Lameyre, J., 1979: Strontium isotope geochemistry in syenite-alkaline granite complexes. In Ahrens, L.H. (Ed.): *Origin and Distribution of the Elements*. (Second Symposium) Physics and Chemistry of the Earth, VII. Pergamon.
- Vinogradov, A.P., Grinenko, V.A., & Ustinov, V.I., 1962: Isotopic composition of sulphur compounds in the Black Sea. *Geokhimiya*, 10: 973-997.
- Virgo, D., Huggins, F.E., & Rosenhauer, M., 1976: Petrologic implications of intrinsic oxygen fugacity measurements on titanium-containing silicate garnets. *Carnegie Inst. Washington Yearbook*, 75: 730-735.

- von Buch, L., 1814: Einige Bernerkungen uber die geognostiche Constitution von Van Diemens Land. (*Mag. fur die Neu Entdeckungen*) in der *Gesamnte Naturkurde*, 6: 234-240.
- Von Platen, H., 1965: Experimental anatexis and genesis of migmatites. *Geol. Jour.*, Special Issue 1: 1368,
- Von Platen, H., 1965: Kristallisation Granitescher Schmelzen. *Beit. Mineral. Petrog.*, 11: 334-381.
- Wade, A., & Prider, R.T., 1940: The leucite bearing rocks of the West Kimberley area, Western Australia. *Quart. Jour. Geol. Soc. London*, 96: 39-98.
- Wager, L.R., 1965: The form and internal structure of the alkaline Kangerdlugssuaq intrusion, east Greenland. *Min. Mag.*, 34: 487-497.
- Waldbaum, D.R., & Thompson, J.B., 1969: Mixing properties of sanidine crystalline solutions: IV. Phase diagrams from equations of state. *Am. Mineral.*, 54: 1274-1298.
- Watkinson, D.H., & Wyllie, P.J., 1971: Experimental study of the composition join $\text{NaAlSiO}_4\text{-CaCO}_3\text{-H}_2\text{O}$ and the genesis of alkalic rock-carbonatite complexes. *Jour. Petrol.*, 12: 357-378.
- Wendlandt, R.F., & Eggler, D.H., 1980: The origins of potassic magmas: 1. Melting relations in the systems $\text{KAlSiO}_4\text{-Mg}_2\text{SiO}_4\text{-SiO}_2$ and $\text{KAlSi}_3\text{O}_8\text{-MgO-SiO}_2\text{-CO}_2$ to 30 kilobars. *Am. Jour. Sci.*, 280: 385-420.
- Wendlandt, R.F., & Eggler, D.H., 1980: The origins of potassic magmas: 2. Stability of phlogopite in natural spinel lherzolite and in the system $\text{KAlSiO}_4\text{-MgO-SiO}_2\text{-H}_2\text{O-CO}_2$ at high pressures and high temperatures. *Am. Jour. Sci.*, 280: 421-458.
- Wilshire, H.G., & Binns, R.A., 1961: Basic and ultrabasic xenoliths from volcanic rocks of New South Wales, Australia. *Jour. Petrol.*, 2: 185-208.
- Wilkinson, J.F.G., 1965: Some feldspars, nephelines and analcimes from the Square Top intrusion, Nundle, N.S.W. *Jour. Petrol.*, 6: 420-444.
- Wilkinson, J.F.G., 1973: Pyroxenite xenoliths from an alkali trachybasalt in the Glen Innes area, N.E. New South Wales. *Contrib. Mineral. Petrog.*, 42: 15-31.
- Winchell, A.N., 1951: *Elements of Optical Mineralogy. Part II: Descriptions of Minerals*: 551. John Wiley.
- Winchester, J.A., & Floyd, P.A., 1976: Geochemical magma type discrimination: application to altered and metamorphosed basic igneous rocks. *Earth Planet. Sci. Letters*, 28: 459-469.
- Winkler, H.G.F., 1976: *Petrogenesis of Metamorphic Rocks*: 334. 4th edition. Springer-Verlag.

- Winkler, H.G.F., Boese, M., & Marcopolous, T., 1975: Low temperature granite melts. *N. Jb. Min. Mon.*, H6: 245-267.
- Winkler, H.G.F., & Lindemann, W., 1972: The system Qtz-Or-An-H₂O within the granitic system Qz-Or-Ab-An-H₂O. *N. Jb. Min. Mon.*, H2: 49-61.
- Wones, D.R., & Eugster, H.P., 1965: Stability of biotite: experiment, theory and application. *Am. Mineral.*, 50: 1228-1272.
- Wood, B.J., 1976: Mixing properties of tschermakitic clinopyroxenes. *Am. Mineral.*, 61: 599-602.
- Wright, J.B., 1965: Petrographic sub-provinces in the Tertiary to Recent volcanics of Kenya. *Geol. Mag.*, 102: 541-557.
- Wright, T.L., 1968: X-ray and optical study of alkali feldspar: an X-ray method for determining the composition and structural state from measurements of 2θ values for three reflections. *Am. Mineral.*, 53: 88-104.
- Wronski, E.B., 1977: Two heat flow values from Tasmania. *Geophys. Jour. Roy. Astr. Soc.*, 48: 131-133.
- Wyllie, P.J., 1977: Crustal anatexis: an experimental review. *Tectonophysics*, 43: 41-71.
- Yoder, H.S., & Eugster, H.P., 1954: Phlogopite synthesis and stability range. *Geochim. Cosmochim. Acta*, 6: 157-185.
- Young, D.A., 1972: A quartz syenite intrusion in the New Jersey Highlands. *Jour. Petrol.*, 13: 511-528.
- Zartman, R.E., Brock, M.R., Heyl, A.V., & Thomas, H.H., 1967: K-Ar and Rb-Sr ages of some alkalic intrusive rocks from central and eastern United States. *Am. Jour. Sci.*, 265: 848-870.

REFERENCES

ADDENDUM

- Abbey, S., 1977: Studies in standard samples. Part 5: 1977 edition of "usable" values. *Geol. Surv. Can.*, Paper 77-34.
- Abbey, S., 1980: Studies in standard samples. Part 6: 1979 edition of "usable" values. *Geol. Surv. Can.*, Paper 80-14.
- Arth, J.G., & Hanson, G.N., 1972: Quartz diorites derived by partial melting of eclogite or amphibolite at mantle depths. *Contrib. Mineral. Petrol.*, 37: 161-174.
- Bailey, D.K., & MacDonald, R. (Eds), 1976: *The Evolution of the Crystalline Rocks*: 484. Academic Press.
- Balashov, Yu.A., 1963: Regularities in the distribution of the rare earths in the earth's crust. *Geochem. (USSR) Eng. Trans.*, 107-124.
- Barker, D.S., 1965: Alkalic rocks at Litchfield, Maine. *Jour. Petrol.*, 6: 1-27.
- Boeke, H.E., 1914: *Zeit. Krist.*, L11: 149.
- Borodin, L.S., & Paulenko, A.S., 1974: The rôle of metasomatic processes in the formation of alkaline rocks. In Sorenson, H. (Ed.) *The Alkaline Rocks*: Chapter VI-7.
- Bose, M.K., 1973: Petrology and geochemistry of the igneous complex of Mt. Girnar, Sujarat, India. *Contrib. Mineral. Petrol.*, 39: 247-266.
- Bowen, N.L., 1937: Recent high-temperature research on silicates and its significance in igneous geology. *Am. Jour. Sci.*, 33: 1-21.
- Bowen, N.L., & Ellestad, R.B., 1937: Leucite and pseudoleucite. *Am. Min.*, 22: 409-415.
- Bowen, N.L., & Tuttle, O.F., 1950: The system $\text{NaAlSi}_3\text{O}_8$ - KAlSi_3O_8 - H_2O . *Jour. Geol.*, 58: 489-511.
- Brown, E.H., 1967: The Greenschist Facies in Part of Eastern Otago, New Zealand. *Contrib. Mineral. Petrol.*, 14: 262-283.
- Browne, W.R., 1914: The geology of the Cooma district. *Jour. Proc. Roy. Soc. N.S.W.*, 48: 172-222.
- Chapman, R.W., & Williams, C.R., 1935: Evolution of the White Mountain magma series. *Am. Min.*, 20: 502-30.
- Coombs, D.S., 1963: Trends and affinities of basaltic magmas and pyroxenes as illustrated on the diopside-olivine-silica diagram. *Min. Soc. Am. Spec. Paper* 1: 227-250.
- Cyzamanske, G.K., & Rye, R.O., 1974: Experimentally determined sulphur isotope fractionations between sphalerite and galena in the temperature range 600°C to 275°C. *Econ. Geol.*, 69: 17-25.

- David, T.W.E., & Skeats, E.W., 1914: Handbook on Australia for Brit. Assoc. meeting: 309.
- Davidson, L.R., 1970: Variation in ferrous iron-magnesium distribution coefficients of metamorphic pyroxenes from Quairading, Western Australia. *Contrib. Mineral. Petrol.*, 19: 239-259.
- Degenhardt, H., 1957: Untersuchungen zur geochemischen Verteilung des Zirkoniums in der Lithosphäre. *Geochem. Cosmochim. Acta*, 11: 279-309.
- Douglas, J.A.V., 1964: Geological investigations in East Greenland, Part VII - The Basistoppen sheet. *Medd. Groenland*, 164(5): 1.
- Fryklund, V.C., & Fleischer, M., 1963: The abundance of scandium in volcanic rocks, a preliminary estimate. *Geochim. Cosmochim. Acta*, 27: 643-664.
- Gast, P., 1968: Trace element fractionation and the origin of tholeiitic and alkaline magma types. *Geochim. et Cosmochim. Acta*, 32: 1057-86.
- Gerasimovsky, V.I., & Belyasev, Yu.I., 1963: Chromium, nickel, vanadium and copper content of alkalic rocks, Kola Peninsula. *Geochemistry*, 1: 22.
- Gilbert, M.C., 1969: Reconnaissance study of the stability of amphiboles at high pressure. *Carnegie Inst. Washington Yearbook*, 67: 167-170.
- Goldschmidt, V.M., 1930: Elemente und Minerale pegmatitischer Gesteine. *Nachr. Gesellsch. Wiss. Göttingen. Math. Phys.*, K1: 370-378.
- Grover, J.L., 1977: Chemical mixing in multicomponent solutions. In Fraser, D.G. (Ed.) *Thermodynamics in Geology*: 410. D. Riedel.
- Gupta, A.K., & Edgar, A.D., 1974: Phase relations in the system nepheline-leucite-anorthite at 1 atmosphere. *Can. Min.*, 12: 354-356.
- Gupta, A.K., & Yagi, K., 1980: *Petrology and Genesis of Leucite-bearing Rocks*: 252. Springer-Verlag.
- Holloway, J.R., 1973: The system pargasite-H₂O-CO₂, a model for melting hydrous minerals with a mixed volatile fluid. I - Experimental results to 8 kb. *Geochim. et Cosmochim. Acta*, 37: 651-666.
- Holloway, J.R., 1976: Fluids in the evolution of granitic magmas: consequences of finite CO₂ solubility. *Bull. Geol. Soc. Am.*, 87: 1513-1518.
- Holloway, J., & Burnham, C.W., 1972: Melting relations of basalt with equilibrium water pressure less than total pressure. *Jour. Petrol.*, 13: 1-29.

- Holmes, A., & Harwood, H.F., 1937: The petrology of the volcanic field of Bafumbria, S.W. Uganda and of other parts of the Birunga Field. *Geol. Surv. Uganda Mem.*, 3.
- Hutton, C.O., 1957: Contributions to the mineralogy of New Zealand. Pt. IV. *Trans. Roy. Soc. N.Z.*, 84: 791-803.
- Jensen, H.I., 1908: The distribution origin and relationships of alkaline rocks. *Proc. Linn. Soc. N.S.W.*, 33: 491-602.
- Johannsen, A., 1938: *A Descriptive Petrography of the Igneous Rocks*: Volume IV. University of Chicago Press.
- King, B.C., 1965: Petrogenesis of the alkaline igneous rock suites of the volcanic and intrusive centres of E. Uganda. *Jour. Petrol.*, 6: 67-100.
- Knight, C.W., 1906: A new occurrence of pseudo-leucite. *Am. Jour. Sci.*, 21: 286-293.
- Kogarko, L.N., 1974: Role of volatiles. In Sorensen, H. (Ed.) *The Alkaline Rocks*: Chapter VI-4. Wiley.
- Kogarko, L.N., & Polyakov, A.J., 1967: The problems on genesis of the agpaitic nepheline syenites. *Geokhim.*, 2: 131-143.
- Kogarko, L.N., Ryabchikov, I.D., & Sorensen, H., 1974: Liquid fractionation. In Sorensen, H. (Ed.) *The Alkaline Rocks*: Chapter VI-5. Wiley.
- Kukhareenko, A.A., Orlova, M.P., Bulak, A.G., Bagdasarov, E.A., Rimskaya-Korsakova, O.M., Nephedor, E.I., Ilynsky, G.A., Sergeev, A.S., & Abakumova, N.B., 1965: Caledonian complex of ultrabasic alkaline rocks and carbonatites of the Kola peninsula and N. Karelia. *Izd. 'Nedra'*, 1-772 (in Russian).
- Kuno, H., 1968: Origin of andesite and its bearing on the island arc structure. *Bull. Volc.*, 32: 141-176.
- Long, L.E., 1964: Rb-Sr chronology of the Cam Chuinneag Intrusion, Rosshire, Scotland. *Jour. Geophys. Res.*, 6: 1589-1597.
- McDougall, I., & Legge, P.J., 1965: Isotopic age determinations on granitic rocks from Tasmania. *Jour. Geol. Soc. Aus.*, 12: 295-332.
- Merrill, R.B., & Wyllie, P.J., 1975: Kaersutite and kaersutite eclogite melting from Kakanui, New Zealand. *Bull. Geol. Soc. Am.*, 86: 555-570.
- Morse, S.A., 1969: Nepheline-kalsilite-silica at 5 kb P_{H_2O} . *Carnegie Inst. Wash. Yearbook*, 68.
- Mysen, B.O., 1976: The role of volatiles in silicate melts: solubility of carbon dioxide and water in feldspar, pyroxene and feldspathoid melts to 30 kb and 1625°C. *Am. Jour. Sci.*, 276: 969-996.

- Nicholls, J., & Carmichael, I.S.E., 1969: A commentary on the akarokite-shoshonite-banakite series of Wyoming, U.S.A. *Schweiz. Min. Petr. Mitt.*, 49: 47-64.
- Nockolds, S.R., & Allen, R., 1953: The geochemistry of some igneous rock series. *Geochim. et Cosmochim. Acta*, 4: 105.
- Nockolds, S.R., & Mitchell, R.L., 1948: The geochemistry of some Caledonian plutonic rocks: a study in the relationship between the major and trace elements of igneous rocks and their minerals. *Trans. Roy. Soc. Edinburgh*, 61: 533-575.
- Norrish, K., & Hutton, J.T., 1969: X-ray spectrographic method for the analysis of a wide range of geological samples. *Geochim. et Cosmochim. Acta*, 33: 431-453.
- Oba, T., 1980: Phase relations in the tremolite-pargasite join. *Contrib. Mineral. Petrol.*, 71: 247-256.
- Parsons, I., 1965: The sub-surface shape of part of the Loch Ailsh intrusion, Assynt. *Geol. Mag.*, 102: 46-58.
- Perchuk, L., 1977: Thermodynamic control of metamorphic processes. In Saxena, S.K., & Bhattacharji, S. (Eds) *Energetics of Geological Processes*: 285-352. Springer-Verlag, New York.
- Peterman, Z.E., & Hedge, C.E., 1971: Related strontium isotopic and chemical variations in oceanic basalts. *Bull. Geol. Soc. Am.*, 83: 493-
- Phemister, J., 1926: *Geol. Surv. Scot. Expl.*, 103: 41.
- Powell, J.L., & Bell, K., 1974: Isotopic composition of strontium in alkalic rocks. In Sorensen, H. (Ed.) *The Alkaline Rocks*: Chapter V-4: 412-421. Wiley.
- Reid, A.M., 1922: In The coal resources of Tasmania: 123-146. *Tas. Geol. Surv. Min. Res. Bull.*, 7.
- Robertson, W.A., & Hastie, L.M., 1961: Palaeomagnetic study of the Cygnet alkaline complex. *Jour. Geol. Soc. Aus.*, 8: 259-268.
- Sabine, P.A., 1953: The petrography and geological significance of the post-Cambrian minor intrusions of Assynt and the adjoining districts of north-west Scotland. *Quart. Jour. Geol. Soc. Lond.*, 109: 127-169.
- Shand, S.J., 1922: The problem of the alkaline rocks. *Proc. Geol. Soc. South Africa*, 25: XIX-XXXII.
- Shand, S.J., 1930: Limestone and the origin of feldspathoidal rocks: an aftermath of the Geological Congress. *Geol. Mag.*, 67: 415-426.
- Shaw, D.M., 1960: The geochemistry of scapolite. Parts I and II. *Jour. Petrol.*, 1: 218-285.

- Shaw, D.M., 1968: A review of K-Rb fractionation trends by covariance analysis. *Geochim. et Cosmochim. Acta*, 32: 573-601.
- Steuhl, H.H., 1962: Di experimentelle Metamorphose und Anatexis eines Parabiottitgneises aus dem Schwarzwald. *Chem. Erde*, 21: 413-449.
- Taylor, S.R., 1964: Abundance of chemical elements in the continental crust: a new table. *Geochim. et Cosmochim. Acta*, 28: 1273-1285.
- Tilley, C.E., 1958: Some new chemical data on assemblages of the Assynt alkali suite. *Trans. Edinburgh Geol. Soc.*, 17: 156-164.
- Upton, B.G.J., 1960: The alkaline igneous complex of Kûngnât Fjeld, South Greenland. *Medd. om Grønland*, 123: 1-145.
- Ussing, N.V., 1912: Geology of the country around Julianehaab, Greenland. *Meddr. Grønland*, 38: 1-376.
- Velde, B., 1965: Phengitic micas: Synthesis, stability and natural occurrence. *Am. Jour. Sci.*, 263: 886-913.
- Vinogradov, A.P., 1962: Average contents of chemical elements in the principal types of igneous rocks in the earth's crust. *Geochem.*, 7: 641.
- Von Knorring, O., & Kennedy, W.Q., 1958: The mineral paragenesis and metamorphic status of garnet-hornblende-pyroxene scapolite gneiss from Shana. *Min. Mag.*, 31: 846-859.
- Wedepohl, K.H., 1972: *Zinc - Handbook of Geochemistry*: II-3, 30 B-O. Springer-Verlag.
- Wedepohl, K.H., 1978: *Niobium - Handbook of Geochemistry*: IIV-4, 41 E. Springer-Verlag.
- White, A.J.R., 1959: Scapolite-bearing marbles and calc-silicate rocks from Tungkillo and Milendella, South Australia. *Geol. Mag.*, 96: 285-306.
- Wilkinson, J.F.G., 1966: Residual glasses from some alkali basaltic lavas from New South Wales. *Min. Mag.*, 35: 847-860.
- Wilkinson, J.F.G., 1968: Analcimes from some potassic igneous rocks and aspects of analcime-rich igneous assemblages. *Contrib. Mineral. Petrol.*, 18: 252-269.
- Winkler, H.G.F., 1966: Der Prozess der Anatexis: Seine Bedeutung für die Genese der Migmatite. *Tschermaks. Miner. Petrogr. Mitt.*, 11: 266-237.
- Winkler, H.G.F., 1967: *Petrogenesis of Metamorphic rocks*: 2nd edition. Springer-Verlag.
- Winkler, H.G.F., 1974: *Petrogenesis of Metamorphic rocks*: 3rd edition. Springer-Verlag.

- Wones, D.R., & Eugster, H.P., 1962: Stability relations of the ferruginous biotite, annite. *Jour. Petrol.*, 3: 82-125.
- Wood, B.J., 1976: Mixing properties of tschermakitic clinopyroxenes. *Am. Min.*, 61: 599-602.
- Wright, T.L., & Stewart, D.B., 1968: X-ray and optical study of alkali feldspar: I. Determination of composition and structural state from refined unit cell parameters and 2V. *Am. Min.*, 53: 38-87.
- Wyllie, P.J., 1974: Limestone assimilation. In Sorensen, H. (Ed.) *The Alkaline Rocks*: Chapter VI-3. Wiley.
- Wyllie, P.J., 1979: Magmas and volatile components. *Am. Min.*, 64: 469-500.
- Wyllie, P.J., & Tuttle, O.F., 1959: Effect of CO₂ on the melting of granite and feldspars. *Am. Jour. Sci.*, 257: 648-655.
- Zielinski, R.A., 1975: Trace element evaluation of a suite of rocks from Reunion Island, Indian Ocean. *Geochim. et Cosmochim. Acta*, 39: 713-734.
- Ferguson, J., 1970: The differentiation of agpaitic magmas: The Ilimaussaq intrusion, south Greenland. *Can. Min.*, 10: 335-349.
- Fersman, A., 1929: Geochemische Migration der Elemente. *Abh. prakt. Geol. Bergwlehre*, 18: 1-116.